# Chapter 10: Linking global to regional climate change

**Coordinating Lead Authors:**
Francisco J. Doblas-Reyes (Spain), Bruce Hewitson (South Africa)

**Lead Authors:**
Mansour Almazroui (Saudi Arabia), Alessandro Dosio (Italy), William Gutowski (USA), Rein Haarsma (Netherlands), Rafiq Hamdi (Belgium), Won-Tae Kwon (Republic of Korea), Benjamin Lamptey (Ghana), Douglas Maraun (Austria/Germany), Anna Amelia Sörensson (Argentina), Tannecia Stephenson (Jamaica), Izuru Takayabu (Japan), Laurent Terray (France), Andrew Turner (UK), Zhiyan Zuo (China)

**Contributing Authors:**
Bodo Ahrens (Germany), Melissa Bukovski (USA), Alex Cannon (Canada), Laura Gallardo (Chile), Hugues Goose (Belgium), Pandora Hope (Australia), Christopher Jack (South Africa), Hiroyuki Kusaka (Japan), Jan Polcher (France/Germany), Ingo Richter (Japan/Germany), Victor Venema (Germany), Piotr Wolski (South Africa), Jakob Zscheischler (Switzerland)

**Review Editors:**
Greg Flato (Canada), Fredolin Tangang (Malaysia), Muhammad Irfan Tariq (Pakistan)

**Date of Draft:** 29 April 2019

**Notes:** TSU Compiled Version

**Executive Summary**

**The AR5 underlined the critical need for better regional information** that is useful and relevant to the decision scale of policy and adaptation communities. To contribute to this gap, Chapter 10 assesses the foundations of how to move from global-mean information to the regional scales of societal need. **Constructing regional messages goes far beyond the application of a downscaling method**, with many complementary emerging approaches. **The AR6 provides additional foundational knowledge of key factors that frame the formulation, interpretation and application of regional messages of change**.

**Observational datasets and model simulations are the two main inputs** for climate-related decision making. **Observational references introduce an additional source of uncertainty for regional climate information**, and benefit from the best performing statistical homogenization methods, which in general improve long-term warming estimates {Section 10.2}.

**Paleo-reanalyses confirm *robust evidence* for the large contribution of internal variability to past changes at the regional scale** during the pre-industrial period, superimposed on a weak common signal due to external forcing {Section 10.2}.

**There is *high confidence* that complex, multi-variate and process-oriented diagnostics are needed to evaluate whether a climate model realistically simulates regional climate**, but they are not sufficient to verify that a climate model is an adequate source of regional climate information for the intended application {Section 10.3}.

Despite the known systematic errors that affect model performance, **there is *high confidence* that GCMs collectively provide useful information for future climate messages at the regional scale**. **There is *robust evidence and high agreement* that increasing global model resolution can help reduce a number of systematic errors**, although resolution per se does not automatically solve all performance limitations. Reducing systematic errors in GCMs is also important for improving the boundary conditions for downscaling {Section 10.3.3}.

**There is *high confidence* that including all relevant forcings in RCMs is a prerequisite for reproducing historical trends**, and that increasing model resolution, performing downscaling and adding model components increase the adequacy-for-purpose for some aspects of regional projections, in particular to represent weather phenomena over complex terrain. **There is *high confidence* that simulations at convection permitting resolution add value** to the representation of deep convection and related phenomena. There is *medium confidence and high agreement* that simulations at convection-permitting resolution are required to realistically represent soil-moisture precipitation feedbacks {Section 10.3.3}.

**There is *high confidence* that while all types of urban parameterizations generally simulate realistic radiation exchanges, they have, however, strong biases in simulating latent heat fluxes**. For the purpose of urban climate modelling there is *robust evidence* that a simple single-layer parameterization might be sufficient {Section 10.3.3}.

**There is *robust evidence and high confidence* that statistical downscaling can enhance aspects of the regional information of climate projections**, but modelling of daily precipitation and spatial fields remains a challenge {Section 10.3.3}.

**Bias adjustment has proven beneficial as an interface between climate model projections and impact modelling**, yet it cannot correct for missing unresolved or fundamentally misrepresented processes that lead to model errors. **There is *high confidence* that bias adjustment can improve the marginal distribution of simulated climate variables** if applied to a climate model that adequately represents the processes relevant for a given application {Box 10.2}. **There is *high confidence* that using bias adjustment for statistical downscaling, in particular of coarse resolution GCMs, has some limitations** and that dynamical downscaling may be required to resolve relevant local processes prior to bias adjustment {Section 10.3.3 and Box 10.2}.

**There is *high confidence* that the multi-model mean and ensemble spread are not sufficient to characterise many aspects of regional climate**. **There is *high confidence* that the interpretation of climate projection uncertainties is improved by storyline approaches**.

**There is *high confidence* that using multi-model ensemble methods, while excluding models that unrealistically simulate processes relevant for a given phenomenon, enhances the value of regional climate messages** {Section 10.3.4}.

**There is *high confidence* that internal variability will significantly influence some future regional precipitation trends** until at least the end of the 21st century. There is *very high confidence* that forced regional-mean temperature signals will have emerged from internal variability at almost all locations by 2050 under the high-end RCPs {Section 10.4}.

**There is *very high confidence* that patterns of 20th century SST variability have caused the Sahel drought and subsequent recovery**, the latter also being aided by amplified Saharan warming. There is *high confidence* that the patterns of SST variability are themselves driven by variations of anthropogenic emissions. **There is *high confidence* for the future West African monsoon and Sahel precipitation change to be dominated by gradients of SST change between the tropics and North Atlantic and of Sahara temperature change** and *medium confidence* (*robust evidence and low agreement*) that the precipitation will increase {Sections 10.4.2 and 10.4.3}.

**There is *high confidence* that anthropogenic forcing has influenced historical changes** (both weakening and recovery) **of the East Asian summer monsoon** but *low confidence* in the magnitude of anthropogenic influence. There is *high confidence* that the transition towards a positive phase of Pacific decadal variability has been one of the main drivers of the monsoon weakening since the 1970s. **There is *high confidence* that precipitation will increase throughout the 21st century** but *low confidence* in the magnitude or spatial pattern {Sections 10.4.2 and 10.4.3}.

**There is *high confidence* that southern Australia warming and rainfall decline since the early 1970s are mainly anthropogenically forced.** There is *high confidence* that the cold season drying trend in southwest Australia will continue under future scenarios, with a greater decline for higher levels of greenhouse gases {Sections 10.4.2 and 10.4.3}.

**There is *low confidence* (*medium evidence and low agreement*) in the relative contributions of anthropogenic and internal drivers to the South Eastern South America summer precipitation increase** since the beginning of the 20th century. The precipitation will *more likely than* not increase based on model simulations, with little knowledge of the responsible mechanisms {Sections 10.4.2 and 10.4.3}.

**There is *high confidence* that a significant (at least 50%) fraction of the Eurasian cooling has been caused by internal atmospheric variability**, but there is *low confidence* in the exact role of Arctic warming and sea-ice loss in this cooling. **There is *high confidence* that Eurasia will experience additional warming during the 21st century with a continental-scale spatial pattern reflecting Arctic amplification** {Sections 10.4.2 and 10.4.3}.

**There is *medium confidence* (*robust evidence and low agreement*) that decreased anthropogenic aerosol emissions over Europe has been the dominant factor behind enhanced European summer warming**. **There is *high confidence* that local soil-moisture feedbacks have contributed to the increase in extreme temperature variability** and consequently, frequency and intensity of heat waves; and *medium confidence* that it has contributed to increased summer-mean temperature. There is *high confidence* that GCMs and RCMs underestimate the observed warming trend. There is *high confidence* that anticipated future reductions in aerosol emissions will enhance European summer warming. **There is *high confidence* that Southern Europe will warm faster than global mean temperature due to local feedbacks** {Sections 10.4.2 and 10.4.3}.

**There is *high confidence* that the observed southwestern North America negative precipitation trend**

**can be attributed to circulation anomalies arising from teleconnections** linked to the tropical Pacific decadal variability. There is *low confidence* in projections of precipitation for the region {Sections 10.4.2 and 10.4.3}.

**There is *robust evidence and high agreement* that a proportion of the observed warming trend in cities can be linked to historical urbanization in rapidly industrialized countries. There is *robust evidence and high agreement* that annual-mean maximum temperature is substantially less affected by urbanization than minimum temperature**. There is *medium evidence and medium agreement* that urban areas induce increases in mean and extreme precipitation over and downwind of a city {Sections 10.4.2 and 10.4.3}.

**There is *high confidence* of rising temperatures in the Himalayan region**, and that the rate of warming is amplified with elevation. **There is *high confidence* that a large fraction (at least 50%) of the warming can be attributed to increases in carbon dioxide and black carbon aerosols and that the decrease in summer precipitation can be mainly attributed to a weakening in the South Asian monsoon**. **There is *medium confidence* that a wetter climate will occur in the Himalayas during the near term of the 21st century**. There is *low confidence* (*medium evidence and low agreement*) in the magnitude and spatial pattern of projected temperature and precipitation changes {Sections 10.4.2 and 10.4.3}.

**There is *low confidence* in the role of historical Arctic warming and sea-ice loss in mid-latitude variability**. The signal is small compared to internal variability, and a number of alternative hypotheses can explain the observed variability. Future climate change is *likely* to affect mid-latitude variability in different ways including through the impact of Arctic warming, but **there is *low confidence* in the relative contributions of Arctic warming and other drivers** {Cross-Chapter Box 10.1}.

**Regional climate change messages are influenced by the values** of those constructing, communicating, and receiving the message. **There is *high confidence* that including users ensures the correct context in forming the message**. **There is *strong evidence* and *high agreement* that support of collaborative learning and information production** involving a diversity of expertise from climate scientists and decision makers **result in better integration of scientific evidence into decision making** {Section 10.5}.

**Distillation of information from multiple** contrasting or even contradictory **data sources remains an important frontier challenge**. **Storylines and narratives are a powerful means of addressing this challenge, making climate change information** more accessible and physically plausible by linking to weather and climate experiences of the recipient {Section 10.5.3}.

**There is *high confidence* (with *high agreement*) that precipitation in the Cape Town region will likely decrease toward the end of the 21st century**. This conclusion is supported by *high agreement* in projections of key circulation mechanisms, including the southward shift of Southern Hemisphere midlatitude westerlies, storm tracks, subtropical jet and subsiding branch of the Hadley cell {Section 10.6.2}.

**It is *likely* that both internal variability and anthropogenic aerosol emissions over the Northern Hemisphere have contributed to the negative trend in South Asian monsoon rainfall over the 20th century**. Given the general agreement among model projections, **it is *likely* that South Asian monsoon rainfall will increase at the end of the 21st century** in response to increased GHG forcing. Persistent daily rainfall extremes are *likely* to become more frequent with the additional half-degree warming between 1.5ºC and 2ºC targets. **There is *robust evidence* of large uncertainty in the spatial distributions of historical and projected changes**. This is made worse by substantial observational uncertainty {Section 10.6.3}.

**There is *high confidence* that the Mediterranean region has experienced faster summer temperature increases in recent decades than the Northern Hemisphere.** There is also *high confidence* that the increase in projected summer temperature for the Mediterranean region will be larger than for the Northern Hemisphere. **There is *high confidence* that summer precipitation in the Mediterranean region will decrease toward the end of the 21st century**. Due to biases in GCMs and RCMs, there is *low to medium confidence* in the projected spatial pattern of precipitation for the

Mediterranean region {Section 10.6.4}.

## 10.1 Foundations for regional climate messages

Expected length: 5 pages, 1 page=950 words
Number of figures: 1
Number of tables: 1

### *10.1.1 Preamble*

Regional climate is determined by a complex interplay of global external forcings and phenomena, large-scale internal modes of climate variability and teleconnections, as well as regional-scale climate processes, feedbacks and forcings. Depending on the specific context, regional climates may span large areas such as those where monsoons happen, but they may also be confined to a particular coast, a mountain range or a human settlement like a city. Users (understood as anyone incorporating climate information into their activities) often request climate information from within this range of scales due to the variety of operating and adaptation decision scales at the regional level. Hence, the term region is used in this chapter to indicate the range of scales of relevance for impact and adaptation without prescribing any formal regional boundaries.

Users may be interested in model-based long-term projections of regional climate change as well as information for the near-term (the next 30 years) (Kushnir et al., 2019a). At the same time, they may wish to understand the causes of past and recent climatic changes. Given the different types of regional climates and the broad range of regional scales, a variety of methodologies and approaches have been developed to construct climate change information for regions. They include global (GCM) and regional (RCM) climate models, statistical downscaling methods, plus the addition of components such as urban parametrizations to take into account the city scale. Regional observations likewise play a key role in the regional message construction process. Good quality observations allow monitoring the regional aspects of climate, are used to adjust inherent model biases, and are the basis for assessing model performance. All these elements, observations and model-based data, can be used to construct contextualised regional climate messages that distill and synthesize material from a range of sources.

The main objective of this chapter is to assess the key foundations for the generation of information about regional climate change. This involves assessing methodologies of producing climate change messages on a regional scale and attributing these changes to large- and regional-scale anthropogenic and natural drivers and forcings. These aspects have been addressed in previous reports (Box 10.1), but this chapter addresses the regional climate change problem in a more systematic way. The chapter is closely linked to three other chapters (11, 12 and Atlas) which also address aspects of regional climate information.

The chapter starts with an introduction of concepts and background information. Section 10.2 addresses the aspects associated with the use of observations in constructing regional climate information. The different modelling approaches developed to construct regional information are introduced and assessed in section 10.3, which also addresses the performance of models in simulating relevant climate phenomena to estimate the credibility of future projections. Section 10.4 assesses the causes of selected recent climate changes to illustrate the complex interplay of processes shaping regional climate change, and to illustrate the use of models for understanding these processes. Section 10.5 explains how messages of regional climate are distilled from different sources of information taking into account the context and user values of specific societal actors with whom the messages are shared. Finally, Section 10.6 assesses the integrated approach to construct regional climate change information through three case studies.

### *10.1.2 Concepts and definitions*

The global coupled atmosphere-ocean-land-cryosphere system, including its feedbacks, shows variability over a wide spectrum of temporal and spatial scales (Hurrell et al., 2009). The concept of a unified and seamless framework for weather and climate prediction (Brown et al., 2012a; Hoskins, 2013) provides the context for understanding and simulating regional climate across multiple space and time scales. This section discusses fundamental concepts and definitions with respect to what can be considered a region, the relevant time scales for regional climate information and region-specific aspects of the baselines used. The section also introduces the sources of uncertainty in model-derived regional climate information and how the quantification of the uncertainties impacts on the confidence statements of the climate messages.

Increasingly there is recognition that the evolution of the weather and climate are linked to the same physical processes in the coupled Earth system operating across multiple space and time scales (outlined in Figure 10.1). Approaches now consider unified modelling and seamless prediction across time scales to benefit from the convergence of methods used in weather and climate forecasting, in particular with regard to the initialization of the climate system and towards maximizing the predictability evident at different time scales (Brown et al., 2012a; Hoskins, 2013). Furthermore, there is evidence that errors inherent in the mean climate simulation in GCMs originate within a few days in initialized NWP versions of the same model (Cavallo et al., 2016; Martin et al., 2010; Sexton et al., 2019). At the spatial scale, interaction is pervasive, which means that unresolved scales in climate models have an impact on the larger scales. This affects both regional and global scales. For instance, global and regional models that resolve ocean mesoscale or atmospheric convection processes help understanding the multiscale interactions in the climate system, identifying those of greatest importance for the region of interest, and documenting their upscale effects on climate (Allen et al., 2018; Hurrell et al., 2006), if any. Besides, the experiments performed help determine how to better represent small-scale processes in relatively coarse resolution models.

**[START FIGURE 10.1 HERE]**

**Figure 10.1:** Schematic diagram derived from the idea of (Orlanski, 1975) displaying relevant interacting space and time scales of relevance to regional climate change information. Also indicated are the processes included in the different models and model components considered in Chapter 10 as a function of the time and space scales. This figure is a companion of Figure 1.15 in Chapter 1 where the region sets adopted in the report are illustrated as a function of the time and space scales.

**[END FIGURE 10.1 HERE]**

### *10.1.2.1 Definition of regions*

Although climate change is a global phenomenon, its manifestations and consequences are different in different regions. Regional climate is not only controlled by large-scale forcings (e.g. GHG emissions, solar radiation, etc.) and processes (e.g. the atmospheric general circulation, large-scale oceanic internal modes of variability), but also driven by regional and local forcings, such as aerosols or land use and the associated complex multiscale interactions. The way in which the climate will change at regional scale, and how it will impact different sectors can differ significantly. Section 10.4 discusses several of these regional processes and their manifestation in regional climate.

The definition of the regional scale and its distinction from the global scale, however, is ambiguous. Chapter 1 provides the definitions of the different region sets adopted in the report using the same frame of multiscale processes as those illustrated in Figure 10.1. Among those processes, large-scale climate and phenomena have been defined in Chapter 2, Cross-Chapter Box 2.1 as ranging from global and hemispheric, to ocean basin and continental. In this chapter, regional scales are defined as those areas from the sub-continental (e.g. the Mediterranean basin) to the local scale (e.g. human settlements such as megacities) without prescribing any formal regional boundaries. The range covered by these regional scales and examples of relevant modes driving signals at the regional scale are given in Figure 10.1.

To accomplish the chapter objective of assessing methodologies for producing climate change information

on a regional scale and its attribution to a range of drivers, a number of examples have been considered. Thirteen case studies have been considered representative of specific regions spanning all continents (except the Antarctic) and with very different spatial extension (Figure 10.2). Section 10.4 describes the selection criteria of ten of these case studies, where all selected regions have experienced a substantial multidecadal climate change in the recent past. The case studies in Section 10.4 focus on the attribution of multi-decadal regional climate change to causal factors that include both external forcing and internal variability drivers. Instead, Section 10.6 describes three other case studies formulated as end-to-end examples of the generation and interpretation of regional climate messages.

**[START FIGURE 10.2 HERE]**

**Figure 10.2:** Regional climate attribution case studies and end-to-end focus region on the generation of regional climate information, discussed in Sections 10.4 and 10.6 respectively. The regions appearing in the figure are the attribution case study regions in Section 4: Caribbean (AR6 region CAR), Central Eurasia (CEU), East Asian monsoon (EASM), Europe (EUR), Hanoi (HAN), Ho Chi Min (HCM), Himalaya (HIMA), Southeast Australia (SAU), Southeastern South America (SESA), Sahel/West African monsoon (SHL), Southwest North America (AR6 region SWN) and Tokyo (TOK). The end-to-end regions in Section 10.6 are: Cape Town (CT), Mediterranean (AR6 MED) and South Asian monsoon (SASM). For visual clarity, cities are marked with blue and the other regions in grey.

**[END FIGURE 10.2 HERE]**

*10.1.2.2 Scales in time and baselines*

Climate variability at global and regional scales is observed on a continuum from weather to macro-weather and climate time scales (Lovejoy, 2013). Lovejoy (2013) used macro-weather to describe the regime found between high frequency weather and low frequency climate regimes. Such thinking has analogies with the current interest in subseasonal-to-seasonal (S2S) time scales (Vitart et al., 2017) and in the seasonal-to-decadal range (Smith et al., 2012). Climate variability emerges from the latter time scale from a combination of slow internal climate processes and external forcings. Although the longest-term, largest-scale climate trends are dominated by external forcing, internal variability plays a vital role to define regional climate for short time scales and increasingly as the spatial scales become smaller (Frankcombe et al., 2015). Only one realization of internal variability is available for the actual climate and it is nontrivial to extract estimates of its characteristics from the available data (Frankcombe et al., 2015). The relatively short observational time series (Section 10.2) is a primary challenge to estimate the forced signal and to isolate low-frequency, multidecadal and longer term internal variability (Bathiany et al., 2018; Frankcombe et al., 2015; Overland et al., 2016).

New et al. (2001) suggested that larger space-scale variations generally occur at longer time scales and are associated with correspondingly large-scale phenomena in the atmosphere or ocean-atmosphere system (see also Figure 10.1). For example, an individual convective storm may exhibit scales of variability from metres and seconds to kilometres and hours, while for El Niño-Southern Oscillation (ENSO), the scales of variability are regional to hemispheric in extent and multi-year in length. However, these different scales are not unrelated. For instance,, using extreme rainfall characteristics (i.e. frequency, intensity and location) Munoz et al. (2015) highlighted that different climate drivers have their own imprint and they also tend to interact with each other. Modern climate models consider this integrated approach, but their present skill for extreme rainfall events and even the representation of large-scale climate drivers still leaves room for improvement.

While some anthropogenic changes generally occur over long periods, other forcings and drivers act over a wide range of time scales, from sub-daily to multi-decadal (see Figure 10.1). Due to the large range of drivers of variability and change, quantifying the interplay between internal modes of decadal variability and any externally forced component is crucial in attempts to attribute regional climate changes (e.g. Hoell et al., 2017; Nath et al., 2018). A climate signal could arise purely due to some anthropogenic influence or

conversely, entirely due to internal variability, but it is most likely the result of a combination of the two (see Section 10.4 and references therein). For instance, decadal variations can be caused by nonlinear atmospheric variability, nonlinear interactions in the atmosphere-ocean-cryosphere system and variability of external factors, such as solar radiation, aerosol loading and atmospheric trace-gas concentrations (Dong et al., 2014). The interplay of internal and forced variability of different time scales is particularly relevant to near-term climate prediction, which aims at predicting the phase of the internal multi-annual variability in the context of changing external factors (Kushnir et al., 2019b).

The magnitude and persistence of climate variability has implications for regional impacts (Bathiany et al., 2018). This is true not just because a longer event accumulates more impacts, but also because it can have impacts greater than the sum of its parts. For instance, a long heat wave can have greater impacts on human mortality than the sum of individual hot days (Gasparrini and Armstrong, 2012), and multi-year droughts can have greater agricultural and economic impacts than the sum of individual dry years (Peck and Adams, 2010).

It is also important to note that in this chapter and subsequent ones the baselines or reference periods used for presentation of climate change may vary from those used in Chapters 1–9, where three baselines are defined for the past, i.e. pre-industrial (1750), early-industrial (1850–1900) and recent (1995–2014), while the future baseline periods are 2021–2040 (near term), 2041–2060 (mid-century) and 2081–2100 (long term). At the global scale, it is known for example that the choice of baseline pre-industrial period affects the estimated probability of exceeding the Paris Agreement warming thresholds (Schurer et al., 2017). The choice of baseline also goes on to provide another source of uncertainty for projections of climate impacts (e.g. for responses of bird species in Africa; Baker et al., 2016). However, these baselines also present challenges for interpreting regional climate messages, since this chapter assesses results obtained from both GCM and RCM simulations, the results of which are found in the literature as using different baselines. Regional simulations described in the recent literature have been mainly performed using very different baselines determined by the availability of the boundary conditions from global simulations: e.g. 1950–2005 for CMIP5 historical and 2006-2100 for future scenarios (Cai et al., 2018; Dong-feng et al., 2017; Vaittinada Ayar et al., 2016), and 1989–2008 when using ERA-Interim reanalyses, although other periods have been used for older scenarios. This mismatch needs to be taken into account when assessing results obtained from both RCMs and GCMs, or when linking the results of this chapter to the assessments performed in previous chapters. This also highlights the need to consider a range of different baselines to satisfy the requirements of the variety of users because the choice of a baseline directly affects the perceived result in impacts studies (Dobor and Hlásny, 2018). Such a variety of baselines is taken into account in the assessment of the case studies in Sections 10.4 and 10.6 as they use a number of information sources. One means of overcoming baseline uncertainty is to define the historical reference period for a given model based on a fixed global-mean temperature change from the pre-industrial (e.g. Sylla et al., 2018, for West Africa); alternative approaches include defining the baseline such that climate deviations departing from it can easily be spotted "by eye" (Burke and Stott, 2017, for the East Asian monsoon).

#### *10.1.2.3 Uncertainty and confidence*

The degree of confidence in climate simulations and the resulting climate information typically depends on quantification of all the uncertainties associated with and the performance assessment of the specific set of simulations used. Since the direct verification of simulations of future climate changes is not possible, model performance and reliable (i.e. trustworthy) uncertainty estimates need to be assessed indirectly through theoretical and process understanding and a systematic comparison with observations (which are also uncertain) of past and current climate (Eyring et al., 2019; Knutti et al., 2010). These uncertainty estimates are then propagated along the chain that uses climate data to generate climate-relevant information (Smith and Matthews, 2015).

Uncertainty and confidence in messages of regional climate change are no different in nature to the way they are used in larger-scale (continental and global) climate problems (see Chapter 1). Uncertainties in model-based future regional climate information arise from different sources and are introduced at various stages in

the modelling process (Booth et al., 2013): 1) forcing uncertainties associated with the future scenario or pathway that is assumed, 2) internal variability sampled by a range of initial conditions, either generated freely by the model itself or as close to the observations as possible as done in near-term climate prediction (Hawkins et al., 2016), and 3) uncertainties related to imperfections in climate models, or structural uncertainty, that are propagated to the climate projections. However, the relative role of each one of these sources is different at regional scales when compared to large-scale indicators and changes substantially from one region and variable to another. The model uncertainty is among the largest contributors to the uncertainty cascade at the regional scale and arises from limited theoretical understanding, uncertainty in model parameters and structural model uncertainty or inability to accurately describe known processes (McNeall et al., 2016). However, new approaches to estimate the internal variability, like the availability of large ensembles of historical simulations and projections, have illustrated how important it is to obtain reliable estimates of regional climate projections (Dai and Bloecker, 2018). Additional elements, like the inconsistency between the GCM and RCM physics and dynamics or the observational uncertainty in bias-adjustment methods, play a role in the uncertainty cascade (Sørland et al., 2018). All these elements contribute to modify the overall confidence in regional climate messages with respect to the typical uncertainty level of the phenomena and indicators at larger scales.

One way to address the internal and structural uncertainties in climate information is to consider results from both multiple models and multiple realizations of the same model (Eyring et al., 2016a). An implicit assumption is that multiple models provide additional and more reliable information than a single model and that higher confidence could be placed on results that are common to an ensemble, known as robustness, although in principle all models could suffer from similar deficiencies leading to an excess of confidence in the results. This illustrates the relevance of considering the independence of the models contributing to create the climate message because when the independence of the elements in the multi-model ensemble is reduced the likelihood of not correctly sampling the uncertainty grows (Boé, 2018). This problem also strongly affects the decisions made to weight different models in the multi-model according to their performance (Abramowitz et al., 2018). The complex scene created by the different sources of uncertainty and the range of models involved in the generation of regional climate information makes that the collection of results available from multi-model, multi-member simulations are often most useful when synthesized, as described in Section 10.5.

### *10.1.3 Regional climate messages*

Regional climate messages connect global climate change to the local and regional scales where adaptation responses and policy decisions take place and play an important role in guiding climate-resilient development. Messages communicate knowledge based on data. At the same time, knowledge is information in context, making the message itself a function of the context. The construction and communication of climate messages are, however, complicated by three categories of key application and contextual issues:

- Practical issues (e.g. spatial and temporal resolution of the data sources).
- Contextual issues related to the construction of the messages (e.g. the type of user (Lemos et al., 2012a)).
- Difficulties associated with the construction of the messages (e.g. the complicated network of actors that are engaged in message construction (Hewitson et al., 2017)).

#### *10.1.3.1 Types of regional climate messages*

The applicability of regional climate messages strongly depend on the context. The approaches adopted in their generation are diverse and include the simple production and delivery of data as information, data that could be as diverse as the extrapolation of observations or the output of physically-based climate models, the assessment of changes in regional climate driving processes, storylines and narratives, and the more complex, fully tailored “distillation” of information drawing on multiple data sources and methods in co-production with user expert judgement.

The choice of approach and the way the outcome is communicated defines the characteristics and the form of the regional climate message. Messages may be provided in the form of summarised raw data, set of user-oriented indicators, data processed with a varied degree of complexity, set of figures and maps with either a brief description or formulated as rich and complex climate adaptation plans. In all cases, the messages are intended to meet a specific demand for regional information and ideally include a description of the assumptions used, an estimate of the associated uncertainty and the sources and propagation of error, uncertainty and possible misunderstandings in its communication.

#### *10.1.3.2 Construction of regional climate messages*

The large number of approaches used to construct regional climate messages from the climate data available creates one of the most fundamental challenges about the delivery of useful and relevant regional information. The choice of approach has deep ramifications for the interpretation of the message. For instance, it is well established that it is invalid to take a time series from a cell of a GCM simulation at face value as an observational estimate of a point within the cell.

Each approach for the construction of regional climate messages has constraints in terms of achievable spatial and temporal resolution, issues of bias and error, or the way they deal with the evolution of climate statistics (non-stationarity). The approaches have different methodological assumptions and relevant decisions are usually made about what method is more suitable to a specific application, bringing again the question of context to the fore. The choice of approach has typically been part of a linear supply chain, starting from the generation of climate data using standard methods (usually climate simulations) which are transformed into maps or derived data products and finally formulating statements that are communicated and delivered to a wide range of users. This methodology has proven to be valuable in many cases, but it is equally fraught with dangers of not well communicating important assumptions and uncertainty, and possible misunderstanding in the hand-over from one community to another one. This has led to the emergence of two new pathways to generate more user-oriented climate messages: a) work seeking to undertake the distillation of multi-model, multi-method data in relation to the context of the information needed and b) bottom-up approaches that begin with the user's articulation of vulnerability in the context of their multi-stressor system and then seeing what climate data might be able to say about exceedance of some relevant threshold. These ideas are assessed in the detail in Sections 10.5 and 10.6.

### ***10.1.4 Sources of regional climate variability***

As explained above, sources of regional climate variability include natural and anthropogenic forcings and other drivers, the local expression of large-scale remote forcings (also known as teleconnections) and local feedbacks. This section briefly introduces these sources. Section 10.4 describes their relevance for the specific regions considered in more detail and Section 10.6 makes reference to them in specific cases where regional climate messages are built.

#### *10.1.4.1 Forcings controlling regional climate*

This section introduces the forcings external to the climate system, including those acting at a global spatial scale (GHG, solar) that have a distinct impact in different regions, and those of a more regional character (land use change, urbanization). Natural (solar, volcanic, natural aerosols) and anthropogenic (GHG, stratospheric ozone depletion, land-use change, anthropogenic aerosols, urbanization) forcings are considered.

##### *10.1.4.1.1 GHG*

Long lived GHG with anthropogenic origin are, over time, well mixed in the atmosphere, meaning that their spatial scale of impact is global. Global GHG warming started with the industrial revolution (see Chapter 2),

but the signal in temperature started to emerge from the natural variability around the end of the 20th century (Chapter 2). Anthropogenic GHGs contribute with 3 W $m^{-2}$ of radiative forcing accounting for *X*ºC GMST increase in the present report (Chapter 2). This global forcing impacts both land areas (in terms of surface temperature for instance) and ocean basins, where both heat and carbon are stored over long time scales. However, there are important differences in the processes involved. Over the ocean, the increased radiative forcing leads to an increase in latent heat flux and a decrease in sensible heat flux; while over land, water availability is limited and increased radiative energy is therefore converted mostly into sensible heat (Sutton et al., 2007). Consequently, GHGs affect the Northern Hemisphere temperatures more than the Southern, since the Northern Hemisphere has more continental surfaces than the Southern one. This hemispheric warming asymmetry can also affect rainfall patterns, as is the case in the Sahel (Section 10.4.2.2.1). As an example of the more regional expression of the GHG forcing, the polar amplification (i.e. the faster warming of the polar regions compared to lower latitude regions; Cross-Chapter Box 10.1) (Smith et al., 2018) is particularly important over the Arctic, leading to recent increases in surface temperature twice as large as those experienced by the GMST (Christensen et al., 2013a; Vihma, 2014; Walsh, 2014). A smaller scale phenomena, crucial e.g. for the world frozen water reserves, is the elevation-dependent warming meaning that warming trends are larger at higher altitudes (Pepin et al., 2015).

#### *10.1.4.1.2 Solar forcing*

The solar cycle is a natural forcing of climate variability. It has a well-known main periodicity of around 11 years with amplitude of 1 W $m^{-2}$ (Chapter 2). Solar forcing also shows longer term trends. It *likely* increased by a daily mean of 0.2 W $m^{-2}$ during the period 1900–1980, a trend that has reversed since 1980 (Chapter 2). Variations in solar forcing can have regional impacts through influences on circulation patterns. This is in particular the case for the leading atmospheric circulation modes of the North Atlantic region (Gray et al., 2013; Sjolte et al., 2018), although the hypothesis is also contested (Chiodo et al., 2019). Impacts on the winter circulation and temperature over Eurasia (Chen et al., 2015) and North America (Li and Xiao, 2018; Liu et al., 2014b) have also been identified.

#### *10.1.4.1.3 Stratospheric ozone*

Stratospheric ozone depletion has been argued to be a driver of the southwards expansion of the descending branch of the Hadley cell (Waugh et al., 2015) that impacts on Southern Hemisphere regions like south eastern South America (González et al., 2014; Wu and Polvani, 2017). Stratospheric ozone depletion is likely to have driven this poleward expansion in competition with other possible drivers, while the recovery of stratospheric ozone during the 21st century could offset the GHG-related climate change in some Southern Hemisphere regions (Barnes et al., 2014a). Further discussion of the impacts of stratospheric ozone on regional climate can be found in Sections 10.4.2.2.4 and 10.4.3.2.4.

#### *10.1.4.1.4 Natural and anthropogenic aerosols*

There are both natural and anthropogenic sources of primary aerosols. Secondary aerosols are those that form and evolve in the atmosphere from natural or antropogenic precursors. Aerosols and their precursors can interact with radiation and act as cloud/ice condensation nuclei, thereby affecting climate with either a cooling or a warming effect depending on their physical and chemical properties (Chapter 6 and Box 6.1). As they are often emitted at a regional scale and their atmospheric lifetime is short (from a few hours to several days), aerosols are dispersed regionally and affect climate at a regional scale. Dynamic and thermodynamic adjustments to their local effects lead to remote responses both in temperature and precipitation, which in this chapter is exemplified in the case study on the East Asia summer monsoon weakening (Section 10.4.2.2.2) and in the end-to-end example on the South Asian summer monsoon (Section 10.6.3).

The majority of aerosols scatter solar radiation, which results in a globally averaged forcing of about -1 W/$m^2$ (Myhre et al., 2013), but with strong regional variations (Shindell and Faluvegi, 2009). Regional implications of clean air policies that reduce emissions of these types of aerosols are exemplified through the Western Europe summer warming case study in Section 10.4.2.2.6. However, black carbon is known to

absorb solar radiation leading to atmospheric warming, with a globally averaged forcing in the range of 0.2 to 1 W/m$^2$ (Gustafsson and Ramanathan, 2016). However, radiative effects at the regional scale can be up to two orders of magnitude larger than the global average (Li et al., 2016c, 2016a; Mallet et al., 2016).

For the volcanic aerosol different impacts are found depending on whether the source is tropical or extratropical. If tropical, explosive eruptions can inject the aerosol into the stratosphere and have global impacts, while smaller eruptions can have brief local or hemispheric impacts. An interaction between the volcanic forcing and ENSO has been found (Liu et al., 2018b, 2018a; Miao et al., 2018), while an extratropical regional impact of tropical volcanic eruptions is emerging (Ménégoz et al., 2018; Swingedouw et al., 2017).

Aerosol-cloud interactions occur via changes in radiative properties and the life cycle of clouds due to aerosols acting as cloud/ice condensation nuclei (Bellouin et al., 2016; Boucher et al., 2014). Aerosol burden and forcing are generally co-located, however temperature and precipitation responses are both local and remote (Kasoar et al., 2018; Li et al., 2016d; Liu et al., 2018d; Samset et al., 2018; Thornhill et al., 2018; Westervelt et al., 2018). Changes in aerosol concentrations in the Northern Hemisphere have been reported to modulate monsoon precipitation in West Africa and the Sahel (Undorf et al., 2018) and in Asia (Zhang et al., 2018a). The impacts of these changes are assessed in Section 10.4.2. However, there is a wide range of mechanisms and feedbacks that need to be better understood to accurately assert the way in which modulation occurs (Li et al., 2016d).

#### *10.1.4.1.5 Land use and management including urbanization*

Regional climate is also shaped by small-scale forcings such as land-use changes or the presence and expansion of cities. These features can have local (e.g. irrigation mitigates temperature extremes at the irrigated site; Section 10.3.3.5.10) and non-local impacts (e.g. increased rainfall downwind of a city; see the case on cities in Section 10.4).

Anthropogenic changes to the continental land surface such as deforestation, afforestation, conversion to croplands, land management (e.g. irrigation and tillage), urbanization and construction of artificial dams can have large impacts on local and regional climate (see Box 10.1). The impact of a specific land-use change will depend on the background climate. As an example, afforestation can induce local warming in boreal areas in winter since it decreases the albedo over snow covered areas, while in tropical regions afforestation leads to cooling through increased latent heat flux that overrules the decrease in albedo. In this chapter, the potential influence of land management such as irrigation on regional climate change is exemplified in the the end-to-end example on the South Asian summer monsoon (10.6.3).

There is *limited evidence* but *high agreement* that the GMST response to urbanization changes is negligible (Zhang et al. 2013; Chen et al., 2016; Hansen et al., 2010; Parker, 2006). However, there is evidence that urbanization may amplify the air temperature response to climate change in different climatic regions (Mahmood et al., 2014) either under present (Doan et al., 2016; Kaplan et al., 2017; Li et al., 2018d) or future conditions (Argüeso et al., 2014; Grossman-Clarke et al., 2017; Kim et al., 2016; Kusaka et al., 2016) with a strong impact on minimum temperatures. For instance, in Flanders (Berckmans et al., 2019) found that future urbanization for the near future (up to 2035) has an impact on minimum temperature (+0.6 °C) that is comparable to the projected climate change signal in the RCP8.5 scenario.

### *10.1.4.2 Internal drivers and their pathways to shaping regional climate*

Regional climate is strongly influenced by internal climate variability on seasonal to multi-decadal time-scales. This variability arises from internal atmospheric variability, oceanic variability and the interaction of ocean modes, and may additionally be forced by other components of the climate system. It also interacts with the forced response of the climate system. These modes are referred to as internal drivers of regional climate. The chapter discusses their influence on regional climate. A more detailed description of the modes themselves can be found in Chapters 2, 3 and 9 while their future projections are assessed in Chapter 4. A

detailed assessment of the role of internal drivers in selected case studies will be provided in Section 10.4.

Regional climate is strongly affected by the global atmospheric circulation. In the mid-latitudes, the dominant associated phenomena are the sub-tropical and polar jet as well as mid-latitude cyclones along the storm tracks. The variability of these phenomena is characterised by large-scale atmospheric modes such as the North Atlantic Oscillation (NAO), the Northern and Southern Annular Modes (NAM and SAM). These modes are additionally modulated by other components of the climate system (ocean, sea-ice, land) and external drivers such as GHG. They possess variability on all time scales, including decadal and longer periods.

The atmospheric modes and phenomena are closely linked to variations in regional climate. For instance, during a positive phase of the winter NAO, when the polar jet is shifted northwards and intensified, winter climate in Northern Europe tends to be milder and wetter, whereas Southern Europe experiences anomalously dry conditions (Tsanis and Tapoglou, 2019). A similar pressure pattern, the summer NAO, influences European climate during summer (Bladé et al., 2012; Dong et al., 2013). For instance, the SAM, which affects the climate of the Southern Hemisphere continents (Hendon et al., 2014a), has variability that can be attributed to natural processes (Smith and Polvani, 2017) while other aspects of the variability are defined by the recent stratospheric ozone changes (Bandoro et al., 2014).

Due to the large ocean heat capacity and large time scales, multiannual to multidecadal modes of ocean variability are key drivers of regional climate change. These modes include the Interdecadal Pacific Variability (IPV), Atlantic Multidecadal Variability (AMV) (Buckley and Marshall, 2016) and Indian Ocean Dipole Mode (IOD). These modes not only affect nearby regions but also remote parts of the globe through atmospheric teleconnections (Dong and Dai, 2015; Meehl et al., 2013) and can act to modulate the impact of the different natural and anthropogenic forcings (Ménégoz et al., 2018). For instance, the AMV may directly influence European climate by warming or cooling the air temperature. Diabatic heating of the atmosphere over the northwestern Atlantic induces a surface baroclinic pressure response that ultimately modulates central to eastern summer temperature (Ghosh et al., 2017). As an example of the modulation of other modes of variability, it is found that tropical SST anomalies during winter associated with the AMV drive an anomalous upper tropospheric streamfunction dipole that influences the NAO, jet stream variability and blocking over Europe (Davini et al., 2015). This generates a regional response in terms of temperature, wind and precipitation.

The dynamics of the ocean modes of variability is simultaneously affected by other modes of variability spanning the full range of length and time scales due to non-linearity (Dong et al., 2018a; Kucharski et al., 2010) (see Figure 10.1). This mutual interdependence can result in changing characteristics of the connection over time as, for example, for IPV and IOD (Dong and McPhaden, 2017), and of their regional climate impact (Martín-Gómez and Barreiro, 2016, 2017). The link of ocean modes to regional climate should therefore be treated with caution because this can vary over time even in a stationary climate (Brands, 2017; Gallant et al., 2013; Pinto et al., 2011; Sterl et al., 2007). Besides, the strong seasonality of the modes and related teleconnections means that their impact on regional climates can be seasonally dependent (Haarsma et al., 2015). Detailed descriptions of how specific ocean modes affect regional climate will be assessed in the individual case studies of Section 10.4.

#### *10.1.4.3 Regional phenomena and feedbacks*

Some regional climates are shaped by the occurrence of phenomena ranging from about 2 to 2,000 km in scale (Figure 10.1). Convective precipitation may occur in a single thunderstorm, but rainfall cells may be organised in mesoscale convective systems, squall lines, weather fronts or even tropical cyclones. Topography strongly influences regional climates and climate change. Coastal regions, cities, oasis, lakes and mountain ranges may induce characteristic circulation features such as urban breezes, oasis breeze, land- and sea breezes, mountain breezes and Fohn winds. This section briefly lists the phenomena and feedbacks that are assessed in Section 10.3.

Key in shaping the regional response to large-scale drivers and forcings are local feedbacks. As an example, soil moisture is coupled both to temperature and precipitation through feedback loops (Hohenegger and Stevens, 2018) that depend on the regional climate and geographical characteristics like the orography (Imamovic et al., 2017). This type of feedback is mentioned in one of the case studies in Section 10.4.

Aerosols affect local-to-regional climate through aerosol-radiation interaction leading to feedbacks on temperature. Under severely polluted conditions, aerosols enhance stratification from morning to daytime and increase their surface concentration leading to a positive feedback loop. For instance, the effect of stratification in Beijing winter haze conditions is estimated to be 10 % ((Gao et al., 2016) and (Kajino et al., (2017)).

An ice sheet albedo feedback is active in the Greenland ice sheet in which the aging of snow or ice should be considered. (Franco et al., 2012) explain the mechanism: when increased warm (southerly) air advection hits the western ice sheet, it increases surface sensible heat that in turn enhances snow aging, reduces the albedo and increases downward short wave, leading to more surface heating that accelerates the melting of snow. To represent such phenomena, aging effects are required in numerical models (Flowers, 2018; Niwano et al., 2018).

**[START BOX 10.1 HERE]**

**BOX 10.1: Regional climate in the special reports SRCCL, SROCC, SR15 and in AR5**

This box summarizes the information on linking global and regional climate change information in the Fifth Assessment Report (AR5), with a special focus on Chapter 14 of the WGI volume, and the three special reports to be published prior to the publication of the Sixth Assessment Report (AR6). This information helps framing the treatment of the production of regional climate information in previous reports and identifies some of the gaps that AR6 needs to address.

**Fifth Assessment Report (AR5)**

**[Placeholder for a summary of the use of regional climate information in AR5.]**

In WGI Chapter 9 regional downscaling methods are mentioned to provide climate information at the scales needed for many climate impact studies. The assessment finds *high confidence* that downscaling adds value both in regions with highly variable topography and for various small-scale phenomena. Regional models necessarily inherit biases from the global models used to provide boundary conditions. Furthermore, the ability to systematically evaluate regional climate models, and statistical downscaling schemes, were hampered because coordinated inter-comparison studies were still emerging. However, several studies demonstrated that added value arises from higher resolution of stationary features like topography and coastlines, and from improved representation of small-scale processes like convective precipitation.

**Special Report on Climate Change and Land (SRCCL)**

**[Placeholder for a summary of the use of regional climate information in the final version of SRCCL.]**

Land surface processes modulate the likelihood, intensity and duration of many extreme events including heatwaves, droughts and heavy precipitations. According to the SRCCL there is *robust evidence and high agreement* that land cover and land use or management exert significant influence on atmospheric states (e.g. temperature, rainfall, wind intensity) and phenomena (e.g. monsoons), at various spatial and temporal scales, through their biophysical impacts on climate. There is *robust evidence* that dry soil moisture anomalies favour summer heat waves. Part of the projected increase in heat waves and droughts can be attributed to soil moisture feedbacks in regions where evapotranspiration is limited by moisture availability (*medium confidence*). Vegetation changes can also amplify or dampen extreme events through changes in albedo and evapotranspiration, which will influence future trends in extreme events (*medium confidence*).

Whatever the land change (e.g. afforestation, urbanization), its location on Earth determines the sign and magnitude of its impacts on climate (*robust evidence, high agreement*). For instance, irrigation in particular may have contributed to a decrease in extreme temperature in strongly irrigated areas (*medium confidence*). The background climate also influences the sign and magnitude of the changes triggered by land-use and land cover change.

Water management and irrigation are generally not accounted by the CMIP5 global models. Additional water can modify regional energy and moisture balance particularly with highly productive agricultural crops with high rate of evapotranspiration. Urbanization increases the risks associated with extreme events (*high confidence*). Urbanization suppresses evaporative cooling and amplifies heatwave intensity (*high confidence*) with a strong impact on minimum temperatures (*very likely, high confidence*). Urban areas stimulate storm occurrence and heavy precipitations in part due to the presence of aerosols. Urbanization also increases the risk of flooding during heavy rain events.

**Special Report on the Ocean and Cryosphere in a Changing Climate (SROCC)**

**[Placeholder for a summary of the use of regional climate information in the final version of SROCC.]**

Observations and models for assessing changes in the ocean and the cryosphere have been developed considerably during the past century but observations in some key regions remain under-sampled and are very short relative to the timescales of natural variability and anthropogenic changes. Retreat of mountain glaciers and thawing of mountain permafrost continues and will continue due to significant warming in those regions, where it is likely to exceed global temperature increase.

It is *virtually certain* that Antarctica and Greenland have lost mass over the past decade and observed glacier mass loss over the last decades is attributable to anthropogenic climate change (*high confidence*). It is *virtually certain* that projected warming will result in continued loss in Arctic sea ice in summer but there is *low confidence* in climate model projections of Antarctic sea ice change because of model biases and disagreement with observed trend. Knowledge and observations of the polar regions are sparse compared with many other regions, due to remoteness and challenges of operation in them.

The sensitivity of small islands and coastal areas to increased sea level differs between emission scenarios and regionally and a consideration of local processes is critical for projections of sea level impacts at local scales.

**Special Report on Global Warming of 1.5°C (SR15)**

**[Placeholder for a summary of the use of regional climate information in the SR15.]**

Most land regions are experiencing greater warming than the global average, with annual average warming already exceeding 1.5°C in many regions. Over one quarter of the global population live in regions that have already experienced more than 1.5°C of warming in at least one season. Land regions will warm more than ocean regions over the coming decades (transient climate conditions).

Transient climate projections reveal observable differences between 1.5°C and 2°C global warming in terms of mean temperature and extremes, both at a global scale and for most land regions. Such studies also reveal detectable differences between 1.5°C and 2°C precipitation extremes in many land regions. Besides, for mean precipitation and various drought measures there is substantially lower risk for human systems and ecosystems in the Mediterranean region at 1.5°C compared to 2°C.

The different pathways to a 1.5ºC warmer world may involve a transition through 1.5°C, with both short and long-term stabilization (without overshoot), or a temporary rise and fall over decades and centuries (overshoot). The influence of these pathways is small for some climate variables at the regional scale (e.g. regional temperature and precipitation extremes) but can be very large for others (e.g. sea level).

Decisions on changes in land use can strongly affect regional climate change through biophysical feedbacks (e.g., changes in land evaporation or surface albedo), potentially affecting regional temperature and precipitation.

**[END BOX 10.1 HERE]**

**[START CROSS-CHAPTER BOX 10.1 HERE]**

**Cross-Chapter Box 10.1: Influence of the Arctic on mid-latitude climate**

Rein Haarsma (Netherlands), Francisco Doblas-Reyes (Spain), Laurent Terray (France), Hervé Douville (France), Nathan Gillet (Canada), R. Krishnan (India), Gerhard Krinner (France), Dirk Notz (Germany), Sonia Seneviratne (Switzerland), Cunde Xiao (China)

The Arctic is warming more than twice as the global mean surface air temperature (Davy et al., 2018), and in some seasons and parts of the temperature distribution up to three times more quickly like in the warming of the coldest nights (Seneviratne et al., 2016). Different mechanisms are responsible for the enhanced warming of the Arctic. These include ice-albedo feedback, lapse rate feedback, Planck feedback and cloud feedback. The rapid Arctic warming has a strong impact on the ocean, atmosphere and cryosphere in that region. To illustrate the latter, late summer and early autumn sea ice extent has decreased by around 13% per decade since 1979 (Cross-Chapter Box 10.1, Figure 1).

**[START CROSS-CHAPTER BOX 10.1, FIGURE 1 HERE]**

**Cross-Chapter Box 10.1, Figure 1:** [Placeholder: Average monthly Arctic sea ice extent for September 1979-2018 (source NSIDC).]

**[END CROSS-CHAPTER BOX 10.1, FIGURE 1 HERE]**

In this box the possible impact of the Arctic warming on the lower latitudes is discussed. This is a topic that has recently raised wide interest (Ogawa et al., 2018; Wang et al., 2018a). Different theories have emerged that describe possible mechanisms of how the Arctic can influence the climate at lower latitudes. This is relevant because, should the Arctic changes play a role to affect part of the mid-latitude variability, the planned continuous decrease of Arctic sea ice cover and Arctic amplification could become an increasingly important factor to determine regional climate change. Below, the different theories are first discussed, followed then by an assessment based on modelling and observational evidence.

**Theories**

Cross-Chapter Box 10.1, Figure 2 shows a diagram summarizing the elements that are involved in the different theories (adapted from Cohen et al., 2014). The diagram illustrates that the proposed theories of the impact of Arctic amplification on mid-latitude weather involve changes in storm tracks, jet stream and planetary waves, modulated by the stratospheric polar vortex. The theories involve the impact on climate means as well as extremes for winter and summer. They can be grouped into categories that focus on different mechanisms.

**[START CROSS-CHAPTER BOX 10.1, FIGURE 2 HERE]**

**Cross-Chapter Box 10.1, Figure 2:** [Placeholder: Schematic of influences on northern hemisphere mid-latitude weather. Adapted from (Cohen et al., 2014).]

**[END CROSS-CHAPTER BOX 10.1, FIGURE 2 HERE]**

*Jet stream fluctuations*

One category of theories propose that Arctic amplification, thereby reducing the poleward temperature difference, could result in a weaker and more meandering jet with Rossby waves of larger amplitude (Francis et al., 2017). This may cause weather systems to travel eastward more slowly and thus, all other things being equal, Arctic amplification could lead to more persistent weather patterns (Francis and Vavrus, 2012). In addition the weaker jet may result in the amplification of quasi-stationary waves with zonal wave numbers 6–8 by a stationary forcing (Coumou et al., 2018; Mann et al., 2018; Petoukhov et al., 2013). The persistent large meandering flow will increase the likelihood of extremes because they frequently occur when atmospheric circulation patterns are persistent, which tends to occur with a strong meridional wind component.

*Storm tracks*

Changes in storm tracks associated with the NAO/AO have a strong influence on the surface temperature and precipitation variability in the North Atlantic sector. When the NAO/AO is in its negative phase, the storm tracks shift equatorward and winters are predominantly more severe across northern Eurasia and the eastern United States, but relatively mild in the Arctic. This temperature pattern is sometimes referred to as the 'warm Arctic–cold continents' pattern (Chen et al., 2018a). Recent observed wintertime temperature trends across the Northern Hemisphere continents project strongly on this temperature-anomaly pattern, reflecting a negative trend in the NAO/AO over the past two decades. Although the atmosphere possesses large internal variability the recent trend in NAO/AO has been ascribed to being forced by the Arctic warming, its associated reduction in sea-ice cover and the increase in Eurasian snow cover (Cohen et al., 2012a; Nakamura et al., 2015; Yang et al., 2016b).

*Polar vortex outbreaks*

Sufficient wave breaking in the polar stratosphere weakens the stratospheric polar vortex and can trigger a sudden stratospheric warming (SSW) event (Hoshi et al., 2019). The circulation anomalies associated with a stratospheric warming event propagate back down to the surface in subsequent weeks, contributing to a persistent negative NAO/AO and cold continental conditions. Arctic warming has been linked to an increase of those stratospheric “outbreaks” (Kim et al., 2014). One of the underlying mechanism point towards enhanced Eurasian snow cover in autumn caused by the more moist air that is advected into Eurasia from the Artic with reduced sea-ice cover. Extensive snow cover may lead to larger planetary waves that increase the vertical propagation of wave energy into the stratosphere (Jaiser et al., 2016), favouring a warmer and weakened stratospheric polar vortex (Cohen et al., 2014).

**Assessment**

It is generally accepted that the above proposed theories are based on our understanding of the climate and rooted in well proven concepts of geophysical fluid dynamics. They are all plausible theories that in principle can describe the link between the Arctic and the midlatitudes (Barnes and Screen, 2015).

Whether they explain part of the observed weather and climate of the mid-latitudes in recent decades must be validated by either observations and/or model simulations. The validation of those theories is hampered by a number of issues that triggers scientific discussion. First, the short period over which the Arctic warming is present and systematically observed, which is only a few decades, makes statistical significance hard to obtain, in particular because of the large internal variability of the atmosphere. Second, the correlations found in observations, even significant, do not necessarily point toward causality. In addition, also lagged correlations that are designed to unravel cause and effect are often hampered by strong persistence. This is the case of sea-ice concentration, which is not always accounted for in statistical tests. The climate system is strongly coupled and the impact of one component of the system onto another is hard to disentangle from observations. Third, model simulations are imperfect representations of reality. Their coarse resolution and the need to parameterize many crucial processes introduce systematic errors and limit their usefulness. In addition, there is the difficulty to design clear cut experiments to separate cause and response, and estimate the role of natural variability.

These issues strongly entered the scientific debate on past influence of the Arctic on the mid-latitude climate. Studies that support the Arctic influence are mostly based on observational relationships between the Artic warming and the reduction of sea-ice and midlatitude extremes and anomalies (Budikova et al., 2017; Cohen et al., 2012a; Francis and Vavrus, 2012, 2015). The criticism is generally focused on the lack of statistical significance and the inability to disentangle cause and effect (Barnes, 2013; Barnes et al., 2014b; Barnes and Polvani, 2013; Barnes and Screen, 2015; Hassanzadeh et al., 2014; Screen and Simmonds, 2013; Sorokina et al., 2016). In Chapter 9 (Section 9.5.4.6) it is stated that there is *low confidence* in the reported relationships between Eurasian snow cover in fall and Northern Hemisphere circulation trends and anomalies in the following winter.

An additional argument in the criticism is the inability of climate models to simulate a significant response, larger than the natural variability, that supports those theories (Chen et al., 2016c; Screen et al., 2014; Walsh, 2014), although some studies find a significant response in summer when the natural variability is less (Petrie et al., 2015). Recently, new studies have emerged that reconcile in a coherent way observations and models (Mori et al., 2019) and enable to separate the different forcings (McCusker et al., 2017; Zappa et al., 2018).

Concerning the impact of Arctic warming on a future warmer climate, it is important to note that mid-latitude variability, apart from its internal variability, is also affected by many drivers outside the Arctic and that those drivers as well as the linkages will change in a warmer world. To note a few: The AMOC, PDO, ENSO, upper tropospheric tropical heating, land-surface processes associated with soil moisture (Hauser et al., 2016; Miralles et al., 2014). The impact of those drivers and the effect of future warming on mid-latitude climate and variability have been documented in many modelling studies. This is difficult to disentangle from the impact of future Artic warming (Blackport and Kushner, 2017; Li et al., 2018b). Also some of the simulated effects of Artic warming counteract the above proposed mechanisms, such as a poleward displacement of the jet (Barnes and Polvani, 2013), although the atmospheric response depends critically on the coupling (Chemke et al., 2019; Deser et al., 2016a; Smith et al., 2017), and the increase of the meridional temperature gradient in the upper troposphere, thereby increasing storm track activity and reducing the frequency of blocking episodes (Barnes and Screen, 2015). Although climate models indicate that future Arctic warming and the associated equator-pole temperature gradient will affect mid-latitude climate and variability (Haarsma et al., 2013b), they do not reveal a dominant impact on extreme weather (Woollings et al., 2014).

An additional complicating aspect is that the Arctic is not warming uniformly and different Arctic regions may generate different regional responses that cancel or enhance one another (McKenna et al., 2018; Screen et al., 2018; Sun et al., 2015). The Artic warming may be also be affected by changes in mid-latitude climate. Anomalous heating associated with enhancement of monsoon precipitation can influence the Arctic ice melt through poleward transport of heat content anomalies by large-scale circulation patterns extending from the low latitudes to the Arctic (Krishnamurti et al., 2015).

Finally, a warmer Arctic climate will without any additional changes in atmospheric dynamics reduce cold extremes in winter and enhance warm extremes in summer due to advection of warmer air from the Arctic into the midlatitudes (Ayarzagüena et al., 2018; Ayarzagüena and Screen, 2016; Screen, 2014).

Based on the discussion above there is *high confidence* that the Arctic can influence mid-latitude climate and variability. However, there is *low confidence* in the exact role and quantitative impact of historical Arctic warming and sea-ice loss on mid-latitude variability. The signal is small compared to internal variability. In addition other theories exist that can explain the observed variability. Future climate change will affect mid-latitude variability in different ways including through the impact of Arctic warming, but there is *low confidence* in the relative contribution of Arctic warming, compared to other drivers.

**[END CROSS-CHAPTER BOX 10.1 HERE]**

## 10.2 Observations

Expected length: 7 pages, 1 page=950 words
Number of figures: 0
Number of tables: 3, in the technical annex

High-quality, long-term observations are essential for climate monitoring, for validating and improving climate models, for data assimilation, to apply post processing techniques, and for increasing our confidence in the attribution of past climate changes, among many other applications. A range of observational products available at the regional scale is assessed from the perspective of their use in the context of regional climate. The different challenges that still exist are also discussed.

### *10.2.1 Type of observations*

The various types of observational products that are particularly relevant for assessing climate and its change at the regional scale are assessed in this section. They include in situ and remote-sensing data, gridded observational datasets and reanalysis products.

#### *10.2.1.1 In situ and remote sensing data*

Climate information for the atmosphere and land mainly comes from two different and complementary sources: surface (this also includes data from the instruments launched from the ground such as upper-air stations/radiosondes) and remote observing systems (this includes space-borne, radar, and lidar observations). Surface observing systems are a critical component of a global monitoring programme, producing the basic data essential for monitoring how climate variability, especially extremes in temperature and precipitation, evolves across different regions. These surface observations are essential in ensuring that climate models can be evaluated with high-quality observations and allowing calibration of satellite sensors. Surface observations can come from a variety of networks such as climate reference networks, mesoscale weather and supersite observation networks, citizen science networks and others, all with their strengths and weaknesses (McPherson, 2013). Supersite observatories are surface observing networks that measure a large amount of atmospheric and soil variables at least hourly over a decade or more (Ackerman and Stokes, 2003; Chiriaco et al., 2018; Haeffelin et al., 2005; Xie et al., 2010). With adequate calibration, quality control and homogenization, they produce the data needed to diagnose processes and change at regional climate scales that involve the influence and interaction of large-scale atmospheric circulation and local processes. Several climate datasets have been developed from in situ station observations, at different spatial scales and temporal frequencies (see Technical Annex): these include sub-daily (Dumitrescu et al., 2016; Okamoto et al., 2005), daily (Aalto et al., 2016; Ashouri et al., 2015; Beck et al., 2017a, 2017b; Camera et al., 2014; Chen et al., 2008; Journée et al., 2015; Schneider et al., 2017), and monthly time scales (Aryee et al., 2018; Cuervo-Robayo et al., 2014; Kaplan et al., 1998; Lee et al., 2007; Rienecker et al., 2011).

Satellite products provide a valuable complement to in situ measurements and are particularly useful over regions with none or sparse in situ data. Most satellite products have global coverage and have been discussed in earlier chapters (e.g. Chapters 2, 8). When considering their application at a regional scale it is important to consider that the spatio-temporal resolution of these products varies considerably, and that there is commonly a trade-off between temporal and spatial resolution. For example, Landsat provides images with a high spatial resolution of around 30 metres, but has a full coverage of the globe as long as 8–16 days (Wulder et al., 2016), while SMOS has a spatial resolution of 25 kilometres, but a shorter full coverage period of 2.5-3 days (Kerr et al., 2012). The Tropical Rainfall Measurement Mission (TRMM; covering 35°N–35°S, 1997–2016) (Simpson et al., 1996) and Global Precipitation Measurements (GPM; 65°N–65°S, 2014–) (Skofronick-Jackson et al., 2017) satellites have provided three-dimensional precipitation radar data with ~5 km pixel size for more than 20 years and feature sub-diurnal sampling. Constellation products such as the Global Satellite Mapping of Precipitation (GSMaP) (Kubota et al., 2007) and Integrated Multi-satellitE Retrievals for GPM (IMERG) (Huffman et al., 2007) provide hourly global precipitation data with

~11 km coverage. Advanced geostationary satellites such as GOES-East and GOES-17 (Goodman et al., 2018), Meteosat-10 and 11 (Schmetz et al., 2002) and Himawari-8 and 9 (Kurihara et al., 2016) are valuable for regional applications since they provide images at very high spatiotemporal resolution, typically 1–2 km, every 10–15 minutes.

There is now a network of satellite based Global Observation System (GOS), mainly for cloud and moisture pattern using the visible or IR channel sensors. The network has been established in 1987 in the framework of the FGGE project (First GARP Global Experiment). Initially the network included two GOESs (USA), METEOSAT (Europe), a Russian satellite and GMS (Japan). The network has been increased including INSAT (India), FY2 (China), and COMS (Korea) with a total number of 10 geostationary satellites. In order to fill the gap around the polar regions there are also some sun-sunchronous orbit satellites now. During the past 40 years, time, resolution and the channel sensors have all increased.

#### *10.2.1.2 Derived products*

Derived products are created from raw datasets collected through surface observations, remote-sensing tools, and research vessels using either statistical interpolation techniques (see Section 10.2.2.4) or numerical atmospheric and land-surface models (Bosilovich et al., 2015). Those modelled products generate atmospheric and land reanalyses, which synthesize observations distributed irregularly in space and time into gridded products (Chaudhuri et al., 2013) (see Technical Annex on observations).

Most global datasets are available at coarse temporal or spatial resolution, or do not include all available station data of a particular region. Therefore efforts have been made to develop regional or country-scale datasets (see Technical Annex on observations). Moreover, both radar and satellite remote sensing are two other sources that can provide a valuable alternative to in situ measurements at regional scale. Various combined products have been described recently, and some of which have been released to the community (Bližňák et al., 2018; Dinku et al., 2014; Krähenmann S. et al., 2018; Manz et al., 2016; Oyler et al., 2015; Panziera et al., 2018; Shen et al., 2018; Yang et al., 2017). However, some are limited by their short length of record, varying between one (Shen et al., 2018b) and 64 years (Oyler et al., 2015).

Reanalysis products are designed to merge irregular observations and models that encompass many physical and dynamical processes. They generate a dynamical coherent estimate of the state of the atmosphere on uniform grids either at global (Dee et al., 2011; Kalnay et al., 1996; Uppala et al., 2006, see chapter 1), regional (Chaney et al., 2014; Dahlgren et al., 2016; Maidment et al., 2014; Mahmood et al., 2018; Attada et al., 2018; Langodan et al., 2017) or country scales (Krähenmann S. et al., 2018; Mahmood et al., 2018; Rostkier-Edelstein et al., 2014; Vidal et al., 2010). Recently, reanalyses using convection permitting regional climate models have been published such as the one described by Wahl et al. (2017) for central Europe.

Regional reanalysis datasets are of large value for regional assessment, since they can employ higher resolution model simulations due to their small spatial coverage. Their accuracy also improves with respect to global reanalyses since they are often developed over regions with a high density of observational data to be assimilated into the model. Current regional reanalysis datasets cover areas like the Arctic, Europe, North America, South Asia and Australia (see the Technical Annex on observations).

### *10.2.2 Challenges*

Considerable challenges remain in using observations for climate monitoring, for improving climate models, for data assimilation and post-processing techniques, and therefore for increasing our confidence in the attribution of past climate changes at the regional level, or in future climate projections. Here problems associated with both the collection and the construction of datasets delivered along with quality control estimates are outlined not only with the traditional temporal resolutions at the monthly or seasonal scale, but also with those at the sub-monthly and sub-diurnal levels. Efforts needed to improve models in under-sampled regions are investigated so that the modelled processes operating on a variety of scales can be

trusted.

There are specific challenges for the typological regions considered in this chapter. Although the urban heat island phenomenon is well documented and studies have increased our understanding, the important measurements of meteorological and external climatic drivers across urban areas remains very limited due to the scarcity of high-density in situ measurement networks. For other regions such as steep mountain terrain, dense networks are required for adequate model evaluation. Finally, while considerable progress has been made by the global and regional modelling communities in order to assess uncertainties in model data, observational datasets, either gridded or station data, are not free of important imperfections and deficiencies.

#### *10.2.2.1 Quality control*

The usefulness of the observational data is conditioned by the outcome of a quality control (QC) process. The objective of the QC is to verify if a reported data value is representative of the measured variable and to what measure the value could be contaminated by unrelated factors. The QC procedure depends strongly on the specific nature of the dataset. It focuses on aspects such as correctly identifying time and location, having values that reliably reflect the expected conditions, and having consistency among the observed measurements. Detailed documentation of data processing optimally enhances the value and defensibility of QC procedures and algorithms.

QC informs the data users that, for instance, many reanalysis products may be inconsistent in the long term because they assimilate inhomogeneous sets of observations over the period data are generated (Kobayashi et al., 2015). As a consequence, the evaluation against independent observations suggest that reanalyses should not be automatically regarded as climate quality products for monitoring trends at the regional level (Torralba et al., 2017). When problems are identified some observational datasets are provided with a quality mask (Contractor et al., 2019) that can be taken into account when using the observations. However, observation-based data are often used without questioning if and how they are quality controlled. Efforts are made to, for example, produce quality-controlled precipitation data at sub-daily scale for the UK (Blenkinsop et al., 2017) and the US (Nelson et al., 2016), yet more concerted efforts are needed to cover more datasets.

QC is also closely related to data scarcity (Section 10.2.2.3), like in cases where the quality of a dataset is affected by gaps in time and space to fit the purpose of a specific application. This is often the case in high-resolution downscaling where adequate observational data may not be available to assess the added value of the increase in resolution (e.g. Di Luca et al., 2016; Zittis et al., 2017). This implies a need for additional efforts to attain quality-controlled high-resolution observational datasets.

#### *10.2.2.2 Homogenization*

Secular station time series contain inhomogeneities (such as artificial jumps or trends), which hamper assessments of long-term trends. Typical reasons for this are the urbanization of a station’s surroundings (Adachi et al., 2012a; Hamdi, 2010; Sun et al., 2016b), or cooling due to its relocation (Tuomenvirta, 2001; Xu et al., 2013; Yan et al., 2010). This can even be important for stations originally placed in villages (Dienst et al., 2017, 2019). Another source of inhomogeneity is transitions in measurement methods that affect most of an observational network over a limited time span, such as the transition to Stevenson screens (Auchmann and Brönnimann, 2012; Böhm et al., 2010; Brunet et al., 2011; Parker, 1994) or to automatic weather stations (WMO, 2017). The main approach to reduce the influence of inhomogeneities in station observations is statistical homogenization produced by comparing a candidate station with neighbouring reference stations (Trewin, 2010). This is a challenging task because candidates and their references normally have multiple inhomogeneities.

Three caveats should be noted. First, most of our understanding of statistical homogenization stems from the homogenization of temperature observations from dense networks. A recent study suggests that our ability to

remove biases quickly diminishes for sparse networks (Lindau and Venema, 2018a). This affects early instrumental data and observations that are not strongly correlated between stations, such as wind and humidity (Chimani et al., 2018). Second, in addition to systematic errors, homogenized data will also suffer from random errors, which are largest at the station level, but also present in network-average signals (Lindau and Venema, 2018b). These errors are spatially correlated and have an impact on aspects like post-processing, interpolation and downscaling (Section 10.2.3.3). Third, the above discussion pertains to the homogenization of monthly and annual means. Homogenization of daily variability around the mean is more difficult. For daily data, specific correction methods are used (Della-Marta and Wanner, 2006; Mestre et al., 2011; Trewin, 2013) that are able to improve the homogeneity of test cases, but recent independent validation efforts were not able to show much improvement (Chimani et al., 2018). The difference may stem from assumptions on the nature of such inhomogeneities, which are not yet well understood.

The best performing statistical homogenization methods in general improve long-term warming estimates. This is based on our understanding of the causes and nature of inhomogeneities combined with the design principles of statistical homogenization methods, as well as on analytical (Lindau and Venema, 2018b), numerical (Venema et al., 2012; Williams et al., 2012) and empirical validation studies (Gubler et al., 2017; Hausfather et al., 2016).

**[Place holder for a confidence statement on the impact of homogenization methods long-term warming estimates and precipitation trend as well]**

### *10.2.2.3 Data scarcity*

Data scarcity arises largely due to the lack of sustainable maintenance of observing stations, inaccessibility of the data held in national networks, and uneven spatial distribution of stations.

Although in several regions numerous stations provide (monthly) data covering more than 100 years for both temperature and precipitation (GCOS, 2015), large areas of the world remain sparsely covered. For instance, the geographical and temporal coverage of stations contributing to the GPCC monthly product vary greatly and the total number of stations providing data declined from 1990 onwards, although this may relate to delays in data acquisition (GCOS, 2015). Data scarcity is especially critical over Africa (Nikulin et al. 2012); for example over South Africa, where the station density is relatively large, the number of weather stations collecting daily temperature used in the CRUTEM4 product has significantly declined since 1980 (Archer et al., 2018).

Even in Europe, where regional high resolution observational datasets exist (e.g. Spain02 over the Iberian Peninsula, at 11 km resolution, EURO4M-APGD over the Alps and UKCP09 over the UK, both at 5 km resolution, and others with even higher resolution over Germany, Sweden and Norway), precipitation station density in the widely used E-OBS gridded dataset varies largely in space and time across regions, with Germany offering ten times more stations than France (Prein and Gobiet, 2017). Low station density is a major source of uncertainty (Isotta et al., 2015). Similarly to the E-OBS dataset, gridded daily temperature and precipitation datasets are being developed for other regions of the world such as Southeast Asia (SA-OBS, van den Besselaar et al., 2017a) and West Africa (WACA&D, Van Den Besselaar et al., 2015) but stations are unevenly distributed and its number varies over time, with gaps due to missing values.

Data scarcity results in critical problems for climate monitoring (e.g. trend analysis of extreme events requires high temporal and spatial resolutions). As an example Lin and Huybers (2019) found that changes in the use of rain gauges after 1975 resulted in spurious trends in extremes of Indian rainfall in a 0.25°gridded dataset covering the 20th century. In fact, the number of stations used to construct the gridded dataset dropped by half after 1990, leading to inhomogeneity and spurious trends.

**[Placeholder for a confidence statement about the fact that data scarcity might bias trend estimates]**

### *10.2.2.4 Gridding*

Derived gridded datasets require merging data from different sources of observations and/or reanalysis data on a uniform grid (see for example (Xie and Arkin, 1997) and Section 10.2.1.2). However, in situ observations are distributed irregularly, especially over sparsely populated areas. This leads to an interpolation challenge.

There are two main approaches to produce gridded datasets: (1) in situ observation-based; (2) combining in situ observations with remote-sensing data. The first approach has been widely employed in regions with high station density using interpolation techniques (such as inverse distance weighting, optimal interpolation, and kriging) (Chen et al., 2008; Frei, 2014; Haylock et al., 2008; Hiebl and Frei, 2016; Inoue et al., 2016; Isotta et al., 2014; Masson and Frei, 2014). This approach can provide high spatial and temporal resolutions according to the scale of observational data. The second approach has been mainly applied in data sparse regions, which have had very low station density, using simple bias adjustment, quantile mapping, and kriging techniques with in situ observations and satellite data (Abera et al., 2016; Cheema and Bastiaanssen, 2012; Dinku et al., 2014). Erdin et al. (2012) have been developing gridded rainfall datasets by combining radar and rain gauge data using kriging. Alternatively, Krähenmann et al. (2018) have produced a high resolution gridded dataset from station data, satellite estimation and model outputs using several merging techniques.

Gridding of station data is affected by uncertainties stemming from measurements errors, inhomogeneities, the distribution of the underlying stations and the interpolation error. The dominant factor is station density (Herrera et al., 2018b). Uncertainty due to interpolation is typically small for temperature but substantial for precipitation (Chubb et al., 2015). The largest errors typically occur in sparsely sampled mountain areas. Interpolation generally brings about smoothing effects like, for instance, the weaker variability of the derived dataset with respect to the in-situ observations. As a result, the effective resolution of gridded data is typically much lower than its nominal resolution. For instance, a 5 km gridded precipitation dataset for the Austrian Alps has an effective resolution of about 10–25 km (Isotta et al., 2014). In an example for precipitation in Spain, the effective resolution converged to the nominal resolution only when at least 6–7 stations where inside the gridbox (Herrera et al., 2018b).To account for the smoothing errors, new stochastic ensemble observation data sets have been introduced. In this approach each ensemble member represents one possible observed field, given the station observations (Von Clarmann, 2014). The gridding problem also pervades in regions such as the Arctic where Dodd et al. (2015) have used ERA-Interim to understand the impact of various interpolation and extrapolation methods for SST on trends, finding that kriging methods produce much better results than bilinear interpolation.

**[Placeholder for a confidence statement about gridding methods]**

### *10.2.2.5 Observations for cities*

The positioning of a monitoring station in a city strictly depends on the scale of the urban area. A typical city extends from a few kilometres to a few tens of kilometres, but its internal features influence the air flow at scales down to the street-canyon scale of a few metres. Oke (2006) published a guideline on urban observations well before the (WMO, 2017) guidelines.

For example, at the neighbourhood scale (up to 1 or 2 km), (repetitive) surface inhomogeneities at the street canyon scale are filtered out, by horizontal averaging over a homogeneous area of the city. In the vertical, the roughness sublayer extends from the surface up to a level at which horizontal homogeneity of the flow is achieved. Both the city (up to 10 or 20 km) and other regional spatial scales (up to 100 or 200 km) focus on the whole boundary layer as many processes in the urban roughness sublayer and the canopy sublayer are less relevant to understand the climate. A typical climate phenomenon relevant to these scales is the urban heat island, characterized by warmer temperatures in the city as compared to the surrounding rural area. Generally, the heat island occurs at night because the rural area cools more rapidly than the city. Temperature differences of up to 10–12 °C have been measured across large cities (Bader et al., 2018;

Kuang, 2019). Urban heat islands can also induce thermodynamically driven regional-scale flows (Oke et al., 2017).

Although the urban heat island phenomenon is well documented and studied (see FAQ 10.2), measurements of meteorological and external climatic drivers across urban areas remain very limited due to the scarcity of high-density, in situ measurement networks. Especially long-term datasets (a year or more) are very scarce but invaluable because they allow more in-depth research on the seasonal evolution of the urban climate. Using a network of monitoring stations in cities can enhance the understanding of urban microclimates and their interaction with climate change and provide key information for end-users, decision-makers, stakeholders and the public.

Recently, urban observational networks (see Technical Annex on observations) have been established, a notable example being the Helsinki Testbed (Koskinen et al., 2011). Another one includes the Tokyo Metropolitan Area Convection Study (TOMACS, Shusse et al., 2015) aiming to study, monitor and predict extreme weather events using dense in situ and radar observation networks (Fujibe, 2015; Seino et al., 2018b). However, there is still a lack of harmonization of collection practices, instrumentation, station locations, and quality control methodologies across cities to facilitate collaborative research (Muller et al., 2013).

#### *10.2.2.6 Mountainous areas*

Because of remoteness, winds, cold temperature, mountains slopes, heavy snow as well as instrumental issues, obtaining measurement over mountainous areas is extremely difficult (Gultepe, 2015). Remote-sensing methods could be considered but they also have limitations. For instance, Zulkafli et al. (2014) showed that different versions of TRMM perform differently over mountainous terrain, with TRMM 3b42 v7 having the smallest bias due to an improved surface clutter algorithm. In order to reduce severe underestimation of heavy rainfall over mountains in microwave-merged products, GSMaP introduced and successfully tested precipitation correction methods over complex terrain (Shige et al., 2013). Another issue with IR-based rainfall estimates over mountains is related to situations where the upper-level anvils are advected by upper-level jets, resulting in rainfall being estimated in locations where it does not really occur (Shige et al., 2017).

Measurements of wind speed, temperature, humidity, and solar radiation are critical, but difficult to deal with, over mountains (Gultepe, 2015). Uncertainty arises due to blowing snow and solar radiation effects, giving uncertainty in relative humidity up to 20% (Gultepe et al., 2014), capturing snow rate become smaller than 50% in a windy case, and posing a serious challenge for model validation. The measured radiative fluxes over slopes need to be corrected for surface slope factors, whereas the estimation (especially with gauges) of snowfall remains challenging because of the wide variety of snow type, shapes, size distributions and particle density (Gultepe et al., 2014).

**[Placeholder for a discussion of the particular challenges of gridded datasets in mountain regions].**

#### *10.2.2.7 Other sources of uncertainty*

The quality and availability of multiple observational references play a central role in the model performance assessment. In fact, when using observations for model validation, there are multiple examples where inter-observational uncertainty is as large as the model error or the inter-model variability. This has been shown for various aspects of the Indian monsoon (Collins et al., 2013) and for precipitation uncertainties over Africa (Dosio et al., 2015a; Nikulin et al., 2012; Sylla et al., 2013b). Dosio et al. (2015) demonstrated uncertainty between precipitation datasets over parts of East Africa up to 3 mm/day, nearly as large as the inter-model standard deviation. Kotlarski et al. (2017) compared three high-resolution observational temperature and precipitation datasets (E-OBS, a compilation of national/regional high-resolution gridded datasets, and the EURO4M-MESAN 0.22° reanalysis based on the HIRLAM high-resolution limited area

model) with five EURO-CORDEX RCMs driven by ERA-Interim. Generally, the differences between RCMs are larger, but for individual regions the uncertainty in the observation datasets can dominate. They also showed that the choice of reference dataset can have an influence in the RCM ranking score. Using a very different perspective, the agreement between model simulations may be used to estimate the uncertainty and quality of observations (Massonnet et al., 2016).

Other example of uncertainty is related to the fact that global observational products such as remote-sensing derived data or reanalyses have higher uncertainty in data sparse regions since in situ data is used to tune the algorithm/model. An example is the estimate of evapotranspiration, for which a large variety of methods based on remote sensing exists (Zhang et al., 2016c). Remotely sensed evapotranspiration products are mostly evaluated against the Fluxnet networks, which has a relatively dense coverage over North America, Europe and Japan (Ichii et al., 2017), but only a few sites over other regions. Consequently, evapotranspiration algorithms in surface and boundary layer parameterizations may be not representative for data sparse regions. Satellite products of evapotranspiration have also been shown to have very large uncertainties over tropical South America (Sörensson and Ruscica, 2018), in particular for the annual cycle and variability, while uncertainties in the mean are largest over arid areas. Some well-documented agricultural droughts over arid areas were found to be unrepresented in satellite products due to uncertainties in the representation of radiation anomalies in the forcing data (Sörensson and Ruscica, 2018).

### *10.2.3 Use of observations*

#### *10.2.3.1 Climate monitoring*

The synthesis of surface climate monitoring information from different countries has the potential to provide a regional or global view of climate variability and change. Many countries do provide national climate monitoring products that summarise climatic conditions at a national scale and show how present conditions compare with those in the past. However, inconsistencies among the methods used by different countries make comparisons among products and their synthesis very challenging and limit their usefulness. Even well identified differences such as the choice of the baseline period for calculating anomalies or the length of available records can make any synthesis difficult. The (WMO, 2017) has defined a shortlist of key indices to be computed at national scale and issued guidelines to produce and disseminate them. This enables a wide range of countries to participate in global monitoring activities such as the Bulletin of the American Meteorological Society's State of the Climate reports (Hartfield et al., 2018).

Space-observing systems such as satellite sensors offer spatial wide and repeatable coverage, long-term service, and the ability to monitor several aspects of weather and climate simultaneously. However, a simple concatenation of data in time would show non-climatic jumps due to changes in calibration and processing algorithms or artificial trends for a satellite series related to orbit stability or changing performance of the instruments (Barrett et al., 2014). Re-calibration and cross-calibration are then an essential prerequisite to arrive at homogenous time series of measurements across different or successive satellites that can be used for climate studies (see Section 10.2.2.2). The next step is to reprocess the data into basic physical measurements (radiance, reflectance etc.) to produce long series known as fundamental climate data records (Merchant et al., 2017) that can then be used to generate Essential Climate Variables (ECVs) and be evaluated against independent climate data.

#### *10.2.3.2 Model evaluation and parametrization improvement*

##### *10.2.3.2.1 Land surface models*

While standard variables such as temperature and precipitation are most widely sampled in observations, detailed information of other surface and atmospheric parameters is necessary in order to improve and develop new parameterizations for the next generation of climate models. Given the potential for strong coupling between the surface and atmosphere, via the boundary layer, there is a great need for more detailed

information on radiation, soil moisture and surface energy fluxes.

Parametrizations are often developed over different soil types and are rendered unsuitable for the semi-arid tropics and monsoon regions. For example, by assimilating AMSR-E brightness temperature observations into a land surface model (Yang et al., 2007), the unknown parameters of the land surface model can be optimized in the Tibetan plateau. Their proposed land data assimilation system, LDAS-UT, can dramatically improve the ability of the land surface model to simulate not only surface soil moisture, but also fluxes. Ivanov et al. (2012) and Manoli et al. (2018) explained the source of the resilience of Amazonian rainforest to water shortage by a numerical eco-hydrological model constrained by in situ observations of tropical leaf phenology. As a result, they successfully mimic the in situ-observed seasonality of gross primary production.

Considering the scale representativeness of surface parameters such as precipitation, soil moisture and surface fluxes is of vital importance. This is exemplified by the different scales on which observations must be taken to develop parameterizations and the scales in which those parameterizations will operate (Taylor et al., 2012, 2013a). A variety of technologies to measure soil moisture at the point scale exist, varying in cost-effectiveness, accuracy and depth of measurement (Dobriyal et al., 2012). Due to the nature of soil moisture that depends on parameters with a large spatial variability such as soil type, vegetation and small-scale variations in topography, these measurements have a spatial representativeness of less than 1 $m^2$ (Liu et al., 2016; Ochsner et al., 2013). In some parts of the world, networks of point-scale measurements are used to compare soil moisture with models and remotely sensed data (Crow et al., 2015; Polcher et al., 2016). The smaller networks are typically of the size of a single climate model grid-square or satellite pixel and are suitable for monitoring watersheds, while networks representative of larger areas (>100 $km^2$) are less common but emerging in some parts of the world, mostly in the USA (Ochsner et al., 2013).

#### *10.2.3.2.2 Precipitation processes*

Adequate modelling of precipitation processes is a challenging issue for numerical models. Recent accumulations of advanced satellite observation data can be used to examine precipitation processes globally, even for their extremes (Hamada et al., 2015; Hamada and Takayabu, 2018; Sohn et al., 2013). Three-dimensional radar observations have made possible to classify precipitation systems according to their statistical characteristics and relate them to large-scale environmental conditions in the East Asian monsoon (e.g. Yokoyama et al., 2017). Based on such relationships, a statistical downscaling of the precipitation characteristics using large-scale conditions from reanalyses and CMIP5 simulation outputs was performed, and then applied to future climate projections (Yokoyama, et al., 2019).

Convective latent heating is an essential part of the diabatic heating of the atmosphere that balances with the large-scale atmospheric circulation. The TRMM precipitation radar is used with the Spectral Latent Heating (SLH) algorithm in conjunction with a cloud-resolving model to estimate three-dimensional convective latent heating over the tropics and subtropics (Shige et al., 2009). A counterpart algorithm produces the Convective Stratiform Heating (CSH) product (Tao et al., 2016). Since the latent heating profiles represent the precipitation characteristics even more directly than precipitation profiles themselves, the SLH product has been used to quantify cumulus congestus regimes and the vertical profile of atmospheric heating (e.g. (Takayabu et al., 2010; Takayabu and Tao, 2019)).

### *10.2.3.3 Statistical downscaling, bias adjustment and weather generators*

Statistical downscaling, bias adjustment and weather generators all require observational data for calibration as well as evaluation (see Section 10.2.3.2). Typically, the so-called perfect prognosis methods use quasi-observations for the predictors (i.e. reanalysis) and actual observations for the predictands. By contrast, bias adjustment methods use observations only for the predictands. Weather generators typically require only observed predictands, although some are conditioned on predictors as well. Very often these methods operate on the daily scale, because of user needs, the limited availability of sub-daily observations and the limited ability of climate models to realistically simulate sub-daily weather (Iizumi et al., 2012). Some methods are calibrated on the monthly scale, but some of the generated time series are then further disaggregated to the

daily scale (e.g. Thober et al., 2014). Some methods, mainly weather generators, represent sub-daily weather (Kaczmarska et al., 2014; Mezghani and Hingray, 2009). Many methods simulate temperature and precipitation only, although some also represent wind, radiation and other variables. The limited availability of high quality and long observational records typically restricts these applications to a few cases (Pryor and Hahmann, 2019).

All limitations and challenges of observational data discussed in Section 10.2.2 apply to the use for statistical post processing of climate model data. High quality and long observational data series are particularly relevant as all statistical post-processing approaches require observations for calibration. In tropical regions, different reanalysis present significant discrepancies for key predictor variables at the daily scale(Brands et al., 2012), indicating that these data may not be suitablefor statistical downscaling.

An important issue for bias adjustment is the correct representation of the required spatial scale. Ideally, bias adjustment is calibrated against area-averaged data of the same spatial scale as the climate model output. Hence, high-quality gridded datasets with an effective resolution close to the nominal resolution are required. Driven by the need to generate regional scale information also in station sparse regions, researchers began to blend information from stations and remote sensing to produce high-resolution calibration observations for the predictands (e.g. (Haiden et al., 2011; Wilby and Yu, 2013); see also 10.2.1.2 and 10.2.2.4). Such developments are particularly important for statistical downscaling and bias adjustment.

#### *10.2.3.4 Assimilation of data including paleoclimate*

Decadal prediction (Kushnir et al., 2019b) must be initialized from the observed state of all components of the climate system (atmosphere, sea, ice, soil, ocean) (Meehl et al., 2014; Mulholland et al., 2015; Towler et al., 2018; Volpi et al., 2017), either in full-field or anomaly initialization mode. The types of observations used include atmospheric and ocean reanalyses, gridded and satellite-derived products of sea-ice, surface height, and gridded ocean temperature and salinity. Full-field initialization brings the model state close to the observed state, while anomaly initialization adds the anomalous component of the observed state to the model climatology to minimize the drift during the forecast (Chiodi and Harrison, 2017; Corti et al., 2015; Ding Ruiqiang et al., 2016; Huddart Benjamin et al., 2017; Weber et al., 2015).

Modern reanalyses constrained by instrumental data cover from the present decade back over the past century, with a few applications for the 19th century (Compo et al., 2011; Laloyaux et al., 2018). The reanalysis period can be extended further back in time using records of past climate variations derived from old documents and natural archives such as tree rings (see Chapter 2). However, several aspects of the methodology are still challenging, in particular the generation of model ensembles, the selection of the data, the estimation of error and the definition of the observation operator that relates simulated variables to the observations (Acevedo et al., 2017; Chen et al., 2018d; Dee et al., 2016; Matsikaris et al., 2015, 2016; Okazaki and Yoshimura, 2017; Steiger et al., 2014).

Following some early concept studies, the first practical applications of paleoclimate data assimilation over past centuries used only selected data to reconstruct past climate changes for analysis of a specific process or case (Widmann et al., 2010). Recently, assimilation of a numerous series obtained from a systematic evaluation of the available records has allowed production of reconstructions that can be widely shared and applied to multiple purposes as in modern reanalyses (Franke et al., 2017; Hakim et al., 2016; Steiger et al., 2018). Most of these paleo-reanalyses are global but there are products using regional models or targeted at specific regions such as Europe, east Africa and Indian ocean (Fallah et al., 2018; Klein and Goosse, 2018).

Paleo-reanalyses are opening a new range of applications and have already provided useful information on seasonal to multidecadal climate variability over the past millennia. They have confirmed a large contribution of internal variability in past changes at regional scale during the pre-industrial period, superimposed on a weak common signal due to forcing changes (Goosse, 2017; Goosse et al., 2012) and the absence of globally coherent warm period in the common era before the recent warming (Neukom et al., 2019).

The paleo-reanalyses are also nice tools to study the co-variance between variables at interannual to centennial timescales. In particular, they have highlighted the processes that can be responsible for change in continental hydrology at multi-decadal timescales (Fallah et al., 2018; Franke et al., 2017; Hakim et al., 2016; Klein and Goosse, 2018; Steiger et al., 2018).

There is *robust evidence* based on paleo-reanalysis that highlighted a strong contribution of the atmospheric circulation in some cold periods of the early 19th century.

### *10.2.4 Outlook for improving observational data for regional climates*

#### *10.2.4.1 Data rescue*

An encouraging development for understanding past climate variations over the last 250 years lies in the field of data rescue, in which hitherto hidden archives of meteorological data are brought to the forefront. At the global level, weather rescue is led by the Atmospheric Circulation Reconstructions over the Earth (ACRE) project (Allan et al., 2011). ACRE recovers land and ocean historical instrument data, which, after quality control, is made available for use as inputs or constraints in global or regional reanalyses. An exemplar product is the 56-member Twentieth Century Reanalysis (20CR; Compo et al., 2011), which is fed entirely by surface pressure observations and the addition of monthly SST or sea-ice as boundary conditions. Alternatively, the ERA-20C reanalysis is a single-member product that assimilates surface pressure and marine winds over 1900–2010 (Poli et al., 2016).

Particular techniques include the transcription of handwritten logbooks of meteorological observations from merchant shipping (e.g., Brönnimann et al., 2011), aided by participatory "citizen science" projects such as Old Weather (oldweather.org). Other projects include Operation Weather Rescue[1], which includes recent efforts to digitise mountain weather data from an observing outpost on the UK's highest mountain at the turn of the 20th century, or work to retrieve archives of Australian climate information (reviewed in Ashcroft et al., 2016).

#### *10.2.4.2 New types of observations including citizen science*

One of the main scientific challenges related to high-resolution regional climate modelling is dealing with the representation of fine-scale process (see e.g. Yano et al., 2018) in observational data sets. Additionally, the reliable WMO-standardized observation networks have a very sparse geographical representation. So regional climate models rely more and more on high-resolution data such as, radar data (Goudenhoofdt and Delobbe, 2016) and GNSS data (i.e. GPS, Berckmans et al., 2018). These efforts have led to the production of homogenously processed long-term datasets for regional climate model evaluation.

Over the past decade more crowdsourcing data is becoming available, through the use of cheap sensors available in real time (IoT technology) that are incorporated in various applications, e.g., in cars, amateur weather stations and smartphones (Sosko and Dalyot, 2017) in citizen science projects (see the review of Muller et al., 2015). While they are far less reliable and accurate than professional observations, they are abundantly available and can give spatial representations with very high spatial resolution. Despite the limitations, this technological trend could prove very useful, and the regional climate community is making efforts to understand the extent to which these methods can be exploited, at least as a complement to traditional datasets (Langendijk et al., 2019; Meier et al., 2017).

[1] https://www.zooniverse.org/projects/edh/weather-rescue

## 10.3 Using models for constructing regional information

Expected length: 30 pages, 1 page=950 words
Number of figures: 12
Number of tables: 1

Much of the information available on future regional climate arises from studies based on climate model simulations. Depending on the scales and application of interest, a hierarchy of models ranging from general circulation models with global coverage to high resolution regional climate models, specific land surface models, and to statistical approaches may be applied in different types of simulation experiments. Model evaluation is central to assess the performance of models in present climate and for corroborating their adequacy for projecting specific aspects of regional climate. An intercomparison of different model types provides insight into the improvements and value added by more complex or higher resolution models. A key objective of evaluation studies is to understand whether a chosen climate model can realistically simulate processes and climate phenomena that are relevant for a given application. Uncertainties, especially those arising from climate model errors and internal climate variability, can be sampled to a certain degree by using ensembles of climate models. This section presents the different types of models and simulation experiments used for generating regional climate change information, the performance of these models and uncertainties associated with regional climate projections.

### *10.3.1 Types of models*

Regional climate change information may be derived from a hierarchy of different model types covering a wide range of spatial scales and processes (Figure 10.3 for an overview). The most relevant models will be introduced in the following and their performance assessed in Section 10.3.3.

**[START FIGURE 10.3 HERE]**

**Figure 10.3:** Typical models and model chains used in regional climate modelling. The dashed lines indicate model chains that might prove useful but have not or only rarely been used. [Placeholder: For the SOD, more text could be given specifying the individual modelling chains and typical resolutions]

**[END FIGURE 10.3 HERE]**

#### *10.3.1.1 GCMs, including high-resolution and variable resolution GCMs*

State of the art GCMs are generally used to derive climate information at continental to global scales both for the past and future climate (Chapters 3 and 4). Although the nominal horizontal resolution in CMIP5 GCMs is typically 100–200 km, which limits their ability to resolve local details, their results have also been applied to study past and future regional climate change.

[**Placeholder: either short discussion of GCM assumptions or link to relevant Chapter]**

There has long been a tension regarding how to best use available simulation resources among choices of increasing model resolution (to capture finer scale processes), enhancing the ensemble size (to better capturing internal variability), improving parameterizations and adding new processes, such as the carbon cycle. Despite these efforts, the progress in reducing biases and providing more credible regional projections by GCMs and ESMs has been limited. Several of the new CMIP6 (Eyring et al., 2016a) MIPs address this limitation: AerChemMIP (Aerosols and Chemistry, Collins et al., 2017), the CFMIP (Cloud Feedback, (Webb et al., 2017), LS3MIP (Land Surface, Snow and Soil Moisture, van den Hurk et al., 2016), LUMIP (Land Use, (Lawrence et al., 2016), OMIP (Ocean) (Griffies et al., 2016), PAMIP (Polar Amplification, (Smith et al., 2019)), and DynVarMIP (Dynamics and Variability, (Gerber and Manzini, 2016). HighResMIP

(High-Resolution, Haarsma et al., 2016) and GMMIP (Global Monsoons, Zhou et al., 2016) specifically address regional climate in GCMs and ESMs.

HighResMIP focuses on producing global climate projections at a horizontal resolution of around 50 km grid spacing or finer, where important mesoscale phenomena such as tropical cyclones start being resolved (Section 10.3.3.5). Higher global resolution also yields improved boundary conditions for regional climate models, although biases that result from for instance inadequate parameterisations typically remain (Roberts et al., 2018).

Apart from increasing resolution everywhere, variable resolution GCMs, that is, with locally enhanced resolution, have also been developed since the 1970s (Krinner and Genthon, 1998; Li, 1999), resulting in a first coordinated effort by Fox-Rabinovitz et al., (2006, 2008). An overview of recent developments has been given by McGregor, (2015). This is a rapidly developing field (Ferguson et al., 2016; Huang et al., 2016; Krinner et al., 2014).

### *10.3.1.2 Regional climate models*

Regional climate models (RCMs) are dynamical models similar to GCMs that are run over a limited area, but with a resolution higher than that of standard GCMs. They are the basis for dynamical downscaling. At the domain boundaries, RCMs take their values from a driving data set, which could be a GCM or a reanalysis. RCMs are typically one-way nested: they do not feed back into the driving model, although two-way nested RCMs exist (Harris and Lin, 2013; Junquas et al., 2016; Lorenz and Jacob, 2005; Takayabu et al., 2015; Yang et al., 2016a).

In general, the assumptions underlying dynamical downscaling in a climate change context are that, for a given application, (1) the relevant large-scale atmospheric circulation features and their response to climate change are realistically and credibly reproduced by the driving GCM (and not distorted by the RCM) and (2) that the RCM realistically simulates the relevant regional- and local-scale processes that control climate variability and change. The second assumption in particular requires that the relevant regional forcings are included and sub-grid parameterisations are, as with GCMs, applicable in the projected climate.

The consistency between the circulation features simulated by the RCM and those inherited through the boundary conditions depends on two factors: 1) the relative importance of the large-scale forcing compared to local-scale phenomena, and 2) the size of the RCM domain; in fact, large (continental scale) domains allow the RCM to generate its own climate. An approach to ensure, if desired, consistency with the driving model (e.g., to synchronize internal variability) is spectral nudging (Kida et al., 1991; von Storch et al., 2000; Waldron et al., 1996), by which selected variables, such as the wind field, are forced to closely follow a prescribed large-scale field over a specified range of spatial scales, whereas smaller scales are generated by the regional model itself.

When RCMs are driven by GCMs, large-scale biases are inherited through the lateral boundary conditions in addition to any inherent biases of the RCM itself (a garbage-in, garbage-out problem, e.g. Dosio et al., 2015; Hall, 2014; Hong and Kanamitsu, 2014; Takayabu et al., 2016).

The CORDEX initiative (COordinated Regional climate Downscaling EXperiment; Giorgi et al., 2009; Giorgi and Gutowski, 2015; Gutowski Jr. et al., 2016) provides ensembles of high-resolution historical and future climate projections for various regions of the world. RCMs in CORDEX have a horizontal resolution between 10 km and 50 km. Much finer spatial resolution is required to fully resolve deep-convection, the dominant cause of precipitation in the tropics. Therefore, an emerging strand in dynamical downscaling employs simulations at convection permitting scales, at a horizontal resolutions of a few kilometres, where deep-convection parameterisations can be switched off (Coppola et al., 2018; Prein et al., 2015; Stratton et al., 2018). Alternatively, some RCMs make use of scale-aware parameterizations that are able to adapt to increasing resolution without switching off the convection scheme (De Troch et al., 2013; Giot et al., 2016; Hamdi et al., 2012b; Plant and Yano, 2015; Termonia et al., 2018a; Yano et al., 2018).

RCMs often consist of an atmospheric and land component only and therefore neglect important processes such as air-sea coupling (in standard RCMs the sea surface temperatures are prescribed from GCM simulations) or cloud-aerosol interaction (aerosols prescribed with a climatology), which may influence regional climate projections. Therefore, in recent years, many RCMs were extended by coupling to additional components like active oceans with sea-ice (Kjellström et al., 2005; Sein et al., 2015; Somot et al., 2008; Van Pham et al., 2014), rivers (Di Sante et al., 2019), glaciers, aerosols (Nabat et al., 2015; Zakey et al., 2006; Zubler et al., 2011). These couplings allow for the investigation of additional climate processes such as regional sea-level change (Adloff et al., 2018) or the control of high-frequency ocean-atmosphere coupling on the climatology of Mediterranean cyclones (Flaounas et al., 2018). If such RCMs are extended by additional components (such as the carbon cycle), they may be named Regional Climate System Models (RCSMs, Somot et al., 2018) or Regional Earth System Models (RESMs, Giorgi and Gao, 2018).

#### *10.3.1.3 Sub-component models*

The influence of cities, small waterbodies, freshwater input to oceans, agriculture and other deviations from the surrounding landscape on regional climate may not be resolved by GCMs or RCMs. Here, a selection of sub-component models developed to represent these influences is introduced. The relevance of including these models in GCM or RCM coupled simulations will be assessed in Section 10.3.3.

##### *10.3.1.3.1 Urban models*

In order to calculate the exchanges of heat, water and momentum between the urban surface and its overlying atmosphere, specific surface-atmosphere exchange schemes dedicated to urban areas must be implemented (Figure 10.4 and FAQ 10.2).

Urban schemes were developed in the last 20 years and vary considerably in complexity. In general, three different types can be distinguished (Best and Grimmond, 2015; Chen et al., 2011; Grimmond et al., 2010, 2011; Masson, 2006):

1. The simplest is the slab or bulk approach, where urban areas are represented by modifying soil and vegetation parameters within land surface models (e.g. Best et al., 2006; Dandou et al., 2005; Liu et al., 2006; Seaman et al., 1989). They usually feature parameters based on the observation that roughness length and displacement height are large over cities. The energy balance is also often modified to account for the radiation trapping in the urban canopy, heat storage, evaporation, and anthropogenic heat fluxes. However, the three-dimensional structure of the city is not resolved.
2. Single-layer urban canopy modules represent cities with a simplified geometry (urban canyon, with three surface types: roof, road and wall) that can approximately capture the main 3D dynamical and thermal physical processes (Figure 10.4) influencing radiative and energy fluxes (Kusaka et al., 2001; Masson, 2000).
3. In multi-layer urban canopy modules urban effects are computed vertically throughout the urban canopy, allowing a direct interaction with the planetary boundary layer (Brown, 2000; Dupont and Mestayer, 2006; Hagishima et al., 2005; Hamdi and Masson, 2008; Martilli et al., 2002; Schubert et al., 2012). As a sub-model of urban canopy modules, building-energy models that estimate anthropogenic heat from a building for given atmospheric conditions have also been developed (e.g. Bueno et al., 2012; Kikegawa et al., 2003; Lipson et al., 2018).

Only a few regional modelling groups are beginning to implement the three types of urban parameterizations within the land-surface component of their RCM (Daniel et al., 2018; Hamdi et al., 2014; KUSAKA et al., 2012; McCarthy et al., 2012; Trusilova et al., 2016).

**[START FIGURE 10.4 HERE]**

**Figure 10.4:** Single-layer urban canopy parametrization in the land surface model of RCMs. [For the SOD, more text will be given explaining the processes and models.]

**[END FIGURE 10.4 HERE]**

*10.3.1.3.2 Land management*

Land management has been implemented in GCMs and RCMs since AR5, two important examples being irrigation and tillage. Irrigation increases the soil moisture, enhancing the latent heat flux and reducing the sensible heat flux and, in turn, local temperature. Various approaches of different complexity are used to calculate crop demand and irrigation supply. Currently no GCM or RCM uses a completely interactive approach, which would be based on crop management and climate interacting to determine demand and account for availability of water on the supply side (McDermid et al., 2017). Furthermore, the influence of crop management on parameters connecting the land-surface model to the atmosphere, such as Leaf Area Index and albedo is not fully understood (McDermid et al., 2017).

The simplest approach to implementing irrigation demand in a model is to define it as the difference between actual and desired soil moisture availability, the latter most commonly set to field capacity (Nazemi and Wheater, 2015). This demand is applied to areas equipped for irrigation and often applied all year round (Pokhrel et al., 2016) resulting in an overestimation of actual irrigation demand. The simplest way to implement supply of water to fill the irrigation demand is to add water from an infinite surface storage until the demand is covered (Nazemi and Wheater, 2015; Pokhrel et al., 2016; Tuinenburg et al., 2014). Another approach forces the model with historical irrigation data constructed from data assessment irrigation data and offline hydrological modelling, which can improve the spatial-temporal heterogeneity of irrigation (Cook et al., 2015b; Shukla et al., 2014; Wada et al., 2014).

Tillage lowers the surface albedo by replacing light-coloured crop residue with darker soil, making the surface absorb more energy. The effect of tillage versus no-tillage systems in coupled simulations has been implemented through changes in albedo and, to account for effects on evaporation, soil resistance (Davin et al., 2014; Hirsch et al., 2017, 2018).

*10.3.1.3.3 Lake models*

Lakes have very different surface properties in comparison to land (lower surface roughness and albedo, and higher thermal conductance and heat capacity), and their presence in a landscape introduces large heterogeneities of temperature and evapotranspiration.

A common way of accounting for the difference between land and lake temperatures has been to put the lake temperature and lake ice conditions equal to those at the closest sea point. This approach is problematic for seasonally ice-covered lakes, since the sea temperature falls much slower during autumn than the actual lake temperature would and therefore creates an artificial heat and moisture source to the atmosphere (Kirillin et al., 2012). Therefore, lake models have been incorporated in RCMs (Bennington et al., 2014; Gula and Peltier, 2012; Martynov et al., 2010; Samuelsson et al., 2010). Most lake models assume that the horizontal gradient of temperature is negligible in comparison to the vertical gradient to justify a 1D approach. Although this can be problematic for large lakes (León et al., 2007) the large computational cost of coupled 2D and 3D lake models prevents this approach (Pietikäinen et al., 2018). A multi-layer model can describe the lake thermocline without parameterization (Xiao et al., 2016) but is computationally expensive. Therefore, the most common approach in RCMs is the two-layer model, including a lake-ice model, with parameterized vertical temperature profiles based on measurements (Golosov et al., 2018; Mironov et al., 2010).

*10.3.1.3.4 Wetlands*

**[placeholder on models for wetlands]**

*10.3.1.3.5 Freshwater input into oceans*

**[placeholder on models for freshwater input to oceans]**

*10.3.1.4 Statistical downscaling, bias adjustment and weather generators*

An alternative or addition to dynamical downscaling is the use of statistical approaches to generate regional projections. In AR5 these methods have been collectively referred to as statistical downscaling, but have received little attention. A major conclusion was that a wide range of different methods exist and a general assessment of their performance is difficult (Flato et al., 2014). Since AR5, several initiatives have been launched to improve the understanding of statistical approaches such as VALUE (Maraun et al., 2015), STARMIP (Vaittinada Ayar et al., 2016) and BADJAM (Galmarini et al., 2019). To precisely distinguish between conceptually different statistical post-processing approaches and their underlying assumptions, the terms perfect prognosis, bias adjustment and weather generators are used in this Chapter, roughly following the VALUE terminology (Maraun et al., 2018). The performance of different implementations of these approaches will be assessed in Section 10.3.3.

*10.3.1.4.1 Perfect prognosis*

Perfect prognosis models are statistical models calibrated between quasi-observed large-scale predictors (e.g. reanalysis) and observed local-scale predictands. Regional climate projections are then generated by replacing the quasi-observed predictors by those from climate model (typically GCM) projections. A set of assumptions underlying the use of perfect prognosis, often simply referred to as the stationarity assumption, has been formulated: (1) the predictors are "perfectly" simulated by the driving model; (2) the chosen predictors are informative of the underlying climate variability on all desired time scales and allow to capture the climate change signal, and (3) the chosen perfect prognosis model is capable of representing the desired aspects of the climate distributions such as extreme events or spatial dependence for a recent period of reference, allowing at least for moderate extrapolations to yet unobserved predictor values (Maraun and Widmann, 2018b).

Typical implementations of perfect prognosis models include regression-like models and the analogue method. All regression-like models (including non-linear regression (e.g. generalized linear models (GLMs) and canonical correlation analysis) rely on a transfer function linking an observed local statistic (such as the temperature at a given day) to some set of large-scale predictors. Stochastic regression models explicitly simulate the variance not explained by the predictors by adding some kind of stochastic noise. The use of advanced machine learning techniques for statistical downscaling purposes is increasing rapidly, especially with deep and convolutional neural networks **[Placeholder for major new methods developed since AR5 plus potentially some older ones]**

Analogue methods are based on the assumption that two similar large-scale weather fields typically result in similar local weather fields. Thus, analogue methods compare a simulated large-scale weather field with an archive of observed weather fields and select, by some distance metric, the observed field closest to the simulated field as analogue. The downscaled weather field is then chosen as the local weather field observed on the instant the analogue occurred. Standard analogue methods cannot sample values outside the observed range. **[Placeholder for major new methods developed since AR5 plus potentially some older ones]**

*10.3.1.4.2 Bias adjustment*

Bias adjustment is a statistical post-processing technique used to pragmatically reduce the errors in climate model outputs. The approach estimates the bias or relative error between a relevant simulated statistic (such as the long-term mean or specific quantiles) and the corresponding observed one over a calibration period; the simulated statistic is then adjusted taking into account the simulated deviation. Bias adjustment methods are applied on spatial scales similar to that of the simulation being corrected, and often used as a simple statistical downscaling method between coarse resolution (e.g. GCM) model output and finer observations.

The most important difference with perfect prognosis is that, whereas perfect prognosis can link any physically sensible predictor at a given day to any local weather variable, bias adjustment can only link long-term statistics of a simulated weather variable to the same long-term statistic of the same observed weather variable.

By construction, the bias in the adjusted statistic vanishes over the calibration period. In a climate change context, bias adjustment is based on the assumption that biases are time-invariant, often referred to as stationarity assumption. This assumption comprises three more specific assumptions, namely that (1) the climate change of the input variable is credibly simulated, (2) the simulated variable is representative of the observed variable, and (3) the chosen bias adjustment method is applicable under future climate conditions (Maraun and Widmann, 2018b).

Typical implementations of bias adjustment are (1) additive adjustments, where the model data is adjusted by adding a constant, (2) rescaling, where the model data is adjusted by a factor, (3) or more flexible quantile mapping approaches that adjust different ranges of a distribution individually. Research on new bias adjustment methods since AR5 has focused mainly on the development of trend-preserving quantile mapping methods and multi-variable methods. Hempel et al. (2013), Pierce et al., (2015) and Switanek et al. (2017) develop variants of quantile mapping that preserve trends in the mean or even further distributional statistics. Multivariate bias adjustment extends univariate methods, which adjust statistics of individual variables separately, to joint adjustment of multiple variables simultaneously. Implementations remove biases in (1) specific measures of multivariate dependence, like correlation structure, via linear transformations (Bárdossy and Pegram, 2012; Cannon, 2016); or, more flexibly, (2) the full multivariate distribution via nonlinear transformations (Cannon, 2018; Robin et al., 2019; Vrac, 2018; Vrac and Friederichs, 2015). Over recent years, several issues have been identified that may arise when using bias adjustment. These are discussed in the Box 10.2.

#### *10.3.1.4.3 Weather generators*

Weather generators are statistical models that simulate weather time series of arbitrary length. They are calibrated to represent observed weather statistics, in particular temporal day-to-day (or even sub-daily) variability. One variant of these models is conditioned on large-scale atmospheric predictors on a day-by-day basis. These models are advanced stochastic perfect prognosis methods underlying the same assumptions. Another widely used variant are change-factor weather generators: the weather generator parameters are calibrated against present and future climate model simulations, and the climate change signal in these parameters is then applied to the parameters calibrated to observations. Such weather generators evolve randomly on a day-by-day basis, and take only long-term changes from the climate model. The assumptions underlying change-factor weather generators are that (1) the change factors are credibly simulated, (2) the simulated variables from which the change factors are derived have to be representative of the corresponding observed variables, and (3) the structure of the weather generator has to capture the relevant statistical climate aspects, and change factors for all relevant aspects have to be included (Maraun and Widmann, 2018b). **[Placeholder on new developments in weather generators]**

### *10.3.2 Types of experiments*

The most commonly used experiments to generate regional climate change information are transient simulations, but a broad range of alternatives exists that may better serve for a specific purpose. For instance, pseudo-global warming studies may be used to mitigate large-scale circulation biases or to study individual events at a very high resolution, sensitivity studies may be conducted to identify important driving processes, and long control simulations may help to understand internal variability. Specific experiments may allow for evaluating downscaling performance. Important experiment types are introduced below.

#### *10.3.2.1 Transient simulations and time-slice experiments*

Transient simulations intend to represent the evolving climate state of the Earth system (see also Chapter 4). They are typically based on some of the CMIP-type coupled GCM simulations, such as those in the DECK and ScenarioMIP part of CMIP6 covering the period 1850–2100 (Eyring et al., 2016), and HighResMIP (although covering only the period 1950–2050 due to computational constrains, Haarsma et al., 2016). Global transient climate simulations may be further downscaled by either dynamical or statistical downscaling. Currently available CORDEX RCM simulations are based on CMIP5 (Gutowski Jr. et al., 2016).

On the contrary, time-slice experiments are designed to represent only a short, specific period of time (typically 30 years); they are often run using GCMs or RCMs in atmosphere-only mode, forced by SSTs derived either from observations, like in the AMIP experiments, or historical simulations and future projections from coupled GCMs. Compared to the transient simulations, they offer advantages in being computationally cheaper (due to the lack of coupled ocean and short duration), which allows for the number of ensemble members (Zhang et al., 2016d), or the resolution (Haarsma et al., 2013a) to be increased. Convection-permitting simulations, both covering the globe or particular regions, are currently conducted for short time slices only (Coppola et al., 2018; Hewitt and Lowe, 2018; Kendon et al., 2017). Some time-slice experiments have been carried out for coupled ocean atmosphere RCMs (Zou and Zhou, 2016, 2017). Time slice experiments may be driven with a historical sequence of SST or with average climatological SST describing the typical seasonal cycle. In the former case, the simulations will reflect the phase of internal, interannual to decadal variability of the driving SST data.

#### *10.3.2.2 Pseudo-global warming experiments*

Often, results from downscaling experiments suffer from large-scale circulation biases in the driving GCMs such as misplaced storm tracks (Section 10.3.3.4). If, in a given application, one can assume that changes in the regional climate aspects of interest are dominated by thermodynamic rather than by circulation changes, so-called pseudo-global warming (PGW) experiments (Schär et al., 1996) may be helpful in mitigating the effects of circulation biases and hence the garbage-in garbage-out problem. In PGW experiments, boundary conditions for the downscaling are taken from reanalysis data, though modified according to the thermodynamic aspects of climate change simulated by GCMs. These changes are added to the reanalysis by modifying the 3-dimensional temperature and moisture fields according to GCM-simulated changes. The dynamical fields are unchanged, such that circulation biases are avoided. The boundary conditions thus exactly represent the observed weather sequence as represented by the reanalysis, but with higher temperatures and adjusted humidity and atmospheric stability.

Recent applications of PGW experiments include an assessment of snow cover changes in Japan (Kawase et al., 2012, 2013), summer climate change in Tokyo (Adachi et al., 2012b), climate change in the Los Angeles area (Walton et al., 2015) and Hawaii (Zhang et al., 2016a), and changes in convective precipitation over the Alps (Keller et al., 2018).

Equivalent simulations can be conducted for individual events, thereby allowing for very high resolution. With counterfactual past climate conditions, such simulations can be used for conditional event attribution (Trenberth et al., 2015, see Chapter 11), with hypothetical future conditions to generate storylines of how specific events may manifest in a warmer climate. The approach has been employed to study extreme events that require very high resolution simulations such as tropical cyclones (Gutmann et al., 2018; Kanada et al., 2017; Lackmann, 2015; Patricola and Wehner, 2018; Takayabu et al., 2015) or convective precipitation events (Hibino et al., 2018; Meredith et al., 2015b; Pall et al., 2017). However, the range of possible events to study is broader and has included, for example, Korean heat waves (Kim et al., 2018) and monsoon onset in West Africa (Lawal et al., 2016). The disadvantage of the approach is that, in many applications, only individual events are simulated and no conclusions can be derived directly on changes in the occurrence probability of these events (Otto et al., 2016; Shepherd, 2016).

#### *10.3.2.3 Sensitivity studies with selected drivers*

Sensitivity studies are used to disentangle and document the impact of a specific driver or process on a given climate change or phenomena. They can be broadly divided in two types, depending on the considered driver being either external forcing or internal variability.

The influence of a single external forcing can be assessed with transient historical simulations within two different frameworks: the "only one" and "all but one" approaches (Bindoff et al., 2013; Gillett et al., 2016). The former entails performing simulations with prescribed (often observed) changes only in the external forcing of interest, the others being fixed at a constant value (often pre-industrial). The latter is based on simulations in which all external forcings are applied but the one of interest. Both approaches in general do not give the same results as the climate response to a range of forcings is not necessarily identical to the sum of climate responses to individual forcings (Jones et al., 2013; Marvel et al., 2015; Ming and Ramaswamy, 2011; Schaller et al., 2013; Shiogama et al., 2013). The "only one" approach is often used to characterize the response to a single forcing in isolation while the "all but one" can be more appropriate to assess the relative influence of a single forcing on an observed change.

The second type of sensitivity study focuses on the influence of internal variability. Since AR5, new approaches such as partial coupling simulations are now routinely used in addition to the standard AMIP-type experiments. These are coupled ocean-atmosphere simulations in which the interaction between the atmosphere and the ocean is only one-way over an oceanic basin or sub-basin and two-way everywhere else. Different implementations have been used such as SST anomaly Newtonian relaxation at the air-sea interface or prescribing daily or higher frequency wind stress anomalies (depending on the coupling frequency) from reanalysis (Deser et al., 2017a; Douville et al., 2015; England et al., 2014; Kosaka and Xie, 2013, 2016; McGregor et al., 2014). Such simulations have been applied to, e.g., identify some of the causal factors responsible for the Global Mean Surface Temperature (GMST) hiatus (see Chapter 3, Cross-Chapter Box 3.1).

Partial coupling experiments are also used to infer the influence of a selected internal driver on regional climate change in the Decadal Climate Prediction Project component-C (DCPP-C) contribution to CMIP6 (Boer et al., 2016) or Tier 2 Atlantic and Pacific pacemaker experiments in GMMIP (Zhou et al., 2016). Similar experiments have been used to study the regional impacts of the AMV (Ruprich-Robert et al., 2017, 2018) or the impact of the NAO on the Atlantic Meridional Overturning Circulation (AMOC) (Delworth and Zeng, 2016).

Another kind of experiment concerns the impact of an observed, projected or idealized change on atmospheric or oceanic circulation and/or regional climate change. A typical example is the influence of Arctic sea-ice loss on the Northern Hemisphere atmospheric circulation and continental climate change based on sea-ice-forced atmospheric and coupled models (see also Cross-Chapter Box 10.1). There is *growing evidence* that model results can be sensitive to many factors including the magnitude and pattern of sea-ice loss, background mean state, stratosphere representation and modelling protocols used to constrain sea-ice extent or volume (Screen et al., 2018).

Another example is the modelling framework used to evaluate the impact of soil moisture and vegetation on large-scale droughts and heatwaves. RCMs are often used to reproduce the effect of land surface conditions on specific extreme events while global GCMs are used to simulate the impact of land surface conditions on the statistics of extremes. The modelling framework consists of a pair of coupled model (RCM or GCM) experiments, with one simulation serving as a control run, and a perturbed simulation with prescribed land conditions (i.e., soil moisture, LAI, and surface albedo) characterizing a specific state of the land surface. The difference between the perturbed and control simulations leads to a robust assessment of the impact of land conditions as causal factors of a climate phenomenon and/or climate extreme (Hauser et al., 2016, 2017; Rasmijn et al., 2018; Seneviratne et al., 2013; Stegehuis et al., 2015; Vogel et al., 2017b).

#### *10.3.2.4 Control simulations*

Over recent years, the role of internal variability has become clearer in the interpretation of climate

projections, in particular at the regional scale (Section 10.3.4.3). A considerable fraction of CMIP5 and CMIP6 resources has therefore been invested in generating an ensemble of control simulations with prescribed constant external forcings. These are often several hundred years long, and sometimes much longer (Pedro et al., 2016; Rackow et al., 2018) As part of the CMIP6 DECK (Eyring et al., 2016a) pre-industrial control (piControl) simulations have been conducted (Menary et al., 2018). Similarly, control simulations with present-day conditions (pdControl) have been performed to represent internal variability under more recent concentrations of forcing agents (Pedro et al., 2016; Williams et al., 2018). Control simulations have been used to study the role of internal variability, teleconnections and many other fundamental aspects of climate models (Krishnamurthy and Krishnamurthy, 2016; Wang et al., 2015b). Unforced internal variability is a fundamental aspect of regional climate as any response to external forcings in experiments with variable forcings will interact with this type of variability (Deser et al., 2017b; Thompson et al., 2015).

#### *10.3.2.5 Downscaling evaluation simulations*

Experiments driven by perfect boundary conditions or predictors (observations or reanalysis) can be useful to evaluate downscaling performance (Frei et al., 2003; Laprise et al., 2013). In such a setting, any discrepancy between the modelled and observed climate arises (approximately, as the boundary conditions are only nearly-perfect) only from errors in the downscaling method (Laprise et al., 2013) or internal climate variability generated by the downscaling method.

Since AR5, this approach has been extensively applied to systematically evaluate the skills of dynamical downscaling, especially in the framework of the CORDEX project, over many regions of the world, such as Europe and the Mediterranean (e.g., (Cavicchia et al., 2018; Dell'Aquila et al., 2018; Drobinski et al., 2018; Fantini et al., 2018; Jury et al., 2018; Knist et al., 2017; Kotlarski et al., 2014) Africa (e.g., Nikulin et al., 2012; Druyan and Fulakeza, 2013; Hernández-Díaz et al., 2013; Panitz et al., 2014; Sarr et al., 2015; Careto et al., 2018); Southeast Asia (Chung et al., 2018; Cruz et al., 2017); South-Asia (Iqbal et al., 2017); East-Asia (Huang et al., 2015; Shen et al., 2018); South America (e.g., Collazo et al., 2018; Reboita et al., 2014; Solman, 2016); Alaska and arctic (Bieniek et al., 2016; Cassano et al., 2017; Diaconescu et al., 2018); North America; Australasia (Firth et al., 2017; Andrys et al., 2015).

A comprehensive inter-comparison of statistical downscaling, bias adjustment and weather generators has been performed over Europe, in order to assess the downscaling skill for marginal, temporal, and spatial aspects, of temperature and precipitation including extremes, and a process based evaluation of specific climatic phenomena (Gutiérrez et al., 2018; Maraun et al., 2018; and references therein).

Alternatively, in the so-called perfect model or pseudo reality simulations (first introduced by Charles et al., 1999), a credible simulation from a high-resolution climate model is used as a hypothetical present day and future reality. A statistical downscaling model is then tested in this so-called "perfect model world" by first calibrating it to present climate conditions and, subsequently, assessing whether it correctly reproduces the future conditions. The assessment of the performance of the various downscaling methods, including added value, will be presented in Section 10.3.3.

### ***10.3.3 Model performance and added value in simulating and projecting regional climate***

Assessing model performance is a prerequisite for projecting regional climate. To quantify performance, many purpose-specific evaluation diagnostics have been developed. Given the availability of a range of different modelling approaches, the question of added value by more complex or higher resolution-models arises. A first evaluation typically covers the representation of relevant surface variables, such as temperature and precipitation, and their spatio-temporal variability. Confidence in future projections may be increased by additionally investigating whether a model realistically represents relevant large-scale and regional processes and phenomena as well as regional feedbacks and forcings controlling climate variability and change in a given region. A key challenge is to link the performance of climate models in simulating past and present

climates to the credibility of future projections.

### *10.3.3.1 Evaluation diagnostics*

A model evaluation may compare some simulated aspect of the climate system with the corresponding observed one. The comparison involves two components: what is compared, and how any mismatch between model and observation is quantified. The former is typically measured by a quantitative statistic or index (in the following referred to as diagnostic; see Chapter 1), the latter by a performance measure or metric (Gleckler et al., 2008; Maraun et al., 2018). Diagnostics and metrics are typically used to assess overall model results (from biases in mean temperature to complex phenomena like cyclone characteristics), but can also be used for trend and process-based evaluation (e.g. the analysis of the energy budget).

Since AR5, model evaluation has made use of a broad combination of diagnostics (Eyring et al., 2016b; Gleckler et al., 2016; Ivanov et al., 2017, 2018; Kotlarski et al., 2014a), ranging from long-term means, specific indices of extreme events (such as those defined by the Expert Team on Climate Change Detection and Indices, Zhang et al., 2011; Sillmann et al., 2013) or a combination of those (such as the Climate Extreme Indices, i.e. the fraction of the area of a region experiencing extremes in surface temperature, daily precipitation, and drought, Dittus et al., 2016). More complex diagnostics have been also designed, in order to characterize specific meteorological phenomena (both observed and modelled), such as ENSO feedbacks (Bellenger et al., 2014), characteristics of the Madden Julian Oscillation (Benedict et al., 2014; Jiang et al., 2015; Kim et al., 2015; MJO Working Group, 2009) and indices based on cyclone tracking (Neu et al., 2013) or front detection (Hope et al., 2014).

New diagnostics for multivariate dependencies are needed to characterise compound events, i.e. the co-occurrence of events causing an extreme impact (Seneviratne et al., 2012; Zscheischler et al., 2018). Such diagnostics can include temperature extremes evaluated against land-atmosphere coupling (Sippel et al., 2016, 2017), the joint occurrence of high runoff and storm surges (Bevacqua et al., 2017; Wahl et al., 2015) and the joint occurrence of heavy precipitation in space (Hobaek Haff et al., 2015), but they depend on the availability of relevant observational data (Section 10.2.2). Multivariate dependences can also be used for designing and evaluating multivariate bias correction and statistical downscaling. There is a growing number of studies highlighting the importance of user-defined or user-relevant diagnostics for model evaluation (Maraun et al., 2015).

Process-based diagnostics are useful for identifying the cause of models errors, although it is not always possible to associate a systematic error with a specific cause (e.g., Eyring et al., 2019). The AR5 discussed two main approaches of process-based evaluation, namely: 1) the isolation of physical components or parameterizations by dedicated experiments as described in Section 10.3.2.4, and 2) a regime-based approach. In the latter approach, the diagnostics are calculated conditionally on relevant regimes, usually synoptic-scale weather patterns, which represent relevant processes. This approach has been used to evaluate the performance of both GCMs (e.g.Catto et al., 2015) and RCMs (Endris et al., 2016; Pinto et al., 2018; Whan and Zwiers, 2017) but also perfect prognosis and bias adjustment methods (Addor et al., 2016; Beranová and Kyselý, 2016; Kjellström et al., 2013; Marteau et al., 2015; Soares et al., 2018; Soares and Cardoso, 2018).

Finally, the performance of climate models in producing useful input data for impact models has been evaluated by comparing the impact as simulated with input from observations and input from climate models, and the observed impact itself. This approach has been used in particular to evaluate the influence of bias adjustment on hydrological (e.g. Rojas et al., 2011), agricultural (e.g. Ruiz-Ramos et al., 2016), forest fire (e.g. Migliavacca et al., 2013) and regional ocean modelling (e.g. Macias et al., 2018). Recently, the Bias ADJustment for Agricultural Modelling (BADJAM) initiative has been established to systematically assess such effects (Galmarini et al., 2019).

Internal variability in both models and observations has to be accounted for when comparing simulated and observed diagnostics, particularly in the case of teleconnections and trends: any mismatch between

observations and a model simulation might simply be caused by internal variability, especially when the diagnostic has been calculated over a short time period (Notz, 2015). In the case of ENSO, Deser et al. (2017c) propose the incorporation of both pattern and amplitude uncertainty in the observational target, allowing for discrimination between true model biases in the forced ENSO response and apparent model biases that arise from limited sampling of non-ENSO-related internal variability.

In any case, the quality and availability of multiple observational references play a central role in the model performance assessment (Section 10.2.2.7).

### *10.3.3.2 Model improvement and added value*

Obtaining regional information from global simulations may involve a range of different methods (see Section 10.3.1). An approach with higher complexity or resolution is useful if it adds further, useful information to that of a reference model (such as a standard GCM). This further useful information is often referred to as added value and is a function of variables, processes and the temporal and spatial scales targeted (Di Luca et al., 2012; Ekström et al., 2015; Falco et al., 2018; Giorgi and Gutowski, 2015; Rummukainen, 2016; Torma et al., 2015). The added value of downscaling is most likely where regional scale processes play an important role in the region's climate, for example in complex or heterogeneous terrain such as mountains (Prein et al., 2016a), along coastlines (Feser et al., 2011) or where convective processes are important (Prein et al., 2015). Precipitation, in particular, is a variable where downscaling potentially can provide a substantial added value, because precipitation events are often regional in scale and short in duration.

There is no common definition for added value. Added value is considered here to be an issue that arises when one methodology attempts to give further value to what another methodology produces. Most frequently, added value is discussed in terms of downscaling methods adding value to GCM output. More generally, model improvement, for example, might include increasing GCM resolution (e.g., Roberts et al., 2018), adding new processes, or simply improving model numerics or parameterizations. Improvement of individual methodologies is covered in Sections 10.3.3.3 to 10.3.3.10.

Assessment of the further detail added to GCM output and the value of attaining it depends in part on the particular interests of the user (Di Luca et al., 2016). However, a common baseline expectation is that the downscaling method should give improved representation of a region's climate compared to the global model driving data (Di Luca et al., 2015), though arguably, there should be a clear physical reason for the improvement. A variety of measures can provide assessment of added value, such as errors versus observations on fine spatial scales (Di Luca et al., 2016), coherence of simulated versus observed spatial patterns (Di Luca et al., 2016), matching of probability distribution functions (Soares and Cardoso, 2018) and field-significance tests of spatially distributed errors (Ivanov et al., 2017, 2018). The added value attained likely depends on the region, season and governing physical processes (e.g., Lenz et al., 2017; Schaaf and Feser, 2018).

A first step in determining added value could be to analyse whether or not the downscaling procedure gives detail on spatial or temporal scales not well-resolved by a GCM. This Potential Added Value (PAV; Di Luca et al., 2012) is not in itself sufficient to demonstrate added value in downscaling (Takayabu et al., 2016), but lack of PAV could indicate that the downscaling method lacks usefulness. An advantage of a PAV analysis is that it sidesteps the challenge of having high resolution observations available to assess if there is true added value. Instead, relatively simple simulation experiments that pair fine and coarse-resolution simulations by the same model are used to see how well applying downscaling to the coarse simulation produces output that agrees with the fine-resolution simulation. Because the evaluation rests on model simulations only, one can assess the PAV for multiple fields and determine if there are physically consistent outcomes that help identify the processes yielding the PAV. Such analysis can provide a physical basis for examining whether or not added value exists with respect to observed and projected climates. So-called "big brother" experiments (Denis et al., 2002; Di Luca et al., 2012) have demonstrated PAV and reasons for its occurrence for some regions (Di Luca et al., 2012; Lenz et al., 2017).

Evaluating added value contributes to estimating the quality of regional information. Several studies have demonstrated the added value of downscaling in specific contexts, both for current climate and for climate projections (Section 10.3.3.4 to 10.3.3.10). However, added value is not guaranteed simply by producing model output at finer resolution; it can depend on several factors, such as general framework of the simulation and the specific climatic variables analysed (Di Luca et al., 2012; Hong and Kanamitsu, 2014; Xue et al., 2014). There is also a need to recognize the role of unforced, internal variability and sampling methodologies that can obscure the climate signals being evaluated (Laprise, 2014).

A further challenge, especially for higher resolution downscaling, is that adequate observational data may not be available to assess added value (e.g. Di Luca et al., 2016; Zittis et al., 2017, see also Section 10.2). This implies a need for additional efforts to attain and quality-control higher resolution observational (or observation-based) data sets and, perhaps also, to apply multivariate analyses to determine physically consistent behaviour that is gained by downscaling. Univariate demonstration of added value is necessary, but even that may not be sufficient, as better agreement with observations in the downscaled variable may be a consequence of compensating errors that are not guaranteed to compensate similarly as climate changes. Multivariate demonstration of added value is more able to demonstrate physical consistency between observed and simulated behaviour (e.g. (Meredith et al., 2015a; Prein et al., 2013a; Reboita et al., 2018)).

### *10.3.3.3 Overall performance of different model types*

The ability to simulate regional climate realistically is a formidable challenge and while improvements to do so, as measured by standard performance metrics, have been steady, they have also been very slow (Fernández et al., 2018). The first level of performance assessment for the construction of regional climate messages tackles the evaluation of the fitness of the most common user variables such as temperature and precipitation. Model performance addresses not only the assessment of a single model, but also the evolution of multi-model ensembles, which are one of the most common tools to build regional climate messages for the future. As an example, Sillmann et al. (2013) found that the spread of metrics among CMIP5 models for several extreme temperature indices are reduced compared to CMIP3 models. In a multi-model context, climate models exhibit large inter-model differences (Matte et al., 2019). This occurs due to the substantial variety in model biases, which largely dominate model performance. They are a symptom of processes not represented correctly in the models, and complicate the extraction of useful climate change information. In certain cases, systematic errors are common across a model class, performance metrics highlighting pervasive problems in the models (Nikiema et al., 2017; Wang et al., 2015a). In the following, the performance of the different model types described in Section 10.3.1, GCMs, RCMs and statistical models, will be discussed. The role of sub-component models will be discussed where appropriate. An overview of dynamical model performance can be found in Figure 10.5 and about statistical model performance in Figure 10.6.

**[START FIGURE 10.5 HERE]**

**Figure 10.5:** [Placeholder: Multipanel with, on the top row, mean bias of the GCM (left) and RCM (right) simulations over the East Asia (ASO), Western Europe (DJF) and/or West Africa (JAS) regions and, at the bottom, sets of box-and-whiskers with one box-and-whisker for each observational reference (observations and/or reanalyses) available and for each simulation considered (CMIP5, CMIP6, CORDEX). One multipanel for temperature and another one for precipitation. The box-and-whisker corresponds to the seasonal mean values for each year and for each point of the region (samples with N points x M years), where the region is a section (illustrated in the maps) of the area shown in the maps above. The box-and-whiskers for each region displayed with a different colour or shade, but if the panel becomes too cluttered then each region displayed separately with one multipanel per region: East Asia and West Africa precipitation and Western Europe temperature.]

**[END FIGURE 10.5 HERE]**

**[START FIGURE 10.6 HERE]**

**Figure 10.6:** [This figure is a placeholder. The abbreviations will be written out, and – depending on the available literature – more aspects may be added] performance of different statistical downscaling methods for daily resolution. BC: bias correction, QM: quantile mapping, REG: (generalised) linear model, det: deterministic, infl.: inflated variance, stoch: white noise randomisation; WT: weather typing; ANA: analog; RI: Richardson-type; POI: Possion clustering; HM: hidden Markov; SS: single-site; MS: multisite; U: unconditional; C: conditional; "+": should work reasonably well based on empirical evidence and/or expert judgement; "o": problems may arise depending on the specific context; "-": weak performance either by construction or inferred from empirical evidence; "?": not studied. The categorisation assumes that predictors are provided by a well performing dynamical model simulating informative and representative predictors, also for climate change. Statements about extremes refer to moderate events occurring at least once every 20 years. From (Maraun and Widmann, 2018b)]

**[END FIGURE 10.6 HERE]**

*10.3.3.3.1 GCMs*

GCMs are known for having pervasive systematic errors in some aspects of their large-scale behaviour (e.g. Oueslati and Bellon, 2015; see Section 10.3.4 and Chapter 3). They also show substantial systematic errors in precipitation and temperature at different regional scales: continental (Prasanna, 2016), national (Lovino et al., 2018) and local (Jiang et al., 2015). The systematic errors, which appear both in the mean and in higher order moments (Ren et al., 2018) of the climatological distribution of the variable (Figure 10.5), can be as high as 100% and have been considered an important limiting factor in model usability (Palmer, 2016). Performance at the regional scale is assessed in terms of the time or spatial averages (Prasanna, 2016), the ability to reproduce the seasonal cycle (Hasson et al., 2016) or a set of extreme indicators. In many cases the performance estimates have been used to select models for an application or more in depth study (Lovino et al., 2018), to select the models that provide boundary conditions to perform RCM simulations (McSweeney et al., 2015) or for weighting the results of the GCM simulations (Sanderson et al., 2015). Regional biases could occur even if all the relevant large-scale processes are correctly represented, but not their interaction.

The special class of high-resolution GCMs (Prodhomme et al., 2016) are expected to resolve some of the regional processes that are not appropriately represented in standard GCMs such as the drought forcing by the circulation (van Haren et al., 2015). There is general agreement that increasing global model resolution improves some long-standing biases (Dawson and Palmer, 2015; Feng et al., 2017; Schiemann et al., 2014), although the resolution increase is not a guarantee of overall improvement. For instance, increasing resolution at GCM scale has been shown to improve Asian monsoon rainfall anchored to orography and the monsoon circulation (Johnson et al., 2016);however, it fails to solve the major dry bias. Some efforts have been undertaken to obtain similar improvements in performance using statistical parameterisations in standard resolution models (Strømmen et al., 2018).

Despite the known systematic errors in temperature and precipitation that affect model performance, there is *high confidence* that GCMs provide useful information for the generation of future climate messages at the regional scale. There is *robust evidence and high agreement* that the increase of global model resolution can help in reducing a number of the systematic errors limiting performance, although resolution per se does not automatically solve all performance limitations shown by GCMs.

*10.3.3.3.2 RCMs*

GCMs tend to have difficulties in simulating climate over complex topography or strong gradients as well as the upscale cascade of energy from unresolved scales (Zanna et al., 2018). This is because small-scale interactions and local feedbacks that take place at small, unresolved scales are missing and result in a degradation of the model performance compared to models with higher resolution. In this case RCMs and variable resolution GCMs can resolve part of these processes in the regions of interest at an acceptable computational cost.

The performance assessment of RCMs is carried out by evaluating simulations of the current climate with

boundary forcings provided by both reanalysis products and GCM historical simulations in a comparison with the best observations available. RCM simulations driven by reanalyses have been extensively used to evaluate many aspects of the downscaling capability (including added value with respect to the driving reanalysis) and are used to identify the errors intrinsic to the RCM (Section 10.3.2.5 and Atlas).

RCMs simulations driven by GCMs provide diagnostics illustrating the total error of the GCM-RCM chain. RCMs are typically not able to mitigate GCM biases in large-scale dynamical processes. Thus, if such biases are substantial, and if the corresponding large-scale processes are important drivers of regional climate, downscaling may be questionable (garbage-in, garbage-out, see Section 10.3.3.4). But when GCMs have weak circulation biases and regional climate change is controlled mainly by regional-scale processes and feedbacks, dynamical downscaling can be particularly useful (Hall, 2014).

Usually, the performance assessment of these experiments focused mainly on temperature and precipitation climatology, including trends and extremes. However, some studies have also investigated the ability of RCMs to correctly reproduce processes and phenomena (Section 10.3.3.4 to 10.3.3.7).

**[Placeholder: assessment statement on RCM performance]**

#### *10.3.3.3.3 Statistical downscaling, bias adjustment and weather generators*

The performance of statistical downscaling models, bias adjustment and weather generators is very much determined by the chosen model structure and, when used, the predictors selected. The model structure aims at describing specific characteristics of a regional diagnostic (e.g. representing variability and extremes or spatial dependence) (Maraun and Widmann, 2018b). The VALUE network has assessed the performance of a range of perfect prognosis methods, bias adjustment methods and weather generators in a perfect predictor experiment where the predictors are taken from reanalysis data (Gutiérrez et al., 2018; Maraun et al., 2015, 2018). Figure 10.6 shows an overview comprising results from VALUE and other studies.

Perfect prognosis methods can perform well when the synoptic forcing (i.e. the explanatory power of large-scale predictors) is strong. Using this approach, downscaling of precipitation is particularly skilful in the presence of strong orographic forcing.

Analogue methods perform well at simulating mean temperature, its variance and high quantiles (Gutiérrez et al., 2018; Hertig et al., 2018), but underrepresent temporal dependence (Maraun et al., 2017a). These methods succeed in representing means, variability and high quantiles within the observed range, and temporal dependence structure of precipitation (Gutiérrez et al., 2018; Hertig et al., 2018; Maraun et al., 2017a). Spatial dependence is typically strongly underestimated and well represented only if the analogues are defined jointly for different locations. The representation of interannual variability depends strongly on the specific analogue method (Maraun et al., 2017a).

Deterministic regression models well represent mean temperature and temporal dependence (Gutiérrez et al., 2018; Maraun et al., 2017a), but typically underestimate variability and high quantiles. Stochastic methods improve the representation of variability and high quantiles (Gutiérrez et al., 2018; Hertig et al., 2018), but typically at the expense of deteriorating temporal dependence (Maraun et al., 2017a). Inflated regression represents well both variability and high quantiles, but the generated variability does not represent local random variability, such that the temporal correlation between predictors and predictands is too high (Maraun, 2016). Spatial dependence of temperature is strongly overestimated by deterministic regression, and underestimated by stochastic methods (Widmann, 2019). Deterministic regression models including inflated regression fail in representing almost all aspects of precipitation.

Overall, there is *robust evidence* that deterministic regression models are not suitable for downscaling daily precipitation, but there is *medium confidence* that single-site stochastic models based on a gamma distribution with sensible predictors perform well for all aspects of precipitation apart from spatial dependence (Maraun et al., 2018).

Bias adjustment methods, if driven with reanalysis predictors, in principle adjust well all the aspects that they are intended to (Maraun and Widmann, 2018b). For temperature, all univariate methods well adjust means, variance and high quantiles (Gutiérrez et al., 2018; Hertig et al., 2018). Temporal and spatial dependence are inherited from the driving model (Maraun et al., 2017a; Widmann, 2019). Spatial fields are thus typically too smooth in space also after bias adjustment (Widmann, 2019). For precipitation, means, intensities, wet-day frequencies and wet-dry and dry-wet transitions are well adjusted (Gutiérrez et al., 2018; Maraun et al., 2017a). The representation of high quantiles depends on the method chosen. In this case flexible quantile mapping performs best (Hertig et al., 2018). Empirical (non-parametric) methods perform better than parametric methods over the observed range, but it is unclear how this translates into extrapolation to unobserved values (Hertig et al., 2018; Stocker et al., 2015). Many quantile mapping methods overestimate interannual variability (Maraun et al., 2017a).

Multivariate bias adjustment methods adjust well all statistical aspects of the multivariate distribution that they intend to adjust. Depending on the method, this includes correlation structure or all aspects of multivariate dependence structure (Cannon, 2016, 2018; Vrac, 2018). Often, marginal distributions are corrected using quantile mapping and hence univariate performance characteristics generally follow those mentioned above. However, adjustment of multivariate dependence necessarily modifies the temporal sequencing of the driving model (Cannon, 2016); hence, there will be a loss of coherence between the modelled and bias adjusted chronology of events, and temporal dependence is no longer fully inherited from the driving model. The extent of the modification depends on the chosen method (Cannon, 2016; Vrac, 2018; Vrac and Friederichs, 2015). If multivariate adjustment includes a spatial dimension, then spatial dependence is adjusted well (Vrac, 2018).

There is *high confidence* that bias adjustment can improve the marginal distribution of simulated climate variables if applied to a climate model that adequately represents the processes relevant for a given application (see Box 10.2 for further details).

Weather generators represent well most aspects that are explicitly calibrated. That is, single-site weather generators represent well mean, variance, high quantiles (for precipitation, if explicitly modelled) and short-term temporal variability for both temperature and precipitation, whereas interannual variability is strongly underestimated, and spatial dependence is not represented at all (Gutiérrez et al., 2018; Hertig et al., 2018; Maraun et al., 2017a; Widmann, 2019). Only little research evaluating the performance of spatial weather generators exists, the results are apparently contradictory and seem to depend strongly on individual model implementations (e.g. Frost et al., 2011; Hu et al., 2013).

There is *high confidence* that weather generators can realistically simulate a wide range of local weather characteristics at single locations, but there is *limited evidence and limited agreement* if weather generators realistically simulate the spatial dependence of weather across multiple sites.

#### *10.3.3.4 Performance at simulating large-scale phenomena and teleconnections relevant for regional climate*

Regional climate is often controlled by large-scale weather phenomena and teleconnections. In particular extreme events are often caused by specific, in some cases persistent, circulation patterns (Chapter 11). The ability of climate models to accurately represent such phenomena is therefore key to reasonably represent not only continental, but also regional climate and its variability. Standard resolution GCMs often suffer from substantial biases in the location, occurrence frequency or intensity of large-scale phenomena. In such cases, any statements about regional climate and climate change will be highly uncertain. In fact, these phenomena are often so large that RCMs over their limited domains cannot improve their representation. This situation is known as garbage-in garbage out problem (10.3.3.4), where the RCM adds detail to an unrealistic large-scale field. In some cases, however, RCMs run over a large-domain may indeed improve large-scale circulation features. Also RCMs may in principle add value to simulating the regional manifestation of teleconnections. Here this discussion will be illustrated with selected examples from the mid-to-high latitudes and tropics.

*Mid-to-high latitude atmospheric variability phenomena: blocking and extratropical cyclones*

A major phenomenon for mid-to-high latitude mean and extreme climate is atmospheric blocking, known to lead to extreme cold conditions in winter and warmth and drought during summer (Sousa et al., 2017, 2018b). Atmospheric blocking is characterized by a quasi-stationary long-lasting, high pressure system that "blocks" and diverts the movement of synoptic cyclones. An overview of model performance in simulating blocking is given in Figure 10.7. The longitudinal distribution of blocking frequency and its seasonality is reasonably well reproduced in the CMIP5 multi-model mean. However, CMIP5 climate models often underestimate winter blocking frequency over Europe and the northeastern Atlantic (Anstey et al., 2013; Davini and D'Andrea, 2016; Dunn-Sigouin and Son, 2013; Masato et al., 2013). This underestimation is dominated by short-lived blocking events with duration shorter than ten days. In contrast, North Pacific blocking frequency is overestimated by most models over broad regions and in all seasons, particularly on the poleward side of the observed blocking frequency maximum. Summertime blocking frequency is slightly overestimated over the subpolar oceans, while it is underestimated over Eurasia (Masato et al., 2013). Multiple reasons have been invoked to explain model biases in blocking: lack of vertical (both tropospheric and stratospheric) and/or horizontal resolution, mean state biases, in particular biases related to the parameterization of orographic effects, the misrepresentation of the Gulf Stream SST front (Anstey et al., 2013; Berckmans et al., 2013; Davini and D'Andrea, 2016; O'Reilly et al., 2016; Pithan et al., 2016). SST biases have been suggested to have a weak relevance only (Davini and D'Andrea, 2016). In a study of five ERA-Interim driven RCMs, Jury et al., (2018) showed that RCMs typically simulate fewer blocking events over Europe than are present in the driving data, irrespective of the RCM horizontal resolution.

**[START FIGURE 10.7 HERE]**

**Figure 10.7:** [Placeholder for a figure showing issues (e.g., blocking) with standard GCMs in simulating specific large-scale phenomena which are relevant for regional climate, and how high resolution GCMs may add value. It should be replaced by a more recent figure, include an intermediate resolution (say T512) and should, if possible, link to a phenomenon from the showcases in Section 10.4. From Dawson et al., GRL, 2012]

**[END FIGURE 10.7 HERE]**

Other related key mid-latitude phenomena are the storm tracks of Atlantic and Pacific extratropical cyclones (Shaw et al., 2016). Similar to CMIP3, most CMIP5 models simulate climatological storm tracks that are too weak and displaced equatorward (Chang et al., 2012). Zappa et al. (2013) evaluated the North Atlantic storm track in CMIP5 models and found that the winter storm track tends to be either too zonal or displaced southward, resulting in too many cyclones in central Europe. The position of the summer North Atlantic storm track is generally well captured but some models underestimate the number of cyclones. In both summer and winter, the intensity of cyclones is often too weak. Yang et al. (2018) found that half of thirteen selected CMIP5 models are able to reproduce the spatial pattern of the winter North Pacific storm-track climatology but most of them underestimate its strength and spatial variation. In addition, most CMIP5 models are unable to reproduce interannual variability in storm-track strength and spatial pattern.

Many arguments have been put forward to explain storm-track model biases. Booth et al. (2017) showed that biases in the surface storm track north of the Gulf Stream are related to biases in SST. Explicit model representation of mesoscale atmospheric features and mesoscale ocean eddies are seen to improve the simulation of the storm track including a systematic increase in eddy intensity, and a stronger and northward shifted storm-track (Foussard et al., 2019; Willison et al., 2013).

In general, RCMs cannot mitigate large-scale circulation errors of the driving GCM. If run over large-domains, reanalysis-driven RCMs can, for specific regions, significantly improve the representation of storm characteristics compared to the driving reanalysis near areas with marked orography and regions with large water masses (Poan et al., 2018). Flaounas et al. (2018) investigated the ability of 12 RCMs and RESMs to reproduce the climatology of Mediterranean cyclones based on different cyclone tracking methods. All RCMs reasonably reproduce the main areas of high cyclone occurrence. The RCMs tend to produce more

intense cyclones over land, likely due to higher horizontal resolution than the driving reanalysis, but tend to underestimate intense cyclone occurrences over the Mediterranean Sea. Air-sea coupling has a rather weak impact on cyclone climatology and intensity. Sánchez-Gómez and Somot (2018) showed that the effect of RCM internal variability on density of cyclone tracks is very significant and larger than for other variables such as precipitation. It is larger in summer than in winter, in particular over the Iberian Peninsula, countries in northern Africa and the eastern Mediterranean, which are regions of enhanced cyclogenesis during the warm season.

*Tropical phenomena: ENSO teleconnections, Madden-Julian oscillation*

The assessment of model performance in simulating ENSO characteristics, including ENSO spatial pattern, frequency, asymmetry between warm and cold events, and diversity, is discussed in Chapter 3. Here the ability of the recent generation of GCMs to adequately simulate ENSO-related teleconnections is reviewed. The model assessment is a challenge due to different types of ENSO and model errors in ENSO spatial patterns, non-stationary aspects of the teleconnection as well as the strong influence of atmospheric internal variability at mid-to-high latitudes (Capotondi et al., 2015; Coats et al., 2013; Deser et al., 2017c; Polade et al., 2013).

Langenbrunner and Neelin (2013) showed that there is little improvement in the CMIP5 ensemble relative to CMIP3 in amplitude and spatial patterns of the ENSO influence on winter precipitation (with model-observation spatial pattern correlation coefficients typically less than 0.5). However, the CMIP5 ensemble accurately represents the amplitude of the precipitation response in regions where observed teleconnections are strong. Moreover, a *high agreement* between models on the teleconnection sign indicates a good performance in representing the observed teleconnections. Hurwitz et al. (2014) showed that CMIP5 models broadly simulate the expected (as seen in the MERRA reanalysis) upper tropospheric responses to Central equatorial Pacific (CP) or Eastern equatorial Pacific (EP) ENSO events in boreal autumn and winter. The CMIP5 models do simulate the correct sign of Arctic stratospheric response (polar vortex weakening during EP and CP Niño events and vortex strengthening during both types of La Niña events).

**[Placeholder: text on RCM influence on the representation of teleconnections]**

SST variations can have profound impacts on land, as evidenced by the near-global teleconnections of ENSO (e.g. Alexander et al., 2002). Consequently, biases in the oceanic components of climate models can lead to the misrepresentation of remote influences over land. The influence of mean-state SST biases on global teleconnection patterns is shown, e.g., by Magnusson et al., (2013) through GCM experiments with and without flux correction.

At the regional scale, the influence of SSTs on climate over land is often reflected in monsoon systems, as these rely on land-sea temperature contrasts. An example can be seen in the tropical Atlantic, where the development of cool SSTs in the eastern equatorial region in early boreal summer contributes to the northward shift of the ITCZ and the development of the West African monsoon (Okumura and Xie, 2004). Many GCMs also show an influence of equatorial Atlantic SSTs on rains over West Africa but feature a cold tongue that develops late and is not as pronounced as observed (Richter et al., 2014). This leads to a corresponding late onset of the rainy season in south West Africa, along the Guinea coast (Dunning et al., 2017). In some models with strong equatorial SST biases this may also be implicated in the delayed onset of the West African monsoon (Roehrig et al., 2013b; Steinig et al., 2018), though overall CMIP5 models tend to reproduce the timing of the monsoon onset rather well (Dunning et al., 2017). In the western part of the equatorial Atlantic basin, it is well documented that the erroneous southward displacement of the Atlantic ITCZ in boreal spring is associated with the dry bias over equatorial South America (Richter et al., 2014; Richter and Xie, 2008). Another example for the impact of mean-state SSTs on precipitation over land is provided by the Indian summer monsoon. Cold SST biases in the Arabian Sea (Levine et al., 2013) and warm SST biases in the western equatorial Indian Ocean (Annamalai et al., 2017)have been implicated in the insufficient monsoon precipitation over India simulated by CMIP5 models, though deficiencies in the atmospheric components of the GCMs also play an important role.

The Madden-Julian oscillation (MJO) is the dominant mode of tropical intra-seasonal variability, and is

characterized by its large spatial extent and intermediate frequencies (zonal wavenumbers 1–3 and 30–90 days period) (Ling et al., 2017; Madden and Julian, 1971). It is characterized by eastward-propagating, planetary-scale envelopes of convective cloud clusters that are tightly coupled with the largescale wind field. The MJO has a strong influence on a range of tropical phenomena from the onset and breaks of the Asian and Australian monsoon systems, the triggering and termination of ENSO events, and tropical cyclone activity. Significant extratropical surface air temperature variations can also arise as a result of teleconnections induced by the MJO. Temperature variations over North America and Europe can arise in response to MJO-induced heating and horizontal temperature advection by northerlies or southerlies associated with a meridionally propagating Rossby wave train (Cassou, 2008; Henderson et al., 2016; Jiang et al., 2017a; Lin et al., 2009; Mundhenk et al., 2016; Seo et al., 2016).

In agreement with results from previous model generations, most CMIP5 models still underestimate MJO amplitude, and struggle to generate a coherent precipitation/convection and wind field eastward propagation (Ahn et al., 2017; Hung et al., 2013; Jiang et al., 2015). Additionally, most CMIP5 models simulate an MJO that propagates too fast compared to observations and intra-seasonal precipitation variability remains poorly simulated among CMIP5 models (Ahn et al., 2017). However, the propagation speed of some CMIP5 models in the Indian Ocean tends to be slower than observed due to a too strong persistence of equatorial precipitation (Hung et al., 2013; Jiang et al., 2015). Improvements in moisture-convection coupling and gross moist stability (i.e., the efficiency of vertical advection to export Moist Static Energy (MSE) out of the convective column) representation might be the most fruitful means to improving simulations of the MJO (Ahn et al., 2017; Kim and Maloney, 2017).

Though GCM representation of the MJO has advanced in recent decades, there is *high confidence* that most models from the current generation of GCMs still have difficulties in achieving a robust and physically-coherent MJO simulation.

#### *10.3.3.5 Performance in simulating regional phenomena and processes*

Regional climate is shaped by a wide range of weather phenomena occurring at scales from about 2000 km to 2 km. These mesoscale phenomena modulate the influence of large-scale weather phenomena and create the characteristic and potentially severe weather conditions people experience regionally.
The climate in different regions will be affected by different mesoscale phenomena, and in a given application, several of these may be relevant. A skilful representation of these phenomena is a necessary condition for providing credible and relevant climate change information for a given region and application. Therefore, it is important to understand the strengths and weaknesses of different model types in simulating these phenomena. Here, the performance of different climate model types to simulate a selection of relevant mesoscale weather phenomena will be assessed.

Perfect prognosis methods typically bridge mesoscales by directly linking synoptic and local scales, and bias adjustment simply adjusts the outputs of the dynamical model. Within the VALUE initiative, Soares et al. (2018) analysed whether statistically downscaled and bias-adjusted model data could represent the observed sensitivity of local weather to a range of phenomena relevant for European climate. The performance of perfect prognosis methods strongly depends on the method, the chosen predictors and the scale at which the predictors are defined. Bias adjustment was, as expected, not able to represent any sensitivity to a phenomenon that was not resolved by the driving model, and in the case of quantile mapping could even inflate well represented sensitivities.

##### *10.3.3.5.1 Convection*

Convection is the process of vertical mixing due to atmospheric instability. Deep moist convection is associated with thunderstorms and related severe weather such as heavy precipitation and strong wind gusts. Convection may occur in single locations, in spatially extended severe events such as supercells, and organised into larger mesoscale convective systems such as squall lines or tropical cyclones (Section 10.3.3.5.8), and embedded in fronts (Section 10.3.3.5.4).

Shallow and deep convection are not explicitly simulated but parameterized in standard GCMs and RCMs. As a consequence, these models suffer from several biases in the representation of convection and related phenomena. AR5 has stated that many CMIP3 and CMIP5 models simulate the peak in the diurnal cycle of precipitation too early, but increasing resolution and better parameterisations help to mitigate this problem (Flato et al., 2014). Similar issues arise for RCMs with parameterised deep convection (Prein et al., 2015). Such standard RCMs also tend to overestimate high cloud cover (Keller et al., 2016; Langhans et al., 2013).

Simulations with non-hydrostatic RCMs at convection-permitting resolution improve the representation of phenomena associated with deep convection, such as the initiation and diurnal cycle of convection (Figure 10.8) (Fosser et al., 2015; Prein et al., 2013a, 2013b; Zhu et al., 2012), the triggering of convection by orographic lifting (Fosser et al., 2015; Langhans et al., 2013), spatial patterns of precipitation (Prein et al., 2013a, 2013b), the scaling of precipitation with temperature (Ban et al., 2014), cloud cover (Böhme et al., 2011; Langhans et al., 2013) and maximum vertical wind speeds (Meredith et al., 2015a). Phenomena such as supercells, mesoscale convective systems or the local weather associated with squall lines are not captured by GCMs and standard RCMs. Convection-permitting RCM simulations, however, have been shown to realistically simulate supercells (Trapp et al., 2011); mesoscale convective systems in the US Great Plains including the maximum rain rate, total precipitation, size and motion (Prein et al., 2017); and heavy precipitation associated with a squall line (Kendon et al., 2014). There is *high confidence* that simulations at convection permitting resolution add value to the representation of deep convection and related phenomena.

**[START FIGURE 10.8 HERE]**

**Figure 10.8:** [Placeholder: Diurnal cycle of precipitation and added value by convection permitting resolution. Black: observations, blue: RCM with parameterised deep convection. Red: RCM at convection permitting resolution. From Prein et al., Rev. Geophys. 2015]

**[END FIGURE 10.8 HERE]**

*10.3.3.5.2 Mountain wind systems including lee-cyclogenesis*

Mountain and valley breezes are localised thermally generated diurnal circulations that have a strong influence on regional temperature and precipitation patterns in mountain regions. During the day, heating of mountain slopes compared to the free atmosphere induces upslope winds; during the night this circulation reverses. This phenomenon is not resolved by GCMs and coarse-resolution RCMs. A reanalysis-driven RCM simulation at 4 km resolution showed good skill in simulating the diurnal cycle of temperature and wind on days of weak synoptic forcing in the US Rocky Mountains (Letcher and Minder, 2017). Similarly the mountain-plain wind circulation over the Tianshan mountains in Central Asia is well simulated by a model running at 4 km resolution (Cai et al. 2019).

Föhn winds are regional-scale synoptically-driven winds that cause orographic precipitation in the windward side of a mountain range, and as a result of the raised condensation level, adiabatic warming in the downwind side. In an RCM study for the Japanese Alps, Ishizaki and Takayabu (2009) found that at least a 10 km resolution was required to realistically simulate Föhn events.

Synoptically-forced winds may be channelled and accelerated in long valleys. For instance, the Tramontana, Mistral and Bora are northerly winds blowing down-valley from central France and the Balkans into the Mediterranean (Flaounas et al., 2013). In winter, these winds may cause severe cold air outbreaks along the coast. Flaounas et al. (2013) have shown that a GCM with a horizontal resolution of roughly 3.75° longitude/1.875° latitude is unable to reproduce these winds because of the coarse representation of orography, whereas a 50 km resolution RCM resolves these winds. Nevertheless, Obermann et al. (2018) found that 50 km resolution simulations still underestimate the resulting wind speeds and exhibit a bias in wind direction, whereas these errors are reduced with increased resolution. Similarly, Cholette et al. (2015) found that a 27 km RCM resolution was not sufficient to adequately simulate the channelling of winds in the

St. Lawrence River Valley in eastern Canada, whereas a 9 km resolution was.

Lee cyclogenesis results from potential vorticity conservation in the lee of major mountain ranges. For instance, the Gulf of Lions is a major region of cyclogenesis. Here many Mediterranean storms originate and travel eastward towards central and Eastern Europe, where they may cause severe damage. Flaounas et al. (2013) found that, whereas a standard CMIP5 GCM substantially underestimated lee cyclogenesis in the Western Mediterranean, dynamically downscaling the GCM to a 50 km horizontal resolution helped to generate cyclones close to the observed frequency.

There is *high confidence* that climate models with finer resolutions are necessary for better simulating mountain wind systems such as mountain breezes and the channelling of winds in valleys.

*10.3.3.5.3 Lake and coastal effects*

Simulating coastal climates and the influence of big lakes are a modelling challenge, due to the complex coastlines, the different heat capacities of land and water, the resulting wind system, and the differential evaporation. Regional features are often not well resolved by GCMs. The AR5 concluded that RCMs can add value to the simulation of coastal climates.

Lucas-Picher et al. (2017) showed that a 0.44°resolution RCM underestimated winds along the Canadian east coast, whereas a 0.11°resolution version better represented the coastline, orography, surface roughness and local atmospheric circulation and thereby simulated more realistic 10-m wind speed.

A particularly relevant coastal phenomenon is the sea breeze, which is caused by the differential heating of water and land during the course of the day and typically reaches several tens of kilometres inland. Reanalyses and GCMs have too coarse a resolution to represent this phenomenon, such that they typically underestimate precipitation over islands and misrepresent its diurnal cycle (Lucas-Picher et al., 2017). RCMs simulate sea breezes and thereby improve the representation of precipitation in coastal areas and islands. Over Cuba and Florida, a long peninsula, only a 0.11°-resolution RCM is able to realistically simulate the inland propagation of precipitation during the course of the day.

RCM simulations at a 20 km horizontal resolution realistically represented the sea breeze circulation in the Mediterranean Gulf of Lions including the intensity, direction and inward propagation (Drobinski et al., 2018). Even though a coupled ocean atmosphere simulation improved the representation of diurnal SST variations, the sea breeze representation itself was not enhanced.

Big lakes modify the downwind climate. In particular during winter they are relatively warm compared to the surrounding land, provide moisture, destabilize the passing air column and produce convective systems; their low surface friction accelerates the moving air, which is in turn slowed-down after reaching land. The resulting convergence causes further uplift and may trigger precipitation. Gula and Peltier, (2012) found that a state-of-the-art GCM does not realistically simulate these effects over the North American Great Lakes, but a 10 km RCM better represents them and thereby simulates realistic downwind precipitation patterns, in particular enhanced snowfall during the winter season. Similar results were found by Wright et al. (2013) and Lucas-Picher et al. (2017).

There is *high confidence* that climate models with finer resolution are necessary for better simulating lake and coastal weather including lake and sea breezes, as well as lake effect precipitation and snow.

In regions like Fenno-Scandinavia or central-eastern Canada with very large fractions of land covered by small and medium sized lakes, as well as in regions with fewer but larger lakes, such as central-eastern Africa, the eastern border between the US and Canada and central Asia, it can be essential to include a lake model in an RCM to realistically represent regional temperatures (Deng et al., 2013; Mallard et al., 2014; Pietikäinen et al., 2018; Samuelsson et al., 2010; Thiery et al., 2015). For the Caspian Sea, it is found that a coupled ocean-atmosphere RCM improved, in addition to representing the circulation in the sea, the simulation of SST fields compared to simulations with a simpler coupled lake model (Turuncoglu et al.,

2012).

There is *medium evidence and high agreement* that it is important to include interactive lake models in RCMs to improve the simulation of regional temperature, in particular in seasonally ice-covered areas with large fractions of lakes. There is *medium evidence* of the local influence of lakes on snow-and rainfall as well as the importance of including lakes in regional climate change simulations.

#### *10.3.3.5.4 Fronts*

Weather fronts are two dimensional surfaces separating air masses of different characteristics and are a key element of mid-latitude cyclones. In particular cold fronts are regions of relatively strong uplift and hence often associated with severe weather. Stationary or slowly moving fronts may cause extended heavy precipitation. Research on how climate models represent fronts, however, is still limited.

Catto et al. (2014) found in both ERA-Interim and CMIP5 models that frequency and strength of fronts were realistically simulated, albeit with some biases in the location of front occurrence maxima. In a follow-up study, Catto et al. (2015) investigated the representation of frontal precipitation for boreal and austral winter. The frequency of frontal precipitation is too high and the intensity is too low, but these compensating biases approximately cancelled out such that the total precipitation bias was small. Blázquez and Solman (2018) found similar results for the Southern Hemisphere during austral winter, and additionally showed that CMIP5 models typically overestimate the fraction of frontal precipitation compared to total precipitation.

Only few studies evaluating fronts in RCMs have been conducted. Kawazoe and Gutowski (2013) diagnosed strong temperature gradients associated with extreme wintertime precipitation events in the framework of the North American Regional Climate Change Assessment Program (NARCCAP) RCM ensemble (Mearns et al., 2012) and found the models agreed well with observation-based gradients in a reanalysis of comparable resolution. De Jesus et al. (2016) diagnosed the representations of cold fronts over southern Brazil by two RCMs, and found that across the year cold fronts were only underestimated by about 5%, but in one of the RCMs, cold fronts during summer were underestimated by 17%.

**[Potential placeholder for an overall assessment statement]**

#### *10.3.3.5.5 Low-level jets*

Low level jets form in regions of sharp horizontal temperature gradients. Coastal low-level jets occur in summer along the cold equatorward eastern boundary currents of the major oceans. They are important factors in shaping regional climate, e.g., by preventing onshore advection of humidity and thereby causing aridity (Soares et al., 2014), or by transporting moisture towards regions of precipitation as in the North American monsoon (Bukovsky et al., 2013).

Reanalysis and most GCMs do not well resolve the details of coastal low-level jets (Bukovsky et al., 2013; Soares et al., 2014). Bukovsky et al. (2013) found RCM simulations at a 50 km resolution to improve the representation of the coastal low level jet in the Gulf of California and the associated precipitation pattern compared to the driving GCM. Lucas-Picher et al. (2017) find indirect evidence via precipitation patterns that 12 km simulations further improve the representation. In a study of the Iberian coastal low-level jet, Soares et al. (2014) dynamically downscaled the ERA-Interim reanalysis to an 8 km resolution. The simulations show a realistic three-dimensional jet structure, and the surface winds compare well with observations.

There is *limited evidence but high agreement* that RCMs add value to the representation of coastal low level jets.

#### *10.3.3.5.6 Mesoscale moisture transport, including atmospheric rivers*

**[Placeholder: Intrusions of moisture into the Arctic]**

Atmospheric rivers are the strong, narrow currents of atmospheric moisture that transport volumes of water comparable to that of large terrestrial rivers (Zhu and Newell, 1998). They generally originate over oceans, occur throughout the world (Gimeno et al., 2016) and contribute to extreme precipitation events (e.g., Mahoney et al., 2016; Rutz et al., 2014) and flooding (Barth et al., 2017; Lavers and Villarini, 2013b, 2013a; Paltan et al., 2017; Ralph and Dettinger, 2011). Their relevance has prompted substantial research on how well numerical models can forecast atmospheric rivers and their impacts (e.g. Cordeira et al., 2017; Gimeno et al., 2014; Nardi et al., 2018; Nayak et al., 2014). For climate simulations, global models can resolve synoptic features associated with atmospheric-river events (Warner et al., 2015). Analysis of 54 GCM simulations by Dong et al., (2018) using CMIP5 AMIP output showed that a major controlling feature is the model internal dynamics, as opposed to changes in SST patterns. Further analyses have evaluated future changes, showing that increasing moisture transport in future climates (Lavers et al., 2013; Warner et al., 2015) and thus implying increasing impact of atmospheric rivers. Using the variable resolution global model MPAS, with 30 km grid spacing over the western U.S. and upwind northeastern Pacific Goldenson et al., (2018) showed contrasting contributions of atmospheric rivers to snowpack in the Cascades and Sierra Nevada. Chen et al. (2018c) confirmed that the WRF model, simulating 35 years of western U.S. climate with 6-km grid spacing could reproduce mean and extreme precipitation in the region, further showing that atmospheric rivers in their simulation had strong correlation with extreme hydrological events.

There is *limited evidence* to date, though *high agreement*, that regional climate models can simulate well the behaviour of atmospheric rivers and their hydrological impacts.

#### *10.3.3.5.7 Tropical cyclones and hurricanes*

In AR5 it was concluded that high-resolution (20–100 km) AGCMs well represented intensities and interannual variability of tropical cyclone numbers; coupled AOGCMs from CMIP3 and CMIP5 models simulated tropical cyclone-like vortices, but with too weak intensities. Post-AR5 studies have shown that CMIP5 models also underestimate the total frequency of tropical cyclones (Camargo, 2013). The North Atlantic is particularly affected as cyclone numbers are relatively low and very sensitive to modest model biases, and easterly waves triggering tropical cyclone development are not well represented.

In the South Atlantic, however, several CMIP5 models simulate many tropical cyclones, where only very few have been observed. Generally, the representation improves with higher resolution (Camargo, 2013).

An inter-comparison study of high-resolution AGCM simulations (Shaevitz et al., 2014) corroborated earlier findings. They showed that these models captured the overall geographical pattern of track densities, although with considerable model dependence. Tropical cyclone intensities appeared in general to be better represented with increasing model resolution. Models forced with observed SSTs were able to capture interannual variability, and in particular the geographic shifts of tropical cyclone tracks related to El Niño and La Niña events.

Takayabu et al. (2015) have compared simulations of Typhoon Hayan at different resolutions ranging from 20 km to 1 km (Figure 10.9). While the eyewall structure in the precipitation pattern was strongly smoothed in the coarse resolution simulations, it was well resolved at the highest resolution. Gentry and Lackmann (2010) found similar improvements in simulating Hurricane Ivan for horizontal resolutions between 8 km and 1 km.

There is *high confidence* that convection permitting resolution is required to realistically simulate the three-dimensional structure of tropical cyclones.

**[START FIGURE 10.9 HERE]**

**Figure 10.9:** [Placeholder: Accumulated precipitation profiles (mm/hour) around the eye of Typhoon Haiyan, simulated by (a) reanalysis, (b) NHRCM (20km), (c) NHRCM (5km), and (d) WRF (1km) models. From

Takayabu et al. Env. Res. Lett., 2015]

**[END FIGURE 10.9 HERE]**

### *10.3.3.6 Performance in simulating regional feedbacks*

Couplings between land and atmosphere or ocean and atmosphere may induce feedback mechanisms such as the snow-albedo feedback and soil moisture feedbacks that modify regional climate. Such feedbacks are particularly relevant as they may also modulate climate change at the regional scale.

**[Placeholder for assessment summary from SROCC and SRCCL]**

The snow-albedo effect is an important process contributing to enhance warming at high elevations. In particular in spring, warming causes snow to melt at the snowline, reducing the albedo and thus increasing the rate of warming. In complex terrain, GCMs often do not represent the orography well enough to realistically simulate the snow-albedo feedback (Hall, 2014; Walton et al., 2015). RCMs have the potential to considerably improve the representation of the snow-albedo effect in complex terrain, but the performance appears to depend strongly on the specific model. Over Europe, some of the EURO-CORDEX RCMs simulate a springtime snow albedo feedback close to the observed, whereas other models considerably overestimate it (Winter et al., 2017). In a multi-physics ensemble based on the WRF RCM, the simulated snow-atmosphere interaction causes a cold bias in northeastern Europe, which is amplified by the albedo feedback (García-Díez et al., 2015). For the Rocky Mountains, WRF simulations with two different land surface models generally reproduce the observed spatial and seasonal variability in snow cover, but exhibit a strong overestimation of snow albedo (Minder et al., 2016). The elevation dependence of historical warming, which is partly caused by the snow albedo effect, is realistically represented across Europe by the ENSEMBLES RCMs (Kotlarski et al., 2015).

There is *high confidence* that RCMs can considerably improve the representation of the snow albedo effect in complex terrain, but the performance appears to depend strongly on the specific model.

Soil-moisture affects the partitioning of incoming energy into latent and sensible heat fluxes and may influence air-temperature, boundary-layer stability and precipitation. In transition zones between wet and dry climates, increasing air temperatures will initially increase evapotranspiration. This in turn will reduce soil moisture and thus also evapotranspiration as well as evaporative cooling, finally leading to an increase in temperature. In a global study (Gevaert et al., 2018), five reanalysis-driven land-surface models simulated the strongest soil-moisture temperature coupling in transition zones, and the models agreed relatively well with flux tower observations. But the strength of coupling varied strongly across models at the regional scale. Also, a realistic partitioning of the incoming radiation into latent and sensible heat fluxes did not necessarily result in a realistic soil-moisture temperature coupling. For the EURO-CORDEX RCMs, Knist et al. (2017) found that the simulated coupling strength agrees well with observations in Northern Europe (weak) and Southern Europe (strong), but in Central Europe many RCMs tend to overestimate the coupling strength.

Evaluating the representation of soil-moisture precipitation feedbacks in climate models is challenging as different processes may induce feedbacks including moisture recycling, boundary-layer dynamics and mesoscale circulations. Moreover, the effects of soil-moisture on precipitation have a spatial and a temporal aspect with different possible feedbacks, and the feedbacks may be region and scale dependent and may even change sign depending on the strength of the background flow (Froidevaux et al., 2014; Guillod et al., 2015; Taylor et al., 2013a; Tuttle and Salvucci, 2016). On seasonal-to-interannual time scales, six CMIP5 models showed a stronger soil-moisture precipitation feedback than estimated by satellite data (Levine et al., 2016). In a study of the sensitivity of day-time convection to soil moisture (Taylor et al., 2013a) found that convection-permitting RCMs could well simulate surface-induced mesoscale circulations and the observed negative feedback, whereas an RCM with parameterised convection, even when run at the same resolution, simulated an unrealistic positive feedback.

There is *medium confidence and high agreement* that simulations at convection permitting resolution are required to realistically represent soil-moisture precipitation feedbacks.

**[Placeholder: representation of ocean atmosphere coupling in GCMs]**

Ocean-atmosphere RCMs have successfully been used to simulate phenomena involving strong regional feedbacks like tropical cyclones in the Indian Ocean (Samson et al., 2014), near-coastline intense precipitation in the Mediterranean (Berthou et al., 2015) or snow bands in the Baltic region (Pham et al., 2017). The positive impact of ocean-coupling on the simulation of strongly convective phenomena of Mediterranean hurricanes, so-called medicanes, can only be diagnosed for relatively fine horizontal grid-resolutions in the atmosphere of about 10 km ((Akhtar et al., 2014; Flaounas et al., 2018). A positive impact of ocean coupling has been quantified in marginal sea regions with reduced large-scale influence (e.g. in the Baltic sea area during weak phases of the North Atlantic oscillation and thus weak influence of Atlantic westerlies in the area (Kjellström et al., 2005; Pham et al., 2018)). There is some evidence available that coupled ocean-components also positively impact RCM simulations of inland climates (precipitation extremes in Central Europe, (Akhtar et al.submitted; Ho-Hagemann et al., 2017).

### *10.3.3.7 Performance in simulating regional anthropogenic drivers of climate and climate change*

*Land management*

The reduction of local mean and extreme temperature in models that include irrigation has been confirmed by many studies and the physical mechanisms behind this are well understood (Cook et al., 2015b; Hirsch et al., 2017; Lu and Kueppers, 2015; Mueller et al., 2016; Thiery et al., 2017). The reduction of hot temperature extremes can reach 2°C (Hirsch et al., 2017) over the worlds' irrigated areas (mainly North America, Eurasia, India and China). Irrigation has also been suggested to have larger scale impacts on circulation and precipitation, in particular over the South Asian monsoon region, where irrigation is most intense in the world amounting to around 0.5 mm/day on a yearly basis (McDermid et al., 2017). The inclusion of irrigation in GCMs and RCMs over this region has been found to be important to represent the monsoon circulation and rainfall correctly (Cook et al., 2015a; Guimberteau et al., 2012; Lucas-Picher et al., 2011; Shukla et al., 2014; Tuinenburg et al., 2014). Similarly, the inclusion of irrigation over northern India and western Pakistan could be important for the correct simulation of precipitation over the Upper Indus Basin in northern Pakistan (Saeed et al., 2013).

There is *medium evidence and high agreement* that representing irrigation is important for a realistic simulation of South Asian monsoon precipitation. **[Placeholder on model performance of surface variables such as temperature and surface fluxes when including irrigation]**

**[Placeholder: Model performance on including realistic no-tillage practices such as (Hirsch et al., 2018) showing more realistic representation of surface variables when a realistic fraction of traditional agricultural practices are replaced by conservation agriculture including no-tillage]**

**[Placeholder on modelling tillage/no tillage practice]**

*Urban Climate and Urbanisation*

**[Placeholder: performance of models in simulating urban climate. Including recent studies comparing urban parameterizations (Best and Grimmond, 2015; Daniel et al., 2018; Grimmond et al., 2010, 2011; Jänicke et al., 2017; KUSAKA et al., 2012; Trusilova et al., 2016) ]**

Looking at the urban scale, it has been observed in different cities over the world that the urban heat island gets intensified during heatwave periods but this feedback is not well represented by RCMs even with an appropriate urban parameterization (Hamdi et al., 2016).

There is *high confidence* that while all types of urban parameterizations generally simulate radiation exchanges in a realistic way; they have, however, strong biases when simulating latent heat fluxes. There is *robust evidence* that a simple single-layer parameterization is sufficient for urban climate modelling.

#### *10.3.3.8 Performance in simulating specific climates*

**[Placeholder for introductory paragraph. Note that the whole section needs revision. It is currently not well integrated into the text as it does not link to previous subsubsections but partly duplicates material from later sections.]**

##### *10.3.3.8.1 Tropical climate*

The South Asian monsoon is an important tropical climatic phenomenon. The CMIP5 models have the ability to capture temperature in the region, however, the monsoon precipitation is relatively too weak in these models (Jain et al., 2018; Rehman et al., 2018). The CMIP5 multi-model mean is found skillful compared to the CMIP3 multi-model mean for the Asian Summer monsoon (Sperber et al., 2013). The performance in simulating the tropical climate characteristics over South Asia is influenced by the errors in the simulation of monsoon teleconnections (Cherchi et al., 2014), summer convective rainfall (Sabeerali et al., 2015), the ratio of convective and large-scale precipitation (Jain et al., 2018), summer mean thermodynamic structure (Boos and Hurley, 2013) and interannual variability (Ramesh and Goswami, 2014). Increasing GCM resolution may overcome some modelling challenges over this region and can improve some features such as monsoon circulation patterns, moist convection processes and representation of low pressure systems (Sabin et al., 2013), although the fundamental dry bias persists even in a GCM at 40 km resolution (Johnson et al., 2016). The west African monsoon is another important tropical climatic phenomena, which is simulated in CMIP5 models a bit better than in CMIP3 models (Roehrig et al., 2013b), although in general CMIP5 models underestimate decadal variability. RCMs are found to give an encouraging simulation of West African monsoon rainfall climatology, mean annual cycle and interannual variability (Sylla et al., 2013a). Hence, model simulation plays important role in understanding the dynamics of West African monsoon via the process of Saharan heat low though it cannot be verified due to the low density of surface observations (Vellinga et al., 2013).

##### *10.3.3.8.2 Subtropical Climate*

The performance of climate model in the subtropics varies widely between model to model and region to region. This is mainly due to unrealistic simulation of strong interactions between mid-latitude and tropical systems that often occur in the subtropical region. The simulation of Arabian Peninsula and South-Eastern South America (SESA) subtropical climates are presented here as examples. The majority of CMIP5 models simulate a cold bias in the surface temperature in the subtropical arid to semi-arid Arabian peninsula (Almazroui et al., 2017). A similar behaviour is seen in the case of precipitation simulation where large numbers of CMIP5 models display a dry bias. However, a majority of CMIP5 models are capable of simulating the annual mean cycle and the interannual variability of temperature and precipitation (Almazroui, 2018). In addition to GCMs, there are a few RCMs used to simulate the subtropical climate. Almazroui (2012) found that an RCM enhances the simulation of temperature and precipitation over the Arabian Peninsula by reducing the dry and warm biases in the driving GCM.

For the SESA region, CMIP5 models show dry bias of annual rainfall (Flato et al., 2014). This dry bias occurs during austral spring, winter and autumn, since the models represent well the summer precipitation (Gulizia and Camilloni, 2015). CMIP5 models however showed an improved representation of winter precipitation in comparison to CMIP3 models (Gulizia and Camilloni, 2015). Solman (2016) analysed the simulations for austral summer and winter separately and found that the GCMs selected for the CLARIS-LPB have a very large dry precipitation bias in summer, and the same is true for the RCMs. In winter, all models show dry biases, and in some cases dynamical downscaling showed a worse bias than that of the driving model. Since this region has a large coupling between soil moisture and atmosphere, and in particular

between soil moisture and temperature (Sörensson and Berbery, 2015; Spennemann et al., 2018), it has been suggested that this warm bias is related to the dry bias (Carril et al., 2012; Menéndez et al., 2019).

#### *10.3.3.8.3 Polar climate*

The feedback of sea-ice anomalies to atmospheric circulation has been increasingly evident in the polar regions. The assessment of CMIP5 models indicate the reduction of sea-ice cover over the Arctic since the late 20th century (Shu et al., 2015). On the other hand, the majority of CMIP5 GCMs simulate an annual sea-ice extent minimum that is too small compared to observations (Turner et al., 2013). Furthermore, several GCMs underestimate the observed seasonal maximum in sea-ice extent over the Antarctic. These model biases in the seasonal cycle of Antarctic sea ice can have strong impacts on the simulated deep convection in the Southern Ocean (Heuzé et al., 2013). Coupled GCMs fairly capture the gross features of the energy budget over Antarctic but largely overestimate the shortwave radiation at the top of the atmosphere during summer season (Previdi et al., 2015). The difference in climatological surface energy fluxes between existing observational datasets precludes any meaningful assessment of model skill in simulating these fluxes over the Antarctic region. Permafrost is another important component of polar climate. High resolution RCMs can simulate atmosphere snow-permafrost interactions in the polar regions. Sophisticated land surface schemes in RCMs can reduce the biases in the temperature and circulation patterns in the Arctic. Changing the land model impacts the 2-m air temperature significantly over land and the atmospheric circulation predominantly over the Arctic Ocean, associated with changes in baroclinic cyclones (Matthes et al., 2017).

#### *10.3.3.8.4 Mediterranean climate*

The Mediterranean climate is characterized by its large seasonal temperature variations, strong winds, heavy precipitation, and cyclones (Akhtar et al., 2018; Obermann et al., 2018). The Mediterranean climate simulated by both GCMs and RCMs suggests pronounced warming in the future, particularly during summer (Giorgi and Lionello, 2008; Lionello and Scarascia, 2018). High-resolution regional atmospheric models coupled with Mediterranean Sea models have shown improvement in the simulation of Mediterranean climate. The high-resolution models improve the representation of hot days and droughts more than heavy precipitation events (Panthou et al., 2018b). Despite quite substantial biases, GCMs results show a realistic representation of the observed spatial patterns of temperature and precipitation over the Mediterranean region (Sanna et al., 2013). Moreover, heat and mass fluxes over the Mediterranean basin are realistically simulated by the majority of climate models. Higher-resolution models may be preferred, but they are not yet able to perform better than their coarse-resolution predecessors in all aspects. The sub-daily SST variation has strong influence on sub-daily wind speed and heat fluxes with less effects at longer time scales, therefore, a coupled atmosphere ocean climate model might be the better choice for studying the Mediterranean climate system (Akhtar et al., 2018).

#### *10.3.3.8.5 Mountain climate*

Simulation of mountain climate is challenging and evaluation of model performance is constrained due to the diverse nature of climate, complex topography and poor background knowledge with sparse in situ hydro-meteorological observations particularly at higher elevations such as in the Himalaya (Krishnan et al., 2019; Smith and Bookhagen, 2018; Bolch et al., 2012). Almost all the CMIP5 models reasonably capture the observed climatological patterns of precipitation in pre-monsoon and winter months in Himalayan mountainous regions (Meher et al., 2017). However, large uncertainty is found in simulation of climate over the Himalaya region particularly in monsoon and annual scale (Meher et al., 2017; Palazzi et al., 2018; Rajbhandari et al., 2019; Wester et al., 2019). The CMIP5 reduced precipitation bias as compared to CMIP3 over Himalayan region (Meher et al., 2017). Overall, the majority of CMIP5 models simulate well the temperature, however a cold bias with reference to the observations in the Tibetan Plateau area (Su et al., 2012). The CMIP5 models largely overestimate annual mean precipitation in the Tibetan Plateau (Su et al., 2012) whereas high resolution RCMs produces reasonably well the diurnal cycle of precipitation, which is typically characterized by a bimodal structure in the complex mountainous regions (Bhatt et al., 2014). In the high mountain regions like the Himalayas, the performance of a climate model improves when including

interactive glaciers (Kumar et al., 2015).

#### *10.3.3.9 Performance at simulating historical regional climate changes*

The AR5 has stated that there is *very high confidence* that models reproduce the general features of the global-scale annual mean surface temperature increase over the historical period (Flato et al., 2014). For regional trends, however, AR5 concluded that the CMIP5 ensemble cannot be taken as a reliable forecast and that the true uncertainty can be larger than the simulated model spread. In particular, many of the models that appear to correctly simulate strong observed regional trends do so because they have a high climate response (Kirtman et al., 2014). In the following, we assess the performance of different model types in simulating past trends at regional scale.

##### *10.3.3.9.1 Performance of GCMs at simulating regional historical trends*

Climatic trends even on multidecadal time scales are a superposition of forced signals and internal climate variability (see Chapter 3). This fact is not only relevant for assessing uncertainties in future projections (Section 10.3.4), but also for both understanding present and past trends (Section 10.4) and assessing model performance in simulating past trends. This section will discuss historical trends from an evaluation perspective. Section 10.4 will subsequently give detail about the different forcings and drivers of regional changes for selected case studies.

In particular at the regional scale, the forced signal may be small compared to internal variability. In these instances, given the limited ability to predict internal variability at multidecadal time scales, an agreement between observed and simulated trends would therefore be expected to occur only by chance (Laprise, 2014). Thus, the AR5, instead of assessing the performance of individual models at reproducing observed trends, has assessed the consistency of observed trends with those simulated by climate model ensembles as a whole (Kirtman et al., 2012). To assess the simulated patterns of change rather than the representation of global climate sensitivity, the influence of the latter is typically accounted for by normalising regional trends with the global-mean temperature trend. AR5 stated that the causes of discrepancies between observed and simulated regional trends are often unknown, but could include an underestimation of the low-frequency variability and unrealistic local forcings (e.g., aerosols) or missing or misrepresented processes in models (Kirtman et al., 2014). These findings have been corroborated and extended since then. Misrepresented trends have been attributed to an underestimation of trends in large-scale circulation patterns (van Haren et al., 2013), missing trends in SST and the occurrence of tropical cyclones (Roxy et al., 2015; Saha et al., 2014). A detailed discussion about which different forcings and drivers may have affected observed trends is given, for selected showcases, in Section 10.4.1.

**[Placeholder: assessment statement about general capability of GCMs in simulating regional trends]**

Statistical models have been used to further assess the influence of observed internal variability on regional-scale past trends (McKinnon et al., 2017; McKinnon and Deser, 2018). Kumar et al. (2016) have thoroughly documented the sensitivity of temperature trends to internal variability with regard to spatio-temporal scales based on CMIP3, CMIP5 and the CESM large ensemble (Kay et al., 2015). They found that the contribution of internal variability to the total uncertainty (as given by the CMIP5 model spread) in regional temperature trends increases from 43% for the full twentieth century to almost 100% for the recent hiatus period, in contrast with lower previous estimates based on parametric methods (Hawkins and Sutton, 2009).

##### *10.3.3.9.2 Performance of downscaling at simulating regional historical trends*

In the context of downscaling, one may address the following questions: (1) whether downscaling methods can reproduce observed trends when driven with observed boundary conditions or predictors, and (2) whether downscaling can add value to GCM simulated trends. Either question is only addressed in few studies.

For temperature in the US, Bukovsky (2012) found that an ensemble of RCMs driven with the NCEP reanalysis skilfully simulated recent spring and, by and large, winter trends, but did not reproduce summer and autumn trends. Similar studies have been carried out for statistical downscaling and bias adjustment, using predictors from reanalyses (or in case of bias adjustment, dynamically downscaled reanalyses). For a range of different perfect prognosis methods, Huth et al. (2015) found that simulated temperature trends were too strong for winter and too weak for summer. The performance was similar for the different methods, indicating the importance of choosing sensible predictors. Similarly, Maraun et al. (2017) found that the performance of perfect prognosis methods depends mostly on the predictor and domain choice (for instance, temperature trends were only captured by those methods including surface temperature as predictor). Bias adjustment methods reproduced the trends of the driving reanalysis, apart from quantile mapping methods, which deteriorated these trends.

Regarding the added value of downscaling, Racherla et al. (2012) found no improvement in the simulation of regional-scale temperature and precipitation trends in a dynamically downscaled GCM compared to the actual GCM itself. Laprise (2014), however, argues that the experiment was ill-designed (Section 10.3.3.7.1): because the weak forced signal was masked by internal variability, the GCM simulated trend cannot be expected to follow the observed trend, and the RCM cannot be expected to decrease the deviation between simulated and observed trends.

Including all relevant regional forcings is important to realistically simulate historical trends. RCM experiments are often set up such that changes in forcing agents are included only via the boundary conditions, but not included inside the domain. Jerez et al. (2018) demonstrated that not explicitly including changing greenhouse gas concentrations may misrepresent temperature trends by 1-2 ºC per century.

**[Placeholder: aerosols as regional driver]**

Similarly, Bukovsky (2012) argued that RCMs may not capture observed summer temperature trends in the US because changes in land cover are not taken into account. Barlage et al. (2015) have revealed that including the behaviour of groundwater in land schemes increases the performance of the WRF model's representativeness of climate variability in the central US. Hamdi et al. (2014) found that a RCM that did not incorporate the historical urbanization in the land-use land cover scheme is not able to reproduce the warming trend observed in urban stations with a larger bias for the minimum temperature trend.

Overall, there is *low evidence* whether dynamical downscaling adds value in simulating regional trends, but there is *high confidence* that including all relevant forcings is a prerequisite for reproducing historical trends.

### *10.3.3.10 Adequacy of climate models for projecting regional climate*

AR5 stated that confidence in climate model projections is based on physical understanding of the climate system and its representation in climate models, and a climate model's credibility is increased if the model is able to simulate past variations in climate. In addition, credibility of downscaled information depends on both the quality of the downscaling method itself and that of the GCM providing the large-scale boundary conditions (Flato et al., 2014).

Parker (2009) argued that climate models are representational tools designed for a particular purpose, and thus one may ask whether a climate model is adequate for the specific purpose of projecting a weather phenomenon under a specific forcing scenario over a particular region. A key consequence of the concept is that any model evaluation has to be specific to a given purpose or application. A general discussion about adequacy-for-purpose can be found in Chapter 1, and an assessment thereof targeting in particular global to continental-scale projections in Chapter 4. Here we focus on the regional context. The issue of model uncertainties, robustness and thus confidence in a specific projection of a multi-model ensemble will be discussed in Section 10.3.4, the broader issue of credibility of different sources of information for constructing regional climate information in Section 10.5.4.

*10.3.3.10.1 General considerations regarding adequacy-for-purpose of regional projections*

Recall from Chapter 1 that a reasonable performance in present climate and understanding the relevant processes, their interactions, and their implementation, constitute necessary but not sufficient conditions to warrant adequacy-for-purpose (Baumberger et al., 2017; Notz, 2015). As already stated in AR5, the evaluation of historical variability and long-term changes may provide more relevant information than just evaluating long-term climatologies (Flato et al., 2014). As discussed in Section 10.3.3.9, this kind of evaluation may provide very useful insight, but has limitations in particular at the regional scale, mainly due to multi-decadal internal climate variability, observational uncertainty and the fact that often not all regional forcings are known (see Section 10.4.1 for examples).

A model is required to sufficiently represent those processes that significantly shape the long-term evolution of the climate characteristics of interest (Baumberger et al., 2017). Thus, diagnostics representing these processes may provide important additional information for corroborating adequacy-for-purpose. This argument is particularly relevant at regional scales, as regional climate is strongly controlled by interacting dynamic and thermodynamic processes and remote drivers ((Shepherd, 2014), see also Section 10.4). For instance, regional changes in mid-latitude wind may depend on the interplay of changes in the polar vortex, polar amplification and tropical amplification (Zappa and Shepherd, 2017). Thus, an assessment of present-day surface winds may not be an informative diagnostic, but rather an assessment of the driving processes. Sections 10.3.3.4 and 10.3.3.5 give illustrative examples of assessments for large-scale and regional-scale processes and phenomena, respectively.

Shepherd (2014) points out that regional climate is strongly affected by aspects of atmospheric circulation. But our theoretical understanding of circulation changes is much weaker than that of purely thermodynamic changes, model performance in simulating the atmospheric circulation is considerably weaker than the performance in simulating thermodynamic changes, and observational constraints on changes in the atmospheric circulation are weak. These limitations are a major source of uncertainty in regional climate projections (Section 10.3.4). But more fundamentally, they also limit our confidence in the adequacy-for-purpose of climate models in projecting regional changes of elements controlled by the atmospheric circulation such as precipitation or wind (Hall, 2014; Shepherd, 2014).

Another factor limiting our confidence in the adequacy-for-purpose of climate models, in particular at the regional scale, are parameterisations of unresolved processes. These are typically developed and tested for weather forecasting purposes, and their applicability in future climate conditions is difficult to assess (Baumberger et al., 2017).

**[Placeholder: Added value and adequacy-for-purpose]**

Increasing model resolution, downscaling, and adding model components may in principle increase the adequacy-for-purpose of a model projection. A general hint of the adequacy-for-purpose of a specific model in a given application may already be gained from Figure 10.3.

If a downscaling model does not represent a phenomenon because its domain is too small, it will likely not add value to the representation of this phenomenon. If the phenomenon is not well represented by the driving model but controls the regional climate aspects of interest for a given application, this compromises the adequacy-for-purpose of the whole downstream modelling chain (garbage-in, garbage-out; Section 10.3.1.2). Examples of such large-scale phenomena are given in Section 10.3.3.4. In contrast, if a model does not represent the phenomena relevant for a specific application because its resolution is too coarse, higher resolution models or further downscaling may be required. Examples of such regional-scale phenomena are given in Section 10.3.3.5.

Increasing resolution or downscaling may be particularly important to increase credibility when it modifies the climate change signal of a lower resolution model in a physically plausible way (Hall, 2014). For instance, Gula and Richard Peltier (2012) showed that a higher resolution allows for a more realistic simulation of lake induced precipitation, resulting in a more credible projection of changes in the snow belts

of the North American Great Lakes (Figure 10.10). Similarly, Giorgi et al. (2016) demonstrated that an ensemble of RCMs better represent high-elevation surface heating and in turn increased convective instability and, finally, a summer convective precipitation response stronger than that simulated by the driving GCMs (Figure 10.11). Walton et al., (2015) showed that a higher resolution model enables a more realistic representation of the snow albedo feedback in mountainous terrain, leading to a more plausible simulation of elevation-dependent warming.

**[START FIGURE 10.10 HERE]**

**Figure 10.10:** [Placeholder: Projected changes in lake effect snow (in percent for the 2050-60 period compared to 1979-2001) over the Great Lakes Basin. (a) GCM: CCSM, (b) RCM: WRF. From Gula and Peltier, J. Climate, 2012]

**[END FIGURE 10.10 HERE]**

**[START FIGURE 10.11 HERE]**

**Figure 10.11:** [Placeholder: Changes in summer precipitation over the Alps simulated by 4 GCM (a-c) and 6 RCM driven with the same GCM (d-f) for three future time slices (top to bottom: 2010–2039; 2040–2069; 2070–2099). Further analysis, comparison with convection permitting simulations and physical arguments. From Giorgi et al., Nat. Geosci. 2016].

**[END FIGURE 10.11 HERE]**

Also including additional components and feedbacks can substantially modify the simulated future climate. For example, Kjellström et al., (2005) and Somot et al., (2008) have shown that an RESM can significantly modify the SST climate change signal of its driving GCM with implications for the climate change signal over both the sea and land. In particular, there is evidence that coupled ocean-atmosphere RCMs may increase the credibility of projections in regions of strong air-sea coupling such as the East Asia-western North Pacific domain (Zou and Zhou, 2016, 2017).

Of course a difference between the climate changes simulated by a coarse or simpler and a higher resolution or more complex model does not automatically imply the latter is superior (e.g. Dosio et al., submitted). For instance, most studies comparing high-resolution convection permitting RCM simulations that explicitly simulate deep convection with simulations of hydrostatic RCMs with parameterized convection find, at least for some regions, a qualitatively different response of short duration extreme summer precipitation (Ban et al., 2015; Chan et al., 2014b, 2014a; Tabari et al., 2016; Vanden Broucke et al., 2018), whereas other studies do not (Fosser et al., 2017). Process studies of convection under warming conditions provide evidence that convection permitting simulations reproduce a physically more plausible warming response of vertical motions in a thunderstorm (Meredith et al., 2015a), but further research is required to test, e.g., the adequacy of the remaining parameterisations for the higher model resolution. Sometimes even the best available models may have limited adequacy. For instance at the urban scale, RCMs, even with appropriate urban parametrization, are not able to correctly represent the intensification of the urban heat island during heat waves (Hamdi et al., 2016).

In general, as discussed above, any statement about improved adequacy-for-purpose has to rest in thorough evaluation and process understanding. Overall, there is *high confidence* that increasing model resolution, downscaling and adding model components increase the adequacy-for-purpose for some aspects of regional projections.

Only little research has addressed the adequacy-for-purpose of statistical downscaling and bias adjustment. Perfect model experiments (Section 10.3.2.7) have been used to assess whether a given model structure with a chosen set of predictors is capable of reproducing the simulated future climates (Dayon et al., 2015;

Gutiérrez et al., 2013; San-Martín et al., 2017). Importantly, it is found that demonstrated that standard analogue methods inherently underestimate future warming trends (Gutiérrez et al., 2013). Emerging discussions on bias adjustment will be assessed in the Box 10.2.

*10.3.3.10.2 Increasing the credibility of regional projection*

Several research strands have been proposed to proactively corroborate the adequacy-for-purpose of climate models (e.g. Baumberger et al., 2017).

Confidence in the adequacy-for-purpose of a model to simulate regional climate change can be increased based on robustness arguments, in particular when comparing the simulated response with higher resolution models that better represent relevant processes (Baumberger et al., 2017). For instance, Giorgi et al. (2016) have further corroborated their findings by convection permitting simulations. These examples point to the importance of using hierarchies of models. Recent coordinated modelling efforts spanning GCMs (CMIP; Eyring et al. 2016a), high resolution GCMs (PRIMAVERA, HighResMIP; Haarsma et al. (2016), standard RCMs (CORDEX; Giorgi and Gutowski, 2015) and convection-permitting RCMs (Coppola et al., 2018) provide a unique opportunity to study the response of processes across a broad range of scales and thereby substantially increase our understanding of which models are adequate for which purpose.

Further confidence may be built by disentangling and understanding the different forcings of observed climatic changes and evaluating how models simulate these changes. Several case studies will be discussed in Section 10.4.1. Finally, targeted experiments such as pseudo global warming studies of how individual weather events may manifest in a future climate (Section 10.3.3.2) may help to explore the limits of plausible changes (Shepherd et al., 2018).

**[Placeholder: paragraph on explicitly testing parameterisations in model simulations or different climates]**

Similarly, the use of perfect model experiments may provide a very useful basis for better understanding the adequacy-for-purpose of statistical downscaling and bias adjustment methods.

**[Placeholder: assessment statement on how to increase credibility]**

### *10.3.4 Managing uncertainties in regional climate projections*

Regional climate projections are affected by mainly three sources of uncertainty (Section 10.5.2): unknown future greenhouse gas emissions, imperfect knowledge and implementation of the response of the climate system to external forcings, and internal variability. In a regional downscaling context, uncertainties arise in every step of the modelling chain. Additionally, statistical methods are calibrated against observational data and thereby also link observational uncertainty to projection uncertainties (Section 10.2.3.3).

To avoid providing overconfident statements about climate change, one aim is to sample the different sources of uncertainty as comprehensively as possible by using hierarchies and ensembles of models.

One strand of research is to characterise the overall uncertainties in a model ensemble by attributing them to different sources of uncertainty, different steps in the modelling chain or even different underlying processes. An important research aim is the reduction of uncertainties by increasing the knowledge of the climate system and improving models. Also new statistical tools have been developed to constrain projections by referring to observations (Section 10.5.2).

#### *10.3.4.1 Propagation of uncertainties*

The generation of regional climate information involves a modelling chain starting from the definition of forcing scenarios to the global modelling, and potentially to dynamical or statistical downscaling and bias

adjustment. The fact that each step is afflicted with uncertainties, which propagate and potentially accumulate along the chain, has been coined the cascade of uncertainty (Wilby and Dessai, 2010). But even when using just a GCM without further downscaling, uncertainty propagates from the direct response to radiative forcing, across scales to the regional-scale manifestation of climate change.

In terms of climate modelling steps (Figure 10.3), the cascade may involve the propagation from

1. GCM to bias adjustment or weather generators
2. GCM to RCM and potentially to bias adjustment or weather generators
3. GCM to perfect prognosis statistical downscaling

Uncertainties in forcings, global climate sensitivity, thermodynamic processes and circulation in GCMs propagate through the uncertainty cascade. Dynamical downscaling involves additional uncertainties related mainly to large-scale thermodynamics and local processes (Hall, 2014). Statistical downscaling, bias adjustment and weather generators express mesoscale to convective-scale atmospheric processes and potentially model errors by a simplified and uncertain statistical model (Maraun and Widmann, 2018b).

**[Placeholder: if space allows, an overview of recent studies that aim to decompose uncertainties]**

The uncertainty propagation often increases the spread in regional climate projections when comparing GCM and downscaled results. But Maraun and Widmann (2018b) argue that increased uncertainties in the modelling chain may in principle arise from a more comprehensive sampling of previously unknown uncertainties. The increase would then be an expression of a better understanding and more skilful modelling and ultimately increased adequacy-for-purpose. For instance, in mountainous terrain high-resolution RCMs may increase the spread in the temperature response across GCMs because they resolve the uncertain snow-albedo feedback, but the very simulation of the feedback might be crucial to credibly represent regional temperature changes.

**[Placeholder for situations where spread is reduced by downscaling]**

**[Placeholder for unsampled uncertainties and unknown unknowns]**

#### *10.3.4.2 Representing and reducing uncertainties*

Uncertainties in climate projections have traditionally been characterized by the multi-model mean change and associated ensemble spread. The change has then further been qualified in terms of the agreement across models and the significance compared to internal climate variability (Chapter 1). Since AR5 several limitations of this “quasi-probabilistic” approach have been identified. Such a treatment fails to address physically plausible, but unlikely high-impact scenarios (Chapter 1; Sutton, 2018), but also considering less extreme projections, the probabilistic approach may be misleading in some cases. Moreover, (Shepherd, 2014) points out the substantial role of uncertainties in atmospheric circulation for regional climate projections (see also Section 10.3.3.4). In consequence, qualitatively different but equally plausible responses of regional climate are possible. In a multi-model mean these different responses would be lumped together, strongly dampened, and qualified as non-robust, whereas in fact high impacts might be expected. Even more, the multi-model mean itself may be implausible and may not manifest at all.

Overall, there is *high confidence* that some regional future climate changes may not be well characterised by multi-model mean and spread, and that additional approaches may be required.

Since AR5, approaches have therefore been developed to better characterise and communicate uncertainties in regional climate projections. Common to these approaches is the attempt to attribute regional uncertainties to uncertainties in remote drivers. The KNMI has communicated climate projections for the Netherlands by presenting a set of different storylines of possible changes. For instance, precipitation changes were presented for different changes of the mid-latitude atmospheric circulation and different levels of European warming (Attema et al., 2014). Manzini et al. (2014) have quantified the impact of uncertainties in tropical

upper troposphere warming, polar amplification, and stratospheric wind change on Northern Hemisphere winter climate change. Based on these results, Zappa and Shepherd (2017) separated the multi-model ensemble into physically consistent sub-groups or storylines of qualitatively different projections in relevant remote drivers of the atmospheric circulation (Figure 10.12).

**[START FIGURE 10.12 HERE]**

**Figure 10.12:** [Placeholder: Cold season U850 response per degree of global warming (m s-1 K-1) according to five plausible storylines in the CMIP5 models. (a) stronger stratospheric vortex and lower tropical amplification; (b) stronger stratospheric vortex and higher tropical amplification; (c) multi model mean response scaled by global warming; (d) weaker stratospheric vortex and lower tropical amplification; (e) weaker stratospheric vortex and higher tropical amplification. From Zappa and Shepherd, J. Climate, 2017]

**[END FIGURE 10.12 HERE]**

These approaches help to physically explain contradicting projections at the regional scale and thus make the conveyed information more defensible (Hewitson et al., 2014). Additionally, storylines help to sub-sample a multi-model ensemble in a way that still represents the full range of possible outcomes, and therefore may help impact modellers to sensibly select a small number of climate model simulations as drivers for impact models (Zappa and Shepherd, 2017). Finally, the attribution of regional uncertainties to drivers may also help to reduce uncertainties in the case where some storylines can be ruled out because the projected changes in the driving processes appear to be physically implausible (Zappa and Shepherd, 2017).

Overall, there is *high confidence* that storylines attributing uncertainties in regional projections to uncertainties in changes of remote drivers improve the interpretation of climate projection uncertainties.

Another approach that has been developed over recent years to characterise and reduce projection uncertainties are emergent constraints (see Chapter 1). The idea is to link the spread in climate model projections via a regression to the spread in present climate model biases for relevant driving processes. Models with lower biases are assigned higher weight in the projections, which in turn reduces the bias of the projection in a physical way and may additionally reduce projection uncertainty. For instance, (Simpson et al., 2016) have reduced the spread in projections of North American winter hydroclimate by linking this spread to model biases in the representation of relevant stationary wave patterns. Other examples of using emergent constraints in a regional context are Brown et al. (2016), Li et al. (2017) and Giannini and Kaplan (2018) (see also Section 10.4.1). Brient and Schneider, (2016) argue that there is a need to account for all uncertainties in emergent constraint statistical models. Studies based on emergent constraints often neglect the structural uncertainty about the adequacy of the assumed linear model between the predictor and predictand. The standard methods can be strongly influenced by low performing models that have a large influence on the inferred slope of the regression line. They can also be prone to selection bias in the pre-processing phase (e.g. cherry-picking spatial averaging to maximize correlations). They rely on ordinary least squares while there usually are uncertainties on both predictor and predictand meaning that a total least square approach would be necessary. They are also based on a multi-model inference procedure that neglects interdependences among climate models (Boé, 2018), which may skew results (in particular when few models are available).

**[Placeholder for assessment statement about use of emergent constraints at regional scale].**

### *10.3.4.3 Role of internal variability*

A regional climate projection based on a single simulation from a single GCM or driving a single RCM alone will inevitably be affected by internal variability due to the chaotic nature of the climate system. This is mainly due to the dominant influence of the chaotic atmospheric circulation on regional climate variability, in particular at mid-to-high latitudes; this implies that internal variability is an irreducible source

of uncertainty for mid-to-long-term projections.

There is *emerging evidence* that the role of internal variability has likely been underestimated in previous assessments of regional climate projections as shown by a large body of studies based on initial condition single-model large ensembles (Maher et al., 2019). Initial-condition large ensembles allow quantification of the influence of internal variability on GCM-based regional climate projections for all simulated variables and spatial and temporal scales. This is a significant change from the CMIP5 multi-model methodology in which differences between realizations coming from different models stem from both model structural differences and internal variability. Another related development is the more frequent use of observation-based statistical models to assess the influence of internal variability on regional-scale GCM and RCM projections (Salazar et al., 2016; Thompson et al., 2015).

The approaches targeting the estimation of regional climate change uncertainty due to internal variability are often based on a signal-to-noise approach based on a specific diagnostic, the signal being the forced response due to anthropogenic forcing and the noise being internal variability. Since AR5, several large (of size 30 or more) initial condition ensembles have been constructed and used to assess signal-to-noise diagnostics (Bengtsson and Hodges, 2018; Deser et al., 2012b; Kay et al., 2015; Sigmond and Fyfe, 2016). Standard diagnostics include a simple assessment of the Signal-to-Noise Ratio (SNR, Figure 10.13) that can be defined as the forced response (ensemble mean) to the noise (ensemble spread) ratio, or a forced to total variance ratio, or a Time of Emergence (ToE) which indicates the time at which a forced climate signal emerges from the secular/decadal "noise" of internal climate variability (Hawkins and Sutton, 2012; Lehner et al., 2017a; Mahlstein et al., 2012). The ToE diagnostic can be based on the SNR exceedance of a subjective threshold or a level of significance for rejecting a null hypothesis of no change in a given climate variable PDF between two different periods. The ToE can also be assessed with regard to the mean change and/or changes in variability including extremes and records (Bador et al., 2016; King et al., 2015; Maraun, 2013b), although Maraun (2013) argued that the ToE can be misleading for the assessment of very rare extremes, as the associated hazard may increase even when the SNR is low (Figure 10.14). The ToE is a subjective diagnostic with different sources of uncertainty as it can be affected by model biases, internal variability, definition of the base period (pre-industrial runs and/or late 19th century), time filtering choices and spatial scale aggregation diagnostics records (Bador et al., 2016; Hawkins and Sutton, 2012; King et al., 2015; Lehner et al., 2017a; Maraun, 2013b).

**[START FIGURE 10.13 HERE]**

**Figure 10.13:** [Placeholder: Signal-to-noise ratio of precipitation changes (2075-2099 average minus 1979-2003 average according to the RCP8.5) in the MRI-AGCM3.2 atmospheric GCM at a 60km resolution as function of spatial (Lxy) and temporal (Lt) averaging scale for different latitudes. From Hibino and Takayabu, J. Met. Soc. Jap. 2016]

**[END FIGURE 10.13 HERE]**

**[START FIGURE 10.14 HERE]**

**Figure 10.14:** [Placeholder: Role of internal variability at different lead times. Sketch to be replaced by example from model simulation for SOD. Dark red: forced signal. Blue: two possible realisations. Magenta shading: likely range of future values. Pink lines: extreme thresholds. The longer the lead time, the stronger the forcing, the higher the signal-to-noise ratio, and thus the more robust statements can be drawn. But even at short lead times with low signal-to-noise ratio, the probability of exceeding high thresholds is steadily increasing, and the probability of exceeding a low threshold is steadily decreasing.]

**[END FIGURE 10.14 HERE]**

Based on the MPI-GE large-ensemble with an ensemble size of 100, (Maher et al., JAMES, submitted) show

that a minimum of 40–50 members are needed to capture both the 21st century SLP-forced trend pattern and the variability of the trend, confirming previous results from (Deser et al., 2012b). Based on a large RCM initial condition ensemble, (Aalbers et al., 2018) found that in summer, at the gridbox scale, significant trends in extremes could not be established everywhere in the domain, not even at the end of the century under RCP8.5. This does not imply that changes in precipitation extremes are unimportant from the perspective of a risk assessment, in particular when considering larger areas. Aggregation of changes over larger areas (e.g. river basins) could lead to a better SNR and better detectability of trends. Some regional-scale studies show that both large-scale internal variability and local-scale internal variability together can still represent a substantial fraction of the total uncertainty related to hydrological cycle variables, even at the end of the 21st century (Gu et al., 2018; Lafaysse et al., 2014).

There is *high confidence* that internal variability introduces substantial irreducible uncertainty in regional-scale climate change attribution and climate change projections. This problem applies to all regions and timescales (from a decade up to a century) and is more acute in the extra-tropics and for climate variables other than temperature, such as precipitation or for atmospheric circulation.

#### *10.3.4.4 Designing and using ensembles for regional climate change assessments*

As noted in Sections 10.3.4.2 and 10.3.4.3, ensembles of climate simulations play an important role in quantifying uncertainties in the simulation output. In addition to providing information on internal variability, ensembles of simulations can indicate scenario uncertainty and model (structural) uncertainty. Chapter 4, especially Box 4.1, discusses issues involved with evaluating ensembles of GCMs simulations and their uncertainties.

In a downscaling context, further considerations are necessary, such as the selection of GCM-RCM combinations when performing dynamical downscaling. The structural uncertainty of both the GCM and the downscaling method can be important (e.g. Dosio, 2017; Dosio et al. 2018; Mearns et al., 2012) as well as further potential uncertainty created by inconsistencies between the GCM and the downscaling method (e.g., Dosio et al., submitted) which could include, for example, differences in topography or modelling of precipitation processes (Mearns et al., 2013).

An important consideration is which GCMs to use. Some RCM-based initiatives consider a matrix of GCM-RCM combinations or one RCM to downscale multiple GCMs. If adequate resources exist, then large numbers of GCM-RCM combinations are possible, as in the ENSEMBLES program (Déqué et al., 2012a). However, downscaling programs can be limited by the resources available, human and computational, for producing ensembles of downscaled output, which limits the number of feasible GCM-RCM combinations. With this limitation in mind, a small set of GCMs might be chosen that span the range of equilibrium climate sensitivity (e.g., Mearns et al., 2012, 2013) or some other measure of sensitivity, such as the projected range of tropical SSTs (Suzuki-Parker et al., 2018).

However, even using a relatively small set of GCMs can still involve substantial computation that strains available resources, both for performing the simulations and for using all simulations in the ensemble for further impacts assessment. The NARCCAP program (Mearns et al., 2012) used only a subset of its possible GCM-RCM combinations that balanced comprehensiveness of sampling the matrix with economy of computation demand (Mearns et al., 2013). If information from all possible combinations is still desired, one can apply statistical methods to a well-balanced, but incompletely filled matrix and extract climatological information for the missing combinations. An advantage of the “sparse, but balanced” matrix for those using the downscaling output for further studies, such as vulnerability, impacts and adaptation assessments is that they have a smaller, yet comprehensive set of GCM-RCM combinations to work with. Alternatively, data-clustering methods can clump together downscaling simulations featuring similar climate-change characteristics, so that only one representative simulation from each cluster may be needed for further impacts analysis, again systematically reducing the necessary number of simulations to work with (Mendlik and Gobiet, 2016; Wilcke and Bärring, 2016).

Whatever the resources, participation of multiple models in a simulation program such as CORDEX for RCMs or CMIP for GCMs creates "ensembles of opportunity", which are ensembles populated by models that participants chose to use for simulation without there necessarily being an overarching guiding principle for the choice. However, as discussed in Chapter 4, these ensembles are likely suboptimal for assessing sources of uncertainty. An important contributor to the suboptimal character of such an ensemble is that the models are not independent. Some may also have larger biases than others. Yet often, the output from models in these ensembles has received equal weight when viewed collectively, as was the case in much of the AR5 assessment (e.g., Flato et al., 2014; Kirtman et al., 2014; Knutti et al., 2013).

One approach to emphasize independent models is to combine models with the same origins into families, effectively an a priori weighting, and create ensemble averages giving equal weight to each of these families of models. A variation of this approach lumps together models that use similar parameterizations for some processes. Much of the work with these approaches has been done using GCMs, which can be a basis for selecting relatively independent GCMs as contributors to a GCM-RCM matrix, for example. Evans et al. (2014) have also used RCM independence as a guiding principle for selecting RCMs to include in their matrix. Alternatively, some have proposed a posteriori weighting, wherein weights are based on a measure of simulation accuracy. Räisänen and Palmer (2001) and Giorgi and Mearns (2002) developed initial applications of this approach to climate-model ensembles. McSweeney et al. (2015) have used accuracy weighting for selecting GCMs appropriate for downscaling in several regions of the world; such weighting has continued to be used for analysing GCMs (see Chapter 4) and RCMs (Déqué et al., 2012a). However, the choice of accuracy measure can be somewhat arbitrary, and if applying the weighting to projections, it assumes that the models replicating present climate the best have the least error in their future scenario climates. Therefore, there is growing support for a process-based binary weighting, i.e., that GCMs should be discarded that unrealistically represent processes controlling the regional climate of interest (Eyring et al., 2019; Maraun et al., 2017b). Chapter 4, Box 4.1 offers a more detailed discussion of the issues surrounding these approaches and their implications for ensemble evaluation and weighting.

There is *high confidence* that ensembles for regional climate projections should be selected such that models unrealistically simulating processes relevant for a given application are discarded, but at the same time the chosen ensemble spans the range of projection uncertainties.

**[START BOX 10.2 HERE]**

**BOX 10.2: Issues in bias adjustment**

Bias adjustment has not been assessed in AR5 (Flato et al., 2014), but it is commonly used at the interface between climate model projections and the assessment of climate hazards and impacts. Over recent years, however, several issues have been identified that may arise from an uncritical use of bias adjustment. A tentative assessment of these issues has been conducted during the IPCC Workshop on Regional Climate Projections and their Use in Impacts and Risk Analysis Studies in 2015 (Stocker et al., 2015). This box will first discuss the justification of bias adjustment and then revisit, extend and update this assessment.

**Justification and need for bias adjustment**

Bias adjustment has become widely used in climate hazard and impact studies (Gangopadhyay et al., 2011; Hagemann et al., 2013; Warszawski et al., 2014) and national assessment reports (Cayan et al., 2013; Georgakakos et al., 2014). However, some authors question its validity when applied to climate change studies, as bias adjustment may alter the spatial-temporal and inter-variable consistency of the model data, violating conservation principles and neglecting feedback mechanisms (Ehret et al., 2012). In addition, the underlying assumption of whether biases are time-invariant or not is still debated (Ehret et al., 2012; Vannitsem, 2011).

However, following a more pragmatic approach, and acknowledging the underlying shortcomings, other studies argue that climate model biases are severe enough to, in principle, justify the use of bias adjustment prior to impact modelling (Maraun et al., 2017b), as these models commonly react very sensitively, often

non linearly, to the input climatic variables and their biases. Examples of impact modelling studies showing an improvement in simulating present day hazard, when fed with bias-adjusted climate model output, include the assessment of hydrological impacts such as river discharge (Montroull et al., 2018; Rojas et al., 2011; Muerth et al., 2013), forest fires (Migliavacca et al., 2013), crop production (Ruiz-Ramos et al., 2016) and regional ocean modelling (Macias et al., 2018). The use of bias adjusted model outputs is also particularly beneficial when threshold based climate indices are required (Dosio, 2016b). There are, however, cases where bias adjustment may not be necessary or useful, for instance:

- when only qualitative statements are required;
- when only changes in mean climate are considered (however, some argue that bias adjustment may improve the change, see below);
- when percentile based indices are considered;

**Time-invariance assumption and modifications of the climate change signal by bias adjustment**

The AR5 has already presented examples of state-dependent climate models biases, i.e., examples where the time-invariance assumption is violated (Flato et al., 2014). Further research since then addressed this issue by means of perfect model experiments (Section 10.3.2.7) and physical reasoning.

Perfect model studies with GCMs found that circulation, energy and water-cycle biases are roughly state-independent (Krinner and Flanner, 2018), whereas temperature biases depend linearly on temperature (Kerkhoff et al., 2014). Bellprat et al. (2013), however, argued that the linear temperature dependence of temperature biases is linked to soil moisture feedbacks and, once soil moisture is depleted, the bias becomes constant. This finding is in line with other results linking the state-dependence of temperature biases to misrepresented temperature feedbacks (e.g. Maraun, 2012, Maraun et al., 2017). The state-dependence implies time-varying biases, i.e., different biases in present and future climate.

It has been shown that bias adjustment methods like quantile mapping can modify simulated climate change trends, with notable impacts on changes to climate indices (e.g., Dosio, 2016; Dosio et al., 2012; Haerter et al., 2011; Hempel et al., 2013; Maurer and Pierce, 2014). Some authors argue that these trend modifications are implicit corrections of state-dependent biases. For instance, by assuming a linear relationship between temperature and its bias (Boberg and Christensen, 2012; Gobiet et al., 2015). However, others argue that quantile mapping is calibrated on short-term (e.g., daily) variability and cannot necessarily be transferred to correct long-term trends (Maraun et al., 2017b). Similar arguments have led to the development of trend preserving quantile mapping methods (see Section 10.3.1.3). Other authors finally claim that bias adjustment has no overwhelming negative or positive effect on precipitation changes, and there is no clear advantage in using a trend-preserving bias adjustment (Maurer and Pierce, 2014). Further research is still required to fully understand the time and state-dependence of climate model biases, and the validity of trend modifications by quantile-mapping approaches.

**Bias adjustment in the presence of large-scale circulation errors**

Recent research has investigated the influence on bias adjustment of circulation errors, such as biases in the frequency of precipitation-relevant weather types (Addor et al. 2016). In this case, a standard bias adjustment (i.e., not accounting for this frequency bias) would remove the overall climatological bias, but residual precipitation biases for individual weather types would remain. Conversely, a bias adjustment applied separately for each weather type would remove weather-type specific biases but not the overall climatological bias. Other works showed that the attempt to correct such frequency biases by e.g., adjusting the number of wet days, may artificially deteriorate the spell-length distribution and either delete or artificially introduce long dry spells (Maraun et al., 2017b).

In presence of biases in the location of dominant circulation patterns, bias adjustment may introduce physically inconsistent and implausible solutions (e.g., a northward-moving North Atlantic storm track accompanied by a southward moving precipitation pattern; (Maraun et al., 2017b)). Bias adjusting the location of circulation features has been proposed (Levy et al., 2013) but this may introduce inconsistencies with the model orography, land-sea contrasts and SSTs (Maraun et al., 2017b). Other authors therefore suggest run-time bias adjustment (Guldberg et al., 2005; Kharin et al., 2012; Krinner et al., 2019).

There is *medium confidence* that the selection of climate models with low biases in the synoptic-scale atmospheric circulation may increase the validity of bias adjustment.

**Bias adjustment prior to dynamical downscaling**

Some authors suggest to mitigate the influence of large-scale temperature or circulation biases by performing a bias adjustment prior to dynamical downscaling (e.g., Colette et al., 2012; Hernández-Díaz et al., 2013). For present climate, this approach has been shown to substantially reduce the RCM biases in mean temperature and precipitation. In a case study for South Africa, White and Toumi (2013) demonstrated that bias adjustment reduces the bias in downscaled monthly mean precipitation, but quantile mapping artificially amplifies its interannual variability. It is found that this approach may introduce dynamical inconsistencies because the adjustment corrects the location of long-term mean patterns, but not the location of day-to-day variability (Maraun et al., 2017b).

Further research is required to understand the validity of bias-adjusted GCM outputs prior to dynamical downscaling.

**Representativeness issues and the use of bias adjustment as statistical downscaling**

Bias adjustment assumes that the simulated variable is representative of the observed target variable, which is not always the case. (Maraun et al., 2017b) investigated a case where observed precipitation was closely correlated with ENSO variability, but GCM-simulated precipitation was essentially uncorrelated with the simulated ENSO variability. In complex terrain, the simulated regional flow may be substantially shifted compared to reality because of the coarse representation of topography in the climate model (Maraun and Widmann, 2015). In both cases, standard bias adjustment is not meaningful.

Bias adjustment is often used to downscale climate model results from gridbox to point scale or finer resolution; for instance, several authors apply bias adjustment directly to GCM outputs instead of using an intermediate dynamical downscaling step (e.g., Johnson and Sharma, 2012). It has been demonstrated that this approach may lead to representativeness issues, as the weather and climate at a point location may substantially differ from the climate model-simulated area average; as a consequence, the attempt to reproduce point-scale variability by quantile mapping the area-averaged climate model output artificially modifies long-term trends and overestimates area-aggregated extreme precipitation (Maraun, 2013a). Similarly, bias adjustment cannot represent, e.g., temperature inversions in unresolved valleys, or sub-grid variations in the climate change signal such as elevation-dependent warming caused by unresolved snow-albedo feedbacks (Maraun et al., 2017b) (Box 10.2, Figure 1). It has therefore been suggested to account for local random variability by combining bias adjustment with stochastic downscaling (Volosciuk et al., 2017), although this approach still does not account for local modifications of the climate change signal. Statistical emulators of high resolution RCMs have been proposed to account for local modifications of the climate change signal (Walton et al., 2015).

Overall, there is *high confidence* that the use of bias adjustment for statistical downscaling, in particular of coarse resolution GCMs, has limitations and that dynamical downscaling may be required to resolve relevant local processes prior to bias adjustment. Examples of such added value of RCMs are given in Sections 10.3.3.3 and 10.3.3.5.

**[START BOX 10.2, FIGURE 1 HERE]**

**Box 10.2, Figure 1:** [Placeholder: Spring (MAM) daily mean temperature in the Sierra Nevada region in California. Top: present climate (1981-2000 average) in (a) the GFDL-CM3 GCM, interpolated to 8km, (b) observations at 8km resolution, (c) WRF RCM at 3km horizontal resolution. Bottom: climate change signal (2081-2100 average minus 1981-2000 average according to RCP8.5) in (d) the GCM, (e) the bias adjusted GCM using quantile mapping, and (f) the RCM. As the GCM does not resolve the snow-albedo feedback, it simulates an implausible regional warming signal. The bias adjustment cannot improve the missing feedback. Only the high-resolution RCM simulation simulates a plausible elevation-dependent climate change signal. From Maraun et al., Nat. Clim.

Change, 2017].

**[END BOX 10.2, FIGURE 1 HERE]**

**Calibrating and evaluating bias adjustment in the presence of observational uncertainty and internal variability**

Observational uncertainties and internal variability may introduce substantial uncertainty in the estimation of biases and thus in the calibration of bias-adjustment methods. Dobor and Hlásny (2018) found a considerable influence of the choice of observational data set and calibration period on the bias adjustment for some regions in Europe. Similarly, Kotlarski et al. (2017) found that RCM biases are typically larger than observational uncertainties, but in some regions, and in particular for wet-day frequencies, spatial patterns and the intensity distribution of daily precipitation the situation may reverse. Switanek et al. (2017) found a strong dependence of the choice of calibration period on the calibration of quantile mapping and ultimately even on the modification of the climate change signal.

Bias adjustment is typically evaluated using cross-validation, i.e., by calibrating the adjustment function to one period of the observational record, and by evaluating it on another, different one. Some studies highlight the difficulties of evaluating bias adjustment using this approach (Maraun et al., 2017b). Maraun and Widmann (2018) demonstrated that, for climate-change simulations, multi-decadal internal climate variability may lead to a rejection of a valid bias adjustment or even lead to a positive evaluation of an invalid bias adjustment. The authors therefore argued that, in the presence of substantial internal variability, bias adjustment of climate cannot sensibly be evaluated by cross-validation, but instead by evaluating aspects that have not been adjusted such as temporal, spatial or multi-variable dependence.

**Recommendations for the use of bias adjustment**

In the light of these issues, several attempts have been made to provide guidelines for the use of bias adjustment. The most important will be summarised below. Ehret et al. (2012) recommend that when using bias adjustment, the raw model output should always be provided alongside the bias adjusted data.

This recommendation was backed up at the IPCC Workshop on Regional Climate Projections and their Use in Impacts and Risk Analysis Studies in 2015 (Stocker et al., 2015). Maraun et al., (2017b) argued that such dissimilarities pointed towards representativeness issues, and a bias adjustment is not sensible. Stocker et al. (2015) and Maraun et al. (2017) both highlighted the relevance of understanding model biases and the misrepresentations of the underlying physical processes prior to any bias adjustment, and encourage the development of physics-informed bias adjustment methods, and the collaboration between bias adjustment users, experts in climate modelling and experts in the considered regional climate.

**[END BOX 10.2 HERE]**

## 10.4 Using climate phenomena / processes

Expected length: 25 pages, 1 page=950 words
Number of figures: 11
Number of tables: 1

### *10.4.1 Introduction*

Regional climate variability results from the complex interaction between local physical processes, and their response to large-scale phenomena such as the ENSO and other low-frequency modes of climate variability such as AMV and PDV.

This section assesses the physical causes of past and future regional climate change in the context of the ongoing anthropogenic influence on the global climate. In this chapter, regional climate change refers to a

transient change in the state of the climate that can be identified by changes in the mean and/or higher moments, and persists for an extended period, typically a few decades or longer. Regional climate change as interpreted here may be due to natural internal processes and/or external forcings such as modulations of the solar cycle, orbital forcing, volcanic eruptions and persistent anthropogenic changes in the composition of the atmosphere or in land use (Section 10.1.4; Chapter 3, Cross-Chapter Box 3.1). Note that this differs from the United Nations Framework Convention on Climate Change (UNFCCC) Article 1 definition, which defines climate change as a change attributable to human activities altering the atmospheric composition.

The section focuses on ten illustrative case studies that span a wide range of regions, time scales, attribution methods and issues (Figure 10.15). Here, a case study is defined by a geographical spatial domain as well as a past period (from a couple to several decades) during which the specific regional climate has undergone a substantial change. Note that substantial does not refer here to significantly rejecting a specific statistical null hypothesis. Instead it is loosely used to describe a change that can have one or more of the following properties: large amplitude and/or spatial extent, a rare occurrence, high-impact in terms of consequence for human and natural systems, thus making a relevant link with the IPCC Working Group II (WGII) assessment report. The list of selected case studies presented roughly follows the order of the regional chapters of the WGII report. Section 10.4.2 provides an assessment of the main causal factors underlying the observed changes for each case study region or area. Future projections for the same regions are then addressed in Section 10.4.3 with a focus on the interplay between internal variability and external forcing in shaping future regional climate change. This section will not provide an exhaustive and complete assessment of past and future regional climate change for all the regions considered in the report (as defined in Box 1.1).

**[START FIGURE 10.15 HERE]**

**Figure 10.15:** Time series of Surface Air Temperature (SAT in °C, blue and red colours) or precipitation (PR in mm per month, green and ochre colours) anomalies (relative to the 1951–1980 period) area-averaged over appropriate regions of 8 out of the 10 selected case studies. The regions are broadly defined by the green (PR) and magenta (SAT) rectangles. The precise region boundaries and case studies are from top to bottom and left to right: a. The south-western North and Central America (25°N–40°N, 94°W–124°W) drought b. The Caribbean small islands (11°N–25°N, 60°W–85°W) summer (JJA) drought c. The south-eastern South America (25°S–40°S, 45°W–65°W) Austral summer (DJF) drought d. The Sahel and the West African monsoon (10°N–20°N, 20°W–40°E) drought and recovery e. The southern Australia (25°S–40°S, 110°E–150°E) rainfall decline f. The East Asia summer (JJA) monsoon weakening and recovery; here the time series is the difference of mean precipitation between two regions: PR (110°E–125°E, 35°N–45°N) – PR (105°E–125°E, 20°N–35°N) g. The central and eastern Eurasia (40°N–65°N, 60°E–140°E) winter (DJF) cooling h. The western Europe (35°N–70°N, 15°W–30°E) summer (JJA) warming. SAT is from the Berkeley surface temperature dataset (Rohde et al., 2013) and PR from GPCC v8 (Becker et al., 2013; Schneider et al., 2017). The white area on each graphic represents the period of interest for attribution. The black line is a simple low-pass filter that has been used in AR4. It has 5 weights 1/12 [1-3-4-3-1] and for annual data, its half-amplitude point is for a 6-year period, and the half-power point is near 8.4 years. The remaining two case studies concerned the Himalaya mountain range and Asian cities. The relevant data and graphics will be included in the figure for the SOD.

**[END FIGURE 10.15 HERE]**

### *10.4.2 Attributing past regional changes to multiple causal factors*

This section focuses on recent research on attribution of past regional climate change for the selected case studies. In this chapter, attribution is defined as the process of evaluating the relative contributions of multiple causal factors (or drivers) to a change. Note that this slightly differs from the usual definition of attribution used in the IPCC AR5 (Hegerl et al., 2010; Box 3.1). In particular, the preliminary detection step is not required to perform attribution since causal factors may also include drivers of internal variability, such as the AMV or PDV among many others, in addition to external natural and anthropogenic forcing. Indeed, to understand changes in climate and attribute cause at the regional scale it is also vital to consider internal variability that might be considered as a noise problem at global scale. In order to make this distinction clear, the term regional-scale (or process-based) attribution will be used in this section.

Importantly, regional-scale attribution also seeks to determine the physical processes and uncertainties involved in the driver's influence. Therefore, this section expands on the detection and attribution work of Chapter 3 by focusing on regional-scale changes arising from both internal variability and external forcing drivers.

Firstly, in Section 10.4.2.1, recent methodologies in the attribution of regional climate change and links to drivers of climate change at the global and regional scale as outlined in Section 10.1.4 are assessed. Next, in Section 10.4.2.2 a series of case studies in which the attribution of regional climate changes in the historical period involves the interplay between the action of large- and local-scale anthropogenic drivers and internal variability are assessed.

### *10.4.2.1 Recent methodologies for regional climate change attribution*

Several emerging methodologies have been increasingly used for regional climate change attribution. These include two statistical approaches, namely, dynamical adjustment techniques and Ensemble Empirical Mode Decomposition (EEMD), and dynamical model-based perturbed parameter model ensembles (or Perturbed Physics Ensembles, PPEs).

The dynamical adjustment method (Deser et al., 2016b; Smoliak et al., 2015) seeks to isolate changes in Surface Air Temperature (SAT) or precipitation that are due purely to atmospheric circulation changes. The residual can then be analysed and attributed to internal changes in both land or ocean surface conditions and the thermodynamical response to external forcing. Smoliak et al. (2015) performed their dynamical adjustment using partial least squares regression of SAT to remove variations arising from Sea-Level Pressure (SLP) changes. Deser et al. (2016) use SLP-based constructed circulation analogues and resampling to estimate the dynamical contribution to changes in SAT. Removing SAT changes associated with circulation patterns allows a cleaner, simplified residual time series of the regional climate variable to be assessed, in order to more easily determine the influence of local and remote ocean and land internal drivers or external forcing agents. A key assumption underlying the dynamical adjustment method is that the total SAT signal is a linear superposition of a SAT change due to atmospheric circulation changes and a residual.

Dynamical adjustment methods have been used by for instance Deser et al. (2016) and O'Reilly et al. (2017). Deser et al. (2016) focused on the causes of observed and simulated trends in North American SAT from 1963 to 2012. A 30-member model ensemble was used, with differing initial states, to identify forced and internally generated components. They demonstrated that the main advantage of this technique is to narrow the spread of SAT trends found by the model ensemble and to bring the dynamically-adjusted observational trend much closer to the forced response estimated by the model ensemble mean. Similarly, O'Reilly et al. (2017) applied dynamical adjustment techniques to more carefully determine the influence of the AMV on continental climates. Variations in SAT and the AMV from 1901 to 2010 were measured, while three SLP datasets were used to construct the patterns of internal circulation variability. Over Europe, temperature anomalies induced thermodynamically by the warm phase of the AMV are further reinforced by circulation anomalies; meanwhile, precipitation signals are largely controlled by dynamical responses to the AMV.

EEMD techniques (e.g., Wilcox et al. (2013)) decompose data, such as time series of historical temperature and precipitation, into oscillatory modes of decreasing frequency (Intrinsic Mode Functions; IMFs). The EEMD thus assumes that the total signal is a linear superposition of independent IMFs. The EEMD last step leaves behind a residual time series with no further oscillations around zero. Typically, the nonlinear trend (e.g., of 20th-century temperature) can be reconstructed by summing the long-term mean, the residual and eventually the preceding IMF to account for a multidecadal forced signal. EEMD is an example of a data-driven, non-parametric approach that can be used to directly provide an estimate of the forced response without the need for model data. Lehner et al. (2018b) have employed EEMD directly on observations, together with dynamical adjustment and traditional model signal detection, designing a step-by-step attribution framework to tackle attribution of SAT and precipitation climate trends in the mid-to-high latitude regions.

A further regional attribution technique is that of PPE: the values of a selected set of model parameters are sampled from a distribution representing their uncertainty, with each ensemble member assigned a different set of parameters. Huang et al. (2018) used a PPE to attribute the drying trend of the Indian monsoon over the latter half of the 20th century to decadal forcing from the PDV (see detailed case study in Section 10.6.1). The PPE members predicted different trends in PDV behaviour across the 20th century and the negative precipitation trend was only replicated in those members with a strong negative-to-positive PDV transition across the 1970s, consistent with the observed PDV behaviour. In a similar manner, Cvijanovic et al. (2017) addressed the possible influence of Arctic sea-ice loss on the North Pacific pressure ridge and, consequently, on southwest USA precipitation. They used a coupled atmosphere-ocean mixed layer setup, rather than the fully coupled set up of Huang et al. (2018). They sampled the uncertainties in selected sea-ice physics parameters (varying parameters within a realistic range) to achieve a "low Arctic sea-ice" state in their perturbed simulations. They then compared the latter with control simulations representative of sea-ice conditions at the end of the 20th century to assess changes purely due to sea-ice loss.

### *10.4.2.2 Regional climate change attribution case studies*

#### *10.4.2.2.1 The Sahel and the West African monsoon drought and recovery*

In this case study the drivers of the long-term drought in the West African monsoon and wider Sahel region are assessed, spanning the decades from the 1950s leading up to the 1990s, in which annual rainfall fell between 20 and 30% (Hulme, 2001). In the assessment the subsequent recovery of these rains is also explained (Figure 10.16).

**[START FIGURE 10.16 HERE]**

**Figure 10.16:** [Placeholder: Schematic diagram illustrating the main drivers of West African monsoon/Sahel rainfall demise and recovery across the 20th century historical period and under future RCPs in the 21st century. The Sahel domain used in the time series is as in Figure 10.15].

**[END FIGURE 10.16 HERE]**

The West African (10°N–20°N, 10°W–20°E) monsoon from 1950 to the present has experienced some of the most severe multi-decadal rainfall variations in the world, including excessive rainfall in the 1950s–1960s, followed by two decades of deficient rainfall, leading to a large negative trend until the mid-to-late 1980s. Recently, there has been a partial recovery of annual rainfall amounts, more significant over the central rather than the western Sahel from August to October (Lebel and Ali, 2009; Sanogo et al., 2015; Maidment et al., 2015). The current period is also characterized by fewer rainy days with a rise in extreme rainfall occurrence, suggesting an intensification of the hydrological cycle (Giannini et al., 2013; Panthou et al., 2014). In a study of rain gauge data over the Sahel (11°N–18°N; 20°W–10°E) since 1950, Panthou et al. (2018) also demonstrated trends towards longer dry spells and greater rainfall intensity or higher frequency of heavy rains. This study was supported by further sub-hourly rainfall records from an observatory in Niger since 1990, in which annual maximum rainfall intensities at these sub-hourly time scales are found to have increased by 2–6% per decade. These distinct changes in different aspects of precipitation suggest a greater complexity than merely a modulation of mean rainfall over several decades. The following assessment covers the role of greenhouse gas and aerosol emissions as well as SST variability in different ocean basins on these changes in West African monsoon and Sahel precipitation.

First, the impact of the different ocean basin SSTs on the West African Monsoon (WAM) is assessed. Nicholson (2013) reviewed studies highlighting the importance of competing mechanisms from equatorial Atlantic SSTs and interhemispheric SST gradients in regulating interannual and decadal variability of the Sahel. Rodríguez-Fonseca et al. (2015) reviewed evidence determining that on interannual time scales, warming across the tropical oceans results in reduced rainfall over the Sahel, while positive SST anomalies over the Mediterranean Sea tend to be associated with increased rainfall. Similarly, at decadal time scales,

warming over the tropics leads to Sahel drought, whereas North Atlantic warming promotes increased rainfall.

Several papers have formalised the SST influence on the WAM in the framework of the AMV. Martin et al. (2014), Martin and Thorncroft (2014) and (Park et al., 2015b) suggested that changes in the SST gradient between the tropics and extratropical Atlantic increased the Northern Hemisphere differential warming and in turn drive Sahel rainfall. This suggested influence of AMV on the WAM has been supported by predictability studies: results from CMIP5 and experiments specifically designed for predictability studies (Gaetani and Mohino, 2013; Mohino et al., 2016; Sheen et al., 2017) showed that initialized decadal hindcasts outperform empirical predictions based on persistence at longer lead times (some skill is also attributed to a non-negligible contribution from external radiative forcing), supporting the key role of SST influence.

The influence of PDV has also been studied but to a lesser extent. Based on a correlation/regression analysis of observations and CMIP5 models, Villamayor and Mohino (2015) suggested that the positive phase of the PDV has a negative impact on Sahel rainfall anomalies regardless of changes induced by anthropogenic forcing.

Other studies have highlighted the role of anthropogenic forcings in addition to variations caused by internal modes of climate variability. For instance, anthropogenic aerosols have been shown to play an important role in modulating temperature and precipitation over Africa. Based on HadGEM2-ES simulations, Dong et al. (2014) studied the impacts of European and Asian anthropogenic sulphur dioxide emissions on boreal summer Sahel rainfall. European emissions lead to an increase in shortwave scattering by increased sulphate burden, leading to a decrease in surface downward shortwave radiation and thus surface cooling over North Africa. This weakens the Saharan heat low and Sahel precipitation. Asian emissions lead to smaller change in sulphate burden over North Africa, but they induce an adjustment of the Walker circulation, which leads again to a weakening of the WAM and a decrease in Sahel precipitation.

The effects of anthropogenic emissions may also be acting at the hemispheric scale. Based on a coupled atmosphere-slab ocean model and following Biasutti and Giannini (2006), Ackerley et al. (2011) have shown that increases in GHG cause an increase in precipitation in the Northern Hemisphere and particularly the Sahel while increases in aerosol loading cause a reduction in Sahel rainfall. They suggested that the mechanism relies upon a hemispheric asymmetry in temperature change that in turn leads to a shift in ITCZ position. Ackerley et al. (2011) further supported their hypothesis by comparing very large perturbed physics ensembles of all-historical forcings and altered aerosols in a coupled GCM. They concluded that aerosol changes are the main driver of observed drying over 1950–1980. This is consistent with the findings of Polson et al. (2014) who used CMIP5 aerosol and greenhouse gas single-forcing experiments to show that aerosol emissions, which are much more widespread in the Northern Hemisphere, have led to declining rainfall across the Northern Hemisphere monsoons, including in the Sahel. Likewise, noting that the southward shift of the ITCZ happens at a similar time in CMIP3 and CMIP5 historical simulations and therefore should have an anthropogenic influence, Hwang et al. (2013) used an atmospheric energetics approach to attribute the southward shift of precipitation to anthropogenic aerosol cooling the Northern Hemisphere.

An important question concerns the causes of the recovery in WAM and Sahel rainfall since the late 1980s. Atmospheric internal variability possibly plays a role in determining the trend magnitude. Five AGCM simulations forced with observed SSTs in the atmospheric component of the IPSL-CM5A-LR model predicted a Sahel rainfall recovery from the 1980s–2000s with a large spread, ranging from +6% to +21% (Roehrig et al., 2013a). A detection study based on three reanalyses (Cook and Vizy, 2015) suggests that the recent recovery in Sahel rainfall is concomitant with the increase of Sahara surface temperature, which is 2–4 times greater than that of tropical-mean temperature (the warmer Sahara drives a stronger thermal low and more intense monsoon flow, enhancing convection over the central and eastern Sahel while it weakens over the western Sahel). The temperature increase in the Saharan heat low over the last 30 years was forced by anomalous night time longwave heating of the surface by water vapour (Evan et al., 2015). Such a result is also represented by the ensemble mean of 15 CMIP5 models (Lavaysse et al., 2016), although not all models

are able to simulate a rainfall-heat low regression pattern as in observations. Vizy and Cook (2017) confirmed the amplified Saharan warming trend in multiple observational and reanalysis products, determining the maximum warming to occur from July to October. A positive feedback process was suggested whereby enhanced Sahara warming draws in more moisture towards the Sahel, cooling the surface, enhancing the meridional temperature gradient and further intensifying the West African monsoon. In related work, Taylor et al. (2017) attributed change to a slightly different mechanism, the frequency of extreme Sahelian storms (mesoscale convective systems) which have tripled since 1982 in satellite observations. While this increase in storms was only weakly correlated to the recovery of Sahel rainfall, it was attributed to the increase in global land temperatures and the increased temperature gradient southward from the Sahara, increasing the wind shear.

Recent work also suggests a prominent influence of the Mediterranean Sea on the WAM recovery. Park et al. (2016) analysed observational and multi-model datasets and conducted SST-sensitivity experiments with two AGCMs and argue that the key area causing the recent Sahel recovery is the Mediterranean Sea. They suggested that anthropogenic warming of the Mediterranean Sea is the key driver of the WAM recovery, in contrast with the late-20th century Sahel drought which was primarily driven by the tropical Atlantic and Indo-Pacific Oceans. Enhanced evaporation and moist air advection from the Mediterranean southward into the Sahel yield enhanced low-level moisture convergence and increased rainfall. However, the AGCM nature of the study by construction could not identify whether the Mediterranean Sea SST warming is caused by external forcing or if internal factors have also contributed.

Advancing on this, Dong and Sutton (2015) suggested that higher atmospheric concentrations of GHG and the associated direct radiative heating leading to an increase in atmospheric temperature were primarily responsible for the Sahel rainfall recovery. Using the HadGEM3-A AGCM, they simulated climate changes over 1964–2011 under different idealized conditions and investigated the roles of global SST, GHG and atmospheric aerosol in the recovery. They suggested that the GHG direct radiative influence is the main cause of Sahel rainfall recovery, with an additional role for changes in anthropogenic aerosol precursor emissions. They also found that recent changes in SSTs, although substantial, did not seem to have a significant impact on the recovery, and that rainfall is likely to be sustained or amplified in the near-term future.

Giannini and Kaplan (2018) determined that since the CMIP5 multi-model mean over the historical period largely follows observations of the decline and recovery in Sahel rainfall (10°N–20°N; 20°W–40°E), then there must be an externally forced driver. They attempted to unify the above mechanisms based on a singular value decomposition of observed and modelled SSTs, themselves forced by a combination of changing anthropogenic aerosol and greenhouse gas emissions. Using the resulting singular vectors as predictors in a bivariate regression of Sahel rainfall, they demonstrated the mapping of the GHG-forced SST pattern onto the combined sum of tropical oceans and North Atlantic SSTs, while the anthropogenic aerosol pattern projected onto cooling in the North Atlantic. Thus, since the 1950s, tropical warming arising from GHG and North Atlantic cooling from aerosol led to regional stabilization, suppressing Sahel rainfall. The subsequent reduction in regional aerosol emissions led to warming in the North Atlantic, and a recovery in the Sahel.

There is *very high confidence* that patterns of 20th century SST variability have caused the Sahel drought and subsequent recovery, and that Saharan warming was a key process in the recovery. There is *high confidence* that the patterns of SST variability are themselves driven by anthropogenic emissions: warming in the tropics and subsequently in the North Atlantic by greenhouse gas emissions; the cooling and subsequent warming of the North Atlantic by emissions of anthropogenic sulphate aerosols and their eventual removal. There is *very high confidence*, aligned with previous reports, that the character of rainfall is changing in the warming world to one of more intense rain events and increased frequency of heavy rainfall.

#### *10.4.2.2.2 The East Asia summer monsoon weakening*

Since the late 1970s, the East Asian Summer Monsoon (EASM) has exhibited a considerable weakening trend, including southward shift of the main rain belt, known as the Southern Flooding and Northern Drought

(SFND) pattern. The major features of the weakened EASM are as follows (Figure 10.17): weakening of the southerly flow, a cooling trend of tropospheric temperature in East Asia, westward extension of the western North Pacific subtropical high (WPSH), zonal expansion of the South Asia high, and a weakening of the land-sea thermal contrast across the East Asian continent and adjacent marginal seas (Hsu et al., 2014). Changes in the EASM have been significantly affected by a range of natural factors including land and oceanic thermal conditions (Zhang, 2015a) and the associated atmospheric teleconnections (Wang et al., 2017b). Recently a few studies have suggested a recovery in the strength of the EASM circulation since the 2000s (Kwon et al., 2007; Zhou et al., 2017; Zhu et al., 2018).

**[START FIGURE 10.17 HERE]**

**Figure 10.17:** [Placeholder: Schematic diagram illustrating main contributing drivers on the decadal change (weakening and recovery) of the East Asia Summer Monsoon (EASM) since the 1970s. The time series shown is the difference of the mean summer (JJA) precipitation (PR) between two regions: PR (110°E–125°E, 35°N–45°N) – PR (105°E–125°E, 20°N–35°N).]

**[END FIGURE 10.17 HERE]**

Among various contributing factors, inter-decadal changes of SST in different ocean basins play an important role in weakening tendency of the EASM since the late 1970s. Several studies have shown that the EASM weakening is accompanied by inter-decadal changes of Pacific SST that shows warming in the tropical central and eastern Pacific but cooling in the central North Pacific, which is similar to the positive phase of the PDV (Ding et al., 2009; Li et al., 2010; Wu et al., 2016c; Zhou et al., 2017). Li et al. (2010) showed that climate models forced with SSTs representing the positive phase of PDV can reasonably reproduce the observed EASM weakening. The proposed mechanisms are the reduced large-scale land-sea thermal contrast (Li et al., 2010) and the Pacific-Japan/East-Asian-Pacific-like atmospheric teleconnection pattern, which develops locally in response to the PDV-associated warm SST anomalies (Qian and Zhou, 2014). The impact of PDV on inter-decadal EASM changes is also noted by the recent recovery of EASM circulation in association with the phase transition of PDV from positive to negative (Zhou et al., 2017). The decadal predictability of East Asian rainfall is found to be influenced by Pacific SST (Li and Wang, 2018). In addition to the influence of PDV, the warming in the tropical Indian Ocean also has been found to be influential on the weakening of EASM (Ding et al., 2009; Yang and Lau, 2004). However, Fu and Li (2013) revealed that SSTs in the tropical Pacific Ocean exert a more significant influence on the EASM compared with those in the Indian Ocean. Several studies have pointed out the influence of AMV on EASM through the circum-global teleconnection pattern propagating from the North Atlantic through the westerly jet (Wu et al., 2016a, 2016b; Zuo et al., 2013). It has contributed to the strong summertime warming in Northeast Asia occurring in the mid-1990s (Monerie et al., 2018) and increase of precipitation over the Huaihe-Huanghe valley since the late 1990s (Li et al., 2017c).

Previous studies have pointed out that the thermal forcing over the Tibetan Plateau during the preceding winter and spring associated with snow cover and sensible heating also plays a considerable role in regulating the EASM (Ding et al., 2009; Duan et al., 2013). In fact, historical records show an abrupt increase in snow cover and related decrease in sensible heat flux in winter and spring over the Tibetan Plateau since around 1977. Analyses using observational data and numerical simulations revealed that the reduction in sensible heat flux is also likely responsible for the weakening of the EASM by cooling the Tibetan Plateau and its overlying atmosphere (Duan et al., 2013). Based on observational data, Ding et al. (2009) also pointed out the importance of increased snow cover over the Tibetan plateau in conjunction with warming of SST over the tropical eastern and central Pacific in affecting weakening of EASM through a reduced land-sea thermal contrast. Supporting the mechanism, Si and Ding (2013) clearly showed an interannual correlation between Tibetan Plateau winter snow amount and East Asia precipitation amount, between 1979 and 2011.

Anthropogenic factors such as GHGs and aerosols may also have an influence on the EASM (Song et al., 2014; Tian et al., 2018; Zhou et al., 2017). Wang et al. (2013) explained the effect of GHGs on the EASM

via two pathways using a coupled general circulation model and multi-ensemble simulations. On one hand, GHGs induce notable Indian Ocean warming that causes a westward shift of the WPSH and southward displacement of the upper tropospheric East Asia westerly jet, leading to increased precipitation in the Yangtze River valley. On the other hand, the surface cooling effects of anthropogenic aerosols in eastern China and evaporative cooling from stronger convection in the Yangtze River valley, lead to a reduced land-sea thermal contrast, which results in weakening of the EASM circulation and hence a drier climate in northern China. Recent papers have argued that GHG and aerosol forcing have different contributions to different parts of the SFND pattern. Changes in GHGs lead to increasing precipitation over southern China, whilst changes in anthropogenic aerosols over East Asia are the dominant factors determining drought conditions over northern China. The increase in anthropogenic aerosols may result in weakening of the EASM circulation (Jiang et al., 2013; Wang et al., 2015a, 2017c; Xie et al., 2016). Song et al. (2014) revealed that aerosol forcing in CMIP5 simulations reasonably reproduces the observed weakening trend of low-level EASM circulation due to the surface cooling effect of aerosol reducing land-sea thermal contrast. Apart from local aerosol emissions, Dong et al. (2016) suggested that the increases in remote emissions over Europe likely contribute to cooling of East Asia and a weakening of the EASM. Zhao and Wu (2017) suggested Land Use and Land Cover (LULC) change as another possible driver of EASM weakening, using an RCM simulation. The roughness changes associated with LULC changes over China between the 1980s and 2010s led to a strengthening of the SFND pattern during the monsoon withdrawal. However, the magnitude of the EASM weakening under anthropogenic forcing alone (i.e., GHGs and aerosols) is much weaker than in the observations. This discrepancy suggests that internal variability may play a major role in monsoon weakening with aerosol and GHG forcing playing a secondary role (Li et al., 2010; Zhou et al., 2017). It should also be noted that the simulated changes in the EASM may largely depend on the sensitivity of the models to GHGs and aerosols and thus the role of anthropogenic factors on EASM change remains uncertain (Zhang, 2015b).

There is *high confidence* that anthropogenic forcing has been influencing historical EASM changes but there is *low confidence* in the magnitude of anthropogenic influence on historical changes in the EASM. There is *high confidence* that the transition towards a positive PDV phase has been one of the main drivers of the EASM weakening since the 1970s.

#### *10.4.2.2.3 The Southern Australian rainfall decline*

In this case study, the drivers of the climate trends across southern Australia in recent decades (Figure 10.18) are assessed, extending the assessment in AR5 (Christensen et al., 2019). A recent review summarises much of the new research (Dey et al., 2019). New research since AR5 reveals nuances in the processes driving the observed changes. On average, southern Australian average annual rainfall totals continue to trend downward, and temperatures are rising in step with many land regions world-wide.

**[START FIGURE 10.18 HERE]**

**Figure 10.18:** [Placeholder Top) schematic showing the main drivers that can influence southern Australia's rainfall; their effect can vary strongly with season. Bottom) Trend in annual rainfall from 1970 to 2018 shows a decline in the far south-west and the whole east coast.]

**[END FIGURE 10.18 HERE]**

Southern Australia has a moderate climate, generally cooler in the south and with average seasonal temperatures ranging up to 33°C in the north of the region in summer and 18°C in winter. Frost occurs in the cooler seasons and there is seasonal snow on the mountains. The westward facing regions of the mainland have a Mediterranean climate with wet winters and very dry summers. The annual average rainfall in the southwest exceeds 600 mm. Inland from this region, annual average rainfall drops to less than 200 mm, and this region of very low annual rainfall extends across the south. In the southeast the annual average rainfall is also above 600 mm and has a reasonably even seasonal cycle, aside from the westward-facing regions that

have higher rainfall totals in winter. There are mountainous regions in the southeast that generally receive more precipitation (including snow) than the surrounding plains (Pepler et al., 2017).

The southwest was known for its reliable rain, and rainfall is generally brought by fronts and cut-off lows (Hope et al., 2014; Pook et al., 2012). Large-scale climate drivers such as ENSO have some influence in the region, but these associations are strongly modulated by their dynamical links with the SAM, (e.g. Lim and Hendon (2015)). Given southern Australia's latitudinal location on the equatorward edge of the mid-latitude storm track, the region can be very sensitive to shifts in the storm track.

In the south-east, rainfall is also associated with fronts and lows, including intense 'east coast lows', that can bring a great deal of rainfall (Pepler et al., 2013). Thunderstorm activity is also important for rainfall in the east of the region (Dowdy and Catto, 2017). ENSO and the Indian Ocean Dipole (IOD) play an important role in driving interannual rainfall variability (Risbey et al., 2009), again modulated by interactions with SAM (Hendon et al., 2014b). Rainfall and temperature are intimately linked in these locations (e.g., Hope and Watterson (2018)). The Antarctic polar vortex has also been found to influence temperatures across southern Australia (Lim et al., 2018), and accounting for this component of the climate systems has clarified the linkage between ENSO and SAM.

Maximum daily average temperatures have increased in both the cool (from May to October) and warm (from November to April) half-years by about 1.1°C from 1900 to 2018 in south-eastern Australia (south of 33°S, east of 135°E), and slightly more in southwestern Australia (the land southwest of the line joining 30°S – 115°E and 35°S –120°E) as measured by the Australian Climate Observations Reference Network-Surface Air Temperature (Trewin, 2013). Individual broad-scale month-long heat events have also been attributed to increasing levels of atmospheric GHGs (Black et al., 2015; Hope et al., 2016).

Across southern Australia there has been a downward trend in rainfall since widespread, reliable records began in 1900. In the southwest, this was seen as a downward shift in the late 1960s, with an absence of 'very wet' winters, resulting in a decline in average annual rainfall of 11% (from 1970 to 2018 compared to 1900 to 1969) (Hope et al., 2006, 2015). Since 1970, the downward trend in rainfall has continued in both the southwest and southeast.

Coupled climate model historical simulations and projections agree that anthropogenic forcing will drive the region to drier conditions during the cool season (Christensen et al., 2013), generally believed to be associated with a contraction of the storm track around Antarctica and the SAM shifting to a more positive phase (Cai et al., 2014). Related to the rainfall decline, and supporting the hypothesis of a shift to positive SAM, there has been a significant increase in pressure across southern Australia (Hope et al., 2015), with reduced baroclinicity (Frederiksen et al., 2017) and an increase in the number of high pressure systems (Pepler et al., 2018). These factors combine to suggest that the rainfall decline is an anthropogenically forced response.

In the south-east, there have been significant drought periods (Freund et al., 2017; Gergis et al., 2012), but there has also been a consistent downward trend in rainfall. Rainfall has been generally low since the start of the Millennium drought in 1997, interspersed with two wet spring/summer periods (2010–2011 and 2016–2017) associated with strong La Niña events. The influence of anthropogenic forcing on the rainfall changes in the southeast is complex because of the varying influences on the relevant large-scale drivers, and climate models can give mixed results (Cai et al., 2014; Chiew et al., 2011). The trends in different seasons provide insight into the drivers, as influences from the higher latitudes are important in winter while tropical drivers and their interactions are more important in the warm season. For instance, the rainfall response to the positive phase of SAM varies strongly by season in this region (Hendon et al., 2007; Hope et al., 2017). The rainfall changes in the southeast align with those in the southwest on a range of timescales (Hope et al., 2010), suggesting the shifts to a more positive SAM are also important for rainfall trends in the southeast.

The difference in response between the warm and cool seasons is amplified in trends in the mountainous regions of the southeast. Grose et al. (2019) found a seasonally enhanced rainfall decrease on the windward slopes in the cool season and a rainfall increase over peaks in summer due to an increase in convective

rainfall (also found by Giorgi et al. (2016) in the European Alps).

In 2016, two attribution studies found minimal influence from anthropogenic forcing to the record high spring rainfall in the southeast (Hope et al., 2018). However, it was also found that the interaction between La Niña and a high-magnitude SAM was amplified by the global observed SST trends (Lim et al., 2016a), that likely have a component of anthropogenic climate change in them. It is also entirely plausible that a seasonal rainfall extreme event might be influenced by anthropogenic forcing (Guerreiro et al., 2018), even in the presence of a background trend towards less mean rainfall.

There is *high confidence* that both southern Australia warming and rainfall decline since the early 1970s are for the most part anthropogenically forced.

*10.4.2.2.4 The Southeastern South America summer wetting*

One of few regions where a robust positive trend in precipitation (Figure 10.19) has been detected since the beginning of the 20th century is South Eastern South America (SESA). SESA is the most densely populated and agriculturally productive area of South America and has several large cities. The positive rainfall trend, which has been particularly strong since the 1960s, has enabled expansion of agriculture into semi-arid areas and has increased crop yields in Argentina (Barros et al., 2015). On the other hand, large parts of the agricultural regions in the Argentinean Pampas in the southern SESA are naturally flood-prone due to the flat topography and poor drainage (Kuppel et al., 2015), which has possibly been aggravated by agricultural expansion and has led to increased water input and rising water tables (Viglizzo et al., 2009; Viglizzo and Frank, 2006). The main rivers of the la Plata Basin in central-northern SESA have increased their mean flows and extreme discharges since the 1970s (Barros et al., 2004, 2015). While in the upper basin this is mainly due to heavy deforestation, in the southern basin it is mainly due to the increase of precipitation (Barros et al., 2015; Saurral et al., 2008). Urban and agricultural expansion together with increased extreme precipitation has led to higher risks for human systems and ecosystems associated with floods from the early 1980s (Barros et al., 2015).

**[START FIGURE 10.19 HERE]**

**Figure 10.19:** [Placeholder a) Austral summer (DJF) precipitation anomaly over SESA (25°S–40°S, 65°W–45°W) from 1920 to 2017 b) Mechanisms that have been suggested to contribute to SESA summer wetting since the beginning of the 20th century.]

**[END FIGURE 10.19 HERE]**

The dominant contribution to the positive annual mean precipitation trend is due to an increase in summer (DJF) precipitation (Díaz and Vera, 2017; Gonzalez et al., 2014; Saurral et al., 2017; Vera and Díaz, 2015), which reached 7 mm per decade in the core region of SESA (Vera and Díaz, 2015) during the period between 1901 and 2005, with respect to a mean DJF precipitation for the whole period of around 380 mm (Gonzalez et al., 2014). The trend is also detectable in daily and monthly extremes (Donat et al., 2013; Doyle et al., 2011; Lorenz et al., 2016; Marengo et al., 2010; Penalba and Robledo, 2010; Re and Barros, 2009).

Using observations and two SST-forced AGCM 16-member ensembles spanning 1901–2007, Seager et al. (2010) estimated that global SSTs are responsible for 40% of the total variability of SESA precipitation. They found *little evidence* that anthropogenic radiative forcing had been an important driver since their ensemble mean of 23 CMIP3 models showed a much weaker trend than observed. Based on an ensemble of season-length model experiments designed to test how SESA precipitation is modulated by tropical Atlantic SSTs, they showed that cold anomalies in the tropical Atlantic favoured wetter conditions by inducing an upper-tropospheric flow towards the equator, which, via advection of vorticity, led to ascending motion over SESA. They concluded that a large part of the wetting trend from the mid-20th century was forced by cooling of the tropical Atlantic resulting from the AMV cold phase (Seager et al., 2010). Monerie et al.

(2019) supported this argument showing the negative relationship between SESA precipitation and the AMV index (Huang et al., 2015a). The idealized AMV warming experiments in (Monerie et al., 2019) also supported the results by Seager et al. (2010) in that the mechanism for AMV control on SESA precipitation is associated with the tropical Atlantic part of the AMV pattern.

However, in contrast to these findings, other studies have attributed the positive precipitation trend to anthropogenic GHG emissions. Using CMIP5 historical simulations, Vera and Díaz (2015) and Díaz and Vera (2017) concluded that climate simulations forced only by natural drivers differed significantly from those forced only with GHG, and that the former lacked the positive rainfall trend. Díaz and Vera (2017) used a subset of CMIP5 historical simulations that best simulate a rainfall dipole with anomalies of opposite sign over SESA and eastern Brazil and showed that the trend since the 1950s is related to changes in rainfall characteristics, favouring the wet phase over SESA. Zhang et al. (2016) also attributed SESA wetting to anthropogenic GHG emissions by conducting a suite of experiments with two high-resolution coupled GCMs. The authors cited a mechanism in which the radiative forcing drives an expansion of the Hadley cell, so that its descending branch moves poleward from SESA, generating anomalous ascending motion and precipitation.

On the other hand, González et al. (2014), using both coupled and atmosphere-only GCMs, found that the positive precipitation trend can be partially explained by the depletion of stratospheric ozone, but not by GHGs; this was confirmed irrespective of the stratosphere vertical resolution. In experiments in which ozone depletion is specified, SESA precipitation is found to increase, while if only GHG forcing is used instead, only small or even negative SESA precipitation signals are found over the 1960–1999 period, with greater model spread. In agreement with these findings, Wu and Polvani (2017) used a subset of the Community Earth System Model Large Ensemble (CESM-LE) in single-forcing experiments to show that the observed trends in precipitation extremes in SESA could be attributed to stratospheric ozone depletion. The depletion causes a southward shift of the jet stream, leading to more intense cyclonic activity over SESA.

Contrary to these two studies, Zhang et al. (2016) found that the positive precipitation trend was not reproducible when forcing two coupled GCMs with observed trends in ozone, all other forcing excluded. However, the authors recognised that their models have a weaker dynamical response to stratospheric ozone than others (Gonzalez et al., 2014; Kang et al., 2011; Polvani et al., 2011). The discrepancy could also be due to different ozone forcing specification: Zhang et al. (2016) used prescribed observed ozone, while Wu and Polvani ( 2017) used ozone concentrations that are calculated within the model; alternatively, the discrepancy may relate to the comparison of different time periods (Wu and Polvani, 2017).

Summarising, the SESA summer precipitation increase during the 20th century and beginning of the 21st has been attributed to the cold phase of the AMV, to increased anthropogenic radiative forcing from GHGs and to stratospheric ozone depletion. Some of the studies that have addressed the cause of the SESA wetting only examined one of these forcings and therefore do not exclude the possible impact of the others (e.g. Díaz and Vera, 2017; Vera and Díaz, 2015), while other studies (e.g. González et al., 2014; Seager et al., 2010; Wu and Polvani, 2017; Zhang et al., 2016) examined two forcings and found that only one of them caused the positive precipitation trend. Therefore there is *medium evidence but low agreement* as to why SESA summer precipitation has increased since the beginning of the 20th century.

#### *10.4.2.2.5 The Central and Eastern Eurasia winter cooling*

Central and Eastern Eurasia is characterized by a wide range of climatic conditions, including subarctic, humid continental, semi-arid and desert climates. It hosts a wide variety of the Earth's biomes from taiga and tundra in the north, down to steppe and desert in the south. It also includes 70% of the Earth's boreal forest and roughly two thirds of the permafrost (Groisman et al., 2009).

A key example of mid-latitude regional climate change across the historical period is the winter Central and Eastern Eurasia land cooling of the late-20th century until around 2014 (Figure 10.20). This recent cooling episode disrupted the warming trend that started in the early 1970s (Figure 10.15) and is in striking contrast to the concurrent Arctic amplification (the propensity for greater surface warming in the Arctic region than at

other latitudes) and sea-ice decline. The occurrence of this dipolar SAT anomalous pattern has been termed the Warm Arctic Cold Eurasia (or Siberia, WACE/WACS) pattern (Inoue et al. 2012; Mori et al. 2014) and is the second EOF mode of mid-to-high latitude Eurasian winter SAT variability (Sorokina et al., 2016).

**[START FIGURE 10.20 HERE]**

**Figure 10.20:** [Placeholder: Attribution of boreal winter (JFM) cooling in Eurasian: surface air temperature (SAT, shading) and sea level pressure (SLP, contours every 1hPa yr-1 interval) 2002-2013 linear trends in °C 12yr-1 and hPa 12yr-1, respectively. a) Observed raw SAT and SLP data b) SAT changes purely due to changes in atmospheric circulation (through dynamical adjustment) and reconstructed SLP based on best analogues c) SAT thermodynamic residual (a)-(b). Bottom row: influence of tropical Pacific changes as simulated by two pacemaker ensembles based on the CESM1 and GFDL-CM2.1 models; the response to anthropogenic and natural forcing has been subtracted from the pacemaker ensemble means based on the ensemble means of large ensembles of historical simulations performed with the two models. The figure will be adapted for the SOD to show other possible influences (for instance from Arctic sea-ice and anthropogenic drivers based on CMIP6 simulations).]

**[END FIGURE 10.20 HERE]**

The winter Eurasia cooling has made an important contribution to the 1998–2012 hiatus in global mean surface temperature (GMST) (Cohen et al., 2012b; Deser et al., 2017a; Li et al., 2015a). Li et al. (2015) used five observational datasets to show that the Eurasian winter cooling trend from 1998 to 2012 dominated the global warming hiatus in terms of a latitudinal contribution. Deser et al. (2017a) showed that Eurasian cooling represented about 70% of the winter SAT hiatus in both observations and a close model analogue drawn from eastern Pacific SST partial coupling experiments (Section 10.3.2.4). The recent winter Eurasian cooling is also related to the re-amplification of the East Asian Winter Monsoon (EAWM) in the mid 2000s (Wang and Chen, 2014).

Eurasia SAT cold anomalies are tightly coupled to recurrent and/or persistent anticyclonic sea level pressure anomalies corresponding to intensification of the surface Siberian High (Gong et al., 2018; Luo et al., 2017). Attribution of the Eurasian cooling is then closely related to attribution of the recent increase in Eurasian blocking (Wang and Chen, 2014) and recovery of the Siberian High (Jeong et al., 2011).

Based on observed correlation/regression analysis and modelling sensitivity experiments, a number of studies since the AR5 have suggested that this anomalous circulation pattern is due to a remote influence of Arctic sea-ice loss, in particular in the Barents-Kara Seas (BKS) (Chen et al. 2016; Inoue et al. 2012; Kug et al. 2015; Mori et al. 2014, 2019; Tang et al. 2013). A first category of proposed mechanisms invokes a weaker meridional temperature gradient leading to weakened zonal winds and reduced Atlantic heat transport, altered cyclone pathways and a wavier atmospheric flow (Francis and Vavrus, 2015). An alternative mechanism suggests an amplification of the Siberian High by a stationary Rossby wave train triggered by anomalous heat fluxes (enhanced ocean heat loss) due to sea-ice retreat. Based on simulations with a single AGCM with a well resolved stratosphere, Zhang et al. (2018) suggested that the stratospheric response to sea ice forcing is crucial in the development of cold conditions over Siberia, indicating the dominant role of the stratospheric pathway. In particular, the downward influence of the stratospheric circulation anomaly significantly intensifies the ridge near the Ural Mountains and the trough over East Asia. The persistently intensified ridge and trough favour more frequent cold air outbreaks and colder winters over Siberia.

Mori et al (2014) studied the repeating severe winters of mid-latitude Eurasia that have occurred despite ongoing anthropogenic warming. In a model assessment, they found no robust atmospheric response (by looking at the Arctic Oscillation) to declining sea ice. Instead, they used a 100-member AGCM ensemble to demonstrate a doubled likelihood of extreme winters in central Eurasia given the loss of ice and due to more frequent Eurasian blocking episodes. Likewise, Kug et al. (2015) used single-model coupled simulations with SST-restoring at northern latitudes to constrain sea-ice loss over the Arctic during the 1980–2013 period. They found that the model response reproduced the observed regression pattern between a BKS sea-

ice concentration (SIC) index as well as SAT and sea level pressure over East Eurasia. Mori et al. (2019) applied maximum covariance analysis to detrended winter SAT from observations combined with a multi-model ensemble of AMIP simulations in order to extract the forced response due to observed SST and SIC changes. They then used single-model sensitivity experiments to assess the relative roles of SST and SIC. Their results suggested that BKS ice loss can explain a substantial fraction (44%) of the 1995–2014 central Eurasia cooling and that atmospheric models systematically underestimate sea-ice forced atmospheric variability. These results might be affected by the fact that the ocean and sea-ice conditions cannot respond to the sea-ice induced atmospheric changes.

In an alternative explanation, a series of observational and modelling studies have questioned whether there is *adequate evidence* that Arctic sea-ice loss can significantly influence atmospheric circulation, blocking, and Eurasian winter temperatures (Wallace et al. 2014). Woollings et al. (2014) found no agreement among a set of 12 CMIP5 models on a significant link at interannual time scales between Eurasian blocking and BKS temperature during both historical and future periods. Based on their set of forced AGCM experiments, Li et al. (2015) showed that Arctic sea-ice loss did not drive the associated regional circulation changes, which can instead be related to internal atmospheric variability. Similarly, both Peings and Magnusdottir (2014) and Screen et al. (2014) failed to detect a significant winter atmospheric circulation response over Eurasia to recent sea-ice loss based on large ensembles of sea-ice forced atmospheric simulations with three different AGCMs. Sun et al. (2016a) employed multi-model ensembles of forced and coupled simulations to show that the observed Eurasian cooling was the consequence of an extreme event of internal atmospheric decadal variability. McCusker et al. (2016) also considered the decreasing SAT over central Eurasia since around 1990 in the face of increased anthropogenic forcing and Arctic amplification. Their 600 years of AGCM simulations forced by different sea-ice loss patterns showed no evidence that Arctic sea-ice loss has led to the central Eurasian cooling. They also used a large ensemble of coupled historical simulations in which Eurasian cooling of the same magnitude as the observed one was found only in a single ensemble member. However, it was shown to be unrelated to BKS sea-ice loss. Hence they concluded that internal atmospheric variability is the cause of the Eurasia SAT decline, a view shared by Sorokina et al. (2016). The latter study investigated causality by looking at lead-lag relationships between BKS sea-ice and heat fluxes, and the WACE pattern on shorter daily, monthly and seasonal time scales in the ERA-Interim reanalysis. Findings showed that the WACE pattern was associated with a weak reduction in BKS ice and reduced BKS heat flux, suggesting that the WACE pattern might primarily be an expression of internal atmospheric variability that could largely determine the BKS sea-ice distribution. Finally, based on large initial-condition historical and pacemaker ensembles, Deser et al. (2017a) showed that internal variability driven by tropical Pacific SSTs and intrinsic atmospheric dynamics contributed almost equally to the dynamically-induced Eurasian cooling, largely offsetting the radiatively induced warming trend.

In an explanation focussing on the role of the tropics, Trenberth et al. (2014) have suggested that many of the regional circulation patterns associated with the 1999–2012 climate hiatus can be blamed on long-term forcing from central and east Pacific SSTs. They used an AGCM forced with the negative PDV-like SST forcing similar to that observed over the same period and demonstrated the excitation of teleconnections to the Atlantic and Northern Hemisphere high latitudes.

Another hypothesis suggested that BKS sea ice reduction may also be related to a larger teleconnection pattern associated with the position of the Gulf Stream in the northwest Atlantic (Sato et al., 2014). Northward shifts in the SST front associated with the Gulf Stream would generate a remote planetary wave response that could favour enhanced advection of warm air and wave energy into the BKS region (Liu et al., 2014a). The induced warming and sea-ice melt would then amplify the wave train, promoting the WACE pattern (Sato et al., 2014; Simmonds and Govekar, 2014).

Studies based on observations and reanalysis do find significant correlations between BKS sea-ice and mid-to-high latitude atmospheric circulation variability including Eurasian blocking. However, causality is challenging to prove because of the complexity of the mechanisms involved and the relatively few degrees of freedom given the shortness of the observed record (Overland, 2016; Overland et al., 2015; Wallace et al., 2014; Walsh, 2014). For instance, blocking over Eurasia might lead to warm southerly winds and moisture intrusions over the BKS region, which have been shown to play a major role in recent BKS SAT and SIC

changes due to the associated increase in downwelling longwave radiation (Park et al., 2015a; Woods et al., 2013; Woods and Caballero, 2016). Furthermore, statistical robustness of lead-lag correlation analysis based on high-frequency data is difficult to achieve due to the large persistence of BKS sea-ice anomalies and, in addition, results can be sensitive to the detrending methodology (Chen et al., 2016b).

Studies based on modelling experiments forced by SST and/or SICs boundary conditions do find an atmospheric response by design when using sufficient ensemble size and/or perturbation amplitude. The differing results and the *poor agreement* among all model studies based on uncoupled simulations may be due to multiple reasons in addition to model structural differences: opposing influence of regional patterns of sea-ice and SST forcing (Chen et al., 2016b) and non-additivity of the response (Sun et al., 2015), influence of season definition, non-linearity of the atmospheric response (Chen et al., 2016c), different and/or limited ensemble sizes (Screen et al., 2014). Further complicating the regional-scale attribution is the presence of tremendous internal variability in large-scale atmospheric circulation and complex three-way ocean-ice-atmosphere interactions in the Earth climate system. This may lead to conditional dependence of the BKS-WACE linkages on the large-scale circulation regime in addition to other remote tropical and mid-latitude influence (Overland, 2016; Wang et al., 2018b). Further discussion of Arctic-midlatitude linkages appears in the Cross-Chapter Box 10.1.

An emerging picture for the Arctic influence on Eurasian cooling is that of an episodic and regional influence that could conditionally amplify the temperature changes due to internal modes of atmospheric circulation. While there is *high confidence* that a significant (at least 50%) fraction of the Eurasian cooling has been caused by internal atmospheric variability, the persistent diversity of results and disagreement among them result in *low confidence* in the exact role and quantitative impact of Arctic warming and sea-ice loss on the recent Eurasian cooling.

#### *10.4.2.2.6 Western Europe summer warming*

Rapid European summer warming has occurred since around 1990 (Bador et al., 2016; Philipona et al., 2009; Ruckstuhl et al., 2008; van der Schrier et al., 2013; van Oldenborgh et al., 2009) at a rate of around 2.5 times the global mean temperature increase (van Oldenborgh et al., 2009) (Figure 10.21). This warming was largest in western and central Europe and in the Mediterranean. In the last two millennia of reconstructed observed temperature records for Europe, there has not been any 30-year period with summer temperatures exceeding those of the last three decades (Luterbacher et al., 2016), where record-breaking heat waves and extreme temperatures also occurred (Lehner et al., 2018; Russo et al., 2015).

**[START FIGURE 10.21 HERE]**

**Figure 10.21:** [Placeholder: The present plot is from the ENSEMBLES project, but should be made for different scenarios and based on CMIP6, HighResMIP, and CORDEX simulations] a) Historical warming (summer SAT 1950-2008 trend) over Europe relative to global mean warming (1 means European warming is equal to global mean warming). [Placeholder figure from Oldenborgh et al. 2008, will be updated for the SOD] b) Summer (JJA) European SAT change for historical period and future scenario.]

**[END FIGURE 10.21 HERE]**

Several mechanisms have been proposed for this warming, but their relative importance and possible interplays are not yet fully understood. Some studies (Besselaar et al. 2015; De Laat and Crok 2013; Dong et al. 2017; Philipona et al. 2009; Ruckstuhl et al. 2008) attributed this warming to the decrease of anthropogenic aerosols over Europe resulting from air pollution policies (Turnock et al., 2016). Also Turnock et al. (2015) and Zubler et al. (2011) found a brightening and increase of solar radiation over Europe. Pfeifroth et al. (2018) showed that this brightening is mainly due to cloud changes caused by the indirect aerosol effect with a minor role for the direct aerosol effect.

The evidence of other possible causes of the rapid warming, such as local feedbacks and atmospheric

circulation changes, is less robust. Soil moisture feedback has amplified the increase in summer temperatures in particular during drought spells (Brulebois et al., 2015; Miralles et al., 2014; Whan et al., 2015; Jaeger and Seneviratne, 2011; Seneviratne et al., 2010), which are related to unusual circulation regimes, in particular blocking patterns (Pfahl and Wernli, 2012; Pfahl, 2014; Horton et al., 2015; Brunner et al., 2017). However, according to Barnes et al. (2014), there is *no robust evidence* that the occurrence of blocking has changed during recent decades. Also Cahynová and Huth (2014) and Vautard and Yiou (2009) argued that European summer warming not associated with changes in the circulation and that local surface and radiative feedbacks are the main drivers.

Several studies have investigated the link between the AMV and European summer warming. Sutton and Dong (2012) argued that the AMV induced a shift around the 1990s towards warmer Southern European (and wetter Northern European) summers. Ghosh et al. (2017) linked the central and Eastern Europe warming to the AMV that showed a shift from its negative to its positive phase coinciding with the European warming trend. This mechanism is associated with a linear baroclinic atmospheric response to the AMV-related surface heat flux. Also O'Reilly et al. (2017) related warm European summer decades to the AMV, but the connectionwas shown to be mainly thermodynamic, whereas Peña-Ortiz et al. (2015) found a link between the length of European summers and multidecadal variability of the AMV.

Both GCMs and RCMs underestimate the observed trend (Lorenz and Jacob, 2010; Ceppi et al., 2012; Dosio, 2016a), indicating that essential processes are missing or that the natural variability is not correctly sampled (Dell'Aquila et al., 2018). Also temperature differences between the Medieval Warm Period, the recent period and the Little Ice Age are larger in the reconstructions than in the simulations (Luterbacher et al., 2016). With respect to missing essential processes, in particular the role of aerosols is discussed (Allen et al., 2013; Bartók, 2017), and the inability to simulate the observed trend is attributed to an underestimation of the anthropogenic aerosol effect in the CMIP protocols (Cherian et al., 2014). Nabat et al. (2014) argued that including realistic aerosol variations enables climate models to correctly reproduce the summer warming trend. However other studies showed models to be sensitive also to local effects, such as convection, microphysics and snow albedo effect (Ceppi et al., 2012; Vautard et al., 2013).

There is *medium confidence* that the decrease of anthropogenic aerosols over Europe has been the dominant factor for the enhanced European summer warming. There is *high confidence* that local feedbacks such as the soil-moisture feedback have contributed to the increase in extreme temperature variability and consequently, frequency and intensity of heat-waves and *medium confidence* that it has contributed to the increase of seasonal mean summer temperature. There is *low-to-medium confidence* that the AMV and atmospheric circulation changes have to a certain degree contributed to the summer warming. There is *low confidence* in the ability of GCMs and RCMs to correctly simulate the observed warming trend, possibly due to incorrect representation of external forcings in both GCMs and RCMs.

#### *10.4.2.2.7 The Southwestern North and Central America drought*

Persistent hydroclimatic drought in the southwestern North America (SWN) remains a much-studied event. Drought is a regular feature of the SWN's climate regime, as can be seen in both the modern record, and through paleoclimate reconstructions as well as in future climate model projections (Cook et al., 2010, 2015a). Since 1980, the region has experienced major multiyear droughts such as the turn-of-the-century drought that lasted from 1999 to 2005, and the most recent 2012–2016 drought that is perhaps unprecedented within the past 10,000 years (Robeson, 2015). Shorter dry spells also happened between these multiyear droughts making the 1980 to present an exceptionally dry period leading to strong declines in Rio Grande and Colorado river flows (Lehner et al., 2017b; Udall and Overpeck, 2017). Droughts are characterized by deficits in total soil moisture content that can be caused by a combination of decreasing precipitation and warming temperature, which promotes greater evapotranspiration. Regional-scale attribution of the SWN drought prevalence since 1980 then mostly focuses on the attribution of change in these two variables.

The observed SWN drying fits the narrative of what might happen in response to increasing greenhouse gas concentrations due to the poleward expansion of the subtropics, that is conducive to drying trends over

subtropical to midlatitude regions (Birner et al., 2014; Hu et al., 2013b; Lucas et al., 2014). However, several studies based on modern reanalyses and CMIP5 models have recently shown that the current contribution of GHGs to Northern Hemisphere tropical expansion is much smaller than in the Southern Hemisphere and will remain difficult to detect due to large internal variability, even by the end of the 21st century (Allen and Kovilakam, 2017; Garfinkel et al., 2015; Grise et al., 2018, 2019). In addition, the widening of the Northern Hemisphere tropical belt exhibits strong seasonality and zonal asymmetry, particularly in autumn and the North Atlantic (Amaya et al., 2018; Grise et al., 2018). There is *high confidence* that the recent tropical expansion results from the important interplay of internal and forced modes of tropical width variations.

A second possible causal factor is the role for ocean-forced or internal atmospheric circulation change. Based on observations and ensembles of SST-driven atmospheric simulations, Seager and Hoerling (2014) suggested that robust tropical Pacific and tropical North Atlantic forcing drove an important fraction of annual mean precipitation and soil moisture changes and that early 21st century multiyear droughts could be attributed to natural decadal swings in tropical Pacific and North Atlantic SSTs. A cold state of the tropical Pacific would lead by well-established atmospheric teleconnections to anomalous high pressure across the North Pacific and southern North America, favouring a weaker jet stream and a diversion of the Pacific storm track away from the southwest (Seager and Ting, 2017). The multiyear drought 2012–2016 has been linked to the multiyear persistence of anomalously high atmospheric pressure over the northeastern Pacific Ocean, which deflected the Pacific storm track northward and suppressed regional precipitation during California's rainy season (Swain et al., 2017). Going into more detail, Prein et al. (2016) used an assessment of changing occurrence of weather regimes to judge that changes in the frequency of certain regimes during 1979–2014 have led to a decline in precipitation by about 25%, chiefly related to the prevalence of anticyclonic circulation patterns in the northeast Pacific.

It has also been suggested that this ocean-controlled influence is limited and internal atmospheric variability has to be invoked to fully explain the observed history of drought on decadal time scales (Seager and Hoerling, 2014; Seager and Ting, 2017). Lasting from roughly 1980 to the present, the regional climate signals show an interesting mix between forced and internal variability. Lehner et al. (2018b) used a dynamical adjustment method and large ensembles of coupled and SST-forced atmospheric experiments to suggest that the observed SWN rainfall decline mainly results from the effects of atmospheric internal variability, which is in part driven by PDV-related phase shift in Pacific SST around 2000. Once aspects of the internal variability are removed by dynamical adjustment, the observed precipitation signal and modelled anthropogenically-forced components look much more similar. Unlike the precipitation deficit, the SWN accompanying warming is driven primarily by anthropogenic forcing from GHGs rather than atmospheric circulation variability and may help to enhance the drought through increased evapotranspiration (Lehner et al., 2018b; Williams et al., 2015).

There is *high confidence* that the anomalous atmospheric circulation that caused the SWN negative precipitation trend can be attributed to teleconnections arising from tropical Pacific SST variations related to PDV. There is *medium confidence* that anthropogenic forcing has made a substantial contribution (~50%) to the SWN warming since 1980.

#### *10.4.2.2.8 The Caribbean small islands summer drought*

Climate variability over the Caribbean region impacts its agriculture, fisheries, health, tourism, water availability, recreation, energy usage and other socioeconomic activities. The region’s location gives rise to influences from synoptic features over the tropical Atlantic (where it is situated) and tropical Pacific basins including the migration of the North Atlantic Subtropical High (NASH) and the ITCZ, easterly winds, the Atlantic warm pool, the intrusion of cold fronts, and the passage of tropical depressions, storms and hurricanes (Ashby et al., 2005; Taylor et al., 2013b).

Caribbean small islands exhibit a climatological mid-summer drought around June/July within a rainfall season from May to October (Figure 10.22). This mid-summer drying is particularly evident over the western/northern Caribbean and Central America. A negative trend in boreal summer (June to August, JJA) precipitation over the Caribbean Sea and parts of Central America has been identified since 1979 in satellite

observations, and since 1950 at land stations (Neelin et al., 2006). The mid-summer drying has also been identified in studies undertaken for individual islands. Declines in summer rainfall (-4.4% per decade) and maximum 5-day rainfall (-32.6 mm per decade) over 1960–2005 were reported for Jamaica from linear regression analyses on station data (Chen et al., 2012). A slight decrease in summer accumulations was observed for Cuba for 1960 to 1995 (Naranjo and Centella, 1994). Three of four stations examined for Puerto Rico exhibited declining JJA rainfall over 1955–2009 with the trend statistically significant for Canóvana (Méndez-lázaro et al., 2019). Recent work suggests that summer drought events may be intensifying. Herrera & Toby (2017) noted that the summer drought of 2015 was record breaking in terms of its spatial extent whereby 99% of the Caribbean experienced drought conditions, and in terms of its severity for 17% of the domain that includes the Caribbean, South America and Central America. The 2015 event was part of a pan-Caribbean drought occurring in 2013–2016 (Herrera et al., 2018a).

**[START FIGURE 10.22 HERE]**

**Figure 10.22:** [Placeholder: Influences that have been suggested to contribute to an intensification of June-August rainfall over the Caribbean. Inset shows average June-August rainfall in mm/month for some northern Caribbean stations by decade from 1971–1980 to 2011–2018 (2011-2016 for the station in Cuba).]

**[END FIGURE 10.22 HERE]**

The climatological mid-summer drying is associated with an intensification and westward shift of the NASH and a related increase in the strength of the low-level easterlies over the Gulf of Mexico and the Caribbean Sea (Giannini et al., 2000; Hastenrath, 1966; Knaff, 1997; Magana et al., 1999; Rauscher et al., 2008; Waylen et al., 1996) and a semi-annual strengthening of the Caribbean Low Level Jet (CLLJ) (Amador, 1998; Wang, 2007; Wang and Lee, 2007). The mid-summer drought has also been linked to warm SST anomalies in the tropical Atlantic and cool eastern equatorial Pacific SST anomalies through their combined modulation of the CLLJ (Whyte et al., 2008). Some other studies have suggested that the intensifying mid-summer drying occurs alongside a general intensification and poleward movement of the subtropical high pressure cells (Christensen et al., 2007), and perhaps with an equatorward contraction of tropical convective regions due to the suppression of convection in a more stable atmosphere (Neelin et al., 2003). Notably SST warming over the Atlantic, though smaller than the warming observed over global tropical areas, has been associated with enhanced divergence and increasing strength of the NASH and potentially the strength of the CLLJ (Rauscher et al., 2011). These factors may be related to the intensified mid-summer drying but there is currently *insufficient evidence* to conclusively suggest this.

Méndez-lázaro et al. (2019) indicated that the summer drying trend could also be linked to the combined effect of ENSO and the NAO rather than to a climate trend. A warm ENSO and positive NAO phase have been shown to result in negative summer rainfall anomalies (Giannini et al., 2000). Mid-summer drought intensity and phenomenahave been associated with the AMV, PDV and ENSO (Fallas-López and Alfaro, 2014).

The work of Herrera et al. (2018) suggested that for the 2013–2016 pan-Caribbean drought, anthropogenic warming accounted for ~15–17% of the drought's severity and ~7% of its spatial extent. This indicates that anthropogenic warming may be influencing the drying trends in summer rainfall though no additional studies to date have presented this case.

There is *low agreement* for the cause of the drying trend over the Caribbean and whether this trend is mainly caused by decadal-scale internal variability or anthropogenic forcing.

*10.4.2.2.9 Asian cities warming*

Cities affect the local weather by perturbing the wind, temperature, moisture, turbulence, and surface energy budget field. Another unique feature of cities is the release of the anthropogenic heat flux from energy

consumption (Bohnenstengel et al., 2014; Ichinose et al., 1999; Ma et al., 2017). One well known phenomenon is the Urban Heat Island (UHI) where urban air temperatures are substantially higher than temperatures in the surrounding rural areas. Three main factors contribute to the establishment of the UHI: 3-D urban geometry, thermal characteristics of impervious surfaces and anthropogenic heat release. There is also a strong contribution of local background climate to the UHI magnitude (Ward et al., 2016; Zhao et al., 2014). Cities can also experience other phenomenon, such as the urban dryness island, which refers to conditions where lower relative humidity is observed in cities relative to nearby rural locations and the urban wind island where cities experience slower wind speeds compared to their adjacent suburbs and countryside (Bader et al., 2018; Wu et al., 2017b).

Most GCM modelling groups consider that the impact of urban land cover on the global weather and climate is negligible compared to that due to other types of land cover. Zhang et al. (2013) and Chen et al. (2016c) introduced an estimate of the anthropogenic heat release globally as an external energy source into the lowest model layer of a global climate model. They found that while the global mean surface air temperature responses are insignificant (0.01°C annual mean), there are statistically significant changes by as much as 1°C in mid and high-latitude in winter and autumn over North America and Eurasia. There is also an equatorward shift of the winter mid-latitude jet, with increasing westerly wind at 20°N and decreasing westerly wind at 40°N. This suggests that the global anthropogenic heat could disturb the normal atmospheric circulation pattern and produce a remote effect on surface air temperature. There is *limited evidence but high agreement* that the global annual mean surface-air temperature response to urbanization is negligible.

At the regional scale, there is *robust evidence and high agreement* that a percentage of the observed warming trend can be linked to historical urbanization in rapidly industrialized countries (Figure 10.23). For example, Sun et al. (2016) found that while China's recorded annual mean temperature increased by 1.44°C during the period 1961–2013, urban warming influences account for about a third (0.49°C). Doan and Kusaka (2016) examined the impact of urbanization on the UHI effect over Greater Ho Chi Minh (GHCM) city since the late 1980s. The evolution of spatial distribution of UHI is closely associated with urban expansion. The increase in the surface air temperature was about 0.3°C in the pre-existing urbanized area and about 0.6°C in newly urbanized area in the last 20 years. The dominant factor in these changes is the conversion of agriculture or grassland into urban areas, which results in increased sensible heating and decreased latent heating. In addition, in the central GHCM, the urbanization impact was estimated at 0.31°C, while the temperature increase was observed at 0.64°C in the last 20 years. This suggests that urbanization may contribute about half of the increased surface air temperature signal in the central GHCM in the past 20 years. Over Europe, Chrysanthou et al. (2014) showed that urbanization explains 0.0026°C per decade of the annual averaged pan-European temperature trend of 0.179°C per decade. The strongest effect of urbanization was found in the summer (0.0070°C per decade) where the trend is more than twice the annual values. Likewise in Brussels, it is found that 38% of the global warming that were observed in Brussels during the period (1955–2006) can be explained by the urban heat island intensification due to the historical expansion of the city of Brussels around the observational station (Hamdi, 2010). Similar effect was reported in other regions (Japan – Fujibe (2009); Puerto Rico – Torres-Valcárcel et al. 2015) and other cities (Bader et al., 2018).

**[START FIGURE 10.23 HERE]**

**Figure 10.23:** [Placeholder: A figure with time series of urban warming reported in the literature in different cities around the world and the spatial map of observed long-term trends in the background]

**[END FIGURE 10.23 HERE]**

There is *robust evidence and high agreement* that the annual-mean maximum temperature is substantially less affected by urbanization than the minimum temperature (Liao et al., 2017; Wang et al., 2017a). In the United States, Hausfather et al. (2013) found that urbanization accounted for between 14 and 21% of the

increase of minimum temperatures since 1895 and 6 to 9% since 1960 (trend between 0.2°C and 0.6°C per century for the period 1960–2010). Therefore, there is *robust evidence and high agreement* that if observations of near-surface air temperatures in growing cities are used in the assessment of global warming trends, these trends may be overestimated, while this urban warming is smaller for a station that originally was established in a densely built-up area. Adjusting global temperature data to remove the impacts of urban affects revealed that for 42% of global stations urban areas warmed at slower rates compared to the surrounding non-urban areas (Bader et al., 2018).

There is *medium evidence and high agreement* that upstream urbanization exacerbates UHI, (e.g. Bassett et al., 2017; Zhang et al., 2009; Zhang and Chen, 2014). Zhang et al. (2009) reported that upstream urbanization exacerbates UHI effects along the Washington-Baltimore corridor in the US. Similar effect was found in the Suzhou-Wuxi area (China) by Zhang and Chen (2014) and more recently over the UK (Bassett et al., 2017) where the urban heat advection from small urban was found to increase mean nocturnal air temperature by 0.6°C at a horizontal distance of 0.5 km. There are also example of interaction between sea breeze front penetration and urban areas either enhancing the sea-breeze front (Li et al., 2015b) or decelerating its penetration inland (Flores Rojas et al., 2018; Hamdi et al., 2012a; Yamato et al., 2017) and therefore impacting the spatial distribution of the urban heat island.

There is *robust evidence and high agreement* of synergistic interactions between the UHI and heat wave episodes making the heat wave more intense in urban than rural areas and the nocturnal UHI during heat wave stronger than its climatological mean e.g. (Founda and Santamouris, 2017; Hamdi et al., 2016; Li and Bou-Zeid, 2013; Wang et al., 2017a).

There is *medium evidence and medium agreement* that urban areas induce increases in mean but also in extreme precipitations over and downwind of the city in different climate regions of the world and especially in the afternoon and early evening: Atlanta (Haberlie et al., 2015; McLeod et al., 2017); different inland and coastal US cities (Ganeshan et al., 2013; Ganeshan and Murtugudde, 2015); Dutch coastal cities (Daniels et al., 2016); Hamburg (Schlünzen et al., 2010); Shanghai (Liang and Ding, 2017). Over Beijing, it is found however (Dou et al., 2015), that depending on the strength of the UHI, maximum precipitation values were found either over the most urbanized area of Beijing in the case of strong UHI (>1.25°C) or along its downwind lateral edges for a weak UHI (<1.25°C). Theoretical analysis (Han and Baik, 2008) and regional climate models using urban canopy parameterizations (Ganeshan and Murtugudde, 2015; Li et al., 2017b; Ooi et al., 2017; Pathirana et al., 2014; Seino et al., 2018a; Song et al., 2016; Trusilova et al., 2008; Zhong et al., 2017; Zhong and Yang, 2015; Zhu et al., 2017) have been used to simulate the impact of urbanization on the precipitation patterns near urban centres. Three mechanisms could be assessed: 1) upward motion induced by the urban heat island circulation can initiate moist convection by creating an urban-induced convergence which may interact with sea-breeze for coastal cities, 2) increased urban roughness which may attract propagating storms toward the urban centres, and 3) urban aerosols which may interact synergistically with the previous mechanisms producing a rainfall enhancement (Schmid and Niyogi, 2014); but other studies suggested that increased aerosols concentrations in urban areas can interrupt precipitation formation process and thereby reducing heavy rainfall (Zhong et al., 2017).

Recently, there are new studies on the urbanization impact on Indian summer monsoon rainfall extremes (Shastri, H., Paul, S., Ghosh, S., Paul, S., Ghosh, S., Karmakar, 2015; Singh et al., 2016) and on the East Asian summer monsoon (Chen et al., 2016d; Jiang et al., 2017b). Overall, these studies reveal the sensitivity of extreme monsoon rainfall events to the increased urbanization but further studies are still needed to reduce uncertainties.

*10.4.2.2.10 Mountains: Himalayas*

The Himalayas, with the largest collection of glaciers and snow cover outside the poles, provide the headwaters for several major rivers in Asia. Since the 1960s, the Himalayas have experienced considerable warming and drying trends. A key feature relevant to the Himalayas is the Elevation-Dependent Warming (EDW), as reviewed in e.g. Pepin et al. (2015). Xu et al. (2016b) described observed surface warming over the Tibetan and Himalayan region of between 2°C and 2.5°C at 5000 m from 1961 to 2006, while

considerably lower (0.5°C) at sea level. Contrasting with increased temperature across the nearby Central and Eastern Himalayas and Tibetan Plateau, Forsythe et al. (2017) have analysed SAT from station observations to show a summer cooling trend over the Karakoram Himalaya for the period 1960–2010.

Yao et al. (2012) have used GPCP data to show that the annual precipitation in the Himalayas exhibits a decreasing trend from 1979 to 2010. Palazzi et al. (2013) also used multiple datasets to find a statistically significant decrease in Himalayan summer rainfall. The rainfall variability and changes over the Himalayan sub-regions can be extremely diverse due to the massive and complex topography. For instance, except during the pre-monsoon period, declining rainfall was detected in Nepalese station data on the southern slopes of the central Himalayas from 1981 to 2015 (Shrestha et al., 2019). Roxy et al. (2015) have used multiple observed datasets to find a statistically significant decrease in summer rainfall during 1901–2012 along the Ganges-Brahmaputra-Meghna basins and the Himalayan foothills. Meher et al. (2018a) have used rain gauge data to show significant declining trends in both rainfall and number of rainy days over the Western Himalaya over 1902–2005. Li et al. (2018) have used four datasets in the western Himalayas of northern India during 1981–2007 to show that winter precipitation exhibits a negative trend, while the precipitation trends are not significant for the other seasons. However, other regions exhibit positive precipitation trends (Li et al., 2018). For example, by using observed data over 1961–2013, Azmat et al. (2017) suggested that a slightly increasing tendency in precipitation has occurred over the Jhelum river basin in the western Himalayas. Li et al. (2018) showed that summer precipitation exhibits a positive trend during the 1981–2007 period in the western Himalayas of northern India.

The following assessment mainly covers the role of GHG and black carbon aerosols on the recent temperature and precipitation trends in the Himalayas (Figure 10.24). First, the impact of GHG and black carbon aerosols on the Himalayas warming is assessed. Using a high-resolution coupled GCM, Xu et al. (2016b) attributed the warming trend in the Himalayas to the increase in GHG and black carbon aerosols. In particular, they suggested that black carbon increase is the major factor in the EDW, and they explained the influence of black carbon in terms of atmospheric warming, snow darkening and the resulting snow-albedo feedback. The earlier findings of Ramanathan and Carmichael (2008) suggested that the black carbon and GHGs in the Himalayan Mountains might be equally responsible for the warming there during the past several decades. Additionally, snow darkening by deposition of light-absorbing aerosols, particularly desert dust, would accelerate warming in the Himalayas, via snow-albedo feedbacks (Gautam et al., 2013; Lau and Kim, 2018). Such darkening of the mid-Himalaya glaciers during 2000–2009 has been found both in simulations and in situ measurements, with light-absorbing constituents (e.g., black carbon and dust) mostly responsible for the regional warming (Ming et al., 2012). In contrast, there is a summer cooling trend over the Karakoram Himalaya that is closely related to the variability in the Karakoram vortex, potentially connected to the position and intensity of the subtropical westerly jet (Forsythe et al., 2017).

**[START FIGURE 10.24 HERE]**

**Figure 10.24:** [Placeholder: Schematic diagram illustrating main contributing drivers on the decadal change of the Himalayas since 1960s.]

**[END FIGURE 10.24 HERE]**

Precipitation in the Himalayas is highly sensitive to westerlies and the South Asian monsoon in the west and east, respectively (Yao et al., 2012). Shrestha et al. (2019) and Yao et al. (2012) stated that the decreasing Himalayan precipitation may be related to the weakening South Asian monsoon intensity, whereas the precipitation increase in the eastern Pamir (situated to the west) is linked to strengthening of the westerlies. (Roxy et al., 2015) also blamed the decreasing trend in summer rainfall along the Ganges-Brahmaputra-Meghna basins and the Himalayan foothills for the weakening South Asian summer monsoon resulting from rapid warming in the Indian Ocean and a relatively subdued warming over the subcontinent. In addition, eastward propagating synoptic-scale weather systems known as Western Disturbances (WDs) contribute substantially to the winter-to-early spring non-monsoonal precipitation over the Western Himalayas. By

using a global variable-grid climate model, Krishnan et al. (2018) highlighted that human-induced climate change is implicated in the rising trend of WDs activity, resulting in enhanced orographic precipitation over the Western Himalayas during recent decades.

Differences in the time periods examined, the stations and datasets compared or the selected elevation range thus contribute to different perceptions of temperature and rainfall trends in the Himalayas in recent decades. Despite the inhomogeneity in the sub-regional warming patterns, there is *high confidence* that the Himalayan region has exhibited rising temperatures, and that the rate of warming is amplified with elevation. There is *high confidence* that a large fraction (at least 50%) of the warming can mainly be attributed to increases in GHG and black carbon aerosols. There is *high confidence* that the decrease in summer precipitation can be mainly attributed to the weakening of South Asian monsoon (Section 10.6.1).

#### *10.4.2.3 Assessment summary*

**[Placeholder: to be filled in for the SOD]**

### *10.4.3 Future regional changes and interplay between internal variability and response to external forcing*

Detailed information about regional impacts of climate change is crucially needed to support adaptation and planning in many economic and social sectors. Yet, regional climate projections are often deemed unreliable to support adaptation policies. This is mainly due to the combination of three different sources of uncertainty: uncertainty about the future greenhouse gas and aerosol emissions as well land-use changes (scenario uncertainty), the weakness of understanding about the multi-scale interactions of large-scale and regional phenomena (also named model or structural uncertainty) and uncertainty related to the lack of predictability of low-frequency internal variability due the chaotic nature of the climate system. This section mostly focuses on the latter and its interplay with the forced climate response to anthropogenic radiative forcing. The different methodologies that are used to estimate and quantify internal variability and its interplay with the forced response are reviewed first. Next, the use of these methods is assessed for our selected use cases and address, when possible, the other sources of uncertainty. Finally, the different methodologies that have been proposed and applied to quantify and possible reduce epistemic uncertainty are reviewed and assessed.

#### *10.4.3.1 Global assessment of interplay between internal variability and response to external forcing*

As described in Section 10.3.4.3, the influence of internal variability on climate projections can be quantified based on simple diagnostics such as Signal-to-Noise Ratio (SNR) and Time of Emergence (ToE). We first briefly assess SNR and ToE global results before focusing on the various case study regions. Based on a SAT variance ratio analysis of five CMIP5 models (each with 4 to 10 members), Lyu et al., (2015) have shown that the unbiased ratio of forced to total variance over the historical period is stronger in the tropics (30–40% in average, up to 70% locally) and decrease poleward (with a range of 5–30%). For SAT, the large variance ratio in tropical areas is mainly due to the forced climate change signal, which is dominant compared with the internal variability background. In contrast, the lower ratio in extratropical areas results from the larger internal variability. The larger ratio of forced variance to total variance generally corresponds to earlier emergence of forced signals from internal variability. The SAT variance ratio, over time intervals with the starting time being fixed at 1860 and the end time increasing from 1870 to 2100, shows that the globally averaged ratios of forced to total variance continue to increase with time under all three RCP GHG scenarios, reflecting the cumulative effect of externally forced climate change. Based on a 40-member ensemble constrained by the SRES-A1B scenario over 2005–2060 and using a simple SNR metric, the interplay between internal variability and the forced response to greenhouse gases was assessed for surface air temperature, precipitation and sea level pressure (Deser et al., 2012a, 2012b). It was found that for temperature, only one realization is needed to detect a significant (at the 95% confidence level) warming in

the 2050s decade compared to the 2010s at nearly all locations, compared to approximately 3–6 (15) ensemble members for tropical and high latitude (middle latitude) precipitation, and approximately 3–6 (9–30) members for tropical (extra-tropical) SLP, depending on location and season. They also underscored the low SNR in the large-scale patterns (e.g. annular modes) of extra-tropical atmospheric circulation response that are primarily due to intrinsic atmospheric dynamics (Deser et al., 2017b). Most of the random uncertainty in temperature and precipitation in the extra-tropics is associated with the annular mode variability in both seasons and hemispheres. Finally, they show that the magnitude of random uncertainty associated with internal variability is rarely less than half that due to model uncertainty for forced linear climate trends during 2005–2060. Similar analyses based on the same large ensemble were also conducted for sea level, the Hadley Cell and Arctic sea ice (Hu and Deser, 2013; Kang et al., 2013; Wettstein and Deser, 2014). Large ensembles simulation from CESM1 (Kay et al., 2015) and CanESM2 (Sigmond and Fyfe, 2016) were used to quantify the internal variability influence on trends in annual surface air temperature and precipitation over different time periods from 1950 up to 2100 (Dai and Bloecker, 2018). Results indicate that regional precipitation trends may remain statistically insignificant over most of the globe until the later part of the 21st century even under a high-emission scenario, while temperature trends since 1979 are already statistically significant over many low-latitude regions and are projected to become significant over most of the globe by the 2030s.

There is *high confidence* that internal variability will significantly influence future regional precipitation trends until at least the end of the 21st century. There is *very high confidence* that the forced mean regional temperature signal will have emerged from internal variability at almost all locations by 2050 under the high-end RCPs.

#### *10.4.3.2 Assessing the interplay of global and regional drivers to understand regional future climate changes for the selected case studies*

This section focuses on the relative contribution of all the important drivers to future climate change for our selected case studies. There are a number of key challenges that are relevant for all selected case studies. Even if successful, the attribution of past changes is useful but not sufficient to robustly infer the relative contribution of the relevant drivers to future regional climate changes. The relative importance of internal variability and anthropogenic factors is not constant in time as external anthropogenic and natural forcing can vary, as well as internal variability and the interaction between the different drivers.

The assessment is necessarily emissions scenario and time-dependent, on a region-by-region basis, among the case studies. Depending on the emissions scenario, period and/or regions, internal variability can counteract, be neutral or exacerbate the forced response due to anthropogenic forcing. The response to anthropogenic forcing can project on internal modes of variability leading to difficulty in identifying the forced response and its spatial pattern. Multi-model analysis cannot easily disentangle structural model uncertainty and uncertainty related to internal variability (only single-model large initial condition ensembles with different models allow a clean separation). Using internal variability from pre-industrial simulations implicitly assumes that internal variability does not change under anthropogenic forcing, which is a strong assumption that does not seem to hold at regional scales (Dai and Bloecker, 2018).

##### *10.4.3.2.1 The Sahel and West African monsoon continued recovery and wetter future*

In this case study the drivers of future projections of West African monsoon and wider Sahel region are assessed, beginning from the recent recovery outlined in Section 10.4.2.2.1. The review of Nicholson (2013) found “universal agreement” that models do not reliably project future climate in the Sahel. More recently, various studies (Biasutti, 2013; James et al., 2015; Roehrig et al., 2013a; Skinner and Diffenbaugh, 2014) have suggested that the magnitude of the future rainfall response depends strongly on the GHG emission scenario (whether RCP4.5 or RCP8.5), while the spatial pattern of change remains consistent between them.

Looking at the time dependency of the signal, based on the 40-member CESM1 large ensemble, Monerie et al. (2017b) showed that for short-term (2010–2049) and medium-term (2030–2069) rainfall projections the

simulated internal variability component is able to obscure the projected response to external forcing. For long-term (2060–2099) projections, the external forcing-induced change dominates. Precipitation changes are found to be more robust over the central Sahel than over the western Sahel. The CESM1 model appears to be representative of the CMIP5 ensemble, since it simulates a reasonably similar change in precipitation, in terms of magnitude, pattern and seasonal cycle as the CMIP5 ensemble mean. However, the multi-decadal variability in Sahel precipitation is underestimated in CESM1 as with all CMIP5 models.

In contrast, the model uncertainty is large in the CMIP5 multi-model ensemble (Biasutti, 2013; Monerie et al., 2017a; Seth et al., 2013). Of these, Monerie et al. (2017a) analysed 32 CMIP5 models under the RCP8.5 emission scenario and classified model precipitation changes (2060–2099 minus 1960–1999) using a hierarchical clustering method. Four groups are found that do not even agree on the sign of future Sahel precipitation change (or temperature and wind change patterns). The inter-model spread was shown to relate to the large spread in: 1) temperature increase over the Sahara and North Atlantic and 2) the strengthening of low and mid-level winds.

Few modelling studies have attempted to account for dynamic vegetation and land-use feedbacks. Berg et al. (2017) performed a comparison of five GLACE-CMIP5 models, using prescribed SST from historical and RCP8.5 scenarios and comparing with and without soil moisture change. The models feature soil moisture-precipitation feedbacks of different sign in the Sahel; in some, soil moisture amplifies the precipitation change, while in other models the future precipitation change is damped. That the atmospheric responses to such large-scale changes in soil moisture are inconsistent supports the view that other drivers such as SST dominate rainfall change. However, the limited number of models considered presents some uncertainty. Vegetation dynamics have also been examined in the regional modelling context by Erfanian et al. (2016) using a single RCM ensemble driven by historical and RCP8.5 scenarios from four GCMs. Although dynamic vegetation clearly reduces physical inconsistencies in the model coupling, RCM biases were increased. The RCM future trends were more consistent than the contradicting GCM ones and showed decreased rain over significant portions of West Africa.

In further regional modelling studies, Vizy et al. (2013) used RCMs at 90 km and 30 km resolutions forced by five CMIP5 models in the RCP8.5 scenario. At the middle and end of the 21st century, summer rainfall is projected to increase over most of the Sahel, resulting from increased rainfall intensity. Those models with stronger Sahara warming feature larger and earlier Sahel rainfall increases, due to intensification of the low-level West African westerly jet. In contrast, Akinsanola and Zhou (2018) used the RCA4 and COSMO-CLM RCMs at 0.44° resolution with inputs from four different GCMs, and showed reductions in wet-day rainfall for 2070–2099 in RCP4.5 and RCP8.5 scenarios. While wet days will become more intense, the tendency for a reduced number of wet days reduces overall rainfall.

Park et al. (2015b) explored the dependence of Sahel rainfall on tropical SST variations and noted that simple relationships between the two were no longer applicable for future climates. Instead, they invoked consideration of the differential warming between extratropical and tropical SSTs to explain the spread in future rainfall projections. Once the differential pattern of warming is considered, it can be used to explain Sahel rainfall variations reliably across the 20th and 21st centuries. Park et al. (2015b) supported their hypothesis with AGCM sensitivity experiments, in which extratropical warming can overcome the drying impact of tropical SST warming. In their Singular Value Decomposition (SVD) analysis, Giannini and Kaplan (2018) arrived at a similar result, such that the sum of tropical and North Atlantic warming controls the Sahel rainfall increase, given that North Atlantic anthropogenic aerosol forcing is largely absent in the long-term for the RCP scenarios.

In drawing comparisons with paleo-climates such as the mid-Holocene, in which vegetation existed much further north, Schewe and Levermann (2017) suggested that the Sahel is capable of abrupt climatic shifts in response to gradual forcing. Using 30 CMIP5 models, seven were identified in which future precipitation increased by large amounts (40–300%), due to northward expansion of the West African monsoon domain. They identified SST controls from the Mediterranean and tropical Atlantic moisture source regions, consistent with works listed above. Beyond a certain SST level, the WAM is found to intensify abruptly; this occurs at the point when the remote stabilizing mechanism (from changes in radiative forcing) is overcome

by a local destabilizing mechanism from land warming. The Mediterranean is found to be a vital source for additional Sahel moisture.

Finally, Yan et al. (2019) suggested that present climate relationships, with parallels to emergent constraints work, can be used to calibrate future projections of Sahel rainfall. Their calibrated approach demonstrates larger future increases in precipitation in the Sahel than when using the standard multi-model mean. They point to choices of convective parametrization as the origin of biases in present day simulations.

In summary, there remains *high confidence* that West African monsoon and Sahel rainfall in future climate scenarios will be dominated by differential patterns (gradients) of SST change between the tropics and North Atlantic and of Sahara temperature change. There is *medium confidence* that in future climate scenarios dominated by greenhouse gas forcing the West African Monsoon and Sahel rainfall will increase.

#### *10.4.3.2.2 East Asia summer monsoon future changes*

The AR5 concluded that EASM precipitation is projected to increase and EASM circulation is projected to slightly increase in the 21st century. This increase in EASM precipitation is mainly due to intensified moisture convergence and increased evaporation in a warmer climate, although some uncertainties exist in the future climate projections among CMIP5 climate models (Kitoh et al., 2013a; Sooraj et al., 2015; Zhou et al., 2018b). (Zhou et al., 2018b) reported that the dominant source of uncertainty in EASM precipitation changes among 18 CMIP5 models is due to uncertain atmospheric circulation changes. Seo et al. (2013) also have reported that the summer monsoonal precipitation is projected to increase by 10%–15% over the major EASM domain in CMIP5 RCP6 experiments, which is mainly attributed to the intensification of the northwest Pacific subtropical high accompanied with increasing 850-hPa geopotential height and increasing moisture convergence. The increase of summertime land-sea thermal contrast during the positive phase of the PDV over the northeastern part of East Asia is commonly found in general circulation models regardless of future forcing scenarios, indicating the robustness of the strengthened EASM response to global warming, and the increasing contrast can be explained by GHG-induced continental warming (Kamae et al., 2014a, 2014b). In addition, Wang et al. (2016) have also suggested that enhanced EASM with a 10% increase in rainfall over the East Asian monsoon region may occur due to future reductions in emissions of anthropogenic aerosols inherent in the RCP4.5 scenario using an aerosol-climate model. The EASM precipitation response to the global warming in the future is different from the recent (since the late 1970s) considerable weakening trend, which is mainly associated with the inter-decadal changes of SST over Pacific Ocean (Ding et al., 2009; Li et al., 2010; Zhou et al., 2017). In future scenarios, the effects of the warming trend due to the increased GHG will overcome other effects (i.e. internal variability).

Under the 1.5°C and 2°C global warming targets AGCM simulations (Mitchell et al., 2016, 2017), the EASM circulation strength and rainfall both increases, although the differences of intensity among scenarios are insignificant (Chen et al., 2018b). Wang et al. (2018b) also reported the significant increase of temperature and precipitation over summer East Asia due to stronger land-sea thermal contrast under a 1.5°C warming scenario derived from an RCP4.5 coupled experiment. Similarly, Liu et al. (2018) showed future changes of monthly precipitation in East Asian region when the global temperature reaches 2°C above the preindustrial using the RCP4.5 scenario, with decreased precipitation over the Meiyu belt and enhanced precipitation to its north and south in June and July, increased precipitation over the high latitudes of East Asia, and finally enhanced EASM precipitation.

Regional downscaling using dynamical models can also give indications of specific local trends within the EASM. Based on the Global/Regional Integrated Model system-Regional Model Program (RMP), Lee et al. (2014) suggested that strong warming and intensified monsoonal precipitation over East Asia would occur for 2006 to 2050, and extreme weather conditions over South Korea would increase and intensify in the near-future (2025–2050) climate because the RMP shows higher reproducibility of climate extremes including precipitation events. Ham et al. (2016) investigated potential future changes in precipitation in the EASM system using a regional spectral model with RCP2.6 and RCP8.5 scenarios and large-scale forcing provided by HadGEM2-AO. The RCM results showed an intensified East Asian monsoon by the strengthening North Pacific subtropical high and Okhotsk high in summer. Gu et al. (2018) also used RCMs from the coordinated

regional downscaling experiment in East Asia (CORDEX-EA); they showed that RCMs can capture the climatology and annual cycle of precipitation better than GCMs during the historical period. The projected precipitation shows consistent increases over China in the future under RCP4.5 scenario, but there are significant inter-RCM differences larger than GCMs, the largest source of uncertainty being internal variability.

In summary, there is *high confidence* that EASM precipitation will increase during the 21st century due to the change of moisture budget. However, there is *low confidence* in the magnitude and detailed spatial patterns of precipitation projections at sub-regional scale.

#### *10.4.3.2.3 Southern Australia future precipitation changes*

The AR5 assessment concluded that it is *likely* that cool season precipitation will decrease over southern Australia associated in part with trends in the SAM, the IOD, and a poleward shift and expansion of the subtropical dry-zone. AR5 also stated that it is *very likely* that Australia will continue to warm through the 21st century, at a rate similar to the global land-surface mean SAT.

New lines of evidence suggest that the cool-season drying trend in south-west Australia will continue under all future scenarios, with a greater decline for higher levels of greenhouse gases (Hope et al., 2015). Confidence in projections can be improved by selecting only climate models that best simulate the weather phenomena and climate features, such as the frequency of blocked days in eastern Australia and the strength of the subtropical jet over Australia, that have a strong influence on Australian rainfall in the current climate. Adopting this approach it was found that 15 climate models passed tests on their representation of local circulation features (Grose et al., 2017). The resulting projected change in rainfall for 2080–2099 (relative to 1986–2005) under RCP8.5 showed that the rainfall reductions in austral winter (July) is even stronger in both the southwest and the southeast of the continent than previously indicated using the full group of climate models. This is consistent with the observed rainfall declines in winter over the last several decades being at the drier end of model projections to 2030. Using this subset of models that best represents rainfall in southern Australia also increases confidence in projections of more summer rainfall in southwest and eastern Australia. Using multiple linear regression of interannual rainfall variability based on atmospheric circulation indices and historical circulation analogues, Grose et al. (2019) brought further evidence constraining the wet end of precipitation projections for the Southern Australia region from the CMIP5 ensemble.

There is *high confidence* that the cool-season drying trend in southwest Australia will continue under future RCP scenarios, with a greater decline for higher levels of greenhouse gases.

#### *10.4.3.2.4 South Eastern South America (SESA) summer future precipitation changes*

As seen in Section 10.4.2.2.4, attribution science has not yet reached a unified view on which internal and external drivers control the observed positive summer precipitation trend over SESA. To reach such a consensus is very important, since it will give clues on how the precipitation in this region, whose economy is largely based on rain-fed agriculture, will evolve in the coming decades. If, as claimed by Díaz and Vera (2017), Vera and Díaz (2015) and Zhang et al. (2016), GHG is the dominant driver of the SESA wetting trend, this trend could be expected to continue and intensify in the future. On the contrary, if stratospheric ozone depletion caused the wetting trend while GHG had very little or no influence, as argued by Gonzalez et al. (2014) and Wu and Polvani (2017), the ozone hole recovery (Strahan and Douglass, 2018) would then lead to a negative trend in precipitation over the SESA region (Wu and Polvani, 2015). If the wet trend was mainly due to the cold phase of the AMV (Seager et al., 2010) it could be expected to continue for a few decades since there are indications that AMV has shifted back to its cold phase since 2005 (Robson et al., 2016), after having a warm phase that started in the mid-1990s. If precipitation variations in SESA could be explained mainly by the AMV, then ultimately it would depend on the causes of AMV variability, traditionally being seen as an internal mode, but more recently claimed to be modulated by natural and anthropogenic forcings such as aerosols (Sutton et al., 2018).

The AR5 assessed future precipitation increases in SESA as *very likely*, based on results from CMIP3 and CMIP5 future projections and downscaled CMIP3 simulations with RCMs. The AR5 also highlighted coherence between projected changes of several physical mechanisms and increased precipitation in the region such as the intensification of the South American low-level jet and the southward expansion of the Hadley Cell, related to a southward displacement of the Atlantic subtropical high. Since the AR5, regionally focussed studies mostly using the CLARIS-LPB RCM ensemble and comparing late 20th century with late 21st century periods have confirmed the projected precipitation increase on different timescales. Menéndez et al. (2016), Sánchez et al. (2015) and Solman (2016) studied seasonal precipitation while Barros et al. (2013) found that the positive trend in monthly extreme precipitation during summer persist, in part due to an increase of low-level atmospheric moisture convergence over eastern SESA. Llopart et al. (2014) downscaled three CMIP5 models with RegCM4 and found that December through April precipitation increased in all downscaled simulations, although only one of the three GCMs employed exhibited a positive future precipitation signal. Similarly, in the CLARIS-LPB ensemble, only one of the three GCMs employed projected future SESA wetting, while all RCMs projected wetting (Sánchez et al., 2015). By viewing the processes involved in more detail, Junquas et al. (2012, 2013) identified a regional dipole between rainfall in SESA and the South Atlantic Convergence Zone (SACZ) and found that in the CMIP3 models rainfall was projected to increase (decreases) in SESA (SACZ) during the 21st century. They attributed this dipole response to a non-zonally uniform pattern of SST warming, including warming over the Indian and Pacific Oceans that excites wave responses over South America. In fact, zonally uniform SST patterns of warming alone would lead to opposite rainfall patterns to those observed. This suggests that the cause of the increased precipitation trend is anthropogenic in origin, with the mechanism mediated by uneven warming patterns in the tropical oceans.

On the other hand, global studies of ToE (Giorgi and Bi, 2009; Nguyen et al., 2018) using CMIP3 and CMIP5 models respectively, did not identify SESA as a hotspot region of regional precipitation changes. Nguyen et al. (2018) looked at different RCP scenarios and time horizons, and only for the RCP8.5 scenario for the end of the 21st century robust precipitation increases of 10–20% were found for SESA, which is substantially less that for their identified hotspot regions.

Thus, according to the AR5, there is general agreement between CMIP5 models on a positive change in precipitation in SESA, as well as the magnitude of the change is greater for the RCPs with higher GHG concentrations and towards the end of the 21st century (see the Supplementary Material of the AR5 Atlas). Analysis of RCMs that downscale CMIP3 and CMIP5 models, published after AR5 (Llopart et al., 2014; Sánchez et al., 2015) shows that RCMs project a positive future change for the end of the 21st century, even though forced by GCMs that have a zero or negative future change. The reason for this has not yet been explained so it remains an open question if the higher resolution of the RCMs is able to resolve some process that the GCMs do not, or if instead they are lacking some forcing factor or misrepresent some teleconnection that the GCMs do include. Furthermore, the lack of consensus around the mechanisms that drove the 20th century positive trend (Section 10.4.2.2.4) and the uncertainty of the future evolution of some of these mechanisms (e.g. AMV, Sutton et al. 2018) leads us to assess a *higher uncertainty* regarding the SESA future wetting than in the AR5. SESA precipitation will more likely than not increase based on model simulations, but the mechanisms behind this increment are still largely unexplored and constitute a knowledge gap.

#### *10.4.3.2.5 Central and eastern Eurasia winter future temperature changes*

Based on CMIP3 and CMIP5 results, AR5 concluded that both northern and central Eurasia are projected to warm in the future, with a stronger than global mean warming trend for northern Eurasia during winter. For central Asia, the warming magnitude is similar between winter and summer.

Based on 22 CMIP5 models and three RCP scenarios, Zhou et al. (2018a) showed that projected warming over Northern Eurasia is much greater than the global mean warming in all RCPs. They also showed that the 2°C warming target is surpassed by around 2050 and 2040 for RCP4.5 and RCP8.5, respectively. Miao et al. (2014) reported increases in SAT for Northern Eurasia under all RCPs used in CMIP5. They used one member for 24 models and three different ensemble averaging techniques. Based on Bayesian model

averaging (Duan and Phillips, 2010), the range of projected SAT increase over the full 21st century varies from ~1°C under RCP2.6, ~3°C under RCP4.5 and up to 7°C under RCP8.5. *Large* inter-model *agreement* is depicted for the large-scale simulated change spatial pattern which reflects a strong Arctic amplification. Monier et al. (2013) used an intermediate complexity model (with a two-dimensional zonal mean atmosphere) coupled with both dynamical (AGCM) and statistical downscaling (pattern scaling) methods to produce quasi-probabilistic projections of climate change over Northern Eurasia. The framework was used to explore the parameter space and the uncertainty linked to climate policy (choice of emission scenario) and climate response (climate sensitivity, strength of the aerosol forcing and ocean heat uptake). They found that under an RCP8.5 scenario, the projected warming and moistening range from 4.5°C to 10°C and 0.2 mm per day to 0.5 mm per day, respectively. They also suggest that internal variability can substantially contribute to the uncertainty in climate change projections (even in 20-year mean temperature changes at the end of the 21st century), in particular for simulations with lower values of climate sensitivity and emissions scenarios.

Other studies have focused on the future changes in the East Asian winter monsoon (EAWM) region (20°N–60°N and 100°E–140°E). Xu et al. (2016a) used 26 CMIP5 climate models under scenarios RCP4.5 and RCP8.5 to present projections for the EAWM region. The Multi-Model Ensemble (MME) mean simulated a strong warming of 3°C for RCP4.5 and 5.5°C for RCP8.5, respectively. The signal-to-noise ratio given by the MME SAT change divided by the inter-model spread was about 4 and is similar for Northeast, mid-latitude and Southeast Asia. It was much lower (around ~1) for precipitation, indicating large uncertainty as far as regional precipitation changes over the EAWM region are concerned. The MME SAT spatial pattern exhibited stronger warming at high latitudes with opposite changes in land-sea contrast changes between mid- and high latitudes. Land warming was greater than Pacific Ocean warming south of 50°N while ocean warming exceeded land warming north of 55°N due to sea-ice melting in the Bering Sea and Okhotsk Seas and associated heating. The reduced mid-latitude land-sea temperature contrast leads to a reduction of northwest–southeast thermal and sea-level pressure differences across Northeast Asia and a weakening of north-easterly winds. The high-latitude North Pacific warming induced a significant intensification and northward shift of the Aleutian Low. These two factors are related to the weakening (strengthening) of the EAWM north (south) of 25°N (Jiang and Tian, 2013e; Kitoh, 2017). Jiang and Tian (2013) selectd 15 CMIP5 and 16 CMIP3 models by their ability to reproduce the key features of the monsoon-related circulation as depicted by the 10-metre wind climatological spatial pattern. They found that there is no significant 21st century trend for the EAWM intensity as a whole. They also note that future East Asian monsoon changes are somewhat model and index dependent.

RCMs can be especially valuable for understanding changes in East Asia, which is characterized by complex topography, coastlines, and land-use distributions, as well as by regional monsoonal circulations that impact local climates (Gao et al., 2012; Gao and Giorgi, 2017). Within the CORDEX East Asia framework, Gu et al. (2018) have shown that five different RCMs driven by a single coupled GCM (which was selected due to its overall performance over East Asia) have a better representation of annual mean SAT and its seasonal cycle than the driving GCM. The RCM projections under RCP4.5 showed enhanced warming over northern and western China compared with southern China. The magnitude of warming for the different China regions was also shown to vary substantially among the five RCMs due to both model uncertainty and internal variability. Gu et al. (2018) also suggested that a full GCM-RCM matrix with more driving GCMs under different GHG scenarios is needed to better quantify the various sources of uncertainty.

As further climate change over Northern Eurasia could lead to significant releases of GHG (CO2 and CH4) to the atmosphere caused by severe permafrost thaw, increasing forest fires, changes in lake and wetland dynamics and changes in land cover, there is a potential for a positive feedback (Groisman et al., 2009, 2017). As the model components needed to quantify the influence of possible positive feedbacks over Northern Eurasia were generally not or only partially included in both CMIP5 and CORDEX models, large uncertainty remains with regard to their potential impact on the rate of future SAT change at global-to-regional scale and related uncertainties.

There is *high confidence* that Eurasia will experience additional warming during the 21st century with a continental-scale spatial pattern reflecting Arctic amplification. However, the above factors lead to *low confidence* in the spatial patterns of sub-continental and regional temperature change. There is *low*

*confidence* in the sign and spatial patterns of regional precipitation changes over the EAWM region.

*10.4.3.2.6 Europe summer future temperature changes*

Europe has different climate regimes that will experience different responses to global warming. Central and Northern European climate, covered by the AR6 regions CEU and NEU are strongly affected by the atmospheric circulation over the Euro-Atlantic region that determines the source of the advected air masses. In these regions, cool summers are characterised by the advection of maritime Atlantic air, whereas warm European summers result from advection of either hot dry continental from the east or hot air from the Mediterranean and Africa (Bladé et al., 2012; Folland et al., 2009; Ghosh et al., 2017). CMIP5 projections of future atmospheric circulations over Europe and the Atlantic differ widely (Hall, 2014; Kjellström et al., 2013, 2018; Kröner et al., 2017; Shepherd, 2014; Shepherd et al., 2018; van den Hurk et al., 2014; Zappa and Shepherd, 2017) which makes it uncertain as to whether the increase in summer temperatures for those European regions will increase faster or slower than the global mean temperature. To narrow down this uncertainty, drivers have been identified for these circulation changes. Among these drivers are the polar amplification, tropical amplification, stratospheric vortex and Atlantic Meridional Overturning Circulation (AMOC) (Haarsma et al., 2015; Shepherd et al., 2018; Zappa and Shepherd, 2017). Apart from changes in atmospheric circulation, local processes and feedbacks will affect future European summer temperatures. The most important one that has been identified is the soil moisture feedback that has been shown to enhance heatwaves due to a shortage of soil moisture (Seneviratne et al., 2010, 2013; Teuling, 2018; Whan et al., 2015). This will be further discussed in Chapter 11. Apart from the impact on heat waves its impact on the mean summer temperatures in Central and Northern Europe is limited (Vautard et al., 2014).

The climate of southern Europe, covered by the AR6 MED region, is also affected by circulation changes (Bladé et al., 2012), but soil moisture feedback and land-surface feedbacks becomes more important due to the semi-arid climate of the region (Knist et al., 2017). Apart from its important role in heatwaves, discussed in Chapter 11, there is *high confidence* that soil moisture feedback will increase the climatological mean summer temperatures (Boé and Terray, 2014; Seneviratne et al., 2013; Vautard et al., 2014) resulting in a larger than global mean temperature rise. This will be discussed in more detail in the integrated Mediterranean case study in Section 10.6.4. This enhanced Mediterranean warming will also have a remote impact on Western Europe due to the development of a heat low that enhances the advection dry continental air (Haarsma et al., 2009). Other identified factors and feedbacks for Europe are SST patterns, land-sea contrast, cloud coverage and lapse-rate, that locally can contribute substantially to the summer warming (Boé and Terray, 2014; Haarsma et al., 2015; Kröner et al., 2017).

Due to the above feedbacks the projected European warming by both GCMs and RCM displays a meridional gradient, with warming varying from similar to the global mean for the northern regions, to about 1.5 times the global mean for the MED region (Christensen et al., 2019, submitted). The transition zone at intermediary latitudes is characterized by a large spread in model results (Déqué et al., 2012b; Terray and Boé, 2013). This is in part due to internal variability, and other feedbacks, mainly related to how strongly evapotranspiration is limited by soil moisture in those models (Boé and Terray, 2014).

There is *high confidence* that reduction in aerosol concentration has been an important contributor to the recent European summer warming (Section 10.4.2.2.6) and that the expected continuing future reduction in aerosol concentrations will enhance European summer warming (Dong et al., 2017).

Recent global high-resolution simulations suggest a stronger drying and increase of European summer temperatures compared to CMIP5 simulations due to a less zonal and more accurate position of the Atlantic storm track and the development of an anticyclone over the eastern North Atlantic, resulting in extra drying in spring that enhances the soil moisture feedback during summer (van der Linden et al., 2019; van Haren et al., 2015). Also on decadal time scales, there is significant natural variability of the atmospheric circulation over Europe (Dong et al., 2017), leading to an additional source of uncertainty for near-term projections (Hawkins and Sutton, 2009; Ravestein et al., 2018).

Atmosphere-land interaction is strongly non-linear in particular in situations of soil drying resulting in

enhanced temperature increase (Douville et al., 2016; Douville and Plazzotta, 2017; Miralles et al., 2014; Seneviratne et al., 2013; Teuling, 2018; van den Hurk et al., 2016; Whan et al., 2015). In particular, Vogel et al., (2017) suggested strong soil moisture-temperature feedback enhancing temperature extremes over Central Europe for the "very dry" CMIP5 models i.e. those showing an increase in net radiation accompanied by strong decrease in soil moisture, precipitation, and latent heat flux.

Regional climate models simulations show enhanced warming over Europe compared to the global mean, even at moderate rates of warming (1.5°C and 2°C, Dosio and Fischer, 2018; Jacob et al., 2018; Kjellström et al., 2018b) . Although RCMs have been found to reduce the bias in simulated summer temperature compared to the driving GCMs, projected changes in seasonal temperature can differ between RCMs and GCMs, with downscaling projecting a smaller warming especially over Scandinavia, eastern Europe and the Alps (Sørland et al., 2018), and over Spain (Fernández et al., 2018). Bartók et al. (2017) showed that the RCMs and GCMs exhibit an opposite trend in surface shortwave radiation (0.17 W $m^{-2}$ per decade for the period of 2006–2100 for the multi-model mean of 5 GCMs compared to -0.72 W $m^{-2}$ per decade for the multi-model mean of the 3 downscaling RCMs); the SSR reduction in the RCMs is not accompanied by an increase in total cloud fraction (whereas significant reduction in cloud cover is projected for the GCMs). They also argued that local processes like evapotranspiration and convective cloud formation may play a significant role. In fact, as both latent heat flux and atmospheric absorption show an increasing trend (similar to that of the GCMs), the amount of moisture in RCMs does not constitute a limiting factor for convective cloud formation.

In addition, the way in which aerosols are handled impacts projected SSR; whereas GCMs can have prescribed (but time varying), semi-interactive, or interactive aerosols (the latter category showing the largest spread in SSR change), most RCMs have prescribed (and time invariant) aerosols, and, in some few cases, even constant GHG concentration, thus relying on the assumption that the direct radiative effect of GHG forcing on the regional climate is small (Jerez et al., 2018).

Finally, coupled RCMs have also been used to assess future SST warming and, consequently, marine heat waves. For instance, Darmaraki et al., (2019) showed that by the end of the century, Mediterranean extreme SST (99th quantile) is expected to warm significantly more than the annual mean, under RCP8.5.

There is *high confidence* that southern Europe will warm faster than the global mean temperature due to local feedbacks. There is *low confidence* that for other parts of Europe the increase in summer temperatures will deviate substantially from the global mean temperature increase.

#### *10.4.3.2.7 Southwestern North and Central America future changes*

Changes in the North American Monsoon System (NAMS) are central to potential drying in northwest Mexico and southwest US. The AR5 (Christensen et al., 2013a) reported no consistent changes in the NAMS behaviour among CMIP5 GCMs. Therefore, *confidence* in NAMS precipitation changes was *low*. Since the AR5, (Seager et al., 2014) have examined near-term (2021–2040) changes in moisture budgets for 22 CMIP5 GCMs that used the RCP8.5 scenario. The multi-model mean shows, for both winter and summer, increases in Evapotranspiration (E) overriding Precipitation (P) changes so that the net change in water balance (P-E) in the southwestern USA is negative. However, similar to the AR5 reporting, the individual models do not show *consistent agreement* in the signs of changes for this region. (Seager et al., 2014) also found in both seasons that changes in mean flow moisture convergence are central to the P-E changes; causes of the circulation changes remain unknown. (Ting et al., 2018) extended the analysis of the 22 CMIP5 GCMs to show that the mechanisms of summer drying are also projected to shift into spring, contributing to a springtime drying, again in the multi-model mean. Looking into the latter half of the twenty-first century (2050–2099), (Cook et al., 2015a) used data from 17 CMIP5 GCMs and found, for both RCP8.5 and RCP4.5, increased drought conditions for the southwestern USA using a version of the Palmer Drought Severity Index and vertically integrated soil moisture. For this time period, there was *high consistency* among the models analysed: 15 of 17 models agreed on substantial increase in drought conditions in latter half of 21st century. Further understanding of ecosystem response is needed, however: (Mankin et al., 2017) showed that feedbacks between plant phenology and climate change need better understanding if uncertainties in water-balance changes for the southwestern USA are to be reduced.

Recent dynamically downscaled simulations do not add more confidence to previous GCM-based projections of precipitation during NAMS, despite better resolving important terrain and circulation features. They generally maintain the uncertainty in precipitation in the northern parts of the NAMS region, including the southwest US, with a higher consensus on drying farther south. In dynamically downscaled CMIP3 simulations, models that simulated a reasonable Gulf of California low-level jet, increased its strength in the future, which in some instances led to small, localized increases in precipitation on the windward side of resolved terrain, as orographic lift and increased moisture overcame the increased stability of a stronger monsoon ridge (Bukovsky et al., 2015). Whereas, in coarser CMIP5 simulations, a stronger land-sea thermal contrast, implying greater onshore flow, did not prevail over greater stability (Torres-Alavez et al., 2014). In downscaled simulations of CMIP5 GCMs from North America CORDEX, there is evidence for an increase in the annual frequency of days in which a monsoon flow regime is present (Prein et al., 2019), which suggests more precipitation in the Southwest US. This projection may be related to mechanisms behind the extension of the monsoon season and increased late season precipitation in CMIP5 GCMs (Torres-Alavez et al., 2014). In contrast, a westward shift projected in the east Pacific Tropical Cyclone (TC) genesis region and a decline in TC numbers nearer the northwest Mexican coast in one regional modelling study (Diro et al., 2014) suggests a decrease in NAMS precipitation forced by TC passage, and a potential overall decrease in NAMS season precipitation, as the forcing contributed by TCs is not negligible to system precipitation (Cavazos et al., 2008). Finally, a large portion of the precipitation in this region is produced by mesoscale convective systems, which generally remain unresolved (Castro et al., 2012) despite increased resolutions in recent studies, further limiting confidence in projections.

There is *low confidence* at this time in projecting future changes in precipitation for the southwestern North America region.

#### *10.4.3.2.8 Caribbean small islands future summer drying*

The mid-summer drying that has been observed historically for the Caribbean, Central America and the Inter-American Seas in general (see Section 10.4.2.2.8) is anticipated to continue to the end of the 21st century. The summer drying in the Caribbean and Central America is one of the *strong and coherent* signals for this region in the CMIP3 models (Neelin et al., 2006). The decline in rainfall is projected to be strongest during the midsummer (June–August) and has been noted in studies using GCMs and RCMs under various emissions scenarios (Campbell et al., 2011; Karmacharya et al., 2017; Karmalkar et al., 2013; Rauscher et al., 2008; Taylor et al., 2018). This drying has also been noted in previous assessment reports of the IPCC (e.g., Christensen et al., 2007). Rauscher et al. (2008) showed that under the A1B scenario for 2061–2090 relative to 1961–1990, decreased precipitation over Central-America and the Intra-America Seas region was projected, mostly in June and July. They used 17 GCMs including three with high horizontal resolution (MIROC-H, HADGEM and ECHAM) because of the complex topography of the region and their ability to replicate the annual cycle of rainfall over the study area fairly well.

Campbell et al. (2011) and Taylor et al. (2007) used the PRECIS regional climate model forced by the HadAM3P under the A2 and B2 scenarios for 2071–2100 relative to 1961–1990 and found a robust summer drying over the Caribbean that extended from June to October. Karmalkar et al. (2013) used 15 GCMs and the PRECIS RCM driven by the HadAM3P and ECHAM4 GCMs and examined projections for 2080–2089 relative to 1970–1989 under the A2 scenario. Projections of a generally drier Caribbean were indicated using the GCM ensemble mean and the RCM driven with the two GCMs though different magnitudes of drying were suggested. Angeles et al. (2007) similarly showed a decrease in summer rainfall over Cuba by the mid-21st century using a fully coupled GCM (the Parallel Climate Model) for the Business as Usual, A2 and B2 scenarios.

Notably, some GCMs do not resolve the islands and are therefore unable to capture land-sea contrasts and topography (Karmalkar et al., 2013). Using these GCMs in the calculation of the ensemble means would have impacted on the magnitude of change projected. While RCM simulations show improvements over the driving GCM primarily through their improved representation of landmasses, their performance would also be dependent on the driving GCM. Additionally the sensitivity of model convection schemes to SST and

cold SST biases in the Caribbean region are likely implicated in the dry bias of the wet season rainfall that emerged in the Karmalkar et al. (2013) study.

More recent studies continue to support the projections of a drier Caribbean towards the end of century. Stennett-Brown et al. (2017) used statistical downscaling to downscale daily maximum and minimum temperature for 44 stations and rainfall for 39 stations for the Caribbean and neighbouring regions. The statistical models projected a sharp decline in July through August (JA) rainfall for northern Caribbean stations using the monthly climatology of mean daily rainfall under the A2 and B2 scenarios for 2070–2099 relative to 1961–1990. Taylor et al. (2018) suggested that the midsummer drought is intensifying with projections of decreasing JA rainfall for global warming targets of 1.0°C, 2.0°C and 2.5°C above pre-industrial levels for RCP4.5 for most of the Caribbean domain. A time-sampling approach was used in this study to determine the approximate future dates when the global mean surface air temperature attains increments of 1.5°, 2.0°, and 2.5°C above preindustrial times. Taylor et al. (2018) used a 42 member CMIP5 ensemble mean and 10 of 13 CMIP5 models examined by Ryu and Hayhoe (2014) that capture the characteristic bimodal rainfall pattern of the main Caribbean with peaks in June and September and for which RCP4.5 data were available.

The future summer drying over the Caribbean is associated with a projected future strengthening of the Caribbean Low Level Jet (CLLJ) (Taylor et al., 2013c). Rauscher et al. (2008) hypothesized that the simulated 21st century drying over Central America represents an early onset and intensification of the mid-summer drought. An analysis of circulation changes indicated that the westward expansion and intensification of the NASH associated with the mid-summer drought occurs earlier using the A1B simulations, along with stronger low-level easterlies. Climatologically, the NASH produces tropical easterly trade winds at its southern flank which set up a pressure gradient that becomes large semi-annually and facilitates an intensification of the easterly winds that form the CLLJ (Martínez et al., 2019; Reichle et al., 2017; Vizy and Cook, 2017; Wang, 2007; Wang and Lee, 2007). Rauscher et al. (2008) further suggested that the eastern Pacific ITCZ is also located further southward in the scenario simulations and that there are some indications that these changes could be forced by ENSO-like warming of the tropical eastern Pacific and increased land–ocean heating contrasts over the North American continent (Rauscher et al., 2008). Other studies also suggest a future intensification of the NASH due to changes in land-sea temperature contrast resulting from increased GHG concentrations (Li et al., 2012).

Rauscher et al. (2011) further proposed that Tropical North Atlantic (TNA) SSTs could also influence the drying over Central America and the Caribbean. TNA SSTs do not warm as much as the surrounding ocean. Therefore, the troposphere senses a TNA that is cooler than the tropical Pacific, potentially exciting a Gill-type response, increasing the strength of the NASH and enabling further drying over the region. The proposed mechanism to date has not decoupled the influence of anthropogenic trends versus natural decadal variability. Additionally, there is *high uncertainty* regarding the nature of ENSO and NAO variations in response to elevated levels of GHGs and there is a limitation to examining future changes in the interannual variability of the Caribbean climate (Karmalkar et al., 2013). AchutaRao and Sperber (2006) suggested that global models differ in their ability to represent ENSO variations and disagree significantly on its future evolution. Studies like DiNezio et al. (2009), Vecchi and Soden (2007) and Vecchi et al. (2006) suggested a perpetual ENSO-like state for the Pacific in the future that would be consistent with a summer drying in the Caribbean.

In summary, there is *medium confidence* that mid-summer drying over the Caribbean will be observed in coming decades due to *low confidence* in the mechanisms that govern this drying trend.

#### *10.4.3.2.9 Asian cities*

It is very uncertain to estimate how the UHI will evolve under climate change conditions because several studies using different methods report contrasting results. Several studies have investigated the changes in the UHI using global climate models coupled to urban canopy parameterizations (McCarthy et al., 2010; Oleson, 2012; Oleson et al., 2011) . The results showed that under simulation constraints of no urban growth both urban and rural areas warmed substantially in response to GHG-induced climate change but generally

the rural areas warmed more and reduced then the urban to rural contrast. The larger storage capacity of urban areas was found to buffer the increase in long-wave radiation, sensible heat flux is reduced accordingly so that urban air temperature warms less than rural air temperature.

Regional climate models have also been coupled to a single-layer urban scheme and results showed that the relative magnitude of UHIs in the UK and Japan would remain the same, while for Brussels, summertime rural areas were found to warm more than urban due to a soil dryness over rural areas limiting then the evapotranspiration (Adachi et al., 2012b; Hamdi et al., 2014; Kusaka et al., 2012; KUSAKA et al., 2012; McCarthy et al., 2012). Other studies generally employ a dynamical downscaling of GCM information with a RCM, while further high-resolution simulations are performed using statistical downscaling approach (Arsiso et al., 2018; Früh et al., 2011; Hatchett et al., 2016; Hoffmann et al., 2018; Sachindra et al., 2016). These studies found an increase of the UHIs in both Hamburg and Melbourne and a decrease during the summer in Addis Ababa under climate change conditions and no urban growth. Finally, in some studies the regionally downscaled model output is used to force an off-line urbanized land surface scheme (Lauwaet et al., 2015; Lemonsu et al., 2013; Rafael et al., 2017). These studies report also contrasting results about the changes in the UHIs. However, the contribution and feedback processes by urban heat island and climate change are not accounted for in these offline mode simulations.

In Asia, there are mature large cities such as Tokyo and others that are developing rapidly like cities in China and Southeast Asia. In this section, studies of future climate projection for Tokyo and two major cities of Vietnam, Ho Chi Minh (HCM) city and Hanoi, which are selected as case studies for developing cities, are assessed. The choice of Vietnam is motivated by the existence of a robust, long-term urban master plan for its cities and that they are among the most studied cities in the Southeast Asian countries with respect to climate change projections.

Studies on future urban climate projection using RCMs are roughly classified into three types: the first type is a high-resolution dynamical downscaling (DDS) experiment for cities while keeping the size of the city the same under future climate conditions. This type is termed the Future Climate-Current Urban (FC-CU) experiment in this section. In this experiment, climate projections performed by a GCM are used as lateral boundary conditions in the same way as a standard DDS except that it is conducted using an RCM at near-kilometre resolution and with dedicated urban parameterization embedded within its land surface model. The second type of downscaling experiment is performed by running an RCM under current conditions using the reanalysis as lateral boundary conditions, termed the Current Climate-Current Urban (CC-CU) experiment in this section. Comparing the results of the CC-CU and FC-CU experiments, it is possible to study the current urban environment under future climate projections. The third type of downscaling experiment is done by combining future climate scenarios together with future city planning scenario, known as Future Climate-Future Urban (FC-FU) experiment. Comparing the results of FC-FU and CC-CU experiments, it is possible to more accurately evaluate the magnitude of both future global warming and urbanization effects.

A pioneering study of urban climate projection (FC-CU) was conducted for Tokyo (Kusaka et al., 2012). The authors presented the projected urban climate for the 2070s' August under the SRES A1B scenario, by using the WRF model at 3-km spatial resolution and coupled to a single-layer urban canopy parameterization. The projected monthly average August temperatures in the 2070s were projected to be about 2.3°C higher than those in the 2000s and comparable to those in the record-breaking hot summer of 2010. The reason why such a research is attracting attention in Japanese mega-cities is that the summer is very hot and humid, and there is a strong concern that the total number of future heat stroke patients and the cooling demand will increase. Indeed, with ongoing urbanization and global warming, the summertime thermal environment in Japan has become so severe that the number of heat stroke causalities count more than 1,000 per year exceeding the number of deaths from natural disasters, including typhoons and tornados (Fumiaki et al., 2018).

Recently, urban climate projections considering future urban planning scenarios, i.e., FC-FU experiments have been conducted and indicated that projected future urban climate of Tokyo under the assumption that the expansion of Tokyo in the past 30 years will continue as it i (Adachi et al., 2012b). It was found that future global warming for the 2070s under the A1B scenario will give a larger contribution to the future

urban warming rather than the future urbanization. Kusaka et al. (2016) computed a future urban climate projection in 2050s under RCP4.5 scenario, assuming both a compact-city and s distributed-city scenarios for greater Tokyo. In the compact city scenario, the projected temperature increase in the plain was reduced by 0.2°C compared to the status quo scenario, while the dispersed city scenario raised the temperature by 0.3°C in the wide area surrounding central Tokyo, suggesting that the alternative urban scenarios have little impact on Tokyo's thermal environment. This result is consistent with the results for Brussels (Hamdi et al., 2015), but different from those for Beijing (Yan et al., 2016), Hanoi (Lee et al., 2017), HCM city (Doan and Kusaka, 2018), and US cities (Georgescu et al., 2013). Part of the reason for this is that Tokyo is a mature metropolis, with little remaining opportunity for significant changes in its urban structure. Urbanization influences precipitation as well as temperature, especially in the case of mega-cities. In Tokyo, summertime heavy rainfall is a major concern; however, almost all of the numerical studies are case studies, focusing on a specific rainfall event. As a first attempt, Kusaka et al. (2014) conducted sensitivity experiment with/without urban areas based on an RCM ensemble. The results showed that the past and the idealized future urbanization cause a statistically significant and robust increase in the amount of heavy precipitation in Tokyo and reduction in the surrounding inland areas.

Hanoi has been experiencing the rapid industrialization and urbanization since the country became a market economy in the late 1980s. During 1990–2010, the total urban population of Hanoi city increased from about 0.9 million to over 3 million, and it is expected to increase to approximately 10 million by 2030 as the urbanization continues. This speed of urban development is the fastest in Southeast Asia (Labbé and Boudreau, 2015). Lee et al. (2017) compared the future urbanization effect of Hanoi with the future global climate change effect for the 2030s horizon under RCP 4.5 and 8.5 scenarios (FC-FU). Here, the Master plan is used for future urban planning scenario. The results indicated that the temperature increase due to global climate change and local urbanization is at most 70% and 30%, respectively. This is completely different from that of Tokyo case as shown in Adachi et al. (2012) and Kusaka et al. (2016). Further investigation have been pursued on the roles of land-use/land-cover (LULC) and Anthropogenic Heat (AH) on the past, present, and future UHI effect over the greater Hanoi ((Doan and Kusaka, 2016) and Doan et al. (2019)). The results showed that the LULC-AH coupled changes during 2010–2030 will have much greater impact on the local UHI effect than those during 1990–2010. In the urban-core area, the monthly mean surface air temperature in July is projected to increase by 0.7°C by 2030, which is a doubling of the increase of 0.35°C during 1990–2010.

On the other hand, Doan and Kusaka (2018) conducted future climate projection for greater HCM city until 2050s. Here, Master plan is used for future urban planning scenario. The results showed that, in rural areas, the spatially averaged monthly mean air temperature in April was projected to increase by 1.2°C and 1.7°C by the 2050s under the RCP4.5 and RCP8.5 scenarios, respectively. In newly urbanized areas, an additional warming of 0.5°C is expected under both scenarios, which corresponds to 20–30% of the global warming. In particular, the additional warming due to urbanization could exceed 0.8°C at night. The impact of future urbanization (0.5°C) is comparable to the difference in the temperature increases achieved under the different RCP scenarios. Therefore, this impact should be considered in studies of the future urban climates of fast-growing cities in developing countries. Comparing the past and future urbanization effects, it is noteworthy that Asian mega-cities such as HCM are still developing and thus urbanization impact is likely to grow and contribute to future climate projection.

Finally, Kusaka et al. (2016) provided the first attempt in quantifying the uncertainties arising from choice of RCM or of future urban planning scenarios. The results showed that the impacts of urban planning scenario and RCM differences are larger during night time, but at most 0.6°C. The results indicate that the uncertainties related to both the RCM and urban planning scenario are significantly less than those arising from global emission scenarios or GCM projections. However, it is worth mentioning that there is a large difference between the RCM with and without urban land use, indicating that this impact is comparable to the differences between GCMs. Therefore, it will be necessary to set the detail land-use map with urban areas and urban canopy parameterization when projecting future urban climate for Asian mega-cities. Impact assessments and adaptation plans for Asian cities will require high spatial resolution climate projections along with: Models that represent urban processes, ensemble dynamical and statistical downscaling, local-impact models.

*10.4.3.2.10 Mountains: Himalayas future changes*

Given the importance of the Himalayas as the source of major Asian rivers, understanding how the regional climate may change in the future is vital for millions of people. Future increases in temperature and precipitation are expected to occur in the Himalayas during the 21st century based on both GCM and RCM climate projections.

Based on results from 21 CMIP5 models, Wu et al. (2017) showed that a general increase in mean temperature occurs over the Hindu Kush Himalayan during the 21st century under both RCP4.5 and RCP8.5, with the largest increase found during 2066–2095 under RCP8.5. Future projections from CMIP3 and CMIP5 suggested annual average temperature increases of 2.5°C–4°C and 2.8°C–4.5ºC over eastern and western Himalayas by the end of 21st century, respectively (Panday et al., 2015). Another study based on multi-model climate projection from CMIP5 showed a significant increase in the average annual temperature rate across all the climate stations over the Eastern Himalayas (Singh and Goyal, 2016). CMIP5 projections under RCP4.5 and RCP8.5 indicated a spread in temperature increases from about 1.5°C to 5°C over the western Himalayas by the mid-21st century (Tiwari et al., 2018). A strong rate of warming (0.03–0.09 °C/year) in the Himalayas across all seasons has also been projected by the CORDEX-SA RCM experiments under different RCP scenarios to the end of 21st century (Dimri et al., 2018). Sanjay et al. (2017) have used RCMs employed in the CORDEX-SA project to find that the Karakoram and northwestern Himalaya would exhibit significant seasonal warming, with slightly higher magnitude in winter than summer, by the end of the 21st century under the RCP8.5 scenario. Significant warming has also been projected in the Chamkhar Chhu basin in Bhutan (eastern Himalayas) and the Beas basin in India (western Himalayas) by two RCMs (Li et al., 2016b). In addition, another study based on RegCM3 simulations indicated an annual mean temperature rise of 0.64°C–5.15 °C in the eastern Himalaya by 2100 (Dash et al., 2012).

CMIP5 projections showed increasingly wetter summers in the Himalayas through the 21st century (Palazzi et al., 2015). Similarly, apart from the northwestern region, future precipitation over most parts of the Hindu Kush-Himalaya region is projected to increase under RCP4.5 and RCP8.5 based on CMIP5 projections (Wu et al., 2017a), including the Central Himalayas (Kadel et al., 2018). Except for a part of the Hindu Kush in the western Himalaya, which showed drier conditions, the CORDEX-SA experiments generally project wetter/drier conditions in the near future (2020–2049) for the western/easternHimalaya, a scenario that intensifies in the far future (2070–2099) (Choudhary and Dimri, 2018). The results from multiple RCMs within CORDEX-SA showed *good consensus* in projecting intensified future summer monsoon precipitation, by about 22% in the hilly sub-regions within the southeastern Himalaya and Tibetan Plateau for the 2066–2095 period under RCP8.5 (Sanjay et al., 2017). Future projections of precipitation in the Himalayan Indus region of Pakistan showed a consistent increase with a reduced rate of change in the far future (2071–2100) compared to the near future (2041–2070) (Ali et al., 2015). By using the RegCM4 RCM, Dash et al. (2015) also found that precipitation over the Himalayas is projected to increase in future across all RCPs. For the cold seasons, a wetter climate would occur in the western Himalaya-Karakoram during the 21st century estimated from CMIP3 and CMIP5 archives (Panday et al., 2015). Palazzi et al., (2015) reported that no significant change can be detected in winter precipitation over the Hindu Kush-Karakoram-Himalaya region throughout the 21st century predicted from the CMIP5 models. A consistent decline in Western Disturbance frequency over the 21st century has been found in CMIP5 RCP8.5 future climate simulations, causing reduced winter rainfall over affected regions within the Himalayas (Hunt et al., 2019, submitted paper).

Studies have confirmed that a warmer and wetter climate is projected to occur over the Himalayas toward the end of the 21st century under a range of scenarios among different models, although some uncertainties exist in the future climate projections (Dimri et al., 2018; Li et al., 2016; Kadel et al., 2018; Panday et al., 2015; Palazzi et al., 2015). These uncertainties arise from various sources, such as different forcings, boundary conditions, GCMs or RCMs selected, and choice of model physics (Choudhary and Dimri, 2018). GCMs from both CMIP3 and CMIP5 were able to simulate the spatial distribution of observed rainfall in pre-monsoon and winter months during 1902–2005 within the western Himalaya (Meher et al., 2017). Panday et al. (2015) showed that both CMIP3 and CMIP5 models capture the 20th century mean annual cycles of temperature and precipitation in the Hindu Kush-Himalaya well, but with a relatively large spread in

capturing observed precipitation regimes. However, the complex topography of the region is not properly resolved in CMIP5 models. Sanjay et al. (2017) suggested that the CORDEX-SA RCM-related uncertainty is found to be large for the projected changes in seasonal temperature and precipitation over Hindu Kush-Himalaya by the end of 21st century. Mishra (2015) found that the CORDEX-SA RCM projections show large uncertainty (1–3.6°C in temperature and 18–60% in precipitation) in the Himalayan region. The CORDEX-SA RCMs overestimate the observed warming and fail to reproduce observed precipitation trends, which raises a question as to their reliability for climate projections in the region. There is also a large systematic cold bias (-6°C to -8°C) in these RCMs (Nengker et al., 2018). The CORDEX-SA RCMs are also unable to capture the inter-annual variability of rainfall over the Himalayas (Ghimire et al., 2018). Both CMIP5 driving GCMs as well as the CORDEX RCMs models underestimate rainfall during summer over the northernmost parts of India covered by the Himalayas; however, the negative bias in CORDEX RCMs was shown to be larger than that of the driving GCMs (Mishra et al., 2018).

Despite the uncertainties in both GCM and RCM climate projections, there is *medium confidence* that a warmer and wetter climate will occur in the Himalayas during the next decades of the 21st century. There is *low confidence* in the magnitude and sub-regional spatial patterns of the projected temperature and precipitation changes.

#### *10.4.3.3 Assessment summary*

**[Placeholder: to be filled in for the SOD]**

## 10.5 Regional messages

Expected length: 8 pages, 1 page=950 words
Number of figures: 3
Number of tables: 0

One of the main objectives of this section is to assess approaches and challenges for producing climate information for informing adaption and policy at regional decision scales (see also Section 10.1.2.1). Here the term “decision scale” is used to recognize the intent that the climate information has an explicit societal application. There is no singular regional spatial or temporal scale of information need, but that scales range from high resolution (e.g. city infrastructure) through to subcontinental (e.g. large watershed management), while temporal scales range from near to medium term (e.g. health and agriculture) to century scale (e.g. large infrastructure). This section considers approaches that range from operational climate services to more ad hoc efforts taken by exploratory programs.

### *10.5.1 Approaches to regional information and climate services*

The diversity of approaches creates one of the most critical and fundamental challenges for the construction of useful information; and the choices made in choosing an approach may have deep consequences. In addition, different methodologies, and even different applications of the same methodology, can lead to contrasting messages (Figure 10.25) that may simply be a result of assumptions implicit in the methodology or choice of methodology.

**[START FIGURE 10.25 HERE]**

**Figure 10.25:** [Placeholder: Illustration of different and potentially conflicting information. The projected rainfall changes for the end of the century shows substantial differences between the EURO-CORDEX ensemble and the ENSEMBLES ensemble. For instance, for Northern France during MAM EURO-CORDEX projects wetting and ENSEMBLES no-change to drying. The difference is due to the different position of the North Atlantic jet in the

EURO-CORDEX ensemble (driven by CMIP5 GCMs) and ENSEMBLES ensemble (driven by CMIP3 GCMs). The plan for evolving the figure after FOD consists in addressing two important questions that are still not answered by these figures: 1) Are the differences significant or just reflection of natural variability. 2) What are the positions of the North Atlantic jet in CMIP3 and CMIP5? To answer these questions: 1) In the SOD a difference map with significance should be included, or probabilistic maps instead of ensemble means, 2) the position of the jet or storm tracks in CMIP will be added.]

**[END FIGURE 10.25 HERE]**

A range of approaches to constructing regional climate information are available, each with constraints in terms of achievable spatial and temporal resolution, issues of bias and error, different vulnerabilities in respects of stationarity, and with notable dependencies on methodological assumptions and decisions about how the methods are applied. These include:

1. Extrapolation of historical trends
2. Direct use of the output from GCMs, including high resolution GCMs
3. Application of downscaling of GCMs
4. Inferring regional climate change from an assessment of changes in driving processes
5. Storylines and narratives drawing on one or more of the prior sources
6. Utilizing expert knowledge and theory
7. Idealised scenario approaches (e.g. Hallegatte et al., 2013)

These approaches may also be used in combination. This is the case, for example, in the ASK method (Allen et al., 2000; Stott et al., 2013; Stott and Kettleborough, 2002), which combines extrapolation with model experiments.

Because approaches to information for societal application are assessed, here knowledge as information is considered in context (Aune, 1971; Baskarada and Koronios, 2013; Liew, 2007), that is, information that has been made part of a specific context and is useful in this context recognizing that data is not necessarily equivalent to information. The rise in demand (Lourenço et al., 2016) has resulted in diverse approaches that include various open access web portal delivery services of data as information (Hewitson et al., 2017), commercialization of climate services (Webber and Donner, 2017), and moves toward fully tailored "distillation" of information drawing on multiple data sets and methods in co-production with expert judgement of users.

Historically, the choice of approach has been embedded in a linear supply chain: extracting the source data, processing into maps or secondary data products, formulating for communication, and delivering to users. Such a chain, although it is intended to meet the interests for regional information, contains many assumptions that are not clear to recipients, and may introduce unforeseen propagation and growth of error, uncertainty and possible misunderstandings in the hand-over from one community to the next. This has led to the emergence of two new pathways: Work seeking to undertake the distillation of multi-model multi-method data in relation to the context of the information need (e.g. Hansen et al. 2009), and bottom-up approaches (Brown et al., 2012b) that begin with the user's articulation of vulnerability in the context of their multi-stressor system and then seeing what climate data might say about exceedance of some important thresholds (Culley et al., 2016).

Increasingly, regional climate change information is being developed through participatory and context-specific dialogues that bring together producers and users across disciplines, and define climate impact as one of the many stressors shaping user decisions (Brown et al., 2012; Lemos et al., 2012).

Thus, provision of climate change information for integration in decision making, from the perspective of the provider, relates to specific contexts for the type of information requirements. For example, to make agricultural management decisions, a farmer requires information about the onset and cessation dates of rains, the seasonal rainfall amount, as well as temporal and spatial information for any wet and dry spells. Thus, the format of the message, the frequency of delivery and the appropriate medium of communicating the message and obtaining feedback is best determined by engaging the end user right from the design stage.

The role of developing context relevant information is the domain of climate services and addresses a wide range of timescales, i.e. on month to century time scales, and so go beyond current operational weather services (Brasseur and Gallardo, 2016). Interest in climate services has grown in recent years. The European Commission established an Expert Group to develop a framework for action towards growing a strong and flourishing climate service sector across Europe (Street, 2016). At international level, the Global Framework for Climate Services (GFCS), a UN structure focused on improving the production, delivery, and application of climate information around the world was first implemented in 2011 (Hewitt et al., 2012). The GFCS prescribed five pillars required to build climate services: (1) a user interface platform, (2) climate services information system, (3) observations and monitoring, (4) research modelling and prediction, and (5) capacity development. Vaughan et al. (2016) conducted an international survey to identify priorities for research under each of the five pillars, revealing an overarching interest in research to improve the connection between information and its intended users. It also reveals significant interest in S2S prediction timescales.

Several types of approaches to provide climate services have been explored. Golding et al. (2017) presented three methods of engagement between providers and users of climate information in China: passive engagement, interactive group activities and focused relationships. They found that the three methods can be useful in different contexts, leading to significant benefits in enhancing engagement, information and establishment of sustainable relationships. Vogel et al. (2017) described an elaborated logic model to structure the evaluation of a climate services programme, which was successfully applied in a case study of the Caribbean Agrometeorological Initiative. Despite high-quality seasonal forecasts, they noted many shortcomings related to the dissemination of information and the willingness of farmers to act on it. Building on GFCS pillars 3 and 5, CLIMANDES (Rosas et al., 2016) is another initiative to introduce climate services in Peru under a pilot twinning project between the national weather service and MeteoSwiss. It was found that while a newly developed internet platform might be useful for decision makers, some communities, such as farmers in the Andes, might be ill equipped to integrate this information into their decision making. It was suggested that climate information needs to be explained in more detail in order to be understood appropriately and to reach countryside communities; in addition, more traditional methods of broadcasting, such as community radio, should be preferred since it is the common communication medium in the rural Andes. Other climate service prototypes exist for example in Uruguay (Vaughan et al., 2017), Argentina (Vera, 2018), Republic of Benin (Amegnaglo et al., 2017) and in Europe with the EUPORIAS project (Buontempo et al., 2018) where users play a key role in shaping the services they will eventually use. Using empirical evidence from Ghana, Naab et al. (2019) argued that if more attention is given to prioritising climate services through development strategies, it can offer reliable options for developing a resilient agricultural sector in sub-Saharan African.

Different climate services providers use different approaches for constructing regional information. For example, the Swedish climate services (Kjellström et al., 2016) is focused on producing country-scale, high-resolution climate projections by means of the Rossby Centre regional climate model RCA4. On the other hand, Cordex.be (Termonia et al., 2018b), an initiative for the foundation of climate services in Belgium, created a multi-model small ensemble of high-resolution projections over Belgium at convection-permitting resolution and also used these to drive seven local impact models. In an Australian context, Ekström et al. (2016) illustrated the potential pitfalls of GCM sub-sampling or the use of a single downscaled product when conducting impact, adaptation, and vulnerability research. They suggested using the broad range of climate change signals from all available model sources in order to best characterize the future and so avoid possible mal-adaptation. Other examples of using high resolution downscaling products for climate services exist, such as dynamical downscaling of global seasonal forecasts over Ethiopia (Tucker et al., 2018) or the future projection of extreme precipitation intensity-duration-frequency (IDF) curves for climate adaptation in New York state (DeGaetano and Castellano, 2017).

There is *high confidence* that the development and value of climate services benefits from working in close collaboration with stakeholders and practitioners in a solution-oriented, co-development approach, whereby users can also participate in the underpinning research by defining their needs and by developing specific requests.

While there exist a diversity of perspectives around what constitutes co-production of climate information

(Bremer and Meisch, 2017), there is *strong evidence and high agreement* that processes that support collaborative learning and information production involving a diversity of expertise including climate science and decision makers, results in enhanced integration of science evidence into decision making (Bremer and Meisch, 2017; Lemos et al., 2012).

This suggests that advanced tools and methods that are co-developed with users on how to formulate and communicate climate information will enhance the capacity of stakeholders to deal with uncertainties.

### *10.5.2 How context frames the message construction*

#### *10.5.2.1 Consideration of different contexts*

Climate messages seek to build knowledge for informing adaptation and policy. However, without context the climate information is not easily relatable to the information need (Baztan et al., 2017; Cash et al., 2003; Lemos et al., 2012). Section 10.1.3 identifies three implicit framing issues in constructing regional messages. Of these, the social context leads the framing of subsequent decisions about the message construction. This requires a nuanced and holistic approach to recognize complex system interdependencies (Daron et al., 2014). For example, a city's dependency on different water resources and the interplay of local and national government legislation with the different decision makers (Scott et al., 2018).

Context plays a role in determining the risks that may affect human systems and ecosystems and consequently the information need. Context thus brings inherent constraints on how messages are constructed to be optimally aligned to the application purpose. Contexts are unlimited in variety, but some key contextual elements may be identified that frame the decisions needed in constructing messages that are useful, and include:

- Whether the problem statement needs to be constructed through consultative activities (Baztan et al., 2017; Willyard et al., 2018) (e.g. thresholds of vulnerability in complex urban or rural systems) or is a more generic vulnerability already identified (e.g., Hallegatte et al., 2013)(e.g. frequency of flood events or recurrence intervals of multi-year drought);
- Societal capacity, cultural or institutional flexibility and willingness to respond to different messages;
- The operational capacity of the different actors (inclusive of users, producers, and communicators);
- Potential contrasts in assumed value systems (Henrich et al., 2010a, 2010b) (e.g. Western versus developing nation world views);
- The relative importance of climate change in relation to climate variability and non-climate stressors on the time/space scales of interest;
- Availability and accessibility of the required data aligned to the information needs;
- The knowledge (or lack of) and magnitude of uncertainty (and the question of deep uncertainty) and/or reconciliation of contrasting messages (e.g. local scale data from GCMs versus RCMs, and their cohesion with changes in large scale climate drivers);
- The challenge of obtaining local observations to assess models and messages in the current climate;
- The need for translation into narratives and/or storylines;

These and other contextual issues frame subsequent decisions about message construction, for example that an engineer typically seeks quantitative information, while the policy community may be more responsive to (complex) storylines and how messages are positioned within an identified risk framework (Figure 10.26). It should be noted that multiple contexts can coexist and potentially result in contested approaches (for example in relation to urban governance versus regional water resource management).

**[START FIGURE 10.26 HERE]**

**Figure 10.26:** [Placeholder: Illustration of a story line approach in conveying regional climate projection. Four possible scenarios are presented depending on the rise of global mean temperature and change in circulation pattern. Source: KNMI 2014 climate scenarios http://www.climatescenarios.nl/scenarios_summary/index.html.]

**[END FIGURE 10.26 HERE]**

*10.5.2.2 Conditioning by values and expertise of different communities*

Messaging is inherently influenced by the values of all parties; those constructing the message, those communicating the message, those hearing the message, and critically those who construct the problem statement which the message seeks to inform. For a message on climate change to be effective it needs to recognize and respond to the values of all parties (e.g., Bessette et al., 2017; Cash et al., 2003) especially taking into account that the world is culturally heterogeneous while the construction of messages is dominantly found in the developed nations' scientific community. Recognizing this is important to give the message saliency and relevance, most notably when informing the complexity of risks for human systems and ecosystems and resilience in developing nations (e.g., Baztan et al., 2017). Part of the challenge with climate messages, especially for messages of impactful change, is that they can be based on a variety of disciplines and target people with a variety of backgrounds, so that the messages may need to accommodate a range of normative lenses (Gorddard et al., 2016; Sarewitz, 2004). Lack of this recognition can make messaging ineffective (Figure 10.27). In addition, political activists may purposely skew messages to motivate support of their partisans (Hamilton, 2011).

**[START FIGURE 10.27 HERE]**

**Figure 10.27:** [Placeholder: To forge this bridge of saliency and relevance, co-producing knowledge with stakeholders is needed. This bridge is now often not existing resulting in wasted knowledge and hampering climate adaptation. Source (Irwin et al., 2018). The plan for evolving after FOD consists in based on this figure to design a new one that in addition also illustrates how a message can be distilled from this bridge.]

**[END FIGURE 10.27 HERE]**

There is a substantial body of evidence that shows that the receptiveness of individuals to climate messages is strongly conditioned by motivated reasoning (Hart and Nisbet, 2012; Kahan, 2012, 2013), wherein a person's reception of climate information is influenced by the values of the community with which the person identifies. This can affect people of any political persuasion which in turn affects how critically or approvingly they accept statements provided by the scientific community. Adherence to a community's values forms part of an individual's social identity (Hart and Nisbet, 2012); fear of losing membership of the community can easily outweigh considerations of how believable statements about climate change might be (Hart and Nisbet, 2012). Individuals thus frame their analysis and understanding of climate messages in the context of cultural values espoused by their community (Bessette et al., 2017; Campbell and Kay, 2014; Hart and Nisbet, 2012; Kahan, 2012, 2013; Tschakert et al., 2017; Vezér et al., 2018).

Overcoming resistance to receiving a climate message is not simply a matter of presenting more information; the so-called Public Irrationality Thesis, which argues that further educating people on a topic will increase their receptiveness to its messages, is ineffective (Kahan, 2013). Rather, giving more information can harden an aversion to climate messages and the aversion, if present, can be stronger for people who are more scientifically literate: they feel more confident sifting through all sources of information to find support for their positions (Kahan, 2012). Divisions over the believability of climate messages can thus become stronger with increased knowledge and, notably, with increased capacity for reflection (Kahan, 2013). A challenge of messaging, then, is that if it is not framed carefully, it may make the sceptical person less receptive to further messages about climate change (Hart and Nisbet, 2012).

Successful framing of climate messages thus seeks to identify interests in targeted groups that yield a common ground between the messenger and the recipients for viewing the messages and responding to them. In doing so, an important factor is recognizing that an aversion to impactful solutions to climate change, such as one that poses economic challenges (e.g., Bessette et al., 2017) may be a greater cause of a person's

negative response to climate messages than the message itself (Campbell and Kay, 2014). Proposed response measures may violate personal or community values, regardless of acceptance of the message of climate change. Successful framing and response have occurred when climate information is presented in a region-focused context with respect to a local challenge posed by climate change. Thus, two U.S. states with fairly conservative leadership, which tends to be more sceptical about climate change, have passed initiatives that respond to specific, local impacts of climate change: rising sea level in Florida and water-resource shortfalls in Arizona (Kahan, 2013). Key factors were recognizing a serious impact and avoiding a central motivation of fighting global climate change.

The effectiveness of climate messages can increase if developed in partnership with the communities for which the message is intended (Tschakert et al., 2016), an approach that can inspire trust among all parties and thus promote a productive relationship (Cash et al., 2003). Such partnerships are expedited if the relevant modelling that leads to the messaging is transparent and accessible (Vezér et al., 2018). This is not always possible with climate and climate impacts simulation, but developing mental models can help, provided they are values-informed (Bessette et al., 2017). This does not preclude the climate-research community from taking steps to develop and convey messages. It does, however, mean that climate services can become an effective means for taking messages from the climate community and crafting them to be consistent with the needs, interests and values of stakeholder communities.

#### *10.5.2.3 The relative roles of spatial and temporal resolution in relation to decision scale*

Climate processes occur on a range of spatial and temporal scales, from global to local, from centuries and longer to days or less (Section 10.1.2 and Figure 10.1). Similarly, decisions by stakeholders cover a range of spatial and temporal scales that can vary with the size of their jurisdiction and scope of activity, which determine their (spatial and temporal) decision scales. However, the link between decision scales and the spatial and temporal resolution of climate and related natural-system information is not straightforward, and failure to recognize mismatches between the two can undermine the effectiveness of messages (Cumming et al., 2006; Sayles, 2018).

The scale of regional climate information does not have to be the same as the decision scale. For example, process-based narratives can create messages that are relevant to making local decisions. Thus, an expectation of increased multi-year drought episodes over a subcontinental region due to changes in circulation patterns can be relevant to decisions by an individual farmer. On the other hand, extreme precipitation processes can occur on scales of tens of km and smaller and thus require high resolution climate information when projected future changes (e.g., Xie et al., 2015). An important factor for effective information is matching the vulnerability of the social and economic systems (which could range from, e.g., a farmer to a national agricultural ministry) with the most prominent changes in the natural system (Andreassen et al., 2018; O'Higgins et al., 2019). More sophisticated matching of spatial and temporal resolution of climate information with decision scales might require engagement across a hierarchy of governance structures at national, regional and local level (e.g., Lagabrielle et al., 2018).

#### *10.5.2.4 Addressing compound events and non-traditional variables*

Users often require and need information from compound events (e.g. concurrent drought and heat (Zscheischler and Seneviratne, 2017); concurrent precipitation and wind extremes (Martius et al., 2016))and in the form of non-traditional variables. The latter is defined as post-processed output from models (e.g. heat stress, heating degree days, cooling degree days, growing degree days, drought indices, fire-weather indices, evaporation surplus). Compound events refer to the combination of multiple drivers and/or hazards that contributes to societal or environmental risk (Zscheischler et al., 2018). Because large impacts are often not linked to single climate extremes, a good understanding of compound events is critical for managing the climate-related risks for human systems and ecosystems (Leonard et al., 2014). Awareness for correlated hazards is increasing in the research community and crucial for risk assessment because compound hazards often lead to disproportionate damages. This has been shown for compound precipitation and wind extremes

and their impacts on infrastructure (Martius et al., 2016), compound storm surge and rainfall extremes and associated flood damage (Wahl et al., 2015) and compound drought and heat and their effect on terrestrial carbon uptake (Zscheischler et al., 2014).

Non-traditional variables depend on multiple climate variables and can directly be computed from climate model output. For instance, heat stress indicators are typically based on some combination of temperature and relative humidity (Lee, 1980). Many impact assessments rely on absolute values of non-traditional variables. For instance, a heat index larger than 40.6 is considered dangerous (Anderson et al., 2013). Similarly, energy consumption for heating and cooling of buildings relies on precise estimates of heating and cooling degree days. Crop models rely on the number of growing degree days. Fire warnings are issued when a specific fire-related indicators exceed a certain threshold (de Jong et al., 2016). Due to biases in climate models, assessing risks associated with climate through projections of non-traditional variables is not straightforward and typically requires some sort of bias adjustment. Most standard bias adjustment methods adjust one variable at a time, thus ignoring potential biases in the dependence structure between the variables that contribute to a non-traditional variable. In some cases, these biases can compensate each other, so that the overall uncertainty in the non-traditional variable is smaller than what one would expect by analysing the contributing variables. For instance, models with a strong warming tend to also show a larger reduction in relative humidity such that heat stress projections seem to be relatively well constrained in the future (Fischer and Knutti, 2012). On the other hand, commonly applied univariate bias adjustment can increase biases and consequently also lead to more uncertain projections. This has been for instance for heat stress (Zscheischler et al., 2019). In general, purely univariate bias adjustment methods fail when: 1) the non-traditional variable depends equally strongly on more than one climatic driver, 2) climate models have biases in the dependence structure of the drivers and 3) univariate biases are relatively small. To address these issues, several approaches that adjust the dependence structure in addition to the marginal distributions have been suggested in the recent years (Cannon, 2018; Gutiérrez et al., 2018; Vrac, 2018; Vrac and Friederichs, 2015). Adjusting for dependencies in driving variables can also improve process-based impacts modelling, as has been shown for hydrological impacts in alpine catchments (Meyer et al., 2019).

When events are very complex or rare, it is often difficult to assign likelihood to the event. In such cases, storylines (Section 10.5.3) can be used to explore potentially devastating events. These are particularly helpful for studying compound and cascading events, which can often not be addressed by standard probabilistic frameworks. This is accomplished by presenting physically self-consistent unfolding of past events, or plausible future events or pathways, which frame risk for human systems and ecosystems in an event-oriented rather than a probabilistic manner, while providing a physical basis for partitioning uncertainty and explore the boundaries of plausibility (Shepherd et al., 2018).

A regional message on climate change is intended to inform decision makers. There is *high confidence* that the inclusion of users ensures that the context contributes to formulating the message. As such, the context becomes a central component in the development of useful regional information for application.

### *10.5.3 Narratives and storylines*

#### *10.5.3.1 Assessing the roles of narratives and storylines*

Narratives and storylines are approaches to communicating climate change messages (e.g. Dessai et al., 2018; Fløttum & Gjerstad, 2017; Moezzi et al., 2017; Scott et al., 2018), which seek to build a cohesive picture of a climate message that moves beyond the presentation of data and figures. The terms narrative and storyline are used inconsistently in the literature, and may, for example, refer to using climate processes and expert elicitation to build narratives of future regional precipitation change (Dessai et al., 2018), plausible storylines of atmospheric circulation change (Zappa and Shepherd, 2017), or the interchangeable use of the concepts of stories, narratives, and storytelling to go beyond analytic approaches (Moezzi et al., 2017). The use of these terms ranges from early compound phrasing of “narrative storylines” (Schneider, 2001) to emergent transdisciplinary narrative framing approaches (Scott et al., 2018) and storylines derived from mutually exclusive but equally plausible changes in the atmospheric circulation (Zappa and Shepherd, 2017).

The approaches of narratives and storylines are together complementary to ensemble means and probabilistic projections. It is possible that important climate-derived risks for human systems and ecosystems may be missed or downplayed considering only mean climate changes (e.g. Sutton, 2018) or in cases where risk is viewed as the probability of an event times the impact of the event (e.g. Oppenheimer et al., 2015). Many low probability events may have high impact and thus pose substantial risk for human systems and ecosystems. Thus, probabilistic projections can obscure what is important for an individual impact assessment (Shepherd et al., 2018), and may also not convey easily the multi-faceted, multivariate nature of an impactful change. Responding appropriately to climate change entails recognising risks for human systems and ecosystems and taking suitable measures, which might include watching for the emergence of projected low-probability events.

The terms narratives and storylines will likely continue to be used interchangeably. This section does not attempt to draw a distinction. It is nonetheless useful to identify two different facets of storylines and narratives. In the one hand the IPCC SR1.5 (Chapter 3, Box 8) considers a subset of storylines out of the many possibilities, whereas Fløttum & Gjerstad (2017) speak of the narrative perspective to identify the presence or absence of relevant elements in a story. The contrast suggests two elements of importance; a story about one of many possible evolutionary developments of events, and a narrative that captures the relevant foundations of regional climate change on which the range of possible stories are based.

For example, one may have a narrative of projected future climate based on the evidence from CMIP5 or CMIP6, yet there be many storylines that connect the narrative to the user context in terms of pathways, events, impacts or consequences. Thus narratives/storylines have a two-fold purpose to develop evidence-based textual descriptions of some state of the past, present, and future climate out of which many possible storylines of evolution and events may be constructed.

Fløttum and Gjerstad (2017) provided a review of the use of storylines/narratives in the climate change discourse, noting that a diverse picture of climate change can be effectively communicated, yet may also compound confusion. Scott et al. (2018) provided an in-depth example of using a narrative approach to climate change and urban water in a transdisciplinary process that is indicative of the emergent co-production paradigm to developing climate change messages.

This approach ideally brings together multiple sources of information, from various climate modelling methodologies through to expert opinion. This allows an assessment of the plausibility of projected changes that may pose substantial risk for human systems and ecosystems and provides foundational messaging in a form that can align with developing relevant storylines for stakeholder needs, values and interests. Because narratives can engage a range of information sources they can provide a basis for distilling climate output from multiple sources along with expert opinion to produce plausible, defensible and actionable climate information.

As discussed in Section 10.5.2, the effectiveness of a climate message, and thus the effectiveness of a storyline, is linked both to the values and perspectives of the intended recipients, and what is believed about the robustness of the source data. Risk, in particular, entails recognising that the magnitude of an impact depends on what is valued by the impacted community. Storylines can be tailored to recognize the values and interests of the intended audiences (Bhave et al., 2018; Hazeleger et al., 2015; Kok et al., 2014), providing the sequences of weather and climate events, such as drought or pluvial episodes, that are part of the climate change scenario in a succinct, physically plausible manner (Hazeleger et al., 2015).

Storylines can blend expert judgement with model output to assess the physical plausibility and consistency of projected changes. It is increasingly recognized that making good use of output from climate models for adaptation and mitigation planning requires expert judgement of projections of changing climate (Dessai et al., 2018; Lempert et al., 2006; Thompson et al., 2016). Storylines built on narratives of the projected change that can arise in many ways, which allows tailoring them for their intended use. For example, Zappa and Shepherd (2017) used their expertise in atmospheric circulation to identify key remote drivers of regional circulation and climate over parts of Europe, showing how differences in their evolution can influence

regional climate change. Storylines of circulation evolution thus become a basis for monitoring ongoing change within a set of plausible futures and for assessing the robustness of simulated projections (James et al., 2015; Stevens et al., 2016). Storylines can prompt novel blends of numerical weather prediction and climate projection to "forecast" behaviour of future high impact, and thus high risk, events during climate states in which they might appear (Hazeleger et al., 2015). Thus, one can achieve a fine-scale, multivariate rendering of event evolution that can show how high-impact weather sequences in the future might change and what responses are needed. The choice of episodes to target can use the expertise of stakeholders who must develop appropriate response measures (e.g., water-resource managers, health professionals, etc.).

Climate-related risks for human systems and ecosystems are typically greater in developing countries, owing in part to their greater vulnerability and lower capacity for adaptation (e.g., Bhave et al., 2016). Storyline development, however, can engage experts on a region's climate (Dessai et al., 2018) or stakeholders (Bhave et al., 2018; Scott et al., 2018) to co-produce storylines that foster adaptive responses to meaningfully account for a region's development needs.

**[Placeholder: Expect new literature in the next year to help refine the definition of the terms; there are some papers in the works on this; leave it at this to be further fleshed out with new emerging literature for the SOD.]**

### *10.5.4 Distillation and multiple lines of evidence*

The preceding sections provide evidence of the diversity of approaches and methods where different approaches and methods are used to construct and distil messages. Similar diversity also exists where climate science interacts with use contexts in which approaches range from data delivery with a focus on visualisation and user friendly interfaces (e.g. portals), through to intensive long term engagement with user communities deploying trans-disciplinary principles. Further diversity exists within the decision contexts themselves where a wide range of decision methods, both formal and informal are deployed. A key question is whether there is a best approach to constructing climate messages to inform decisions at a regional or smaller scale, and if there is best practice.

The term distillation lacks a clear definition yet speaks to the challenges of constructing or distilling messages of value to society from a diverse range of evidence. Central to the concept is the recognition that there are multiple data sources and many analysis methods that collectively may inform a useful regional climate change message. Choices about how to approach this can fundamentally alter the derived conclusions.

The available evidence includes observations and reanalysis of historical climate, projections of future or alternate climate states based on model simulation experiments, and statistically and dynamically downscaled climate projections.

There are two traditional complementary approaches to dealing with contrasts between sources. First is to attempt to identify the most valid or skilful evidence while the second approach is to integrate differences into uncertainty estimates. The most common example is the estimation of the uncertainty in future climate projections using multi-model ensemble projections. It should be noted that differences between observational datasets are seldom integrated into uncertainty. However, a number of assumptions need to be made and these have consequences for the use of the resultant information or messages.

Not reducing uncertainty in any way, like for instance distilling messages that span the full range of all available theoretical, observational and model evidence, also involves assuming that all available evidence is valid and should be considered, and that the resultant range of possible outcomes describes the possibility space that decision makers need to consider. It may also involve the assumption that this possibility space is complete, or it may assume that the possibility space described by all available evidence remains too limited and that possibilities outside of this space are also possible (Stainforth et al., 2007). Robust Decision Making (RDM) (Lempert et al., 2006b; Lempert and Collins, 2007; Walker et al., 2013; Weaver et al., 2013) are a

class of approaches that recognize this and assume very large climate uncertainty in order to identify points of failure or optimal decision spaces before, in some cases, assigning probabilities to those failure points.

Climate information distillation is essentially the process of making informed assumptions in order to distil messages for decision contexts. The core element of distillation is the trade-off between uncertainty and the risk of error. Assuming that any future is possible then probability of being wrong is small (arguably zero, depending on our imagination). As the range of possible futures is narrowed down by making assumptions (informed or uninformed), then the probability that the future unfolds outside of our projected range is increased. This is not a zero sum game in that knowledge about the climate system means that uncertainty can be reduced substantively without an equivalent increase in the risk of error. In other words, advances in climate science have allowed us to, and continue to provide the opportunity to, reduce uncertainty without necessarily increasing the risk of error (Hawkins and Sutton, 2009, 2011).

Normally, the assumptions made in the process of producing climate information are made by climate scientists. The decision to use particular datasets, particular models or model ensembles, downscaling method selection, exclusion or weighting models, presenting particular ensemble quantile statistics, etc. are almost always made by climate scientists. Distillation raises questions about who makes these assumptions, or at least how they are informed. As noted above, there is strong evidence that understanding the use context is important in producing climate information messages. Hence, distillation starts with understanding the use context. However, it is important to note that the use context should be far more general than often considered in climate services literature. For example, in providing climate change data to drive an analysis of impact models (e.g. (McSweeney et al., 2015)), the impact modelling analysis is the use case and needs to inform the assumptions made.

Climate information production often occurs under the over-arching assumption that uncertainty is a problem and reducing uncertainty is the priority (Eisenack et al., 2014). This is both a psychological barrier (Morton et al., 2011), as well as pragmatic barrier in cases where uncertainty appears to limit the ability to make decisions (Mukheibir and Ziervogel, 2007). However, where in depth engagements with decision contexts are undertaken, these initial barriers are often dismantled to reveal a more complex and nuanced intersection with climate uncertainty (Lemos et al., 2012b; Moss, 2016; Rice et al., 2009). Hence the first step in climate information distillation is interrogating the use context. Of course there are many cases where the use context is essentially unknown. Rather than diminishing a focus on the use context, these cases may produce more focus on the use and potential misuse (Arnold, 2011; Street, 2016; Lamb, 2017) and inform that assumptions and choices made in producing the information.

Going further than understanding the use case involves including non-climate scientists in the process of making assumptions, or at least guiding assumptions (Bhave et al., 2018; Collins and Ison, 2009; Wildschut, 2017). Importantly, the application of trans-disciplinary engagement processes that emphasise the role of non-scientists in the learning and knowledge production process, builds relationships and trust between information users and producers which is arguably as important for the uptake of climate science into decision making as the nature of the climate information itself. Transparency and humility are also emphasized as they allow non-scientists to make informed decisions about the information they are being presented with, be involved in decisions about approaches and assumptions, and take ownership of the resultant information (Pettenger, 2016; Verrax, 2017).

Reducing uncertainty involves making assumptions. In the case of the ensemble mean, the assumptions are that the ensemble mean is more skilful than any single model, and that this means that the climate is more likely to evolve in line with this mean than with any other model. Another is to map out various percentiles across the range of projected changes. For example, in the AR5 Atlas, maps were presented of the 25th, median, and 75th percentiles of the CMIP5 ensemble projected changes of key variables.

Many approaches to reducing uncertainty exist. The use of emergent constraints (Allen and Ingram, 2002; Borodina et al., 2017; Brown et al., 2018; Collins et al., 2012; Cox et al., 2018; Knutti et al., 2017; Li et al., 2017a, 2018a; Nijsse and Dijkstra, 2018; Stott and Forest, 2007) is fairly widespread. The approach is dependent on identifying suitable observational constraints and on the robustness of the identified constraints

(Bracegirdle and Stephenson, 2013; Brown et al., 2018; Knutti et al., 2017; Masson and Knutti, 2013). The assumptions made are that the identified relationship between observed trends and simulated trends are physically plausible and robust, and that these relationships hold linearly into the future time period. Making these assumptions involves some level of statistical evidence but also a level of expert judgement.

Model exclusion or weighting can also be applied (Giorgi and Mearns, 2002b, 2003; McSweeney et al., 2012, 2015; Smith and Chandler, 2010; Walsh et al., 2008) based on the assumption that models that are able to better represent some observed climate statistical parameters are more reliable or accurate and hence their projected changes should be emphasised when developing statistics of future projected changes across a multi-model ensemble.

**[Placeholder for description and unpacking of other emerging methods]**

*10.5.4.1 Multiple lines of evidence*

**[Placeholder: Multiple lines of evidence are where results from observations, physical theory, past climate changes and climate model simulations, and dynamical and statistical downscaling, are assessed through expert judgement. This necessarily involves a measure of subjectivity and is readily biased by availability and accessibility of different data resources and by the capacity of the assessor in drawing these together, including value judgements and consideration of the how the problem statement is formulated (see Section 10.5.2).]**

*10.5.4.2 Differences, congruence and credibility of information sources*

**[Placeholder: GCMs produce drying, but RCMs better resolve the orography over mountainous areas, while ESD approaches can again be different and are contingent on the historical record. In addition, information from the large-scale drivers can lead to competing inferences.]**

## 10.6 Fully-integrated end-to-end case studies

Expected length: 9 pages, 1 page=950 words
Number of figures: 4
Number of tables: 0

### *10.6.1 Introduction*

Examining the activities around the construction of regional climate messages for communication and application exposes the strengths and weaknesses in the linking of different elements, and of the assumptions and consequences of decisions made in the process. This section explores these issues through three contrasting case studies. The end-to-end case studies are framed within a human dimension to contextualise the regional climate message. The recent Cape Town drought, the South Asian monsoon and the Mediterranean summer warming have been chosen for study since most of the aspects of regional climate outlined thus far in Chapter 10 are directly relevant to each case.

The three end-to-end case studies considered follow a similar structure:

- Introduction contextualising the human dimension
- Issues pertaining to the region's climate such as the sort of hydroclimatic zone covered
- Relevant anthropogenic and natural drivers
- Observational issues
- Assessment of global models over the historical period
- Results from global projections
- Messages from downscaled studies

- Potential for abrupt change
- Storyline and narrative approaches
- Assessment summary integrating the multiple lines of evidence

### *10.6.2 Cape Town drought*

#### *10.6.2.1 Introduction*

Cape Town's "Day Zero" water crisis in 2018 threatened a shut-down of water supply to 3.4 million inhabitants of the city and resulted in domestic water use restriction of 50 l/person/day lasting for 9 months, punitive water tariffs, and temporary closure of irrigation systems. Problems with water supply in many large cities in developing countries are endemic and rarely reported internationally. The water crisis in Cape Town attracted considerable international attention to a city with functional government structures, well developed services (compared to other urban centres in Africa), a centre of international tourism, and an economic hub with GDP of $22 billion (~$6,000 per capita) (CoCT, 2018) that exceeds that of many developing countries. The crisis was widely seen as a harbinger of future problems to be faced by the city, and a highlight of vulnerability of many cities in the world resulting from interplay of three factors: 1) the fast urban-population growth, 2) the economic, policy, infrastructural and water resource paradigms and constraints, and 3) anthropogenic climate change.

The Cape Town's crisis was a result of a combination of a strong multi-year meteorological drought (Figure 10.28), the severity of which is estimated at 1 in 300 years (Wolski, 2018), and factors related to the nature of the water supply system, operational water management and water resource policies. Cape Town was very successful in implementing water saving actions after the previous drought of 2000–2003, reducing water losses from over 22% to 14% (DWA, 2013; Frame and Killick, 2007), in effect decoupling a previous link between population and growth in water demand. As a consequence, Cape Town won a Water Smart City award only three years prior to the crisis. The water-saving actions, together with changing priorities in water resource provision from infrastructure-oriented towards resource and demand management, have likely led to delays in implementation of the expansion of water supply infrastructure (Muller, 2018). The expansion plan, formulated a decade prior to the crisis, fully anticipated long-term climate change-related drying in the region (DWAF, 2007). The crisis also exposed structural deficiencies of water management and inadequacy of the policy model where decisions about local water resources are taken at a national level, particularly in a situation of political tension (Visser, 2018).

**[START FIGURE 10.28 HERE]**

**Figure 10.28:** [Placeholder: Monthly rainfall during the 2015-2017 period. Average of 51 quality controlled and gap-filled series from stations within the Cape Town region.]

**[END FIGURE 10.28 HERE]**

Economic and social impacts of the crisis were significant. Loss of revenue of companies of all sizes resulted from the scaling down of water-dependent activities, but also from the need to invest in water efficient technologies and processes. The upside, however, is that the latter likely increased city's resilience in the long-term. Tourism was affected too through reduced arrivals and bookings, although only temporarily (CTT, 2018). In the agricultural sector, 30,000 people were laid-off and production dropped by 20% (Louw and Boonzaaier, 2018). The crisis initially polarized the society, with conflict emerging between various water users and erosion of trust in the government, but eventually social cohesion and an acute awareness of water resource emerged (Robins, 2019).

#### *10.6.2.2 The regional climate of Cape Town and surrounding area*

An evaluation of the relative role of rainfall and temperature signal in the 2015–2017 hydrological drought gives a strong indication that lack of rainfall was the primary driver (Otto et al., 2018). Thus, the remainder of this section focuses on rainfall.

Cape Town is located at the southwestern tip of Africa, with an approximately 100 km x 300 km region receiving 80% of its rainfall during the austral winter, spanning March to October, with core in June to August. The region is surrounded by arid and semi-arid regions with summer rainfall regime. In the vicinity of Cape Town, rainfall is strongly heterogeneous, ranging from ~300 mm/year in coastal plains to >2,000 mm/year in mountain ranges. Cape Town's water supply relies on surface water reservoirs located in and supplied from a few small areas of ~800 $km^2$ in total mountain catchments. Cape Town's region receives 85% of its rainfall from a series of cold fronts forming within the mid-latitude cyclones. The remainder is brought in by the infrequent cut-off lows that occur throughout the year (Favre et al., 2013). This creates a very strong water resource dependency on a single rainfall delivery mechanism, which is potentially strongly affected by anthropogenic climate change (see Section 10.6.2.3).

The climatic event underlying the crisis was a multi-year drought, with strong rainfall anomalies in shoulder seasons (March to May, and less strongly in September to November), and average rainfall in June and July (Mahlalela et al., 2018; Sousa et al., 2018a). The anomaly resulted from fewer rainfall events and lower average intensity of events. The anomaly manifested strongest in the mountains (Wolski et al., 2019).

### *10.6.2.3 Relevant anthropogenic and natural drivers*

Considering the primary rainfall delivery mechanism, frontal rain, the dominant large-scale drivers of relevance are those that affect the cyclogenesis, frontogenesis and the latitudinal position and moisture supply of the mid-latitude westerlies. The region's rainfall is linked to the Southern Annular Mode (SAM; Reason and Rouault, 2005), the dominant monthly and interannual mode of Southern Hemisphere atmospheric variability, and a measure of the pressure gradient across high latitudes. The mechanisms through which SAM affects the region rainfall involve shifting and weakening in the subtropical jet, as well as changes in the low-level moisture flux, convergence and relative vorticity over the region (Reason and Rouault, 2005). Note that, while in the post-1950 period, the SAM displays a long-term trend, the Cape Town region's rainfall does not (see below), and the SAM-rainfall relationship manifests at shorter time scales, as evidenced by the need to detrend both SAM and rainfall anomalies in order to detect significant correlations (Mahlalela et al., 2018; Reason and Rouault, 2005). There is, therefore, *weak evidence* that a trend in SAM manifests as a trend in the Cape Town region's rainfall.

The SAM varies with a characteristic decorrelation time of ~2 weeks, but its low frequency variability is influenced by GHGs (Fyfe et al., 2012), stratospheric ozone (Arblaster et al., 2011; Thompson et al., 2011) and ENSO (Lim et al., 2016b). The influence of ENSO on SAM manifests mostly in austral summer. The influence of GHGs on SAM is similar in nature to that resulting from the depletion of ozone in the Antarctic, with the historical trend in SAM related mostly to ozone depletion. The ongoing ozone recovery compensates for the GHG increase, but the GHG increase is projected to dominate after 2045 (Barnes et al., 2014a). The influence of ozone, however, manifests mostly in the austral summer SAM state, and it is thus not certain whether or not ozone dynamics have impacts on austral winter rainfall in general, and the Cape Town region's winter and early winter rainfall in particular.

The Cape Town region's rainfall is also potentially affected by other hemispheric phenomena such as the expansion of the tropics and, specifically, the South Atlantic high-pressure system and the position of the sub-tropical and polar jets. The relationships between the latter phenomenon and Cape Town rainfall have not been thoroughly investigated outside of the context of the 2015–2017 drought, but the drought itself was associated with the poleward expansion of the subtropical anticyclones in the South Atlantic and South Indian Oceans and (a resulting) poleward displacement in the moisture corridor across the South Atlantic (Sousa et al. 2018), as well as a weaker subtropical jet (Mahlalela et al., 2018).

Rainfall in the Cape Town region also responds to SST anomalies in the Southeast Atlantic, including the Agulhas Current retroflection region, which may drive intensification of the low-pressure systems, leading to the trailing front strengthening as it makes landfall over the Cape Town region (Reason and Jagadheesha, 2005). There are also linkages at seasonal time scale between the Cape Town region's rainfall and Antarctic sea ice (Blamey and Reason, 2007). The relationship between ENSO and Cape Town's rainfall is weak and time-inconsistent, manifesting the strongest impact in May to June (Philippon et al., 2012).

#### *10.6.2.4 Observational issues for this region*

Compared to other African countries, South Africa and the Cape Town region have good instrumental weather data. Records start in late 1800s, with in excess of 10 gauges reporting since 1920s, expanding to ~80 gauges in 1980s, and reduction in number or rain gauges since. Few records are available in the mountains receiving more than 1,000 mm/year. In view of strong heterogeneity of rainfall, the changes in number of stations contributing to datasets such as CRU and GPCP results in their unreliability in the region (Wolski et al., 2019; Figure 10.28).

#### *10.6.2.5 Historical climate and its representation in CMIP models*

Although the 2015–2017 drought was unprecedented in the historical record, Cape Town has experienced droughts of substantial magnitude, notably in the 1930s, 1970s and more recently in 2000-2003. Long term (>90 years) rainfall trends are mixed in sign, location-dependent, and weak (Kruger and Nxumalo, 2017; Wolski et al., 2019), mixed in sign in mid-term (~50 years; MacKellar et al., 2014), and mostly decreasing in the post 1981 period, particularly in March to May and December to February (Sousa et al., 2018a; Wolski et al., 2019), leading to a later onset and an earlier cessation of the rainy season. Temperature trends are in the order of 0.15–0.2˚C/decade (Kruger and Shongwe, 2004), locally reaching 0.3˚C/decade (MacKellar et al., 2014).

Due to the small scale of the Cape Town region, it is difficult to robustly compare CMIP5 GCM simulations to observations. However, in general, the CMIP5 models capture well the nature of seasonality, such as the dominance of austral winter rains, although details like the distribution of rains between the core and tails of the rainy season are not well captured (Mahlalela et al., 2018). For the post-1960s period, the large majority of CMIP3 and CMIP5 GCMs simulate a strong decline in total annual rainfall, which is not consistent with the lack of robust trend in observations (Figure 10.29).

Move Figure 10.29 here?

Models capture the overall manifestations of the observed main hemispherical processes, such as the expansion of tropics, positive trend in SAM and the poleward shift of the westerly jet, but they fail to capture details of their observed climatology and variability (Simpson and Polvani, 2016), and the magnitudes of simulated trends vary and in general the models underestimate observed trends (Purich et al., 2013; Staten et al., 2018). In general, CMIP5 models fail to capture the influence of ENSO on SAM on a month-to-month basis, but they capture SAM trends and the SAM-regional rainfall association (Lim et al., 2016b), although not consistently across all seasons, particularly in March to May (Purich et al., 2013).

**[START FIGURE 10.29 HERE]**

**Figure 10.29:** [Placeholder: Historical and projected rainfall over Cape Town region. Gridded datasets: averaged over 17ºE-19ºE, 32ºS-35ºS, with the observations an average of 10 quality-controlled, gap-filled time series for station located within the same bounding box. All data, apart from station-based data, are bias corrected in mean (but not in variance) over the 1981-2010 period. CMIP5 data include multiple runs of individual models. CORDEX data are simulations with 6 RCMs forced by one to ten GCMs. High-resolution simulations with C-CAM use forcings from 6 GCMs. Note that CRU4.01 dataset in the Cape Town region uses data from eight stations prior to 2000, and only 3-4 stations afterwards.]

**[END FIGURE 10.29 HERE]**

### *10.6.2.6 GCM future projections*

CMIP3 and CMIP5 models show *strong consistency* in a drying signal for the Cape Town region, with the reduction in total annual rainfall ranging up to 20% by the end of the twenty-first century (Figure 10.29). This is a *robust signal* across the ensembles compared to the summer rainfall region of southern Africa, where the climate change signal varies spatially: stronger drying in the west and moderate drying or weak wetting in the east. Rainfall changes projected for the Cape Town region are consistent with projected changes in hemispherical-scale processes and regional scale dynamics that point toward reduced frequency of frontal systems affecting that region. There is a *robust signal* in CMIP5 models for the Southern Hemisphere in terms of poleward expansion of the tropics (Hu et al., 2013b), poleward displacement of mid-latitude storm tracks (Chang et al., 2012), increase in strength and a poleward shift of the westerly winds (Bracegirdle et al., 2018) and sub-tropical jet-streams (Chenoli et al., 2017), and an increase in SAM (Lim et al., 2016b).

However, there is also a *robust increase* in the frequency of Atmospheric Rivers (ARs) and integrated water vapour transport towards the Southwest coast of southern Africa in the projected climate (Espinoza et al., 2018). That signal is opposite to the signal detected during the 2015–2017 drought, when ARs affecting the region had lower than climatological frequency (Sousa et al., 2018a). This behaviour has strong implications for the region, as most topographically high locations receive rainfall from persistent ARs (Blamey et al., 2018). A thorough understanding of the role of ARs in the Cape Town region under changing climate is missing.

### *10.6.2.7 Messages from downscaling studies*

Dynamical downscaling studies implemented with a stretched-grid CCAM model (Engelbrecht et al., 2009) revealed a signal compatible with the GCM ensemble, i.e. consistent drying throughout the region, amplifying in time, irrespective of the considered GHG emission scenario and the generation of GCMs (DEA, 2013). More recent high resolution (8-km) simulations, confirm a similar direction of future change (Section 10.6.2.2). A multi-model CORDEX ensemble indicates a *robust signal* of reduction of total annual rainfall in the future (Figure 10.29), although there is *less agreement* on how changes in rainfall occurrence may evolve in the region, such as whether through fewer consecutive rain days or longer dry spells (Abiodun et al., 2017; Maúre et al., 2018). By comparing the CORDEX ensemble with the driving GCMs for the end of the century under RCP8.5, Dosio et al. 2019, (submitted) showed that the drying is associated with an increase in the number of consecutive dry days and a reduction in number of rainy days. These results are consistent with the driving GCMs for all the precipitation indices, and they are robust independently of the choice of the RCM or GCM.

Statistical downscaling results using a perfect-prog method (Hewitson and Crane, 2006), in contrast to the overall drying simulated by GCMs, indicated possible wetting in the region, particularly in the mountainous catchments (DEA, 2013). While the result was theoretically justifiable by thermodynamic considerations in a warming climate, it is likely that this was a spurious effect resulting from the fact that the method was applied using predictor variables that inadequately reflect drivers of rainfall variability in the region (Wolski et al., 2018). There is not enough understanding of the interplay of dynamic and thermodynamic effects on rainfall in the strongly topographically diverse region of Cape Town, however, to dismiss the perfect-prog projections outright, although they remain discounted in view of other sources of information.

### *10.6.2.8 Potential for abrupt change*

Since the rainfall delivery mechanisms in the region are strongly conditional on the north-south migration of

the mid-latitude westerlies, a question arises as to whether it is possible for the region to experience a threshold-controlled rainfall regime shift, and whether the 2015–2017 drought is simply a manifestation of such as shift. Such a situation might have occurred in Perth, Australia, which is located in a climatological setting almost identical to that of Cape Town. In Perth, patterns in the 120-year river runoff record have been interpreted as several events of step change (as for example illustrated in Figure 11.3 of Christensen et al. (2007)) shifting the region to a "permanent drought" situation. However, Bates et al. (2010), Hughes et al. (2012), and Smith and Power (2014) showed that the decline in the annual inflow is more consistent with a smooth declining trend than with a sequence of sharp breaks.

In terms of paleoclimate indicators of regime shifts, multi-proxy and modelling studies indicate that mid-Holocene and more recent climate evolution in the winter South African rainfall region had a character of gradual desertification and wetting, with no abrupt changes (Weldeab et al., 2013). In these multi-proxy analyses, Weldeab et al., (2013) found that the gradual aridification was accompanied by an increase in an easterly hot wind flowing off the edge of South Africa's interior plateau, a weakening of the southern Benguela Current upwelling and Agulhas Current leakage into the southern Atlantic from the Indian Ocean. These effects are consistent with a southward migration of the mid-latitude westerlies. The behaviour indicates that at least within range of the climate variability experienced in the paleo-history, an abrupt shift of the rainfall regime in the Cape Town region is unlikely.

#### *10.6.2.9 Storyline and narrative approaches for the case*

There is a consistency in rainfall projections with projections of drivers of rainfall, and with the general understanding of the influence of warming on the circulation dynamics and rainfall patterns in the region. Thus, the expansion of the south Atlantic high-pressure system, related to widespread warming of the tropics and poleward shift of the subsiding limb of the Hadley cell, is associated with the southward displacement of the sub-tropical jet, and southward migration of mid-latitude westerlies and storm tracks, in addition to changes in the Antarctic Oscillation and SAM. These effects are also relatively consistent with recent (post-1980s) declines in rainfall in the Cape Town region. There is, however, little consistency in the long-term, with previous droughts in the 20th century not clearly reflecting GHG-related trends, and with an overall weak or increasing rainfall at the time scale of 90 or more years (Kruger and Nxumalo, 2017; Wolski et al., 2019; Figure 10.29). In spite of this inconsistency, the overall message is that of a drier future, with either a warmer and drier climate or a much warmer and considerably drier climate. These messages are reinforced by results of a 2015–2017 drought multi-method attribution study (Otto et al., 2018), which estimated the probability of the event to have increased by a factor of 3 since pre-industrial times (although with a wide 95% confidence interval of 1.5 to 6), and to have a further factor of 3 increase in a world experiencing further warming to 1.5˚C above pre-industrial levels.

#### *10.6.2.10 Assessment summary*

There is *high agreement* among multiple sources giving *high confidence* that precipitation in the Cape Town region will *likely* decrease toward the end of the 21st century. This conclusion is supported by the *high agreement* in projections of key circulation mechanisms, including the southward shift in the Southern Hemisphere of the midlatitude westerlies, storm tracks, subtropical jet and subsiding branch of the Hadley cell. A potentially counteracting feature is the behaviour of atmospheric rivers, whose impact on the region's precipitation needs further study.

### ***10.6.3 Indian summer monsoon***

#### *10.6.3.1 Introduction*

Societies in South Asia are finely attuned to the summer monsoon; for India alone, the monsoon between June and September provides 80% of the annual rainfall, supplying the majority of water resources for

agriculture, industry, drinking and sanitation of over a billion people. As such, any variations in the monsoon on time scales from days to decades can have large impacts (Challinor et al., 2006; Gadgil and Gadgil, 2006). There is therefore a pressing need to understand if the monsoon will change in the future under anthropogenic forcing and to quantify any such changes.

In studies going back several decades, the monsoon has been suggested to increase in strength in future projections under idealised enhanced CO2 forcing, supported by the theory of greater availability of moisture in the future, warmer climate. It was therefore puzzling that little trend was observed in central India up to the turn of the 21st century, with increases in extreme rainfall events compensating for decreases in light and moderate rain (Goswami et al., 2006b). Further analysis of trends in a variety of datasets has shown consistent negative trends since the 1950s (Bollasina et al., 2011). This opposition between idealised or theoretical future projections and observed historical trends makes the region an ideal topic for the more in-depth assessment described here.

Simulation of the Indian monsoon over the historical period in CMIP-class GCMs is poor, with consistent deficiencies in summer rainfall and a weakened monsoon circulation in CMIP3 and CMIP5 models (Sperber et al., 2013; also Chapter 8). The region is also the subject of coordinated modelling efforts under the Global Monsoon MIP (GMMIP; Zhou et al., 2016) and regional efforts such as CORDEX South Asia (Choudhary et al., 2018; Gutowski Jr. et al., 2016), sometimes with contradictory outcomes. Research has begun to apply emergent-constraint techniques to the Indian monsoon (Li et al., 2017a), while alternatively, narratives approaches are also beginning to be employed (Stainforth, 2018).

#### *10.6.3.2 The regional climate of India*

The geography of India gives rise to distinct differences in societal experience of the monsoon and its impacts. India is bounded on its west coast by the Western Ghats mountains, leading to significant orographic enhancement and heavy rains as the monsoon flow (known as the Somali jet) hits from the southwest; these rains supply rivers with water for much of the southern peninsula. To the east of the Western Ghats, south-eastern India sits under a rain shadow (this is the only major part of India to receive more rainfall during the winter monsoon season). The northern plains region contains the Ganges river basin and has India's most intensive agriculture, the crops either being rainfed or irrigated from the Ganges, associated canals, or groundwater pumping. Synoptic systems known as monsoon depressions are incident upon India's north-east coast, bringing much of the rain to the northern plains. Further north, the Himalayas also experience heavy precipitation; in the eastern Himalayas, this is dominated by the summer monsoon, while the western Himalayas receive most precipitation from western disturbances during winter (Palazzi et al., 2013).

#### *10.6.3.3 Relevant anthropogenic and natural drivers*

Numerous studies in the AR5 and before have shown the relevance of various anthropogenic and natural drivers for the Indian monsoon. While the attribution of observed changes in the monsoon to these drivers and the implications for future projections will be discussed later in Sections 10.6.3.5 and 10.6.3.6 the drivers are summarised briefly here:

- The increase in GHG concentrations (chiefly of $CO_2$) are suggested as a strong contributor to changes in the Indian monsoon, with potential impacts on the meridional temperature contrast driving the monsoon circulation (Roxy et al., 2015; Ueda et al., 2006), on the monsoon winds in the lower troposphere (Cherchi et al., 2011), or on the availability of moisture, chiefly derived from the Indian Ocean (May, 2011).
- Anthropogenic aerosol emissions can potentially alter the monsoon from both remote regions and locally. Preferential emissions of sulphate aerosol from industrial processes in the Northern Hemisphere could lead to changes in the inter-hemispheric energy transports and weakening of the monsoon (Polson et al., 2014; Undorf et al., 2018). Meanwhile, India has large emissions of sulphate aerosols and also black carbon (soot) from extensive use of cooking fires (Guo et al., 2016),

although the effect of black carbon on the monsoon is uncertain (Lau and Kim, 2006; Nigam and Bollasina, 2010).

- Over the late-20th century India underwent a green revolution with massive expansion of agriculture, culminating in the overall loss of natural vegetation such as forest and shrublands and its replacement with crops. To support this new agriculture, India has one of the largest regions of the world equipped for irrigation, in the northern plains, which have been identified in models as a region of strong land-atmosphere coupling (Koster, 2004).
- Increasingly, the movement of large parts of the population to urban areas has led to their expansion, potentially with local climate impacts (Shastri et al., 2015; Singh et al., 2016) such as altered sensitivity of extreme rainfall to the circulation.
- Natural drivers such as desert dust emissions from the Arabian Peninsula, Iraq, Syria and Iran have a role to play in heating the troposphere locally, and in interacting with black carbon aerosols (Lau, 2014).
- Finally, internal modes of variability in the oceans such as AMV and PDV are known to yield decadal forcing on the Asian monsoon (Goswami et al., 2006a; Krishnan and Sugi, 2003), which may interfere with interpretation of climate signals.

#### *10.6.3.4 Observational issues for India*

India has an extensive network of rain gauges dating back to the 19th century.This has led to the production of several gridded products for analysis of climate trends (e.g. around 2,000 quality controlled gauges consistently reporting since the early 1950s (Rajeevan et al., 2006)). A smaller subset of 306 stations has operated since the early 19th century and reveals pronounced decadal variability (e.g., Sontakke et al., 2008). A more recent 0.5°-gridded dataset begins in the 1970s, but it is clearly acknowledged as unsuitable for climate trend analysis, since there are critical inhomogeneities in station distribution and reporting over time (Rajeevan and Bhate, 2008). These data are suitable for use in mesoscale analysis only.

More recently, a 0.25°-gridded dataset has been introduced covering the period from 1901 onwards (Pai et al., 2015) based on Shepherd's method for gridding station data. Findings include the increased intensity of daily rainfall and extreme events over four analysed regions, especially in the latter half of the 20th century. However, as discussed in Section 10.2.2.3, critical assessment of the methods used in conjunction with the inhomogeneities in the input data, in particular their variation over time, leads to the suggestion (Lin and Huybers, 2019) that changes in the input gauges have introduced an artificial jump in higher frequencies of more extreme rainfall since 1975 over central India. At its worst, Lin and Huybers (2019) stated that this may have acted to mask declines in mean rainfall; they highlighted the desire for openness of raw meteorological information to allow improved assessments.

Finally, the large number of locally produced and international observational products for India and differences between them can indicate some of the uncertainty in observational datasets, which might pose challenges when evaluating climate models (as suggested in 10.3.3.3). Collins et al., (2013) found evidence of cases (such as the seasonal mean monsoon rainfall) in which large biases clearly separated CMIP5 models from the available observational products. However, in other cases, such as measures of variability or teleconnections, the spread across observational products overlaps with that in the CMIP5 ensemble, with a significant portion of the models lie within the observational range. Such observational uncertainty presents difficulties in evaluating models.

#### *10.6.3.5 Drying over the historical period*

The Indian summer monsoon is a pertinent example of the need to consider multiple factors in the attribution of regional climate changes and is societally important both due to the size of the area covered and its population. That rainfall in India was not increasing over the course of the 20th century had been regarded as a puzzle (Goswami et al., 2006b), because the trend was not in line with the expected wetter trend arising from future projections under greenhouse warming (e.g., Kitoh, 2017; Kitoh et al., 2013a; Turner and

Annamalai, 2012). Notwithstanding the large dry biases in historical coupled GCM simulations of the Indian monsoon (Sperber et al., 2013), various studies have suggested that aerosol forcing is the cause for the declining rainfall trend. Attribution work using single-forcing historical experiments in CMIP5 has suggested this for the Northern Hemisphere monsoons generally (Polson et al., 2014) and specifically for the Asian monsoon region (Guo et al., 2015, 2016). This is due to the dominance of aerosol emissions in industrialized regions of the Northern Hemisphere, cooling it relative to the Southern Hemisphere and thus decreasing moisture transport across the equator (Bollasina et al., 2011). The aerosol hypothesis is supported by (Salzmann et al., 2014), who noted a negative monsoon rainfall trend in 15 CMIP5 GCMs forced by aerosol and GHG, compared to a positive trend when forced by GHG only. (Salzmann et al., 2014) however cautioned that over smaller regions such as northern-central India, there was a large spread between individual model realisations of comparable magnitude to the purported aerosol-induced signal, suggesting that internal variability may also play a role.

Alternatively, the impact of rapidly warming Indian Ocean SSTs, themselves partly arising due to greenhouse warming, has been blamed. (Roxy et al., 2015) forced a coupled GCM in the equatorial Indian Ocean (the region of strongest SST warming signal) with a nudged trend in SST to demonstrate a weakening response of the Indian monsoon. (Annamalai et al., 2013) used a coupled climate model to suggest instead that preferential warming of the western North Pacific may lead to a Rossby wave response to its west that produces dry advection and descending motion over India, weakening the monsoon. A different viewpoint for the decreasing rainfall lies in the relative cooling of the troposphere over the Asian landmass compared to that of the adjacent Indian Ocean (e.g. Zuo et al., 2012, 2013)), following the mechanism of (Ueda et al., 2006) in which the thickness of the troposphere over the equator increases, decreasing the meridional temperature gradient. The cause for the relative cooling may lie in robust multi-decadal variations over the Asian landmass, which is related to internal variability, especially the AMV (Zuo et al., 2013, Zuo et al., 2018).

Internal variability in the Pacific could also be a significant driver. Huang et al. (2018) compared 57 members of a perturbed physics ensemble of the coupled HadCM3C model run over the historical period. Those members in which the Indian negative rainfall trend is replicated are accompanied by a strong phase change in the Interdecadal Pacific Oscillation (IPO) from negative to positive, consistent with the observed trend in SST. Recently, (Jin and Wang, 2017) have demonstrated increasing Indian monsoon rainfall since 2002 in a variety of observed datasets, suggesting the increase is due either to a change in dominance of a particular forcing (for example from aerosol to greenhouse gases) or to a phase change in a mode of internal variability such as the IPO.

Finally, other authors have raised the possibility that local land-use/land-cover changes and land management are drivers of Indian monsoon drying. For example, Paul et al. (2016) forced the regional WRF model with land cover patterns from 1987 and 2005, representing a shift from forest cover to agricultural land, and found a weakening of summer monsoon rainfall. Ramarao et al. (2015) have noted the overall anthropogenic impact on the drying trend and noted the potential for the warmer surface to decrease evapotranspiration as a result, potentially feeding back on the supply of moisture. India is the world's most irrigated region with around 0.5 mm/day on a yearly basis (McDermid et al., 2017), and including irrigation in GCMs and RCMs slows the monsoon circulation and diminishes the rainfall (Cook et al., 2015a; Guimberteau et al., 2012; Lucas-Picher et al., 2011; Shukla et al., 2014; Tuinenburg et al., 2014). However, the methodologies used to implement irrigation in these studies were simplified relative to actual practice and did not take into account spatial heterogeneity or overestimated both demand and supply (Nazemi and Wheater, 2015; Pokhrel et al., 2016)(see also 10.3.1.4.2).

Krishnan et al. (2016) tried to unify some of the above mechanisms. Using single all-forcings and natural-forcings-only simulations of the historical period in the LMDZ4 model, they demonstrated the positive influence of increased GHG concentrations (and GHG-associated SST patterns) on rainfall. Meanwhile just examining the influence of the radiative effect of GHG forcing, together with imposed SSTs, a slight weakening of the monsoon circulation was found. This was related to an increase in the static stability. When the monsoon was driven by all forcings other than GHGs, declining rainfall was found. Based on other literature, Krishnan et al., (2016) hypothesized that the combination of anthropogenic aerosol, land-use

change, and rapid Indian Ocean warming may be to blame for the declining Indian monsoon.

Thus, understanding the 20th century Indian monsoon drying trend relies on a mixture of control exerted from anthropogenic forcing and internal variability. Common factors are the relative cooling of the Eurasian land mass or Northern Hemisphere, and relative equatorial warming in the Indian Ocean. Understanding the interplay between these controls will be important for understanding future change in the region.

*10.6.3.6 GCM future projections*

In the AR5, Christensen et al. (2013) concluded that the Indian monsoon rainfall is likely to strengthen under future climate scenarios (Figure 10.30), while the circulation will weaken. More recent work has examined changes in the future mean-state monsoon rainfall at RCP4.5 and RCP8.5. Latif et al. (2018) found increased June-to-September rainfall over the Indo-Pakistan region, attributed to strengthened northward moisture transport over the Indian Ocean. However, they selected a subset of models given their agreement at simulating the pattern of observed rainfall trends in the 20th-century historical period. Since the trend over the 20th century is likely to have been driven by other drivers than GHG (see Section 10.6.3.5) and the dominant forcing at the end of the 21st century in RCPs is GHG emissions, the result might be different if using different criteria (e.g., the performance in terms of mean circulation patterns) to select the subset of models.

**[START FIGURE 10.30 HERE]**

**Figure 10.30:** [Placeholder: Maps of precipitation changes for Central, North, East and South Asia in 2080-2099 with respect to 1986-2005 in June to August in the SRES A1B scenario with 24 CMIP3 models (left), and in the RCP4.5 scenario with 39 CMIP5 models (middle). The map at the right-hand-side represents the precipitation changes in 2075-2099 with respect to 1979-2003 in the SRES A1B scenario with the 12 member 60 km mesh Meteorological Research Institute (MRI)-Atmospheric General Circulation Model 3.2 (AGCM3.2) multi-physics, multi-sea surface temperature (SST) ensembles (Kitoh et al., 2013b). Precipitation changes are normalized by the global annual mean surface air temperature changes in each scenario. Light hatching denotes where more than 66% of models (or members) have the same sign with the ensemble mean changes, while dense hatching denotes where more than 90% of models (or members) have the same sign with the ensemble mean changes. Adapted from Fig. 14.24 of Christensen et al. (2013). To be replaced in SOD by corresponding figure using CMIP5, CMIP6 and CORDEX output.]

**[END FIGURE 10.30 HERE]**

Alternatively, Singh and AchutaRao (2018) aimed to quantify sources of uncertainty in Indian regions using a 40-member CESM1 large ensemble. For precipitation, internal variability remains quite large and comparable to model uncertainty until at least the latter part of the 21st century. Much of the rainfall uncertainty is found for the more arid northwest region, with the west-central region exhibiting lower uncertainties. Considerable increases in rainfall are seen during September to November, which could be interpreted as an extension to the monsoon season. These results are based on a single large ensemble and there is no real process-based evaluation of the model.

Mechanisms for Indian monsoon change were explored in more detail by Li and Ting (2017), in order to determine the relative impacts of SST change and direct radiative forcing from GHG, using CMIP5 coupled and AGCM output. Rainfall increases were found to be dominated by the fast, radiative, response to GHG increase. However, in response to SST forcing, there was much greater model spread, likely arising from a competition between dynamic and thermodynamic responses in the moisture budget. While the thermodynamic response was found to be robust between models, the dynamic one is not. (Li and Ting, 2017) therefore conclude that the weak multi-model ensemble mean response of Indian monsoon rainfall in CMIP5 emerges from the combination of different processes arising on different time scales.

More detail of changes to the overall rainy season was examined by Sabeerali and Ajayamohan (2018), who used the CMIP5 RCP8.5 multi-model ensemble to project shortening of the rainy season, due to alteration of onset and withdrawal dates, in contrast to the single-model study of Singh and AchutaRao (2018). Most models were found to exhibit preferential warming over the western tropical Indian Ocean, leading to tropospheric warming aloft and reducing the upper tropospheric temperature gradient. This was found to be coincident with weakened easterly wind shear in the vertical, also reducing the period in which the tropospheric meridional temperature gradient is favourable for the monsoon.

Endo et al. (2018) explored the changing meridional temperature gradient in more detail in nine CMIP5 GCMs. In coupled experiments, lower tropospheric monsoon winds are found to strengthen and move northwards, in response to the stronger land-sea temperature contrast in RCP8.5 experiments. Meanwhile the tropical easterly jet in the upper troposphere was found to weaken, consistent with weakening of the meridional gradient at upper levels and with the mechanisms above. AMIP experiments were then used to isolate the role of the SST, finding that the strengthened meridional temperature gradient in the lower troposphere can be explained by the GHG radiative forcing alone.

Sooraj et al. (2015) selected a subset of seven CMIP5 models that simulated well the monsoon during the historical period. In the RCP4.5 future scenario, they found a robust reduction in the large-scale upper-tropospheric meridional temperature gradient, ascribed to tropospheric heating and enhanced ascent over the tropical Pacific. This was combined with an increase in atmospheric stability to weaken the Asian monsoon circulation. By decomposing the climate signal into dynamic and thermodynamic components, the dynamic part was found to give a tendency for decreasing monsoon rainfall, while the thermodynamic part gave a positive tendency; the positive tendency was greater in magnitude.

Finally, the RCP4.5 experiments of Krishnan et al. (2016) in the LMDZ AGCM forced by coupled-model derived future warming patterns superimposed onto AMIP SSTs, showed the 20th century drying of India to continue into the 21st century, before a rainfall recovery in the second half of that period.

In summary, future scenarios dominated by GHG increases such as the RCPs tend to suggest likely increases in monsoon rainfall, dominated by thermodynamic mechanisms leading to increases in the available moisture. However, there is large uncertainty as to how the rainfall evolution is spatially distributed, which is explored further in the subsequent text on downscaling studies.

#### *10.6.3.7 Messages from downscaling studies*

While the studies previously mentioned used GCM output directly for attributing past climate trends or projecting the future, others attempted to add value to the results based on GCMs by employing downscaling methods.

Starting with statistical downscaling methods, Akhter et al. (2019) used principal component-based linear regression to test a variety of large-scale fields from the NCEP-NCAR re-analysis to determine their suitability for downscaling precipitation in seven different regions of India. Fields such as precipitable water and relative humidity seem to be consistently good predictors. Their finding that increasing the domain size leads to worsened results points to the complex nature of India's hydroclimatic zones. Applying statistical methods to the future, albeit in older SRES A2 projections, Vigaud et al. (2013) used the CDF-transform method to bias adjust GCM outputs for southern India. The method is applied month-wise to maintain seasonality. During the historical validation period, using Indian Meteorological Department gauge data for observational comparison, the method was shown to improve the pattern, mean and seasonal cycle of modelled rainfall versus the GCMs used. Increases in monsoon rainfall were found for the future in southern India.

Salvi et al. (2013) attempted statistical downscaling for the whole of India at 0.5°-resolution based on five ensemble members of the CCCMA model in SRES scenarios of the 21st century and using a regression-based perfect prognosis method. They noted increases over the heavy rainfall regions of the west coast and

northeast India, while decreases were found in the north, west and southeast regions. Madhusoodhanan et al. (2018) used statistical downscaling at 0.05°-resolution to provide added detail in future rainfall projections over India based on inputs from 20 CMIP5 models. The statistical downscaling was judged to add value to the simulation of monsoon rainfall. While their method provided *medium confidence* of rainfall changes over the Western Ghats, Himalayan foothills and India, overall, with most models suggesting increased rainfall in future, they found significant inter-model differences in the pattern of change. However, the accuracy of their method is dependent on the quality of the observational data used for training that, as explained above, offers substantial challenges. In addition, the large disparity in resolution between the output and driving GCM suggest that the downscaled product may provide high spatial detail at the expense of neglecting key physical processes that cannot be resolved at the GCM scale, such as topographically determined circulation distributions.

Given ongoing concerns about the added value of dynamical downscaling for regional climate projection, Singh et al. (2017) raised this issue in relation to the Indian monsoon. They compared nine RCMs from CORDEX South Asia against their driving CMIP5 models, with respect to present-day (1951 or 1970 to 2005) monsoon characteristics including rainfall patterns and processes related to intraseasonal variability such as northward propagation. They found no consistent improvement in any present-day monsoon characteristics other than the spatial pattern (e.g. the representation of rainfall close to better-resolved orography); some characteristics were made worse.

In contrast, Varikoden et al. (2018) assessed the 1951–2005 historical period in the CORDEX South Asia models and found considerable improvement in the representation of historical rainfall patterns compared to the five driving GCMs. In particular, they noted better simulation of the long-term mean specifically over the Western Ghats mountains (consistent with Singh et al., 2017), reducing the dry bias; improvements were not evident however over the northern plains, which are dominated by a type of synoptic variability known as monsoon depressions.

Similarly, Sabin et al. (2013) used the variable-resolution LMDZ model to compare two ten-member ensembles: one operating with a uniform 1°-resolution and a second using a version zoomed to ~35 km over South Asia, while coarsening the grid outside and conserving the total number of grid points. Such modifications led to an improved simulation of orographic precipitation as well as the monsoon trough.

Finally, by using a GCM to produce a perturbed parameter ensemble ("HadCM3-QUMP") with the PRECIS RCM, Bal et al. (2016) made projections under SRES A1B for the 2020s, 2050s and 2080s in a continuous integration since 1970. They noted increases in rainfall of 15–24% for India.

There are mixed messages as to whether downscaling methods add value to climate projections of the Indian monsoon; it is a common theme however that rainfall patterns tied to orography are better represented by dynamical downscaling, giving *medium confidence* to the precipitation changes tied to orography.

#### *10.6.3.8 Potential for abrupt change*

Given the interest in physically plausible high impact scenarios (Sutton, 2018), it is worth considering whether the Indian monsoon may undergo abrupt change, which would involve failure of the reversal of the meridional tropospheric temperature gradient during spring, collapse of the monsoon circulation and thus failure of the monsoon rains over a season or more. Such ideas pertaining to collapse of the monsoon were originally explored in the wider review of (Lenton et al., 2008), where it was suggested that monsoon collapse could occur if regional planetary albedo exceeded 0.5, perhaps pertaining to aerosol emissions or land-use change. This finding was based entirely on the results from a single conceptual box model (Zickfeld, 2005). As reported in Hoegh-Guldberg et al. (2018), given the small radiative forcing in 1.5°C or 2°C equilibrium scenarios, or the absence of large aerosol emissions at the end of the 21st century in RCPs, there is *limited evidence* of abrupt changes in the Indian monsoon. There has been no credible evidence for abrupt monsoon collapse under the radiative forcings present in the RCP scenarios.

#### *10.6.3.9 Storyline and narrative approaches for India*

Since the AR5, considerable focus has been given to understanding regional climate impacts in future scenarios at target levels of global-mean warming in line with the Paris Agreement; such comparisons are often made between 1.5°C and 2°C above pre-industrial conditions. The IPCC Special Report on Global Warming of 1.5˚C (SR15; Hoegh-Guldberg et al., 2018), suggested that since the radiative forcings involved in these time-slice scenarios are rather lower than those at the end of the 21st century in the typical RCP4.5 and RCP8.5 scenarios, then there is only *low confidence* in projections of monsoon change at 1.5°C and 2°C, and of any differences between them. However, further literature is emerging examining such equilibrium-temperature experiments for monsoon regions. Chevuturi et al. (2018) compared five AGCMs from the HAPPI (Half a degree Additional warming, Prognosis and Projected Impacts) project, forced by SST patterns representative of 1.5˚C and 2.0˚C warming. While there is considerable model spread, the mean and extreme monsoon rainfall both amplify. Persistent daily rainfall extremes are *likely* to become more frequent with the additional half-degree warming.

The only study so far to have examined climate narratives for the Indian monsoon is that of Dessai et al. (2018). Using an expert elicitation approach, they constructed physically plausible futures of the monsoon substantiated by climate processes, focusing on the Cauvery river basin in southern India. Possible outcomes of the monsoon were provided based on the changes in two drivers: the availability of moisture from the Arabian Sea and the strength of the low-level flow. The key outcome is that the mechanistic narratives identified in the expert elicitation process were able to explain 70% of the variance in monsoon rainfall over 1979–2013, the implication being that climate uncertainties could be easily communicated to stakeholders.

#### *10.6.3.10 Assessment summary*

It is *likely* that both internal variability and anthropogenic aerosol emissions over the Northern Hemisphere have contributed to the negative rainfall trend in the Indian monsoon over the 20th century. There is *robust evidence* of a large uncertainty in the spatial distribution of the historical and projected changes. This is made worse by the substantial observational uncertainty. Given the *general agreement* among model projections, it is *likely* that Indian monsoon rainfall will increase at the end of the 21st century in response to increased GHG forcing; this arises due to the dominance of thermodynamic mechanisms. *No contradictory evidence* is found from downscaling methods. There is *low agreement* on how the monsoon onset might change in the future.

### ***10.6.4 Mediterranean summer warming***

#### *10.6.4.1 Introduction*

The Mediterranean is historically loosely denoted as the region that surrounds the Mediterranean Sea. In the Mediterranean, human society and natural environment have co-evolved over several millennia, experiencing significant climatic variations and laying the ground for diverse and culturally rich communities. The region is characterized by a complex morphology of mountain chains and strong land-sea contrasts, a dense and growing human population and various environmental pressures. Within the Mediterranean, large regional differences exist: whereas the population of the European Mediterranean countries has been relatively stable or even declining during the last decade, the population of countries in Mediterranean areas of the Middle East and North Africa (MENA) has quadrupled between 1960 and 2015, and the degree of urbanization has risen from 35 to 64% during the same period (World Bank Group, 2017). Agricultural land management is intensifying, particularly through enhanced irrigation; as many southern and eastern land systems seem to have the potential for further increase in yields (Mueller et al., 2012), agricultural management is likely to change further, with consequences for water resources, biodiversity and landscape functioning (Cramer et al., 2018).

The Mediterranean climate is characterized by mild humid winters and dry hot summers. As a consequence, water scarcity is a recurrent problem for the region especially in summer, requiring substantial infrastructural efforts, like dams and irrigation systems (Saadi et al., 2015). The dry hot Mediterranean climate is also a potential factor of risk for wild fires, which are the most important natural threat to forests and wooded areas of the Mediterranean basin. The region also suffers from severe heatwaves causing a mortality-risk in particular for older adults, young children and people with pre-existing and chronic medical conditions (CDC, 2018).

#### *10.6.4.2 The regional climate of the Mediterranean*

The Mediterranean has a semi-arid climate. Dynamically the dry summers are associated with large scale subsidence that is related to the downward branch of the Hadley circulation. Seasonal variability is strongly linked to the NAO in winter and the Summer NAO (SNAO) in summer (Bladé et al., 2012; Folland et al., 2009). During high SNAO the Mediterranean is anomalously wet, associated with an upper level through over the Balkans (Bladé et al., 2012). The local climate is strongly affected by the Mediterranean Sea, which acts as an evaporation source that dominates the hydrological cycle. The sea also modifies remotely the hydrological cycle in other locations such as the Sahel (Park et al., 2016). Strong storms can develop over the Mediterranean. The most intense ones, known as Medicanes, are particular destructive and exhibit several similarities with tropical cyclones (Cavicchia et al., 2014). Due to its semi-arid climate, the Mediterranean region is characterized by strong land-atmosphere coupling and feedbacks (Seneviratne et al., 2006) generating prolonged droughts and intense heatwaves, which can also affect other European regions (Zampieri et al., 2009).

#### *10.6.4.3 Observational issues for the Mediterranean*

The Mediterranean region has a wide variety of countries and economies. This has led to differences in the existence and availability of observations. In addition, the occurring of political problems and civil strife has undermined the continuity of observational records where they have been taken. As a consequence, there is generally a lack of basin-wide observational datasets, especially before the advent of substantial satellite observations in the 1970s.

#### *10.6.4.4 Warming over the historical period*

The European part of the Mediterranean region has been warming faster than the global mean in recent decades. Basin-wide, annual mean temperatures are now 1.4°C above late-19th-century levels (Cramer et al., 2018; Lionello and Scarascia, 2018; van der Schrier et al., 2013). For each of the most recent decades, the surface of the Mediterranean Sea has warmed by around 0.4°C (Macias et al., 2013). The enhanced Mediterranean warming is related to the much wider enhanced European warming discussed in Section 10.4.2.2.6.

Several studies have linked the enhanced Mediterranean warming to a shift to the positive phase of the AMV around the 1990s (Macias et al., 2013; O'Reilly et al., 2017; Sutton and Dong, 2012), with the underlying mechanism either being thermodynamic, where the enhanced North Atlantic warming directly warms the Mediterranean, or dynamic, with a linear atmospheric response downstream over Europe. However, the recent warming has also been linked to aerosol concentrations. As discussed in Section 10.4.2.2.6, there is *medium confidence* that reduction of aerosol concentrations, an outcome of air pollution control legislation, has also been a dominant factor for the enhanced warming by changing the optical properties of clouds (Besselaar et al., 2015; Crippa et al., 2016; De Laat and Crok, 2013; Dong et al., 2017; Philipona et al., 2009; Ruckstuhl et al., 2008; Turnock et al., 2015, 2016). By means of model sensitivity experiments, Nabat et al., (2014) also associated the increase in Mediterranean SST to the decrease in aerosol concentrations.

Due to its semi-arid climate, strong atmosphere-land coupling has contributed to the larger increase of mean

summer temperature compared to the increase of the annual mean temperature (Zampieri et al., 2009). In particular during drought spells, soil moisture limitation of evaporation provides a positive feedback and enhances the intensity of heat waves (Lorenz et al., 2016). By comparing reanalysis-driven RCM simulations with observations, Knist et al. ( 2017) found that RCMs are able to reproduce soil moisture interannual variability, spatial patterns, and annual cycles of surface fluxes over the period 1990–2008, revealing a strong land-atmosphere coupling especially in southern Europe in summer.

*10.6.4.5 GCM future projections*

The Mediterranean is expected to be one of the most prominent and vulnerable climate change "hotspots" (Diffenbaugh and Giorgi, 2012) because there is *agreement* among different climate projections of a *substantial* warming, particularly in summer. CMIP5 simulations project an enhanced future warming for the 21st century compared to global mean and enhanced drying (Figure 10.31; Mariotti et al., 2015). Warming projections are particularly large in summer, 40–50% larger than global warming and, for the land areas located north of the basin, locally up to 100% larger than global warming (Cramer et al., 2018; Lionello and Scarascia, 2018). Peculiar to the Mediterranean is that the warming of the daily maximum is larger than for the daily minimum. Consequently, the difference between daytime maxima and night-time minima is expected to increase, particularly in summer (Lionello and Scarascia, 2018). Simulations have also projected a northward and eastward expansion of the Mediterranean climate and the replacement of the southern part by a more arid climate with an increased summer drying in both old and newly established Mediterranean climates (Alessandri et al., 2015).

**[START FIGURE 10.31 HERE]**

**Figure 10.31:** [Placeholder: Maps of precipitation changes for Europe and Mediterranean in 2080-2099 with respect to 1986-2005 in June to August in the SRES A1B scenario with 24 CMIP3 models (left), and in the RCP4.5 scenario with 39 CMIP5 models (middle). The map at the right-hand-side represents the precipitation changes in 2075-2099 with respect to 1979-2003 in the SRES A1B scenario with the 12 member 60 km mesh Meteorological Research Institute (MRI)-Atmospheric General Circulation Model 3.2 (AGCM3.2) multi-physics, multi-sea surface temperature (SST) ensembles (Endo et al., 2012). Precipitation changes are normalized by the global annual mean surface air temperature changes in each scenario. Light hatching denotes where more than 66% of models (or members) have the same sign with the ensemble mean changes, while dense hatching denotes where more than 90% of models (or members) have the same sign with the ensemble mean changes. Adapted from Fig. 14.22 Christensen et al. (2013). To be replaced in SOD by corresponding figure using CMIP6 and CORDEX output.]

**[END FIGURE 10.31 HERE]**

Apart from the enhanced warming compared to global mean temperature rise, the Mediterranean climate projections are characterised by reduced precipitation in all seasons (Lionello and Scarascia, 2018; Mariotti et al., 2015; Rajczak and Schär, 2017; Spinoni et al., 2018). Land-surface feedbacks increase this drying thereby contributing to the enhanced warming (Lorenz et al., 2016; Russo et al., 2019; Whan et al., 2015). An additional mechanism for Mediterranean drying, with a feedback on summer temperatures, is the "monsoon-desert mechanism" that relates diabatic heating associated with the South Asian summer monsoon rainfall with subsidence over the eastern Mediterranean (Cherchi et al., 2016).

The Mediterranean summer climate is affected by large-scale circulation patterns of which the SNAO is the most important (Bladé et al., 2012; Folland et al., 2009). It is also connected with the Hadley circulation. Its northward shift in summer connects the hot and arid eastern part of the Mediterranean with the Asian and African monsoon (Mariotti et al., 2015). These large-scale drivers of the Mediterranean summer climate often show large biases in global models decreasing confidence in the regional projections (Bladé et al., 2012). Correctly simulating their impact on the Mediterranean climate can partly offset the anthropogenic warming signal (Barcikowska et al., 2019).

### *10.6.4.6 Messages from downscaling studies*

To unravel the complex interactions and feedbacks involving ocean-atmosphere-land-biogeochemical processes that modulate the climate and environment of the Mediterranean region on a range of spatial and temporal scales, regional downscaling projects are being developed to provide an integrated view on the future of the Mediterranean. A recent example is Med-CORDEX (Ruti et al., 2016; Somot et al., 2018), which aims at coordinating the Mediterranean climate modelling community in developing fully coupled regional climate simulations, in part by improving all relevant components of the system from atmosphere and ocean dynamics to land surface, hydrology, and biogeochemical processes. Other activities have included ENSEMBLES (Fernández et al., 2018) and ESCENA (Jiménez-Guerrero et al., 2013) and the ongoing EURO-CORDEX (Jacob et al., 2014).

From an analysis of EURO-CORDEX results, studies showed that southern Europe is projected to face a *robust non-linear* increase in temperature larger than the global mean, especially for both hot and cold extremes (Jacob et al., 2018; Kjellström et al., 2018; Maule et al., 2017). In particular, Dosio and Fischer (2018) showed that the increase in the number of tropical nights is more than 60% larger in many places in southern Europe and the Mediterranean under 2°C warming compared to 1.5°C. Over the region, the projected temperature increase, including a higher probability of severe heat waves (Russo et al., 2015), together with a reduction in precipitation (Jacob et al., 2014; Dosio, 2016; Rajczak and Schär, 2017) results in projected increase of drought frequency and severity (Spinoni et al., 2018). Also, the severity of marine heat waves of the Mediterranean Sea is projected to increase (Darmaraki et al., 2019).

In their analysis of the effect of model resolution and sea coupling in MED-CORDEX RCMs, Panthou et al. (2018) found out that models reproduce well the observed spatial patterns of hot days and droughts, although they tend to overestimate extreme return levels of hot days. In particular, higher resolution simulations showed a clear improvement in the representation of droughts, while the additional degrees of freedom in coupled simulations did not downgrade the performance. Similarly, Akhtar et al. (2018) argued that higher resolution improved the wind speed (particularly near coastal areas) and subsequently the turbulent heat flux simulations. Both fields were also better simulated with an interactive ocean model, compared to simulations with prescribed SST.

Finally, Macias et al. (2018) argued that simulated SST in RCMs are significantly improved when wind speed values were bias-corrected towards observed values, whereas other variables like air temperature and cloud cover had a more marginal importance in reducing the SST bias.

Despite the large efforts of these regional downscaling projects, the GCM-RCM matrix is still sparse and lacking a systematic design to explore the uncertainty sources (e.g. GCM, RCM, scenario, resolution). Focusing on the Iberian peninsula, Fernández et al. (2018) argued that the driving GCM is the main contributor to uncertainty in the grand-ensemble. Consistent but implausible temperature changes in RCMs can occur. An example is a strong temperature increase over the Pyrenees due to excessive snow cover in the present climate (Fernández et al., 2018). Based on an older set of RCMs simulations (ENSEMBLES), Déqué et al. (2012) also argued that the largest source of uncertainty in the climate response over Southern Europe is the choice of the driving GCM. Similarly, Macias et al., (2018) claimed that the choice of the GCM has the largest impact on the simulated SST bias exhibited by the RCM. Finally, Bartók et al. (2017) found that RCMs projected a change in surface solar radiation (on average, -0.60 W/m2 per decade over Europe) opposite to that of the driving GCMs, with the large discrepancies being over spring and summer, due mainly to different trends in cloud cover in global and regional climate models.

### *10.6.4.7 Potential for abrupt change*

A growing number of studies are investigating the impacts of warming levels above the Paris Agreement (which would limit warming to 1.5°C above the pre-industrial level) on the hydrological cycle, vegetation

and their socio-economic consequences. Based on EURO-CORDEX results, Barredo et al. (2018) showed that, by the end of the century under RCP8.5 the present Mediterranean climate zone is projected to contract by 16%, mainly due to the expansion of the arid zone, which is projected to increase by more than twice its present extent, equivalent to three times the size of Greece. Combining Holocene pollen profiles and CMIP5 climate scenarios, Guiot and Cramer (2016) argued that above 2°C of warming, climatic change will generate Mediterranean land ecosystem changes that are unmatched in the Holocene, a period characterized by recurring precipitation deficits rather than temperature anomalies. The changes will likely lead to substantial expansion of deserts in much of southern Europe and northern Africa. Samaniego et al., (2018), using an ensemble of hydrological and land-surface models, estimated that a warming of 3˚C will increase the drought area by 40% affecting up to 42% more of the population.

#### *10.6.4.8 Storyline and narrative approaches for the Mediterranean*

The atmospheric circulation is influenced by large scale often slowly varying components of the climate system, such as the ocean, sea-ice and soil moisture. Historic and future changes of the atmospheric circulation depend, among other factors, on how these drivers have changed and will change. Zappa and Shepherd (2017) have analysed this for the Mediterranean region and identified different possible evolutions of those drivers and their impact on the Mediterranean winter climate. Important identified drivers are tropical and polar amplification of global warming and the polar stratospheric vortex, with implications for precipitation. Based on the possible future different evolutions of the drivers and their regional impacts, different story lines can be developed (Shepherd et al., 2018). As an example, scenarios have been developed for the Netherlands based on the story line approach (Attema et al., 2014). Multiple scenarios are being explored and the resulting implications for adaptation planning have been co-developed with end users and stakeholders. For the Mediterranean, the approach of Zappa and Shepherd (2017) could be applied to the summer and developed into story lines.

#### *10.6.4.9 Assessment summary*

The Mediterranean has a semi-arid climate with a dense and growing human population and various environmental pressures. There is *high confidence* that the Mediterranean region has experienced a summer temperature increase in recent decades that is faster than the increase for the Northern Hemisphere summer mean. There is also *high confidence* that the projected summer temperature increase will be larger than the Northern Hemisphere mean, resulting in an increase in frequency and intensity of heat waves.

There is *robust evidence* and, thus, *high confidence* that summer precipitation in the Mediterranean region will decrease toward the end of the 21st century. There is *high confidence* that this will substantially affect the hydrological cycle and vegetation, with implications for the socio-economic structure. Due to the biases in GCMs and RCMs, there is *low to medium confidence* in the spatial distribution of projections of precipitation for the Mediterranean region. Natural variability on decadal time scales enhances this uncertainty. Nevertheless, the approach of storylines and narratives enables provisioning useful information for decision makers and stakeholders in this realm of uncertainty.

## Frequently Asked Questions

### FAQ 10.1: To produce useful regional climate information, what must we consider?

*Both physically and culturally, the world is diverse. Providing citizens useful information on how climate is changing can help with decision-making but only when relevant for the people involved. Useful climate information, when relevant, robust and well understood makes a difference to the decision. To achieve this requires awareness of the context where the information will be used, and establishing a common ground of understanding by all involved as to the robustness and appropriate formulation of the needed information.*

The development and use of climate change information are inherently influenced by the values of all parties: those constructing the information, those communicating the information, those hearing the information, and critically those who identify a problem that the climate information seeks to inform. Consequently, partnerships between these participating communities, and most especially with those for whom the information is intended, can substantially enhance the usefulness of the climate information in addressing the problem.

Effective partnerships recognize and respond to the values of all parties involved, especially when taking into account that the world and regions within it are culturally heterogeneous. By recognizing this heterogeneity, the information can be made more relevant and credible, most notably when informing the complexity of risks for human systems and ecosystems and resilience in developing nations, which may be more vulnerable to damaging impacts of climate change.

Many sources can provide useful descriptions of climate. These can include extending historical trends forward into the future, using model simulations of the global and/or regional climate change, and inferring regional change by evaluating changes in the weather behaviour that influences a region. Constructing useful climate information needs to consider all sources, in order to capture the fullest possible representation of projected changes, and then distil from them the information that links to the needs and concerns of the stakeholders and members of the community impacted by the changes. The distillation process (FAQ 10.1, Figure 1) ideally engages with the intended recipients of the climate information and, especially those stakeholders whose work involves non-climatic factors, such as in issues of human health, agriculture or water resources. Distilling climate information should further recognize that the geographic regions and time periods governing stakeholders' interest (for example, the growing season of an agricultural zone) may not be well aligned with the time and space resolution of available climate data, and thus may require additional development to extract useful climate information.

Successful framing of climate information and effective societal response have occurred when climate information is presented in the context of the local challenge posed by climate change. For example, the U.S. state of Arizona passed an initiative that responded to a specific, local impact of climate change, water-resource shortfalls in Arizona, even though some of the state's government leaders were unsure about global climate change. The success of the climate information came from recognizing a serious impact and avoiding the central, but likely controversial, motivation of fighting global climate change. Similarly, the city officials of Lusaka in Zambia engaged in sustained collaboration with climate scientists and effectively changed the city's approach to changing climate through a partnership that constructs and communicates climate information relevant to governing an African city vulnerable to climate change.

Stakeholders often need information from complex, compound events (e.g. floods after a drought) and in terms of quantities that, for those simulating climate, may not be primary concerns, such as receiving heat-stress conditions or a drought index. One way that complex information can be linked to the application is by stories. Storylines give climate change information that links with the recipients' experiences of existing weather and climate. This makes the climate information more accessible and physically comprehensible. The development of storylines uses the experience and expertise of stakeholders who seek to develop appropriate response measures (e.g., water-resource managers, health professionals, etc.). With appropriate choices, storylines can engage nuances of the climate information in a meaningful way by linking them to familiar details of a region's weather, thus enhancing the information's usefulness.

**[START FAQ 10.1, FIGURE 1 HERE]**

**FAQ 10.1, Figure 1:** [Placeholder: Schematic of possible figure showing the distillation of multiple factors into useful climate information. Underlying figure of the distillation flask found at http://www.clker.com/clipart-23858.html]

**[END FAQ 10.1, FIGURE 1 HERE]**

**FAQ 10.2: How does the growth of cities interact with climate change?**

*Cities feel the impact of climate change in a unique way. Tall buildings in close proximity to each other 'trap' heat, creating a so-called 'urban heat island', which causes cities to experience higher than average temperatures than their surrounding areas. Urbanization and the increasing severity of climate change further aggravate this effect.*

Cities are on front line in both cause and effect of climate change. On one hand, cities are responsible for up to 70% of current emissions of greenhouse gases, yet occupy less than 1% of global land mass. By 2030, almost 60% of the world's population will live in urban areas and every year sees the addition of 67 million new urban dwellers, 90% of these is added to cities in developing countries. On the other hand, cities and people who live in them are highly vulnerable to climate extremes including more frequent, longer and more intense heat waves. Urban areas are already vulnerable to increased thermal stress during heat-waves and projected rates of urban growth means that vulnerability will increase. This became apparent in 2003 in Paris, France, when daily mortality tripled during a heat wave in early August, or in 2010, in Ahmedabad, India, when a heatwave killed more than 1,100 people.

Due to the low albedo (reflectivity) of impervious surfaces, such as rooftops and asphalt roadways, differential heat storage (big heat capacity of building materials), anthropogenic heat, reduced wind speed (greater surface roughness), and light trapping within the canyons formed by taller structures, cities 'trap' heat. They are therefore often associated with elevated surface air temperature, a phenomenon referred to as the urban heat island (UHI) where night-time urban air temperature is substantially higher (several degrees) than corresponding temperatures in the surrounding rural areas. In different cities around the world, it has been found that during heat waves episodes, the UHI gets intensified compared to its climatological mean values.

Although the urban heat island phenomenon is well documented, and studies have increased our understanding, important measurements of meteorological and external climatic drivers across urban areas remain very limited due to the scarcity of high-density, in-situ measurement networks. Especially, long-term datasets (a year or more) are very scarce but invaluable because they allow more in-depth research on the seasonal evolution of the urban climate. In many cities, especially in the developing world, the historical record is too short, discontinuous, or the quality too uncertain to support trend analysis and climate change attribution. For example, it is very important to know whether, and to what extent, estimates of global warming trends are influenced by the growth of the urban heat island (UHI) in cities around the world due to the urban sprawl. In fact, if observations of near-surface air temperatures in growing cities are used in the assessment of global warming trends, these trends may be overestimated. For this reason, computations of global warming trends either avoid using measurements from cities or else adjust urban measurements to account for UHI influences.

Estimating how the UHI will evolve under climate change conditions is uncertain because several studies using a variety of methods report contrasting results. However, there is *clear evidence* that future urbanization may amplify the projected air temperature in different climatic regions *with a strong impact on minimum temperatures that could be comparable in magnitude to the global climate change warming.*

**[START FAQ 10.2, FIGURE 1 HERE]?**

Figure : [Placeholder: Infographic explaining the urban heat island effect and how urbanization aggravates this effect or schematic summarizing why cities are important to climate change.]

**[START FAQ 10.2, FIGURE 1 HERE]?**

## References


Aalbers, E. E., Lenderink, G., van Meijgaard, E., and van den Hurk, B. J. J. M. (2018). Local-scale changes in mean and heavy precipitation in Western Europe, climate change or internal variability? *Clim. Dyn.* 50, 4745–4766. doi:10.1007/s00382-017-3901-9.

Aalto, J., Pirinen, P., and Jylhä, K. (2016). New gridded daily climatology of Finland: Permutation-based uncertainty estimates and temporal trends in climate. *J. Geophys. Res. Atmos.* 121, 3807–3823. doi:10.1002/2015JD024651.

Abera, W., Brocca, L., and Rigon, R. (2016). Comparative evaluation of different satellite rainfall estimation products and bias correction in the Upper Blue Nile (UBN) basin. *Atmos. Res.* 178–179, 471–483. doi:10.1016/j.atmosres.2016.04.017.

Abiodun, B. J., Adegoke, J., Abatan, A. A., Ibe, C. A., Egbebiyi, T. S., Engelbrecht, F., et al. (2017). Potential impacts of climate change on extreme precipitation over four African coastal cities. *Clim. Change* 143, 399–413. doi:10.1007/s10584-017-2001-5.

Abramowitz, G., Herger, N., Gutmann, E., Hammerling, D., Knutti, R., Leduc, M., et al. (2018). Model dependence in multi-model climate ensembles: weighting, sub-selection and out-of-sample testing. *Earth Syst. Dyn. Discuss.*, 1–20. doi:10.5194/esd-2018-51.

Acevedo, W., Fallah, B., Reich, S., and Cubasch, U. (2017). Assimilation of pseudo-tree-ring-width observations into an atmospheric general circulation model. *Clim. Past* 13, 545–557. doi:10.5194/cp-13-545-2017.

AchutaRao, K., and Sperber, K. . (2006). ENSO simulation in coupled ocean-atmosphere models: are the current models better? 27, 1–15. doi:https://doi.org/10.1007/s00382-006-0119-7.

Ackerley, D., Booth, B. B. B., Knight, S. H. E., Highwood, E. J., Frame, D. J., Allen, M. R., et al. (2011). Sensitivity of Twentieth-Century Sahel rainfall to sulfate aerosol and CO2 forcing. *J. Clim.* doi:10.1175/JCLI-D-11-00019.1.

Ackerman, T. P., and Stokes, G. M. (2003). The Atmospheric Radiation Measurement Program. *Phys. Today* 56, 38–44. doi:10.1063/1.1554135.

Adachi, S. A., Kimura, F., Kusaka, H., Inoue, T., and Ueda, H. (2012a). Comparison of the impact of global climate changes and urbanization on summertime future climate in the Tokyo metropolitan area. *J. Appl. Meteorol. Climatol.* 51, 1441–1454. doi:10.1175/JAMC-D-11-0137.1.

Adachi, S. A., Kimura, F., Kusaka, H., Inoue, T., and Ueda, H. (2012b). Comparison of the Impact of Global Climate Changes and Urbanization on Summertime Future Climate in the Tokyo Metropolitan Area. *J. Appl. Meteorol. Climatol.* 51, 1441–1454. doi:10.1175/JAMC-D-11-0137.1.

Addor, N., Rohrer, M., Furrer, R., and Seibert, J. (2016). Propagation of biases in climate models from the synoptic to the regional scale: Implications for bias adjustment. *J. Geophys. Res. Atmos.* 121, 2075–2089. doi:10.1002/2015JD024040.

Adloff, F., Jordà, G., Somot, S., Sevault, F., Arsouze, T., Meyssignac, B., et al. (2018). Improving sea level simulation in Mediterranean regional climate models. *Clim. Dyn.* 51, 1167–1178. doi:10.1007/s00382-017-3842-3.

Ahn, M.-S., Kim, D., Sperber, K. R., Kang, I.-S., Maloney, E., Waliser, D., et al. (2017). MJO simulation in CMIP5 climate models: MJO skill metrics and process-oriented diagnosis. *Clim. Dyn.* 49, 4023–4045. doi:10.1007/s00382-017-3558-4.

Akhtar, N., Brauch, J., and Ahrens, B. (2018). Climate modeling over the Mediterranean Sea: impact of resolution and ocean coupling. *Clim. Dyn.* 51, 933–948. doi:10.1007/s00382-017-3570-8.

Akhtar, N., Brauch, J., Dobler, A., Béranger, K., and Ahrens, B. (2014). Medicanes in an ocean–atmosphere coupled regional climate model. *Nat. Hazards Earth Syst. Sci.* 14, 2189–2201. doi:10.5194/nhess-14-2189-2014.

Akhtar, N., Krug, A., Brauch, J., Arsouze, T., Dieterich, C., and Ahrens, B. European Marginal Seas in a regional atmosphere-ocean coupled model and their impact on Vb-cyclones and associated precipitation. *Clim. Dyn.* doi:Submitted.

Akhter, J., Das, L., Meher, J. K., and Deb, A. (2019). Evaluation of different large-scale predictor-based statistical downscaling models in simulating zone-wise monsoon precipitation over India. *Int. J. Climatol.* 39, 465–482. doi:10.1002/joc.5822.

Akinsanola, A. A., and Zhou, W. (2019). Projections of West African summer monsoon rainfall extremes from two CORDEX models. *Clim. Dyn.* 52, 2017–2028. doi:10.1007/s00382-018-4238-8.

Alessandri, A., De Felice, M., Zeng, N., Mariotti, A., Pan, Y., Cherchi, A., et al. (2015). Robust assessment of the expansion and retreat of Mediterranean climate in the 21 st century. *Sci. Rep.* 4, 7211. doi:10.1038/srep07211.

Alexander, M. A., Bladé, I., Newman, M., Lanzante, J. R., Lau, N.-C., and Scott, J. D. (2002). The Atmospheric Bridge: The Influence of ENSO Teleconnections on Air–Sea Interaction over the Global Oceans. *J. Clim.* 15, 2205–2231. doi:10.1175/1520-0442(2002)015<2205:TABTIO>2.0.CO;2.

Ali, S., Li, D., Congbin, F., and Khan, F. (2015). Twenty first century climatic and hydrological changes over Upper Indus Basin of Himalayan region of Pakistan. *Environ. Res. Lett.* 10, 014007. doi:10.1088/1748-9326/10/1/014007.

Allan, R., Brohan, P., Compo, G. P., Stone, R., Luterbacher, J., and Brönnimann, S. (2011). The International Atmospheric Circulation Reconstructions over the Earth (ACRE) Initiative. *Bull. Am. Meteorol. Soc.* 92, 1421–1425. doi:10.1175/2011BAMS3218.1.

Allen, M. R., Dube, O. P., Solecki, W., Aragón–Durand, F., Cramer, W., Humphreys, S., et al. (2018). "Framing and Context," in *Global warming of 1.5°C. An IPCC Special Report on the impacts of global warming of 1.5°C above pre-industrial levels and related global greenhouse gas emission pathways, in the context of strengthening the global response to the threat of climate change*, eds. V. Masson-Delmotte, P. Zhai, H.-O. Pörtner, D. Roberts, J. Skea, P. R. Shukla, et al. (Geneva, Switzerland: In Press).

Allen, M. R., and Ingram, W. J. (2002). Constraints on future changes in climate and the hydrologic cycle. *Nature* 419, 228–232. doi:10.1038/nature01092.

Allen, M. R., Stott, P. A., Mitchell, J. F. B., Schnur, R., and Delworth, T. L. (2000). Quantifying the uncertainty in forecasts of anthropogenic climate change. *Nature* 407, 617–620. doi:10.1038/35036559.

Allen, R. J., and Kovilakam, M. (2017). The Role of Natural Climate Variability in Recent Tropical Expansion. *J. Clim.* 30, 6329–6350. doi:10.1175/JCLI-D-16-0735.1.

Allen, R. J., Norris, J. R., and Wild, M. (2013). Evaluation of multidecadal variability in CMIP5 surface solar radiation and inferred underestimation of aerosol direct effects over Europe, China, Japan, and India. *J. Geophys. Res. Atmos.* 118, 6311–6336. doi:10.1002/jgrd.50426.

Almazroui, M. (2012). Dynamical downscaling of rainfall and temperature over the Arabian Peninsula using RegCM4. *Clim. Res.* doi:10.3354/cr01073.

Almazroui, M. (2018). Assessment of CMIP5 global climate models and projected changes in surface air temperature over the Arabian Peninsula in the twenty-first century. *Arab. J. Geosci.* 11, 650. doi:10.1007/s12517-018-4011-7.

Almazroui, M., Nazrul Islam, M., Saeed, S., Alkhalaf, A. K., and Dambul, R. (2017). Assessment of Uncertainties in Projected Temperature and Precipitation over the Arabian Peninsula Using Three Categories of Cmip5 Multimodel Ensembles. *Earth Syst. Environ.* doi:10.1007/s41748-017-0027-5.

Amador, J. A. (1998). A climatic feature of the tropical Americas : The trade wind easterly jet The Intra-Americas Sea Low-level Jet Overview and Future Research. doi:10.1196/annals.1446.012.

Amaya, D. J., Siler, N., Xie, S.-P., and Miller, A. J. (2018). The interplay of internal and forced modes of Hadley Cell expansion: lessons from the global warming hiatus. *Clim. Dyn.* 51, 305–319. doi:10.1007/s00382-017-3921-5.

Amegnaglo, C. J., Anaman, K. A., Mensah-Bonsu, A., Onumah, E. E., and Amoussouga Gero, F. (2017). Contingent valuation study of the benefits of seasonal climate forecasts for maize farmers in the Republic of Benin, West Africa. *Clim. Serv.* 6, 1–11. doi:10.1016/J.CLISER.2017.06.007.

Anderson, G. B., Bell, M. L., and Peng, R. D. (2013). Methods to Calculate the Heat Index as an Exposure Metric in Environmental Health Research. *Environ. Health Perspect.* 121, 1111–1119. doi:10.1289/ehp.1206273.

Andreassen, H. P., Gangaas, K. E., and Kaltenborn, B. P. (2018). Matching social-ecological systems by understanding the spatial scale of environmental attitudes. *Nat. Conserv.* 30, 69–81. doi:10.3897/natureconservation.30.28289.

Andrys, J., Lyons, T. J., and Kala, J. (2015). Multidecadal Evaluation of WRF Downscaling Capabilities over Western Australia in Simulating Rainfall and Temperature Extremes. *J. Appl. Meteorol. Climatol.* 54, 370–394. doi:10.1175/JAMC-D-14-0212.1.

Angeles, M. E., Gonzalez, J. E., Erickson, D. J., and Hernandez, J. L. (2007). Predictions of future climate change in the caribbean region using global general circulation models. 27, 555–569. doi:10.1002/joc.

Annamalai, H., Hafner, J., Sooraj, K. P., and Pillai, P. (2013). Global warming shifts the monsoon circulation, drying South Asia. *J. Clim.* 26, 2701–2718. doi:10.1175/JCLI-D-12-00208.1.

Annamalai, H., Taguchi, B., McCreary, J. P., Nagura, M., and Miyama, T. (2017). Systematic Errors in South Asian Monsoon Simulation: Importance of Equatorial Indian Ocean Processes. *J. Clim.* 30, 8159–8178. doi:10.1175/JCLI-D-16-0573.1.

Anstey, J. A., Davini, P., Gray, L. J., Woollings, T. J., Butchart, N., Cagnazzo, C., et al. (2013). Multi-model analysis of Northern Hemisphere winter blocking: Model biases and the role of resolution. *J. Geophys. Res. Atmos.* 118, 3956–3971. doi:10.1002/jgrd.50231.

Arblaster, J. M., Meehl, G. A., and Karoly, D. J. (2011). Future climate change in the Southern Hemisphere: Competing effects of ozone and greenhouse gases. *Geophys. Res. Lett.* 38, n/a-n/a. doi:10.1029/2010GL045384.

Archer, E., Engelbrecht, F., Hänsler, A., Landman, W., Tadross, M., and Helmschrot, J. (2018). Seasonal prediction and regional climate projections for southern Africa. *Biodivers. Ecol.* 6, 14–21. doi:10.7809/b-e.00296.

Argüeso, D., Evans, J. P., Fita, L., and Bormann, K. J. (2014). Temperature response to future urbanization and climate change. *Clim. Dyn.* 42, 2183–2199. doi:10.1007/s00382-013-1789-6.

Arnold, D. G. "Introduction: climate change and ethics," in *The Ethics of Global Climate Change*, ed. D. G. Arnold (Cambridge: Cambridge University Press), 1–15. doi:10.1017/CBO9780511732294.001.

Arsiso, B. K., Mengistu Tsidu, G., Stoffberg, G. H., and Tadesse, T. (2018). Influence of urbanization-driven land use/cover change on climate: The case of Addis Ababa, Ethiopia. *Phys. Chem. Earth*. doi:10.1016/j.pce.2018.02.009.

Aryee, J. N. A., Amekudzi, L. K., Quansah, E., Klutse, N. A. B., Atiah, W. A., and Yorke, C. (2018). Development of high spatial resolution rainfall data for Ghana. *Int. J. Climatol.* 38, 1201–1215. doi:10.1002/joc.5238.

Ashby, S. a., Taylor, M. A., and Chen, A. A. (2005). Statistical models for predicting rainfall in the Caribbean. *Theor. Appl. Climatol.* 82, 65–80. doi:10.1007/s00704-004-0118-8.

Ashcroft, L., Allan, R., Bridgman, H., Gergis, J., Pudmenzky, C., and Thornton, K. (2016). Current climate data rescue

activities in Australia. *Adv. Atmos. Sci.* 33, 1323–1324. doi:10.1007/s00376-016-6189-5.
Ashouri, H., Hsu, K. L., Sorooshian, S., Braithwaite, D. K., Knapp, K. R., Cecil, L. D., et al. (2015). PERSIANN-CDR: Daily precipitation climate data record from multisatellite observations for hydrological and climate studies. *Bull. Am. Meteorol. Soc.* doi:10.1175/BAMS-D-13-00068.1.
Attada Raju, and Parekh, A., and Chowdary J S., and and Gnanaseelan C (2018). Reanalysis of the Indian summer monsoon: four dimensional data assimilation of AIRS retrievals in a regional data assimilation and modeling framework. *Clim. Dyn.* 50, 2905–2923. doi:10.1007/s00382-017-3781-z.
Attema, J., Bakker, A., Beersma, J., Bessembinder, J., Boers, R., Brandsma, T., et al. (2014). KNMI'14: Climate Change scenarios for the 21st Century–A Netherlands perspective. *Sci. Rep. WR2014-01*. Available at: http://www.klimaatscenarios.nl/brochures/images/KNMI_WR_2014-01_version26May2014.pdf.
Auchmann, R., and Brönnimann, S. (2012). A physics-based correction model for homogenizing sub-daily temperature series. *J. Geophys. Res. Atmos.* 117. doi:10.1029/2012JD018067.
Aune, B. (1971). Two Theories of Scientific Knowledge. *Crítica Rev. Hispanoam. Filos.* 5, 3–20. Available at: http://www.jstor.org/stable/40103960.
Ayarzagüena, B., Polvani, L. M., Langematz, U., Akiyoshi, H., Bekki, S., Butchart, N., et al. (2018). No robust evidence of future changes in major stratospheric sudden warmings: a multi-model assessment from CCMI. *Atmos. Chem. Phys.* 18, 11277–11287. doi:10.5194/acp-18-11277-2018.
Ayarzagüena, B., and Screen, J. A. (2016). Future Arctic sea ice loss reduces severity of cold air outbreaks in midlatitudes. *Geophys. Res. Lett.* 43, 2801–2809. doi:10.1002/2016GL068092.
Azmat, M., Liaqat, U. W., Qamar, M. U., and Awan, U. K. (2017). Impacts of changing climate and snow cover on the flow regime of Jhelum River, Western Himalayas. *Reg. Environ. Chang.* 17, 813–825. doi:10.1007/s10113-016-1072-6.
Bader, D. A., Blake, R., Grimm, A., Hamdi, R., Kim, Y., Horton, R., et al. (2018). "Urban Climate Science," in *Climate Change and Cities: Second Assessment Report of the Urban Climate Change Research Network*, eds. C. Rosenzweig, P. Romero-Lankao, S. Mehrotra, S. Dhakal, S. Ali Ibrahim, and W. D. Solecki (Cambridge: Cambridge University Press), 27–60. doi:DOI: 10.1017/9781316563878.009.
Bador, M., Terray, L., and Boé, J. (2016). Emergence of human influence on summer record-breaking temperatures over Europe. *Geophys. Res. Lett.* 43, 404–412. doi:10.1002/2015GL066560.
Baker, D. J., Hartley, A. J., Butchart, S. H. M., and Willis, S. G. (2016). Choice of baseline climate data impacts projected species' responses to climate change. *Glob. Chang. Biol.* 22, 2392–2404. doi:10.1111/gcb.13273.
Bal, P. K., Ramachandran, A., Palanivelu, K., Thirumurugan, P., Geetha, R., and Bhaskaran, B. (2016). Climate change projections over India by a downscaling approach using PRECIS. *Asia-Pacific J. Atmos. Sci.* 52, 353–369. doi:10.1007/s13143-016-0004-1.
Ban, N., Schmidli, J., and Schär, C. (2014). Evaluation of the convection-resolving regional climate modeling approach in decade-long simulations. *J. Geophys. Res. Atmos.* 119, 7889–7907. doi:10.1002/2014JD021478.
Ban, N., Schmidli, J., and Schär, C. (2015). Heavy precipitation in a changing climate: Does short-term summer precipitation increase faster? *Geophys. Res. Lett.* 42, 1165–1172. doi:10.1002/2014GL062588.
Bandoro, J., Solomon, S., Donohoe, A., Thompson, D. W. J., and Santer, B. D. (2014). Influences of the Antarctic Ozone Hole on Southern Hemispheric Summer Climate Change. *J. Clim.* 27, 6245–6264. doi:10.1175/JCLI-D-13-00698.1.
Barcikowska, M. J., Kapnick, S. B., Krishnamurty, L., Russo, S., Cherchi, A., and Folland, C. K. (2019). Changes in the future summer Mediterranean climate: contribution of teleconnections and local factors. *Earth Syst. Dyn. Discuss.*, 1–43. doi:10.5194/esd-2018-85.
Bárdossy, A., and Pegram, G. (2012). Multiscale spatial recorrelation of RCM precipitation to produce unbiased climate change scenarios over large areas and small. *Water Resour. Res.* 48. doi:10.1029/2011WR011524.
Barlage, M., Tewari, M., Chen, F., Miguez-Macho, G., Yang, Z. L., and Niu, G. Y. (2015). The effect of groundwater interaction in North American regional climate simulations with WRF/Noah-MP. *Clim. Change*. doi:10.1007/s10584-014-1308-8.
Barnes, E. A. (2013). Revisiting the evidence linking Arctic amplification to extreme weather in midlatitudes. *Geophys. Res. Lett.* 40, 4734–4739. doi:10.1002/grl.50880.
Barnes, E. A., Barnes, N. W., and Polvani, L. M. (2014a). Delayed Southern Hemisphere Climate Change Induced by Stratospheric Ozone Recovery, as Projected by the CMIP5 Models. *J. Clim.* 27, 852–867. doi:10.1175/JCLI-D-13-00246.1.
Barnes, E. A., Dunn-Sigouin, E., Masato, G., and Woollings, T. (2014b). Exploring recent trends in Northern Hemisphere blocking. *Geophys. Res. Lett.* 41, 638–644. doi:10.1002/2013GL058745.
Barnes, E. A., and Polvani, L. (2013). Response of the Midlatitude Jets, and of Their Variability, to Increased Greenhouse Gases in the CMIP5 Models. *J. Clim.* 26, 7117–7135. doi:10.1175/JCLI-D-12-00536.1.
Barnes, E. A., and Screen, J. A. (2015). The impact of Arctic warming on the midlatitude jet-stream: Can it? Has it? Will it? *Wiley Interdiscip. Rev. Clim. Chang.* 6, 277–286. doi:10.1002/wcc.337.
Barredo, J. I., Mauri, A., Caudullo, G., and Dosio, A. (2018). Assessing Shifts of Mediterranean and Arid Climates Under RCP4.5 and RCP8.5 Climate Projections in Europe. *Pure Appl. Geophys.* 175, 3955–3971.

doi:10.1007/s00024-018-1853-6.
Barrett, B., Nitze, I., Green, S., and Cawkwell, F. (2014). Assessment of multi-temporal, multi-sensor radar and ancillary spatial data for grasslands monitoring in Ireland using machine learning approaches. *Remote Sens. Environ.* 152, 109–124. doi:https://doi.org/10.1016/j.rse.2014.05.018.
Barros, V., Chamorro, L., Coronel, G., and Baez, J. (2004). The Major Discharge Events in the Paraguay River: Magnitudes, Source Regions, and Climate Forcings. *J. Hydrometeorol.* 5, 1161–1170. doi:10.1175/JHM-378.1.
Barros, V. R., Boninsegna, J. A., Camilloni, I. A., Chidiak, M., Magrín, G. O., and Rusticucci, M. (2015). Climate change in Argentina: trends, projections, impacts and adaptation. *Wiley Interdiscip. Rev. Clim. Chang.* 6, 151–169. doi:10.1002/wcc.316.
Barros, V. R., Garavaglia, C. R., and Doyle, M. E. (2013). Twenty-first century projections of extreme precipitations in the Plata Basin. *Int. J. River Basin Manag.* 11, 373–387. doi:10.1080/15715124.2013.819358.
Barth, N. A., Villarini, G., Nayak, M. A., and White, K. (2017). Mixed populations and annual flood frequency estimates in the western United States: The role of atmospheric rivers. *Water Resour. Res.* 53, 257–269. doi:10.1002/2016WR019064.
Bartók, B. (2017). Aerosol radiative effects under clear skies over Europe and their changes in the period of 2001-2012. *Int. J. Climatol.* 37, 1901–1909. doi:10.1002/joc.4821.
Bartók, B., Wild, M., Folini, D., Lüthi, D., Kotlarski, S., Schär, C., et al. (2017). Projected changes in surface solar radiation in CMIP5 global climate models and in EURO-CORDEX regional climate models for Europe. *Clim. Dyn.* 49, 2665–2683. doi:10.1007/s00382-016-3471-2.
Baskarada, S., and Koronios, A. (2013). Data, Information, Knowledge, Wisdom (DIKW): A Semiotic Theoretical and Empirical Exploration of the Hierarchy and its Quality Dimension. *Australas. J. Inf. Syst.* 18. doi:10.3127/ajis.v18i1.748.
Bassett, R., Cai, X., Chapman, L., Heaviside, C., and Thornes, J. E. (2017). The Effects of Heat Advection on UK Weather and Climate Observations in the Vicinity of Small Urbanized Areas. *Boundary-Layer Meteorol.* 165, 181–196. doi:10.1007/s10546-017-0263-0.
Bates, B. C., Chandler, R. E., Charles, S. P., and Campbell, E. P. (2010). Assessment of apparent nonstationarity in time series of annual inflow, daily precipitation, and atmospheric circulation indices: A case study from southwest Western Australia. *Water Resour. Res.* 46. doi:10.1029/2010WR009509.
Bathiany, S., Dakos, V., Scheffer, M., and Lenton, T. M. (2018). Climate models predict increasing temperature variability in poor countries. *Sci. Adv.* 4, 1–11. doi:10.1126/sciadv.aar5809.
Baumberger, C., Knutti, R., and Hirsch Hadorn, G. (2017). Building confidence in climate model projections: an analysis of inferences from fit. *Wiley Interdiscip. Rev. Clim. Chang.* 8, e454. doi:10.1002/wcc.454.
Baztan, J., Cordier, M., Huctin, J.-M., Zhu, Z., and Vanderlinden, J.-P. (2017). Life on thin ice: Insights from Uummannaq, Greenland for connecting climate science with Arctic communities. *Polar Sci.* 13, 100–108. doi:10.1016/j.polar.2017.05.002.
Beck, H. E., van Dijk, A. I. J. M., de Roo, A., Dutra, E., Fink, G., Orth, R., et al. (2017a). Global evaluation of runoff from 10 state-of-the-art hydrological models. *Hydrol. Earth Syst. Sci.* 21, 2881–2903. doi:10.5194/hess-21-2881-2017.
Beck, H. E., Vergopolan, N., Pan, M., Levizzani, V., van Dijk, A. I. J. M., Weedon, G. P., et al. (2017b). Global-scale evaluation of 22 precipitation datasets using gauge observations and hydrological modeling. *Hydrol. Earth Syst. Sci.* 21, 6201–6217. doi:10.5194/hess-21-6201-2017.
Becker, A., Finger, P., Meyer-Christoffer, A., Rudolf, B., Schamm, K., Schneider, U., et al. (2013). A description of the global land-surface precipitation data products of the Global Precipitation Climatology Centre with sample applications including centennial (trend) analysis from 1901–present. *Earth Syst. Sci. Data* 5, 71–99. doi:10.5194/essd-5-71-2013.
Bellenger, H., Guilyardi, E., Leloup, J., Lengaigne, M., and Vialard, J. (2014). ENSO representation in climate models: from CMIP3 to CMIP5. *Clim. Dyn.* 42, 1999–2018. doi:10.1007/s00382-013-1783-z.
Bellouin, N., Baker, L., Hodnebrog, Ø., Olivié, D., Cherian, R., Macintosh, C., et al. (2016). Regional and seasonal radiative forcing by perturbations to aerosol and ozone precursor emissions. *Atmos. Chem. Phys.* 16, 13885–13910. doi:10.5194/acp-16-13885-2016.
Bellprat, O., Kotlarski, S., Lüthi, D., and Schär, C. (2013). Physical constraints for temperature biases in climate models. *Geophys. Res. Lett.* 40, 4042–4047. doi:10.1002/grl.50737.
Benedict, J. J., Maloney, E. D., Sobel, A. H., and Frierson, D. M. W. (2014). Gross Moist Stability and MJO Simulation Skill in Three Full-Physics GCMs. *J. Atmos. Sci.* 71, 3327–3349. doi:10.1175/JAS-D-13-0240.1.
Bengtsson, L., and Hodges, K. I. (2018). Can an ensemble climate simulation be used to separate climate change signals from internal unforced variability? *Clim. Dyn.* doi:10.1007/s00382-018-4343-8.
Bennington, V., Notaro, M., and Holman, K. D. (2014). Improving Climate Sensitivity of Deep Lakes within a Regional Climate Model and Its Impact on Simulated Climate. *J. Clim.* 27, 2886–2911. doi:10.1175/JCLI-D-13-00110.1.
Benzanilla, A., New, M., Centella, A., Charlery, J., Taylor, M. A., Karmalkar, A. V., et al. (2015). A review of observed and projected changes in climate for the islands in the Caribbean. *Atmósfera* 26, 283–309.

doi:10.1016/s0187-6236(13)71076-2.
Beranová, R., and Kyselý, J. (2016). Links between circulation indices and precipitation in the Mediterranean in an ensemble of regional climate models. *Theor. Appl. Climatol.* 123, 693–701. doi:10.1007/s00704-015-1381-6.
Berckmans, J., Hamdi, R., and Dendoncker, N. (2019). Bridging the gap between policy-driven land use changes and 1 regional climate projections 2. *J. Geophys. Res.*
Berckmans, J., Van Malderen, R., Pottiaux, E., Pacione, R., and Hamdi, R. (2018). Validating the water vapour content from a reanalysis product and aregional climate model over Europe based on GNSS observations. *Atmos. Chem. Phys. Discuss.* 2018, 1–24. doi:10.5194/acp-2018-1097.
Berckmans, J., Woollings, T., Demory, M.-E., Vidale, P.-L., and Roberts, M. (2013). Atmospheric blocking in a high resolution climate model: influences of mean state, orography and eddy forcing. *Atmos. Sci. Lett.* 14, 34–40. doi:10.1002/asl2.412.
Berg, A., Lintner, B. R., Findell, K., and Giannini, A. (2017). Uncertain soil moisture feedbacks in model projections of Sahel precipitation. *Geophys. Res. Lett.* 44, 6124–6133. doi:10.1002/2017GL073851.
Berthou, S., Mailler, S., Drobinski, P., Arsouze, T., Bastin, S., Béranger, K., et al. (2015). Sensitivity of an intense rain event between atmosphere-only and atmosphere-ocean regional coupled models: 19 September 1996. *Q. J. R. Meteorol. Soc.* 141, 258–271. doi:10.1002/qj.2355.
Besselaar, E. J. M., Sanchez-Lorenzo, A., Wild, M., Klein Tank, A. M. G., and Laat, A. T. J. (2015). Relationship between sunshine duration and temperature trends across Europe since the second half of the twentieth century. *J. Geophys. Res. Atmos.* 120, 10,810-823,836. doi:10.1002/2015JD023640.
Bessette, D. L., Mayer, L. A., Cwik, B., Vezér, M., Keller, K., Lempert, R. J., et al. (2017). Building a Values-Informed Mental Model for New Orleans Climate Risk Management. *Risk Anal.* 37, 1993–2004. doi:10.1111/risa.12743.
Best, M. J., and Grimmond, C. S. B. (2015). Key Conclusions of the First International Urban Land Surface Model Comparison Project. *Bull. Am. Meteorol. Soc.* 96, 805–819. doi:10.1175/BAMS-D-14-00122.1.
Best, M. J., Grimmond, C. S. B., and Villani, M. G. (2006). Evaluation of the urban tile in MOSES using surface energy balance observations. *Boundary-Layer Meteorol.* doi:10.1007/s10546-005-9025-5.
Bevacqua, E., Maraun, D., Hobæk Haff, I., Widmann, M., and Vrac, M. (2017). Multivariate statistical modelling of compound events via pair-copula constructions: analysis of floods in Ravenna (Italy). *Hydrol. Earth Syst. Sci.* 21, 2701–2723. doi:10.5194/hess-21-2701-2017.
Bhatt, B. C., Sobolowski, S., and King, M. P. (2014). Assessment of downscaled current and future projections of diurnal rainfall patterns for the Himalaya. *J. Geophys. Res. Atmos.* doi:10.1002/2014JD022134.
Bhave, A. G., Conway, D., Dessai, S., and Stainforth, D. A. (2016). Barriers and opportunities for robust decision making approaches to support climate change adaptation in the developing world. *Clim. Risk Manag.* 14, 1–10. doi:10.1016/j.crm.2016.09.004.
Bhave, A. G., Conway, D., Dessai, S., and Stainforth, D. A. (2018). Water Resource Planning Under Future Climate and Socioeconomic Uncertainty in the Cauvery River Basin in Karnataka, India. *Water Resour. Res.* 54, 708–728. doi:10.1002/2017WR020970.
Biasutti, M. (2013). Forced Sahel rainfall trends in the CMIP5 archive. *J. Geophys. Res. Atmos.* 118, 1613–1623. doi:10.1002/jgrd.50206.
Biasutti, M., and Giannini, A. (2006). Robust Sahel drying in response to late 20th century forcings. *Geophys. Res. Lett.* 33, L11706. doi:10.1029/2006GL026067.
Bieniek, P. A., Bhatt, U. S., Walsh, J. E., Rupp, T. S., Zhang, J., Krieger, J. R., et al. (2016). Dynamical Downscaling of ERA-Interim Temperature and Precipitation for Alaska. *J. Appl. Meteorol. Climatol.* 55, 635–654. doi:10.1175/JAMC-D-15-0153.1.
Bindoff, N. L., Stott, P. A., AchutaRao, K. M., Allen, M. R., Gillett, N. P., and Gutzler, D., et al. (2013). "Detection and Attribution of Climate Change: from Global to Regional," in *Climate Change 2013 - The Physical Science Basis*, ed. Intergovernmental Panel on Climate Change (Cambridge: Cambridge University Press), 867–952. doi:10.1017/CBO9781107415324.022.
Birner, T., Davis, S. M., and Seidel, D. J. (2014). The changing width of Earth's tropical belt. *Phys. Today* 67, 38–44. doi:10.1063/PT.3.2620.
Black, M., Karoly, D., and King, A. (2015). The contribution of anthropogenic forcing to the Adelaide and Melbourne, Australia, heat waves of January 2014. *Bull. Am. Meteorol. Soc.* 96, S145–S148.
Blackport, R., and Kushner, P. J. (2017). Isolating the Atmospheric Circulation Response to Arctic Sea Ice Loss in the Coupled Climate System. *J. Clim.* 30, 2163–2185. doi:10.1175/JCLI-D-16-0257.1.
Bladé, I., Liebmann, B., Fortuny, D., and van Oldenborgh, G. J. (2012). Observed and simulated impacts of the summer NAO in Europe: implications for projected drying in the Mediterranean region. *Clim. Dyn.* 39, 709–727. doi:10.1007/s00382-011-1195-x.
Blamey, R. C., Kolusu, S. R., Mahlalela, P., Todd, M. C., and Reason, C. J. C. (2018). The role of regional circulation features in regulating El Niño climate impacts over southern Africa: A comparison of the 2015/2016 drought with previous events. *Int. J. Climatol.* 38, 4276–4295. doi:10.1002/joc.5668.
Blamey, R., and Reason, C. (2007). Relationships between Antarctic sea-ice and South African winter rainfall. *Clim. Res.* 33, 183–193. doi:10.3354/cr033183.

Blázquez, J., and Solman, S. A. (2018). Fronts and precipitation in CMIP5 models for the austral winter of the Southern Hemisphere. *Clim. Dyn.* 50, 2705–2717. doi:10.1007/s00382-017-3765-z.

Blenkinsop, S., Lewis, E., Chan, S. C., and Fowler, H. J. (2017). Quality-control of an hourly rainfall dataset and climatology of extremes for the UK. *Int. J. Climatol.* 37, 722–740. doi:10.1002/joc.4735.

Bližňák, V., Kašpar, M., and Müller, M. (2018). Radar-based summer precipitation climatology of the Czech Republic. *Int. J. Climatol.* 38, 677–691. doi:10.1002/joc.5202.

Boberg, F., and Christensen, J. H. (2012). Overestimation of Mediterranean summer temperature projections due to model deficiencies. *Nat. Clim. Chang.* 2, 1–4. doi:10.1038/nclimate1454.

Boé, J. (2018). Interdependency in Multimodel Climate Projections: Component Replication and Result Similarity. *Geophys. Res. Lett.* 45, 2771–2779. doi:10.1002/2017GL076829.

Boé, J., and Terray, L. (2014). Land–sea contrast, soil-atmosphere and cloud-temperature interactions: interplays and roles in future summer European climate change. *Clim. Dyn.* 42, 683–699. doi:10.1007/s00382-013-1868-8.

Boer, G. J., Smith, D. M., Cassou, C., Doblas-Reyes, F., Danabasoglu, G., Kirtman, B., et al. (2016). The Decadal Climate Prediction Project (DCPP) contribution to CMIP6. *Geosci. Model Dev.* 9, 3751–3777. doi:10.5194/gmd-9-3751-2016.

Böhm, R., Jones, P. D., Hiebl, J., Frank, D., Brunetti, M., and Maugeri, M. (2010). The early instrumental warm-bias: A solution for long central European temperature series 1760-2007. *Clim. Change*. doi:10.1007/s10584-009-9649-4.

Böhme, T., Stapelberg, S., Akkermans, T., Crewell, S., Fischer, J., Reinhardt, T., et al. (2011). Long-term evaluation of COSMO forecasting using combined observational data of the GOP period. *Meteorol. Zeitschrift* 20, 119–132. doi:10.1127/0941-2948/2011/0225.

Bohnenstengel, S. I., Hamilton, I., Davies, M., and Belcher, S. E. (2014). Impact of anthropogenic heat emissions on London's temperatures. *Q. J. R. Meteorol. Soc.* 140, 687–698. doi:10.1002/qj.2144.

Bolch, T., Kulkarni, A., Kääb, A., Huggel, C., Paul, F., Cogley, J. G., et al. (2012). The state and fate of himalayan glaciers. *Science (80-. ).* 336, 310–314. doi:10.1126/science.1215828.

Bollasina, M. A., Ming, Y., and Ramaswamy, V. (2011). Anthropogenic aerosols and the weakening of the south asian summer monsoon. *Science (80-. ).* 334, 502–505. doi:10.1126/science.1204994.

Boos, W. R., and Hurley, J. V. (2013). Thermodynamic bias in the multimodel mean boreal summer monsoon. *J. Clim.* doi:10.1175/JCLI-D-12-00493.1.

Booth, B. B. B., Bernie, D., McNeall, D., Hawkins, E., Caesar, J., Boulton, C., et al. (2013). Scenario and modelling uncertainty in global mean temperature change derived from emission-driven global climate models. *Earth Syst. Dyn.* 4, 95–108. doi:10.5194/esd-4-95-2013.

Booth, J. F., Kwon, Y.-O., Ko, S., Small, R. J., and Msadek, R. (2017). Spatial Patterns and Intensity of the Surface Storm Tracks in CMIP5 Models. *J. Clim.* 30, 4965–4981. doi:10.1175/JCLI-D-16-0228.1.

Borodina, A., Fischer, E. M., and Knutti, R. (2017). Emergent Constraints in Climate Projections: A Case Study of Changes in High-Latitude Temperature Variability. *J. Clim.* 30, 3655–3670. doi:10.1175/JCLI-D-16-0662.1.

Bosilovich, M. G., Chern, J.-D., Mocko, D., Robertson, F. R., and da Silva, A. M. (2015). Evaluating Observation Influence on Regional Water Budgets in Reanalyses. *J. Clim.* 28, 3631–3649. doi:10.1175/JCLI-D-14-00623.1.

Boucher, O., Randall, D., and et al. (2014). "Anthropogenic and Natural Radiative Forcing," in *Climate Change 2013 - The Physical Science Basis*, ed. Intergovernmental Panel on Climate Change (Cambridge: Cambridge University Press), 659–740. doi:10.1017/CBO9781107415324.018.

Bracegirdle, T. J., Hyder, P., and Holmes, C. R. (2018). CMIP5 Diversity in Southern Westerly Jet Projections Related to Historical Sea Ice Area: Strong Link to Strengthening and Weak Link to Shift. *J. Clim.* 31, 195–211. doi:10.1175/JCLI-D-17-0320.1.

Bracegirdle, T. J., and Stephenson, D. B. (2013). On the Robustness of Emergent Constraints Used in Multimodel Climate Change Projections of Arctic Warming. *J. Clim.* 26, 669–678. doi:10.1175/JCLI-D-12-00537.1.

Brands, S. (2017). Which ENSO teleconnections are robust to internal atmospheric variability? *Geophys. Res. Lett.* 44, 1483–1493. doi:10.1002/2016GL071529.

Brands, S., Gutiérrez, J. M., Herrera, S., and Cofiño, A. S. (2012). On the Use of Reanalysis Data for Downscaling. *J. Clim.* 25, 2517–2526. doi:10.1175/JCLI-D-11-00251.1.

Brasseur, G. P., and Gallardo, L. (2016). Climate services: Lessons learned and future prospects. *Earth's Futur.* 4, 79–89. doi:10.1002/2015EF000338.

Bremer, S., and Meisch, S. (2017). Co-production in climate change research: reviewing different perspectives. *Wiley Interdiscip. Rev. Clim. Chang.* 8, e482. doi:10.1002/wcc.482.

Brient, F., and Schneider, T. (2016). Constraints on Climate Sensitivity from Space-Based Measurements of Low-Cloud Reflection. *J. Clim.* 29, 5821–5835. doi:10.1175/JCLI-D-15-0897.1.

Brönnimann, S., Compo, G. P., Spadin, R., Allan, R., and Adam, W. (2011). Early ship-based upper-air data and comparison with the Twentieth Century Reanalysis. *Clim. Past* 7, 265–276. doi:10.5194/cp-7-265-2011.

Brown, A., Milton, S., Cullen, M., Golding, B., Mitchell, J., and Shelly, A. (2012a). Unified Modeling and Prediction of Weather and Climate. *Bull. Amer. Meteor. Soc.* 93, 1865–1877. doi:10.1175/BAMS-D-12-00018.1.

Brown, C., Ghile, Y., Laverty, M., and Li, K. (2012b). Decision scaling: Linking bottom-up vulnerability analysis with climate projections in the water sector. *Water Resour. Res.* 48, 1–12. doi:10.1029/2011WR011212.

Brown, J. R., Moise, A. F., Colman, R., and Zhang, H. (2016). Will a Warmer World Mean a Wetter or Drier Australian Monsoon? *J. Clim.* 29, 4577–4596. doi:10.1175/JCLI-D-15-0695.1.

Brown, M. J. (2000). Urban parameterizations for mesoscale meteorological models. *Mesoscale Atmos. Dispers.* 9, 193–255.

Brown, P. T., Stolpe, M. B., and Caldeira, K. (2018). Assumptions for emergent constraints. *Nature* 563, E1–E3. doi:10.1038/s41586-018-0638-5.

Brulebois, E., Castel, T., Richard, Y., Chateau-Smith, C., and Amiotte-Suchet, P. (2015). Hydrological response to an abrupt shift in surface air temperature over France in 1987/88. *J. Hydrol.* 531, 892–901. doi:https://doi.org/10.1016/j.jhydrol.2015.10.026.

Brunet, M., Asin, J., Sigró, J., Bañón, M., García, F., Aguilar, E., et al. (2011). The minimization of the screen bias from ancient Western Mediterranean air temperature records: an exploratory statistical analysis. *Int. J. Climatol.* 31, 1879–1895. doi:10.1002/joc.2192.

Brunner, L., Hegerl, G. C., and Steiner, A. K. (2017). Connecting Atmospheric Blocking to European Temperature Extremes in Spring. *J. Clim.* 30, 585–594. doi:10.1175/JCLI-D-16-0518.1.

Buckley, M. W., and Marshall, J. (2016). Observations, inferences, and mechanisms of the Atlantic Meridional Overturning Circulation: A review. *Rev. Geophys.* 54, 5–63. doi:10.1002/2015RG000493.

Budikova, D., Ford, T. W., and Ballinger, T. J. (2017). Connections between north-central United States summer hydroclimatology and Arctic sea ice variability. *Int. J. Climatol.* 37, 4434–4450. doi:10.1002/joc.5097.

Bueno, B., Pigeon, G., Norford, L. K., Zibouche, K., and Marchadier, C. (2012). Development and evaluation of a building energy model integrated in the TEB scheme. *Geosci. Model Dev.* 5, 433–448. doi:10.5194/gmd-5-433-2012.

Bukovsky, M. S. (2012). Temperature Trends in the NARCCAP Regional Climate Models. *J. Clim.* 25, 3985–3991. doi:10.1175/JCLI-D-11-00588.1.

Bukovsky, M. S., Carrillo, C. M., Gochis, D. J., Hammerling, D. M., McCrary, R. R., and Mearns, L. O. (2015). Toward assessing NARCCAP regional climate model credibility for the North American monsoon: Future climate simulations. *J. Clim.* 28, 6707–6728. doi:10.1175/JCLI-D-14-00695.1.

Bukovsky, M. S., Gochis, D. J., and Mearns, L. O. (2013). Towards Assessing NARCCAP Regional Climate Model Credibility for the North American Monsoon: Current Climate Simulations*. *J. Clim.* 26, 8802–8826. doi:10.1175/JCLI-D-12-00538.1.

Buontempo, C., Hanlon, H. M., Bruno Soares, M., Christel, I., Soubeyroux, J. M., Viel, C., et al. (2018). What have we learnt from EUPORIAS climate service prototypes? *Clim. Serv.* 9, 21–32. doi:10.1016/j.cliser.2017.06.003.

Burke, C., and Stott, P. (2017). Impact of Anthropogenic Climate Change on the East Asian Summer Monsoon. *J. Clim.* 30, 5205–5220. doi:10.1175/JCLI-D-16-0892.1.

Cahynová, M., and Huth, R. (2014). Atmospheric circulation influence on climatic trends in Europe: an analysis of circulation type classifications from the COST733 catalogue. *Int. J. Climatol.* 36, 2743–2760. doi:10.1002/joc.4003.

Cai, L., Alexeev, V. A., Arp, C. D., Jones, B. M., Liljedahl, A. K., and Gädeke, A. (2018). The Polar WRF Downscaled Historical and Projected Twenty-First Century Climate for the Coast and Foothills of Arctic Alaska. 5, 1–15. doi:10.3389/feart.2017.00111.

Cai, P., Hamdi, R., He, H., Luo, G., Wang, J., Zhang, M., et al. Numerical study of the interaction between oasis and urban areas within an arid mountains-desert system in Xinjiang, China using ALARO-SURFEX 3.

Cai, W., Purich, A., Cowan, T., van Rensch, P., and Weller, E. (2014). Did Climate Change–Induced Rainfall Trends Contribute to the Australian Millennium Drought? *J. Clim.* 27, 3145–3168. doi:10.1175/JCLI-D-13-00322.1.

Camargo, S. J. (2013). Global and Regional Aspects of Tropical Cyclone Activity in the CMIP5 Models. *J. Clim.* 26, 9880–9902. doi:10.1175/JCLI-D-12-00549.1.

Camera, C., Bruggeman, A., Hadjinicolaou, P., Pashiardis, S., and Lange, M. A. (2014). Evaluation of interpolation techniques for the creation of gridded daily precipitation (1 × 1 km2); Cyprus, 1980–2010. *J. Geophys. Res. Atmos.* 119, 693–712. doi:10.1002/2013JD020611.

Campbell, J. D., Taylor, M. A., Stephenson, T. S., Watson, R. A., and Whyte, F. S. (2011). Future climate of the Caribbean from a regional climate model. *Int. J. Climatol.* 31, 1866–1878. doi:10.1002/joc.2200.

Campbell, T. H., and Kay, A. C. (2014). Solution aversion: On the relation between ideology and motivated disbelief. *J. Pers. Soc. Psychol.* 107, 809–824. doi:10.1037/a0037963.

Cannon, A. J. (2016). Multivariate Bias Correction of Climate Model Output: Matching Marginal Distributions and Intervariable Dependence Structure. *J. Clim.* 29, 7045–7064. doi:10.1175/JCLI-D-15-0679.1.

Cannon, A. J. (2018). Multivariate quantile mapping bias correction: an N-dimensional probability density function transform for climate model simulations of multiple variables. *Clim. Dyn.* 50, 31–49. doi:10.1007/s00382-017-3580-6.

Capotondi, A., Wittenberg, A. T., Newman, M., Di Lorenzo, E., Yu, J.-Y., Braconnot, P., et al. (2015). Understanding ENSO Diversity. *Bull. Am. Meteorol. Soc.* 96, 921–938. doi:10.1175/BAMS-D-13-00117.1.

Careto, J. A. M., Cardoso, R. M., Soares, P. M. M., and Trigo, R. M. (2018). Land-Atmosphere Coupling in CORDEX-Africa: Hindcast Regional Climate Simulations. *J. Geophys. Res. Atmos.* 123, 11,048-11,067.

doi:10.1029/2018JD028378.
Carril, A. F., Menéndez, C. G., Remedio, A. R. C., Robledo, F., Sörensson, A., Tencer, B., et al. (2012). Performance of a multi-RCM ensemble for South Eastern South America. *Clim. Dyn.* 39, 2747–2768. doi:10.1007/s00382-012-1573-z.
Cash, D. W., Clark, W. C., Alcock, F., Dickson, N. M., Eckley, N., Guston, D. H., et al. (2003). Knowledge Systems for Sustainable Development. *Proc. Natl. Acad. Sci.* 100, 8086–8091. doi:10.1073/pnas.1231332100.
Cassano, J. J., DuVivier, A., Roberts, A., Hughes, M., Seefeldt, M., Brunke, M., et al. (2017). Development of the Regional Arctic System Model (RASM): Near-Surface Atmospheric Climate Sensitivity. *J. Clim.* 30, 5729–5753. doi:10.1175/JCLI-D-15-0775.1.
Cassou, C. (2008). Intraseasonal interaction between the Madden–Julian Oscillation and the North Atlantic Oscillation. *Nature* 455, 523–527. doi:10.1038/nature07286.
Castro, C. L., Chang, H. I., Dominguez, F., Carrillo, C., Schemm, J. K., and Juang, H. M. H. (2012). Can a regional climate model improve the ability to forecast the North American monsoon? *J. Clim.* 25, 8212–8237. doi:10.1175/JCLI-D-11-00441.1.
Catto, J. L., Jakob, C., and Nicholls, N. (2015). Can the CMIP5 models represent winter frontal precipitation? *Geophys. Res. Lett.* 42, 8596–8604. doi:10.1002/2015GL066015.
Catto, J. L., Nicholls, N., Jakob, C., and Shelton, K. L. (2014). Atmospheric fronts in current and future climates. *Geophys. Res. Lett.* 41, 7642–7650. doi:10.1002/2014GL061943.
Cavallo, S. M., Berner, J., and Snyder, C. (2016). Diagnosing Model Errors from Time-Averaged Tendencies in the Weather Research and Forecasting (WRF) Model. *Mon. Weather Rev.* 144, 759–779. doi:10.1175/MWR-D-15-0120.1.
Cavazos, T., Turrent, C., and Lettenmaier, D. P. (2008). Extreme precipitation trends associated with tropical cyclones in the core of the North American monsoon. *Geophys. Res. Lett.* 35, 1–5. doi:10.1029/2008GL035832.
Cavicchia, L., Scoccimarro, E., Gualdi, S., Marson, P., Ahrens, B., Berthou, S., et al. (2018). Mediterranean extreme precipitation: a multi-model assessment. *Clim. Dyn.* 51, 901–913. doi:10.1007/s00382-016-3245-x.
Cavicchia, L., von Storch, H., and Gualdi, S. (2014). A long-term climatology of medicanes. *Clim. Dyn.* 43, 1183–1195. doi:10.1007/s00382-013-1893-7.
Cayan, D., Kunkel, K., Castro, C., Gershunov, A., Barsugli, J., Ray, A., et al. (2013). "Future climate: Projected average," in *Assessment of Climate Change in the Southwest United States: A Report Prepared for the National Climate Assessment* (Island Press), 101–125.
CDC (2018). Heat Stress.
Ceppi, P., Scherrer, S. C., Fischer, A. M., and Appenzeller, C. (2012). Revisiting Swiss temperature trends 1959-2008. *Int. J. Climatol.* 32, 203–213. doi:10.1002/joc.2260.
Challinor, A., Slingo, J., Turner, A., and Wheeler, T. (2006). Indian Monsoon: Contribution to the Stern Review.
Chan, S. C., Kendon, E. J., Fowler, H. J., Blenkinsop, S., and Roberts, N. M. (2014a). Projected increases in summer and winter UK sub-daily precipitation extremes from high-resolution regional climate models. *Environ. Res. Lett.* 9, 084019. doi:10.1088/1748-9326/9/8/084019.
Chan, S. C., Kendon, E. J., Fowler, H. J., Blenkinsop, S., Roberts, N. M., and Ferro, C. A. T. (2014b). The value of high-resolution Met Office regional climate models in the simulation of multihourly precipitation extremes. *J. Clim.* 27, 6155–6174. doi:10.1175/JCLI-D-13-00723.1.
Chaney, N. W., Sheffield, J., Villarini, G., and Wood, E. F. (2014). Development of a High-Resolution Gridded Daily Meteorological Dataset over Sub-Saharan Africa: Spatial Analysis of Trends in Climate Extremes. *J. Clim.* 27, 5815–5835. doi:10.1175/JCLI-D-13-00423.1.
Chang, E. K. M., Guo, Y., and Xia, X. (2012). CMIP5 multimodel ensemble projection of storm track change under global warming. *J. Geophys. Res. Atmos.* 117, n/a-n/a. doi:10.1029/2012JD018578.
Charles, S., Bates, B., Whetton, P., and Hughes, J. (1999). Validation of downscaling models for changed climate conditions: case study of southwestern Australia. *Clim. Res.* 12, 1–14. doi:10.3354/cr012001.
Chaudhuri, A. H., Ponte, R. M., Forget, G., and Heimbach, P. (2013). A Comparison of Atmospheric Reanalysis Surface Products over the Ocean and Implications for Uncertainties in Air–Sea Boundary Forcing. *J. Clim.* 26, 153–170. doi:10.1175/JCLI-D-12-00090.1.
Cheema, M. J. M., and Bastiaanssen, W. G. M. (2012). Local calibration of remotely sensed rainfall from the TRMM satellite for different periods and spatial scales in the Indus Basin. *Int. J. Remote Sens.* 33, 2603–2627. doi:10.1080/01431161.2011.617397.
Chemke, R., Polvani, L. M., and Deser, C. (2019). The Effect of Arctic Sea Ice Loss on the Hadley Circulation. *Geophys. Res. Lett.* 46, 963–972. doi:10.1029/2018GL081110.
Chen, A. A., Taylor, M. A., Brown, P., and Campbell, J. D. (2012). *State of the Jamaican Climate 2012 [ State of the Jamaican Climate 2012 ]*.
Chen, B., Dong, L., Liu, X., Shi, G. Y., Chen, L., Nakajima, T., et al. (2016a). Exploring the possible effect of anthropogenic heat release due to global energy consumption upon global climate: a climate model study. *Int. J. Climatol.* 36, 4790–4796. doi:10.1002/joc.4669.
Chen, F., Kusaka, H., Bornstein, R., Ching, J., Grimmond, C. S. B., Grossman-Clarke, S., et al. (2011). The integrated

WRF/urban modelling system: development, evaluation, and applications to urban environmental problems. *Int. J. Climatol.* 31, 273–288. doi:10.1002/joc.2158.

Chen, H., Ma, H., Li, X., and Sun, S. (2015). Solar influences on spatial patterns of Eurasian winter temperature and atmospheric general circulation anomalies. *J. Geophys. Res. Atmos.* 120, 8642–8657. doi:10.1002/2015JD023415.

Chen, H. W., Alley, R. B., and Zhang, F. (2016b). Interannual Arctic sea ice variability and associated winter weather patterns: A regional perspective for 1979-2014. *J. Geophys. Res. Atmos.* 121, 14,433-14,455. doi:10.1002/2016JD024769.

Chen, H. W., Zhang, F., and Alley, R. B. (2016c). The Robustness of Midlatitude Weather Pattern Changes due to Arctic Sea Ice Loss. *J. Clim.* 29, 7831–7849. doi:10.1175/JCLI-D-16-0167.1.

Chen, H., Zhang, Y., Yu, M., Hua, W., Sun, S., Li, X., et al. (2016d). Large-scale urbanization effects on eastern Asian summer monsoon circulation and climate. *Clim. Dyn.* 47, 117–136. doi:10.1007/s00382-015-2827-3.

Chen, L., Francis, J., and Hanna, E. (2018a). The "Warm-Arctic/Cold-continents" pattern during 1901–2010. *Int. J. Climatol.* 38, 5245–5254. doi:10.1002/joc.5725.

Chen, L., Qu, X., Huang, G., and Gong, Y. (2018b). Projections of East Asian summer monsoon under 1.5 °C and 2 °C warming goals. *Theor. Appl. Climatol.* doi:10.1007/s00704-018-2720-1.

Chen, M., Shi, W., Xie, P., Silva, V. B. S., Kousky, V. E., Wayne Higgins, R., et al. (2008). Assessing objective techniques for gauge-based analyses of global daily precipitation. *J. Geophys. Res.* 113, D04110. doi:10.1029/2007JD009132.

Chen, X., Leung, L. R., Gao, Y., Liu, Y., Wigmosta, M., and Richmond, M. (2018c). Predictability of Extreme Precipitation in Western U.S. Watersheds Based on Atmospheric River Occurrence, Intensity, and Duration. *Geophys. Res. Lett.*, 693–701. doi:10.1029/2018GL079831.

Chen, X., Xing, P., Luo, Y., Nie, S., Zhao, Z., Huang, J., et al. (2018d). Multiscale combination of climate model simulations and proxy records over the last millennium. *Theor. Appl. Climatol.* 132, 763–777. doi:10.1007/s00704-017-2119-4.

Chenoli, S. N., Ahmad Mazuki, M. Y., Turner, J., and Samah, A. A. (2017). Historical and projected changes in the Southern Hemisphere Sub-tropical Jet during winter from the CMIP5 models. *Clim. Dyn.* 48, 661–681. doi:10.1007/s00382-016-3102-y.

Cherchi, A., Alessandri, A., Masina, S., and Navarra, A. (2011). Effects of increased CO2 levels on monsoons. *Clim. Dyn.* 37, 83–101. doi:10.1007/s00382-010-0801-7.

Cherchi, A., Annamalai, H., Masina, S., and Navarra, A. (2014). South Asian summer monsoon and the eastern Mediterranean climate: The monsoon-desert mechanism in CMIP5 simulations. *J. Clim.* doi:10.1175/JCLI-D-13-00530.1.

Cherchi, A., Annamalai, H., Masina, S., Navarra, A., and Alessandri, A. (2016). Twenty-first century projected summer mean climate in the Mediterranean interpreted through the monsoon-desert mechanism. *Clim. Dyn.* 47, 2361–2371. doi:10.1007/s00382-015-2968-4.

Cherian, R., Quaas, J., Salzmann, M., and Wild, M. (2014). Pollution trends over Europe constrain global aerosol forcing as simulated by climate models. *Geophys. Res. Lett.* 41, 2176–2181. doi:10.1002/2013GL058715.

Chevuturi, A., Klingaman, N. P., Turner, A. G., and Hannah, S. (2018). Projected Changes in the Asian-Australian Monsoon Region in 1.5°C and 2.0°C Global-Warming Scenarios. *Earth's Futur.* 6. doi:10.1002/2017EF000734.

Chiew, F. H. S., Young, W. J., Cai, W., and Teng, J. (2011). Current drought and future hydroclimate projections in southeast Australia and implications for water resources management. *Stoch. Environ. Res. Risk Assess.* 25, 601–612. doi:10.1007/s00477-010-0424-x.

Chimani, B., Venema, V., Lexer, A., Andre, K., Auer, I., and Nemec, J. (2018). Inter-comparison of methods to homogenize daily relative humidity. *Int. J. Climatol.* 38, 3106–3122. doi:10.1002/joc.5488.

Chiodi, A. M., and Harrison, D. E. (2017). Simulating ENSO SSTAs from TAO/TRITON Winds: The Impacts of 20 Years of Buoy Observations in the Pacific Waveguide and Comparison with Reanalysis Products. *J. Clim.* 30, 1041–1059. doi:10.1175/JCLI-D-15-0865.1.

Chiodo, G., Oehrlein, J., Polvani, L. M., Fyfe, J. C., and Smith, A. K. (2019). Insignificant influence of the 11-year solar cycle on the North Atlantic Oscillation. *Nat. Geosci.* 12, 94–99. doi:10.1038/s41561-018-0293-3.

Chiriaco, M., Dupont, J.-C., Bastin, S., Badosa, J., Lopez, J., Haeffelin, M., et al. (2018). ReOBS: a new approach to synthesize long-term multi-variable dataset and application to the SIRTA supersite. *Earth Syst. Sci. Data* 10, 919–940. doi:10.5194/essd-10-919-2018.

Cholette, M., Laprise, R., and Thériault, J. (2015). Perspectives for Very High-Resolution Climate Simulations with Nested Models: Illustration of Potential in Simulating St. Lawrence River Valley Channelling Winds with the Fifth-Generation Canadian Regional Climate Model. *Climate* 3, 283–307. doi:10.3390/cli3020283.

Choudhary, A., and Dimri, A. P. (2018). Assessment of CORDEX-South Asia experiments for monsoonal precipitation over Himalayan region for future climate. *Clim. Dyn.* 50, 3009–3030. doi:10.1007/s00382-017-3789-4.

Choudhary, A., Dimri, A. P., and Maharana, P. (2018). Assessment of CORDEX-SA experiments in representing precipitation climatology of summer monsoon over India. *Theor. Appl. Climatol.* 134, 283–307. doi:10.1007/s00704-017-2274-7.

Christensen, J. H., Hewitson, B., Busuioc, A., Chen, A., Gao, X., Held, I., et al. (2007). "Regional Climate Projections,"

in *Climate Change 2007: The Physical Science Basis*, ed. IPCC (Cham: Cambridge University Press), 847–940. doi:10.1007/978-3-319-68418-5_10.

Christensen, J. H., Kumar, K. K., Aldrian, E., An, S.-I., Cavalcanti, I. F. A., de Castro, M., et al. (2013a). "Climate Phenomena and their Relevance for Future Regional Climate Change," in *Climate Change 2013: The Physical Science Basis. Contribution of Working Group I to the Fifth Assessment Report of the Intergovernmental Panel on Climate Change*, eds. T. F. Stocker, D. Qin, G.-K. Plattner, M. Tignor, S. K. Allen, J. Boschung, et al. (Cambridge: Cambridge University Press), 1217–1308.

Christensen, J. H., Kumar, K. K., Aldrian, E., An, S.-I., Cavalcanti, I. F. A., de Castro, M., et al. (2013b). "Climate Phenomena and their Relevance for Future Regional Climate Change," in *Climate Change 2013 - The Physical Science Basis*, ed. Intergovernmental Panel on Climate Change (Cambridge: Cambridge University Press), 1217–1308. doi:10.1017/CBO9781107415324.028.

Christensen, J. H., Larsen, M. A. D., Christensen, O. B., Drews, M., and Stendel, M. (2019a). Robustness of European climate projections from dynamical downscaling. *Clim. Dyn.*, submitted.

Christensen, J. H., Matte, D., Larsen, M. A. D., Christensen, O. B., Drews, M., and Stendel, M. (2019b). Robustness and scalability of regional climate projections over Europe. *Front. Environ. Sci.* 6, submitted. doi:10.3389/fenvs.2018.00163.

Chrysanthou, A., van der Schrier, G., van den Besselaar, E. J. M., Klein Tank, A. M. G. G., and Brandsma, T. (2014). The effects of urbanization on the rise of the European temperature since 1960. *Geophys. Res. Lett.* 41, 7716–7722. doi:10.1002/2014GL061154.

Chubb, T., Manton, M. J., Peace, A. D., and Bilish, S. P. (2015). Estimation of Wind-Induced Losses from a Precipitation Gauge Network in the Australian Snowy Mountains. *J. Hydrometeorol.* 16, 2619–2638. doi:10.1175/jhm-d-14-0216.1.

Chung, J. X., Juneng, L., Tangang, F., and Jamaluddin, A. F. (2018). Performances of BATS and CLM land-surface schemes in RegCM4 in simulating precipitation over CORDEX Southeast Asia domain. *Int. J. Climatol.* 38, 794–810. doi:10.1002/joc.5211.

Coats, S., Smerdon, J. E., Cook, B. I., and Seager, R. (2013). Stationarity of the tropical pacific teleconnection to North America in CMIP5/PMIP3 model simulations. *Geophys. Res. Lett.* 40, 4927–4932. doi:10.1002/grl.50938.

CoCT (2018). Economic Performance Indicators for Cape Town. Cape Town Available at: http://resource.capetown.gov.za/documentcentre/Documents/City research reports and review/CCT EPIC 2018Q1 FINAL 20180702.pdf%0A%0A.

Cohen, J. L., Furtado, J. C., Barlow, M. A., Alexeev, V. A., and Cherry, J. E. (2012a). Arctic warming, increasing snow cover and widespread boreal winter cooling. *Environ. Res. Lett.* 7, 014007. doi:10.1088/1748-9326/7/1/014007.

Cohen, J. L., Furtado, J. C., Barlow, M., Alexeev, V. A., and Cherry, J. E. (2012b). Asymmetric seasonal temperature trends. *Geophys. Res. Lett.* 39, n/a-n/a. doi:10.1029/2011GL050582.

Cohen, J., Screen, J. A., Furtado, J. C., Barlow, M., Whittleston, D., Coumou, D., et al. (2014). Recent Arctic amplification and extreme mid-latitude weather. *Nat. Geosci.* 7, 627–637. doi:10.1038/ngeo2234.

Colette, A., Vautard, R., and Vrac, M. (2012). Regional climate downscaling with prior statistical correction of the global climate forcing. *Geophys. Res. Lett.* 39, n/a-n/a. doi:10.1029/2012GL052258.

Collazo, S., Lhotka, O., Rusticucci, M., and Kyselý, J. (2018). Capability of the SMHI-RCA4 RCM driven by the ERA-Interim reanalysis to simulate heat waves in Argentina. *Int. J. Climatol.* 38, 483–496. doi:10.1002/joc.5190.

Collins, K., and Ison, R. (2009). Jumping off Arnstein's ladder: social learning as a new policy paradigm for climate change adaptation. *Environ. Policy Gov.* 19, 358–373. doi:10.1002/eet.523.

Collins, M., AchutaRao, K., Ashok, K., Bhandari, S., Mitra, A. K., Prakash, S., et al. (2013). Observational challenges in evaluating climate models. *Nat. Clim. Chang.* 3, 940–941. doi:10.1038/nclimate2012.

Collins, M., Chandler, R. E., Cox, P. M., Huthnance, J. M., Rougier, J., and Stephenson, D. B. (2012). Quantifying future climate change. *Nat. Clim. Chang.* 2, 403–409. doi:10.1038/nclimate1414.

Collins, W. J., Lamarque, J.-F., Schulz, M., Boucher, O., Eyring, V., Hegglin, M. I., et al. (2017). AerChemMIP: quantifying the effects of chemistry and aerosols in CMIP6. *Geosci. Model Dev.* 10, 585–607. doi:10.5194/gmd-10-585-2017.

Compo, G. P., Whitaker, J. S., Sardeshmukh, P. D., Matsui, N., Allan, R. J., Yin, X., et al. (2011). The Twentieth Century Reanalysis Project. *Q. J. R. Meteorol. Soc.* 137, 1–28. doi:10.1002/qj.776.

Contractor, S., Donat, M. G., Alexander, L. V., Ziese, M., Meyer-Christoffer, A., Schneider, U., et al. (2019). Rainfall Estimates on a Gridded Network (REGEN) – A global land-based gridded dataset of daily precipitation from 1950–2013. *Hydrol. Earth Syst. Sci. Discuss.*, 1–30. doi:10.5194/hess-2018-595.

Cook, B. I., Ault, T. R., and Smerdon, J. E. (2015a). Unprecedented 21st century drought risk in the American Southwest and Central Plains. *Sci. Adv.* 1, e1400082. doi:10.1126/sciadv.1400082.

Cook, B. I., Shukla, S. P., Puma, M. J., and Nazarenko, L. S. (2015b). Irrigation as an historical climate forcing. *Clim. Dyn.* 44, 1715–1730. doi:10.1007/s00382-014-2204-7.

Cook, E. R., Seager, R., Heim, R. R., Vose, R. S., Herweijer, C., and Woodhouse, C. (2010). Megadroughts in North America: placing IPCC projections of hydroclimatic change in a long-term palaeoclimate context. *J. Quat. Sci.*

25, 48–61. doi:10.1002/jqs.1303.
Cook, K. H., and Vizy, E. K. (2015). Detection and analysis of an amplified warming of the Sahara Desert. *J. Clim.* doi:10.1175/JCLI-D-14-00230.1.
Coppola, E., Sobolowski, S., Pichelli, E., Raffaele, F., Ahrens, B., Anders, I., et al. (2018). A first-of-its-kind multi-model convection permitting ensemble for investigating convective phenomena over Europe and the Mediterranean. *Clim. Dyn.* doi:10.1007/s00382-018-4521-8.
Cordeira, J. M., Ralph, F. M., Martin, A., Gaggini, N., Spackman, J. R., Neiman, P. J., et al. (2017). Forecasting Atmospheric Rivers during CalWater 2015. *Bull. Am. Meteorol. Soc.* 98, 449–459. doi:10.1175/bams-d-15-00245.1.
Corti, S., Palmer, T., Balmaseda, M., Weisheimer, A., Drijfhout, S., Dunstone, N., et al. (2015). Impact of Initial Conditions versus External Forcing in Decadal Climate Predictions: A Sensitivity Experiment. *J. Clim.* 28, 4454–4470. doi:10.1175/JCLI-D-14-00671.1.
Coumou, D., Di Capua, G., Vavrus, S., Wang, L., and Wang, S. (2018). The influence of Arctic amplification on mid-latitude summer circulation. *Nat. Commun.* 9, 2959. doi:10.1038/s41467-018-05256-8.
Cox, P. M., Huntingford, C., and Williamson, M. S. (2018). Emergent constraint on equilibrium climate sensitivity from global temperature variability. *Nature* 553, 319–322. doi:10.1038/nature25450.
Cramer, W., Guiot, J., Fader, M., Garrabou, J., Gattuso, J.-P., Iglesias, A., et al. (2018). Climate change and interconnected risks to sustainable development in the Mediterranean. *Nat. Clim. Chang.* 8, 972–980. doi:10.1038/s41558-018-0299-2.
Crippa, M., Janssens-Maenhout, G., Dentener, F., Guizzardi, D., Sindelarova, K., Muntean, M., et al. (2016). Forty years of improvements in European air quality: regional policy-industry interactions with global impacts. *Atmos. Chem. Phys.* 16, 3825–3841. doi:10.5194/acp-16-3825-2016.
Crow, W. T., Lei, F., Hain, C., Anderson, M. C., Scott, R. L., Billesbach, D., et al. (2015). Robust estimates of soil moisture and latent heat flux coupling strength obtained from triple collocation. *Geophys. Res. Lett.* 42, 8415–8423. doi:10.1002/2015GL065929.
Cruz, F. T., Narisma, G. T., Dado, J. B., Singhruck, P., Tangang, F., Linarka, U. A., et al. (2017). Sensitivity of temperature to physical parameterization schemes of RegCM4 over the CORDEX-Southeast Asia region. *Int. J. Climatol.* 37, 5139–5153. doi:10.1002/joc.5151.
CTT (2018). Cape Town Tourism Research Report. Cape Town.
Cuervo-Robayo, A. P., Téllez-Valdés, O., Gómez-Albores, M. A., Venegas-Barrera, C. S., Manjarrez, J., and Martínez-Meyer, E. (2014). An update of high-resolution monthly climate surfaces for Mexico. *Int. J. Climatol.* 34, 2427–2437. doi:10.1002/joc.3848.
Culley, S., Noble, S., Yates, A., Timbs, M., Westra, S., Maier, H. R., et al. (2016). A bottom-up approach to identifying the maximum operational adaptive capacity of water resource systems to a changing climate. *Water Resour. Res.* 52, 6751–6768. doi:10.1002/2015WR018253.
Cumming, G. S., Cumming, D. H. M., and Redman, C. L. (2006). Scale Mismatches in Social-Ecological Systems : Causes , Consequences , and Solutions. *Ecol. Soc.* 11, Aritcle 14. Available at: http://www.ecologyandsociety.org/vol11/iss1/art14/.
Cvijanovic, I., Santer, B. D., Bonfils, C., Lucas, D. D., Chiang, J. C. H., and Zimmerman, S. (2017). Future loss of Arctic sea-ice cover could drive a substantial decrease in California's rainfall. *Nat. Commun.* 8, 1947. doi:10.1038/s41467-017-01907-4.
Dahlgren, P., Landelius, T., Kållberg, P., and Gollvik, S. (2016). A high-resolution regional reanalysis for Europe. Part 1: Three-dimensional reanalysis with the regional HIgh-Resolution Limited-Area Model (HIRLAM). *Q. J. R. Meteorol. Soc.* 142, 2119–2131. doi:10.1002/qj.2807.
Dai, A., and Bloecker, C. E. (2018). Impacts of internal variability on temperature and precipitation trends in large ensemble simulations by two climate models. *Clim. Dyn.* doi:10.1007/s00382-018-4132-4.
Dandou, A., Tombrou, M., Akylas, E., Soulakellis, N., and Bossioli, E. (2005). Development and evaluation of an urban parameterization scheme in the Penn State/NCAR Mesoscale Model (MM5). *J. Geophys. Res. D Atmos.* doi:10.1029/2004JD005192.
Daniel, M., Lemonsu, A., Déqué, M., Somot, S., Alias, A., and Masson, V. (2018). Benefits of explicit urban parameterization in regional climate modeling to study climate and city interactions. *Clim. Dyn.* 1, 3. doi:10.1007/s00382-018-4289-x.
Daniels, E. E., Lenderink, G., Hutjes, R. W. A., and Holtslag, A. A. M. (2016). Observed urban effects on precipitation along the Dutch West coast. *Int. J. Climatol.* 36, 2111–2119. doi:10.1002/joc.4458.
Darmaraki, S., Somot, S., Sevault, F., Nabat, P., Cabos Narvaez, W. D., Cavicchia, L., et al. (2019). Future evolution of Marine Heatwaves in the Mediterranean Sea. *Clim. Dyn.* doi:10.1007/s00382-019-04661-z.
Daron, J. D., Sutherland, K., Jack, C., and Hewitson, B. C. (2014). The role of regional climate projections in managing complex socio-ecological systems. *Reg. Environ. Chang.* 15, 1–12. doi:10.1007/s10113-014-0631-y.
Dash, S. K., Mishra, S. K., Pattnayak, K. C., Mamgain, A., Mariotti, L., Coppola, E., et al. (2015). Projected seasonal mean summer monsoon over India and adjoining regions for the twenty-first century. *Theor. Appl. Climatol.* 122, 581–593. doi:10.1007/s00704-014-1310-0.

Dash, S. K., Sharma, N., Pattnayak, K. C., Gao, X. J., and Shi, Y. (2012). Temperature and precipitation changes in the north-east India and their future projections. *Glob. Planet. Change* 98–99, 31–44. doi:10.1016/j.gloplacha.2012.07.006.

Davin, E. L., Seneviratne, S. I., Ciais, P., Olioso, A., and Wang, T. (2014). Preferential cooling of hot extremes from cropland albedo management. *Proc. Natl. Acad. Sci.* 111, 9757–9761. doi:10.1073/pnas.1317323111.

Davini, P., and D'Andrea, F. (2016). Northern Hemisphere Atmospheric Blocking Representation in Global Climate Models: Twenty Years of Improvements? *J. Clim.* 29, 8823–8840. doi:10.1175/JCLI-D-16-0242.1.

Davini, P., Hardenberg, J. von, and Corti, S. (2015). Tropical origin for the impacts of the Atlantic Multidecadal Variability on the Euro-Atlantic climate. *Environ. Res. Lett.* 10, 094010. doi:10.1088/1748-9326/10/9/094010.

Davy, R., Chen, L., and Hanna, E. (2018). Arctic amplification metrics. *Int. J. Climatol.* 38, 4384–4394. doi:10.1002/joc.5675.

Dawson, A., and Palmer, T. N. (2015). Simulating weather regimes: impact of model resolution and stochastic parameterization. *Clim. Dyn.* 44, 2177–2193. doi:10.1007/s00382-014-2238-x.

Dayon, G., Boé, J., and Martin, E. (2015). Transferability in the future climate of a statistical downscaling method for precipitation in France. *J. Geophys. Res. Atmos.* 120, 1023–1043. doi:10.1002/2014JD022236.

de Jesus, E., da Rocha, R., Reboita, M., Llopart, M., Mosso Dutra, L., and Remedio, C. A. R. (2016). Contribution of cold fronts to seasonal rainfall in simulations over the southern La Plata Basin. *Clim. Res.* 68, 243–255. Available at: https://www.int-res.com/abstracts/cr/v68/n2-3/p243-255/.

de Jong, M. C., Wooster, M. J., Kitchen, K., Manley, C., Gazzard, R., and McCall, F. F. (2016). Calibration and evaluation of the Canadian Forest Fire Weather Index (FWI) System for improved wildland fire danger rating in the United Kingdom. *Nat. Hazards Earth Syst. Sci.* 16, 1217–1237. doi:10.5194/nhess-16-1217-2016.

De Laat, A. T. J., and Crok, M. (2013). A late 20th century European climate shift: fingerprint of regional brightening? *Atmos. Clim. Sci.* 3, 291.

De Troch, R., Hamdi, R., Van de Vyver, H., Geleyn, J.-F., and Termonia, P. (2013). Multiscale Performance of the ALARO-0 Model for Simulating Extreme Summer Precipitation Climatology in Belgium. *J. Clim.* 26, 8895–8915. doi:10.1175/JCLI-D-12-00844.1.

DEA (2013). Long-Term Adaptation Scenarios Flagship Research Programme (LTAS) for South Africa. Climate Trends and Scenarios for South Africa. Pretoria, South Africa Available at: www.environment.gov.za.

Dee, D. P., Uppala, S. M., Simmons, A. J., Berrisford, P., Poli, P., Kobayashi, S., et al. (2011). The ERA-Interim reanalysis: Configuration and performance of the data assimilation system. *Q. J. R. Meteorol. Soc.* doi:10.1002/qj.828.

Dee, S. G., Steiger, N. J., Emile-Geay, J., and Hakim, G. J. (2016). On the utility of proxy system models for estimating climate states over the common era. *J. Adv. Model. Earth Syst.* 8, 1164–1179. doi:10.1002/2016MS000677.

DeGaetano, A. T., and Castellano, C. M. (2017). Future projections of extreme precipitation intensity-duration-frequency curves for climate adaptation planning in New York State. *Clim. Serv.* 5, 23–35. doi:10.1016/J.CLISER.2017.03.003.

Dell'Aquila, A., Mariotti, A., Bastin, S., Calmanti, S., Cavicchia, L., Deque, M., et al. (2018). Evaluation of simulated decadal variations over the Euro-Mediterranean region from ENSEMBLES to Med-CORDEX. *Clim. Dyn.* 51, 857–876. doi:10.1007/s00382-016-3143-2.

Della-Marta, P. M., and Wanner, H. (2006). A Method of Homogenizing the Extremes and Mean of Daily Temperature Measurements. *J. Clim.* 19, 4179–4197. doi:10.1175/JCLI3855.1.

Delworth, T. L., and Zeng, F. (2016). The Impact of the North Atlantic Oscillation on Climate through Its Influence on the Atlantic Meridional Overturning Circulation. *J. Clim.* 29, 941–962. doi:10.1175/JCLI-D-15-0396.1.

Deng, B., Liu, S., Xiao, W., Wang, W., Jin, J., and Lee, X. (2013). Evaluation of the CLM4 Lake Model at a Large and Shallow Freshwater Lake*. *J. Hydrometeorol.* 14, 636–649. doi:10.1175/JHM-D-12-067.1.

Denis, B., Laprise, R., Caya, D., and Côté, J. (2002). Downscaling ability of one-way nested regional climate models: The Big-Brother Experiment. *Clim. Dyn.* 18, 627–646. doi:10.1007/s00382-001-0201-0.

Déqué, M., Somot, S., Sanchez-Gomez, E., Goodess, C. M., Jacob, D., Lenderink, G., et al. (2012a). The spread amongst ENSEMBLES regional scenarios: regional climate models, driving general circulation models and interannual variability. *Clim. Dyn.* 38, 951–964. doi:10.1007/s00382-011-1053-x.

Déqué, M., Somot, S., Sanchez-Gomez, E., Goodess, C. M., Jacob, D., Lenderink, G., et al. (2012b). The spread amongst ENSEMBLES regional scenarios: regional climate models, driving general circulation models and interannual variability. *Clim. Dyn.* 38, 951–964. doi:10.1007/s00382-011-1053-x.

Deser, C., Guo, R., and Lehner, F. (2017a). The relative contributions of tropical Pacific sea surface temperatures and atmospheric internal variability to the recent global warming hiatus. *Geophys. Res. Lett.* 44, 7945–7954. doi:10.1002/2017GL074273.

Deser, C., Hurrell, J. W., and Phillips, A. S. (2017b). The role of the North Atlantic Oscillation in European climate projections. *Clim. Dyn.* 49, 3141–3157. doi:10.1007/s00382-016-3502-z.

Deser, C., Knutti, R., Solomon, S., and Phillips, A. S. (2012a). Communication of the role of natural variability in future North American climate. *Nat. Clim. Chang.* 2, 775–779. doi:10.1038/nclimate1562.

Deser, C., Phillips, A., Bourdette, V., and Teng, H. (2012b). Uncertainty in climate change projections: the role of

internal variability. *Clim. Dyn.* 38, 527–546. doi:10.1007/s00382-010-0977-x.
Deser, C., Simpson, I. R., McKinnon, K. A., and Phillips, A. S. (2017c). The Northern Hemisphere Extratropical Atmospheric Circulation Response to ENSO: How Well Do We Know It and How Do We Evaluate Models Accordingly? *J. Clim.* 30, 5059–5082. doi:10.1175/JCLI-D-16-0844.1.
Deser, C., Sun, L., Tomas, R. A., and Screen, J. (2016a). Does ocean coupling matter for the northern extratropical response to projected Arctic sea ice loss? *Geophys. Res. Lett.* 43, 2149–2157. doi:10.1002/2016GL067792.
Deser, C., Terray, L., and Phillips, A. S. (2016b). Forced and Internal Components of Winter Air Temperature Trends over North America during the past 50 Years: Mechanisms and Implications*. *J. Clim.* 29, 2237–2258. doi:10.1175/JCLI-D-15-0304.1.
Dessai, S., Bhave, A., Birch, C., Conway, D., Garcia-Carreras, L., Gosling, J. P., et al. (2018). Building narratives to characterise uncertainty in regional climate change through expert elicitation. *Environ. Res. Lett.* 13, 074005. doi:10.1088/1748-9326/aabcdd.
Dey, R., Lewis, S. C., Arblaster, J. M., and Abram, N. J. (2019). A review of past and projected changes in Australia's rainfall. *Wiley Interdiscip. Rev. Clim. Chang.*, e00577. doi:10.1002/wcc.577.
Di Luca, A., Argüeso, D., Evans, J. P., de Elía, R., and Laprise, R. (2016). Quantifying the overall added value of dynamical downscaling and the contribution from different spatial scales. *J. Geophys. Res. Atmos.* 121, 1575–1590. doi:10.1002/2015JD024009.
Di Luca, A., de Elía, R., and Laprise, R. (2012). Potential for added value in precipitation simulated by high-resolution nested Regional Climate Models and observations. *Clim. Dyn.* 38, 1229–1247. doi:10.1007/s00382-011-1068-3.
Di Luca, A., de Elía, R., and Laprise, R. (2015). Challenges in the Quest for Added Value of Regional Climate Dynamical Downscaling. *Curr. Clim. Chang. Reports*, 10–21. doi:10.1007/s40641-015-0003-9.
Di Sante, F., Coppola, E., Farneti, R., and Giorgi, F. (2019). Indian Summer Monsoon as simulated by the regional earth system model RegCM-ES: the role of local air–sea interaction. *Clim. Dyn.* doi:10.1007/s00382-019-04612-8.
Diaconescu, E. P., Mailhot, A., Brown, R., and Chaumont, D. (2018). Evaluation of CORDEX-Arctic daily precipitation and temperature-based climate indices over Canadian Arctic land areas. *Clim. Dyn.* 50, 2061–2085. doi:10.1007/s00382-017-3736-4.
Díaz, L. B., and Vera, C. S. (2017). Austral summer precipitation interannual variability and trends over Southeastern South America in CMIP5 models. *Int. J. Climatol.* 37, 681–695. doi:10.1002/joc.5031.
Dienst, M., Lindén, J., Engström, E., and Esper, J. (2017). Removing the relocation bias from the 155-year Haparanda temperature record in Northern Europe. *Int. J. Climatol.* 37, 4015–4026. doi:10.1002/joc.4981.
Dienst, M., Lindén, J., Saladié, Ò., and Esper, J. (2019). Detection and elimination of UHI effects in long temperature records from villages – A case study from Tivissa, Spain. *Urban Clim.* 27, 372–383. doi:https://doi.org/10.1016/j.uclim.2018.12.012.
Diffenbaugh, N. S., and Giorgi, F. (2012). Climate change hotspots in the CMIP5 global climate model ensemble. *Clim. Change* 114, 813–822. doi:10.1007/s10584-012-0570-x.
Dimri, A. P., Kumar, D., Choudhary, A., and Maharana, P. (2018). Future changes over the Himalayas: Mean temperature. *Glob. Planet. Change* 162, 235–251. doi:10.1016/j.gloplacha.2018.01.014.
Dimri, A. P., Yasunari, T., Wiltshire, A., Kumar, P., Mathison, C., Ridley, J., et al. (2013). Application of regional climate models to the Indian winter monsoon over the western Himalayas. *Sci. Total Environ.* 468–469, S36–S47. doi:10.1016/j.scitotenv.2013.01.040.
DiNezio, P. N., Clement, A. C., Vecchi, G. A., Soden, B. J., Kirtman, B. P., and Lee, S.-K. (2009). Climate Response of the Equatorial Pacific to Global Warming. *J. Clim.* 22, 4873–4892. doi:10.1175/2009JCLI2982.1.
Ding Ruiqiang, and Li, J., and Zheng Fei, and Feng Jie, and and Liu Deqiang (2016). Estimating the limit of decadal-scale climate predictability using observational data. *Clim. Dyn.* 46, 1563–1580. doi:10.1007/s00382-015-2662-6.
Ding, Y., Sun, Y., Wang, Z., Zhu, Y., and Song, Y. (2009). Inter-decadal variation of the summer precipitation in China and its association with decreasing Asian summer monsoon Part II: Possible causes. *Int. J. Climatol.* 29, 1926–1944. doi:10.1002/joc.1759.
Dinku, T., Hailemariam, K., Maidment, R., Tarnavsky, E., and Connor, S. (2014). Combined use of satellite estimates and rain gauge observations to generate high-quality historical rainfall time series over Ethiopia. *Int. J. Climatol.* 34, 2489–2504. doi:10.1002/joc.3855.
Diro, G. T., Giorgi, F., Fuentes-Franco, R., Walsh, K. J. E., Giuliani, G., and Coppola, E. (2014). Tropical cyclones in a regional climate change projection with RegCM4 over the CORDEX Central America domain. *Clim. Change* 125, 79–94. doi:10.1007/s10584-014-1155-7.
Dittus, A. J., Karoly, D. J., Lewis, S. C., Alexander, L. V., and Donat, M. G. (2016). A Multiregion Model Evaluation and Attribution Study of Historical Changes in the Area Affected by Temperature and Precipitation Extremes. *J. Clim.* 29, 8285–8299. doi:10.1175/JCLI-D-16-0164.1.
Doan, Q.-V., and Kusaka, H. (2016). Numerical study on regional climate change due to the rapid urbanization of greater Ho Chi Minh City's metropolitan area over the past 20 years. *Int. J. Climatol.* doi:10.1002/joc.4582.
Doan, V. Q., and Kusaka, H. (2018). Projections of urban climate in the 2050s in a fast-growing city in Southeast Asia: The greater Ho Chi Minh City metropolitan area, Vietnam. *Int. J. Climatol.* 38, 4155–4171. doi:10.1002/joc.5559.

Doan, V. Q., Kusaka, H., and Nguyen, T. M. (2019). Roles of past, present, and future land use and anthropogenic heat release changes on urban heat island effects in Hanoi, Vietnam: Numerical experiments with a regional climate model. *Sustain. Cities Soc.* 47, 101479. doi:10.1016/j.scs.2019.101479.

Doan, Q. Van, Kusaka, H., and Ho, Q. B. (2016). Impact of future urbanization on temperature and thermal comfort index in a developing tropical city: Ho Chi Minh City. *Urban Clim.* 17, 20–31. doi:10.1016/j.uclim.2016.04.003.

Dobor, L., and Hlásny, T. (2018). Choice of reference climate conditions matters in impact studies: Case of bias-corrected CORDEX data set. *Int. J. Climatol.* doi:10.1002/joc.5930.

Dobriyal, P., Qureshi, A., Badola, R., and Hussain, S. A. (2012). A review of the methods available for estimating soil moisture and its implications for water resource management. *J. Hydrol.* 458–459, 110–117. doi:https://doi.org/10.1016/j.jhydrol.2012.06.021.

Dodd, E. M. A., Merchant, C. J., Rayner, N. A., and Morice, C. P. (2015). An Investigation into the Impact of using Various Techniques to Estimate Arctic Surface Air Temperature Anomalies. *J. Clim.* 28, 1743–1763. doi:10.1175/JCLI-D-14-00250.1.

Donat, M. G., Alexander, L. V., Yang, H., Durre, I., Vose, R., Dunn, R. J. H., et al. (2013). Updated analyses of temperature and precipitation extreme indices since the beginning of the twentieth century: The HadEX2 dataset. *J. Geophys. Res. Atmos.* 118, 2098–2118. doi:10.1002/jgrd.50150.

Dong-feng, Z., Zhen-yu, H. A. N., and Ying, S. H. I. (2017). ScienceDirect Comparison of climate projections between driving CSIRO-Mk3 . 6 . 0 and downscaling simulation of RegCM4 . 4 over China. *Adv. Clim. Chang. Res.* 8, 245–255. doi:10.1016/j.accre.2017.10.001.

Dong, B., and Dai, A. (2015). The influence of the Interdecadal Pacific Oscillation on Temperature and Precipitation over the Globe. *Clim. Dyn.* 45, 2667–2681. doi:10.1007/s00382-015-2500-x.

Dong, B., Dai, A., Vuille, M., and Timm, O. E. (2018a). Asymmetric Modulation of ENSO Teleconnections by the Interdecadal Pacific Oscillation. *J. Clim.* 31, 7337–7361. doi:10.1175/JCLI-D-17-0663.1.

Dong, B., and Sutton, R. (2015). Dominant role of greenhouse-gas forcing in the recovery of Sahel rainfall. *Nat. Clim. Chang.* doi:10.1038/nclimate2664.

Dong, B., Sutton, R. T., Chen, W., Liu, X., Lu, R., and Sun, Y. (2016). Abrupt summer warming and changes in temperature extremes over Northeast Asia since the mid-1990s: Drivers and physical processes. *Adv. Atmos. Sci.* 33, 1005–1023. doi:10.1007/s00376-016-5247-3.

Dong, B., Sutton, R. T., Highwood, E., and Wilcox, L. (2014). The impacts of European and Asian anthropogenic sulfur dioxide emissions on Sahel rainfall. *J. Clim.* doi:10.1175/JCLI-D-13-00769.1.

Dong, B., Sutton, R. T., and Shaffrey, L. (2017). Understanding the rapid summer warming and changes in temperature extremes since the mid-1990s over Western Europe. *Clim. Dyn.* 48, 1537–1554. doi:10.1007/s00382-016-3158-8.

Dong, B., Sutton, R. T., Woollings, T., and Hodges, K. (2013). Variability of the North Atlantic summer storm track: mechanisms and impacts on European climate. *Environ. Res. Lett.* 8, 034037. doi:10.1088/1748-9326/8/3/034037.

Dong, L., Leung, L. R., Song, F., and Lu, J. (2018b). Roles of SST versus internal atmospheric variability in winter extreme precipitation variability along the U.S. West Coast. *J. Clim.* 31, 8039–8058. doi:10.1175/JCLI-D-18-0062.1.

Dong, L., and McPhaden, M. J. (2017). Why Has the Relationship between Indian and Pacific Ocean Decadal Variability Changed in Recent Decades? *J. Clim.* 30, 1971–1983. doi:10.1175/JCLI-D-16-0313.1.

Dosio, A. (2016a). Projections of climate change indices of temperature and precipitation from an ensemble of bias-adjusted high-resolution EURO-CORDEX regional climate models. *J. Geophys. Res. Atmos.* 121, 5488–5511. doi:10.1002/2015JD024411.

Dosio, A. (2016b). Projections of climate change indices of temperature and precipitation from an ensemble of bias-adjusted high-resolution EURO-CORDEX regional climate models. *J. Geophys. Res. Atmos.* 121, 5488–5511. doi:10.1002/2015JD024411.

Dosio, A. (2017). Projection of temperature and heat waves for Africa with an ensemble of CORDEX Regional Climate Models. *Clim. Dyn.* 49, 493–519. doi:10.1007/s00382-016-3355-5.

Dosio, A., and Fischer, E. M. (2018). Will Half a Degree Make a Difference? Robust Projections of Indices of Mean and Extreme Climate in Europe Under 1.5°C, 2°C, and 3°C Global Warming. *Geophys. Res. Lett.* 45, 935–944. doi:10.1002/2017GL076222.

Dosio, A., Jones, R., Jack, C., Lennard, C., Nikulin, G., and Hewitson, B. What can we know about future precipitation in Africa? Robustness, significance and added value of projections from a large ensemble of regional climate models. *Clim. Dyn.* doi:SUBMITTED.

Dosio, A., Panitz, H.-J., Schubert-Frisius, M., and Lüthi, D. (2015a). Dynamical downscaling of CMIP5 global circulation models over CORDEX-Africa with COSMO-CLM: evaluation over the present climate and analysis of the added value. *Clim. Dyn.* 44, 2637–2661. doi:10.1007/s00382-014-2262-x.

Dosio, A., Panitz, H.-J., Schubert-Frisius, M., and Lüthi, D. (2015b). Dynamical downscaling of CMIP5 global circulation models over CORDEX-Africa with COSMO-CLM: evaluation over the present climate and analysis of the added value. *Clim. Dyn.* 44, 2637–2661. doi:10.1007/s00382-014-2262-x.

Dosio, A., Paruolo, P., and Rojas, R. (2012). Bias correction of the ENSEMBLES high resolution climate change projections for use by impact models: Analysis of the climate change signal. *J. Geophys. Res. Atmos.* 117, n/a-n/a.

doi:10.1029/2012JD017968.
Dou, J., Wang, Y., Bornstein, R., and Miao, S. (2015). Observed Spatial Characteristics of Beijing Urban Climate Impacts on Summer Thunderstorms. *J. Appl. Meteorol. Climatol.* 54, 94–105. doi:10.1175/JAMC-D-13-0355.1.
Douville, H., Colin, J., Krug, E., Cattiaux, J., and Thao, S. (2016). Midlatitude daily summer temperatures reshaped by soil moisture under climate change. *Geophys. Res. Lett.* 43, 812–818. doi:10.1002/2015GL066222.
Douville, H., and Plazzotta, M. (2017). Midlatitude Summer Drying: An Underestimated Threat in CMIP5 Models? *Geophys. Res. Lett.* 44, 9967–9975. doi:10.1002/2017GL075353.
Douville, H., Voldoire, A., and Geoffroy, O. (2015). The recent global warming hiatus: What is the role of Pacific variability? *Geophys. Res. Lett.* 42, 880–888. doi:10.1002/2014GL062775.
Dowdy, A. J., and Catto, J. L. (2017). Extreme weather caused by concurrent cyclone, front and thunderstorm occurrences. *Sci. Rep.* 7, 40359. doi:10.1038/srep40359.
Doyle, M. E., Saurral, R. I., and Barros, V. R. (2011). Trends in the distributions of aggregated monthly precipitation over the La Plata Basin. *Int. J. Climatol.* 32, n/a-n/a. doi:10.1002/joc.2429.
Drobinski, P., Bastin, S., Arsouze, T., Béranger, K., Flaounas, E., and Stéfanon, M. (2018). North-western Mediterranean sea-breeze circulation in a regional climate system model. *Clim. Dyn.* 51, 1077–1093. doi:10.1007/s00382-017-3595-z.
Druyan, L., and Fulakeza, M. (2013). Downscaling reanalysis over continental Africa with a regional model: NCEP versus ERA Interim forcing. *Clim. Res.* 56, 181–196. doi:10.3354/cr01152.
Duan, A., Wang, M., Lei, Y., and Cui, Y. (2013). Trends in Summer Rainfall over China Associated with the Tibetan Plateau Sensible Heat Source during 1980–2008. *J. Clim.* 26, 261–275. doi:10.1175/JCLI-D-11-00669.1.
Duan, Q., and Phillips, T. J. (2010). Bayesian estimation of local signal and noise in multimodel simulations of climate change. *J. Geophys. Res.* 115, D18123. doi:10.1029/2009JD013654.
Dumitrescu, A., Birsan, M.-V., and Manea, A. (2016). Spatio-temporal interpolation of sub-daily (6 h) precipitation over Romania for the period 1975–2010. *Int. J. Climatol.* 36, 1331–1343. doi:10.1002/joc.4427.
Dunn-Sigouin, E., and Son, S.-W. (2013). Northern Hemisphere blocking frequency and duration in the CMIP5 models. *J. Geophys. Res. Atmos.* 118, 1179–1188. doi:10.1002/jgrd.50143.
Dunning, C. M., Allan, R. P., and Black, E. (2017). Identification of deficiencies in seasonal rainfall simulated by CMIP5 climate models. *Environ. Res. Lett.* 12, 114001. doi:10.1088/1748-9326/aa869e.
Dupont, S., and Mestayer, P. G. (2006). Parameterization of the urban energy budget with the submesoscale soil model. *J. Appl. Meteorol. Climatol.* doi:10.1175/JAM2417.1.
DWA (2013). Metropolitan Municipality Non-Revenue /Water Loss Assessment. Retrieved from www.dwa.gov.za/wsks/UserControls/Do. Available at: www.dwa.gov.za/wsks/UserControls/DownloadImportFiles.aspx?FileID=211.
DWAF (2007). WESTERN CAPE WATER SUPPLY SYSTEM RECONCILIATION STRATEGY STUDY. Cape Town Available at: http://www.dwa.gov.za/Projects/RS_WC_WSS/Docs/Reconciliation Strategy.pdf.
Ehret, U., Zehe, E., Wulfmeyer, V., Warrach-Sagi, K., and Liebert, J. (2012). HESS Opinions "Should we apply bias correction to global and regional climate model data?" *Hydrol. Earth Syst. Sci.* 16, 3391–3404. doi:10.5194/hess-16-3391-2012.
Eisenack, K., Moser, S. C., Hoffmann, E., Klein, R. J. T., Oberlack, C., Pechan, A., et al. (2014). Explaining and overcoming barriers to climate change adaptation. *Nat. Clim. Chang.* 4, 867–872. doi:10.1038/nclimate2350.
Ekström, M., Grose, M., Heady, C., Turner, S., and Teng, J. (2016). The method of producing climate change datasets impacts the resulting policy guidance and chance of mal-adaptation. *Clim. Serv.* 4, 13–29. doi:10.1016/J.CLISER.2016.09.003.
Ekström, M., Grose, M. R., and Whetton, P. H. (2015). An appraisal of downscaling methods used in climate change research. *Wiley Interdiscip. Rev. Clim. Chang.* 6, 301–319. doi:10.1002/wcc.339.
Endo, H., Kitoh, A., and Ueda, H. (2018). A Unique Feature of the Asian Summer Monsoon Response to Global Warming: The Role of Different Land–Sea Thermal Contrast Change between the Lower and Upper Troposphere. *SOLA* 14, 57–63. doi:10.2151/sola.2018-010.
Endris, H. S., Lennard, C., Hewitson, B., Dosio, A., Nikulin, G., and Panitz, H.-J. (2016). Teleconnection responses in multi-GCM driven CORDEX RCMs over Eastern Africa. *Clim. Dyn.* 46, 2821–2846. doi:10.1007/s00382-015-2734-7.
Engelbrecht, F. A., McGregor, J. L., and Engelbrecht, C. J. (2009). Dynamics of the Conformal-Cubic Atmospheric Model projected climate-change signal over southern Africa. *Int. J. Climatol.* 29, 1013–1033. doi:10.1002/joc.1742.
England, M. H., McGregor, S., Spence, P., Meehl, G. A., Timmermann, A., Cai, W., et al. (2014). Recent intensification of wind-driven circulation in the Pacific and the ongoing warming hiatus. *Nat. Clim. Chang.* 4, 222–227. doi:10.1038/nclimate2106.
Erdin, R., Frei, C., and Künsch, H. R. (2012). Data Transformation and Uncertainty in Geostatistical Combination of Radar and Rain Gauges. *J. Hydrometeorol.* 13, 1332–1346. doi:10.1175/jhm-d-11-096.1.
Erfanian, A., Wang, G., Yu, M., and Anyah, R. (2016). Multimodel ensemble simulations of present and future climates over West Africa: Impacts of vegetation dynamics. *J. Adv. Model. Earth Syst.* 8, 1411–1431.

doi:10.1002/2016MS000660.
Espinoza, V., Waliser, D. E., Guan, B., Lavers, D. A., and Ralph, F. M. (2018). Global Analysis of Climate Change Projection Effects on Atmospheric Rivers. *Geophys. Res. Lett.* 45, 4299–4308. doi:10.1029/2017GL076968.
Evan, A. T., Flamant, C., Lavaysse, C., Kocha, C., and Saci, A. (2015). Water vapor-forced greenhouse warming over the Sahara desert and the recent recovery from the Sahelian drought. *J. Clim.* doi:10.1175/JCLI-D-14-00039.1.
Evans, J. P., Ji, F., Lee, C., Smith, P., Argüeso, D., and Fita, L. (2014). Design of a regional climate modelling projection ensemble experiment – NARCliM. *Geosci. Model Dev.* 7, 621–629. doi:10.5194/gmd-7-621-2014.
Eyring, V., Bony, S., Meehl, G. A., Senior, C. A., Stevens, B., Stouffer, R. J., et al. (2016a). Overview of the Coupled Model Intercomparison Project Phase 6 (CMIP6) experimental design and organization. *Geosci. Model Dev.* 9, 1937–1958. doi:10.5194/gmd-9-1937-2016.
Eyring, V., Cox, P. M., Flato, G. M., Gleckler, P. J., Abramowitz, G., Caldwell, P., et al. (2019). Taking climate model evaluation to the next level. *Nat. Clim. Chang.* 9, 102–110. doi:10.1038/s41558-018-0355-y.
Eyring, V., Righi, M., Lauer, A., Evaldsson, M., Wenzel, S., Jones, C., et al. (2016b). ESMValTool (v1.0) – a community diagnostic and performance metrics tool for routine evaluation of Earth system models in CMIP. *Geosci. Model Dev.* 9, 1747–1802. doi:10.5194/gmd-9-1747-2016.
Falco, M., Carril, A. F., Menéndez, C. G., Zaninelli, P. G., Li, L. Z. X., and Falco M., Carril A.F., Menéndez C., Zaninelli P.G., L. L. Z. . (2018). Assessment of CORDEX simulations over South America: added value on seasonal climatology and resolution considerations. *Clim. Dyn.* doi:10.1007/s00382-018-4412-z.
Fallah, B., Russo, E., Acevedo, W., Mauri, A., Becker, N., and Cubasch, U. (2018). Towards high-resolution climate reconstruction using an off-line data assimilation and COSMO-CLM 5.00 model. *Clim. Past* 14, 1345–1360. doi:10.5194/cp-14-1345-2018.
Fallas-López, B., and Alfaro, E. J. (2014). Predicción estacional de las temperaturas máximas y mínimas en América Central. *Trópicos Meteorológicos y Ocean. 13 5-26* 13, 5–26.
Fantini, A., Raffaele, F., Torma, C., Bacer, S., Coppola, E., Giorgi, F., et al. (2018). Assessment of multiple daily precipitation statistics in ERA-Interim driven Med-CORDEX and EURO-CORDEX experiments against high resolution observations. *Clim. Dyn.* 51, 877–900. doi:10.1007/s00382-016-3453-4.
Favre, A., Hewitson, B., Lennard, C., Cerezo-Mota, R., and Tadross, M. (2013). Cut-off Lows in the South Africa region and their contribution to precipitation. *Clim. Dyn.* 41, 2331–2351. doi:10.1007/s00382-012-1579-6.
Feng, X., Huang, B., Kirtman, B. P., Kinter, J. L., and Chiu, L. S. (2017). A multi-model analysis of the resolution influence on precipitation climatology in the Gulf Stream region. *Clim. Dyn.* 48, 1685–1704. doi:10.1007/s00382-016-3167-7.
Ferguson, J. O., Jablonowski, C., Johansen, H., McCorquodale, P., Colella, P., and Ullrich, P. A. (2016). Analyzing the Adaptive Mesh Refinement (AMR) Characteristics of a High-Order 2D Cubed-Sphere Shallow-Water Model. *Mon. Weather Rev.* 144, 4641–4666. doi:10.1175/MWR-D-16-0197.1.
Fernández, J., Frías, M. D., Cabos, W. D., Cofiño, A. S., Domínguez, M., Fita, L., et al. (2018). Consistency of climate change projections from multiple global and regional model intercomparison projects. *Clim. Dyn.* doi:10.1007/s00382-018-4181-8.
Feser, F., Rockel, B., von Storch, H., Winterfeldt, J., and Zahn, M. (2011). Regional Climate Models Add Value to Global Model Data: A Review and Selected Examples. *Bull. Am. Meteorol. Soc.* 92, 1181–1192. doi:10.1175/2011BAMS3061.1.
Fick, S. E., and Hijmans, R. J. (2017). WorldClim 2: new 1-km spatial resolution climate surfaces for global land areas. *Int. J. Climatol.* 37, 4302–4315. doi:10.1002/joc.5086.
Firth, R., Kala, J., Lyons, T. J., and Andrys, J. (2017). An Analysis of Regional Climate Simulations for Western Australia's Wine Regions—Model Evaluation and Future Climate Projections. *J. Appl. Meteorol. Climatol.* 56, 2113–2138. doi:10.1175/JAMC-D-16-0333.1.
Fischer, E. M., and Knutti, R. (2012). Robust projections of combined humidity and temperature extremes. *Nat. Clim. Chang.* 3, 126. Available at: https://doi.org/10.1038/nclimate1682.
Flaounas, E., Drobinski, P., and Bastin, S. (2013). Dynamical downscaling of IPSL-CM5 CMIP5 historical simulations over the Mediterranean: benefits on the representation of regional surface winds and cyclogenesis. *Clim. Dyn.* 40, 2497–2513. doi:10.1007/s00382-012-1606-7.
Flaounas, E., Kelemen, F. D., Wernli, H., Gaertner, M. A., Reale, M., Sanchez-Gomez, E., et al. (2018). Assessment of an ensemble of ocean–atmosphere coupled and uncoupled regional climate models to reproduce the climatology of Mediterranean cyclones. *Clim. Dyn.* 51, 1023–1040. doi:10.1007/s00382-016-3398-7.
Flato, G., Marotzke, J., Abiodun, B., Braconnot, P., Chou, S. C., Collins, W., et al. (2014). *Climate Change 2013 - The Physical Science Basis.* , ed. Intergovernmental Panel on Climate Change Cambridge: Cambridge University Press doi:10.1017/CBO9781107415324.
Flores Rojas, J. L., Pereira Filho, A. J., Karam, H. A., Vemado, F., and Masson, V. (2018). Effects of Explicit Urban-Canopy Representation on Local Circulations Above a Tropical Mega-City. *Boundary-Layer Meteorol.* 166, 83–111. doi:10.1007/s10546-017-0292-8.
Fløttum, K., and Gjerstad, Ø. (2017). Narratives in climate change discourse. *Wiley Interdiscip. Rev. Clim. Chang.* 8,

e429. doi:10.1002/wcc.429.
Flowers, G. E. (2018). Hydrology and the future of the Greenland Ice Sheet. *Nat. Commun.* doi:10.1038/s41467-018-05002-0.
Folland, C. K., Knight, J., Linderholm, H. W., Fereday, D., Ineson, S., and Hurrell, J. W. (2009). The Summer North Atlantic Oscillation: Past, Present, and Future. *J. Clim.* 22, 1082–1103. doi:10.1175/2008JCLI2459.1.
Forsythe, N., Fowler, H. J., Li, X. F., Blenkinsop, S., and Pritchard, D. (2017). Karakoram temperature and glacial melt driven by regional atmospheric circulation variability. *Nat. Clim. Chang.* 7, 664–670. doi:10.1038/nclimate3361.
Fosser, G., Khodayar, S., and Berg, P. (2015). Benefit of convection permitting climate model simulations in the representation of convective precipitation. *Clim. Dyn.* 44, 45–60. doi:10.1007/s00382-014-2242-1.
Fosser, G., Khodayar, S., and Berg, P. (2017). Climate change in the next 30 years: What can a convection-permitting model tell us that we did not already know? *Clim. Dyn.* 48, 1987–2003. doi:10.1007/s00382-016-3186-4.
Founda, D., and Santamouris, M. (2017). Synergies between Urban Heat Island and Heat Waves in Athens (Greece), during an extremely hot summer (2012). *Sci. Rep.* 7, 1–11. doi:10.1038/s41598-017-11407-6.
Foussard, A., Lapeyre, G., and Plougonven, R. (2019). Storm Track Response to Oceanic Eddies in Idealized Atmospheric Simulations. *J. Clim.* 32, 445–463. doi:10.1175/JCLI-D-18-0415.1.
Fox-Rabinovitz, M., Côté, J., Dugas, B., Déqué, M., and McGregor, J. L. (2006). Variable resolution general circulation models: Stretched-grid model intercomparison project (SGMIP). *J. Geophys. Res.* 111, D16104. doi:10.1029/2005JD006520.
Fox-Rabinovitz, M., Cote, J., Dugas, B., Deque, M., McGregor, J. L., and Belochitski, A. (2008). Stretched-grid Model Intercomparison Project: decadal regional climate simulations with enhanced variable and uniform-resolution GCMs. *Meteorol. Atmos. Phys.* 100, 159–178. doi:10.1007/s00703-008-0301-z.
Frame, J., and Killick, M. (2007). Integrated water resource planning in the city of Cape Town. *Water SA* 30. doi:10.4314/wsa.v30i5.5188.
Francis, J. A., and Vavrus, S. J. (2012). Evidence linking Arctic amplification to extreme weather in mid-latitudes. *Geophys. Res. Lett.* 39. doi:10.1029/2012GL051000.
Francis, J. A., and Vavrus, S. J. (2015). Evidence for a wavier jet stream in response to rapid Arctic warming. *Environ. Res. Lett.* 10, 014005. doi:10.1088/1748-9326/10/1/014005.
Francis, J. A., Vavrus, S. J., and Cohen, J. (2017). Amplified Arctic warming and mid-latitude weather: new perspectives on emerging connections. *Wiley Interdiscip. Rev. Clim. Chang.* 8, e474. doi:10.1002/wcc.474.
Franco, B., Fettweis, X., and Erpicum, M. (2012). Future projections of the Greenland ice sheet energy balance driving the surface melt, developed using the regional climate MAR model. *Cryosph. Discuss.* doi:10.5194/tcd-6-2265-2012.
Frankcombe, L. M., England, M. H., Mann, M. E., and Steinman, B. A. (2015). Separating internal variability from the externally forced climate response. *J. Clim.* 28, 8184–8202. doi:10.1175/JCLI-D-15-0069.1.
Franke, J., Brönnimann, S., Bhend, J., and Brugnara, Y. (2017). A monthly global paleo-reanalysis of the atmosphere from 1600 to 2005 for studying past climatic variations. *Sci. data* 4, 170076. doi:10.1038/sdata.2017.76.
Frederiksen, C. S., Frederiksen, J. S., Sisson, J. M., and Osbrough, S. L. (2017). Trends and projections of Southern Hemisphere baroclinicity: the role of external forcing and impact on Australian rainfall. *Clim. Dyn.* 48, 3261–3282. doi:10.1007/s00382-016-3263-8.
Frei, C. (2014). Interpolation of temperature in a mountainous region using nonlinear profiles and non-Euclidean distances. *Int. J. Climatol.* 1605, 1585–1605. doi:10.1002/joc.3786.
Frei, C., Christensen, J. H., Déqué, M., Jacob, D., Jones, R. G., and Vidale, P. L. (2003). Daily precipitation statistics in regional climate models: Evaluation and intercomparison for the European Alps. *J. Geophys. Res. Atmos.* 108, n/a-n/a. doi:10.1029/2002JD002287.
Freund, M., Henley, B. J., Karoly, D. J., Allen, K. J., and Baker, P. J. (2017). Multi-century cool- and warm-season rainfall reconstructions for Australia's major climatic regions. *Clim. Past* 13, 1751–1770. doi:10.5194/cp-13-1751-2017.
Froidevaux, P., Schlemmer, L., Schmidli, J., Langhans, W., and Schär, C. (2014). Influence of the Background Wind on the Local Soil Moisture–Precipitation Feedback. *J. Atmos. Sci.* 71, 782–799. doi:10.1175/JAS-D-13-0180.1.
Frost, A. J., Charles, S. P., Timbal, B., Chiew, F. H. S., Mehrotra, R., Nguyen, K. C., et al. (2011). A comparison of multi-site daily rainfall downscaling techniques under Australian conditions. *J. Hydrol.* 408, 1–18. doi:10.1016/j.jhydrol.2011.06.021.
Früh, B., Becker, P., Deutschländer, T., Hessel, J.-D., Kossmann, M., Mieskes, I., et al. (2011). Estimation of Climate-Change Impacts on the Urban Heat Load Using an Urban Climate Model and Regional Climate Projections. *J. Appl. Meteorol. Climatol.* 50, 167–184. doi:10.1175/2010JAMC2377.1.
Fu, J., and Li, S. (2013). The influence of regional SSTs on the interdecadal shift of the East Asian summer monsoon. *Adv. Atmos. Sci.* 30, 330–340. doi:10.1007/s00376-012-2062-3.
Fujibe, F. (2009). Detection of urban warming in recent temperature trends in Japan. *Int. J. Climatol.* 29, 1811–1822. doi:10.1002/joc.1822.
Fujibe, F. (2015). Relationship between Interannual Variations of Extreme Hourly Precipitation and Air/Sea-Surface Temperature in Japan. *SOLA* 11, 5–9. doi:10.2151/sola.2015-002.

Fumiaki, F., Jun, M., and Hideto, S. (2018). Spatial and Temporal Features of Heat Stroke Mortality in Japan and Their Relation to Temperature Variations, 1999–2014. *Geogr. Rev. Japan Ser. B* 91, 17–27. doi:10.4157/geogrevjapanb.91.17.

Fyfe, J. C., Gillett, N. P., and Marshall, G. J. (2012). Human influence on extratropical Southern Hemisphere summer precipitation. *Geophys. Res. Lett.* 39, n/a-n/a. doi:10.1029/2012GL054199.

Gadgil, S. S., and Gadgil, S. S. (2006). The Indian monsoon, GDP and agriculture. *Econ. Polit. Wkly.* doi:10.2307/4418949.

Gaetani, M., and Mohino, E. (2013). Decadal prediction of the sahelian precipitation in CMIP5 simulations. *J. Clim.* doi:10.1175/JCLI-D-12-00635.1.

Gallant, A. J. E., Phipps, S. J., Karoly, D. J., Mullan, A. B., and Lorrey, A. M. (2013). Nonstationary Australasian Teleconnections and Implications for Paleoclimate Reconstructions. *J. Clim.* 26, 8827–8849. doi:10.1175/JCLI-D-12-00338.1.

Galmarini, S., Cannon, A. J., Ceglar, A., Christensen, O. B., de Noblet-Ducoudré, N., Dentener, F., et al. (2019). Adjusting climate model bias for agricultural impact assessment: How to cut the mustard. *Clim. Serv.* doi:10.1016/j.cliser.2019.01.004.

Ganeshan, M., and Murtugudde, R. (2015). Nocturnal propagating thunderstorms may favor urban “hot-spots”: A model-based study over Minneapolis. *Urban Clim.* 14, 606–621. doi:10.1016/j.uclim.2015.10.005.

Ganeshan, M., Murtugudde, R., and Imhoff, M. L. (2013). A multi-city analysis of the UHI-influence on warm season rainfall. *Urban Clim.* 6, 1–23. doi:https://doi.org/10.1016/j.uclim.2013.09.004.

Gangopadhyay, S., Pruitt, T., Brekke, L., and Raff, D. (2011). Hydrologic projections for the western United States. *Eos, Trans. Am. Geophys. Union* 92, 441–442. doi:10.1029/2011EO480001.

Gao, M., Carmichael, G. R., Wang, Y., Saide, P. E., Yu, M., Xin, J., et al. (2016). Modeling study of the 2010 regional haze event in the North China Plain. *Atmos. Chem. Phys.* 16, 1673–1691. doi:10.5194/acp-16-1673-2016.

Gao, X., and Giorgi, F. (2017). Use of the RegCM System over East Asia: Review and Perspectives. *Engineering* 3, 766–772. doi:10.1016/J.ENG.2017.05.019.

Gao, X., Shi, Y., Zhang, D., Wu, J., Giorgi, F., Ji, Z., et al. (2012). Uncertainties in monsoon precipitation projections over China: results from two high-resolution RCM simulations. *Clim. Res.* 52, 213–226. doi:10.3354/cr01084.

García-Díez, M., Fernández, J., and Vautard, R. (2015). An RCM multi-physics ensemble over Europe: multi-variable evaluation to avoid error compensation. *Clim. Dyn.* 45, 3141–3156. doi:10.1007/s00382-015-2529-x.

Garfinkel, C. I., Waugh, D. W., and Polvani, L. M. (2015). Recent Hadley cell expansion: The role of internal atmospheric variability in reconciling modeled and observed trends. *Geophys. Res. Lett.* 42, 10,824-10,831. doi:10.1002/2015GL066942.

Gasparrini, A., and Armstrong, B. (2012). UKPMC Funders Group The impact of heat waves on mortality. *Epidemiology* 22, 68–73. doi:10.1097/EDE.0b013e3181fdcd99.The.

Gautam, R., Hsu, N. C., Lau, W. K.-M., and Yasunari, T. J. (2013). Satellite observations of desert dust-induced Himalayan snow darkening. *Geophys. Res. Lett.* 40, 988–993. doi:10.1002/grl.50226.

GCOS (2015). *Status of the Global Observing System for Climate*. doi:10.13140/RG.2.2.23178.26566.

Gentry, M. S., and Lackmann, G. M. (2010). Sensitivity of Simulated Tropical Cyclone Structure and Intensity to Horizontal Resolution. *Mon. Weather Rev.* 138, 688–704. doi:10.1175/2009MWR2976.1.

Georgakakos, A., Fleming, P., Dettinger, M., Peters-Lidard, C., Richmond, T. C., Reckhow, K., et al. (2014). “Water Resources,” in *Climate Change Impacts in the United States: The Third National Climate Assessment* (U.S. Global Change Research Program), 69–112.

Georgescu, M., Moustaoui, M., Mahalov, A., and Dudhia, J. (2013). Summer-time climate impacts of projected megapolitan expansion in Arizona. *Nat. Clim. Chang.* 3, 37–41. doi:10.1038/nclimate1656.

Gerber, E. P., and Manzini, E. (2016). The Dynamics and Variability Model Intercomparison Project (DynVarMIP) for CMIP6: assessing the stratosphere–troposphere system. *Geosci. Model Dev.* 9, 3413–3425. doi:10.5194/gmd-9-3413-2016.

Gergis, J., Gallant, A. J. E., Braganza, K., Karoly, D. J., and Allen, K. (2012). On the long-term context of the 1997–2009 ’Big Dry’in South-Eastern Australia: insights from a 206-year multi-proxy rainfall reconstruction. *Clim. Change*.

Gevaert, A. I., Miralles, D. G., de Jeu, R. A. M., Schellekens, J., and Dolman, A. J. (2018). Soil Moisture-Temperature Coupling in a Set of Land Surface Models. *J. Geophys. Res. Atmos.* doi:10.1002/2017JD027346.

Ghimire, S., Choudhary, A., and Dimri, A. P. (2018). Assessment of the performance of CORDEX-South Asia experiments for monsoonal precipitation over the Himalayan region during present climate: part I. *Clim. Dyn.* 50, 2311–2334. doi:10.1007/s00382-015-2747-2.

Ghosh, R., Müller, W. A., Baehr, J., and Bader, J. (2017). Impact of observed North Atlantic multidecadal variations to European summer climate: a linear baroclinic response to surface heating. *Clim. Dyn.* 48, 3547–3563. doi:10.1007/s00382-016-3283-4.

Giannini, a, Kushnir, Y., and Cane, M. a (2000). {Interannual} variability of the {Carribbean} rainfall {ENSO} and the {Atlantic} {Ocean}. *J. Clim.* 13, 297–311. doi:Doi 10.1175/1520-0442(2000)013<0297:Ivocre>2.0.Co;2.

Giannini, A., and Kaplan, A. (2018). The role of aerosols and greenhouse gases in Sahel drought and recovery. *Clim.*

*Change*. doi:10.1007/s10584-018-2341-9.
Giannini, A., Salack, S., Lodoun, T., Ali, A., Gaye, A. T., and Ndiaye, O. (2013). A unifying view of climate change in the Sahel linking intra-seasonal, interannual and longer time scales. *Environ. Res. Lett.* 8, 024010. doi:10.1088/1748-9326/8/2/024010.
Gillett, N. P., Shiogama, H., Funke, B., Hegerl, G., Knutti, R., Matthes, K., et al. (2016). The Detection and Attribution Model Intercomparison Project (DAMIP v1.0) contribution to CMIP6. *Geosci. Model Dev.* 9, 3685–3697. doi:10.5194/gmd-9-3685-2016.
Gimeno, L., Dominguez, F., Nieto, R., Trigo, R., Drumond, A., Reason, C., et al. (2016). Major Mechanisms of Atmospheric Moisture Transport and Their Role in Extreme Precipitation Events. *Ssrn*. doi:10.1146/annurev-environ-110615-085558.
Gimeno, L., Nieto, R., VÃ¡zquez, M., and Lavers, D. A. (2014). Atmospheric rivers: a mini-review. *Front. Earth Sci.* 2, 1–6. doi:10.3389/feart.2014.00002.
Giorgi, F., and Bi, X. (2009). Time of emergence (TOE) of GHG-forced precipitation change hot-spots. *Geophys. Res. Lett.* 36, L06709. doi:10.1029/2009GL037593.
GIORGI, F., and GAO, X.-J. (2018). Regional earth system modeling: review and future directions. *Atmos. Ocean. Sci. Lett.* 11, 189–197. doi:10.1080/16742834.2018.1452520.
Giorgi, F., and Gutowski, W. J. (2015). Regional Dynamical Downscaling and the CORDEX Initiative. *Annu. Rev. Environ. Resour.* 40, 467–490. doi:10.1146/annurev-environ-102014-021217.
Giorgi, F., Jones, C., and Asrar, G. R. (2009). Addressing climate information needs at the regional level: the CORDEX framework. *WMO Bull.* 58, 175–183.
Giorgi, F., and Lionello, P. (2008). Climate change projections for the Mediterranean region. *Glob. Planet. Change*. doi:10.1016/j.gloplacha.2007.09.005.
Giorgi, F., and Mearns, L. O. (2002a). Calculation of average, uncertainty range, and reliability of regional climate changes from AOGCM simulations via the "Reliability Ensemble Averaging" (REA) method. *J. Clim.* 15, 1141–1158. doi:10.1175/1520-0442(2002)015<1141:COAURA>2.0.CO;2.
Giorgi, F., and Mearns, L. O. (2002b). Calculation of Average, Uncertainty Range, and Reliability of Regional Climate Changes from AOGCM Simulations via the "Reliability Ensemble Averaging" (REA) Method. *J. Clim.* 15, 1141–1158. doi:10.1175/1520-0442(2002)015<1141:COAURA>2.0.CO;2.
Giorgi, F., and Mearns, L. O. (2003). Probability of regional climate change based on the Reliability Ensemble Averaging (REA) method. *Geophys. Res. Lett.* 30. doi:10.1029/2003GL017130.
Giorgi, F., Torma, C., Coppola, E., Ban, N., Schär, C., and Somot, S. (2016). Enhanced summer convective rainfall at Alpine high elevations in response to climate warming. *Nat. Geosci.* 9, 584–589. doi:10.1038/ngeo2761.
Giot, O., Termonia, P., Degrauwe, D., De Troch, R., Caluwaerts, S., Smet, G., et al. (2016). Validation of the ALARO-0 model within the EURO-CORDEX framework. *Geosci. Model Dev.* 9, 1143–1152. doi:10.5194/gmd-9-1143-2016.
Gleckler, P., Doutriaux, C., Durack, P., Taylor, K., Zhang, Y., Williams, D., et al. (2016). A More Powerful Reality Test for Climate Models. *Eos (Washington. DC).* 97. doi:10.1029/2016EO051663.
Gleckler, P. J., Taylor, K. E., and Doutriaux, C. (2008). Performance metrics for climate models. *J. Geophys. Res.* 113, D06104. doi:10.1029/2007JD008972.
Gobiet, A., Suklitsch, M., and Heinrich, G. (2015). The effect of empirical-statistical correction of intensity-dependent model errors on the temperature climate change signal. *Hydrol. Earth Syst. Sci.* 19, 4055–4066. doi:10.5194/hess-19-4055-2015.
Goldenson, N., Leung, L. R., Bitz, C. M., and Blanchard-Wrigglesworth, E. (2018). Influence of Atmospheric Rivers on Mountain Snowpack in the Western United States. *J. Clim.* 31, 9921–9940. doi:10.1175/JCLI-D-18-0268.1.
Golding, N., Hewitt, C., and Zhang, P. (2017). Effective engagement for climate services: Methods in practice in China. *Clim. Serv.* 8, 72–76. doi:10.1016/J.CLISER.2017.11.002.
Golosov, S., Zverev, I., Shipunova, E., and Terzhevik, A. (2018). Modified parameterization of the vertical water temperature profile in the FLake model. *Tellus A Dyn. Meteorol. Oceanogr.* 70, 1–7. doi:10.1080/16000870.2018.1441247.
Gong, H., Wang, L., Zhou, W., Chen, W., Wu, R., Liu, L., et al. (2018). Revisiting the Northern Mode of East Asian Winter Monsoon Variation and Its Response to Global Warming. *J. Clim.* 31, 9001–9014. doi:10.1175/JCLI-D-18-0136.1.
Gonzalez, P. L. M., Polvani, L. M., Seager, R., and Correa, G. J. P. (2014). Stratospheric ozone depletion: a key driver of recent precipitation trends in South Eastern South America. *Clim. Dyn.* 42, 1775–1792. doi:10.1007/s00382-013-1777-x.
Goodman, S. J., Schmit, T. J., Daniels, J., Denig, W., and Metcalf, K. (2018). "GOES: Past, Present, and Future," in *Comprehensive Remote Sensing* (Elsevier), 119–149. doi:10.1016/B978-0-12-409548-9.10315-X.
Goosse, H. (2017). Reconstructed and simulated temperature asymmetry between continents in both hemispheres over the last centuries. *Clim. Dyn.* 48, 1483–1501. doi:10.1007/s00382-016-3154-z.
Goosse, H., Crespin, E., Dubinkina, S., Loutre, M.-F., Mann, M. E., Renssen, H., et al. (2012). The role of forcing and internal dynamics in explaining the "Medieval Climate Anomaly." *Clim. Dyn.* 39, 2847–2866.

doi:10.1007/s00382-012-1297-0.
Gorddard, R., Colloff, M. J., Wise, R. M., Ware, D., and Dunlop, M. (2016). Environmental Science & Policy Values , rules and knowledge : Adaptation as change in the decision context. *Environ. Sci. Policy* 57, 60–69. doi:10.1016/j.envsci.2015.12.004.
Goswami, B. N., Madhusoodanan, M. S., Neema, C. P., and Sengupta, D. (2006a). A physical mechanism for North Atlantic SST influence on the Indian summer monsoon. *Geophys. Res. Lett.* 33, L02706. doi:10.1029/2005GL024803.
Goswami, B. N., Venugopal, V., Sangupta, D., Madhusoodanan, M. S., and Xavier, P. K. (2006b). Increasing trend of extreme rain events over India in a warming environment. *Science (80-. ).* 314, 1442–1445. doi:10.1126/science.1132027.
Goudenhoofdt, E., and Delobbe, L. (2016). Generation and Verification of Rainfall Estimates from 10-Yr Volumetric Weather Radar Measurements. *J. Hydrometeorol.* 17, 1223–1242. doi:10.1175/JHM-D-15-0166.1.
Gray, L. J., Scaife, A. A., Mitchell, D. M., Osprey, S., Ineson, S., Hardiman, S., et al. (2013). A lagged response to the 11 year solar cycle in observed winter Atlantic/European weather patterns. *J. Geophys. Res. Atmos.* 118, 13,405-413,420. doi:10.1002/2013JD020062.
Griffies, S. M., Danabasoglu, G., Durack, P. J., Adcroft, A. J., Balaji, V., Böning, C. W., et al. (2016). OMIP contribution to CMIP6: experimental and diagnostic protocol for the physical component of the Ocean Model Intercomparison Project. *Geosci. Model Dev.* 9, 3231–3296. doi:10.5194/gmd-9-3231-2016.
Grimmond, C. S. B., Blackett, M., Best, M. J., Baik, J.-J., Belcher, S. E., Beringer, J., et al. (2011). Initial results from Phase 2 of the international urban energy balance model comparison. *Int. J. Climatol.* 31, 244–272. doi:10.1002/joc.2227.
Grimmond, C. S. B., Blackett, M., Best, M. J., Barlow, J., Baik, J.-J., Belcher, S. E., et al. (2010). The International Urban Energy Balance Models Comparison Project: First Results from Phase 1. *J. Appl. Meteorol. Climatol.* 49, 1268–1292. doi:10.1175/2010JAMC2354.1.
Grise, K. M., Davis, S. M., Simpson, I. R., Waugh, D. W., Fu, Q., Allen, R. J., et al. (2019). Recent Tropical Expansion: Natural Variability or Forced Response? *J. Clim.* 32, 1551–1571. doi:10.1175/JCLI-D-18-0444.1.
Grise, K. M., Davis, S. M., Staten, P. W., and Adam, O. (2018). Regional and Seasonal Characteristics of the Recent Expansion of the Tropics. *J. Clim.* 31, 6839–6856. doi:10.1175/JCLI-D-18-0060.1.
Groisman, P., Shugart, H., Kicklighter, D., Henebry, G., Tchebakova, N., Maksyutov, S., et al. (2017). Northern Eurasia Future Initiative (NEFI): facing the challenges and pathways of global change in the twenty-first century. *Prog. Earth Planet. Sci.* 4, 41. doi:10.1186/s40645-017-0154-5.
Groisman, P. Y., Clark, E. A., Kattsov, V. M., Lettenmaier, D. P., Sokolik, I. N., Aizen, V. B., et al. (2009). The Northern Eurasia Earth Science Partnership: An Example of Science Applied to Societal Needs. *Bull. Am. Meteorol. Soc.* 90, 671–688. doi:10.1175/2008BAMS2556.1.
Grose, M., Foster, S., Risbey, J., Osbrough, S., and Wilson, L. (2019). Using indices of atmospheric circulation to refine southern Australian winter rainfall climate projections. *J. Clim.*
Grose, M. R., Risbey, J. S., Moise, A. F., Osbrough, S., Heady, C., Wilson, L., et al. (2017). Constraints on Southern Australian Rainfall Change Based on Atmospheric Circulation in CMIP5 Simulations. *J. Clim.* 30, 225–242. doi:10.1175/JCLI-D-16-0142.1.
Grossman-Clarke, S., Schubert, S., and Fenner, D. (2017). Urban effects on summertime air temperature in Germany under climate change. *Int. J. Climatol.* 37, 905–917. doi:10.1002/joc.4748.
Gu, H., Yu, Z., Yang, C., Ju, Q., Yang, T., and Zhang, D. (2018). High-resolution ensemble projections and uncertainty assessment of regional climate change over China in CORDEX East Asia. *Hydrol. Earth Syst. Sci.* 22, 3087–3103. doi:10.5194/hess-22-3087-2018.
Gubler, S., Hunziker, S., Begert, M., Croci-Maspoli, M., Konzelmann, T., Brönnimann, S., et al. (2017). The influence of station density on climate data homogenization. *Int. J. Climatol.* 37, 4670–4683. doi:10.1002/joc.5114.
Guerreiro, S. B., Fowler, H. J., Barbero, R., Westra, S., Lenderink, G., Blenkinsop, S., et al. (2018). Detection of continental-scale intensification of hourly rainfall extremes. *Nat. Clim. Chang.* 8, 803–807. doi:10.1038/s41558-018-0245-3.
Guillod, B. P., Orlowsky, B., Miralles, D. G., Teuling, A. J., and Seneviratne, S. I. (2015). Reconciling spatial and temporal soil moisture effects on afternoon rainfall. *Nat. Commun.* 6. doi:10.1038/ncomms7443.
Guimberteau, M., Laval, K., Perrier, A., and Polcher, J. (2012). Global effect of irrigation and its impact on the onset of the Indian summer monsoon. *Clim. Dyn.* 39, 1329–1348. doi:10.1007/s00382-011-1252-5.
Guiot, J., and Cramer, W. (2016). Climate change: The 2015 Paris Agreement thresholds and Mediterranean basin ecosystems. *Science (80-. ).* 354, 465–468. doi:10.1126/science.aah5015.
Gula, J., and Peltier, W. R. (2012). Dynamical Downscaling over the Great Lakes Basin of North America Using the WRF Regional Climate Model: The Impact of the Great Lakes System on Regional Greenhouse Warming. *J. Clim.* 25, 7723–7742. doi:10.1175/JCLI-D-11-00388.1.
Guldberg, A., Kaas, E., Deque, M., Yang, S., and Thorsen, S. V. (2005). Reduction of systematic errors by empirical model correction: impact on seasonal prediction skill. *Tellus A* 57, 575–588. doi:10.1111/j.1600-0870.2005.00120.x.

Gulizia, C., and Camilloni, I. (2015). Comparative analysis of the ability of a set of CMIP3 and CMIP5 global climate models to represent precipitation in South America. *Int. J. Climatol.* 35, 583–595. doi:10.1002/joc.4005.
Gultepe, I. (2015). "Chapter Three - Mountain Weather: Observation and Modeling," in *Advances in Geophysics*, ed. R. Dmowska (Elsevier), 229–312. doi:https://doi.org/10.1016/bs.agph.2015.01.001.
Gultepe, I., Isaac, G. A., Joe, P., Kucera, P. A., Theriault, J. M., and Fisico, T. (2014). Roundhouse (RND) Mountain Top Research Site: Measurements and Uncertainties for Winter Alpine Weather Conditions. *Pure Appl. Geophys.* 171, 59–85. doi:10.1007/s00024-012-0582-5.
Guo, L., Turner, A. G., and Highwood, E. J. (2015). Impacts of 20th century aerosol emissions on the South Asian monsoon in the CMIP5 models. *Atmos. Chem. Phys.* 15, 6367–6378. doi:10.5194/acp-15-6367-2015.
Guo, L., Turner, A. G., and Highwood, E. J. (2016). Local and remote impacts of aerosol species on indian summer monsoon rainfall in a GCM. *J. Clim.* 29, 6937–6955. doi:10.1175/JCLI-D-15-0728.1.
Gustafsson, Ö., and Ramanathan, V. (2016). Convergence on climate warming by black carbon aerosols. *Proc. Natl. Acad. Sci.* 113, 4243 LP – 4245. doi:10.1073/pnas.1603570113.
Gutiérrez, J. M., Maraun, D., Widmann, M., Huth, R., Hertig, E., Benestad, R., et al. (2018). An intercomparison of a large ensemble of statistical downscaling methods over Europe: Results from the VALUE perfect predictor cross-validation experiment. *Int. J. Climatol.* doi:10.1002/joc.5462.
Gutiérrez, J. M., San-Martín, D., Brands, S., Manzanas, R., and Herrera, S. (2013). Reassessing Statistical Downscaling Techniques for Their Robust Application under Climate Change Conditions. *J. Clim.* 26, 171–188. doi:10.1175/JCLI-D-11-00687.1.
Gutmann, E. D., Rasmussen, R. M., Liu, C., Ikeda, K., Bruyere, C. L., Done, J. M., et al. (2018). Changes in hurricanes from a 13-Yr convection-permitting pseudo- global warming simulation. *J. Clim.* doi:10.1175/JCLI-D-17-0391.1.
Gutowski Jr., W. J., Giorgi, F., Timbal, B., Frigon, A., Jacob, D., Kang, H.-S., et al. (2016). WCRP COordinated Regional Downscaling EXperiment (CORDEX): a diagnostic MIP for CMIP6. *Geosci. Model Dev.* 9, 4087–4095. doi:10.5194/gmd-9-4087-2016.
Haarsma, R. J., Hazeleger, W., Severijns, C., Vries, H., Sterl, A., Bintanja, R., et al. (2013a). More hurricanes to hit western Europe due to global warming. *Geophys. Res. Lett.* 40, 1783–1788. doi:10.1002/grl.50360.
Haarsma, R. J., Roberts, M. J., Vidale, P. L., Senior, C. A., Bellucci, A., Bao, Q., et al. (2016). High Resolution Model Intercomparison Project (HighResMIP v1.0) for CMIP6. *Geosci. Model Dev.* 9, 4185–4208. doi:10.5194/gmd-9-4185-2016.
Haarsma, R. J., Selten, F., Hurk, B. Vd, Hazeleger, W., and Wang, X. (2009). Drier Mediterranean soils due to greenhouse warming bring easterly winds over summertime central Europe. *Geophys. Res. Lett.* doi:10.1029/2008GL036617.
Haarsma, R. J., Selten, F. M., and Drijfhout, S. S. (2015). Decelerating Atlantic meridional overturning circulation main cause of future west European summer atmospheric circulation changes. *Environ. Res. Lett.* 10, 094007. doi:10.1088/1748-9326/10/9/094007.
Haarsma, R. J., Selten, F., and van Oldenborgh, G. J. (2013b). Anthropogenic changes of the thermal and zonal flow structure over Western Europe and Eastern North Atlantic in CMIP3 and CMIP5 models. *Clim. Dyn.* 41, 2577–2588. doi:10.1007/s00382-013-1734-8.
Haberlie, A. M., Ashley, W. S., and Pingel, T. J. (2015). The effect of urbanisation on the climatology of thunderstorm initiation. *Q. J. R. Meteorol. Soc.* 141, 663–675. doi:10.1002/qj.2499.
Haeffelin, M., Barthès, L., Bock, O., Boitel, C., Bony, S., Bouniol, D., et al. (2005). SIRTA, a ground-based atmospheric observatory for cloud and aerosol research. *Ann. Geophys.* 23, 253–275. doi:10.5194/angeo-23-253-2005.
Haerter, J. O., Hagemann, S., Moseley, C., and Piani, C. (2011). Climate model bias correction and the role of timescales. *Hydrol. Earth Syst. Sci.* 15, 1065–1079. doi:10.5194/hess-15-1065-2011.
Hagemann, S., Chen, C., Clark, D. B., Folwell, S., Gosling, S. N., Haddeland, I., et al. (2013). Climate change impact on available water resources obtained using multiple global climate and hydrology models. *Earth Syst. Dyn.* 4, 129–144. doi:10.5194/esd-4-129-2013.
Hagishima, A., Tanimoto, J., and Narita, K. I. (2005). Intercomparisons of experimental convective heat transfer coefficients and mass transfer coefficients of urban surfaces. *Boundary-Layer Meteorol.* doi:10.1007/s10546-005-2078-7.
Haiden, T., Kann, A., Wittmann, C., Pistotnik, G., Bica, B., and Gruber, C. (2011). The Integrated Nowcasting through Comprehensive Analysis (INCA) System and Its Validation over the Eastern Alpine Region. *Weather Forecast.* 26, 166–183. doi:10.1175/2010WAF2222451.1.
Hakim, G. J., Emile-Geay, J., Steig, E. J., Noone, D., Anderson, D. M., Tardif, R., et al. (2016). The last millennium climate reanalysis project: Framework and first results. *J. Geophys. Res. Atmos.* 121, 6745–6764. doi:10.1002/2016JD024751.
Hall, A. (2014). Projecting regional change. *Science (80-. ).* 346, 1461–1462. doi:10.1126/science.aaa0629.
Hallegatte, S., Green, C., Nicholls, R. J., and Corfee-Morlot, J. (2013). Future flood losses in major coastal cities. *Nat. Clim. Chang.* 3, 802–806. doi:10.1038/nclimate1979.
Ham, S., Lee, J.-W., and Yoshimura, K. (2016). Assessing Future Climate Changes in the East Asian Summer and

Winter Monsoon Using Regional Spectral Model. *J. Meteorol. Soc. Japan. Ser. II* 94A, 69–87. doi:10.2151/jmsj.2015-051.
Hamada, A., and Takayabu, Y. N. (2018). Large-scale environmental conditions related to midsummer extreme rainfall events around Japan in the TRMM region. *J. Clim.* doi:10.1175/JCLI-D-17-0632.1.
Hamada, A., Takayabu, Y. N., Liu, C., and Zipser, E. J. (2015). Weak linkage between the heaviest rainfall and tallest storms. *Nat. Commun.* 6, 6213. doi:10.1038/ncomms7213.
Hamdi, R. (2010). Estimating Urban Heat Island Effects on the Temperature Series of Uccle (Brussels, Belgium) Using Remote Sensing Data and a Land Surface Scheme. *Remote Sens.* 2, 2773–2784. doi:10.3390/rs2122773.
Hamdi, R., Degrauwe, D., and Termonia, P. (2012a). Coupling the Town Energy Balance (TEB) Scheme to an Operational Limited-Area NWP Model: Evaluation for a Highly Urbanized Area in Belgium. *Weather Forecast.* 27, 323–344. doi:10.1175/WAF-D-11-00064.1.
Hamdi, R., Duchêne, F., Berckmans, J., Delcloo, A., Vanpoucke, C., and Termonia, P. (2016). Evolution of urban heat wave intensity for the Brussels Capital Region in the ARPEGE-Climat A1B scenario. *Urban Clim.* 17, 176–195. doi:10.1016/J.UCLIM.2016.08.001.
Hamdi, R., Giot, O., De Troch, R., Deckmyn, A., and Termonia, P. (2015). Future climate of Brussels and Paris for the 2050s under the A1B scenario. *Urban Clim.* 12, 160–182. doi:10.1016/j.uclim.2015.03.003.
Hamdi, R., and Masson, V. (2008). Inclusion of a Drag Approach in the Town Energy Balance (TEB) Scheme: Offline 1D Evaluation in a Street Canyon. *J. Appl. Meteorol. Climatol.* 47, 2627–2644. doi:10.1175/2008JAMC1865.1.
Hamdi, R., Van de Vyver, H., De Troch, R., and Termonia, P. (2014). Assessment of three dynamical urban climate downscaling methods: Brussels's future urban heat island under an A1B emission scenario. *Int. J. Climatol.* 34, 978–999. doi:10.1002/joc.3734.
Hamdi, R., Van de Vyver, H., and Termonia, P. (2012b). New cloud and microphysics parameterisation for use in high-resolution dynamical downscaling: application for summer extreme temperature over Belgium. *Int. J. Climatol.* 32, 2051–2065. doi:10.1002/joc.2409.
Hamilton, L. C. (2011). Education, politics and opinions about climate change evidence for interaction effects. *Clim. Change* 104, 231–242. doi:10.1007/s10584-010-9957-8.
Han, J.-Y., and Baik, J.-J. (2008). A Theoretical and Numerical Study of Urban Heat Island–Induced Circulation and Convection. *J. Atmos. Sci.* 65, 1859–1877. doi:10.1175/2007JAS2326.1.
Hansen, J., Ruedy, R., Sato, M., and Lo, K. (2010). GLOBAL SURFACE TEMPERATURE CHANGE. *Rev. Geophys.* 48. doi:10.1029/2010RG000345.
Hansen, J. W., Mishra, A., Rao, K. P. C., Indeje, M., and Ngugi, R. K. (2009). Potential value of GCM-based seasonal rainfall forecasts for maize management in semi-arid Kenya. *Agric. Syst.* 101, 80–90. doi:10.1016/j.agsy.2009.03.005.
Haren, R. van, Oldenborgh, G. J. van, Lenderink, G., and Hazeleger, W. (2013). Evaluation of modeled changes in extreme precipitation in Europe and the Rhine basin. *Environ. Res. Lett.* 8, 014053. doi:10.1088/1748-9326/8/1/014053.
Harris, I., Jones, P. D., Osborn, T. J., and Lister, D. H. (2014). Updated high-resolution grids of monthly climatic observations - the CRU TS3.10 Dataset. *Int. J. Climatol.* 34, 623–642. doi:10.1002/joc.3711.
Harris, L. M., and Lin, S.-J. (2013). A Two-Way Nested Global-Regional Dynamical Core on the Cubed-Sphere Grid. *Mon. Weather Rev.* 141, 283–306. doi:10.1175/MWR-D-11-00201.1.
Hart, P. S., and Nisbet, E. C. (2012). Boomerang Effects in Science Communication: How Motivated Reasoning and Identity Cues Amplify Opinion Polarization About Climate Mitigation Policies. *Communic. Res.* 39, 701–723. doi:10.1177/0093650211416646.
Hartfield, G., Blunden, J., and Arndt, D. S. (2018). State of the Climate in 2017. *Bull. Am. Meteorol. Soc.* 99, Si-S310. doi:10.1175/2018BAMSStateoftheClimate.1.
Hassanzadeh, P., Kuang, Z., and Farrell, B. F. (2014). Responses of midlatitude blocks and wave amplitude to changes in the meridional temperature gradient in an idealized dry GCM. *Geophys. Res. Lett.* 41, 5223–5232. doi:10.1002/2014GL060764.
Hasson, S., Lucarini, V., and Pascale, S. (2013). Hydrological cycle over South and Southeast Asian river basins as simulated by PCMDI/CMIP3 experiments. *Earth Syst. Dyn.* 4, 199–217. doi:10.5194/esd-4-199-2013.
Hasson, S. ul, Pascale, S., Lucarini, V., and Böhner, J. (2016). Seasonal cycle of precipitation over major river basins in South and Southeast Asia: A review of the CMIP5 climate models data for present climate and future climate projections. *Atmos. Res.* 180, 42–63. doi:10.1016/j.atmosres.2016.05.008.
Hastenrath, S. (1966). On general circulation and energy budget in the area of the Central American seas. *J. Atmos. Sci.* 23, 694–711.
Hatchett, B. J., Koračin, D., Mejía, J. F., and Boyle, D. P. (2016). Assimilating urban heat island effects into climate projections. *J. Arid Environ.* 128, 59–64. doi:10.1016/j.jaridenv.2016.01.007.
Hauser, M., Orth, R., and Seneviratne, S. I. (2016). Role of soil moisture versus recent climate change for the 2010 heat wave in western Russia. *Geophys. Res. Lett.* 43, 2819–2826. doi:10.1002/2016GL068036.
Hauser, M., Orth, R., and Seneviratne, S. I. (2017). Investigating soil moisture–climate interactions with prescribed soil moisture experiments: an assessment with the Community Earth System Model (version 1.2). *Geosci. Model Dev.*

10, 1665–1677. doi:10.5194/gmd-10-1665-2017.
Hausfather, Z., Cowtan, K., Menne, M. J., and Williams Jr., C. N. (2016). Evaluating the impact of U.S. Historical Climatology Network homogenization using the U.S. Climate Reference Network. *Geophys. Res. Lett.* 43, 1695–1701. doi:10.1002/2015GL067640.
Hausfather, Z., Menne, M. J., Williams, C. N., Masters, T., Broberg, R., and Jones, D. (2013). Quantifying the effect of urbanization on u.s. Historical climatology network temperature records. *J. Geophys. Res. Atmos.* 118, 481–494. doi:10.1029/2012JD018509.
Hawkins, E., Smith, R. S., Gregory, J. M., and Stainforth, D. A. (2016). Irreducible uncertainty in near-term climate projections. *Clim. Dyn.* 46, 3807–3819. doi:10.1007/s00382-015-2806-8.
Hawkins, E., and Sutton, R. (2009). The Potential to Narrow Uncertainty in Regional Climate Predictions. *Bull. Am. Meteorol. Soc.* 90, 1095–1108. doi:10.1175/2009BAMS2607.1.
Hawkins, E., and Sutton, R. (2011). The potential to narrow uncertainty in projections of regional precipitation change. *Clim. Dyn.* 37, 407–418. doi:10.1007/s00382-010-0810-6.
Hawkins, E., and Sutton, R. (2012). Time of emergence of climate signals. *Geophys. Res. Lett.* 39, n/a-n/a. doi:10.1029/2011GL050087.
Haylock, M. R., Hofstra, N., Klein Tank, A. M. G., Klok, E. J., Jones, P. D., and New, M. (2008). A European daily high-resolution gridded data set of surface temperature and precipitation for 1950–2006. *J. Geophys. Res.* 113, D20119. doi:10.1029/2008JD010201.
Hazeleger, W., Van Den Hurk, B. J. J. M., Min, E., Van Oldenborgh, G. J., Petersen, A. C., Stainforth, D. A., et al. (2015). Tales of future weather. *Nat. Clim. Chang.* 5, 107–113. doi:10.1038/nclimate2450.
Hegerl, G., Hoegh-Guldberg, O., Casassa, G., Hoerling, M., Kovats, S., Parmesan, C., et al. (2010). Good Practice Guidance Paper on Detection and Attribution Related to Anthropogenic Climate Change. *Meet. Rep. Intergov. Panel Clim. Chang. Expert Meet. Detect. Attrib. Anthropog. Clim. Chang.*, 1–9. Available at: http://nova.wh.whoi.edu/palit/Stocker et al_2009_Report_IPCC Expert Meeting on Detection and Attribution Related to Anthropogenic Climate Change.
Hempel, S., Frieler, K., Warszawski, L., Schewe, J., and Piontek, F. (2013). A trend-preserving bias correction – the ISI-MIP approach. *Earth Syst. Dyn.* 4, 219–236. doi:10.5194/esd-4-219-2013.
Henderson, S. A., Maloney, E. D., and Barnes, E. A. (2016). The Influence of the Madden–Julian Oscillation on Northern Hemisphere Winter Blocking. *J. Clim.* 29, 4597–4616. doi:10.1175/JCLI-D-15-0502.1.
Hendon, H. H., Lim, E.-P., and Nguyen, H. (2014a). Seasonal Variations of Subtropical Precipitation Associated with the Southern Annular Mode. *J. Clim.* 27, 3446–3460. doi:10.1175/JCLI-D-13-00550.1.
Hendon, H. H., Lim, E., Arblaster, J. M., and Anderson, D. L. T. (2014b). Causes and predictability of the record wet east Australian spring 2010. *Clim. Dyn.* 42, 1155–1174. doi:10.1007/s00382-013-1700-5.
Hendon, H., Thompson, D., and Wheeler, M. (2007). Australian Rainfall and Surface Temperature Variations Associated with the Southern Hemisphere Annular Mode. *J. Clim.* 20, 2452–2465.
Henrich, J., Heine, S. J., and Norenzayan, A. (2010a). The weidest people in the world? *Behav. Brain Sci.* 33, 61–135. doi:10.1017/S0140525X0999152X.
Henrich, J., Heine, S., and Norenzayan, A. (2010b). Beyond WEIRD: Towards a broad-based behavioral science. *Behav. Brain Sci.* 33, 111–135. doi:10.1017/S0140525X10000725.
Hernández-Díaz, L., Laprise, R., Sushama, L., Martynov, A., Winger, K., and Dugas, B. (2013). Climate simulation over CORDEX Africa domain using the fifth-generation Canadian Regional Climate Model (CRCM5). *Clim. Dyn.* 40, 1415–1433. doi:10.1007/s00382-012-1387-z.
Herrera, D., and Ault, T. (2017). Insights from a New High-Resolution Drought Atlas for the Caribbean Spanning 1950–2016. *J. Clim.* 30, 7801–7825. doi:10.1175/JCLI-D-16-0838.1.
Herrera, D., Ault, T. R., Carrillo, C. M., and Cook, B. I. (2018a). Exacerbation of the 2013-2016 Pan-Caribbean Drought by Anthropogenic Exacerbation of the 2013 – 2016 Pan-Caribbean Drought by Anthropogenic Warming. doi:10.1029/2018GL079408.
Herrera, S., Kotlarski, S., Soares, P. M. M., Cardoso, R. M., Jaczewski, A., Gutiérrez, J. M., et al. (2018b). Uncertainty in gridded precipitation products: Influence of station density, interpolation method and grid resolution. *Int. J. Climatol.* doi:10.1002/joc.5878.
Hertig, E., Maraun, D., Bartholy, J., Pongracz, R., Vrac, M., Mares, I., et al. (2018). Comparison of statistical downscaling methods with respect to extreme events over Europe: Validation results from the perfect predictor experiment of the COST Action VALUE. *Int. J. Climatol.* doi:10.1002/joc.5469.
Heuzé, C., Heywood, K. J., Stevens, D. P., and Ridley, J. K. (2013). Southern Ocean bottom water characteristics in CMIP5 models. *Geophys. Res. Lett.* doi:10.1002/grl.50287.
Hewitson, B. C., and Crane, R. G. (2006). Consensus between GCM climate change projections with empirical downscaling: precipitation downscaling over South Africa. *Int. J. Climatol.* 26, 1315–1337. doi:10.1002/joc.1314.
Hewitson, B. C., Daron, J., Crane, R. G., Zermoglio, M. F., and Jack, C. (2014). Interrogating empirical-statistical downscaling. *Clim. Change* 122, 539–554. doi:10.1007/s10584-013-1021-z.
Hewitson, B., Waagsaether, K., Wohland, J., Kloppers, K., and Kara, T. (2017). Climate information websites: an evolving landscape. *Wiley Interdiscip. Rev. Clim. Chang.* 8, e470. doi:10.1002/wcc.470.

Hewitt, C. D., and Lowe, J. A. (2018). Toward a European Climate Prediction System. *Bull. Am. Meteorol. Soc.* 99, 1997–2001. doi:10.1175/BAMS-D-18-0022.1.
Hewitt, C., Mason, S., and Walland, D. (2012). The Global Framework for Climate Services. *Nat. Clim. Chang.* 2, 831. Available at: http://dx.doi.org/10.1038/nclimate1745.
Hibino, K., Takayabu, I., Wakazuki, Y., and Ogata, T. (2018). Physical Responses of Convective Heavy Rainfall to Future Warming Condition: Case Study of the Hiroshima Event. *Front. Earth Sci.* 6, 35. doi:10.3389/feart.2018.00035.
Hiebl, J., and Frei, C. (2016). Daily temperature grids for Austria since 1961 — concept , creation and applicability. *Theor Appl Clim.*, 161–178. doi:10.1007/s00704-015-1411-4.
Hirsch, A. L., Prestele, R., Davin, E. L., Seneviratne, S. I., Thiery, W., and Verburg, P. H. (2018). Modelled biophysical impacts of conservation agriculture on local climates. *Glob. Chang. Biol.* 0. doi:10.1111/gcb.14362.
Hirsch, A. L., Wilhelm, M., Davin, E. L., Thiery, W., and Seneviratne, S. I. (2017). Can climate-effective land management reduce regional warming? *J. Geophys. Res. Atmos.* 122, 2269–2288. doi:10.1002/2016JD026125.
Ho-Hagemann, H. T. M., Gröger, M., Rockel, B., Zahn, M., Geyer, B., and Meier, H. E. M. (2017). Effects of air-sea coupling over the North Sea and the Baltic Sea on simulated summer precipitation over Central Europe. *Clim. Dyn.* 49, 3851–3876. doi:10.1007/s00382-017-3546-8.
Hobaek Haff, I., Frigessi, A., and Maraun, D. (2015). How well do regional climate models simulate the spatial dependence of precipitation? An application of pair-copula constructions. *J. Geophys. Res. Atmos.* 120, 2624–2646. doi:10.1002/2014JD022748.
Hoegh-Guldberg, O., Jacob, D., Taylor, M., Bindi, M., Abdul Halim, S., Achlatis Australia, M., et al. (2018). "Impacts of 1.5°C of Global Warming on Natural and Human Systems," in *Global Warming of 1.5°C. An IPCC Special Report on the impacts of global warming of 1.5°C above pre-industrial levels and related global greenhouse gas emission pathways, in the context of strengthening the global response to the threat of climate change*, eds. V. Masson-Delmotte, P. Zhai, H.-O. Pörtner, D. Roberts, J. Skea, P. R. Shukla, et al., 175–311.
Hoell, A., Hoerling, M., Eischeid, J., Quan, X.-W., and Liebmann, B. (2017). Reconciling Theories for Human and Natural Attribution of Recent East Africa Drying. *J. Clim.* 30, 1939–1957. doi:10.1175/JCLI-D-16-0558.1.
Hoffmann, P., Schoetter, R., and Schlünzen, K. H. (2018). Statistical-dynamical downscaling of the urban heat island in Hamburg, Germany. *Meteorol. Zeitschrift* 27, 89–109. doi:10.1127/metz/2016/0773.
Hohenegger, C., and Stevens, B. (2018). The role of the permanent wilting point in controlling the spatial distribution of precipitation. *Proc. Natl. Acad. Sci.* 115, 5692–5697. doi:10.1073/pnas.1718842115.
Hong, S.-Y., and Kanamitsu, M. (2014). Dynamical downscaling: Fundamental issues from an NWP point of view and recommendations. *Asia-Pacific J. Atmos. Sci.* 50, 83–104. doi:10.1007/s13143-014-0029-2.
Hope, P., Grose, M. R., Timbal, B., Dowdy, A. J., Bhend, J., Katzfey, J. J., et al. (2015). Seasonal and regional signature of the projected southern Australian rainfall reduction. *Aust. Meteorol. Oceanogr. J.* 65, 54–71.
Hope, P. K., Drosdowsky, W., and Nicholls, N. (2006). Shifts in the synoptic systems influencing southwest Western Australia. *Clim. Dyn.* 26, 751–764. doi:10.1007/s00382-006-0115-y.
Hope, P., Keay, K., Pook, M., Catto, J., Simmonds, I., Mills, G., et al. (2014). A Comparison of Automated Methods of Front Recognition for Climate Studies: A Case Study in Southwest Western Australia. *Mon. Weather Rev.* 142, 343–363. doi:10.1175/MWR-D-12-00252.1.
Hope, P., Lim, E.-P., Hendon, H., and Wang, G. (2018). The Effect of Increasing CO 2 on the Extreme September 2016 Rainfall Across Southeastern Australia. *Bull. Am. Meteorol. Soc.* 99, S133–S138. doi:10.1175/BAMS-D-17-0094.1.
Hope, P., Timbal, B., and Fawcett, R. (2010). Associations between rainfall variability in the southwest and southeast of Australia and their evolution through time. *Int. J. Climatol.* 30, 1360–1371. doi:DOI:10.1002/joc.1964-1097-0088.
Hope, P., Timbal, B., Hendon, H., Ekström, M., and Potter, N. (2017). A Synthesis of Findings from the Victorian Climate Initiative. 56.
Hope, P., Wang, G., Lim, E.-P., Hendon, H. H., and Arblaster, J. M. (2016). What caused the record-breaking heat across Australia in October 2015? *Bull. Am. Meteorol. Soc.* 96, S1–S172. doi:10.1175/BAMS-D-15-00157.1.
Hope, P., and Watterson, I. (2018). Persistence of cool conditions after heavy rain in Australia. *J. South. Hemisph. Earth Syst. Sci.* 68. doi:10.22499/3.6801.004.
Horton, D. E., Johnson, N. C., Singh, D., Swain, D. L., Rajaratnam, B., and Diffenbaugh, N. S. (2015). Contribution of changes in atmospheric circulation patterns to extreme temperature trends. *Nature* 522, 465–469. doi:10.1038/nature14550.
Hoshi, K., Ukita, J., Honda, M., Nakamura, T., Yamazaki, K., Miyoshi, Y., et al. (2019). Weak Stratospheric Polar Vortex Events Modulated by the Arctic Sea-Ice Loss. *J. Geophys. Res. Atmos.* 124, 858–869. doi:10.1029/2018JD029222.
Hoskins, B. (2013). The potential for skill across the range of the seamless weather-climate prediction problem: A stimulus for our science. *Q. J. R. Meteorol. Soc.* 139, 573–584. doi:10.1002/qj.1991.
Hsu, H.-H., Zhou, T., and Matsumoto, J. (2014). East Asian, Indochina and Western North Pacific Summer Monsoon - An Update. *Asia-Pac. J. Atmos. Sci.* 50, 45–68. doi:10.1007/13143-014-0027-4.

Hu, A., and Deser, C. (2013). Uncertainty in future regional sea level rise due to internal climate variability. *Geophys. Res. Lett.* 40, 2768–2772. doi:10.1002/grl.50531.
Hu, Y., Maskey, S., and Uhlenbrook, S. (2013a). Downscaling daily precipitation over the Yellow River source region in China: a comparison of three statistical downscaling methods. *Theor. Appl. Climatol.* 112, 447–460. doi:10.1007/s00704-012-0745-4.
Hu, Y., Tao, L., and Liu, J. (2013b). Poleward expansion of the hadley circulation in CMIP5 simulations. *Adv. Atmos. Sci.* 30, 790–795. doi:10.1007/s00376-012-2187-4.
Huang, B., Banzon, V. F., Freeman, E., Lawrimore, J., Liu, W., Peterson, T. C., et al. (2015a). Extended Reconstructed Sea Surface Temperature Version 4 (ERSST.v4). Part I: Upgrades and Intercomparisons. *J. Clim.* 28, 911–930. doi:10.1175/JCLI-D-14-00006.1.
Huang, B., Polanski, S., and Cubasch, U. (2015b). Assessment of precipitation climatology in an ensemble of CORDEX-East Asia regional climate simulations. *Clim. Res.* 64, 141–158. doi:10.3354/cr01302.
Huang, X., Rhoades, A. M., Ullrich, P. A., and Zarzycki, C. M. (2016). An evaluation of the variable-resolution CESM for modeling California's climate. *J. Adv. Model. Earth Syst.* 8, 345–369. doi:10.1002/2015MS000559.
Huang, X., Zhou, T., Chen, X., Clark, R., Man, W., Murphy, J., et al. (2018). Indian summer monsoon drying trend caused by internal variability. *Nat. Clim. Chang.*
Huddart Benjamin, and Subramanian, A., and Zanna Laure, and and Palmer Tim (2017). Seasonal and decadal forecasts of Atlantic Sea surface temperatures using a linear inverse model. *Clim. Dyn.* 49, 1833–1845. doi:10.1007/s00382-016-3375-1.
Huffman, G. J., Bolvin, D. T., Braithwaite, D., Hsu, K., Joyce, R., Xie, P., et al. (2014). Algorithm Theoretical Basis Document ( ATBD ) NASA Global Precipitation Measurement ( GPM ) Integrated Multi-satellitE Retrievals for GPM ( I- MERG ) Prepared by :
Huffman, G. J., Bolvin, D. T., Nelkin, E. J., Wolff, D. B., Adler, R. F., Gu, G., et al. (2007). The TRMM Multisatellite Precipitation Analysis (TMPA): Quasi-Global, Multiyear, Combined-Sensor Precipitation Estimates at Fine Scales. *J. Hydrometeorol.* 8, 38–55. doi:10.1175/JHM560.1.
Hughes, J. D., Petrone, K. C., and Silberstein, R. P. (2012). Drought, groundwater storage and stream flow decline in southwestern Australia. *Geophys. Res. Lett.* 39, n/a-n/a. doi:10.1029/2011GL050797.
Hulme, M. (2001). Climatic perspectives on Sahelian desiccation: 1973–1998. *Glob. Environ. Chang.* 11, 19–29. doi:10.1016/S0959-3780(00)00042-X.
Hung, M.-P., Lin, J.-L., Wang, W., Kim, D., Shinoda, T., and Weaver, S. J. (2013). MJO and Convectively Coupled Equatorial Waves Simulated by CMIP5 Climate Models. *J. Clim.* 26, 6185–6214. doi:10.1175/JCLI-D-12-00541.1.
Hurrell, J., Bader, D., Delworth, T., Kirtman, B., Pan, J. M. H., and Wielicki, B. (2006). White Paper on Seamless Prediction.
Hurrell, J., Meehl, G. A., Bader, D., Delworth, T. L., Kirtman, B., and Wielicki, B. (2009). A Unified Modeling Approach to Climate System Prediction. *Bull. Am. Meteorol. Soc.* 90, 1819–1832. doi:10.1175/2009BAMS2752.1.
Hurwitz, M. M., Calvo, N., Garfinkel, C. I., Butler, A. H., Ineson, S., Cagnazzo, C., et al. (2014). Extra-tropical atmospheric response to ENSO in the CMIP5 models. *Clim. Dyn.* 43, 3367–3376. doi:10.1007/s00382-014-2110-z.
Huth, R., Mikšovský, J., Štěpánek, P., Belda, M., Farda, A., Chládová, Z., et al. (2015). Comparative validation of statistical and dynamical downscaling models on a dense grid in central Europe: temperature. *Theor. Appl. Climatol.* 120, 533–553. doi:10.1007/s00704-014-1190-3.
Hwang, Y.-T., Frierson, D. M. W., and Kang, S. M. (2013). Anthropogenic sulfate aerosol and the southward shift of tropical precipitation in the late 20th century. *Geophys. Res. Lett.* 40, 2845–2850. doi:10.1002/grl.50502.
Ichii, K., Ueyama, M., Kondo, M., Saigusa, N., Kim, J., Alberto, M. C., et al. (2017). New data-driven estimation of terrestrial $CO_2$ fluxes in Asia using a standardized database of eddy covariance measurements, remote sensing data, and support vector regression. *J. Geophys. Res. Biogeosciences*. doi:10.1002/2016JG003640.
Ichinose, T., Shimodozono, K., and Hanaki, K. (1999). Impact of anthropogenic heat on urban climate in Tokyo. *Atmos. Environ.* 33, 3897–3909. doi:10.1016/S1352-2310(99)00132-6.
Iizumi, T., Semenov, M. A., Nishimori, M., Ishigooka, Y., and Kuwagata, T. (2012). ELPIS-JP: a dataset of local-scale daily climate change scenarios for Japan. *Philos. Trans. R. Soc. A Math. Phys. Eng. Sci.* 370, 1121–1139. doi:10.1098/rsta.2011.0305.
Imamovic, A., Schlemmer, L., and Schär, C. (2017). Collective Impacts of Orography and Soil Moisture on the Soil Moisture-Precipitation Feedback. *Geophys. Res. Lett.* 44, 11,682-11,691. doi:10.1002/2017GL075657.
Inoue, J., Hori, M. E., and Takaya, K. (2012). The Role of Barents Sea Ice in the Wintertime Cyclone Track and Emergence of a Warm-Arctic Cold-Siberian Anomaly. *J. Clim.* 25, 2561–2568. doi:10.1175/JCLI-D-11-00449.1.
Inoue, T., Ngo-Duc, T., Matsumoto, J., Phan-Van, T., Nguyen-Xuan, T., Trinh-Tuan, L., et al. (2016). The Vietnam Gridded Precipitation (VnGP) Dataset: Construction and Validation. *SOLA*. doi:10.2151/sola.2016-057.
Iqbal, W., Syed, F. S., Sajjad, H., Nikulin, G., Kjellström, E., and Hannachi, A. (2017). Mean climate and representation of jet streams in the CORDEX South Asia simulations by the regional climate model RCA4.

*Theor. Appl. Climatol.* 129, 1–19. doi:10.1007/s00704-016-1755-4.
Irwin, E. G., Culligan, P. J., Fischer-Kowalski, M., Law, K. L., Murtugudde, R., and Pfirman, S. (2018). Bridging barriers to advance global sustainability. *Nat. Sustain.* 1, 324–326. doi:10.1038/s41893-018-0085-1.
Ishizaki, N., and Takayabu, I. (2009). On the Warming Events over Toyama Plain by Using NHRCM. *SOLA* 5, 129–132. doi:10.2151/sola.2009-033.
Isotta, F. A., Frei, C., Weilguni, V., Perˇ, M., Lass, P., Rudolf, B., et al. (2014). The climate of daily precipitation in the Alps : development and analysis of a high-resolution grid dataset from pan-Alpine rain-gauge data. *Int. J. Climatol.* 1675, 1657–1675. doi:10.1002/joc.3794.
Isotta, F. A., Vogel, R., and Frei, C. (2015). Evaluation of European regional reanalyses and downscalings for precipitation in the Alpine region. *Meteorol. Zeitschrift* 24, 15–37. doi:10.1127/metz/2014/0584.
Ivanov, M., Warrach-Sagi, K., and Wulfmeyer, V. (2017). Field significance of performance measures in the context of regional climate model evaluation. Part 1: temperature. *Theor. Appl. Climatol.*, 1–19. doi:10.1007/s00704-017-2100-2.
Ivanov, M., Warrach-Sagi, K., and Wulfmeyer, V. (2018). Field significance of performance measures in the context of regional climate model evaluation. Part 2: precipitation. *Theor. Appl. Climatol.* 132, 239–261. doi:10.1007/s00704-017-2077-x.
Ivanov, V. Y., Hutyra, L. R., Wofsy, S. C., Munger, J. W., Saleska, S. R., de Oliveira, R. C., et al. (2012). Root niche separation can explain avoidance of seasonal drought stress and vulnerability of overstory trees to extended drought in a mature Amazonian forest. *Water Resour. Res.* 48. doi:10.1029/2012WR011972.
Jacob, D., Kotova, L., Teichmann, C., Sobolowski, S. P., Vautard, R., Donnelly, C., et al. (2018). Climate Impacts in Europe Under +1.5°C Global Warming. *Earth's Futur.* 6, 264–285. doi:10.1002/2017EF000710.
Jacob, D., Petersen, J., Eggert, B., Alias, A., Christensen, O. B., Bouwer, L. M., et al. (2014). EURO-CORDEX: new high-resolution climate change projections for European impact research. *Reg. Environ. Chang.* 14, 563–578. doi:10.1007/s10113-013-0499-2.
Jaeger, E. B., and Seneviratne, S. I. (2011). Impact of soil moisture–atmosphere coupling on European climate extremes and trends in a regional climate model. *Clim. Dyn.* 36, 1919–1939. doi:10.1007/s00382-010-0780-8.
Jain, S., Salunke, P., K. Mishra, S., and Sahany, S. (2018). *Performance of CMIP5 models in the simulation of Indian summer monsoon*. doi:10.1007/s00704-018-2674-3.
Jaiser, R., Nakamura, T., Handorf, D., Dethloff, K., Ukita, J., and Yamazaki, K. (2016). Atmospheric winter response to Arctic sea ice changes in reanalysis data and model simulations. *J. Geophys. Res. Atmos.* 121, 7564–7577. doi:10.1002/2015JD024679.
James, R., Washington, R., and Jones, R. (2015). Process-based assessment of an ensemble of climate projections for West Africa. *J. Geophys. Res. Atmos.* 120, 1221–1238. doi:10.1002/2014JD022513.
Jänicke, B., Meier, F., Fenner, D., Fehrenbach, U., Holtmann, A., and Scherer, D. (2017). Urban-rural differences in near-surface air temperature as resolved by the Central Europe Refined analysis (CER): sensitivity to planetary boundary layer schemes and urban canopy models. *Int. J. Climatol.* 37, 2063–2079. doi:10.1002/joc.4835.
Jeong, J.-H., Ou, T., Linderholm, H. W., Kim, B.-M., Kim, S.-J., Kug, J.-S., et al. (2011). Recent recovery of the Siberian High intensity. *J. Geophys. Res. Atmos.* 116, n/a-n/a. doi:10.1029/2011JD015904.
Jerez, S., López-Romero, J. M., Turco, M., Jiménez-Guerrero, P., Vautard, R., and Montávez, J. P. (2018). Impact of evolving greenhouse gas forcing on the warming signal in regional climate model experiments. *Nat. Commun.* 9, 1304. doi:10.1038/s41467-018-03527-y.
Jiang, D., and Tian, Z. (2013). East Asian monsoon change for the 21st century: Results of CMIP3 and CMIP5 models. *Chinese Sci. Bull.* 58, 1427–1435. doi:10.1007/s11434-012-5533-0.
Jiang, X., Waliser, D. E., Xavier, P. K., Petch, J., Klingaman, N. P., Woolnough, S. J., et al. (2015). Vertical structure and physical processes of the Madden-Julian oscillation: Exploring key model physics in climate simulations. *J. Geophys. Res. Atmos.* 120, 4718–4748. doi:10.1002/2014JD022375.
Jiang, Y., Liu, X., Yang, X.-Q., and Wang, M. (2013). A numerical study of the effect of different aerosol types on East Asian summer clouds and precipitation. *Atmos. Environ.* 70, 51–63. doi:10.1016/j.atmosenv.2012.12.039.
Jiang, Z., Feldstein, S. B., and Lee, S. (2017a). The relationship between the Madden-Julian Oscillation and the North Atlantic Oscillation. *Q. J. R. Meteorol. Soc.* 143, 240–250. doi:10.1002/qj.2917.
Jiang, Z., Huo, F., Ma, H., Song, J., and Dai, A. (2017b). Impact of Chinese urbanization and aerosol emissions on the East Asian summer monsoon. *J. Clim.* 30, 1019–1039. doi:10.1175/JCLI-D-15-0593.1.
Jiménez-Guerrero, P., Montávez, J., Domínguez, M., Romera, R., Fita, L., Fernández, J., et al. (2013). Mean fields and interannual variability in RCM simulations over Spain: the ESCENA project. *Clim. Res.* 57, 201–220. doi:10.3354/cr01165.
Jin, Q., and Wang, C. (2017). A revival of Indian summer monsoon rainfall since 2002. *Nat. Clim. Chang.* 7, 587–594. doi:10.1038/NCLIMATE3348.
Johnson, F., and Sharma, A. (2012). A nesting model for bias correction of variability at multiple time scales in general circulation model precipitation simulations. *Water Resour. Res.* 48. doi:10.1029/2011WR010464.
Johnson, S. J., Levine, R. C., Turner, A. G., Martin, G. M., Woolnough, S. J., Schiemann, R., et al. (2016). The resolution sensitivity of the South Asian monsoon and Indo-Pacific in a global 0.35° AGCM. *Clim. Dyn.* 46, 807–

831. doi:10.1007/s00382-015-2614-1.
Jones, A. D., Collins, W. D., and Torn, M. S. (2013). On the additivity of radiative forcing between land use change and greenhouse gases. *Geophys. Res. Lett.* 40, 4036–4041. doi:10.1002/grl.50754.
Journée, M., Delvaux, C., and Bertrand, C. (2015). Precipitation climate maps of Belgium. *Adv. Sci. Res.* 12, 73–78. doi:10.5194/asr-12-73-2015.
Junquas, C., Li, L., Vera, C. S., Le Treut, H., and Takahashi, K. (2016). Influence of South America orography on summertime precipitation in Southeastern South America. *Clim. Dyn.* 46, 3941–3963. doi:10.1007/s00382-015-2814-8.
Junquas, C., Vera, C., Li, L., and Le Treut, H. (2012). Summer precipitation variability over Southeastern South America in a global warming scenario. *Clim. Dyn.* 38, 1867–1883. doi:10.1007/s00382-011-1141-y.
Junquas, C., Vera, C. S., Li, L., and Le Treut, H. (2013). Impact of projected SST changes on summer rainfall in southeastern South America. *Clim. Dyn.* 40, 1569–1589. doi:10.1007/s00382-013-1695-y.
Jury, M. W., Herrera, S., Gutiérrez, J. M., and Barriopedro, D. (2018). Blocking representation in the ERA-Interim driven EURO-CORDEX RCMs. *Clim. Dyn.* doi:10.1007/s00382-018-4335-8.
Kaczmarska, J., Isham, V., and Onof, C. (2014). Point process models for fine-resolution rainfall. *Hydrol. Sci. J.* 59, 1972–1991. doi:10.1080/02626667.2014.925558.
Kadel, I., Yamazaki, T., Iwasaki, T., and Abdillah, M. (2018). Projection of future monsoon precipitation over the central Himalayas by CMIP5 models under warming scenarios. *Clim. Res.* 75, 1–21. doi:10.3354/cr01497.
Kahan, D. M. (2012). Ideology, Motivated Reasoning, and Cognitive Reflection: An Experimental Study. *Ssrn* 8, 407–424. doi:10.2139/ssrn.2182588.
Kahan, D. M. (2013). "Making Climate-Science Communication Evidence-Based — All the Way Down," in *SSRN Electronic Journal*, eds. M. Boykoff and D. Crow (Routledge Press). doi:10.2139/ssrn.2216469.
Kajino, M., Ueda, H., Han, Z., Kudo, R., Inomata, Y., and Kaku, H. (2017). Synergy between air pollution and urban meteorological changes through aerosol-radiation-diffusion feedback—A case study of Beijing in January 2013. *Atmos. Environ.* 171, 98–110. doi:https://doi.org/10.1016/j.atmosenv.2017.10.018.
Kalnay, E., Kanamitsu, M., Kistler, R., Collins, W., Deaven, D., Gandin, L., et al. (1996). The NCEP/NCAR 40-Year Reanalysis Project. *Bull. Am. Meteorol. Soc.* 77, 437–471. doi:10.1175/1520-0477(1996)077<0437:TNYRP>2.0.CO;2.
Kamae, Y., Watanabe, M., Kimoto, M., and Shiogama, H. (2014a). Summertime land–sea thermal contrast and atmospheric circulation over East Asia in a warming climate—Part I: Past changes and future projections. *Clim. Dyn.* 43, 2553–2568. doi:10.1007/s00382-014-2073-0.
Kamae, Y., Watanabe, M., Kimoto, M., and Shiogama, H. (2014b). Summertime land–sea thermal contrast and atmospheric circulation over East Asia in a warming climate—Part II: Importance of CO2-induced continental warming. *Clim. Dyn.* 43, 2569–2583. doi:10.1007/s00382-014-2146-0.
Kanada, S., Tsuboki, K., Aiki, H., Tsujino, S., and Takayabu, I. (2017). Future Enhancement of Heavy Rainfall Events Associated with a Typhoon in the Midlatitude Regions. *SOLA* 13, 246–251. doi:10.2151/sola.2017-045.
Kang, S. M., Deser, C., and Polvani, L. M. (2013). Uncertainty in Climate Change Projections of the Hadley Circulation: The Role of Internal Variability. *J. Clim.* 26, 7541–7554. doi:10.1175/JCLI-D-12-00788.1.
Kang, S. M., Polvani, L. M., Fyfe, J. C., and Sigmond, M. (2011). Impact of Polar Ozone Depletion on Subtropical Precipitation. *Science (80-. ).* 332, 951–954. doi:10.1126/science.1202131.
Kaplan, A., Cane, M. A., Kushnir, Y., Clement, A. C., Benno Blumenthal, M., and Rajagopalan, B. (1998). Analyses of global sea surface temperature 1856-1991. *J. Geophys. Res.* doi:10.1029/97JC01736.
Kaplan, S., Georgescu, M., Alfasi, N., and Kloog, I. (2017). Impact of future urbanization on a hot summer: a case study of Israel. *Theor. Appl. Climatol.* 128, 325–341. doi:10.1007/s00704-015-1708-3.
Karmacharya, J., Jones, R., Moufouma-Okia, W., and New, M. (2017). Evaluation of the added value of a high-resolution regional climate model simulation of the South Asian summer monsoon climatology. *Int. J. Climatol.* 37, 3630–3643. doi:10.1002/joc.4944.
Karmalkar, A. V., Taylor, M. A., Campbell, J., and Stephenson, T. (2013). A review of observed and projected changes in climate for the islands in the Caribbean. *Atmósfera* 26, 283–309. doi:10.1016/S0187-6236(13)71076-2.
Kasoar, M., Shawki, D., and Voulgarakis, A. (2018). Similar spatial patterns of global climate response to aerosols from different regions. *npj Clim. Atmos. Sci.* 1, 12. doi:10.1038/s41612-018-0022-z.
Kawase, H., Hara, M., Yoshikane, T., Ishizaki, N. N., Uno, F., Hatsushika, H., et al. (2013). Altitude dependency of future snow cover changes over Central Japan evaluated by a regional climate model. *J. Geophys. Res. Atmos.* doi:10.1002/2013JD020429.
Kawase, H., Yoshikane, T., Hara, M., Fujita, M., Ishizaki, N. N., Kimura, F., et al. (2012). Downscaling of Snow Cover Changes in the Late 20th Century Using a Past Climate Simulation Method over Central Japan. *SOLA* 8, 61–64. doi:10.2151/sola.2012-016.
Kawazoe, S., and Gutowski, W. J. (2013). Regional, Very Heavy Daily Precipitation in NARCCAP Simulations. *J. Hydrometeorol.* 14, 1212–1227. doi:10.1175/JHM-D-12-068.1.
Kay, J. E., Deser, C., Phillips, A., Mai, A., Hannay, C., Strand, G., et al. (2015). The Community Earth System Model (CESM) Large Ensemble Project: A Community Resource for Studying Climate Change in the Presence of

Internal Climate Variability. *Bull. Am. Meteorol. Soc.* 96, 1333–1349. doi:10.1175/BAMS-D-13-00255.1.
Keller, M., Fuhrer, O., Schmidli, J., Stengel, M., Stöckli, R., and Schär, C. (2016). Evaluation of convection-resolving models using satellite data: The diurnal cycle of summer convection over the Alps. *Meteorol. Zeitschrift* 25, 165–179. doi:10.1127/metz/2015/0715.
Keller, M., Kröner, N., Fuhrer, O., Lüthi, D., Schmidli, J., Stengel, M., et al. (2018). The sensitivity of Alpine summer convection to surrogate climate change: an intercomparison between convection-parameterizing and convection-resolving models. *Atmos. Chem. Phys.* 18, 5253–5264. doi:10.5194/acp-18-5253-2018.
Kendon, E. J., Ban, N., Roberts, N. M., Fowler, H. J., Roberts, M. J., Chan, S. C., et al. (2017). Do Convection-Permitting Regional Climate Models Improve Projections of Future Precipitation Change? *Bull. Am. Meteorol. Soc.* 98, 79–93. doi:10.1175/BAMS-D-15-0004.1.
Kendon, E. J., Roberts, N. M., Fowler, H. J., Roberts, M. J., Chan, S. C., and Senior, C. A. (2014). Heavier summer downpours with climate change revealed by weather forecast resolution model. *Nat. Clim. Chang.* 4, 570. Available at: http://dx.doi.org/10.1038/nclimate2258.
Kerkhoff, C., Künsch, H. R., and Schär, C. (2014). Assessment of Bias Assumptions for Climate Models. *J. Clim.* 27, 6799–6818. doi:10.1175/JCLI-D-13-00716.1.
Kerr, Y. H., Waldteufel, P., Richaume, P., Wigneron, J. P., Ferrazzoli, P., Mahmoodi, A., et al. (2012). The SMOS Soil Moisture Retrieval Algorithm. *IEEE Trans. Geosci. Remote Sens.* 50, 1384–1403. doi:10.1109/TGRS.2012.2184548.
Kharin, V. V., Boer, G. J., Merryfield, W. J., Scinocca, J. F., and Lee, W.-S. (2012). Statistical adjustment of decadal predictions in a changing climate. *Geophys. Res. Lett.* 39, n/a-n/a. doi:10.1029/2012GL052647.
Kida, H., Koide, T., Sasaki, H., and Chiba, M. (1991). A New Approach for Coupling a Limited Area Model to a GCM for Regional Climate Simulations. *J. Meteorol. Soc. Japan. Ser. II* 69, 723–728. doi:10.2151/jmsj1965.69.6_723.
Kikegawa, Y., Genchi, Y., Yoshikado, H., and Kondo, H. (2003). Development of a numerical simulation system toward comprehensive assessments of urban warming countermeasures including their impacts upon the urban buildings' energy-demands. *Appl. Energy*. doi:10.1016/S0306-2619(03)00009-6.
Kim, B.-M., Son, S.-W., Min, S.-K., Jeong, J.-H., Kim, S.-J., Zhang, X., et al. (2014). Weakening of the stratospheric polar vortex by Arctic sea-ice loss. *Nat. Commun.* 5, 4646. doi:10.1038/ncomms5646.
Kim, D., Ahn, M.-S., Kang, I.-S., and Del Genio, A. D. (2015). Role of Longwave Cloud–Radiation Feedback in the Simulation of the Madden–Julian Oscillation. *J. Clim.* 28, 6979–6994. doi:10.1175/JCLI-D-14-00767.1.
Kim, D., and Maloney, E. D. (2017). "Simulation of the Madden-Julian Oscillation Using General Circulation Models," in, 119–130. doi:10.1142/9789813200913_0009.
Kim, H., Kim, Y. K., Song, S. K., and Lee, H. W. (2016). Impact of future urban growth on regional climate changes in the Seoul Metropolitan Area, Korea. *Sci. Total Environ.* 571, 355–363. doi:10.1016/j.scitotenv.2016.05.046.
Kim, Y. H., Min, S. K., Stone, D. A., Shiogama, H., and Wolski, P. (2018). Multi-model event attribution of the summer 2013 heat wave in Korea. *Weather Clim. Extrem.* 20, 33–44. doi:10.1016/j.wace.2018.03.004.
King, A. D., Donat, M. G., Fischer, E. M., Hawkins, E., Alexander, L. V, Karoly, D. J., et al. (2015). The timing of anthropogenic emergence in simulated climate extremes. *Environ. Res. Lett.* 10, 094015. doi:10.1088/1748-9326/10/9/094015.
Kirillin, G., Leppäranta, M., Terzhevik, A., Granin, N., Bernhardt, J., Engelhardt, C., et al. (2012). Physics of seasonally ice-covered lakes: a review. *Aquat. Sci.* 74, 659–682. doi:10.1007/s00027-012-0279-y.
Kirtman, B. P., Bitz, C., Bryan, F., Collins, W., Dennis, J., Hearn, N., et al. (2012). Impact of ocean model resolution on CCSM climate simulations. *Clim. Dyn.* 39, 1303–1328. doi:10.1007/s00382-012-1500-3.
Kirtman, B., Power, S., Adedoyin, J., Boer, G., Bojariu, R., Camilloni, I., et al. (2014). IPCC Assessment Report 2014. Near-term Climate Change Projections and Predictability. 982–985. doi:10.1017/CBO9781107415324.023.
Kitoh, A. (2017). The Asian Monsoon and its Future Change in Climate Models: A Review. *J. Meteorol. Soc. Japan. Ser. II* 95, 7–33. doi:10.2151/jmsj.2017-002.
Kitoh, A., Endo, H., Krishna Kumar, K., Cavalcanti, I. F. A., Goswami, P., and Zhou, T. (2013a). Monsoons in a changing world: A regional perspective in a global context. *J. Geophys. Res. Atmos.* 118, 3053–3065. doi:10.1002/jgrd.50258.
Kitoh, A., Endo, H., Krishna Kumar, K., Cavalcanti, I. F. A., Goswami, P., and Zhou, T. (2013b). Monsoons in a changing world: A regional perspective in a global context. *J. Geophys. Res. Atmos.* 118, 3053–3065. doi:10.1002/jgrd.50258.
Kjellström, E., Bärring, L., Nikulin, G., Nilsson, C., Persson, G., and Strandberg, G. (2016). Production and use of regional climate model projections – A Swedish perspective on building climate services. *Clim. Serv.* 2–3, 15–29. doi:10.1016/j.cliser.2016.06.004.
Kjellström, E., Döscher, R., and Meier, H. E. M. (2005). Atmospheric response to different sea surface temperatures in the Baltic Sea: coupled versus uncoupled regional climate model experiments. *Hydrol. Res.* 36, 397–409. doi:10.2166/nh.2005.0030.
Kjellström, E., Nikulin, G., Strandberg, G., Christensen, O. B., Jacob, D., Keuler, K., et al. (2018). European climate change at global mean temperature increases of 1.5 and 2 °C above pre-industrial conditions as simulated by the EURO-CORDEX regional climate models. *Earth Syst. Dyn.* 9, 459–478. doi:10.5194/esd-9-459-2018.

Kjellström, E., Thejll, P., Rummukainen, M., Christensen, J., Boberg, F., Christensen, O., et al. (2013). Emerging regional climate change signals for Europe under varying large-scale circulation conditions. *Clim. Res.* 56, 103–119. doi:10.3354/cr01146.
Klein, F., and Goosse, H. (2018). Reconstructing East African rainfall and Indian Ocean sea surface temperatures over the last centuries using data assimilation. *Clim. Dyn.* 50, 3909–3929. doi:10.1007/s00382-017-3853-0.
Knaff, J. (1997). Implications of Summertime Sea Level Pressure Anomalies in the Tropical Atlantic Region. 789–804.
Knist, S., Goergen, K., Buonomo, E., Christensen, O. B., Colette, A., Cardoso, R. M., et al. (2017). Land-atmosphere coupling in EURO-CORDEX evaluation experiments. *J. Geophys. Res. Atmos.* 122, 79–103. doi:10.1002/2016JD025476.
Knutti, R., Arblaster, J., Dufresne, J., Fichefet, T., Friedlingstein, P., Gao, X., et al. (2013). Long-term Climate Change: Projections, Commitments and Irreversibility. doi:10.1002/mds.26688.
Knutti, R., Furrer, R., Tebaldi, C., Cermak, J., and Meehl, G. A. (2010). Challenges in combining projections from multiple climate models. *J. Clim.* 23, 2739–2758. doi:10.1175/2009JCLI3361.1.
Knutti, R., Sedláček, J., Sanderson, B. M., Lorenz, R., Fischer, E. M., and Eyring, V. (2017). A climate model projection weighting scheme accounting for performance and interdependence. *Geophys. Res. Lett.* doi:10.1002/2016GL072012.
Kobayashi, S., Ota, Y., Harada, Y., Ebita, A., Moriya, M., Onoda, H., et al. (2015). The JRA-55 Reanalysis: General Specifications and Basic Characteristics. *J. Meteorol. Soc. Japan. Ser. II* 93, 5–48. doi:10.2151/jmsj.2015-001.
Kok, K., Bärlund, I., Flörke, M., Holman, I., Gramberger, M., Sendzimir, J., et al. (2014). European participatory scenario development: strengthening the link between stories and models. *Clim. Change* 128, 187–200. doi:10.1007/s10584-014-1143-y.
Kosaka, Y., and Xie, S.-P. (2016). The tropical Pacific as a key pacemaker of the variable rates of global warming. *Nat. Geosci.* 9, 669–673. doi:10.1038/ngeo2770.
Kosaka, Y., and Xie, S. P. (2013). Recent global-warming hiatus tied to equatorial Pacific surface cooling. *Nature*. doi:10.1038/nature12534.
Koskinen, J. T., Poutiainen, J., Schultz, D. M., Joffre, S., Koistinen, J., Saltikoff, E., et al. (2011). The Helsinki Testbed: A Mesoscale Measurement, Research, and Service Platform. *Bull. Am. Meteorol. Soc.* 92, 325–342. doi:10.1175/2010BAMS2878.1.
Koster, R. D. (2004). Regions of Strong Coupling Between Soil Moisture and Precipitation. *Science (80-. ).* 305, 1138–1140. doi:10.1126/science.1100217.
Kotlarski, S., Keuler, K., Christensen, O. B., Colette, A., Déqué, M., Gobiet, A., et al. (2014a). Regional climate modeling on European scales: a joint standard evaluation of the EURO-CORDEX RCM ensemble. *Geosci. Model Dev.* 7, 1297–1333. doi:10.5194/gmd-7-1297-2014.
Kotlarski, S., Keuler, K., Christensen, O. B., Colette, A., Déqué, M., Gobiet, A., et al. (2014b). Regional climate modeling on European scales: A joint standard evaluation of the EURO-CORDEX RCM ensemble. *Geosci. Model Dev.* 7, 1297–1333. doi:10.5194/gmd-7-1297-2014.
Kotlarski, S., Lüthi, D., and Schär, C. (2015). The elevation dependency of 21st century European climate change: an RCM ensemble perspective. *Int. J. Climatol.* 35, 3902–3920. doi:10.1002/joc.4254.
Kotlarski, S., Szabó, P., Herrera, S., Räty, O., Keuler, K., Soares, P. M., et al. (2017a). Observational uncertainty and regional climate model evaluation: a pan-European perspective. *Int. J. Climatol.* 0. doi:10.1002/joc.5249.
Kotlarski, S., Szabó, P., Herrera, S., Räty, O., Keuler, K., Soares, P. M., et al. (2017b). Observational uncertainty and regional climate model evaluation: a pan-European perspective. *Int. J. Climatol.* doi:10.1002/joc.5249.
Krähenmann S., and Walter, A., and Brienen S., and Imbery F., and and Matzarakis A (2018). High-resolution grids of hourly meteorological variables for Germany. *Theor. Appl. Climatol.* 131, 899–926. doi:10.1007/s00704-016-2003-7.
Krinner, G., Beaumet, J., Favier, V., Déqué, M., and Brutel-Vuilmet, C. (2019). Empirical Run-Time Bias Correction for Antarctic Regional Climate Projections With a Stretched-Grid AGCM. *J. Adv. Model. Earth Syst.* 11, 64–82. doi:10.1029/2018MS001438.
Krinner, G., and Flanner, M. G. (2018). Striking stationarity of large-scale climate model bias patterns under strong climate change. *Proc. Natl. Acad. Sci.* 115, 9462–9466. doi:10.1073/pnas.1807912115.
Krinner, G., and Genthon, C. (1998). GCM simulations of the Last Glacial Maximum surface climate of Greenland and Antarctica. *Clim. Dyn.* 14, 741–758. doi:10.1007/s003820050252.
Krinner, G., Largeron, C., Ménégoz, M., Agosta, C., and Brutel-Vuilmet, C. (2014). Oceanic Forcing of Antarctic Climate Change: A Study Using a Stretched-Grid Atmospheric General Circulation Model. *J. Clim.* 27, 5786–5800. doi:10.1175/JCLI-D-13-00367.1.
Krishnamurthy, L., and Krishnamurthy, V. (2016). Teleconnections of Indian monsoon rainfall with AMO and Atlantic tripole. *Clim. Dyn.* 46, 2269–2285. doi:10.1007/s00382-015-2701-3.
Krishnamurti, T. N., Krishnamurti, R., Das, S., Kumar, V., Jayakumar, A., and Simon, A. (2015). A Pathway Connecting the Monsoonal Heating to the Rapid Arctic Ice Melt*. *J. Atmos. Sci.* 72, 5–34. doi:10.1175/JAS-D-14-0004.1.
Krishnan, R., Sabin, T. P., Madhura, R. K., Vellore, R. K., Mujumdar, M., Sanjay, J., et al. (2018). Non-monsoonal

precipitation response over the Western Himalayas to climate change. *Clim. Dyn.* doi:10.1007/s00382-018-4357-2.

Krishnan, R., Sabin, T. P., Vellore, R., Mujumdar, M., Sanjay, J., Goswami, B. N., et al. (2016). Deciphering the desiccation trend of the South Asian monsoon hydroclimate in a warming world. *Clim. Dyn.* 47, 1007–1027. doi:10.1007/s00382-015-2886-5.

Krishnan, R., Shrestha, A. B., Ren, G., Rajbhandari, R., Saeed, S., Sanjay, J., et al. (2019). "Unravelling Climate Change in the Hindu Kush Himalaya: Rapid Warming in the Mountains and Increasing Extremes BT - The Hindu Kush Himalaya Assessment: Mountains, Climate Change, Sustainability and People," in, eds. P. Wester, A. Mishra, A. Mukherji, and A. B. Shrestha (Cham: Springer International Publishing), 57–97. doi:10.1007/978-3-319-92288-1_3.

Krishnan, R., and Sugi, M. (2003). Pacific decadal oscillation and variability of the Indian summer monsoon rainfall. *Clim. Dyn.* 21, 233–242. doi:10.1007/s00382-003-0330-8.

Kröner, N., Kotlarski, S., Fischer, E., Lüthi, D., Zubler, E., and Schär, C. (2017). Separating climate change signals into thermodynamic, lapse-rate and circulation effects: theory and application to the European summer climate. *Clim. Dyn.* 48, 3425–3440. doi:10.1007/s00382-016-3276-3.

Kruger, A. C., and Nxumalo, M. P. (2017). Historical rainfall trends in South Africa: 1921–2015. *Water SA* 43, 285. doi:10.4314/wsa.v43i2.12.

Kruger, A. C., and Shongwe, S. (2004). Temperature trends in South Africa: 1960-2003. *Int. J. Climatol.* 24, 1929–1945. doi:10.1002/joc.1096.

Kuang, W. (2019). New evidences on anomalous phenomenon of buildings in regulating urban climate from observations in Beijing , China. *Earth Sp. Sci.* minor revi.

Kubota, T., Shige, S., Hashizume, H., Aonashi, K., Takahashi, N., Seto, S., et al. (2007). Global Precipitation Map Using Satellite-Borne Microwave Radiometers by the GSMaP Project: Production and Validation. *IEEE Trans. Geosci. Remote Sens.* doi:10.1109/TGRS.2007.895337.

Kucharski, F., Kang, I.-S., Straus, D., and King, M. P. (2010). Teleconnections in the Atmosphere and Oceans. *Bull. Am. Meteorol. Soc.* 91, 381–383. doi:10.1175/2009BAMS2834.1.

Kug, J.-S., Jeong, J.-H., Jang, Y.-S., Kim, B.-M., Folland, C. K., Min, S.-K., et al. (2015). Two distinct influences of Arctic warming on cold winters over North America and East Asia. *Nat. Geosci.* 8, 759–762. doi:10.1038/ngeo2517.

Kumar, P., Kotlarski, S., Moseley, C., Sieck, K., Frey, H., Stoffel, M., et al. (2015). Response of Karakoram-Himalayan glaciers to climate variability and climatic change: A regional climate model assessment. *Geophys. Res. Lett.* doi:10.1002/2015GL063392.

Kumar, S., Kinter, J. L., Pan, Z., and Sheffield, J. (2016). Twentieth century temperature trends in CMIP3, CMIP5, and CESM-LE climate simulations: Spatial-temporal uncertainties, differences, and their potential sources. *J. Geophys. Res. Atmos.* 121, 9561–9575. doi:10.1002/2015JD024382.

Kuppel, S., Houspanossian, J., Nosetto, M. D., and Jobbágy, E. G. (2015). What does it take to flood the Pampas?: Lessons from a decade of strong hydrological fluctuations. *Water Resour. Res.* 51, 2937–2950. doi:10.1002/2015WR016966.

Kurihara, Y., Murakami, H., and Kachi, M. (2016). Sea surface temperature from the new Japanese geostationary meteorological Himawari-8 satellite. *Geophys. Res. Lett.* 43, 1234–1240. doi:10.1002/2015GL067159.

Kusaka, H., Chen, F., Tewari, M., Dudhia, J., Gill, D. O., Duda, M. G., et al. (2012). Numerical Simulation of Urban Heat Island Effect by the WRF Model with 4-km Grid Increment: An Inter-Comparison Study between the Urban Canopy Model and Slab Model. *J. Meteorol. Soc. Japan. Ser. II*. doi:10.2151/jmsj.2012-B03.

KUSAKA, H., HARA, M., and TAKANE, Y. (2012). Urban Climate Projection by the WRF Model at 3-km Horizontal Grid Increment: Dynamical Downscaling and Predicting Heat Stress in the 2070^|^rsquo;s August for Tokyo, Osaka, and Nagoya Metropolises. *J. Meteorol. Soc. Japan. Ser. II* 90B, 47–63. doi:10.2151/jmsj.2012-B04.

Kusaka, H., Kondo, H., Kikegawa, Y., and Kimura, F. (2001). A simple single-layer urban canopy model for atmospheric models: Comparison with multi-layer and slab models. *Boundary-Layer Meteorol.* doi:10.1023/A:1019207923078.

Kusaka, H., Nawata, K., Suzuki-Parker, A., Takane, Y., and Furuhashi, N. (2014). Mechanism of Precipitation Increase with Urbanization in Tokyo as Revealed by Ensemble Climate Simulations. *J. Appl. Meteorol. Climatol.* 53, 824–839. doi:10.1175/JAMC-D-13-065.1.

Kusaka, H., Suzuki-Parker, A., Aoyagi, T., Adachi, S. A., and Yamagata, Y. (2016). Assessment of RCM and urban scenarios uncertainties in the climate projections for August in the 2050s in Tokyo. *Clim. Change* 137, 427–438. doi:10.1007/s10584-016-1693-2.

Kushnir, Y., Scaife, A. A., Arritt, R., Balsamo, G., Boer, G., Doblas-Reyes, F., et al. (2019a). Towards operational predictions of the near-term climate. *Nat. Clim. Chang.* doi:10.1038/s41558-018-0359-7.

Kushnir, Y., Scaife, A. A., Arritt, R., Balsamo, G., Boer, G., Doblas-Reyes, F., et al. (2019b). Towards operational predictions of the near-term climate. *Nat. Clim. Chang.* 9, 94–101. doi:10.1038/s41558-018-0359-7.

Kwon, M. H., Jhun, J. G., and Ha, K. J. (2007). Decadal change in east Asian summer monsoon circulation in the mid-1990s. *Geophys. Res. Lett.* doi:10.1029/2007GL031977.

Labbé, D., and Boudreau, J.-A. (2015). Local Integration Experiments in the New Urban Areas of Hanoi. *South East Asia Res.* 23, 245–262. doi:10.5367/sear.2015.0259.
Lackmann, G. M. (2015). Hurricane Sandy before 1900 and after 2100. *Bull. Am. Meteorol. Soc.* 96, 547–560. doi:10.1175/BAMS-D-14-00123.1.
Lafaysse, M., Hingray, B., Mezghani, A., Gailhard, J., and Terray, L. (2014). Internal variability and model uncertainty components in future hydrometeorological projections: The Alpine Durance basin. *Water Resour. Res.* 50, 3317–3341. doi:10.1002/2013WR014897.
Lagabrielle, E., Lombard, A. T., Harris, J. M., and Livingstone, T. C. (2018). Multi-scale multi-level marine spatial planning: A novel methodological approach applied in south africa. *PLoS One* 13, 1–29. doi:10.1371/journal.pone.0192582.
Laloyaux, P., de Boisseson, E., Balmaseda, M., Bidlot, J.-R., Broennimann, S., Buizza, R., et al. (2018). CERA-20C: A Coupled Reanalysis of the Twentieth Century. *J. Adv. Model. Earth Syst.* 10, 1172–1195. doi:10.1029/2018MS001273.
Lamb, M. (2017). *Ethics for Climate Change Communicators*. Oxford University Press doi:10.1093/acrefore/9780190228620.013.564.
Langenbrunner, B., and Neelin, J. D. (2013). Analyzing ENSO Teleconnections in CMIP Models as a Measure of Model Fidelity in Simulating Precipitation. *J. Clim.* 26, 4431–4446. doi:10.1175/JCLI-D-12-00542.1.
Langendijk, G. S., Aubry-Wake, C., Osman, M., Gulizia, C., Attig-Bahar, F., Behrens, E., et al. (2019). Three Ways Forward to Improve Regional Information for Extreme Events: An Early Career Perspective. *Front. Environ. Sci.* 7. doi:10.3389/fenvs.2019.00006.
Langhans, W., Schmidli, J., Fuhrer, O., Bieri, S., and Schär, C. (2013). Long-Term Simulations of Thermally Driven Flows and Orographic Convection at Convection-Parameterizing and Cloud-Resolving Resolutions. *J. Appl. Meteorol. Climatol.* 52, 1490–1510. doi:10.1175/JAMC-D-12-0167.1.
Langodan, S., Cavaleri, L., Vishwanadhapalli, Y., Pomaro, A., Bertotti, L., and Hoteit, I. (2017). The climatology of the Red Sea – part 1: the wind. *Int. J. Climatol.* 37, 4509–4517. doi:10.1002/joc.5103.
Laprise, R. (2014). Comment on "The added value to global model projections of climate change by dynamical downscaling: A case study over the continental U.S. using the GISS-ModelE2 and WRF models" by Racherla et al. *J. Geophys. Res. Atmos.* 119, 3877–3881. doi:10.1002/2013JD019945.
Laprise, R., Hernández-Díaz, L., Tete, K., Sushama, L., Šeparović, L., Martynov, A., et al. (2013). Climate projections over CORDEX Africa domain using the fifth-generation Canadian Regional Climate Model (CRCM5). *Clim. Dyn.* 41, 3219–3246. doi:10.1007/s00382-012-1651-2.
Latif, M., Hannachi, A., and Syed, F. S. (2018). Analysis of rainfall trends over Indo-Pakistan summer monsoon and related dynamics based on CMIP5 climate model simulations. *Int. J. Climatol.* 38, e577–e595. doi:10.1002/joc.5391.
Lau, K.-M., and Kim, K.-M. (2006). Observational relationships between aerosol and Asian monsoon rainfall, and circulation. *Geophys. Res. Lett.* 33, L21810. doi:10.1029/2006GL027546.
Lau, W. (2014). Desert dust and monsoon rain. *Nat. Geosci.* 7, 255–256. doi:10.1038/ngeo2115.
Lau, W. K. M., and Kim, K. M. (2018). Impact of snow darkening by deposition of light-absorbing aerosols on snow cover in the Himalayas-Tibetan Plateau and influence on the Asian summer monsoon: A possible mechanism for the blanford hypothesis. *Atmosphere (Basel).* 9. doi:10.3390/atmos9110438.
Lauwaet, D., Hooyberghs, H., Maiheu, B., Lefebvre, W., Driesen, G., Van Looy, S., et al. (2015). Detailed Urban Heat Island Projections for Cities Worldwide: Dynamical Downscaling CMIP5 Global Climate Models. *Climate* 3, 391–415. doi:10.3390/cli3020391.
Lavaysse, C., Flamant, C., Evan, A., Janicot, S., and Gaetani, M. (2016). Recent climatological trend of the Saharan heat low and its impact on the West African climate. *Clim. Dyn.* doi:10.1007/s00382-015-2847-z.
Lavers, D. A., Allan, R. P., Villarini, G., Lloyd-Hughes, B., Brayshaw, D. J., and Wade, A. J. (2013). Future changes in atmospheric rivers and their implications for winter flooding in Britain. *Environ. Res. Lett.* 8. doi:10.1088/1748-9326/8/3/034010.
Lavers, D. A., and Villarini, G. (2013a). Atmospheric Rivers and Flooding over the Central United States. *J. Clim.* 26, 7829–7836. doi:10.1175/JCLI-D-13-00212.1.
Lavers, D. A., and Villarini, G. (2013b). The nexus between atmospheric rivers and extreme precipitation across Europe. *Geophys. Res. Lett.* 40, 3259–3264. doi:10.1002/grl.50636.
Lawal, K. A., Abatan, A. A., Angélil, O., Olaniyan, E., Olusoji, V. H., Oguntunde, P. G., et al. (2016). 13. The late onset of the 2015 wet season in Nigeria. *Bull. Am. Meteorol. Soc.* 97, S63–S69. doi:10.1175/BAMS-D-16-0131.1.
Lawrence, D. M., Hurtt, G. C., Arneth, A., Brovkin, V., Calvin, K. V., Jones, A. D., et al. (2016). The Land Use Model Intercomparison Project (LUMIP) contribution to CMIP6: rationale and experimental design. *Geosci. Model Dev.* 9, 2973–2998. doi:10.5194/gmd-9-2973-2016.
Lebel, T., and Ali, A. (2009). Recent trends in the Central and Western Sahel rainfall regime (1990-2007). *J. Hydrol.* doi:10.1016/j.jhydrol.2008.11.030.
Lee, D. H. K. (1980). Seventy-five years of searching for a heat index. *Environ. Res.* 22, 331–356. doi:10.1016/0013-9351(80)90146-2.

Lee, H. S., Trihamdani, A. R., Kubota, T., Iizuka, S., and Phuong, T. T. T. (2017). Impacts of land use changes from the Hanoi Master Plan 2030 on urban heat islands: Part 2. Influence of global warming. *Sustain. Cities Soc.* 31, 95–108. doi:https://doi.org/10.1016/j.scs.2017.02.015.

Lee, H. T., Gruber, A., Ellingson, R. G., and Laszlo, I. (2007). Development of the HIRS outgoing longwave radiation climate dataset. *J. Atmos. Ocean. Technol.* doi:10.1175/2007JTECHA989.1.

Lee, J.-W., Hong, S.-Y., Chang, E.-C., Suh, M.-S., and Kang, H.-S. (2014). Assessment of future climate change over East Asia due to the RCP scenarios downscaled by GRIMs-RMP. *Clim. Dyn.* 42, 733–747. doi:10.1007/s00382-013-1841-6.

Lehner, F., Deser, C., and Sanderson, B. M. (2018a). Future risk of record-breaking summer temperatures and its mitigation. *Clim. Change* 146, 363–375. doi:10.1007/s10584-016-1616-2.

Lehner, F., Deser, C., Simpson, I. R., and Terray, L. (2018b). Attributing the U.S. Southwest's Recent Shift Into Drier Conditions. *Geophys. Res. Lett.* 45, 6251–6261. doi:10.1029/2018GL078312.

Lehner, F., Deser, C., and Terray, L. (2017a). Toward a New Estimate of "Time of Emergence" of Anthropogenic Warming: Insights from Dynamical Adjustment and a Large Initial-Condition Model Ensemble. *J. Clim.* 30, 7739–7756. doi:10.1175/JCLI-D-16-0792.1.

Lehner, F., Wahl, E. R., Wood, A. W., Blatchford, D. B., and Llewellyn, D. (2017b). Assessing recent declines in Upper Rio Grande runoff efficiency from a paleoclimate perspective. *Geophys. Res. Lett.* 44, 4124–4133. doi:10.1002/2017GL073253.

Lemonsu, A., Kounkou-Arnaud, R., Desplat, J., Salagnac, J. L., and Masson, V. (2013). Evolution of the Parisian urban climate under a global changing climate. *Clim. Change* 116, 679–692. doi:10.1007/s10584-012-0521-6.

Lemos, M. C., Kirchhoff, C. J., and Ramprasad, V. (2012a). Narrowing the climate information usability gap. *Nat. Clim. Chang.* 2, 789. doi:10.1038/nclimate1614.

Lemos, M. C., Kirchhoff, C. J., and Ramprasad, V. (2012b). Narrowing the climate information usability gap. *Nat. Clim. Chang.* 2, 789–794. doi:10.1038/nclimate1614.

Lempert, R. J., and Collins, M. T. (2007). Managing the Risk of Uncertain Threshold Responses: Comparison of Robust, Optimum, and Precautionary Approaches. *Risk Anal.* 27, 1009–1026. doi:10.1111/j.1539-6924.2007.00940.x.

Lempert, R. J., Groves, D. G., Popper, S. W., and Bankes, S. C. (2006). A General, Analytic Method for Generating Robust Strategies and Narrative Scenarios. *Manage. Sci.* 52, 514–528. doi:10.1287/mnsc.1050.0472.

Lenton, T. M., Held, H., Kriegler, E., Hall, J. W., Lucht, W., Rahmstorf, S., et al. (2008). Tipping elements in the Earth's climate system. *Proc. Natl. Acad. Sci.* 105, 1786–1793. doi:10.1073/pnas.0705414105.

Lenz, C. J., Früh, B., and Adalatpanah, F. D. (2017). Is there potential added value in COSMO–CLM forced by ERA reanalysis data? *Clim. Dyn.* 49, 4061–4074. doi:10.1007/s00382-017-3562-8.

León, L., Lam, D., Schertzer, W., Swayne, D., Imberger, and J (2007). Towards coupling a 3D hydrodynamic lake model with the Canadian Regional Climate Model: Simulation on Great Slave Lake. *Environ. Model. Softw.* 22, 787–796. doi:10.1016/j.envsoft.2006.03.005.

Leonard, M., Westra, S., Phatak, A., Lambert, M., van den Hurk, B., McInnes, K., et al. (2014). A compound event framework for understanding extreme impacts. *Wiley Interdiscip. Rev. Clim. Chang.* 5, 113–128. doi:10.1002/wcc.252.

Letcher, T. W., and Minder, J. R. (2017). The Simulated Response of Diurnal Mountain Winds to Regionally Enhanced Warming Caused by the Snow Albedo Feedback. *J. Atmos. Sci.* 74, 49–67. doi:10.1175/JAS-D-16-0158.1.

Levine, P. A., Randerson, J. T., Swenson, S. C., and Lawrence, D. M. (2016). Evaluating the strength of the land-atmosphere moisture feedback in Earth system models using satellite observations. *Hydrol. Earth Syst. Sci.* 20, 4837–4856. doi:10.5194/hess-20-4837-2016.

Levine, R. C., Turner, A. G., Marathayil, D., and Martin, G. M. (2013). The role of northern Arabian Sea surface temperature biases in CMIP5 model simulations and future projections of Indian summer monsoon rainfall. *Clim. Dyn.* 41, 155–172. doi:10.1007/s00382-012-1656-x.

Levy, A. A. L., Ingram, W., Jenkinson, M., Huntingford, C., Hugo Lambert, F., and Allen, M. (2013). Can correcting feature location in simulated mean climate improve agreement on projected changes? *Geophys. Res. Lett.* 40, 354–358. doi:10.1002/2012GL053964.

Li, B., Gasser, T., Ciais, P., Piao, S., Tao, S., Balkanski, Y., et al. (2016a). The contribution of China's emissions to global climate forcing. *Nature* 531, 357–361. doi:10.1038/nature17165.

Li, C., Stevens, B., and Marotzke, J. (2015a). Eurasian winter cooling in the warming hiatus of 1998-2012. *Geophys. Res. Lett.* 42, 8131–8139. doi:10.1002/2015GL065327.

Li, C., Zwiers, F., Zhang, X., and Li, G. (2018a). How much information is required to well-constrain local estimates of future precipitation extremes? *Earth's Futur.*, 2018EF001001. doi:10.1029/2018EF001001.

Li, D., and Bou-Zeid, E. (2013). Synergistic interactions between urban heat islands and heat waves: The impact in cities is larger than the sum of its parts. *J. Appl. Meteorol. Climatol.* 52, 2051–2064. doi:10.1175/JAMC-D-13-02.1.

Li, D., and Xiao, Z. (2018). Can solar cycle modulate the ENSO effect on the Pacific/North American pattern? *J. Atmos. Solar-Terrestrial Phys.* 167, 30–38. doi:https://doi.org/10.1016/j.jastp.2017.10.007.

Li, F., Orsolini, Y. J., Wang, H., Gao, Y., and He, S. (2018b). Atlantic Multidecadal Oscillation Modulates the Impacts of Arctic Sea Ice Decline. *Geophys. Res. Lett.* 45, 2497–2506. doi:10.1002/2017GL076210.

Li, G., Xie, S.-P., He, C., and Chen, Z. (2017a). Western Pacific emergent constraint lowers projected increase in Indian summer monsoon rainfall. *Nat. Clim. Chang.* 7, 708–712. doi:10.1038/nclimate3387.

Li, H., Cui, X., and Zhang, D.-L. (2017b). Sensitivity of the initiation of an isolated thunderstorm over the Beijing metropolitan region to urbanization, terrain morphology and cold outflows. *Q. J. R. Meteorol. Soc.* 143, 3153–3164. doi:10.1002/qj.3169.

Li, H., Dai, A., Zhou, T., and Lu, J. (2010). Responses of East Asian summer monsoon to historical SST and atmospheric forcing during 1950–2000. *Clim. Dyn.* 34, 501–514. doi:10.1007/s00382-008-0482-7.

Li, H., Haugen, J. E., and Xu, C. Y. (2018c). Precipitation pattern in the Western Himalayas revealed by four datasets. *Hydrol. Earth Syst. Sci.* 22, 5097–5110. doi:10.5194/hess-22-5097-2018.

Li, H., Xu, C. Y., Beldring, S., Tallaksen, L. M., and Jain, S. K. (2016b). Water resources under climate change in himalayan basins. *Water Resour. Manag.* 30, 843–859. doi:10.1007/s11269-015-1194-5.

Li, J., and Wang, B. (2018). Origins of the decadal predictability of East Asian land summer monsoon rainfall. *J. Clim.* doi:10.1175/JCLI-D-17-0790.1.

Li, K., Liao, H., Mao, Y., and Ridley, D. A. (2016c). Source sector and region contributions to concentration and direct radiative forcing of black carbon in China. *Atmos. Environ.* 124, 351–366. doi:10.1016/j.atmosenv.2015.06.014.

Li, M., Mao, Z., Song, Y., Liu, M., and Huang, X. (2015b). Impacts of the decadal urbanization on thermally induced circulations in eastern China. *J. Appl. Meteorol. Climatol.* 54, 259–282. doi:10.1175/JAMC-D-14-0176.1.

Li, W., Li, L., Ting, M., and Liu, Y. (2012). Intensification of Northern Hemisphere subtropical highs in a warming climate. *Nat. Geosci.* 5, 830. Available at: https://doi.org/10.1038/ngeo1590.

Li, X., Mitra, C., Dong, L., and Yang, Q. (2018d). Understanding land use change impacts on microclimate using Weather Research and Forecasting (WRF) model. *Phys. Chem. Earth, Parts A/B/C* 103, 115–126. doi:https://doi.org/10.1016/j.pce.2017.01.017.

Li, X., and Ting, M. (2017). Understanding the Asian summer monsoon response to greenhouse warming: the relative roles of direct radiative forcing and sea surface temperature change. *Clim. Dyn.* 49, 2863–2880. doi:10.1007/s00382-016-3470-3.

Li, Y., Ding, Y., and Li, W. (2017c). Interdecadal variability of the Afro-Asian summer monsoon system. *Adv. Atmos. Sci.* 34, 833–846. doi:10.1007/s00376-017-6247-7.

Li, Z.-X. (1999). Ensemble Atmospheric GCM Simulation of Climate Interannual Variability from 1979 to 1994. *J. Clim.* 12, 986–1001. doi:10.1175/1520-0442(1999)012<0986:EAGSOC>2.0.CO;2.

Li, Z., Lau, W. K.-M., Ramanathan, V., Wu, G., Ding, Y., Manoj, M. G., et al. (2016d). Aerosol and monsoon climate interactions over Asia. *Rev. Geophys.* 54, 866–929. doi:10.1002/2015RG000500.

Liang, P., and Ding, Y. (2017). The long-term variation of extreme heavy precipitation and its link to urbanization effects in Shanghai during 1916–2014. *Adv. Atmos. Sci.* 34, 321–334. doi:10.1007/s00376-016-6120-0.

Liao, W., Wang, D., Liu, X., Wang, G., and Zhang, J. (2017). Estimated influence of urbanization on surface warming in Eastern China using time-varying land use data. *Int. J. Climatol.* 37, 3197–3208. doi:10.1002/joc.4908.

Liew, A. (2007). Understanding Data, Information, Knowledge And Their Inter-Relationships. *J. Knowl. Manag. Pract.* 7. Available at: http://www.tlainc.com/articl134.htm.

Lim, E.-P., Hendon, H. H., Arblaster, J. M., Chung, C., Moise, A. F., Hope, P., et al. (2016a). Interaction of the recent 50 year SST trend and La Niña 2010: amplification of the Southern Annular Mode and Australian springtime rainfall. *Clim. Dyn.* 47, 2273–2291. doi:10.1007/s00382-015-2963-9.

Lim, E.-P., Hendon, H. H., Arblaster, J. M., Delage, F., Nguyen, H., Min, S.-K., et al. (2016b). The impact of the Southern Annular Mode on future changes in Southern Hemisphere rainfall. *Geophys. Res. Lett.* 43, 7160–7167. doi:10.1002/2016GL069453.

Lim, E.-P., Hendon, H. H., and Thompson, D. W. J. (2018). On the Seasonal Evolution and Impacts of Stratosphere-Troposphere Coupling in the Southern Hemisphere. *J. Geophys. Res. Atmos.* doi:10.1029/2018JD029321.

Lim, E.-P. P., and Hendon, H. H. (2015). Understanding and predicting the strong Southern Annular Mode and its impact on the record wet east Australian spring 2010. *Clim. Dyn.* 44, 2807–2824. doi:10.1007/s00382-014-2400-5.

Lin, H., Brunet, G., and Derome, J. (2009). An Observed Connection between the North Atlantic Oscillation and the Madden–Julian Oscillation. *J. Clim.* 22, 364–380. doi:10.1175/2008JCLI2515.1.

Lin, M., and Huybers, P. (2019). If Rain Falls in India and No One Reports It, Are Historical Trends in Monsoon Extremes Biased? *Geophys. Res. Lett.* doi:10.1029/2018GL079709.

Lindau, R., and Venema, V. (2018a). On the reduction of trend errors by the ANOVA joint correction scheme used in homogenization of climate station records. *Int. J. Climatol.* 38, 5255–5271. doi:10.1002/joc.5728.

Lindau, R., and Venema, V. K. C. (2018b). The joint influence of break and noise variance on the break detectioncapability in time series homogenization. *Adv. Stat. Climatol. Meteorol. Oceanogr.* 4, 1–18. doi:10.5194/ascmo-4-1-2018.

Ling, J., Li, C., Li, T., Jia, X., Khouider, B., Maloney, E., et al. (2017). Challenges and Opportunities in MJO Studies. *Bull. Am. Meteorol. Soc.* 98, ES53–ES56. doi:10.1175/BAMS-D-16-0283.1.

Lionello, P., and Scarascia, L. (2018). The relation between climate change in the Mediterranean region and global warming. *Reg. Environ. Chang.* 18, 1481–1493. doi:10.1007/s10113-018-1290-1.
Lipson, M. J., Thatcher, M., Hart, M. A., and Pitman, A. (2018). A building energy demand and urban land surface model. *Q. J. R. Meteorol. Soc.* 144, 1572–1590. doi:10.1002/qj.3317.
Liu, F., Li, J., Wang, B., Liu, J., Li, T., Huang, G., et al. (2018a). Divergent El Niño responses to volcanic eruptions at different latitudes over the past millennium. *Clim. Dyn.* 50, 3799–3812. doi:10.1007/s00382-017-3846-z.
Liu, F., Xing, C., Sun, L., Wang, B., Chen, D., and Liu, J. (2018b). How Do Tropical, Northern Hemispheric, and Southern Hemispheric Volcanic Eruptions Affect ENSO Under Different Initial Ocean Conditions? *Geophys. Res. Lett.*, 2018GL080315. doi:10.1029/2018GL080315.
Liu, J., Xu, H., and Deng, J. (2018c). Projections of East Asian summer monsoon change at global warming of 1 . 5 and 2 ◦ C. *Earth Syst. Dynam.* 9, 427–439. doi:10.5194/esd-9-427-2018.
Liu, L., Shawki, D., Voulgarakis, A., Kasoar, M., Samset, B. H., Myhre, G., et al. (2018d). A PDRMIP Multimodel Study on the Impacts of Regional Aerosol Forcings on Global and Regional Precipitation. *J. Clim.* 31, 4429–4447. doi:10.1175/JCLI-D-17-0439.1.
Liu, L., Zhang, R., and Zuo, Z. (2016). The Relationship between Soil Moisture and LAI in Different Types of Soil in Central Eastern China. *J. Hydrometeorol.* 17, 2733–2742. doi:10.1175/JHM-D-15-0240.1.
Liu, Y., Chen, F., Warner, T., and Basara, J. (2006). Verification of a Mesoscale Data-Assimilation and Forecasting System for the Oklahoma City Area during the Joint Urban 2003 Field Project. *J. Appl. Meteorol. Climatol.* 45, 912–929. doi:10.1175/JAM2383.1.
Liu, Y., Wang, L., Zhou, W., and Chen, W. (2014a). Three Eurasian teleconnection patterns: spatial structures, temporal variability, and associated winter climate anomalies. *Clim. Dyn.* 42, 2817–2839. doi:10.1007/s00382-014-2163-z.
Liu, Z., Yoshimura, K., Buenning, N. H., and He, X. (2014b). Solar cycle modulation of the Pacific{\textendash}North American teleconnection influence on North American winter climate. *Environ. Res. Lett.* 9, 24004. doi:10.1088/1748-9326/9/2/024004.
Llopart, M., Coppola, E., Giorgi, F., da Rocha, R. P., and Cuadra, S. V (2014). Climate change impact on precipitation for the Amazon and La Plata basins. *Clim. Change* 125, 111–125. doi:10.1007/s10584-014-1140-1.
Lorenz, P., and Jacob, D. (2005). Influence of regional scale information on the global circulation: A two-way nesting climate simulation. *Geophys. Res. Lett.* 32, n/a-n/a. doi:10.1029/2005GL023351.
Lorenz, P., and Jacob, D. (2010). Validation of temperature trends in the ENSEMBLES regional climate model runs driven by ERA40. *Clim. Res.* 44, 167–177. doi:10.3354/cr00973.
Lorenz, R., Argüeso, D., Donat, M. G., Pitman, A. J., van den Hurk, B., Berg, A., et al. (2016). Influence of land-atmosphere feedbacks on temperature and precipitation extremes in the GLACE-CMIP5 ensemble. *J. Geophys. Res. Atmos.* 121, 607–623. doi:10.1002/2015JD024053.
Lourenço, T. C., Swart, R., Goosen, H., and Street, R. (2016). The rise of demand-driven climate services. *Nat. Clim. Chang.* 6, 13–14. doi:10.1038/nclimate2836.
Louw, P., and Boonzaaier, J. (2018). DROUGHT POLICY BRIEF WESTERN CAPE AGRICULTURE. Die Wilgers, South Africa Available at: www.bfap.co.za.
Lovejoy, S. (2013). Lovejoy_2013_WhatIsClimate. 94, 4–6.
Lovino, M. A., Müller, O. V, Berbery, E. H., and Müller, G. V (2018). Evaluation of CMIP5 retrospective simulations of temperature and precipitation in northeastern Argentina. *Int. J. Climatol.* 38, e1158–e1175. doi:10.1002/joc.5441.
Lu, Y., and Kueppers, L. (2015). Increased heat waves with loss of irrigation in the United States. *Environ. Res. Lett.* 10, 64010. Available at: http://stacks.iop.org/1748-9326/10/i=6/a=064010.
Lucas-Picher, P., Christensen, J. H., Saeed, F., Kumar, P., Asharaf, S., Ahrens, B., et al. (2011). Can Regional Climate Models Represent the Indian Monsoon? *J. Hydrometeorol.* 12, 849–868. doi:10.1175/2011JHM1327.1.
Lucas-Picher, P., Laprise, R., and Winger, K. (2017). Evidence of added value in North American regional climate model hindcast simulations using ever-increasing horizontal resolutions. *Clim. Dyn.* 48, 2611–2633. doi:10.1007/s00382-016-3227-z.
Lucas, C., Timbal, B., and Nguyen, H. (2014). The expanding tropics: a critical assessment of the observational and modeling studies. *Wiley Interdiscip. Rev. Clim. Chang.* 5, 89–112. doi:10.1002/wcc.251.
Luo, D., Yao, Y., Dai, A., Simmonds, I., and Zhong, L. (2017). Increased quasi stationarity and persistence of winter ural blocking and Eurasian extreme cold events in response to arctic warming. Part II: A theoretical explanation. *J. Clim.* doi:10.1175/JCLI-D-16-0262.1.
Luterbacher, J., Werner, J. P., Smerdon, J. E., Fernández-Donado, L., González-Rouco, F. J., Barriopedro, D., et al. (2016). European summer temperatures since Roman times. *Environ. Res. Lett.* 11, 024001. doi:10.1088/1748-9326/11/2/024001.
Lutz, A. F., Immerzeel, W. W., Biemans, H., ter Maat, H., Veldore, V., and Shrestha, A. (2016a). Selection of Climate Models for Developing Representative Climate Projections for the Hindu Kush Himalayan Region. *Hi-Aware*, 46.
Lutz, A. F., ter Maat, H. W., Biemans, H., Shrestha, A. B., Wester, P., and Immerzeel, W. W. (2016b). Selecting representative climate models for climate change impact studies: an advanced envelope-based selection approach.

*Int. J. Climatol.* 36, 3988–4005. doi:10.1002/joc.4608.
Lyu, K., Zhang, X., Church, J. A., and Hu, J. (2015). Quantifying internally generated and externally forced climate signals at regional scales in CMIP5 models. *Geophys. Res. Lett.* 42, 9394–9403. doi:10.1002/2015GL065508.
Ma, S., Pitman, A., Hart, M., Evans, J. P., Haghdadi, N., and MacGill, I. (2017). The impact of an urban canopy and anthropogenic heat fluxes on Sydney's climate. *Int. J. Climatol.* 37, 255–270. doi:10.1002/joc.5001.
Macias, D., Garcia-Gorriz, E., Dosio, A., Stips, A., and Keuler, K. (2018). Obtaining the correct sea surface temperature: bias correction of regional climate model data for the Mediterranean Sea. *Clim. Dyn.* 51, 1095–1117. doi:10.1007/s00382-016-3049-z.
Macias, D., Garcia-Gorriz, E., and Stips, A. (2013). Understanding the Causes of Recent Warming of Mediterranean Waters. How Much Could Be Attributed to Climate Change? *PLoS One* 8, e81591. doi:10.1371/journal.pone.0081591.
MacKellar, N., New, M., and Jack, C. (2014). Observed and modelled trends in rainfall and temperature for South Africa: 1960–2010. *S. Afr. J. Sci.* 110, 1–13. doi:10.1590/sajs.2014/20130353.
Madden, R. A., and Julian, P. R. (1971). Detection of a 40–50 Day Oscillation in the Zonal Wind in the Tropical Pacific. *J. Atmos. Sci.* 28, 702–708. doi:10.1175/1520-0469(1971)028<0702:DOADOI>2.0.CO;2.
Madhusoodhanan, C. G., Shashikanth, K., Eldho, T. I., and Ghosh, S. (2018). Can statistical downscaling improve consensus among CMIP5 models for Indian summer monsoon rainfall projections? *Int. J. Climatol.* 38, 2449–2461. doi:10.1002/joc.5352.
Magana, V., Amador, J., and Medina, S. (1999). The Midsummer Drought over Mexico and Central America. 1577–1588.
Magnusson, L., Alonso-Balmaseda, M., Corti, S., Molteni, F., and Stockdale, T. (2013). Evaluation of forecast strategies for seasonal and decadal forecasts in presence of systematic model errors. *Clim. Dyn.* 41, 2393–2409. doi:10.1007/s00382-012-1599-2.
Maher, N., Milinski, S., Suarez-Gutierrez, L., Botzet, M., Kornblueh, L., Takano, Y., et al. (2019). The Max Planck Institute Grand Ensemble – Enabling the Exploration of Climate System Variability. *J. Adv. Model. Earth Syst.*
Mahlalela, P. T., Blamey, R. C., and Reason, C. J. C. (2018). Mechanisms behind early winter rainfall variability in the southwestern Cape, South Africa. *Clim. Dyn.* doi:10.1007/s00382-018-4571-y.
Mahlstein, I., Hegerl, G., and Solomon, S. (2012). Emerging local warming signals in observational data. *Geophys. Res. Lett.* 39, n/a-n/a. doi:10.1029/2012GL053952.
Mahmood, R., Pielke, R. A., Hubbard, K. G., Niyogi, D., Dirmeyer, P. A., Mcalpine, C., et al. (2014). Land cover changes and their biogeophysical effects on climate. *Int. J. Climatol.* 34, 929–953. doi:10.1002/joc.3736.
Mahmood, S., Davie, J., Jermey, P., Renshaw, R., George, J. P., Rajagopal, E. N., et al. (2018). Indian monsoon data assimilation and analysis regional reanalysis: Configuration and performance. *Atmos. Sci. Lett.* 19, e808. doi:10.1002/asl.808.
Mahoney, K., Jackson, D. L., Neiman, P., Hughes, M., Darby, L., Wick, G., et al. (2016). Understanding the Role of Atmospheric Rivers in Heavy Precipitation in the Southeast United States. *Mon. Weather Rev.* 144, 1617–1632. doi:10.1175/mwr-d-15-0279.1.
Maidment, R. I., Allan, R. P., and Black, E. (2015). Recent observed and simulated changes in precipitation over Africa. *Geophys. Res. Lett.* 42, 8155–8164. doi:10.1002/2015GL065765.
Maidment, R. I., Grimes, D., Allan, R. P., Tarnavsky, E., Stringer, M., Hewison, T., et al. (2014). The 30 year TAMSAT African Rainfall Climatology And Time series (TARCAT) data set. *J. Geophys. Res. Atmos.* 119, 10, 610–619, 644. doi:10.1002/2014JD021927.
Mallard, M. S., Nolte, C. G., Bullock, O. R., Spero, T. L., and Gula, J. (2014). Using a coupled lake model with WRF for dynamical downscaling. *J. Geophys. Res. Atmos.* 119, 7193–7208. doi:10.1002/2014JD021785.
Mallet, M., Dulac, F., Formenti, P., Nabat, P., Sciare, J., Roberts, G., et al. (2016). Overview of the Chemistry-Aerosol Mediterranean Experiment/Aerosol Direct Radiative Forcing on the Mediterranean Climate (ChArMEx/ADRIMED) summer 2013 campaign. *Atmos. Chem. Phys.* 16, 455–504. doi:10.5194/acp-16-455-2016.
Mankin, J. S., Smerdon, J. E., Cook, B. I., Williams, A. P., and Seager, R. (2017). The Curious Case of Projected Twenty-First-Century Drying but Greening in the American West. *J. Clim.* 30, 8689–8710. doi:10.1175/jcli-d-17-0213.1.
Mann, M. E., Rahmstorf, S., Kornhuber, K., Steinman, B. A., Miller, S. K., Petri, S., et al. (2018). Projected changes in persistent extreme summer weather events: The role of quasi-resonant amplification. *Sci. Adv.* 4, eaat3272. doi:10.1126/sciadv.aat3272.
Manoli, G., Ivanov, V. Y., and Fatichi, S. (2018). Dry-Season Greening and Water Stress in Amazonia: The Role of Modeling Leaf Phenology. *J. Geophys. Res. Biogeosciences* 123, 1909–1926. doi:10.1029/2017JG004282.
Manz, B., Buytaert, W., Zulkafli, Z., Lavado, W., Willems, B., Robles, L. A., et al. (2016). High-resolution satellite-gauge merged precipitation climatologies of the Tropical Andes. *J. Geophys. Res. Atmos.* 121, 1190–1207. doi:10.1002/2015JD023788.
Manzini, E., Karpechko, A. Y., Anstey, J., Baldwin, M. P., Black, R. X., Cagnazzo, C., et al. (2014). Northern winter climate change: Assessment of uncertainty in CMIP5 projections related to stratosphere-troposphere coupling. *J.*

*Geophys. Res. Atmos.* 119, 7979–7998. doi:10.1002/2013JD021403.
Maraun, D. (2012). Nonstationarities of regional climate model biases in European seasonal mean temperature and precipitation sums. *Geophys. Res. Lett.* 39, n/a-n/a. doi:10.1029/2012GL051210.
Maraun, D. (2013a). Bias Correction, Quantile Mapping, and Downscaling: Revisiting the Inflation Issue. *J. Clim.* 26, 2137–2143. doi:10.1175/JCLI-D-12-00821.1.
Maraun, D. (2013b). When will trends in European mean and heavy daily precipitation emerge? *Environ. Res. Lett.* 8, 014004. doi:10.1088/1748-9326/8/1/014004.
Maraun, D. (2016). Reply to "Comment on 'Bias Correction, Quantile Mapping, and Downscaling: Revisiting the Inflation Issue.'" *J. Clim.* 29, 8669–8671. doi:10.1175/JCLI-D-16-0592.1.
Maraun, D., Huth, R., Gutiérrez, J. M., Martín, D. S., Dubrovsky, M., Fischer, A., et al. (2017a). The VALUE perfect predictor experiment: evaluation of temporal variability. *Int. J. Climatol.* doi:10.1002/joc.5222.
Maraun, D., Shepherd, T. G., Widmann, M., Zappa, G., Walton, D., Gutiérrez, J. M., et al. (2017b). Towards process-informed bias correction of climate change simulations. *Nat. Clim. Chang.* 7, 664–773. doi:10.1038/nclimate3418.
Maraun, D., and Widmann, M. (2015). The representation of location by a regional climate model in complex terrain. *Hydrol. Earth Syst. Sci.* 19, 3449–3456. doi:10.5194/hess-19-3449-2015.
Maraun, D., and Widmann, M. (2018a). Cross-validation of bias-corrected climate simulations is misleading. *Hydrol. Earth Syst. Sci.* 22, 4867–4873. doi:10.5194/hess-22-4867-2018.
Maraun, D., and Widmann, M. (2018b). *Statistical Downscaling and Bias Correction for Climate Research*. Cambridge: Cambridge University Press doi:10.1017/9781107588783.
Maraun, D., Widmann, M., and Gutiérrez, J. M. (2018). Statistical downscaling skill under present climate conditions: A synthesis of the VALUE perfect predictor experiment. *Int. J. Climatol.* doi:10.1002/joc.5877.
Maraun, D., Widmann, M., Gutiérrez, J. M., Kotlarski, S., Chandler, R. E., Hertig, E., et al. (2015). VALUE: A framework to validate downscaling approaches for climate change studies. *Earth's Futur.* 3, 1–14. doi:10.1002/2014EF000259.
Marengo, J. A., Rusticucci, M., Penalba, O., and Renom, M. (2010). An intercomparison of observed and simulated extreme rainfall and temperature events during the last half of the twentieth century: part 2: historical trends. *Clim. Change* 98, 509–529. doi:10.1007/s10584-009-9743-7.
Mariotti, A., Pan, Y., Zeng, N., and Alessandri, A. (2015). Long-term climate change in the Mediterranean region in the midst of decadal variability. *Clim. Dyn.* 44, 1437–1456. doi:10.1007/s00382-015-2487-3.
Marteau, R., Richard, Y., Pohl, B., Smith, C. C., and Castel, T. (2015). High-resolution rainfall variability simulated by the WRF RCM: application to eastern France. *Clim. Dyn.* 44, 1093–1107. doi:10.1007/s00382-014-2125-5.
Martilli, A., Clappier, A., and Rotach, M. W. (2002). An urban surface exchange parameterisation for mesoscale models. *Boundary-Layer Meteorol.* doi:10.1023/A:1016099921195.
Martín-Gómez, V., and Barreiro, M. (2016). Analysis of oceans' influence on spring time rainfall variability over Southeastern South America during the 20th century. *Int. J. Climatol.* 36, 1344–1358. doi:10.1002/joc.4428.
Martín-Gómez, V., and Barreiro, M. (2017). Effect of future climate change on the coupling between the tropical oceans and precipitation over Southeastern South America. *Clim. Change* 141, 315–329. doi:10.1007/s10584-016-1888-6.
Martin, E. R., Thorncroft, C., and Booth, B. B. B. (2014). The multidecadal atlantic SST-sahel rainfall teleconnection in CMIP5 simulations. *J. Clim.* doi:10.1175/JCLI-D-13-00242.1.
Martin, E. R., and Thorncroft, C. D. (2014). The impact of the AMO on the West African monsoon annual cycle. *Q. J. R. Meteorol. Soc.* doi:10.1002/qj.2107.
Martin, G. M., Milton, S. F., Senior, C. A., Brooks, M. E., Ineson, S., Reichler, T., et al. (2010). Analysis and Reduction of Systematic Errors through a Seamless Approach to Modeling Weather and Climate. *J. Clim.* 23, 5933–5957. doi:10.1175/2010JCLI3541.1.
Martinez, C., Goddard, L., Kushnir, Y., and Ting, M. (2019). Seasonal climatology and dynamical mechanisms of rainfall in the Caribbean. *Clim. Dyn.* doi:10.1007/s00382-019-04616-4.
Martius, O., Pfahl, S., and Chevalier, C. (2016). A global quantification of compound precipitation and wind extremes. *Geophys. Res. Lett.* 43, 7709–7717. doi:10.1002/2016GL070017.
Martynov, A., Sushama, L., and Laprise, R. (2010). Simulation of temperate freezing lakes by one-dimensional lake models: performance assessment for interactive coupling with regional climate models. *Boreal Environ. Res.* 15, 143–164.
Martynov, A., Sushama, L., Laprise, R., Winger, K., and Dugas, B. (2012). Interactive lakes in the Canadian Regional Climate Model, version 5: the role of lakes in the regional climate of North America. *Tellus A Dyn. Meteorol. Oceanogr.* 64, 16226. doi:10.3402/tellusa.v64i0.16226.
Marvel, K., Schmidt, G. A., Shindell, D., Bonfils, C., LeGrande, A. N., Nazarenko, L., et al. (2015). Do responses to different anthropogenic forcings add linearly in climate models? *Environ. Res. Lett.* 10, 104010. doi:10.1088/1748-9326/10/10/104010.
Masato, G., Hoskins, B. J., and Woollings, T. (2013). Winter and Summer Northern Hemisphere Blocking in CMIP5 Models. *J. Clim.* 26, 7044–7059. doi:10.1175/JCLI-D-12-00466.1.

Masson, D., and Frei, C. (2014). Spatial analysis of precipitation in a high-mountain region : exploring methods with multi-scale topographic predictors and circulation types. *Hydrol. Earth Syst. Sci.*, 18, 4543–4563. doi:10.5194/hess-18-4543-2014.

Masson, D., and Knutti, R. (2013). Predictor Screening, Calibration, and Observational Constraints in Climate Model Ensembles: An Illustration Using Climate Sensitivity. *J. Clim.* 26, 887–898. doi:10.1175/JCLI-D-11-00540.1.

Masson, V. (2000). A Physically-Based Scheme for the Urban Energy Budget in Atmospheric Models.

Masson, V. (2006). Urban surface modeling and the meso-scale impact of cities. *Theor. Appl. Climatol.* doi:10.1007/s00704-005-0142-3.

Massonnet, F., Bellprat, O., Guemas, V., and Doblas-Reyes, F. J. (2016). Using climate models to estimate the quality of global observational data sets. *Science (80-. ).* 354, 452. Available at: http://science.sciencemag.org/content/354/6311/452.abstract.

Matsikaris, A., Widmann, M., and Jungclaus, J. (2015). On-line and off-line data assimilation in palaeoclimatology: a case study. *Clim. Past* 11, 81–93. doi:10.5194/cp-11-81-2015.

Matsikaris, A., Widmann, M., and Jungclaus, J. (2016). Influence of proxy data uncertainty on data assimilation for the past climate. *Clim. Past* 12, 1555–1563. doi:10.5194/cp-12-1555-2016.

Matte, D., Larsen, M. A. D., Christensen, O. B., and Christensen, J. H. (2019). Robustness and scalability of regional climate projections over Europe. *Front. Environ. Sci.* 6. doi:10.3389/fenvs.2018.00163.

Matthes, H., Rinke, A., Zhou, X., and Dethloff, K. (2017). Uncertainties in coupled regional Arctic climate simulations associated with the used land surface model. *J. Geophys. Res.* 122, 7755–7771. doi:10.1002/2016JD026213.

Maule, C. F., Mendlik, T., and Christensen, O. B. (2017). The effect of the pathway to a two degrees warmer world on the regional temperature change of Europe. *Clim. Serv.* 7, 3–11. doi:10.1016/j.cliser.2016.07.002.

Maúre, G., Pinto, I., Ndebele-Murisa, M., Muthige, M., Lennard, C., Nikulin, G., et al. (2018). The southern African climate under 1.5 °C and 2 °C of global warming as simulated by CORDEX regional climate models. *Environ. Res. Lett.* 13, 065002. doi:10.1088/1748-9326/aab190.

Maurer, E. P., and Pierce, D. W. (2014). Bias correction can modify climate model simulated precipitation changes without adverse effect on the ensemble mean. *Hydrol. Earth Syst. Sci.* 18, 915–925. doi:10.5194/hess-18-915-2014.

May, W. (2011). The sensitivity of the Indian summer monsoon to a global warming of 2°C with respect to pre-industrial times. *Clim. Dyn.* 37, 1843–1868. doi:10.1007/s00382-010-0942-8.

McCarthy, M. P., Best, M. J., and Betts, R. A. (2010). Climate change in cities due to global warming and urban effects. *Geophys. Res. Lett.* 37. doi:10.1029/2010GL042845.

McCarthy, M. P., Harpham, C., Goodess, C. M., and Jones, P. D. (2012). Simulating climate change in UK cities using a regional climate model, HadRM3. *Int. J. Climatol.* 32, 1875–1888. doi:10.1002/joc.2402.

McCusker, K. E., Fyfe, J. C., and Sigmond, M. (2016). Twenty-five winters of unexpected Eurasian cooling unlikely due to Arctic sea-ice loss. *Nat. Geosci.* 9, 838–842. doi:10.1038/ngeo2820.

McCusker, K. E., Kushner, P. J., Fyfe, J. C., Sigmond, M., Kharin, V. V., and Bitz, C. M. (2017). Remarkable separability of circulation response to Arctic sea ice loss and greenhouse gas forcing. *Geophys. Res. Lett.* 44, 7955–7964. doi:10.1002/2017GL074327.

McDermid, S. S., Mearns, L. O., and Ruane, A. C. (2017). Representing agriculture in Earth System Models: Approaches and priorities for development. *J. Adv. Model. Earth Syst.* 9, 2230–2265. doi:10.1002/2016MS000749.

McGregor, J. L. (2015). Recent developments in variable-resolution global climate modelling. *Clim. Change* 129, 369–380. doi:10.1007/s10584-013-0866-5.

McGregor, S., Timmermann, A., Stuecker, M. F., England, M. H., Merrifield, M., Jin, F.-F., et al. (2014). Recent Walker circulation strengthening and Pacific cooling amplified by Atlantic warming. *Nat. Clim. Chang.* 4, 888–892. doi:10.1038/nclimate2330.

McKenna, C. M., Bracegirdle, T. J., Shuckburgh, E. F., Haynes, P. H., and Joshi, M. M. (2018). Arctic Sea Ice Loss in Different Regions Leads to Contrasting Northern Hemisphere Impacts. *Geophys. Res. Lett.* 45, 945–954. doi:10.1002/2017GL076433.

McKinnon, K. A., and Deser, C. (2018). Internal Variability and Regional Climate Trends in an Observational Large Ensemble. *J. Clim.* 31, 6783–6802. doi:10.1175/JCLI-D-17-0901.1.

McKinnon, K. A., Poppick, A., Dunn-Sigouin, E., and Deser, C. (2017). An "Observational Large Ensemble" to Compare Observed and Modeled Temperature Trend Uncertainty due to Internal Variability. *J. Clim.* 30, 7585–7598. doi:10.1175/JCLI-D-16-0905.1.

McLeod, J., Shepherd, M., and Konrad, C. E. (2017). Spatio-temporal rainfall patterns around Atlanta, Georgia and possible relationships to urban land cover. *Urban Clim.* 21, 27–42. doi:10.1016/j.uclim.2017.03.004.

McNeall, D., Williams, J., Booth, B., Betts, R., Challenor, P., Wiltshire, A., et al. (2016). The impact of structural error on parameter constraint in a climate model. *Earth Syst. Dyn.* 7, 917–935. doi:10.5194/esd-7-917-2016.

McPherson, R. A. (2013). "High-Resolution Surface Observations for Climate Monitoring," in *Climate Variability - Regional and Thematic Patterns* (InTech). doi:10.5772/56044.

McSweeney, C. F., Jones, R. G., and Booth, B. B. B. (2012). Selecting Ensemble Members to Provide Regional

Climate Change Information. *J. Clim.* 25, 7100–7121. doi:10.1175/JCLI-D-11-00526.1.
McSweeney, C. F., Jones, R. G., Lee, R. W., and Rowell, D. P. (2015). Selecting CMIP5 GCMs for downscaling over multiple regions. *Clim. Dyn.* 44, 3237–3260. doi:10.1007/s00382-014-2418-8.
Mearns, L. O., Arritt, R., Biner, S., Bukovsky, M. S., McGinnis, S., Sain, S., et al. (2012). The North American Regional Climate Change Assessment Program. *Bull. Am. Meteorol. Soc.* 93, 1337–1362. doi:10.1175/BAMS-D-11-00223.1.
Mearns, L. O., Sain, S., Leung, L. R., Bukovsky, M. S., McGinnis, S., Biner, S., et al. (2013). Climate change projections of the North American Regional Climate Change Assessment Program (NARCCAP). *Clim. Change* 120. doi:10.1007/s10584-013-0831-3.
Meehl, G. A., Goddard, L., Boer, G., Burgman, R., Branstator, G., Cassou, C., et al. (2014). Decadal Climate Prediction: An Update from the Trenches. *Bull. Am. Meteorol. Soc.* 95, 243–267. doi:10.1175/BAMS-D-12-00241.1.
Meehl, G. A., Hu, A., Arblaster, J. M., Fasullo, J., and Trenberth, K. E. (2013). Externally Forced and Internally Generated Decadal Climate Variability Associated with the Interdecadal Pacific Oscillation. *J. Clim.* 26, 7298–7310. doi:10.1175/JCLI-D-12-00548.1.
Meher, J. K., Das, L., Akhter, J., Benestad, R. E., and Mezghani, A. (2017). Performance of CMIP3 and CMIP5 GCMs to Simulate Observed Rainfall Characteristics over the Western Himalayan Region. *J. Clim.* 30, 7777–7799. doi:10.1175/JCLI-D-16-0774.1.
Meher, J. K., Das, L., Benestad, R. E., and Mezghani, A. (2018). Analysis of winter rainfall change statistics over the Western Himalaya: the influence of internal variability and topography. *Int. J. Climatol.* 38, e475–e496. doi:10.1002/joc.5385.
Meier, F., Fenner, D., Grassmann, T., Otto, M., and Scherer, D. (2017). Crowdsourcing air temperature from citizen weather stations for urban climate research. *Urban Clim.* 19, 170–191. doi:https://doi.org/10.1016/j.uclim.2017.01.006.
Menary, M. B., Kuhlbrodt, T., Ridley, J., Andrews, M. B., Dimdore-Miles, O. B., Deshayes, J., et al. (2018). Preindustrial Control Simulations With HadGEM3-GC3.1 for CMIP6. *J. Adv. Model. Earth Syst.* 10, 3049–3075. doi:10.1029/2018MS001495.
Méndez-lázaro, A. P. A., Nieves-santiango, A., and Miranda-, J. (2019). Trends in total rainfall , heavy rain events , and number of dry days in San Juan , Puerto Rico , 1955-2009.
Mendlik, T., and Gobiet, A. (2016). Selecting climate simulations for impact studies based on multivariate patterns of climate change. *Clim. Change* 135, 381–393. doi:10.1007/s10584-015-1582-0.
Ménégoz, M., Cassou, C., Swingedouw, D., Ruprich-Robert, Y., Bretonnière, P.-A., and Doblas-Reyes, F. (2018). Role of the Atlantic Multidecadal Variability in modulating the climate response to a Pinatubo-like volcanic eruption. *Clim. Dyn.* 51, 1863–1883. doi:10.1007/s00382-017-3986-1.
Menéndez, C. G., Giles, J., Ruscica, R., Zaninelli, P., Coronato, T., Falco, M., et al. (2019). Temperature variability and soil–atmosphere interaction in South America simulated by two regional climate models. *Clim. Dyn.* doi:10.1007/s00382-019-04668-6.
Menéndez, C., Zaninelli, P., Carril, A., and Sánchez, E. (2016). Hydrological cycle, temperature, and land surface-atmosphere interaction in the La Plata Basin during summer: response to climate change. *Clim. Res.* 68, 231–241. doi:10.3354/cr01373.
Merchant, C. J., Paul, F., Popp, T., Ablain, M., Bontemps, S., Defourny, P., et al. (2017). Uncertainty information in climate data records from Earth observation. *Earth Syst. Sci. Data* 9, 511–527. doi:10.5194/essd-9-511-2017.
Meredith, E. P., Maraun, D., Semenov, V. A., and Park, W. (2015a). Evidence for added value of convection-permitting models for studying changes in extreme precipitation. *J. Geophys. Res. Atmos.* 120, 12500–12513. doi:10.1002/2015JD024238.
Meredith, E. P., Semenov, V. A., Maraun, D., Park, W., and Chernokulsky, A. V. (2015b). Crucial role of Black Sea warming in amplifying the 2012 Krymsk precipitation extreme. *Nat. Geosci.* 8, 615–619. doi:10.1038/ngeo2483.
Mestre, O., Gruber, C., Prieur, C., Caussinus, H., and Jourdain, S. (2011). SPLIDHOM: A Method for Homogenization of Daily Temperature Observations. *J. Appl. Meteorol. Climatol.* 50, 2343–2358. doi:10.1175/2011JAMC2641.1.
Meyer, J., Kohn, I., Stahl, K., Hakala, K., Seibert, J., and Cannon, A. J. (2019). Effects of univariate and multivariate bias correction on hydrological impact projections in alpine catchments. *Hydrol. Earth Syst. Sci.* 23, 1339–1354. doi:10.5194/hess-23-1339-2019.
Mezghani, A., and Hingray, B. (2009). A combined downscaling-disaggregation weather generator for stochastic generation of multisite hourly weather variables over complex terrain: Development and multi-scale validation for the Upper Rhone River basin. *J. Hydrol.* 377, 245–260. doi:10.1016/j.jhydrol.2009.08.033.
Miao, C., Duan, Q., Sun, Q., Huang, Y., Kong, D., Yang, T., et al. (2014). Assessment of CMIP5 climate models and projected temperature changes over Northern Eurasia. *Environ. Res. Lett.* 9, 055007. doi:10.1088/1748-9326/9/5/055007.
Miao, J., Wang, T., Wang, H., and Sun, J. (2018). Interannual Weakening of the Tropical Pacific Walker Circulation Due to Strong Tropical Volcanism. *Adv. Atmos. Sci.* 35, 645–658. doi:10.1007/s00376-017-7134-y.
Migliavacca, M., Dosio, A., Camia, A., Hobourg, R., Houston-Durrant, T., Kaiser, J. W., et al. (2013). Modeling

biomass burning and related carbon emissions during the 21st century in Europe. *J. Geophys. Res. Biogeosciences* 118, 1732–1747. doi:10.1002/2013JG002444.
Minder, J. R., Letcher, T. W., and Skiles, S. M. (2016). An evaluation of high-resolution regional climate model simulations of snow cover and albedo over the Rocky Mountains, with implications for the simulated snow-albedo feedback. *J. Geophys. Res. Atmos.* 121, 9069–9088. doi:10.1002/2016JD024995.
Ming, J., Du, Z., Xiao, C., Xu, X., and Zhang, D. (2012). Darkening of the mid-Himalaya glaciers since 2000 and the potential causes. *Environ. Res. Lett.* 7, 014021. doi:10.1088/1748-9326/7/1/014021.
Ming, Y., and Ramaswamy, V. (2011). A Model Investigation of Aerosol-Induced Changes in Tropical Circulation. *J. Clim.* 24, 5125–5133. doi:10.1175/2011JCLI4108.1.
Miralles, D. G., Teuling, A. J., van Heerwaarden, C. C., and Vilà-Guerau de Arellano, J. (2014). Mega-heatwave temperatures due to combined soil desiccation and atmospheric heat accumulation. *Nat. Geosci.* 7, 345. Available at: http://dx.doi.org/10.1038/ngeo2141.
Mironov, D., Heise, E., Kourzeneva, E., Ritter, B., Schneider, N., and Terzhevik, A. (2010). Implementation of the lake parameterisation scheme FLake into numerical weather prediction model COSMO. *Boreal Environ. Res.* 15, 218–230.
Mishra, S. K., Sahany, S., and Salunke, P. (2018). CMIP5 vs. CORDEX over the Indian region: how much do we benefit from dynamical downscaling? *Theor. Appl. Climatol.* 133, 1133–1141. doi:10.1007/s00704-017-2237-z.
Mishra, V. (2015). Climatic uncertainty in Himalayan water towers. *J. Geophys. Res. Atmos.* 120, 2689–2705. doi:10.1002/2014JD022650.
Mitchell, D., AchutaRao, K., Allen, M., Bethke, I., Beyerle, U., Ciavarella, A., et al. (2017). Half a degree additional warming, prognosis and projected impacts (HAPPI): background and experimental design. *Geosci. Model Dev.* 10, 571–583. doi:10.5194/gmd-10-571-2017.
Mitchell, D., James, R., Forster, P. M., Betts, R. A., Shiogama, H., and Allen, M. (2016). Realizing the impacts of a 1.5 °C warmer world. *Nat. Clim. Chang.* 6, 735–737. doi:10.1038/nclimate3055.
MJO Working Group (2009). MJO Simulation Diagnostics. *J. Clim.* 22, 3006–3030. doi:10.1175/2008JCLI2731.1.
Moezzi, M., Janda, K. B., and Rotmann, S. (2017). Using stories, narratives, and storytelling in energy and climate change research. *Energy Res. Soc. Sci.* 31, 1–10. doi:https://doi.org/10.1016/j.erss.2017.06.034.
Mohino, E., Keenlyside, N., and Pohlmann, H. (2016). Decadal prediction of Sahel rainfall: where does the skill (or lack thereof) come from? *Clim. Dyn.* 47, 3593–3612. doi:10.1007/s00382-016-3416-9.
Monerie, P.-A., Robson, J., Dong, B., Hodson, D. L. R., and Klingaman, N. P. (2019). Effect of the Atlantic Multidecadal Variability on the Global Monsoon. *Geophys. Res. Lett.* doi:10.1029/2018GL080903.
Monerie, P.-A., Sanchez-Gomez, E., and Boé, J. (2017a). On the range of future Sahel precipitation projections and the selection of a sub-sample of CMIP5 models for impact studies. *Clim. Dyn.* 48, 2751–2770. doi:10.1007/s00382-016-3236-y.
Monerie, P.-A., Sanchez-Gomez, E., Pohl, B., Robson, J., and Dong, B. (2017b). Impact of internal variability on projections of Sahel precipitation change. *Environ. Res. Lett.* 12, 114003. doi:10.1088/1748-9326/aa8cda.
Monerie, P. A., Robson, J., Dong, B., and Dunstone, N. (2018). A role of the Atlantic Ocean in predicting summer surface air temperature over North East Asia? *Clim. Dyn.* 51, 473–491. doi:10.1007/s00382-017-3935-z.
Monier, E., Sokolov, A., Schlosser, A., Scott, J., and Gao, X. (2013). Probabilistic projections of 21st century climate change over Northern Eurasia. *Environ. Res. Lett.* 8, 045008. doi:10.1088/1748-9326/8/4/045008.
Montroull, N. B., Saurral, R. I., and Camilloni, I. A. (2018). Hydrological impacts in La Plata basin under 1.5, 2 and 3 °C global warming above the pre-industrial level. *Int. J. Climatol.* 38, 3355–3368. doi:10.1002/joc.5505.
Mori, M., Kosaka, Y., Watanabe, M., Nakamura, H., and Kimoto, M. (2019). A reconciled estimate of the influence of Arctic sea-ice loss on recent Eurasian cooling. *Nat. Clim. Chang.* 9, 123–129. doi:10.1038/s41558-018-0379-3.
Mori, M., Watanabe, M., Shiogama, H., Inoue, J., and Kimoto, M. (2014). Robust Arctic sea-ice influence on the frequent Eurasian cold winters in past decades. *Nat. Geosci.* 7, 869–873. doi:10.1038/ngeo2277.
Morton, T. A., Rabinovich, A., Marshall, D., and Bretschneider, P. (2011). The future that may (or may not) come: How framing changes responses to uncertainty in climate change communications. *Glob. Environ. Chang.* 21, 103–109. doi:10.1016/j.gloenvcha.2010.09.013.
Moss, R. H. (2016). "Assessing decision support systems and levels of confidence to narrow the climate information 'usability gap,'" in, 143–155. doi:10.1007/978-3-319-41802-5_11.
Mueller, N. D., Butler, E. E., McKinnon, K. A., Rhines, A., Tingley, M., Holbrook, N. M., et al. (2016). Cooling of US Midwest summer temperature extremes from cropland intensification. *Nat. Clim. Chang.* 6, 317–322. doi:10.1038/nclimate2825.
Mueller, N. D., Gerber, J. S., Johnston, M., Ray, D. K., Ramankutty, N., and Foley, J. A. (2012). Closing yield gaps through nutrient and water management. *Nature* 490, 254. Available at: https://doi.org/10.1038/nature11420.
Muerth, M. J., Gauvin St-Denis, B., Ricard, S., Velázquez, J. A., Schmid, J., Minville, M., et al. (2013). On the need for bias correction in regional climate scenarios to assess climate change impacts on river runoff. *Hydrol. Earth Syst. Sci.* 17, 1189–1204. doi:10.5194/hess-17-1189-2013.
Mukheibir, P., and Ziervogel, G. (2007). Developing a Municipal Adaptation Plan (MAP) for climate change: the city of Cape Town. *Environ. Urban.* 19, 143–158. doi:10.1177/0956247807076912.

Mulholland, D. P., Laloyaux, P., Haines, K., and Balmaseda, M. A. (2015). Origin and Impact of Initialization Shocks in Coupled Atmosphere–Ocean Forecasts. *Mon. Weather Rev.* 143, 4631–4644. doi:10.1175/MWR-D-15-0076.1.
Muller, C. L., Chapman, L., Grimmond, C. S. B., Young, D. T., and Cai, X. (2013). Sensors and the city: a review of urban meteorological networks. *Int. J. Climatol.* 33, 1585–1600. doi:10.1002/joc.3678.
Muller, C. L., Chapman, L., Johnston, S., Kidd, C., Illingworth, S., Foody, G., et al. (2015). Crowdsourcing for climate and atmospheric sciences: current status and future potential. *Int. J. Climatol.* 35, 3185–3203. doi:10.1002/joc.4210.
Muller, M. (2018). Cape Town's drought: don't blame climate change. *Nature* 559, 174–176. doi:10.1038/d41586-018-05649-1.
Mundhenk, B. D., Barnes, E. A., and Maloney, E. D. (2016). All-Season Climatology and Variability of Atmospheric River Frequencies over the North Pacific. *J. Clim.* 29, 4885–4903. doi:10.1175/JCLI-D-15-0655.1.
Muñoz, A. G., Goddard, L., Robertson, A. W., Kushnir, Y., and Baethgen, W. (2015). Cross-time scale interactions and rainfall extreme events in southeastern South America for the austral summer. Part I: Potential predictors. *J. Clim.* 28, 7894–7913. doi:10.1175/JCLI-D-14-00693.1.
Myhre, G., Shindell, D., and Al., E. (2013). "Clouds and Aerosols," in *Climate Change 2013 - The Physical Science Basis*, ed. Intergovernmental Panel on Climate Change (Cambridge: Cambridge University Press), 571–658. doi:10.1017/CBO9781107415324.016.
Naab, F. Z., Abubakari, Z., and Ahmed, A. (2019). The role of climate services in agricultural productivity in Ghana: The perspectives of farmers and institutions. *Clim. Serv.* doi:10.1016/j.cliser.2019.01.007.
Nabat, P., Somot, S., Mallet, M., Sanchez-Lorenzo, A., and Wild, M. (2014). Contribution of anthropogenic sulfate aerosols to the changing Euro-Mediterranean climate since 1980. *Geophys. Res. Lett.* 41, 5605–5611. doi:10.1002/2014GL060798.
Nabat, P., Somot, S., Mallet, M., Sevault, F., Chiacchio, M., and Wild, M. (2015). Direct and semi-direct aerosol radiative effect on the Mediterranean climate variability using a coupled regional climate system model. *Clim. Dyn.* 44, 1127–1155. doi:10.1007/s00382-014-2205-6.
Nakamura, T., Yamazaki, K., Iwamoto, K., Honda, M., Miyoshi, Y., Ogawa, Y., et al. (2015). A negative phase shift of the winter AO/NAO due to the recent Arctic sea-ice reduction in late autumn. *J. Geophys. Res. Atmos.* 120, 3209–3227. doi:10.1002/2014JD022848.
Naranjo, L., and Centella, A. (1994). Recent trends in the climate of Cuba.
Nardi, K. M., Barnes, E. A., and Ralph, F. M. (2018). Assessment of Numerical Weather Prediction Model Reforecasts of the Occurrence, Intensity, and Location of Atmospheric Rivers along the West Coast of North America. *Mon. Weather Rev.* 146, 3343–3362. doi:10.1175/mwr-d-18-0060.1.
Nath, R., Luo, Y., Chen, W., and Cui, X. (2018). On the contribution of internal variability and external forcing factors to the Cooling trend over the Humid Subtropical Indo-Gangetic Plain in India. *Sci. Rep.* 8, 18047. doi:10.1038/s41598-018-36311-5.
Nayak, M. A., Villarini, G., and Lavers, D. A. (2014). On the skill of numerical weather prediction models to forecast atmospheric rivers over the central United States. *Geophys. Res. Lett.* 41, 4354–4362. doi:10.1002/2014GL060299.
Nazemi, A., and Wheater, H. S. (2015). On inclusion of water resource management in Earth system models – Part 1: Problem definition and representation of water demand. *Hydrol. Earth Syst. Sci.* 19, 33–61. doi:10.5194/hess-19-33-2015.
Neelin, J. D., Chou, C., and Su, H. (2003). Tropical drought regions in global warming and El Nin ˜ o teleconnections. 30, 1–4. doi:10.1029/2003GL018625.
Neelin, J. D., Münnich, M., Su, H., Meyerson, J. E., and Holloway, C. E. (2006). Tropical drying trends in global warming models and observations. *Proc. Natl. Acad. Sci. U. S. A.* 103, 6110–6115. doi:10.1073/pnas.0601798103.
Nelson, B. R., Prat, O. P., Seo, D.-J., and Habib, E. (2016). Assessment and Implications of NCEP Stage IV Quantitative Precipitation Estimates for Product Intercomparisons. *Weather Forecast.* 31, 371–394. doi:10.1175/waf-d-14-00112.1.
Nengker, T., Choudhary, A., and Dimri, A. P. (2018). Assessment of the performance of CORDEX-SA experiments in simulating seasonal mean temperature over the Himalayan region for the present climate: Part I. *Clim. Dyn.* 50, 2411–2441. doi:10.1007/s00382-017-3597-x.
Neu, U., Akperov, M. G., Bellenbaum, N., Benestad, R., Blender, R., Caballero, R., et al. (2013). IMILAST: A Community Effort to Intercompare Extratropical Cyclone Detection and Tracking Algorithms. *Bull. Am. Meteorol. Soc.* 94, 529–547. doi:10.1175/BAMS-D-11-00154.1.
Neukom, R., Steiger, Nathan, Gómez-Navarro, J. J., Wang, J., & Werner, J. P. (2019). No evidence for globally coherent warm and cold periods over the pre-industrial Common Era. *Nature*.
New, M., Todd, M., Hulme, M., and Jones, P. (2001). PRECIPITATION MEASUREMENTS AND TRENDS IN THE. 1922, 1899–1922.
Nguyen, T.-H., Min, S.-K., Paik, S., and Lee, D. (2018). Time of emergence in regional precipitation changes: an updated assessment using the CMIP5 multi-model ensemble. *Clim. Dyn.* 51, 3179–3193. doi:10.1007/s00382-

018-4073-y.
Nicholson, S. E. (2013). The West African Sahel: A Review of Recent Studies on the Rainfall Regime and Its Interannual Variability. *ISRN Meteorol.* 2013, 1–32. doi:10.1155/2013/453521.
Nigam, S., and Bollasina, M. (2010). "Elevated heat pump" hypothesis for the aerosol-monsoon hydroclimate link: "Grounded" in observations? *J. Geophys. Res.* 115, D16201. doi:10.1029/2009JD013800.
Nijsse, F. J. M. M., and Dijkstra, H. A. (2018). A mathematical approach to understanding emergent constraints. *Earth Syst. Dyn.* 9, 999–1012. doi:10.5194/esd-9-999-2018.
Nikiema, P. M., Sylla, M. B., Ogunjobi, K., Kebe, I., Gibba, P., and Giorgi, F. (2017). Multi-model CMIP5 and CORDEX simulations of historical summer temperature and precipitation variabilities over West Africa. *Int. J. Climatol.* 37, 2438–2450. doi:10.1002/joc.4856.
Nikulin, G., Jones, C., Giorgi, F., Asrar, G., Büchner, M., Cerezo-Mota, R., et al. (2012). Precipitation Climatology in an Ensemble of CORDEX-Africa Regional Climate Simulations. *J. Clim.* 25, 6057–6078. doi:10.1175/JCLI-D-11-00375.1.
Niwano, M., Aoki, T., Hashimoto, A., Matoba, S., Yamaguchi, S., Tanikawa, T., et al. (2018). NHM-SMAP: Spatially and temporally high-resolution nonhydrostatic atmospheric model coupled with detailed snow process model for Greenland Ice Sheet. *Cryosphere*. doi:10.5194/tc-12-635-2018.
Notaro, M., Holman, K., Zarrin, A., Fluck, E., Vavrus, S., and Bennington, V. (2013). Influence of the Laurentian Great Lakes on Regional Climate*. *J. Clim.* 26, 789–804. doi:10.1175/JCLI-D-12-00140.1.
Notz, D. (2015). How well must climate models agree with observations? *Philos. Trans. R. Soc. A Math. Phys. Eng. Sci.* 373, 20140164. doi:10.1098/rsta.2014.0164.
O'Higgins, T., Nogueira, A. A., and Lillebø, A. I. (2019). A simple spatial typology for assessment of complex coastal ecosystem services across multiple scales. *Sci. Total Environ.* 649, 1452–1466. doi:10.1016/j.scitotenv.2018.08.420.
O'Reilly, C. H., Minobe, S., and Kuwano-Yoshida, A. (2016). The influence of the Gulf Stream on wintertime European blocking. *Clim. Dyn.* 47, 1545–1567. doi:10.1007/s00382-015-2919-0.
O'Reilly, C. H., Woollings, T., and Zanna, L. (2017). The Dynamical Influence of the Atlantic Multidecadal Oscillation on Continental Climate. *J. Clim.* 30, 7213–7230. doi:10.1175/JCLI-D-16-0345.1.
Obermann, A., Bastin, S., Belamari, S., Conte, D., Gaertner, M. A., Li, L., et al. (2018). Mistral and Tramontane wind speed and wind direction patterns in regional climate simulations. *Clim. Dyn.* 51, 1059–1076. doi:10.1007/s00382-016-3053-3.
Ochsner, T. E., Cosh, M. H., Cuenca, R. H., Dorigo, W. A., Draper, C. S., Hagimoto, Y., et al. (2013). State of the Art in Large-Scale Soil Moisture Monitoring. *Soil Sci. Soc. Am. J.* 77, 1888. doi:10.2136/sssaj2013.03.0093.
Ogawa, F., Keenlyside, N., Gao, Y., Koenigk, T., Yang, S., Suo, L., et al. (2018). Evaluating Impacts of Recent Arctic Sea Ice Loss on the Northern Hemisphere Winter Climate Change. *Geophys. Res. Lett.* 45, 3255–3263. doi:10.1002/2017GL076502.
Okamoto, K., Ushio, T., Iguchi, T., Takahashi, N., and Iwanami, K. (2005). The Global Satellite Mapping of Precipitation (GSMaP) project. *Int. Geosci. Remote Sens. Symp.* 5, 3414–3416. doi:10.1109/IGARSS.2005.1526575.
Okazaki, A., and Yoshimura, K. (2017). Development and evaluation of a system of proxy data assimilationfor paleoclimate reconstruction. *Clim. Past* 13, 379–393. doi:10.5194/cp-13-379-2017.
Oke, T. (2006). Initial guidance to obtain representative meteorological observations at urban sites. *WMO Bull.*
Oke, T. R., Mills, G., Christen, A., and Voogt, J. A. (2017). *Urban Climates*. Cambridge: Cambridge University Press doi:DOI: 10.1017/9781139016476.
OKUMURA, Y., and XIE, S. P. (2004). Interaction of the Atlantic Equatorial Cold Tongue and the African Monsoon. *J. Clim.* 17, 3589–3602.
Oleson, K. (2012). Contrasts between Urban and rural climate in CCSM4 CMIP5 climate change scenarios. *J. Clim.* 25, 1390–1412. doi:10.1175/JCLI-D-11-00098.1.
Oleson, K. W., Bonan, G. B., Feddema, J., and Jackson, T. (2011). An examination of urban heat island characteristics in a global climate model. *Int. J. Climatol.* 31, 1848–1865. doi:10.1002/joc.2201.
Ooi, M. C. G., Chan, A., Ashfold, M. J., Morris, K. I., Oozeer, M. Y., and Salleh, S. A. (2017). Numerical study on effect of urban heating on local climate during calm inter-monsoon period in greater Kuala Lumpur, Malaysia. *Urban Clim.* 20, 228–250. doi:10.1016/j.uclim.2017.04.010.
Oppenheimer, M., Campos, M., Warren, R., Birkmann, J., Luber, G., O'Neill, B., et al. (2015). Emergent risks and key vulnerabilities. *Clim. Chang. 2014 Impacts, Adapt. Vulnerability Part A Glob. Sect. Asp.*, 1039–1100. doi:10.1017/CBO9781107415379.024.
Orlanski, I. (1975). A Rational Subdivision of Scales for Atmospheric Processes. *Bull. Am. Meteorol. Soc.* 56, 527–530. Available at: http://www.jstor.org/stable/26216020.
Otto, F. E. L., van Oldenborgh, G. J., Eden, J., Stott, P. A., Karoly, D. J., and Allen, M. R. (2016). The attribution question. *Nat. Clim. Chang.* 6, 813–816. doi:10.1038/nclimate3089.
Otto, F. E. L., Wolski, P., Lehner, F., Tebaldi, C., van Oldenborgh, G. J., Hogesteeger, S., et al. (2018). Anthropogenic influence on the drivers of the Western Cape drought 2015–2017. *Environ. Res. Lett.* 13, 124010.

doi:10.1088/1748-9326/aae9f9.
Oueslati, B., and Bellon, G. (2015). The double ITCZ bias in CMIP5 models: interaction between SST, large-scale circulation and precipitation. *Clim. Dyn.* 44, 585–607. doi:10.1007/s00382-015-2468-6.
Overland, J. E. (2016). A difficult Arctic science issue: Midlatitude weather linkages. *Polar Sci.* 10, 210–216. doi:10.1016/j.polar.2016.04.011.
Overland, J. E., Dethloff, K., Francis, J. A., Hall, R. J., Hanna, E., Kim, S.-J., et al. (2016). Nonlinear response of mid-latitude weather to the changing Arctic. *Nat. Clim. Chang.* 6, 992–999. doi:10.1038/nclimate3121.
Overland, J., Francis, J. A., Hall, R., Hanna, E., Kim, S.-J., and Vihma, T. (2015). The Melting Arctic and Midlatitude Weather Patterns: Are They Connected?*. *J. Clim.* 28, 7917–7932. doi:10.1175/JCLI-D-14-00822.1.
Oyler, J. W., Ballantyne, A., Jencso, K., Sweet, M., and Running, S. W. (2015). Creating a topoclimatic daily air temperature dataset for the conterminous United States using homogenized station data and remotely sensed land skin temperature. *Int. J. Climatol.* 35, 2258–2279. doi:10.1002/joc.4127.
Pai, D. S., Sridhar, L., Badwaik, M. R., and Rajeevan, M. (2015). Analysis of the daily rainfall events over India using a new long period (1901–2010) high resolution (0.25° × 0.25°) gridded rainfall data set. *Clim. Dyn.* 45, 755–776. doi:10.1007/s00382-014-2307-1.
Palazzi, E., Mortarini, L., Terzago, S., and von Hardenberg, J. (2018). Elevation-dependent warming in global climate model simulations at high spatial resolution. *Clim. Dyn.*, 1–18. doi:10.1007/s00382-018-4287-z.
Palazzi, E., Von Hardenberg, J., and Provenzale, A. (2013). Precipitation in the hindu-kush karakoram himalaya: Observations and future scenarios. *J. Geophys. Res. Atmos.* 118, 85–100. doi:10.1029/2012JD018697.
Palazzi, E., von Hardenberg, J., Terzago, S., and Provenzale, A. (2015). Precipitation in the Karakoram-Himalaya: a CMIP5 view. *Clim. Dyn.* 45, 21–45. doi:10.1007/s00382-014-2341-z.
Pall, P., Patricola, C. M., Wehner, M. F., Stone, D. A., Paciorek, C. J., and Collins, W. D. (2017). Diagnosing conditional anthropogenic contributions to heavy Colorado rainfall in September 2013. *Weather Clim. Extrem.* 17, 1–6. doi:10.1016/j.wace.2017.03.004.
Palmer, T. N. (2016). A personal perspective on modelling the climate system. *Proc. R. Soc. A Math. Phys. Eng. Sci.* 472, 20150772. doi:10.1098/rspa.2015.0772.
Paltan, H., Waliser, D., Lim, W. H., Guan, B., Yamazaki, D., Pant, R., et al. (2017). Global Floods and Water Availability Driven by Atmospheric Rivers. *Geophys. Res. Lett.* 44, 10,387-10,395. doi:10.1002/2017gl074882.
Panday, P. K., Thibeault, J., and Frey, K. E. (2015). Changing temperature and precipitation extremes in the Hindu Kush-Himalayan region: An analysis of CMIP3 and CMIP5 simulations and projections. *Int. J. Climatol.* 35, 3058–3077. doi:10.1002/joc.4192.
Panitz, H.-J., Dosio, A., Büchner, M., Lüthi, D., and Keuler, K. (2014). COSMO-CLM (CCLM) climate simulations over CORDEX-Africa domain: analysis of the ERA-Interim driven simulations at 0.44° and 0.22° resolution. *Clim. Dyn.* 42, 3015–3038. doi:10.1007/s00382-013-1834-5.
Panthou, G., Lebel, T., Vischel, T., Quantin, G., Sane, Y., Ba, A., et al. (2018a). Rainfall intensification in tropical semi-arid regions: the Sahelian case. *Environ. Res. Lett.* 13, 064013. doi:10.1088/1748-9326/aac334.
Panthou, G., Vischel, T., and Lebel, T. (2014). Recent trends in the regime of extreme rainfall in the Central Sahel. *Int. J. Climatol.* doi:10.1002/joc.3984.
Panthou, G., Vrac, M., Drobinski, P., Bastin, S., and Li, L. (2018b). Impact of model resolution and Mediterranean sea coupling on hydrometeorological extremes in RCMs in the frame of HyMeX and MED-CORDEX. *Clim. Dyn.* 51, 915–932. doi:10.1007/s00382-016-3374-2.
Panziera, L., Gabella, M., Germann, U., and Martius, O. (2018). A 12-year radar-based climatology of daily and sub-daily extreme precipitation over the Swiss Alps. *Int. J. Climatol.* 38, 3749–3769. doi:10.1002/joc.5528.
Park, D.-S. R., Lee, S., and Feldstein, S. B. (2015a). Attribution of the Recent Winter Sea Ice Decline over the Atlantic Sector of the Arctic Ocean*. *J. Clim.* 28, 4027–4033. doi:10.1175/JCLI-D-15-0042.1.
Park, J.-Y., Bader, J., and Matei, D. (2015b). Northern-hemispheric differential warming is the key to understanding the discrepancies in the projected Sahel rainfall. *Nat. Commun.* 6, 5985. doi:10.1038/ncomms6985.
Park, J. Y., Bader, J., and Matei, D. (2016). Anthropogenic Mediterranean warming essential driver for present and future Sahel rainfall. *Nat. Clim. Chang.* doi:10.1038/nclimate3065.
Parker, D. E. (1994). Effects of changing exposure of thermometers at land stations. *Int. J. Climatol.* 14, 1–31. doi:10.1002/joc.3370140102.
Parker, D. E. (2006). A Demonstration That Large-Scale Warming Is Not Urban. *J. Clim.* 19, 2882–2895. doi:10.1175/JCLI3730.1.
Parker, W. S. (2009). II—Wendy S. Parker: Confirmation and adequacy-for-Purpose in Climate Modelling. *Aristot. Soc. Suppl. Vol.* 83, 233–249. doi:10.1111/j.1467-8349.2009.00180.x.
Pathirana, A., Denekew, H. B., Veerbeek, W., Zevenbergen, C., and Banda, A. T. (2014). Impact of urban growth-driven landuse change on microclimate and extreme precipitation - A sensitivity study. *Atmos. Res.* 138, 59–72. doi:10.1016/j.atmosres.2013.10.005.
Patricola, C. M., and Wehner, M. F. (2018). Anthropogenic influences on major tropical cyclone events. *Nature* 563, 339–346. doi:10.1038/s41586-018-0673-2.
Paul, S., Ghosh, S., Oglesby, R., Pathak, A., Chandrasekharan, A., and Ramsankaran, R. (2016). Weakening of Indian

Summer Monsoon Rainfall due to Changes in Land Use Land Cover. *Sci. Rep.* 6. doi:10.1038/srep32177.
Peck, D. E., and Adams, R. M. (2010). Farm-level impacts of prolonged drought : is a multiyear event more than the sum of its parts ? 43–60. doi:10.1111/j.1467-8489.2009.00478.x.
Pedro, J. B., Martin, T., Steig, E. J., Jochum, M., Park, W., and Rasmussen, S. O. (2016). Southern Ocean deep convection as a driver of Antarctic warming events. *Geophys. Res. Lett.* 43, 2192–2199. doi:10.1002/2016GL067861.
Peings, Y., and Magnusdottir, G. (2014). Response of the Wintertime Northern Hemisphere Atmospheric Circulation to Current and Projected Arctic Sea Ice Decline: A Numerical Study with CAM5. *J. Clim.* 27, 244–264. doi:10.1175/JCLI-D-13-00272.1.
Peña-Ortiz, C., Barriopedro, D., and García-Herrera, R. (2015). Multidecadal Variability of the Summer Length in Europe*. *J. Clim.* 28, 5375–5388. doi:10.1175/JCLI-D-14-00429.1.
Penalba, O. C., and Robledo, F. A. (2010). Spatial and temporal variability of the frequency of extreme daily rainfall regime in the La Plata Basin during the 20th century. *Clim. Change* 98, 531–550. doi:10.1007/s10584-009-9744-6.
Pepin, N., Bradley, R. S., Diaz, H. F., Baraer, M., Caceres, E. B., Forsythe, N., et al. (2015). Elevation-dependent warming in mountain regions of the world. *Nat. Clim. Chang.* 5, 424–430. doi:10.1038/nclimate2563.
Pepler, A., Coutts-Smith, A., and Timbal, B. (2013). The role of East Coast Lows on rainfall patterns and inter-annual variability across the East Coast of Australia. *Int. J. Climatol.*
Pepler, A., Dowdy, A., and Hope, P. (2018). A global climatology of surface anticyclones, their variability, associated drivers and long-term trends. *Clim. Dyn.* doi:10.1007/s00382-018-4451-5.
Pepler, A. S., Alexander, L. V., Evans, J. P., and Sherwood, S. C. (2017). The influence of topography on midlatitude cyclones on Australia's east coast. *J. Geophys. Res. Atmos.* 122, 9173–9184. doi:10.1002/2017JD027345.
Pessacg, N. L., Solman, S. A., Samuelsson, P., Sanchez, E., Marengo, J., Li, L., et al. (2014). The surface radiation budget over South America in a set of regional climate models from the CLARIS-LPB project. *Clim. Dyn.* 43, 1221–1239. doi:10.1007/s00382-013-1916-4.
Petoukhov, V., Rahmstorf, S., Petri, S., and Schellnhuber, H. J. (2013). Quasiresonant amplification of planetary waves and recent Northern Hemisphere weather extremes. *Proc. Natl. Acad. Sci.* 110, 5336–5341. doi:10.1073/pnas.1222000110.
Petrie, R. E., Shaffrey, L. C., and Sutton, R. T. (2015). Atmospheric Impact of Arctic Sea Ice Loss in a Coupled Ocean–Atmosphere Simulation*. *J. Clim.* 28, 9606–9622. doi:10.1175/JCLI-D-15-0316.1.
Pettenger, M. E. (2016). *The Social Construction of Climate Change*. Routledge doi:10.4324/9781315552842.
Pfahl, S. (2014). Characterising the relationship between weather extremes in Europe and synoptic circulation features. *Nat. Hazards Earth Syst. Sci.* 14, 1461–1475. doi:10.5194/nhess-14-1461-2014.
Pfahl, S., and Wernli, H. (2012). Quantifying the relevance of atmospheric blocking for co-located temperature extremes in the Northern Hemisphere on (sub-)daily time scales. *Geophys. Res. Lett.* 39, n/a-n/a. doi:10.1029/2012GL052261.
Pfeifroth, U., Bojanowski, J. S., Clerbaux, N., Manara, V., Sanchez-Lorenzo, A., Trentmann, J., et al. (2018). Satellite-based trends of solar radiation and cloud parameters in Europe. *Adv. Sci. Res.* 15, 31–37. doi:10.5194/asr-15-31-2018.
Pham, T. Van, Brauch, J., Früh, B., and Ahrens, B. (2017). Simulation of snowbands in the Baltic Sea area with the coupled atmosphere-ocean-ice model COSMO-CLM/NEMO. *Meteorol. Zeitschrift* 26, 71–82. doi:10.1127/metz/2016/0775.
Pham, T. Van, Brauch, J., Früh, B., and Ahrens, B. (2018). Added decadal prediction skill with the coupled regional climate model COSMO-CLM/NEMO. *Meteorol. Zeitschrift* 27, 391–399. doi:10.1127/metz/2018/0872.
Philipona, R., Behrens, K., and Ruckstuhl, C. (2009). How declining aerosols and rising greenhouse gases forced rapid warming in Europe since the 1980s. *Geophys. Res. Lett.* 36. doi:10.1029/2008GL036350.
Philippon, N., Rouault, M., Richard, Y., and Favre, A. (2012). The influence of ENSO on winter rainfall in South Africa. *Int. J. Climatol.* 32, 2333–2347. doi:10.1002/joc.3403.
Pierce, D. W., Cayan, D. R., Maurer, E. P., Abatzoglou, J. T., and Hegewisch, K. C. (2015). Improved Bias Correction Techniques for Hydrological Simulations of Climate Change*. *J. Hydrometeorol.* 16, 2421–2442. doi:10.1175/JHM-D-14-0236.1.
Pietikäinen, J.-P., Markkanen, T., Sieck, K., Jacob, D., Korhonen, J., Räisänen, P., et al. (2018). The regional climate model REMO (v2015) coupled with the 1-D freshwater lake model FLake (v1): Fenno-Scandinavian climate and lakes. *Geosci. Model Dev.* 11, 1321–1342. doi:10.5194/gmd-11-1321-2018.
Pinto, I., Jack, C., and Hewitson, B. (2018). Process-based model evaluation and projections over southern Africa from Coordinated Regional Climate Downscaling Experiment and Coupled Model Intercomparison Project Phase 5 models. *Int. J. Climatol.* 38, 4251–4261. doi:10.1002/joc.5666.
Pinto, J. G., Reyers, M., and Ulbrich, U. (2011). The variable link between PNA and NAO in observations and in multi-century CGCM simulations. *Clim. Dyn.* 36, 337–354. doi:10.1007/s00382-010-0770-x.
Pithan, F., Shepherd, T. G., Zappa, G., and Sandu, I. (2016). Climate model biases in jet streams, blocking and storm tracks resulting from missing orographic drag. *Geophys. Res. Lett.* 43, 7231–7240. doi:10.1002/2016GL069551.

Plant, R. S., and Yano, J.-I. (2015). *Parameterization of Atmospheric Convection*. IMPERIAL COLLEGE PRESS doi:10.1142/p1005.

Poan, E. D., Gachon, P., Laprise, R., Aider, R., and Dueymes, G. (2018). Investigating added value of regional climate modeling in North American winter storm track simulations. *Clim. Dyn.* 50, 1799–1818. doi:10.1007/s00382-017-3723-9.

Pokhrel, Y. N., Hanasaki, N., Wada, Y., and Kim, H. (2016). Recent progresses in incorporating human land-water management into global land surface models toward their integration into Earth system models. *Wiley Interdiscip. Rev. Water* 3, 548–574. doi:10.1002/wat2.1150.

Polade, S. D., Gershunov, A., Cayan, D. R., Dettinger, M. D., and Pierce, D. W. (2013). Natural climate variability and teleconnections to precipitation over the Pacific-North American region in CMIP3 and CMIP5 models. *Geophys. Res. Lett.* 40, 2296–2301. doi:10.1002/grl.50491.

Polcher, J., Piles, M., Gelati, E., Barella-Ortiz, A., and Tello, M. (2016). Comparing surface-soil moisture from the SMOS mission and the ORCHIDEE land-surface model over the Iberian Peninsula. *Remote Sens. Environ.* 174, 69–81. doi:https://doi.org/10.1016/j.rse.2015.12.004.

Poli, P., Hersbach, H., Dee, D. P., Berrisford, P., Simmons, A. J., Vitart, F., et al. (2016). ERA-20C: An Atmospheric Reanalysis of the Twentieth Century. *J. Clim.* 29, 4083–4097. doi:10.1175/JCLI-D-15-0556.1.

Polson, D., Bollasina, M., Hegerl, G. C., and Wilcox, L. J. (2014). Decreased monsoon precipitation in the Northern Hemisphere due to anthropogenic aerosols. *Geophys. Res. Lett.* 41, 6023–6029. doi:10.1002/2014GL060811.

Polvani, L. M., Waugh, D. W., Correa, G. J. P., and Son, S.-W. (2011). Stratospheric Ozone Depletion: The Main Driver of Twentieth-Century Atmospheric Circulation Changes in the Southern Hemisphere. *J. Clim.* 24, 795–812. doi:10.1175/2010JCLI3772.1.

Pook, M. J., Risbey, J. S., and McIntosh, P. C. (2012). The Synoptic Climatology of Cool-Season Rainfall in the Central Wheatbelt of Western Australia. *Mon. Weather Rev.* 140, 28–43. doi:10.1175/MWR-D-11-00048.1.

Prasanna, V. (2016). Assessment of South Asian Summer Monsoon Simulation in CMIP5-Coupled Climate Models During the Historical Period (1850--2005). *Pure Appl. Geophys.* 173, 1379–1402. doi:10.1007/s00024-015-1126-6.

Prein, A., Bukovsky, M., Mearns, L., Bruyère, C., and Done, J. (2019). Simulating North American weather types with regional climate models. *Frontiers (Boulder).*

Prein, A. F., and Gobiet, A. (2017). Impacts of uncertainties in European gridded precipitation observations on regional climate analysis. *Int. J. Climatol.* 37, 305–327. doi:10.1002/joc.4706.

Prein, A. F., Gobiet, A., Suklitsch, M., Truhetz, H., Awan, N. K., Keuler, K., et al. (2013a). Added value of convection permitting seasonal simulations. *Clim. Dyn.* 41, 2655–2677. doi:10.1007/s00382-013-1744-6.

Prein, A. F., Gobiet, A., Truhetz, H., Keuler, K., Goergen, K., Teichmann, C., et al. (2016a). Precipitation in the EURO-CORDEX 0.11∘ and 0.44∘ simulations: high resolution, high benefits? *Clim. Dyn.* 46, 383–412. doi:10.1007/s00382-015-2589-y.

Prein, A. F., Holland, G. J., Rasmussen, R. M., Clark, M. P., and Tye, M. R. (2016b). Running dry: The U.S. Southwest's drift into a drier climate state. *Geophys. Res. Lett.* 43, 1272–1279. doi:10.1002/2015GL066727.

Prein, A. F., Holland, G. J., Rasmussen, R. M., Done, J., Ikeda, K., Clark, M. P., et al. (2013b). Importance of Regional Climate Model Grid Spacing for the Simulation of Heavy Precipitation in the Colorado Headwaters. *J. Clim.* 26, 4848–4857. doi:10.1175/JCLI-D-12-00727.1.

Prein, A. F., Langhans, W., Fosser, G., Ferrone, A., Ban, N., Goergen, K., et al. (2015). A review on regional convection-permitting climate modeling: Demonstrations, prospects, and challenges. *Rev. Geophys.* 53, 323–361. doi:10.1002/2014RG000475.

Prein, A. F., Liu, C., Ikeda, K., Trier, S. B., Rasmussen, R. M., Holland, G. J., et al. (2017). Increased rainfall volume from future convective storms in the US. *Nat. Clim. Chang.* 7, 880–884. doi:10.1038/s41558-017-0007-7.

Previdi, M., Smith, K. L., and Polvani, L. M. (2015). How well do the CMIP5 models simulate the antarctic atmospheric energy budget? *J. Clim.* doi:10.1175/JCLI-D-15-0027.1.

Prodhomme, C., Battï¿½, L., Massonnet, F., Davini, P., Bellprat, O., Guemas, V., et al. (2016). Benefits of increasing the model resolution for the seasonal forecast quality in EC-earth. *J. Clim.* 29. doi:10.1175/JCLI-D-16-0117.1.

Pryor, S. C., and Hahmann, A. N. (2019). "Downscaling Wind," in *Oxford Research Encyclopedia of Climate Science* (Oxford University Press). doi:10.1093/acrefore/9780190228620.013.730.

Purich, A., Cowan, T., Min, S.-K., and Cai, W. (2013). Autumn Precipitation Trends over Southern Hemisphere Midlatitudes as Simulated by CMIP5 Models. *J. Clim.* 26, 8341–8356. doi:10.1175/JCLI-D-13-00007.1.

Qian, C., and Zhou, T. (2014). Multidecadal variability of North China aridity and its relationship to PDO during 1900-2010. *J. Clim.* 27, 1210–1222. doi:10.1175/JCLI-D-13-00235.1.

Racherla, P. N., Shindell, D. T., and Faluvegi, G. S. (2012). The added value to global model projections of climate change by dynamical downscaling: A case study over the continental U.S. using the GISS-ModelE2 and WRF models. *J. Geophys. Res. Atmos.* 117, D20118. doi:10.1029/2012JD018091.

Rackow, T., Goessling, H. F., Jung, T., Sidorenko, D., Semmler, T., Barbi, D., et al. (2018). Towards multi-resolution global climate modeling with ECHAM6-FESOM. Part II: climate variability. *Clim. Dyn.* 50, 2369–2394. doi:10.1007/s00382-016-3192-6.

Rafael, S., Martins, H., Marta-Almeida, M., Sï¿½, E., Coelho, S., Rocha, A., et al. (2017). Quantification and mapping of urban fluxes under climate change: Application of WRF-SUEWS model to Greater Porto area (Portugal). *Environ. Res.* 155, 321–334. doi:10.1016/j.envres.2017.02.033.

Räisänen, J., and Palmer, T. N. (2001). A probability and decision-model analysis of a multimodel ensemble of climate change simulations. *J. Clim.* 14, 3212–3226. doi:10.1175/1520-0442(2001)014<3212:APADMA>2.0.CO;2.

Rajbhandari, R., Syed, M. A., Krishnan, R., Vellore, R., Xu, Y., Ren, Y., et al. (2019). "Unravelling Climate Change in the Hindu Kush Himalaya: Rapid Warming in the Mountains and Increasing Extremes," in *The Hindu Kush Himalaya Assessment* (Cham: Springer International Publishing), 57–97. doi:10.1007/978-3-319-92288-1_3.

Rajczak, J., and Schär, C. (2017). Projections of Future Precipitation Extremes Over Europe: A Multimodel Assessment of Climate Simulations. *J. Geophys. Res. Atmos.* 122, 10,773-10,800. doi:10.1002/2017JD027176.

Rajeevan, M., and Bhate, J. (2008). A High Resolution Daily Gridded for Mesoscale Meteorological Studies M Rajeevan. 96.

Rajeevan, M., Bhate, J., Kale, J. D., and Lal, B. (2006). High resolution daily gridded rainfall data for the Indian region: Analysis of break and active monsoon spells. *Curr. Sci.* doi:10.1007/s12040-007-0019-1.

Ralph, F. M., and Dettinger, M. D. (2011). Storms Floods and the Science of Atmospheric Rivers. *EOS, Trans. Am. Geophys. Union* 92, 2009–2011.

Ramanathan, V., and Carmichael, G. (2008). Global and regional climate changes due to black carbon. *Nat. Geosci.* 1, 221–227. doi:10.1038/ngeo156.

Ramarao, M. V. S., Krishnan, R., Sanjay, J., and Sabin, T. P. (2015). Understanding land surface response to changing South Asian monsoon in a warming climate. *Earth Syst. Dyn.* 6, 569–582. doi:10.5194/esd-6-569-2015.

Ramesh, K. V., and Goswami, P. (2014). Assessing reliability of regional climate projections: The case of Indian monsoon. *Sci. Rep.* doi:10.1038/srep04071.

Rasmijn, L. M., van der Schrier, G., Bintanja, R., Barkmeijer, J., Sterl, A., and Hazeleger, W. (2018). Future equivalent of 2010 Russian heatwave intensified by weakening soil moisture constraints. *Nat. Clim. Chang.* 8, 381–385. doi:10.1038/s41558-018-0114-0.

Rauscher, S. A., Giorgi, F., Diffenbaugh, N. S., and Seth, Æ. A. (2008). Extension and Intensification of the Meso-American mid-summer drought in the twenty-first century. 551–571. doi:10.1007/s00382-007-0359-1.

Rauscher, S. A., Kucharski, F., and Enfield, D. B. (2011). The Role of Regional SST Warming Variations in the Drying of Meso-America in Future Climate Projections *. *J. Clim.* 24, 2003–2016. doi:10.1175/2010JCLI3536.1.

Ravestein, P., van der Schrier, G., Haarsma, R., Scheele, R., and van den Broek, M. (2018). Vulnerability of European intermittent renewable energy supply to climate change and climate variability. *Renew. Sustain. Energy Rev.* 97, 497–508. doi:https://doi.org/10.1016/j.rser.2018.08.057.

Re, M., and Barros, V. R. (2009). Extreme rainfalls in SE South America. *Clim. Change* 96, 119–136. doi:10.1007/s10584-009-9619-x.

Reason, C. J. C., and Jagadheesha, D. (2005). Relationships between South Atlantic SST Variability and Atmospheric Circulation over the South African Region during Austral Winter. *J. Clim.* 18, 3339–3355. doi:10.1175/JCLI3474.1.

Reason, C. J. C., and Rouault, M. (2005). Links between the Antarctic Oscillation and winter rainfall over western South Africa. *Geophys. Res. Lett.* 32, n/a-n/a. doi:10.1029/2005GL022419.

Reboita, M., Fernandez, J., Pereira Llopart, M., Porfirio da Rocha, R., Albertani Pampuch, L., and Cruz, F. (2014). Assessment of RegCM4.3 over the CORDEX South America domain: sensitivity analysis for physical parameterization schemes. *Clim. Res.* 60, 215–234. doi:10.3354/cr01239.

Reboita, M. S., da Rocha, R. P., de Souza, M. R., and Llopart, M. (2018). Extratropical cyclones over the southwestern South Atlantic Ocean: HadGEM2-ES and RegCM4 projections. *Int. J. Climatol.* 38, 2866–2879. doi:10.1002/joc.5468.

Rehman, N., Adnan, M., and Ali, S. (2018). *Assessment of CMIP5 climate models over South Asia and climate change projections over Pakistan under representative concentration pathways*. doi:10.1504/IJGW.2018.095994.

Reichle, R. H., De Lannoy, G. J. M., Liu, Q., Ardizzone, J. V, Colliander, A., Conaty, A., et al. (2017). Assessment of the SMAP Level-4 Surface and Root-Zone Soil Moisture Product Using In Situ Measurements. *J. Hydrometeorol.* 18, 2621–2645. doi:10.1175/JHM-D-17-0063.1.

Ren, Y., Song, L., Xiao, Y., and Du, L. (2018). Underestimated interannual variability of East Asian summer rainfall under climate change. *Theor. Appl. Climatol.* doi:10.1007/s00704-018-2398-4.

Rice, J. L., Woodhouse, C. A., and Lukas, J. J. (2009). Science and Decision Making: Water Management and Tree-Ring Data in the Western United States. *JAWRA J. Am. Water Resour. Assoc.* 45, 1248–1259. doi:10.1111/j.1752-1688.2009.00358.x.

Richter, I., and Xie, S.-P. (2008). On the origin of equatorial Atlantic biases in coupled general circulation models. *Clim. Dyn.* 31, 587–598. doi:10.1007/s00382-008-0364-z.

Richter, I., Xie, S.-P., Behera, S. K., Doi, T., and Masumoto, Y. (2014). Equatorial Atlantic variability and its relation to mean state biases in CMIP5. *Clim. Dyn.* 42, 171–188. doi:10.1007/s00382-012-1624-5.

Rienecker, M. M., Suarez, M. J., Gelaro, R., Todling, R., Bacmeister, J., Liu, E., et al. (2011). MERRA: NASA's Modern-Era Retrospective Analysis for Research and Applications. *J. Clim.* 24, 3624–3648. doi:10.1175/JCLI-D-

11-00015.1.
Risbey, J. S., Pook, M. J., and McIntosh, P. C. (2009). On the remote drivers of rainfall variability in Australia. *Mon. Weather*.
Roberts, M. J., Vidale, P. L., Senior, C., Hewitt, H. T., Bates, C., Berthou, S., et al. (2018). The benefits of global high-resolution for climate simulation: process-understanding and the enabling of stakeholder decisions at the regional scale. *Bull. Am. Meteorol. Soc.* 0, null. doi:10.1175/BAMS-D-15-00320.1.
Robeson, S. M. (2015). Revisiting the recent California drought as an extreme value. *Geophys. Res. Lett.* 42, 6771–6779. doi:10.1002/2015GL064593.
Robin, Y., Vrac, M., Naveau, P., and Yiou, P. (2019). Multivariate stochastic bias corrections with optimal transport. *Hydrol. Earth Syst. Sci.* 23, 773–786. doi:10.5194/hess-23-773-2019.
Robins, S. (2019). 'Day Zero', Hydraulic Citizenship and the Defence of the Commons in Cape Town: A Case Study of the Politics of Water and its Infrastructures (2017–2018). *J. South. Afr. Stud.*, 1–25. doi:10.1080/03057070.2019.1552424.
Robson, J., Ortega, P., and Sutton, R. (2016). A reversal of climatic trends in the North Atlantic since 2005. *Nat. Geosci.* 9, 513–517. doi:10.1038/ngeo2727.
Rodríguez-Fonseca, B., Mohino, E., Mechoso, C. R., Caminade, C., Biasutti, M., Gaetani, M., et al. (2015). Variability and Predictability of West African Droughts: A Review on the Role of Sea Surface Temperature Anomalies. *J. Clim.* 28, 4034–4060. doi:10.1175/JCLI-D-14-00130.1.
Roehrig, R., Bouniol, D., Guichard, F., Hourdin, F. déric, and Redelsperger, J. L. (2013a). The present and future of the west african monsoon: A process-oriented assessment of CMIP5 simulations along the AMMA transect. *J. Clim.* doi:10.1175/JCLI-D-12-00505.1.
Roehrig, R., Bouniol, D., Guichard, F., Hourdin, F., and Redelsperger, J.-L. (2013b). The Present and Future of the West African Monsoon: A Process-Oriented Assessment of CMIP5 Simulations along the AMMA Transect. *J. Clim.* 26, 6471–6505. doi:10.1175/JCLI-D-12-00505.1.
Rohde, R., Muller, R., Jacobsen, R., Muller, E., and Wickham, C. (2013). A New Estimate of the Average Earth Surface Land Temperature Spanning 1753 to 2011. *Geoinformatics Geostatistics An Overv.* 01. doi:10.4172/2327-4581.1000101.
Rojas, R., Feyen, L., Dosio, A., and Bavera, D. (2011). Improving pan-European hydrological simulation of extreme events through statistical bias correction of RCM-driven climate simulations. *Hydrol. Earth Syst. Sci.* 15, 2599–2620. doi:10.5194/hess-15-2599-2011.
Rosas, G., Gubler, S., Oria, C., Acuña, D., Avalos, G., Begert, M., et al. (2016). Towards implementing climate services in Peru – The project CLIMANDES. *Clim. Serv.* 4, 30–41. doi:10.1016/J.CLISER.2016.10.001.
Rostkier-Edelstein, D., Liu, Y., Wu, W., Kunin, P., Givati, A., and Ge, M. (2014). Towards a high-resolution climatography of seasonal precipitation over Israel. *Int. J. Climatol.* 34, 1964–1979. doi:10.1002/joc.3814.
Roxy, M. K., Ritika, K., Terray, P., Murtugudde, R., Ashok, K., and Goswami, B. N. (2015). Drying of Indian subcontinent by rapid Indian Ocean warming and a weakening land-sea thermal gradient. *Nat. Commun.* 6, 7423. doi:10.1038/ncomms8423.
Ruckstuhl, C., Philipona, R., Behrens, K., Collaud Coen, M., Dürr, B., Heimo, A., et al. (2008). Aerosol and cloud effects on solar brightening and the recent rapid warming. *Geophys. Res. Lett.* 35. doi:10.1029/2008GL034228.
Ruiz-Ramos, M., Rodríguez, A., Dosio, A., Goodess, C. M., Harpham, C., Mínguez, M. I., et al. (2016). Comparing correction methods of RCM outputs for improving crop impact projections in the Iberian Peninsula for 21st century. *Clim. Change* 134, 283–297. doi:10.1007/s10584-015-1518-8.
Rummukainen, M. (2016). Added value in regional climate modeling. *Wiley Interdiscip. Rev. Clim. Chang.* 7, 145–159. doi:10.1002/wcc.378.
Ruprich-Robert, Y., Delworth, T., Msadek, R., Castruccio, F., Yeager, S., and Danabasoglu, G. (2018). Impacts of the Atlantic Multidecadal Variability on North American Summer Climate and Heat Waves. *J. Clim.* 31, 3679–3700. doi:10.1175/JCLI-D-17-0270.1.
Ruprich-Robert, Y., Msadek, R., Castruccio, F., Yeager, S., Delworth, T., and Danabasoglu, G. (2017). Assessing the Climate Impacts of the Observed Atlantic Multidecadal Variability Using the GFDL CM2.1 and NCAR CESM1 Global Coupled Models. *J. Clim.* 30, 2785–2810. doi:10.1175/JCLI-D-16-0127.1.
Ruscica, R. C., Sörensson, A. A., and Menéndez, C. G. (2014). Hydrological links in Southeastern South America: soil moisture memory and coupling within a hot spot. *Int. J. Climatol.* 34, 3641–3653. doi:10.1002/joc.3930.
Ruscica, R. C., Sörensson, A. A., and Menéndez, C. G. (2015). Pathways between soil moisture and precipitation in southeastern South America. *Atmos. Sci. Lett.* 16, 267–272. doi:10.1002/asl2.552.
Russo, A., Gouveia, C. M., Dutra, E., Soares, P. M. M., and Trigo, R. M. (2019). The synergy between drought and extremely hot summers in the Mediterranean. *Environ. Res. Lett.* 14, 14011. doi:10.1088/1748-9326/aaf09e.
Russo, S., Sillmann, J., and Fischer, E. M. (2015). Top ten European heatwaves since 1950 and their occurrence in the coming decades. *Environ. Res. Lett.* 10, 124003. doi:10.1088/1748-9326/10/12/124003.
Ruti, P. M., Somot, S., Giorgi, F., Dubois, C., Flaounas, E., Obermann, A., et al. (2016). Med-CORDEX Initiative for Mediterranean Climate Studies. *Bull. Am. Meteorol. Soc.* 97, 1187–1208. doi:10.1175/BAMS-D-14-00176.1.
Rutz, J. J., Steenburgh, W. J., and Ralph, F. M. (2014). Climatological Characteristics of Atmospheric Rivers and Their

Inland Penetration over the Western United States. *Mon. Weather Rev.* 142, 905–921. doi:10.1175/mwr-d-13-00168.1.
Ryu, J. H., and Hayhoe, K. (2014). Understanding the sources of Caribbean precipitation biases in CMIP3 and CMIP5 simulations. *Clim. Dyn.* 42, 3233–3252. doi:10.1007/s00382-013-1801-1.
Saadi, S., Todorovic, M., Tanasijevic, L., Pereira, L. S., Pizzigalli, C., and Lionello, P. (2015). Climate change and Mediterranean agriculture: Impacts on winter wheat and tomato crop evapotranspiration, irrigation requirements and yield. *Agric. Water Manag.* 147, 103–115. doi:10.1016/j.agwat.2014.05.008.
Sabeerali, C. T., and Ajayamohan, R. S. (2018). On the shortening of Indian summer monsoon season in a warming scenario. *Clim. Dyn.* 50, 1609–1624. doi:10.1007/s00382-017-3709-7.
Sabeerali, C. T., Rao, S. A., Dhakate, A. R., Salunke, K., and Goswami, B. N. (2015). Why ensemble mean projection of south Asian monsoon rainfall by CMIP5 models is not reliable? *Clim. Dyn.* doi:10.1007/s00382-014-2269-3.
Sabin, T. P., Krishnan, R., Ghattas, J., Denvil, S., Dufresne, J.-L., Hourdin, F., et al. (2013). High resolution simulation of the South Asian monsoon using a variable resolution global climate model. *Clim. Dyn.* 41, 173–194. doi:10.1007/s00382-012-1658-8.
Sachindra, D. A., Ng, A. W. M., Muthukumaran, S., and Perera, B. J. C. (2016). Impact of climate change on urban heat island effect and extreme temperatures: a case-study. *Q. J. R. Meteorol. Soc.* 142, 172–186. doi:10.1002/qj.2642.
Saeed, F., Hagemann, S., Saeed, S., and Jacob, D. (2013). Influence of mid-latitude circulation on upper Indus basin precipitation: the explicit role of irrigation. *Clim. Dyn.* 40, 21–38. doi:10.1007/s00382-012-1480-3.
Saha, A., Ghosh, S., Sahana, A. S., and Rao, E. P. (2014). Failure of CMIP5 climate models in simulating post-1950 decreasing trend of Indian monsoon. *Geophys. Res. Lett.* 41, 7323–7330. doi:10.1002/2014GL061573.
Salazar, E., Hammerling, D., Wang, X., Sansó, B., Finley, A. O., and Mearns, L. O. (2016). Observation-based blended projections from ensembles of regional climate models. *Clim. Change* 138, 55–69. doi:10.1007/s10584-016-1722-1.
Salunke, P., Jain, S., and Kanta Mishra, S. (2018). *Performance of the CMIP5 models in the simulation of the Himalaya-Tibetan Plateau monsoon*. doi:10.1007/s00704-018-2644-9.
Salvi, K., Kannan, S., and Ghosh, S. (2013). High-resolution multisite daily rainfall projections in India with statistical downscaling for climate change impacts assessment. *J. Geophys. Res. Atmos.* 118, 3557–3578. doi:10.1002/jgrd.502802013.
Salzmann, M., Weser, H., and Cherian, R. (2014). Robust response of Asian summer monsoon to anthropogenic aerosols in CMIP5 models. *J. Geophys. Res. Atmos.* 119, 11,321-11,337. doi:10.1002/2014JD021783.
Samaniego, L., Thober, S., Kumar, R., Wanders, N., Rakovec, O., Pan, M., et al. (2018). Anthropogenic warming exacerbates European soil moisture droughts. *Nat. Clim. Chang.* 8, 421–426. doi:10.1038/s41558-018-0138-5.
Samset, B. H., Sand, M., Smith, C. J., Bauer, S. E., Forster, P. M., Fuglestvedt, J. S., et al. (2018). Climate Impacts From a Removal of Anthropogenic Aerosol Emissions. *Geophys. Res. Lett.* 45, 1020–1029. doi:10.1002/2017GL076079.
Samson, G., Masson, S., Lengaigne, M., Keerthi, M. G., Vialard, J., Pous, S., et al. (2014). The NOW regional coupled model: Application to the tropical Indian Ocean climate and tropical cyclone activity. *J. Adv. Model. Earth Syst.* 6, 700–722. doi:10.1002/2014MS000324.
Samuelsson, P., Kourzeneva, E., and Mironov, D. (2010). The impact of lakes on the European climate as simulated by a regional climate model. *Boreal Environ. Res.* 15, 113–129.
San-Martín, D., Manzanas, R., Brands, S., Herrera, S., and Gutiérrez, J. M. (2017). Reassessing Model Uncertainty for Regional Projections of Precipitation with an Ensemble of Statistical Downscaling Methods. *J. Clim.* 30, 203–223. doi:10.1175/JCLI-D-16-0366.1.
Sanchez-Gomez, E., and Somot, S. (2018). Impact of the internal variability on the cyclone tracks simulated by a regional climate model over the Med-CORDEX domain. *Clim. Dyn.* 51, 1005–1021. doi:10.1007/s00382-016-3394-y.
Sánchez, E., Solman, S., Remedio, A. R. C., Berbery, H., Samuelsson, P., Da Rocha, R. P., et al. (2015). Regional climate modelling in CLARIS-LPB: a concerted approach towards twentyfirst century projections of regional temperature and precipitation over South America. *Clim. Dyn.* 45, 2193–2212. doi:10.1007/s00382-014-2466-0.
Sanderson, B. M., Knutti, R., and Caldwell, P. (2015). Addressing Interdependency in a Multimodel Ensemble by Interpolation of Model Properties. *J. Clim.* 28, 5150–5170. doi:10.1175/JCLI-D-14-00361.1.
Sanjay, J., Krishnan, R., Shrestha, A. B., Rajbhandari, R., and Ren, G.-Y. (2017). Downscaled climate change projections for the Hindu Kush Himalayan region using CORDEX South Asia regional climate models. *Adv. Clim. Chang. Res.* 8, 185–198. doi:10.1016/j.accre.2017.08.003.
Sanna, A., Lionello, P., and Gualdi, S. (2013). *Coupled atmosphere ocean climate model simulations in the Mediterranean region: Effect of a high-resolution marine model on cyclones and precipitation*. doi:10.5194/nhess-13-1567-2013.
Sanogo, S., Fink, A. H., Omotosho, J. A., Ba, A., Redl, R., and Ermert, V. (2015). Spatio-temporal characteristics of the recent rainfall recovery in West Africa. *Int. J. Climatol.* doi:10.1002/joc.4309.
Sarewitz, D. (2004). How science makes environmental controversies worse. *Environ. Sci. Policy* 7, 385–403. doi:10.1016/j.envsci.2004.06.001.

Sarr, A. B., Camara, M., and Diba, I. (2015). Spatial Distribution of Cordex Regional Climate Models Biases over West Africa. *Int. J. Geosci.* 06, 1018–1031. doi:10.4236/ijg.2015.69081.
Sato, K., Inoue, J., and Watanabe, M. (2014). Influence of the Gulf Stream on the Barents Sea ice retreat and Eurasian coldness during early winter. *Environ. Res. Lett.* 9, 084009. doi:10.1088/1748-9326/9/8/084009.
Saurral, R. I., Barros, V. R., and Lettenmaier, D. P. (2008). Land use impact on the Uruguay River discharge. *Geophys. Res. Lett.* 35, n/a-n/a. doi:10.1029/2008GL033707.
Saurral, R. I., Camilloni, I. A., and Barros, V. R. (2017). Low-frequency variability and trends in centennial precipitation stations in southern South America. *Int. J. Climatol.* 37, 1774–1793. doi:10.1002/joc.4810.
Sayles, J. S. (2018). Effects of social-ecological scale mismatches on estuary restoration at the project and landscape level in Puget Sound, USA. *Ecol. Restor.* 36, 62–75. doi:10.3368/er.36.1.62c.
Schaaf, B., and Feser, F. (2018). Is there added value of convection-permitting regional climate model simulations for storms over the German Bight and Northern Germany? *Meteorol. Hydrol. Water Manag.* 6, 21–37. doi:10.26491/mhwm/85507.
Schaller, N., Cermak, J., Wild, M., and Knutti, R. (2013). The sensitivity of the modeled energy budget and hydrological cycle to CO<sub>2</sub> and solar forcing. *Earth Syst. Dyn.* 4, 253–266. doi:10.5194/esd-4-253-2013.
Schär, C., Frei, C., Lüthi, D., and Davies, H. C. (1996). Surrogate climate-change scenarios for regional climate models. *Geophys. Res. Lett.* 23, 669–672. doi:10.1029/96GL00265.
Schewe, J., and Levermann, A. (2017). Non-linear intensification of Sahel rainfall as a possible dynamic response to future warming. *Earth Syst. Dyn.* 8, 495–505. doi:10.5194/esd-8-495-2017.
Schiemann, R., Demory, M.-E., Mizielinski, M. S., Roberts, M. J., Shaffrey, L. C., Strachan, J., et al. (2014). The sensitivity of the tropical circulation and Maritime Continent precipitation to climate model resolution. *Clim. Dyn.* 42, 2455–2468. doi:10.1007/s00382-013-1997-0.
Schlünzen, K. H., Hoffmann, P., Rosenhagen, G., and Riecke, W. (2010). Long-term changes and regional differences in temperature and precipitation in the metropolitan area of Hamburg. *Int. J. Climatol.* 30, 1121–1136. doi:10.1002/joc.1968.
Schmetz, J., Pili, P., Tjemkes, S., Just, D., Kerkmann, J., Rota, S., et al. (2002). An Introduction to Meteosat Second Generation (MSG). *Bull. Am. Meteorol. Soc.* 83, 977–992. doi:10.1175/1520-0477(2002)083<0977:AITMSG>2.3.CO;2.
Schmid, P. E., and Niyogi, D. (2014). Modeling urban precipitation modification by spatially heterogeneous aerosols. *J. Appl. Meteorol. Climatol.* 56, 2141–2153. doi:10.1175/JAMC-D-16-0320.1.
Schneider, S. H. (2001). What is “dangerous” climate change? *Nature* 411, 17–19. doi:10.1038/35075167.
Schneider, U., Finger, P., Meyer-Christoffer, A., Rustemeier, E., Ziese, M., Becker, A., et al. (2017). Evaluating the Hydrological Cycle over Land Using the Newly-Corrected Precipitation Climatology from the Global Precipitation Climatology Centre (GPCC). *Atmosphere (Basel).* 8, 52. doi:10.3390/atmos8030052.
Schubert, S., Grossman-Clarke, S., and Martilli, A. (2012). A Double-Canyon Radiation Scheme for Multi-Layer Urban Canopy Models. *Boundary-Layer Meteorol.* doi:10.1007/s10546-012-9728-3.
Schurer, A. P., Mann, M. E., Hawkins, E., Tett, S. F. B., and Hegerl, G. C. (2017). Importance of the pre-industrial baseline for likelihood of exceeding Paris goals. *Nat. Clim. Chang.* 7, 563–567. doi:10.1038/nclimate3345.
Scott, D., Iipinge, K. N., Mfune, J. K. E., Muchadenyika, D., Makuti, O. V, and Ziervogel, G. (2018). The Story of Water in Windhoek: A Narrative Approach to Interpreting a Transdisciplinary Process. *Water* 10. doi:10.3390/w10101366.
Screen, J. A. (2014). Arctic amplification decreases temperature variance in northern mid- to high-latitudes. *Nat. Clim. Chang.* 4, 577–582. doi:10.1038/nclimate2268.
Screen, J. A., Deser, C., Simmonds, I., and Tomas, R. (2014). Atmospheric impacts of Arctic sea-ice loss, 1979–2009: separating forced change from atmospheric internal variability. *Clim. Dyn.* 43, 333–344. doi:10.1007/s00382-013-1830-9.
Screen, J. A., Deser, C., Smith, D. M., Zhang, X., Blackport, R., Kushner, P. J., et al. (2018). Consistency and discrepancy in the atmospheric response to Arctic sea-ice loss across climate models. *Nat. Geosci.* 11, 155–163. doi:10.1038/s41561-018-0059-y.
Screen, J. A., and Simmonds, I. (2013). Exploring links between Arctic amplification and mid-latitude weather. *Geophys. Res. Lett.* 40, 959–964. doi:10.1002/grl.50174.
Seager, R., and Hoerling, M. (2014). Atmosphere and Ocean Origins of North American Droughts. *J. Clim.* 27, 4581–4606. doi:10.1175/JCLI-D-13-00329.1.
Seager, R., Naik, N., Baethgen, W., Robertson, A., Kushnir, Y., Nakamura, J., et al. (2010). Tropical Oceanic Causes of Interannual to Multidecadal Precipitation Variability in Southeast South America over the Past Century*. *J. Clim.* 23, 5517–5539. doi:10.1175/2010JCLI3578.1.
Seager, R., Neelin, D., Simpson, I., Liu, H., Henderson, N., Shaw, T., et al. (2014). Dynamical and thermodynamical causes of large-scale changes in the hydrological cycle over North America in response to global warming. *J. Clim.* 27, 7921–7948. doi:10.1175/JCLI-D-14-00153.1.
Seager, R., and Ting, M. (2017). Decadal Drought Variability Over North America: Mechanisms and Predictability.

*Curr. Clim. Chang. Reports* 3, 141–149. doi:10.1007/s40641-017-0062-1.
Seaman, N. L., Ludwig, F. L., Donall, E. G., Warner, T. T., and Bhumralkar, C. M. (1989). Numerical Studies of Urban Planetary Boundary-Layer Structure under Realistic Synoptic Conditions. *J. Appl. Meteorol.* 28, 760–781. doi:10.1175/1520-0450(1989)028<0760:NSOUPB>2.0.CO;2.
Sein, D. V., Mikolajewicz, U., Gröger, M., Fast, I., Cabos, W., Pinto, J. G., et al. (2015). Regionally coupled atmosphere-ocean-sea ice-marine biogeochemistry model ROM: 1. Description and validation. *J. Adv. Model. Earth Syst.* 7, 268–304. doi:10.1002/2014MS000357.
Seino, N., Aoyagi, T., and Tsuguti, H. (2018a). Numerical simulation of urban impact on precipitation in Tokyo: How does urban temperature rise affect precipitation? *Urban Clim.* 23, 8–35. doi:10.1016/j.uclim.2016.11.007.
Seino, N., Oda, R., Sugawara, H., and Aoyagi, T. (2018b). Observations and Simulations of the Mesoscale Environment in TOMACS Urban Heavy Rain Events. *J. Meteorol. Soc. Japan. Ser. II* advpub. doi:10.2151/jmsj.2018-029.
Seneviratne, S. I., Corti, T., Davin, E. L., Hirschi, M., Jaeger, E. B., Lehner, I., et al. (2010). Investigating soil moisture–climate interactions in a changing climate: A review. *Earth-Science Rev.* 99, 125–161. doi:10.1016/j.earscirev.2010.02.004.
Seneviratne, S. I., Donat, M. G., Pitman, A. J., Knutti, R., and Wilby, R. L. (2016). Allowable CO2 emissions based on regional and impact-related climate targets. *Nature* 529, 477–483. doi:10.1038/nature16542.
Seneviratne, S. I., Lüthi, D., Litschi, M., and Schär, C. (2006). Land-atmosphere coupling and climate change in Europe. *Nature*. doi:10.1038/nature05095.
Seneviratne, S. I., Nicholls, N., Easterling, D., Goodess, C. M., Kanae, S., Kossin, J., et al. (2012). "Changes in climate extremes and their impacts on the natural physical environment," in *Managing the Risks of Extreme Events and Disasters to Advance Climate Change Adaptation: Special Report of the Intergovernmental Panel on Climate Change*, 109–230. doi:10.1017/CBO9781139177245.006.
Seneviratne, S. I., Wilhelm, M., Stanelle, T., van den Hurk, B., Hagemann, S., Berg, A., et al. (2013). Impact of soil moisture-climate feedbacks on CMIP5 projections: First results from the GLACE-CMIP5 experiment. *Geophys. Res. Lett.* 40, 5212–5217. doi:10.1002/grl.50956.
Seo, K.-H., Lee, H.-J., and Frierson, D. M. W. (2016). Unraveling the Teleconnection Mechanisms that Induce Wintertime Temperature Anomalies over the Northern Hemisphere Continents in Response to the MJO. *J. Atmos. Sci.* 73, 3557–3571. doi:10.1175/JAS-D-16-0036.1.
Seo, K.-H., Ok, J., Son, J.-H., and Cha, D.-H. (2013). Assessing Future Changes in the East Asian Summer Monsoon Using CMIP5 Coupled Models. *J. Clim.* 26, 7662–7675. doi:10.1175/JCLI-D-12-00694.1.
Seth, A., Rauscher, S. A., Biasutti, M., Giannini, A., Camargo, S. J., and Rojas, M. (2013). CMIP5 Projected Changes in the Annual Cycle of Precipitation in Monsoon Regions. *J. Clim.* 26, 7328–7351. doi:10.1175/JCLI-D-12-00726.1.
Sexton, D. M. H., Karmalkar, A. V, Murphy, J. M., Williams, K. D., Boutle, I. A., Morcrette, C. J., et al. (2019). Finding plausible and diverse variants of a climate model. Part 1: establishing the relationship between errors at weather and climate time scales. *Clim. Dyn.* doi:10.1007/s00382-019-04625-3.
Shaevitz, D. A., Camargo, S. J., Sobel, A. H., Jonas, J. A., Kim, D., Kumar, A., et al. (2014). Characteristics of tropical cyclones in high-resolution models in the present climate. *J. Adv. Model. Earth Syst.* 6, 1154–1172. doi:10.1002/2014MS000372.
Shashikanth, K., Salvi, K., Ghosh, S., and Rajendran, K. (2014). Do CMIP5 simulations of Indian summer monsoon rainfall differ from those of CMIP3? *Atmos. Sci. Lett.* 15, 79–85. doi:10.1002/asl2.466.
Shastri, H., Paul, S., Ghosh, S., Paul, S., Ghosh, S., Karmakar, S. (2015). Impacts of urbanization on Indian summer monsoon rainfall extremes. *J. Geophys. Res. Atmos.* 120, 495–516. doi:10.1002/2014JD022061.Received.
Shastri, H., Paul, S., Ghosh, S., and Karmakar, S. (2015). Impacts of urbanization on Indian summer monsoon rainfall extremes. *J. Geophys. Res. Atmos.* 120, 495–516. doi:10.1002/2014JD022061.
Shaw, T. A., Baldwin, M., Barnes, E. A., Caballero, R., Garfinkel, C. I., Hwang, Y.-T., et al. (2016). Storm track processes and the opposing influences of climate change. *Nat. Geosci.* 9, 656. Available at: http://dx.doi.org/10.1038/ngeo2783.
Sheen, K. L., Smith, D. M., Dunstone, N. J., Eade, R., Rowell, D. P., and Vellinga, M. (2017). Skilful prediction of Sahel summer rainfall on inter-annual and multi-year timescales. *Nat. Commun.* 8, 14966. doi:10.1038/ncomms14966.
Shen, W., Song, J., Liu, G., Zhuang, Y., Wang, Y., and Tang, J. (2018a). The effect of convection scheme on tropical cyclones simulations over the CORDEX East Asia domain. *Clim. Dyn.* doi:10.1007/s00382-018-4405-y.
Shen, Y., Hong, Z., Pan, Y., Yu, J., and Maguire, L. (2018b). China's 1 km Merged Gauge, Radar and Satellite Experimental Precipitation Dataset. *Remote Sens.* 10. doi:10.3390/rs10020264.
Shepherd, T. G. (2014). Atmospheric circulation as a source of uncertainty in climate change projections. *Nat. Geosci.* 7, 703. Available at: http://dx.doi.org/10.1038/ngeo2253.
Shepherd, T. G. (2016). A Common Framework for Approaches to Extreme Event Attribution. *Curr. Clim. Chang. Reports* 2, 28–38. doi:10.1007/s40641-016-0033-y.
Shepherd, T. G., Boyd, E., Calel, R. A., Chapman, S. C., Dessai, S., Dima-West, I. M., et al. (2018). Storylines: an

alternative approach to representing uncertainty in physical aspects of climate change. *Clim. Change* 151, 555–571. doi:10.1007/s10584-018-2317-9.
Shige, S., Kida, S., Ashiwake, H., Kubota, T., and Aonashi, K. (2013). Improvement of TMI Rain Retrievals in Mountainous Areas. *J. Appl. Meteorol. Climatol.* 52, 242–254. doi:10.1175/JAMC-D-12-074.1.
Shige, S., Nakano, Y., and Yamamoto, M. K. (2017). Role of Orography, Diurnal Cycle, and Intraseasonal Oscillation in Summer Monsoon Rainfall over the Western Ghats and Myanmar Coast. *J. Clim.* 30, 9365–9381. doi:10.1175/JCLI-D-16-0858.1.
Shige, S., Takayabu, Y. N., KIDA, S., Tao, W. K., Zeng, X., Yokoyama, C., et al. (2009). Spectral retrieval of latent heating profiles from TRMM PR data. Part IV: comparisons of lookup tables from two-and three-dimensional cloud-resolving model simulations. *J. Clim.* doi:10.1175/2009JCLI2919.1.
Shindell, D., and Faluvegi, G. (2009). Climate response to regional radiative forcing during the twentieth century. *Nat. Geosci.* 2, 294–300. doi:10.1038/ngeo473.
Shiogama, H., Stone, D. A., Nagashima, T., Nozawa, T., and Emori, S. (2013). On the linear additivity of climate forcing-response relationships at global and continental scales. *Int. J. Climatol.* 33, 2542–2550. doi:10.1002/joc.3607.
Shrestha, B. A., and Devkota, P. L. (2010). Climate Change in the Eastern Himalayas : Observed Trends and Model Projections.
Shrestha, S., Yao, T., and Adhikari, T. R. (2019). Analysis of rainfall trends of two complex mountain river basins on the southern slopes of the Central Himalayas. *Atmos. Res.* 215, 99–115. doi:10.1016/j.atmosres.2018.08.027.
Shu, Q., Song, Z., and Qiao, F. (2015). Assessment of sea ice simulations in the CMIP5 models. *Cryosphere*. doi:10.5194/tc-9-399-2015.
Shukla, S. P., Puma, M. J., and Cook, B. I. (2014). The response of the South Asian Summer Monsoon circulation to intensified irrigation in global climate model simulations. *Clim. Dyn.* 42, 21–36. doi:10.1007/s00382-013-1786-9.
Shusse, Y., Shoji, Y., Maesaka, T., Sugawara, H., Misumi, R., Seino, N., et al. (2015). Tokyo Metropolitan Area Convection Study for Extreme Weather Resilient Cities. *Bull. Am. Meteorol. Soc.* doi:10.1175/bams-d-14-00209.1.
Si, D., and Ding, Y. (2013). Decadal change in the correlation pattern between the tibetan plateau winter snow and the East Asian summer precipitation during 1979-2011. *J. Clim.* doi:10.1175/JCLI-D-12-00587.1.
Sigmond, M., and Fyfe, J. C. (2016). Tropical Pacific impacts on cooling North American winters. *Nat. Clim. Chang.* 6, 970–974. doi:10.1038/nclimate3069.
Sillmann, J., Kharin, V. V., Zhang, X., Zwiers, F. W., and Bronaugh, D. (2013). Climate extremes indices in the CMIP5 multimodel ensemble: Part 1. Model evaluation in the present climate. *J. Geophys. Res. Atmos.* 118, 1716–1733. doi:10.1002/jgrd.50203.
Simmonds, I., and Govekar, P. D. (2014). What are the physical links between Arctic sea ice loss and Eurasian winter climate? *Environ. Res. Lett.* 9, 101003. doi:10.1088/1748-9326/9/10/101003.
Simpson, I. R., and Polvani, L. M. (2016). Revisiting the relationship between jet position, forced response, and annular mode variability in the southern midlatitudes. *Geophys. Res. Lett.* 43, 2896–2903. doi:10.1002/2016GL067989.
Simpson, I. R., Seager, R., Ting, M., and Shaw, T. A. (2016). Causes of change in Northern Hemisphere winter meridional winds and regional hydroclimate. *Nat. Clim. Chang.* 6, 65–70. doi:10.1038/nclimate2783.
Simpson, J., Kummerow, C., Tao, W.-K., and Adler, R. F. (1996). On the Tropical Rainfall Measuring Mission (TRMM). *Meteorol. Atmos. Phys.* 60, 19–36. doi:10.1007/BF01029783.
Singh, H. K. A., Hakim, G. J., Tardif, R., Emile-Geay, J., and Noone, D. C. (2018). Insights into Atlantic multidecadal variability using the Last Millennium Reanalysis framework. *Clim. Past* 14, 157–174. doi:10.5194/cp-14-157-2018.
Singh, J., Vittal, H., Karmakar, S., Ghosh, S., and Niyogi, D. (2016). Urbanization causes nonstationarity in Indian Summer Monsoon Rainfall extremes. *Geophys. Res. Lett.* 43, 11,269-11,277. doi:10.1002/2016GL071238.
Singh, R., and AchutaRao, K. (2018). Quantifying uncertainty in twenty-first century climate change over India. *Clim. Dyn.* doi:10.1007/s00382-018-4361-6.
Singh, S., Ghosh, S., Sahana, A. S., Vittal, H., and Karmakar, S. (2017). Do dynamic regional models add value to the global model projections of Indian monsoon? *Clim. Dyn.* 48, 1375–1397. doi:10.1007/s00382-016-3147-y.
Singh, V., and Goyal, M. K. (2016). Changes in climate extremes by the use of CMIP5 coupled climate models over eastern Himalayas. *Environ. Earth Sci.* 75, 839. doi:10.1007/s12665-016-5651-0.
Sippel, S., Otto, F. E. L., Flach, M., and van Oldenborgh, G. J. (2016). The Role of Anthropogenic Warming in 2015 Central European Heat Waves. *Bull. Am. Meteorol. Soc.* 97, S51–S56. doi:10.1175/BAMS-D-16-0150.1.
Sippel, S., Zscheischler, J., Mahecha, M. D., Orth, R., Reichstein, M., Vogel, M., et al. (2017). Refining multi-model projections of temperature extremes by evaluation against land–atmosphere coupling diagnostics. *Earth Syst. Dyn.* 8, 387–403. doi:10.5194/esd-8-387-2017.
Sjolte, J., Sturm, C., Adolphi, F., Vinther, B. M., Werner, M., Lohmann, G., et al. (2018). Solar and volcanic forcing of North Atlantic climate inferred from a process-based reconstruction. *Clim. Past* 14, 1179–1194. doi:10.5194/cp-14-1179-2018.
Skinner, C. B., and Diffenbaugh, N. S. (2014). Projected changes in African easterly wave intensity and track in

response to greenhouse forcing. *Proc. Natl. Acad. Sci.* 111, 6882–6887. doi:10.1073/pnas.1319597111.
Skofronick-Jackson, G., Petersen, W. A., Berg, W., Kidd, C., Stocker, E. F., Kirschbaum, D. B., et al. (2017). The Global Precipitation Measurement (GPM) Mission for Science and Society. *Bull. Am. Meteorol. Soc.* 98, 1679–1695. doi:10.1175/BAMS-D-15-00306.1.
Smith, A. B., and Matthews, J. L. (2015). Quantifying uncertainty and variable sensitivity within the US billion-dollar weather and climate disaster cost estimates. *Nat. Hazards* 77, 1829–1851. doi:10.1007/s11069-015-1678-x.
Smith, D. M., Dunstone, N. J., Scaife, A. A., Fiedler, E. K., Copsey, D., and Hardiman, S. C. (2017). Atmospheric Response to Arctic and Antarctic Sea Ice: The Importance of Ocean–Atmosphere Coupling and the Background State. *J. Clim.* 30, 4547–4565. doi:10.1175/JCLI-D-16-0564.1.
Smith, D. M., Scaife, A. A., and Kirtman, B. P. (2012). What is the current state of scientific knowledge with regard to seasonal and decadal forecasting? *Environ. Res. Lett.* 7, 015602. doi:10.1088/1748-9326/7/1/015602.
Smith, D. M., Screen, J. A., Deser, C., Cohen, J., Fyfe, J. C., García-Serrano, J., et al. (2018). The Polar Amplification Model Intercomparison Project (PAMIP) contribution to CMIP6: investigating the causes and consequences of polar amplification. *Geosci. Model Dev. Discuss.*, 1–42. doi:10.5194/gmd-2018-82.
Smith, D. M., Screen, J. A., Deser, C., Cohen, J., Fyfe, J. C., García-Serrano, J., et al. (2019). The Polar Amplification Model Intercomparison Project (PAMIP) contribution to CMIP6: investigating the causes and consequences of polar amplification. *Geosci. Model Dev.* 12, 1139–1164. doi:10.5194/gmd-12-1139-2019.
Smith, I., and Chandler, E. (2010). Refining rainfall projections for the Murray Darling Basin of south-east Australia—the effect of sampling model results based on performance. *Clim. Change* 102, 377–393. doi:10.1007/s10584-009-9757-1.
Smith, I., and Power, S. (2014). Past and future changes to inflows into Perth (Western Australia) dams. *J. Hydrol. Reg. Stud.* 2, 84–96. doi:10.1016/j.ejrh.2014.08.005.
Smith, K. L., and Polvani, L. M. (2017). Spatial patterns of recent Antarctic surface temperature trends and the importance of natural variability: lessons from multiple reconstructions and the CMIP5 models. *Clim. Dyn.* 48, 2653–2670. doi:10.1007/s00382-016-3230-4.
Smith, T., and Bookhagen, B. (2018). Changes in seasonal snow water equivalent distribution in high mountain Asia (1987 to 2009). *Sci. Adv.* 4. doi:10.1126/sciadv.1701550.
Smoliak, B. V., Wallace, J. M., Lin, P., and Fu, Q. (2015). Dynamical Adjustment of the Northern Hemisphere Surface Air Temperature Field: Methodology and Application to Observations*. *J. Clim.* 28, 1613–1629. doi:10.1175/JCLI-D-14-00111.1.
Soares, P. M. M., and Cardoso, R. M. (2018). A simple method to assess the added value using high-resolution climate distributions: application to the EURO-CORDEX daily precipitation. *Int. J. Climatol.* 38, 1484–1498. doi:10.1002/joc.5261.
Soares, P. M. M., Cardoso, R. M., Semedo, Ál., Chinita, M. J., and Ranjha, R. (2014). Climatology of the Iberia coastal low-level wind jet: weather research forecasting model high-resolution results. *Tellus A Dyn. Meteorol. Oceanogr.* 66, 22377. doi:10.3402/tellusa.v66.22377.
Soares, P. M. M., Maraun, D., Brands, S., Jury, M. W., Gutiérrez, J. M., San-Martín, D., et al. (2018). Process-based evaluation of the VALUE perfect predictor experiment of statistical downscaling methods. *Int. J. Climatol.* doi:10.1002/joc.5911.
Sohn, B. J., Ryu, G.-H., Song, H.-J., Ou, M.-L., Sohn, B. J., Ryu, G.-H., et al. (2013). Characteristic Features of Warm-Type Rain Producing Heavy Rainfall over the Korean Peninsula Inferred from TRMM Measurements. *Mon. Weather Rev.* 141, 3873–3888. doi:10.1175/MWR-D-13-00075.1.
Solman, S. A. (2016). Systematic temperature and precipitation biases in the CLARIS-LPB ensemble simulations over South America and possible implications for climate projections. *Clim. Res.* 68, 117–136. Available at: https://www.int-res.com/abstracts/cr/v68/n2-3/p117-136/.
Somot, S., Ruti, P., Ahrens, B., Coppola, E., Jordà, G., Sannino, G., et al. (2018). Editorial for the Med-CORDEX special issue. *Clim. Dyn.* 51, 771–777. doi:10.1007/s00382-018-4325-x.
Somot, S., Sevault, F., Déqué, M., and Crépon, M. (2008). 21st century climate change scenario for the Mediterranean using a coupled atmosphere–ocean regional climate model. *Glob. Planet. Change* 63, 112–126. doi:10.1016/j.gloplacha.2007.10.003.
Song, F., Zhou, T., and Qian, Y. (2014). Responses of East Asian summer monsoon to natural and anthropogenic forcings in the 17 latest CMIP5 models. *Geophys. Res. Lett.* 41, 596–603. doi:10.1002/2013GL058705.
Song, Y., Liu, H., Wang, X., Zhang, N., and Sun, J. (2016). Numerical Simulation of the Impact of Urban Non-uniformity on Precipitation. 33, 783–793.
Sontakke, N. A., Singh, N., and Singh, H. N. (2008). Instrumental period rainfall series of the Indian region (AD 1813—2005): revised reconstruction, update and analysis. *The Holocene* 18, 1055–1066. doi:10.1177/0959683608095576.
Sooraj, K. P., Terray, P., and Mujumdar, M. (2015). Global warming and the weakening of the Asian summer monsoon circulation: assessments from the CMIP5 models. *Clim. Dyn.* 45, 233–252. doi:10.1007/s00382-014-2257-7.
Sörensson, A. A., and Berbery, E. H. (2015). A Note on Soil Moisture Memory and Interactions with Surface Climate for Different Vegetation Types in the La Plata Basin. *J. Hydrometeorol.* 16, 716–729. doi:10.1175/JHM-D-14-

0102.1.
Sörensson, A. A., and Ruscica, R. C. (2018). Intercomparison and Uncertainty Assessment of Nine Evapotranspiration Estimates Over South America. *Water Resour. Res.* 54, 2891–2908. doi:10.1002/2017WR021682.
Sørland, S. L., Schär, C., Lüthi, D., and Kjellström, E. (2018). Bias patterns and climate change signals in GCM-RCM model chains. *Environ. Res. Lett.* 13, 074017. doi:10.1088/1748-9326/aacc77.
Sorokina, S. A., Li, C., Wettstein, J. J., and Kvamstø, N. G. (2016). Observed Atmospheric Coupling between Barents Sea Ice and the Warm-Arctic Cold-Siberian Anomaly Pattern. *J. Clim.* 29, 495–511. doi:10.1175/JCLI-D-15-0046.1.
Sosko, S., and Dalyot, S. (2017). Crowdsourcing User-Generated Mobile Sensor Weather Data for Densifying Static Geosensor Networks. *ISPRS Int. J. Geo-Information* 6, 61. doi:10.3390/ijgi6030061.
Sousa, P. M., Blamey, R. C., Reason, C. J. C., Ramos, A. M., and Trigo, R. M. (2018a). The "Day Zero" Cape Town drought and the poleward migration of moisture corridors. *Environ. Res. Lett.* 13. doi:10.1088/1748-9326/aaebc7.
Sousa, P. M., Trigo, R. M., Barriopedro, D., Soares, P. M. M., Ramos, A. M., and Liberato, M. L. R. (2017). Responses of European precipitation distributions and regimes to different blocking locations. *Clim. Dyn.* 48, 1141–1160. doi:10.1007/s00382-016-3132-5.
Sousa, P. M., Trigo, R. M., Barriopedro, D., Soares, P. M. M., and Santos, J. A. (2018b). European temperature responses to blocking and ridge regional patterns. *Clim. Dyn.* 50, 457–477. doi:10.1007/s00382-017-3620-2.
Spennemann, P. C., Salvia, M., Ruscica, R. C., Sörensson, A. A., Grings, F., and Karszenbaum, H. (2018). Land-atmosphere interaction patterns in southeastern South America using satellite products and climate models. *Int. J. Appl. Earth Obs. Geoinf.* 64, 96–103. doi:10.1016/j.jag.2017.08.016.
Sperber, K. R., Annamalai, H., Kang, I.-S., Kitoh, A., Moise, A., Turner, A., et al. (2013). The Asian summer monsoon: an intercomparison of CMIP5 vs. CMIP3 simulations of the late 20th century. *Clim. Dyn.* 41, 2711–2744. doi:10.1007/s00382-012-1607-6.
Spinoni, J., Vogt, J. V., Naumann, G., Barbosa, P., and Dosio, A. (2018). Will drought events become more frequent and severe in Europe? *Int. J. Climatol.* 38, 1718–1736. doi:10.1002/joc.5291.
Stainforth, D. ., Allen, M. ., Tredger, E. ., and Smith, L. . (2007). Confidence, uncertainty and decision-support relevance in climate predictions. *Philos. Trans. R. Soc. A Math. Phys. Eng. Sci.* 365, 2145–2161. doi:10.1098/rsta.2007.2074.
Stainforth, S. D. and A. B. and C. B. and D. C. and L. G.-C. and J. P. G. and N. M. and D. (2018). Building narratives to characterise uncertainty in regional climate change through expert elicitation. *Environ. Res. Lett.* 13, 74005. doi:10.1088/1748-9326/aabcdd.
Staten, P. W., Lu, J., Grise, K. M., Davis, S. M., and Birner, T. (2018). Re-examining tropical expansion. *Nat. Clim. Chang.* 8, 768–775. doi:10.1038/s41558-018-0246-2.
Stegehuis, A. I., Vautard, R., Ciais, P., Teuling, A. J., Miralles, D. G., and Wild, M. (2015). An observation-constrained multi-physics WRF ensemble for simulating European mega heat waves. *Geosci. Model Dev.* 8, 2285–2298. doi:10.5194/gmd-8-2285-2015.
Steiger, N. J., Hakim, G. J., Steig, E. J., Battisti, D. S., and Roe, G. H. (2014). Assimilation of Time-Averaged Pseudoproxies for Climate Reconstruction. *J. Clim.* 27, 426–441. doi:10.1175/JCLI-D-12-00693.1.
Steiger, N. J., Smerdon, J. E., Cook, E. R., and Cook, B. I. (2018). A reconstruction of global hydroclimate and dynamical variables over the Common Era. *Sci. Data* 5, 180086.
Steinig, S., Harlaß, J., Park, W., and Latif, M. (2018). Sahel rainfall strength and onset improvements due to more realistic Atlantic cold tongue development in a climate model. *Sci. Rep.* 8, 2569. doi:10.1038/s41598-018-20904-1.
Stennett-Brown, R. K., Jones, J. J. P., Stephenson, T. S., and Taylor, M. A. (2017). Future Caribbean temperature and rainfall extremes from statistical downscaling. *Int. J. Climatol.* 37, 4828–4845. doi:10.1002/joc.5126.
Sterl, A., van Oldenborgh, G. J., Hazeleger, W., and Burgers, G. (2007). On the robustness of ENSO teleconnections. *Clim. Dyn.* 29, 469–485. doi:10.1007/s00382-007-0251-z.
Stevens, B., Sherwood, S. C., Bony, S., and Webb, M. J. (2016). Earth ' s Future Prospects for narrowing bounds on Earth ' s equilibrium climate sensitivity Earth ' s Future. 1–11. doi:10.1002/2016EF000376.Received.
Stocker, T. F., Dahe, Q., Plattner, G.-K., and Tignor, M. (2015). IPCC Workshop on Regional Climate Projections and their Use in Impacts and Risk Analysis Studies. Sao Jose dos Campos.
Stott, P. A., and Forest, C. E. (2007). Ensemble climate predictions using climate models and observational constraints. *Philos. Trans. R. Soc. A Math. Phys. Eng. Sci.* 365, 2029–2052. doi:10.1098/rsta.2007.2075.
Stott, P. A., and Kettleborough, J. A. (2002). Origins and estimates of uncertainty in predictions of twenty-first century temperature rise. *Nature* 416, 723–726. doi:10.1038/416723a.
Stott, P., Good, P., Jones, G., Gillett, N., and Hawkins, E. (2013). The upper end of climate model temperature projections is inconsistent with past warming. *Environ. Res. Lett.* 8, 014024. doi:10.1088/1748-9326/8/1/014024.
Strahan, S. E., and Douglass, A. R. (2018). Decline in Antarctic Ozone Depletion and Lower Stratospheric Chlorine Determined From Aura Microwave Limb Sounder Observations. *Geophys. Res. Lett.* 45, 382–390. doi:10.1002/2017GL074830.
Stratton, R. A., Senior, C. A., Vosper, S. B., Folwell, S. S., Boutle, I. A., Earnshaw, P. D., et al. (2018). A Pan-African

Convection-Permitting Regional Climate Simulation with the Met Office Unified Model: CP4-Africa. *J. Clim.* 31, 3485–3508. doi:10.1175/JCLI-D-17-0503.1.

Street, R. B. (2016). Towards a leading role on climate services in Europe: A research and innovation roadmap. *Clim. Serv.* 1, 2–5. doi:10.1016/j.cliser.2015.12.001.

Strømmen, K., Christensen, H. M., Berner, J., and Palmer, T. N. (2018). The impact of stochastic parametrisations on the representation of the Asian summer monsoon. *Clim. Dyn.* 50, 2269–2282. doi:10.1007/s00382-017-3749-z.

Su, F., Duan, X., Chen, D., Hao, Z., and Cuo, L. (2012). Evaluation of the Global Climate Models in the CMIP5 over the Tibetan Plateau. *J. Clim.* 26, 3187–3208. doi:10.1175/JCLI-D-12-00321.1.

Sun, L., Deser, C., and Tomas, R. A. (2015). Mechanisms of Stratospheric and Tropospheric Circulation Response to Projected Arctic Sea Ice Loss. *J. Clim.* 28, 7824–7845. doi:10.1175/JCLI-D-15-0169.1.

Sun, L., Perlwitz, J., and Hoerling, M. (2016a). What caused the recent "Warm Arctic, Cold Continents" trend pattern in winter temperatures? *Geophys. Res. Lett.* 43, 5345–5352. doi:10.1002/2016GL069024.

Sun, Y., Zhang, X., Ren, G., Zwiers, F. W., and Hu, T. (2016b). Contribution of urbanization to warming in China. *Nat. Clim. Chang.* 6, 706–709. doi:10.1038/nclimate2956.

Sutton, R. T. (2018). Ideas: a simple proposal to improve the contribution of IPCC WG1 to the assessment and communication of climate change risks. *Earth Syst. Dyn. Discuss.*, 1–3. doi:10.5194/esd-2018-36.

Sutton, R. T., and Dong, B. (2012). Atlantic Ocean influence on a shift in European climate in the 1990s. *Nat. Geosci.* 5, 788. Available at: https://doi.org/10.1038/ngeo1595.

Sutton, R. T., Dong, B., and Gregory, J. M. (2007). Land/sea warming ratio in response to climate change: IPCC AR4 model results and comparison with observations. *Geophys. Res. Lett.* 34, L02701. doi:10.1029/2006GL028164.

Sutton, R. T., McCarthy, G. D., Robson, J., Sinha, B., Archibald, A. T., and Gray, L. J. (2018). Atlantic Multidecadal Variability and the U.K. ACSIS Program. *Bull. Am. Meteorol. Soc.* 99, 415–425. doi:10.1175/BAMS-D-16-0266.1.

Suzuki-Parker, A., Kusaka, H., Takayabu, I., Dairaku, K., Ishizaki, N. N., and Ham, S. (2018). Contributions of GCM/RCM Uncertainty in Ensemble Dynamical Downscaling for Precipitation in East Asian Summer Monsoon Season. *SOLA* 14, 97–104. doi:10.2151/sola.2018-017.

Swain, D. L., Singh, D., Horton, D. E., Mankin, J. S., Ballard, T. C., and Diffenbaugh, N. S. (2017). Remote Linkages to Anomalous Winter Atmospheric Ridging Over the Northeastern Pacific. *J. Geophys. Res. Atmos.* 122, 12,194-12,209. doi:10.1002/2017JD026575.

Swingedouw, D., Mignot, J., Ortega, P., Khodri, M., Menegoz, M., Cassou, C., et al. (2017). Impact of explosive volcanic eruptions on the main climate variability modes. *Glob. Planet. Change* 150, 24–45. doi:https://doi.org/10.1016/j.gloplacha.2017.01.006.

Switanek, M. B., Troch, P. A., Castro, C. L., Leuprecht, A., Chang, H.-I., Mukherjee, R., et al. (2017). Scaled distribution mapping: a bias correction method that preserves raw climate model projected changes. *Hydrol. Earth Syst. Sci.* 21, 2649–2666. doi:10.5194/hess-21-2649-2017.

Sylla, M. B., Diallo, I., and Pal, J. S. (2013a). West African Monsoon in State-of-the-Science Regional Climate Models. *Clim. Var. - Reg. Themat. Patterns*, 3–36. doi:10.5772/55140.

Sylla, M. B., Giorgi, F., Coppola, E., and Mariotti, L. (2013b). Uncertainties in daily rainfall over Africa: assessment of gridded observation products and evaluation of a regional climate model simulation. *Int. J. Climatol.* 33, 1805–1817. doi:10.1002/joc.3551.

Sylla, M. B., Pal, J. S., Faye, A., Dimobe, K., and Kunstmann, H. (2018). Climate change to severely impact West African basin scale irrigation in 2 °C and 1.5 °C global warming scenarios. *Sci. Rep.* 8, 14395. doi:10.1038/s41598-018-32736-0.

Tabari, H., De Troch, R., Giot, O., Hamdi, R., Termonia, P., Saeed, S., et al. (2016). Local impact analysis of climate change on precipitation extremes: are high-resolution climate models needed for realistic simulations? *Hydrol. Earth Syst. Sci.* 20, 3843–3857. doi:10.5194/hess-20-3843-2016.

Takayabu, I., Hibino, K., Sasaki, H., Shiogama, H., Mori, N., Shibutani, Y., et al. (2015). Climate change effects on the worst-case storm surge: a case study of Typhoon Haiyan. *Environ. Res. Lett.* 10, 064011. doi:10.1088/1748-9326/10/6/064011.

Takayabu, I., Kanamaru, H., DAIRAKU, K., Benestad, R., Storch, H. von, and CHRISTENSEN, J. H. (2016). Reconsidering the Quality and Utility of Downscaling. *J. Meteorol. Soc. Japan. Ser. II* 94A, 31–45. doi:10.2151/jmsj.2015-042.

Takayabu, Y. N., Shige, S., Tao, W. K., and Hirota, N. (2010). Shallow and deep latent heating modes over tropical oceans observed with TRMM PR spectral latent heating data. *J. Clim.* doi:10.1175/2009JCLI3110.1.

Takayabu, Y. N., and Tao, W.-K. (2019). "Latent heating retrievals from satellite observations," in *Satellite Precipitation Measurement*.

Tang, Q., Zhang, X., Yang, X., and Francis, J. A. (2013). Cold winter extremes in northern continents linked to Arctic sea ice loss. *Environ. Res. Lett.* 8, 014036. doi:10.1088/1748-9326/8/1/014036.

Tao, W.-K., Takayabu, Y. N., Lang, S., Shige, S., Olson, W., Hou, A., et al. (2016). TRMM Latent Heating Retrieval: Applications and Comparisons with Field Campaigns and Large-Scale Analyses. *Meteorol. Monogr.* doi:10.1175/AMSMONOGRAPHS-D-15-0013.1.

Taylor, C. M., Belusic, D., Guichard, F., Parker, D. J., Vischel, T., Bock, O., et al. (2017). Frequency of extreme Sahelian storms tripled since 1982 in satellite observations. *Nature* 544, 475–478. doi:10.1038/nature22069.

Taylor, C. M., Birch, C. E., Parker, D. J., Dixon, N., Guichard, F., Nikulin, G., et al. (2013a). Modeling soil moisture-precipitation feedback in the Sahel: Importance of spatial scale versus convective parameterization. *Geophys. Res. Lett.* 40, 6213–6218. doi:10.1002/2013GL058511.

Taylor, C. M., de Jeu, R. A. M., Guichard, F., Harris, P. P., and Dorigo, W. A. (2012). Afternoon rain more likely over drier soils. *Nature* 489, 423–426. doi:10.1038/nature11377.

Taylor, M. A., Clarke, L. A., Centella, A., Bezanilla, A., Stephenson, T. S., Jones, J. J., et al. (2018). Future Caribbean Climates in a World of Rising Temperatures: The 1.5 vs 2.0 Dilemma. *J. Clim.* 31, 2907–2926. doi:10.1175/JCLI-D-17-0074.1.

Taylor, M. A., Stephenson, T. S., Chen, A. A., and Stephenson, K. A. (2013b). Climate Change and the Caribbean: Review and Response. *Caribb. Stud.* 40, 169–200. doi:10.1353/crb.2012.0020.

Taylor, M. A., Whyte, F. S., Stephenson, T. S., and Campbell, J. D. (2013c). Why dry? Investigating the future evolution of the Caribbean Low Level Jet to explain projected Caribbean drying. *Int. J. Climatol.* 33, 784–792. doi:10.1002/joc.3461.

Taylor, M., Centella, A., Charlery, J., Borrajero, I., Bezanilla, A., Campbell, J., et al. (2007). Glimpses of the future: A Briefing from the PRECIS Caribbean Climate Change Project. *Caribb. Community Clim. Chang. Cent.*, 22. Available at: http://www.researchgate.net/publication/237150646_Glimpses_of_the_Future_A_Briefing_from_the_PRECIS_Caribbean_Climate_Change_Project.

Termonia, P., Fischer, C., Bazile, E., Bouyssel, F., Brožková, R., Bénard, P., et al. (2018a). The ALADIN System and its canonical model configurations AROME CY41T1 and ALARO CY40T1. *Geosci. Model Dev.* 11, 257–281. doi:10.5194/gmd-11-257-2018.

Termonia, P., Van Schaeybroeck, B., De Cruz, L., De Troch, R., Caluwaerts, S., Giot, O., et al. (2018b). The CORDEX.be initiative as a foundation for climate services in Belgium. *Clim. Serv.* doi:10.1016/J.CLISER.2018.05.001.

Terray, L., and Boé, J. (2013). Quantifying 21st-century France climate change and related uncertainties. *Comptes Rendus Geosci.* 345, 136–149. doi:10.1016/j.crte.2013.02.003.

Teuling, A. J. (2018). A hot future for European droughts. *Nat. Clim. Chang.* 8, 364–365. doi:10.1038/s41558-018-0154-5.

Thiery, W., Davin, E. L., Lawrence, D. M., Hirsch, A. L., Hauser, M., and Seneviratne, S. I. (2017). Present-day irrigation mitigates heat extremes. *J. Geophys. Res. Atmos.* 122, 1403–1422. doi:10.1002/2016JD025740.

Thiery, W., Davin, E. L., Panitz, H.-J., Demuzere, M., Lhermitte, S., and van Lipzig, N. (2015). The Impact of the African Great Lakes on the Regional Climate. *J. Clim.* 28, 4061–4085. doi:10.1175/JCLI-D-14-00565.1.

Thober, S., Mai, J., Zink, M., and Samaniego, L. (2014). Stochastic temporal disaggregation of monthly precipitation for regional gridded data sets. *Water Resour. Res.* 50, 8714–8735. doi:10.1002/2014WR015930.

Thompson, D. W. J., Barnes, E. A., Deser, C., Foust, W. E., and Phillips, A. S. (2015). Quantifying the Role of Internal Climate Variability in Future Climate Trends. *J. Clim.* 28, 6443–6456. doi:10.1175/JCLI-D-14-00830.1.

Thompson, D. W. J., Solomon, S., Kushner, P. J., England, M. H., Grise, K. M., and Karoly, D. J. (2011). Signatures of the Antarctic ozone hole in Southern Hemisphere surface climate change. *Nat. Geosci.* 4, 741–749. doi:10.1038/ngeo1296.

Thompson, E., Frigg, R., and Helgeson, C. (2016). Expert Judgment for Climate Change Adaptation. *Philos. Sci.* 83, 1110–1121. doi:10.1086/687942.

Thornhill, G. D., Ryder, C. L., Highwood, E. J., Shaffrey, L. C., and Johnson, B. T. (2018). The effect of South American biomass burning aerosol emissions on the regional climate. *Atmos. Chem. Phys.* 18, 5321–5342. doi:10.5194/acp-18-5321-2018.

Tian, F., Dong, B., Robson, J., and Sutton, R. (2018). Forced decadal changes in the East Asian summer monsoon: the roles of greenhouse gases and anthropogenic aerosols. *Clim. Dyn.* 51, 3699–3715. doi:10.1007/s00382-018-4105-7.

Ting, M., Seager, R., Li, C., Liu, H., and Henderson, N. (2018). Mechanism of Future Spring Drying in the Southwestern United States in CMIP5 Models. *J. Clim.* 31, 4265–4279. doi:10.1175/JCLI-D-17-0574.1.

Tiwari, S., Kar, S. C., and Bhatla, R. (2018). Mid-21st century projections of hydroclimate in Western Himalayas and Satluj River basin. *Glob. Planet. Change* 161, 10–27. doi:10.1016/j.gloplacha.2017.10.013.

Torma, C., Giorgi, F., and Coppola, E. (2015). Added value of regional climate modeling over areas characterized by complex terrain-Precipitation over the Alps. *J. Geophys. Res. Atmos.* 120, 3957–3972. doi:10.1002/2014JD022781.

Torralba, V., Doblas-Reyes, F. J., and Gonzalez-Reviriego, N. (2017). Uncertainty in recent near-surface wind speed trends: A global reanalysis intercomparison. *Environ. Res. Lett.* doi:10.1088/1748-9326/aa8a58.

Torres-Alavez, A., Cavazos, T., and Turrent, C. (2014). Land-sea thermal contrast and intensity of the North American monsoon under climate change conditions. *J. Clim.* 27, 4566–4580. doi:10.1175/JCLI-D-13-00557.1.

Torres-Valcárcel, Á. R., Harbor, J., Torres-Valcárcel, A. L., and González-Avilés, C. J. (2015). Historical differences in

temperature between urban and non-urban areas in Puerto Rico. *Int. J. Climatol.* 35, 1648–1661. doi:10.1002/joc.4083.

Towler, E., PaiMazumder, D., and Done, J. (2018). Toward the Application of Decadal Climate Predictions. *J. Appl. Meteorol. Climatol.* 57, 555–568. doi:10.1175/JAMC-D-17-0113.1.

Trapp, R. J., Robinson, E. D., Baldwin, M. E., Diffenbaugh, N. S., and Schwedler, B. R. J. (2011). Regional climate of hazardous convective weather through high-resolution dynamical downscaling. *Clim. Dyn.* 37, 677–688. doi:10.1007/s00382-010-0826-y.

Trenberth, K. E., Fasullo, J. T., Branstator, G., and Phillips, A. S. (2014). Seasonal aspects of the recent pause in surface warming. *Nat. Clim. Chang.* 4, 911–916. doi:10.1038/nclimate2341.

Trenberth, K. E., Fasullo, J. T., and Shepherd, T. G. (2015). Attribution of climate extreme events. *Nat. Clim. Chang.* 5, 725–730. doi:10.1038/nclimate2657.

Trewin, B. (2010). Exposure, instrumentation, and observing practice effects on land temperature measurements. *Wiley Interdiscip. Rev. Clim. Chang.* 1, 490–506. doi:10.1002/wcc.46.

Trewin, B. (2013). A daily homogenized temperature data set for Australia. *Int. J. Climatol.* 33, 1510–1529. doi:10.1002/joc.3530.

Trusilova, K., Jung, M., Churkina, G., Karsten, U., Heimann, M., and Claussen, M. (2008). Urbanization impacts on the climate in Europe: Numerical experiments by the PSU-NCAR mesoscale model (MM5). *J. Appl. Meteorol. Climatol.* 47, 1442–1455. doi:10.1175/2007JAMC1624.1.

Trusilova, K., Schubert, S., Wouters, H., Früh, B., Grossman-Clarke, S., Demuzere, M., et al. (2016). The urban land use in the COSMO-CLM model: a comparison of three parameterizations for Berlin. *Meteorol. Zeitschrift* 25, 231–244. doi:10.1127/metz/2015/0587.

Tsanis, I., and Tapoglou, E. (2019). Winter North Atlantic Oscillation impact on European precipitation and drought under climate change. *Theor. Appl. Climatol.* 135, 323–330. doi:10.1007/s00704-018-2379-7.

Tschakert, P., Barnett, J., Ellis, N., Lawrence, C., Tuana, N., New, M., et al. (2017). Climate change and loss, as if people mattered: values, places, and experiences. *Wiley Interdiscip. Rev. Clim. Chang.* 8, 1–19. doi:10.1002/wcc.476.

Tschakert, P., Tuana, N., Westskog, H., Koelle, B., and Afrika, A. (2016). TCHANGE: The role of values and visioning in transformation science. *Curr. Opin. Environ. Sustain.* 20, 21–25. doi:10.1016/j.cosust.2016.04.003.

Tucker, S., Jones, R. G., Buonomo, E., Burgin, L., and Gallo, F. (2018). Dynamical downscaling of GloSea5 over Ethiopia. *Clim. Serv.* 9, 57–71. doi:10.1016/J.CLISER.2018.02.001.

Tuinenburg, O. A., Hutjes, R. W. A., Stacke, T., Wiltshire, A., and Lucas-Picher, P. (2014). Effects of Irrigation in India on the Atmospheric Water Budget. *J. Hydrometeorol.* 15, 1028–1050. doi:10.1175/JHM-D-13-078.1.

Tuomenvirta, H. (2001). Homogeneity adjustments of temperature and precipitation series—Finnish and Nordic data. *Int. J. Climatol.* 21, 495–506. doi:10.1002/joc.616.

Turner, A. G., and Annamalai, H. (2012). Climate change and the South Asian summer monsoon. *Nat. Clim. Chang.* 2, 587–595. doi:10.1038/nclimate1495.

Turner, J., Bracegirdle, T. J., Phillips, T., Marshall, G. J., and Scott Hosking, J. (2013). An initial assessment of antarctic sea ice extent in the CMIP5 models. *J. Clim.* doi:10.1175/JCLI-D-12-00068.1.

Turnock, S. T., Butt, E. W., Richardson, T. B., Mann, G. W., Reddington, C. L., Forster, P. M., et al. (2016). The impact of European legislative and technology measures to reduce air pollutants on air quality, human health and climate. *Environ. Res. Lett.* 11, 24010. Available at: http://stacks.iop.org/1748-9326/11/i=2/a=024010.

Turnock, S. T., Spracklen, D. V, Carslaw, K. S., Mann, G. W., Woodhouse, M. T., Forster, P. M., et al. (2015). Modelled and observed changes in aerosols and surface solar radiation over Europe between 1960 and 2009. *Atmos. Chem. Phys.* 15, 9477–9500. doi:10.5194/acp-15-9477-2015.

Turuncoglu, U. U., Giuliani, G., Elguindi, N., and Giorgi, F. (2012). Modeling the Caspian Sea and its catchment area using a coupled regional atmosphere-ocean model (RegCM-ROMS): model design and preliminary results. *Geosci. Model Dev. Discuss.* 5, 3907–3955. doi:10.5194/gmdd-5-3907-2012.

Tuttle, S., and Salvucci, G. (2016). Empirical evidence of contrasting soil moisture-precipitation feedbacks across the United States. *Science (80-. ).* 352, 825–828. doi:10.1126/science.aaa7185.

Udall, B., and Overpeck, J. (2017). The twenty-first century Colorado River hot drought and implications for the future. *Water Resour. Res.* 53, 2404–2418. doi:10.1002/2016WR019638.

Ueda, H., Iwai, A., Kuwako, K., and Hori, M. E. (2006). Impact of anthropogenic forcing on the Asian summer monsoon as simulated by eight GCMs. *Geophys. Res. Lett.* doi:10.1029/2005GL025336.

Undorf, S., Polson, D., Bollasina, M. A., Ming, Y., Schurer, A., and Hegerl, G. C. (2018). Detectable Impact of Local and Remote Anthropogenic Aerosols on the 20th Century Changes of West African and South Asian Monsoon Precipitation. *J. Geophys. Res. Atmos.* 123, 4871–4889. doi:10.1029/2017JD027711.

Uppala, S. M., KÅllberg, P. W., Simmons, A. J., Andrae, U., Bechtold, V. D. C., Fiorino, M., et al. (2006). The ERA-40 re-analysis. *Q. J. R. Meteorol. Soc.* 131, 2961–3012. doi:10.1256/qj.04.176.

Vaittinada Ayar, P., Vrac, M., Bastin, S., Carreau, J., Déqué, M., and Gallardo, C. (2016). Intercomparison of statistical and dynamical downscaling models under the EURO- and MED-CORDEX initiative framework: present climate evaluations. *Clim. Dyn.* 46, 1301–1329. doi:10.1007/s00382-015-2647-5.

Van Den Besselaar, E. J. M., Klein Tank, A. M. G., Van Der Schrier, G., Abass, M. S., Baddour, O., Van Engelen, A. F. V., et al. (2015). International Climate Assessment & Dataset: Climate Services across Borders. *Bull. Am. Meteorol. Soc.* 96, 16–21. doi:10.1175/BAMS-D-13-00249.1.

van den Besselaar, E. J. M. M., van der Schrier, G., Cornes, R. C., Iqbal, A. S., and Klein Tank, A. M. G. (2017). SA-OBS: A Daily Gridded Surface Temperature and Precipitation Dataset for Southeast Asia. *J. Clim.* 30, 5151–5165. doi:10.1175/JCLI-D-16-0575.1.

van den Hurk, B., Kim, H., Krinner, G., Seneviratne, S. I., Derksen, C., Oki, T., et al. (2016). LS3MIP (v1.0) contribution to CMIP6: the Land Surface, Snow and Soil moisture Model Intercomparison Project – aims, setup and expected outcome. *Geosci. Model Dev.* 9, 2809–2832. doi:10.5194/gmd-9-2809-2016.

van den Hurk, B., van Oldenborgh, G. J., Lenderink, G., Hazeleger, W., Haarsma, R., and de Vries, H. (2014). Drivers of mean climate change around the Netherlands derived from CMIP5. *Clim. Dyn.* 42, 1683–1697. doi:10.1007/s00382-013-1707-y.

van der Linden, E. C., Haarsma, R. J., and van der Schrier, G. (2019). Impact of climate model resolution on soil moisture projections in central-western Europe. *Hydrol. Earth Syst. Sci.* 23, 191–206. doi:10.5194/hess-23-191-2019.

van der Schrier, G., van den Besselaar, E. J. M., Klein Tank, A. M. G., and Verver, G. (2013). Monitoring European average temperature based on the E-OBS gridded data set. *J. Geophys. Res. Atmos.* 118, 5120–5135. doi:10.1002/jgrd.50444.

van Haren, R., Haarsma, R. J., de Vries, H., van Oldenborgh, G. J., and Hazeleger, W. (2015). Resolution dependence of circulation forced future central European summer drying. *Environ. Res. Lett.* 10, 55002. Available at: http://stacks.iop.org/1748-9326/10/i=5/a=055002.

van Oldenborgh, G. J., Drijfhout, S., van Ulden, A., Haarsma, R., Sterl, A., Severijns, C., et al. (2009). Western Europe is warming much faster than expected. *Clim. Past* 5, 1–12. doi:10.5194/cp-5-1-2009.

Van Pham, T., Brauch, J., Dieterich, C., Frueh, B., and Ahrens, B. (2014). New coupled atmosphere-ocean-ice system COSMO-CLM/NEMO: assessing air temperature sensitivity over the North and Baltic Seas. *Oceanologia* 56, 167–189. doi:10.5697/oc.56-2.167.

Vanden Broucke, S., Wouters, H., Demuzere, M., and van Lipzig, N. P. M. (2018). The influence of convection-permitting regional climate modeling on future projections of extreme precipitation: dependency on topography and timescale. *Clim. Dyn.* doi:10.1007/s00382-018-4454-2.

Vannitsem, S. (2011). Bias correction and post-processing under climate change. *Nonlinear Process. Geophys.* 18, 911–924. doi:10.5194/npg-18-911-2011.

Varikoden, H., Mujumdar, M., Revadekar, J. V., Sooraj, K. P., Ramarao, M. V. S., Sanjay, J., et al. (2018). Assessment of regional downscaling simulations for long term mean, excess and deficit Indian Summer Monsoons. *Glob. Planet. Change* 162, 28–38. doi:10.1016/j.gloplacha.2017.12.002.

Vaughan, C., Buja, L., Kruczkiewicz, A., and Goddard, L. (2016). Identifying research priorities to advance climate services. *Clim. Serv.* 4, 65–74. doi:10.1016/J.CLISER.2016.11.004.

Vaughan, C., Dessai, S., Hewitt, C., Baethgen, W., Terra, R., and Berterretche, M. (2017). Creating an enabling environment for investment in climate services: The case of Uruguay's National Agricultural Information System. *Clim. Serv.* 8, 62–71. doi:10.1016/J.CLISER.2017.11.001.

Vautard, R., Gobiet, A., Jacob, D., Belda, M., Colette, A., Déqué, M., et al. (2013). The simulation of European heat waves from an ensemble of regional climate models within the EURO-CORDEX project. *Clim. Dyn.* 41, 2555–2575. doi:10.1007/s00382-013-1714-z.

Vautard, R., Gobiet, A., Sobolowski, S., Kjellström, E., Stegehuis, A., Watkiss, P., et al. (2014). The European climate under a 2 °C global warming. *Environ. Res. Lett.* 9, 034006. doi:10.1088/1748-9326/9/3/034006.

Vautard, R., and Yiou, P. (2009). Control of recent European surface climate change by atmospheric flow. *Geophys. Res. Lett.* 36. doi:10.1029/2009GL040480.

Vecchi, G. A., and Soden, B. J. (2007). Global Warming and the Weakening of the Tropical Circulation. *J. Clim.* 20, 4316–4340. doi:10.1175/JCLI4258.1.

Vecchi, G. A., Soden, B. J., Wittenberg, A. T., Held, I. M., Leetmaa, A., and Harrison, M. J. (2006). Weakening of tropical Pacific atmospheric circulation due to anthropogenic forcing. *Nature* 441, 73. Available at: https://doi.org/10.1038/nature04744.

Vellinga, M., Arribas, A., and Graham, R. (2013). Seasonal forecasts for regional onset of the West African monsoon. *Clim. Dyn.* doi:10.1007/s00382-012-1520-z.

Venema, V. K. C., Mestre, O., Aguilar, E., Auer, I., Guijarro, J. A., Domonkos, P., et al. (2012). Benchmarking homogenization algorithms for monthly data. *Clim. Past* 8, 89–115. doi:10.5194/cp-8-89-2012.

Vera, C. (2018). Farmers transformed how we investigate climate. *Nature* 562, 9–9. doi:10.1038/d41586-018-06856-6.

Vera, C. S., and Díaz, L. (2015). Anthropogenic influence on summer precipitation trends over South America in CMIP5 models. *Int. J. Climatol.* 35, 3172–3177. doi:10.1002/joc.4153.

Verrax, F. (2017). Engineering ethics and post-normal science: A French perspective. *Futures* 91, 76–79. doi:10.1016/j.futures.2017.01.009.

Vezér, M., Bakker, A., Keller, K., and Tuana, N. (2018). Epistemic and ethical trade-offs in decision analytical

modelling: A case study of flood risk management in New Orleans. *Clim. Change* 147, 1–10. doi:10.1007/s10584-017-2123-9.
Vidal, J.-P., Martin, E., Franchistéguy, L., Baillon, M., and Soubeyroux, J.-M. (2010). A 50-year high-resolution atmospheric reanalysis over France with the Safran system. *Int. J. Climatol.* 30, 1627–1644. doi:10.1002/joc.2003.
Vigaud, N., Vrac, M., and Caballero, Y. (2013). Probabilistic downscaling of GCM scenarios over southern India. *Int. J. Climatol.* 33, 1248–1263. doi:10.1002/joc.3509.
Viglizzo, E. F., and Frank, F. C. (2006). Ecological interactions, feedbacks, thresholds and collapses in the Argentine Pampas in response to climate and farming during the last century. *Quat. Int.* 158, 122–126. doi:10.1016/j.quaint.2006.05.022.
Viglizzo, E. F., Jobbágy, E. G., Carreño, L., Frank, F. C., Aragón, R., De Oro, L., et al. (2009). The dynamics of cultivation and floods in arable lands of Central Argentina. *Hydrol. Earth Syst. Sci.* 13, 491–502. doi:10.5194/hess-13-491-2009.
Vihma, T. (2014). Effects of Arctic Sea Ice Decline on Weather and Climate: A Review. *Surv. Geophys.* 35, 1175–1214. doi:10.1007/s10712-014-9284-0.
Villamayor, J., and Mohino, E. (2015). Robust Sahel drought due to the Interdecadal Pacific Oscillation in CMIP5 simulations. *Geophys. Res. Lett.* doi:10.1002/2014GL062473.
Visser, W. P. (2018). A perfect storm: The ramifications of Cape Town's drought crisis. *J. Transdiscipl. Res. South. Africa* 14, 1–10. doi:10.4102/td.v14i1.567.
Vitart, F., Ardilouze, C., Bonet, A., Brookshaw, A., Chen, M., Codorean, C., et al. (2017). The Subseasonal to Seasonal (S2S) Prediction Project Database. *Bull. Am. Meteorol. Soc.* 98, 163–173. doi:10.1175/BAMS-D-16-0017.1.
Vizy, E. K., and Cook, K. H. (2017). Seasonality of the Observed Amplified Sahara Warming Trend and Implications for Sahel Rainfall. *J. Clim.* 30, 3073–3094. doi:10.1175/JCLI-D-16-0687.1.
Vizy, E. K., Cook, K. H., Crétat, J., and Neupane, N. (2013). Projections of a Wetter Sahel in the Twenty-First Century from Global and Regional Models. *J. Clim.* 26, 4664–4687. doi:10.1175/JCLI-D-12-00533.1.
Vogel, J., Letson, D., and Herrick, C. (2017a). A framework for climate services evaluation and its application to the Caribbean Agrometeorological Initiative. *Clim. Serv.* 6, 65–76. doi:10.1016/J.CLISER.2017.07.003.
Vogel, M. M., Orth, R., Cheruy, F., Hagemann, S., Lorenz, R., van den Hurk, B. J. J. M., et al. (2017b). Regional amplification of projected changes in extreme temperatures strongly controlled by soil moisture-temperature feedbacks. *Geophys. Res. Lett.* 44, 1511–1519. doi:10.1002/2016GL071235.
Volosciuk, C., Maraun, D., Vrac, M., and Widmann, M. (2017). A combined statistical bias correction and stochastic downscaling method for precipitation. *Hydrol. Earth Syst. Sci.* 21, 1693–1719. doi:10.5194/hess-21-1693-2017.
Volpi, D., Guemas, V., Doblas-Reyes, F. J., Hawkins, E., and Nichols, N. K. (2017). Decadal climate prediction with a refined anomaly initialisation approach. *Clim. Dyn.* 48, 1841–1853. doi:10.1007/s00382-016-3176-6.
Von Clarmann, T. (2014). Smoothing error pitfalls. *Atmos. Meas. Tech.* 7, 3023–3034. doi:10.5194/amt-7-3023-2014.
von Storch, H., Langenberg, H., and Feser, F. (2000). A Spectral Nudging Technique for Dynamical Downscaling Purposes. *Mon. Weather Rev.* 128, 3664–3673. doi:10.1175/1520-0493(2000)128<3664:ASNTFD>2.0.CO;2.
Vrac, M. (2018). Multivariate bias adjustment of high-dimensional climate simulations: the Rank Resampling for Distributions and Dependences (R<sup>2</sup>D<sup>2</sup>) bias correction. *Hydrol. Earth Syst. Sci.* 22, 3175–3196. doi:10.5194/hess-22-3175-2018.
Vrac, M., and Friederichs, P. (2015). Multivariate—Intervariable, Spatial, and Temporal—Bias Correction*. *J. Clim.* 28, 218–237. doi:10.1175/JCLI-D-14-00059.1.
Wada, Y., Wisser, D., and Bierkens, M. F. P. (2014). Global modeling of withdrawal, allocation and consumptive use of surface water and groundwater resources. *Earth Syst. Dyn.* doi:10.5194/esd-5-15-2014.
Wahl, S., Bollmeyer, C., Crewell, S., Figura, C., Friederichs, P., Hense, A., et al. (2017). A novel convective-scale regional reanalysis COSMO-REA2: Improving the representation of precipitation. *Meteorol. Zeitschrift* 26, 345–361. doi:10.1127/metz/2017/0824.
Wahl, T., Jain, S., Bender, J., Meyers, S. D., and Luther, M. E. (2015). Increasing risk of compound flooding from storm surge and rainfall for major US cities. *Nat. Clim. Chang.* 5, 1093. Available at: https://doi.org/10.1038/nclimate2736.
Waldron, K. M., Paegle, J., and Horel, J. D. (1996). Sensitivity of a Spectrally Filtered and Nudged Limited-Area Model to Outer Model Options. *Mon. Weather Rev.* 124, 529–547. doi:10.1175/1520-0493(1996)124<0529:SOASFA>2.0.CO;2.
Walker, W., Haasnoot, M., and Kwakkel, J. (2013). Adapt or Perish: A Review of Planning Approaches for Adaptation under Deep Uncertainty. *Sustainability* 5, 955–979. doi:10.3390/su5030955.
Wallace, J. M., Held, I. M., Thompson, D. W. J., Trenberth, K. E., and Walsh, J. E. (2014). Global Warming and Winter Weather. *Science (80-. ).* 343, 729–730. doi:10.1126/science.343.6172.729.
Walsh, J. E. (2014). Intensified warming of the Arctic: Causes and impacts on middle latitudes. *Glob. Planet. Change* 117, 52–63. doi:10.1016/j.gloplacha.2014.03.003.
Walsh, J. E., Chapman, W. L., Romanovsky, V., Christensen, J. H., and Stendel, M. (2008). Global Climate Model

Performance over Alaska and Greenland. *J. Clim.* 21, 6156–6174. doi:10.1175/2008JCLI2163.1.
Walton, D. B., Sun, F., Hall, A., and Capps, S. (2015). A Hybrid Dynamical–Statistical Downscaling Technique. Part I: Development and Validation of the Technique. *J. Clim.* 28, 4597–4617. doi:10.1175/JCLI-D-14-00196.1.
Wang, C. (2007). Variability of the Caribbean Low-Level Jet and its relations to climate. 411–422. doi:10.1007/s00382-007-0243-z.
Wang, C., and Lee, S. (2007). Atlantic warm pool, Caribbean low-level jet, and their potential impact on Atlantic hurricanes. *Geophys. Res. Lett.* 34, L02703. doi:10.1029/2006GL028579.
Wang, J., Yan, Z., Quan, X. W., and Feng, J. (2017a). Urban warming in the 2013 summer heat wave in eastern China. *Clim. Dyn.* 48, 3015–3033. doi:10.1007/s00382-016-3248-7.
Wang, K., Deser, C., Sun, L., and Tomas, R. A. (2018a). Fast Response of the Tropics to an Abrupt Loss of Arctic Sea Ice via Ocean Dynamics. *Geophys. Res. Lett.* 45, 4264–4272. doi:10.1029/2018GL077325.
Wang, L., and Chen, W. (2014). The East Asian winter monsoon: re-amplification in the mid-2000s. *Chinese Sci. Bull.* 59, 430–436. doi:10.1007/s11434-013-0029-0.
Wang, L., Liu, Y., Zhang, Y., Chen, W., and Chen, S. (2018b). Time-varying structure of the wintertime Eurasian pattern: role of the North Atlantic sea surface temperature and atmospheric mean flow. *Clim. Dyn.* doi:10.1007/s00382-018-4261-9.
Wang, L., Xu, P., Chen, W., and Liu, Y. (2017b). Interdecadal variations of the Silk Road pattern. *J. Clim.* doi:10.1175/JCLI-D-17-0340.1.
Wang, T. J., Zhuang, B. L., Li, S., Liu, J., Xie, M., Yin, C. Q., et al. (2015a). The interactions between anthropogenic aerosols and the East Asian summer monsoon using RegCCMS. *J. Geophys. Res. Atmos.* 120, 5602–5621. doi:10.1002/2014JD022877.
Wang, T., Miao, J., Sun, J., and Fu, Y. (2018c). ScienceDirect Intensified East Asian summer monsoon and associated precipitation mode shift under the 1 . 5 C global warming target. *Adv. Clim. Chang. Res.* 9, 102–111. doi:10.1016/j.accre.2017.12.002.
Wang, T., Wang, H. J., Otterå, O. H., Gao, Y. Q., Suo, L. L., Furevik, T., et al. (2013). Anthropogenic forcing of shift in precipitation in Eastern China in late 1970s. *Atmos. Chem. Phys. Discuss.* 13, 11997–12032. doi:10.5194/acpd-13-11997-2013.
Wang, Z., Li, Y., Liu, B., and Liu, J. (2015b). Global climate internal variability in a 2000-year control simulation with Community Earth System Model (CESM). *Chinese Geogr. Sci.* 25. doi:10.1007/s11769-015-0754-1.
Wang, Z., Lin, L., Yang, M., Xu, Y., and Li, J. (2017c). Disentangling fast and slow responses of the East Asian summer monsoon to reflecting and absorbing aerosol forcings. *Atmos. Chem. Phys.* 17, 11075–11088. doi:10.5194/acp-17-11075-2017.
Wang, Z., Zhang, H., and Zhang, X. (2016). Projected response of East Asian summer monsoon system to future reductions in emissions of anthropogenic aerosols and their precursors. *Clim. Dyn.* 47, 1455–1468. doi:10.1007/s00382-015-2912-7.
Ward, K., Lauf, S., Kleinschmit, B., and Endlicher, W. (2016). Heat waves and urban heat islands in Europe: A review of relevant drivers. *Sci. Total Environ.* 569–570, 527–539. doi:10.1016/j.scitotenv.2016.06.119.
Warner, M. D., Mass, C. F., and Salathé, E. P. (2015). Changes in Winter Atmospheric Rivers along the North American West Coast in CMIP5 Climate Models. *J. Hydrometeorol.* 16, 118–128. doi:10.1175/jhm-d-14-0080.1.
Warszawski, L., Frieler, K., Huber, V., Piontek, F., Serdeczny, O., and Schewe, J. (2014). The Inter-Sectoral Impact Model Intercomparison Project (ISI–MIP): Project framework. *Proc. Natl. Acad. Sci.* 111, 3228–3232. doi:10.1073/pnas.1312330110.
Waugh, D. W., Garfinkel, C. I., and Polvani, L. M. (2015). Drivers of the Recent Tropical Expansion in the Southern Hemisphere: Changing SSTs or Ozone Depletion? *J. Clim.* 28, 6581–6586. doi:10.1175/JCLI-D-15-0138.1.
Waylen, P. R., Caviedes, C. N., and Quesada, M. E. (1996). Interannual Variability of Monthly Precipitation in Costa Rica. *J. Clim.* 9, 2606–2613. doi:10.1175/1520-0442(1996)009<2606:IVOMPI>2.0.CO;2.
Weaver, C. P., Lempert, R. J., Brown, C., Hall, J. A., Revell, D., and Sarewitz, D. (2013). Improving the contribution of climate model information to decision making: the value and demands of robust decision frameworks. *Wiley Interdiscip. Rev. Clim. Chang.* 4, 39–60. doi:10.1002/wcc.202.
Webb, M. J., Andrews, T., Bodas-Salcedo, A., Bony, S., Bretherton, C. S., Chadwick, R., et al. (2017). The Cloud Feedback Model Intercomparison Project (CFMIP) contribution to CMIP6. *Geosci. Model Dev.* 10, 359–384. doi:10.5194/gmd-10-359-2017.
Webber, S., and Donner, S. D. (2017). Climate service warnings: cautions about commercializing climate science for adaptation in the developing world. *Wiley Interdiscip. Rev. Clim. Chang.* 8, e424. doi:10.1002/wcc.424.
Weber, R. J. T., Carrassi, A., and Doblas-Reyes, F. J. (2015). Linking the anomaly initialization approach to the mapping paradigm: A proof-of-concept study. *Mon. Weather Rev.* 143. doi:10.1175/MWR-D-14-00398.1.
Weedon, G. P., Balsamo, G., Bellouin, N., Gomes, S., Best, M. J., and Viterbo, P. (2014). The WFDEI meteorological forcing data set: WATCH Forcing data methodology applied to ERA-Interim reanalysis data. *Water Resour. Res.* doi:10.1002/2014WR015638.
Weldeab, S., Stuut, J.-B. W., Schneider, R. R., and Siebel, W. (2013). Holocene climate variability in the winter rainfall zone of South Africa. *Clim. Past* 9, 2347–2364. doi:10.5194/cp-9-2347-2013.

Wester, P., Mishra, A., Mukherji, A., and Shrestha, A. B. (2019). *The Hindu Kush Himalaya Assessment*. doi:10.1007/978-3-319-92288-1.
Westervelt, D. M., Conley, A. J., Fiore, A. M., Lamarque, J.-F., Shindell, D. T., Previdi, M., et al. (2018). Connecting regional aerosol emissions reductions to local and remote precipitation responses. *Atmos. Chem. Phys.* 18, 12461–12475. doi:10.5194/acp-18-12461-2018.
Wettstein, J. J., and Deser, C. (2014). Internal Variability in Projections of Twenty-First-Century Arctic Sea Ice Loss: Role of the Large-Scale Atmospheric Circulation. *J. Clim.* 27, 527–550. doi:10.1175/JCLI-D-12-00839.1.
Whan, K., Zscheischler, J., Orth, R., Shongwe, M., Rahimi, M., Asare, E. O., et al. (2015). Impact of soil moisture on extreme maximum temperatures in Europe. *Weather Clim. Extrem.* 9, 57–67. doi:https://doi.org/10.1016/j.wace.2015.05.001.
Whan, K., and Zwiers, F. (2017). The impact of ENSO and the NAO on extreme winter precipitation in North America in observations and regional climate models. *Clim. Dyn.* 48, 1401–1411. doi:10.1007/s00382-016-3148-x.
White, R. H., and Toumi, R. (2013). The limitations of bias correcting regional climate model inputs. *Geophys. Res. Lett.* 40, 2907–2912. doi:10.1002/grl.50612.
Whyte, F. S., Taylor, M. A., Stephenson, T. S., and Campbell, J. D. (2008). Features of the Caribbean low level jet. 128, 119–128. doi:10.1002/joc.
Widmann, M. (2019). Validation of spatial variability in downscaling results from the VALUE perfect predictor experiment. *Int. J. Climatol.*
Widmann, M., Goosse, H., van der Schrier, G., Schnur, R., and Barkmeijer, J. (2010). Using data assimilation to study extratropical Northern Hemisphere climate over the last millennium. *Clim. Past* 6, 627–644. doi:10.5194/cp-6-627-2010.
Wilby, R. L., and Dessai, S. (2010). Robust adaptation to climate change. *Weather* 65, 180–185. doi:10.1002/wea.543.
Wilby, R. L., and Yu, D. (2013). Rainfall and temperature estimation for a data sparse region. *Hydrol. Earth Syst. Sci.* 17, 3937–3955. doi:10.5194/hess-17-3937-2013.
Wilcke, R. A. I., and Bärring, L. (2016). Selecting regional climate scenarios for impact modelling studies. *Environ. Model. Softw.* 78, 191–201. doi:10.1016/j.envsoft.2016.01.002.
Wilcox, L. J., Highwood, E. J., and Dunstone, N. J. (2013). The influence of anthropogenic aerosol on multi-decadal variations of historical global climate. *Environ. Res. Lett.* doi:10.1088/1748-9326/8/2/024033.
Wildschut, D. (2017). The need for citizen science in the transition to a sustainable peer-to-peer-society. *Futures* 91, 46–52. doi:10.1016/j.futures.2016.11.010.
Williams, A. P., Seager, R., Abatzoglou, J. T., Cook, B. I., Smerdon, J. E., and Cook, E. R. (2015). Contribution of anthropogenic warming to California drought during 2012-2014. *Geophys. Res. Lett.* 42, 6819–6828. doi:10.1002/2015GL064924.
Williams, C. N., Menne, M. J., and Thorne, P. W. (2012). Benchmarking the performance of pairwise homogenization of surface temperatures in the United States. *J. Geophys. Res. Atmos.* 117. doi:10.1029/2011JD016761.
Williams, K. D., Copsey, D., Blockley, E. W., Bodas-Salcedo, A., Calvert, D., Comer, R., et al. (2018). The Met Office Global Coupled Model 3.0 and 3.1 (GC3.0 and GC3.1) Configurations. *J. Adv. Model. Earth Syst.* 10, 357–380. doi:10.1002/2017MS001115.
Willison, J., Robinson, W. A., and Lackmann, G. M. (2013). The Importance of Resolving Mesoscale Latent Heating in the North Atlantic Storm Track. *J. Atmos. Sci.* 70, 2234–2250. doi:10.1175/JAS-D-12-0226.1.
Willmott, C. J., and Matsuura, K. (1995). Smart Interpolation of Annually Averaged Air Temperature in the United States. *J. Appl. Meteorol.* 34, 2577–2586. doi:10.1175/1520-0450(1995)034<2577:SIOAAA>2.0.CO;2.
Willyard, C., Scudellari, M., and Nordling, L. (2018). How three research groups are tearing down the ivory tower. *Nature* 562, 24–28. doi:10.1038/d41586-018-06858-4.
Winter, K. J.-P. M., Kotlarski, S., Scherrer, S. C., and Schär, C. (2017). The Alpine snow-albedo feedback in regional climate models. *Clim. Dyn.* 48, 1109–1124. doi:10.1007/s00382-016-3130-7.
WMO (2017). WMO Guidelines on Generating a Defined Set of National Climate Monitoring Products 2017.
Wolski, P. (2018). How severe is Cape Town's "Day Zero" drought? *Significance* 15, 24–27. doi:10.1111/j.1740-9713.2018.01127.x.
Wolski, P., Jack, C., and Conradie, S. (2019). Rainfall trends and anomalies underlying 2015-2017 Cape Town drought and water crisis. *Int. J. Climatol.*, (in prep.).
Wolski, P., Jack, C., Tadross, M., van Aardenne, L., and Lennard, C. (2018). Interannual rainfall variability and SOM-based circulation classification. *Clim. Dyn.* 50, 479–492. doi:10.1007/s00382-017-3621-1.
Woods, C., and Caballero, R. (2016). The Role of Moist Intrusions in Winter Arctic Warming and Sea Ice Decline. *J. Clim.* 29, 4473–4485. doi:10.1175/JCLI-D-15-0773.1.
Woods, C., Caballero, R., and Svensson, G. (2013). Large-scale circulation associated with moisture intrusions into the Arctic during winter. *Geophys. Res. Lett.* 40, 4717–4721. doi:10.1002/grl.50912.
Woollings, T., Harvey, B., and Masato, G. (2014). Arctic warming, atmospheric blocking and cold European winters in CMIP5 models. *Environ. Res. Lett.* 9, 014002. doi:10.1088/1748-9326/9/1/014002.
World Bank Group (2017). Middle East & North Africa Data. Available at: Middle East & North Africa Data [Accessed September 3, 2017].

Wright, D. M., Posselt, D. J., and Steiner, A. L. (2013). Sensitivity of Lake-Effect Snowfall to Lake Ice Cover and Temperature in the Great Lakes Region. *Mon. Weather Rev.* 141, 670–689. doi:10.1175/MWR-D-12-00038.1.

Wu, B., Lin, J., and Zhou, T. (2016a). Interdecadal circumglobal teleconnection pattern during boreal summer. *Atmos. Sci. Lett.* 17, 446–452. doi:10.1002/asl.677.

Wu, B., Zhou, T., and Li, T. (2016b). Impacts of the Pacific–Japan and Circumglobal Teleconnection Patterns on the Interdecadal Variability of the East Asian Summer Monsoon. *J. Clim.* 29, 3253–3271. doi:10.1175/JCLI-D-15-0105.1.

Wu, G., Li, Z., Fu, C., Zhang, X., Zhang, R., Zhang, R., et al. (2016c). Advances in studying interactions between aerosols and monsoon in China. *Sci. China Earth Sci.* 59, 1–16. doi:10.1007/s11430-015-5198-z.

Wu, J., Xu, Y., and Gao, X.-J. (2017a). Projected changes in mean and extreme climates over Hindu Kush Himalayan region by 21 CMIP5 models. *Adv. Clim. Chang. Res.* 8, 176–184. doi:10.1016/j.accre.2017.03.001.

Wu, J., Zha, J., and Zhao, D. (2017b). Evaluating the effects of land use and cover change on the decrease of surface wind speed over China in recent 30 years using a statistical downscaling method. *Clim. Dyn.* 48, 131–149. doi:10.1007/s00382-016-3065-z.

Wu, Y., and Polvani, L. M. (2015). Contrasting Short- and Long-Term Projections of the Hydrological Cycle in the Southern Extratropics. *J. Clim.* 28, 5845–5856. doi:10.1175/JCLI-D-15-0040.1.

Wu, Y., and Polvani, L. M. (2017). Recent Trends in Extreme Precipitation and Temperature over Southeastern South America: The Dominant Role of Stratospheric Ozone Depletion in the CESM Large Ensemble. *J. Clim.* 30, 6433–6441. doi:10.1175/JCLI-D-17-0124.1.

Wulder, M. A., White, J. C., Loveland, T. R., Woodcock, C. E., Belward, A. S., Cohen, W. B., et al. (2016). The global Landsat archive: Status, consolidation, and direction. *Remote Sens. Environ.* 185, 271–283. doi:10.1016/j.rse.2015.11.032.

Xavier, A. C., King, C. W., and Scanlon, B. R. (2016). Daily gridded meteorological variables in Brazil (1980–2013). *Int. J. Climatol.* 36, 2644–2659. doi:10.1002/joc.4518.

Xiao, C., Lofgren, B. M., Wang, J., and Chu, P. Y. (2016). Improving the lake scheme within a coupled WRF-lake model in the Laurentian Great Lakes. *J. Adv. Model. Earth Syst.* 8, 1969–1985. doi:10.1002/2016MS000717.

Xie, P., and Arkin, P. A. (1997). Global Precipitation: A 17-Year Monthly Analysis Based on Gauge Observations, Satellite Estimates, and Numerical Model Outputs. *Bull. Am. Meteorol. Soc.* 78, 2539–2558. doi:10.1175/1520-0477(1997)078<2539:GPAYMA>2.0.CO;2.

Xie, S.-P., Deser, C., Vecchi, G. A., Collins, M., Delworth, T. L., Hall, A., et al. (2015). Towards predictive understanding of regional climate change. *Nat. Clim. Chang.* 5, 921. Available at: http://dx.doi.org/10.1038/nclimate2689.

Xie, S., McCoy, R. B., Klein, S. A., Cederwall, R. T., Wiscombe, W. J., Jensen, M. P., et al. (2010). CLOUDS AND MORE: ARM Climate Modeling Best Estimate Data. *Bull. Am. Meteorol. Soc.* 91, 13–20. doi:10.1175/2009BAMS2891.1.

Xie, X., Wang, H., Liu, X., Li, J., Wang, Z., and Liu, Y. (2016). Distinct effects of anthropogenic aerosols on the East Asian summer monsoon between multidecadal strong and weak monsoon stages. *J. Geophys. Res. Atmos.* 121, 7026–7040. doi:10.1002/2015JD024228.

Xu, M., Xu, H., and Ma, J. (2016a). Responses of the East Asian winter monsoon to global warming in CMIP5 models. *Int. J. Climatol.* 36, 2139–2155. doi:10.1002/joc.4480.

Xu, W., Li, Q., Wang, X. L., Yang, S., Cao, L., and Feng, Y. (2013). Homogenization of Chinese daily surface air temperatures and analysis of trends in the extreme temperature indices. *J. Geophys. Res. Atmos.* 118, 9708–9720. doi:10.1002/jgrd.50791.

Xu, Y., Ramanathan, V., and Washington, W. M. (2016b). Observed high-altitude warming and snow cover retreat over Tibet and the Himalayas enhanced by black carbon aerosols. *Atmos. Chem. Phys.* 16, 1303–1315. doi:10.5194/acp-16-1303-2016.

Xue, Y., Janjic, Z., Dudhia, J., Vasic, R., and De Sales, F. (2014). A review on regional dynamical downscaling in intraseasonal to seasonal simulation/prediction and major factors that affect downscaling ability. *Atmos. Res.* 147–148, 68–85. doi:10.1016/j.atmosres.2014.05.001.

Yamato, H., Mikami, T., and Takahashi, H. (2017). Impact of sea breeze penetration over urban areas on midsummer temperature distributions in the Tokyo Metropolitan area. *Int. J. Climatol.* 37, 5154–5169. doi:10.1002/joc.5152.

Yan, Y., Lu, R., and Li, C. (2019). Relationship between the Future Projections of Sahel Rainfall and the Simulation Biases of Present South Asian and Western North Pacific Rainfall in Summer. *J. Clim.* 32, 1327–1343. doi:10.1175/JCLI-D-17-0846.1.

Yan, Z., Li, Z., li, Q., and Jones, P. (2010). Effects of site change and urbanisation in the Beijing temperature series 1977–2006. *Int. J. Climatol.* 30, 1226–1234. doi:10.1002/joc.1971.

Yan, Z. W., Wang, J., Xia, J. J., and Feng, J. M. (2016). Review of recent studies of the climatic effects of urbanization in China. *Adv. Clim. Chang. Res.* doi:10.1016/j.accre.2016.09.003.

Yang, F., and Lau, K. M. (2004). Trend and variability of China precipitation in spring and summer: Linkage to sea-surface temperatures. *Int. J. Climatol.* 24, 1625–1644. doi:10.1002/joc.1094.

Yang, H., Jiang, Z., and Li, L. (2016a). Biases and improvements in three dynamical downscaling climate simulations

over China. *Clim. Dyn.* 47, 3235–3251. doi:10.1007/s00382-016-3023-9.
YANG, K., WATANABE, T., KOIKE, T., LI, X., FUJII, H., TAMAGAWA, K., et al. (2007). Auto-calibration System Developed to Assimilate AMSR-E Data into a Land Surface Model for Estimating Soil Moisture and the Surface Energy Budget. *J. Meteorol. Soc. Japan. Ser. II* 85A, 229–242. doi:10.2151/jmsj.85A.229.
Yang, M., Li, X., Zuo, R., Chen, X., and Wang, L. (2018). Climatology and Interannual Variability of Winter North Pacific Storm Track in CMIP5 Models. *Atmosphere (Basel).* 9, 79. doi:10.3390/atmos9030079.
Yang, X.-Y., Yuan, X., and Ting, M. (2016b). Dynamical Link between the Barents–Kara Sea Ice and the Arctic Oscillation. *J. Clim.* 29, 5103–5122. doi:10.1175/JCLI-D-15-0669.1.
Yang, Z., Hsu, K., Sorooshian, S., Xu, X., Braithwaite, D., Zhang, Y., et al. (2017). Merging high-resolution satellite-based precipitation fields and point-scale rain gauge measurements-A case study in Chile. *J. Geophys. Res. Atmos.* 122, 5267–5284. doi:10.1002/2016JD026177.
Yano, J.-I., Ziemiański, M. Z., Cullen, M., Termonia, P., Onvlee, J., Bengtsson, L., et al. (2018). Scientific Challenges of Convective-Scale Numerical Weather Prediction. *Bull. Am. Meteorol. Soc.* 99, 699–710. doi:10.1175/BAMS-D-17-0125.1.
Yao, T., Thompson, L., Yang, W., Yu, W., Gao, Y., Guo, X., et al. (2012). Different glacier status with atmospheric circulations in Tibetan Plateau and surroundings. *Nat. Clim. Chang.* 2, 663–667. doi:10.1038/nclimate1580.
Yokoyama, C., Y. N. Takayabu, O. Arakawa, and T. O. (2019). A study on future projections of precipitation characteristics around Japan in early summer combining GPM DPR observation and CMIP5 large-scale environments. *J. Clim.*
Yokoyama, C., Takayabu, Y. N., and Horinouchi, T. (2017). Precipitation Characteristics over East Asia in Early Summer: Effects of the Subtropical Jet and Lower-Tropospheric Convective Instability. *J. Clim.* 30, 8127–8147. doi:10.1175/JCLI-D-16-0724.1.
Zakey, A. S., Solmon, F., and Giorgi, F. (2006). Implementation and testing of a desert dust module in a regional climate model. *Atmos. Chem. Phys.* 6, 4687–4704. doi:10.5194/acp-6-4687-2006.
Zampieri, M., D'Andrea, F., Vautard, R., Ciais, P., de Noblet-Ducoudré, N., and Yiou, P. (2009). Hot European Summers and the Role of Soil Moisture in the Propagation of Mediterranean Drought. *J. Clim.* 22, 4747–4758. doi:10.1175/2009JCLI2568.1.
Zanna, L., Brankart, J. M., Huber, M., Leroux, S., Penduff, T., and Williams, P. D. (2018). Uncertainty and scale interactions in ocean ensembles: From seasonal forecasts to multidecadal climate predictions. *Q. J. R. Meteorol. Soc.* 0. doi:10.1002/qj.3397.
Zappa, G., Pithan, F., and Shepherd, T. G. (2018). Multimodel Evidence for an Atmospheric Circulation Response to Arctic Sea Ice Loss in the CMIP5 Future Projections. *Geophys. Res. Lett.* 45, 1011–1019. doi:10.1002/2017GL076096.
Zappa, G., Shaffrey, L. C., and Hodges, K. I. (2013). The Ability of CMIP5 Models to Simulate North Atlantic Extratropical Cyclones*. *J. Clim.* 26, 5379–5396. doi:10.1175/JCLI-D-12-00501.1.
Zappa, G., and Shepherd, T. G. (2017). Storylines of Atmospheric Circulation Change for European Regional Climate Impact Assessment. *J. Clim.* 30, 6561–6577. doi:10.1175/JCLI-D-16-0807.1.
Zhang, C., Wang, Y., Hamilton, K., and Lauer, A. (2016a). Dynamical downscaling of the climate for the Hawaiian islands. Part II: Projection for the late twenty-first century. *J. Clim.* doi:10.1175/JCLI-D-16-0038.1.
Zhang, D. L., Shou, Y. X., and Dickerson, R. R. (2009). Upstream urbanization exacerbates urban heat island effects. *Geophys. Res. Lett.* 36, 1–5. doi:10.1029/2009GL041082.
Zhang, G. J., Cai, M., and Hu, A. (2013). Energy consumption and the unexplained winter warming over northern Asia and North America. *Nat. Clim. Chang.* 3, 466–470. doi:10.1038/nclimate1803.
Zhang, H., Delworth, T. L., Zeng, F., Vecchi, G., Paffendorf, K., and Jia, L. (2016b). Detection, Attribution, and Projection of Regional Rainfall Changes on (Multi-) Decadal Time Scales: A Focus on Southeastern South America. *J. Clim.* 29, 8515–8534. doi:10.1175/JCLI-D-16-0287.1.
Zhang, H., Xie, B., and Wang, Z. (2018a). Effective Radiative Forcing and Climate Response to Short-Lived Climate Pollutants Under Different Scenarios. *Earth's Futur.* 6, 857–866. doi:10.1029/2018EF000832.
Zhang, K., Kimball, J. S., and Running, S. W. (2016c). A review of remote sensing based actual evapotranspiration estimation. *Wiley Interdiscip. Rev. Water* 3, 834–853. doi:10.1002/wat2.1168.
Zhang, N., and Chen, Y. (2014). A case study of the upwind urbanization influence on the urban heat Island effects along the Suzhou-Wuxi corridor. *J. Appl. Meteorol. Climatol.* 53, 333–345. doi:10.1175/JAMC-D-12-0219.1.
Zhang, P., Wu, Y., Simpson, I. R., Smith, K. L., Zhang, X., De, B., et al. (2018b). A stratospheric pathway linking a colder Siberia to Barents-Kara Sea sea ice loss. *Sci. Adv.* 4, eaat6025. doi:10.1126/sciadv.aat6025.
Zhang, R. (2015a). Changes in East Asian summer monsoon and summer rainfall over eastern China during recent decades. *Sci. Bull.* 60, 1222–1224. doi:10.1007/s11434-015-0824-x.
Zhang, R. H. (2015b). Natural and human-induced changes in summer climate over the East Asian monsoon region in the last half century: A review. *Adv. Clim. Chang. Res.* 6, 131–140. doi:10.1016/j.accre.2015.09.009.
Zhang, T., Hoerling, M. P., Perlwitz, J., and Xu, T. (2016d). Forced Atmospheric Teleconnections during 1979–2014. *J. Clim.* 29, 2333–2357. doi:10.1175/JCLI-D-15-0226.1.
Zhang, X., Alexander, L., Hegerl, G. C., Jones, P., Tank, A. K., Peterson, T. C., et al. (2011). Indices for monitoring

changes in extremes based on daily temperature and precipitation data. *Wiley Interdiscip. Rev. Clim. Chang.* 2, 851–870. doi:10.1002/wcc.147.
Zhao, D., and Wu, J. (2017). The impact of land use and land cover changes on East Asian summer monsoon precipitation using the WRF-mosaic approach. *Atmos. Sci. Lett.* 18, 450–457. doi:10.1002/asl.788.
Zhao, L., Lee, X., Smith, R. B., and Oleson, K. (2014). Strong contributions of local background climate to urban heat islands. *Nature* 511, 216–219. doi:10.1038/nature13462.
Zhong, S., Qian, Y., Zhao, C., Leung, R., Wang, H., Yang, B., et al. (2017). Urbanization-induced urban heat island and aerosol effects on climate extremes in the Yangtze River Delta region of China. *Atmos. Chem. Phys.* 17, 5439–5457. doi:10.5194/acp-17-5439-2017.
Zhong, S., and Yang, X. Q. (2015). Mechanism of urbanization impact on a summer cold-frontal rainfall process in the greater Beijing metropolitan area. *J. Appl. Meteorol. Climatol.* 54, 1234–1247. doi:10.1175/JAMC-D-14-0264.1.
Zhou, B., Zhai, P., Chen, Y., and Yu, R. (2018a). Projected changes of thermal growing season over Northern Eurasia in a 1.5 °C and 2 °C warming world. *Environ. Res. Lett.* 13, 035004. doi:10.1088/1748-9326/aaa6dc.
Zhou, S., Huang, G., and Huang, P. (2018b). Changes in the East Asian summer monsoon rainfall under global warming: moisture budget decompositions and the sources of uncertainty. *Clim. Dyn.* 51, 1363–1373. doi:10.1007/s00382-017-3959-4.
Zhou, T., Song, F., Ha, K. J., and Chen, X. (2017). "Decadal changes of East Asian summer monsoon: Contributions of internal variability and external forcing," in *The Global Monsoon System: Research and Forecasting*, ed. M. C. Chang, C. P., Kuo, H. C., Lau, N. C., Johnson, Richard H., Wang, Bin, Wheeler (World Scientific), 327–336. Available at: https://doi.org/10.1142/10305.
Zhou, T., Turner, A. G., Kinter, J. L., Wang, B., Qian, Y., Chen, X., et al. (2016). GMMIP (v1.0) contribution to CMIP6: Global Monsoons Model Inter-comparison Project. *Geosci. Model Dev.* 9, 3589–3604. doi:10.5194/gmd-9-3589-2016.
Zhu, P., Dudhia, J., Field, P. R., Wapler, K., Fridlind, A., Varble, A., et al. (2012). A limited area model (LAM) intercomparison study of a TWP-ICE active monsoon mesoscale convective event. *J. Geophys. Res. Atmos.* 117, n/a-n/a. doi:10.1029/2011JD016447.
Zhu, X.-C., Guo, Y.-Y., and Zhang, Hai-Yan, LI, Xiu-Zhen, Chen, Rui-Dan, Wen, Z.-P. (2018). A southward withdrawal of the northern edge of the East Asian summer monsoon around the early 1990s. *Atmos. Ocean. Sci. Lett.* 11, 136–142. doi:10.1080/16742834.2018.1410058.
Zhu, X., Li, D., Zhou, W., Ni, G., Cong, Z., and Sun, T. (2017). An idealized LES study of urban modification of moist convection. *Q. J. R. Meteorol. Soc.* 143, 3228–3243. doi:10.1002/qj.3176.
Zhu, Y., and Newell, R. E. (1998). A Proposed Algorithm for Moisture Fluxes from Atmospheric Rivers. *Mon. Weather Rev.* 126, 725–735. doi:10.1175/1520-0493(1998)126<0725:apafmf>2.0.co;2.
Zickfeld, K. (2005). Is the Indian summer monsoon stable against global change? *Geophys. Res. Lett.* 32, L15707. doi:10.1029/2005GL022771.
Zittis, G., Bruggeman, A., Camera, C., Hadjinicolaou, P., and Lelieveld, J. (2017). The added value of convection permitting simulations of extreme precipitation events over the eastern Mediterranean. *Atmos. Res.* 191, 20–33. doi:10.1016/j.atmosres.2017.03.002.
Zou, L., and Zhou, T. (2016). Future summer precipitation changes over CORDEX-East Asia domain downscaled by a regional ocean-atmosphere coupled model: A comparison to the stand-alone RCM. *J. Geophys. Res. Atmos.* 121, 2691–2704. doi:10.1002/2015JD024519.
Zou, L., and Zhou, T. (2017). Dynamical downscaling of East Asian winter monsoon changes with a regional ocean-atmosphere coupled model. *Q. J. R. Meteorol. Soc.* 143, 2245–2259. doi:10.1002/qj.3082.
Zscheischler, J., Fischer, E. M., and Lange, S. (2019). The effect of univariate bias adjustment on multivariate hazard estimates. *Earth Syst. Dyn.* 10, 31–43. doi:10.5194/esd-10-31-2019.
Zscheischler, J., Michalak, A. M., Schwalm, C., Mahecha, M. D., Huntzinger, D. N., Reichstein, M., et al. (2014). Impact of large-scale climate extremes on biospheric carbon fluxes: An intercomparison based on MsTMIP data. *Global Biogeochem. Cycles* 28, 585–600. doi:10.1002/2014GB004826.
Zscheischler, J., and Seneviratne, S. I. (2017). Dependence of drivers affects risks associated with compound events. *Sci. Adv.* 3, e1700263. doi:10.1126/sciadv.1700263.
Zscheischler, J., Westra, S., van den Hurk, B. J. J. M., Seneviratne, S. I., Ward, P. J., Pitman, A., et al. (2018). Future climate risk from compound events. *Nat. Clim. Chang.* 8, 469–477. doi:10.1038/s41558-018-0156-3.
Zubler, E. M., Folini, D., Lohmann, U., Lüthi, D., Schär, C., and Wild, M. (2011). Simulation of dimming and brightening in Europe from 1958 to 2001 using a regional climate model. *J. Geophys. Res.* 116, D18205. doi:10.1029/2010JD015396.
Zulkafli, Z., Buytaert, W., Onof, C., Manz, B., Tarnavsky, E., Lavado, W., et al. (2014). A Comparative Performance Analysis of TRMM 3B42 (TMPA) Versions 6 and 7 for Hydrological Applications over Andean–Amazon River Basins. *J. Hydrometeorol.* 15, 581–592. doi:10.1175/JHM-D-13-094.1.
Zuo, Z., Yang, S., Kumar, A., Zhang, R., Xue, Y., and Jha, B. (2012). Role of thermal condition over Asia in the weakening Asian summer monsoon under global warming background. *J. Clim.* doi:10.1175/JCLI-D-11-00742.1.
Zuo, Z., Yang, S., Xu, K., Zhang, R., He, Q., Zhao, T., et al. (2018). Land surface air temperature variations over

Eurasia and possible causes in the past century. *Int. J. Climatol.* 38, 1925–1937. doi:10.1002/joc.5306.
Zuo, Z., Yang, S., Zhang, R., Jiang, P., Zhang, L., and Wang, F. (2013). Long-term variations of broad-scale Asian summer monsoon circulation and possible causes. *J. Clim.* doi:10.1175/JCLI-D-12-00691.1.

## Figures

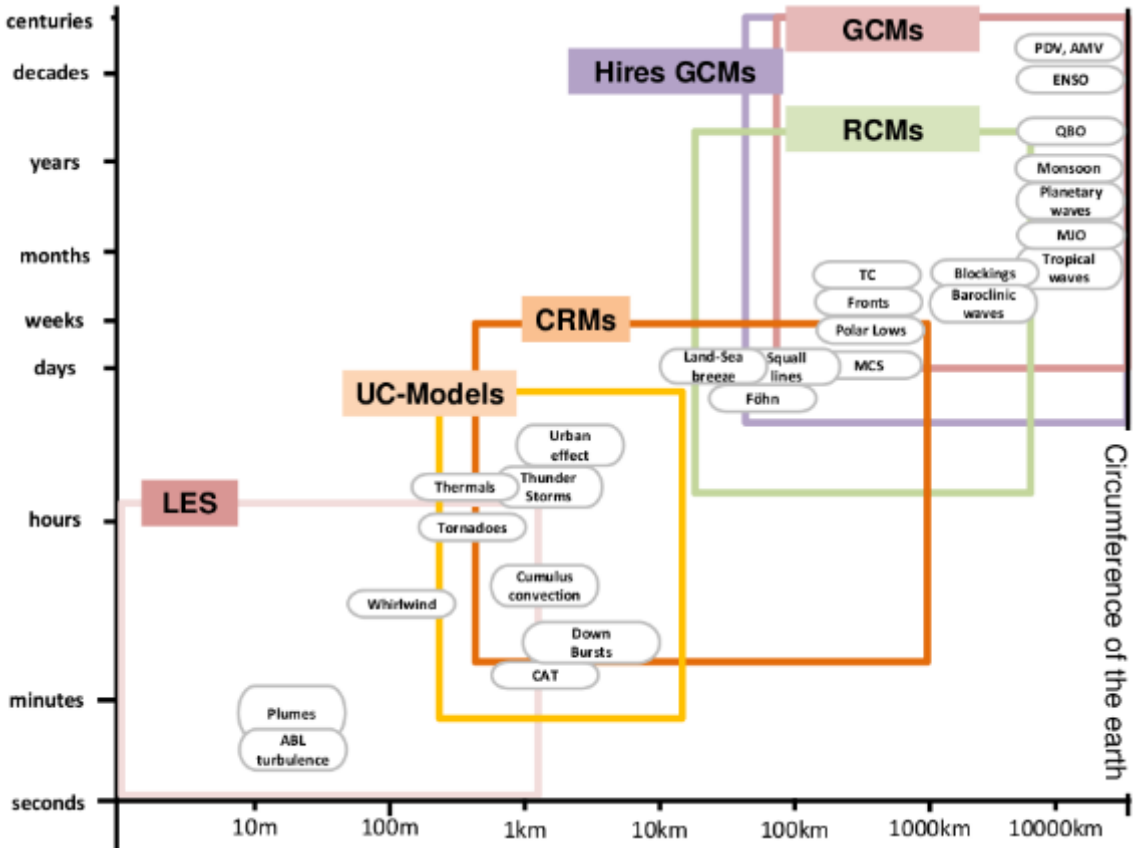


**Figure 10.1:** Schematic diagram derived from the idea of (Orlanski, 1975) displaying relevant interacting space and time scales of relevance to regional climate change information. Also indicated are the processes included in the different models and model components considered in Chapter 10 as a function of the time and space scales. This figure is a companion of Figure 1.15 in Chapter 1 where the region sets adopted in the report are illustrated as a function of the time and space scales.

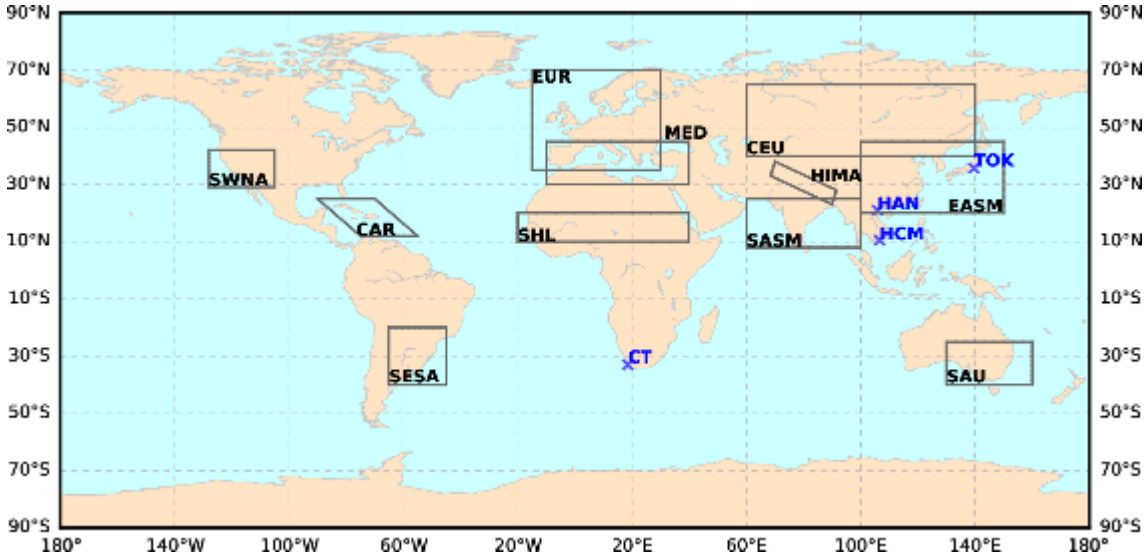


**Figure 10.2:** Regional climate attribution case studies and end-to-end focus region on the generation of regional climate information, discussed in Sections 10.4 and 10.6 respectively. The regions appearing in the figure are the attribution case study regions in Section 4: Caribbean (AR6 region CAR), Central Eurasia (CEU), East Asian monsoon (EASM), Europe (EUR), Hanoi (HAN), Ho Chi Min (HCM), Himalaya (HIMA), Southeast Australia (SAU), Southeastern South America (SESA), Sahel/West African monsoon (SHL), Southwest North America (AR6 region SWNA) and Tokyo (TOK). The end-to-end regions in Section 10.6 are: Cape Town (CT), Mediterranean (AR6 MED) and South Asian monsoon (SASM). For visual clarity, cities are marked with blue and the other regions in grey.

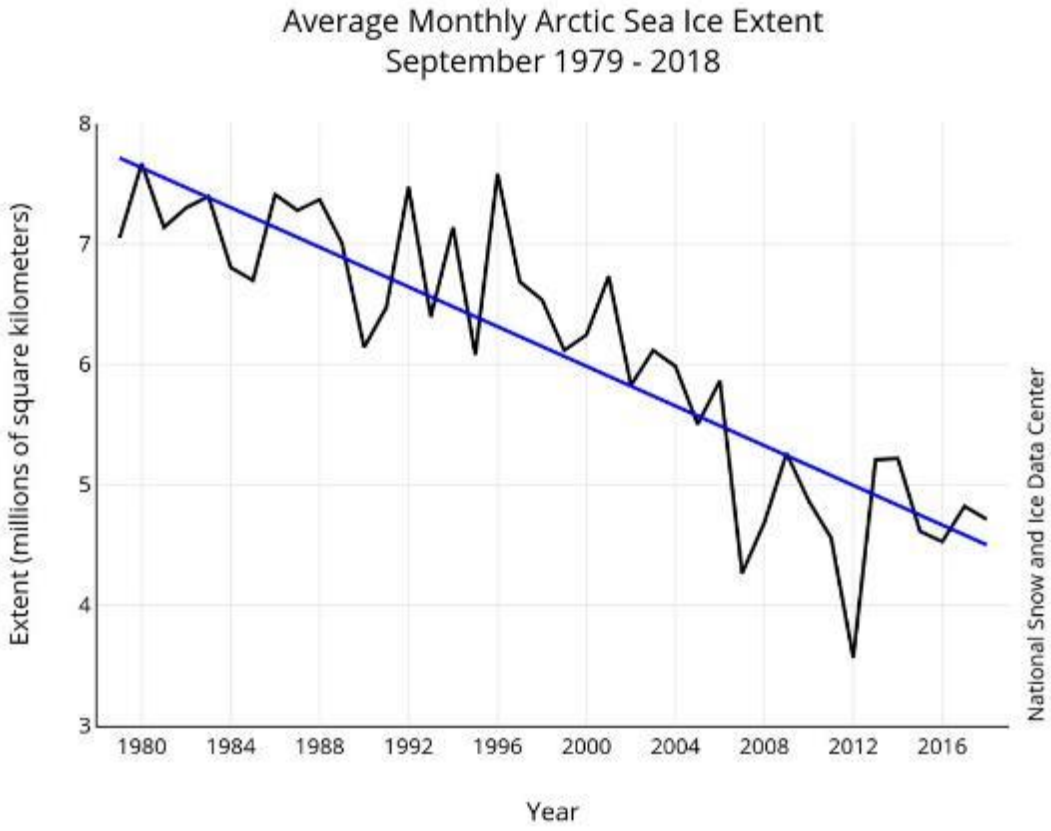


**Cross-Chapter Box 10.1, Figure 1:** [Placeholder: Average monthly Arctic sea ice extent September 1979-2018 (source NSIDC).]

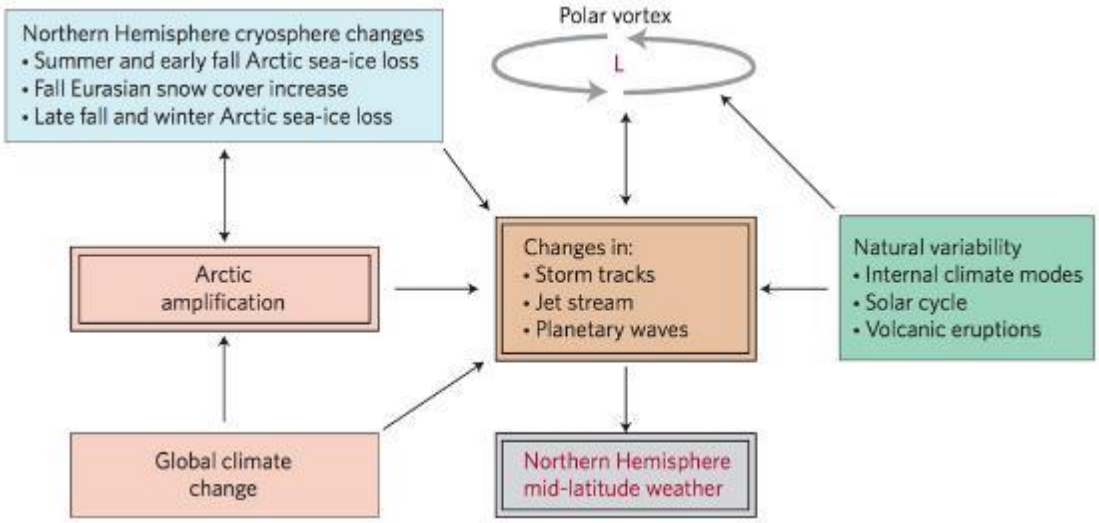


**Cross-Chapter Box 10.1, Figure 2:** [Placeholder: Schematic of influences on northern hemisphere mid-latitude weather. Adapted from (Cohen et al., 2014).]

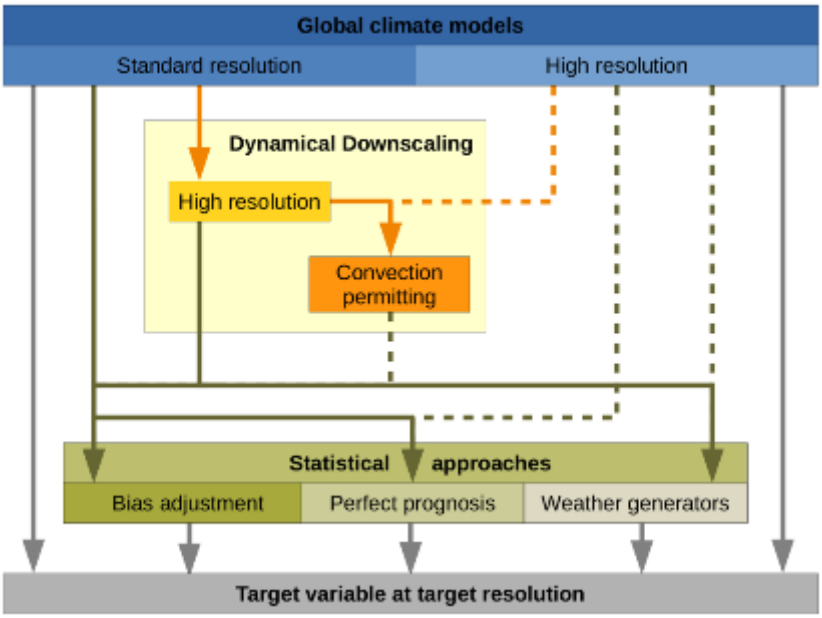


**Figure 10.3:** Typical models and model chains used in regional climate modelling. The dashed lines indicate model chains that might prove useful but have not or only rarely been used. [Placeholder: For the SOD, more text could be given specifying the individual modelling chains and typical resolutions]

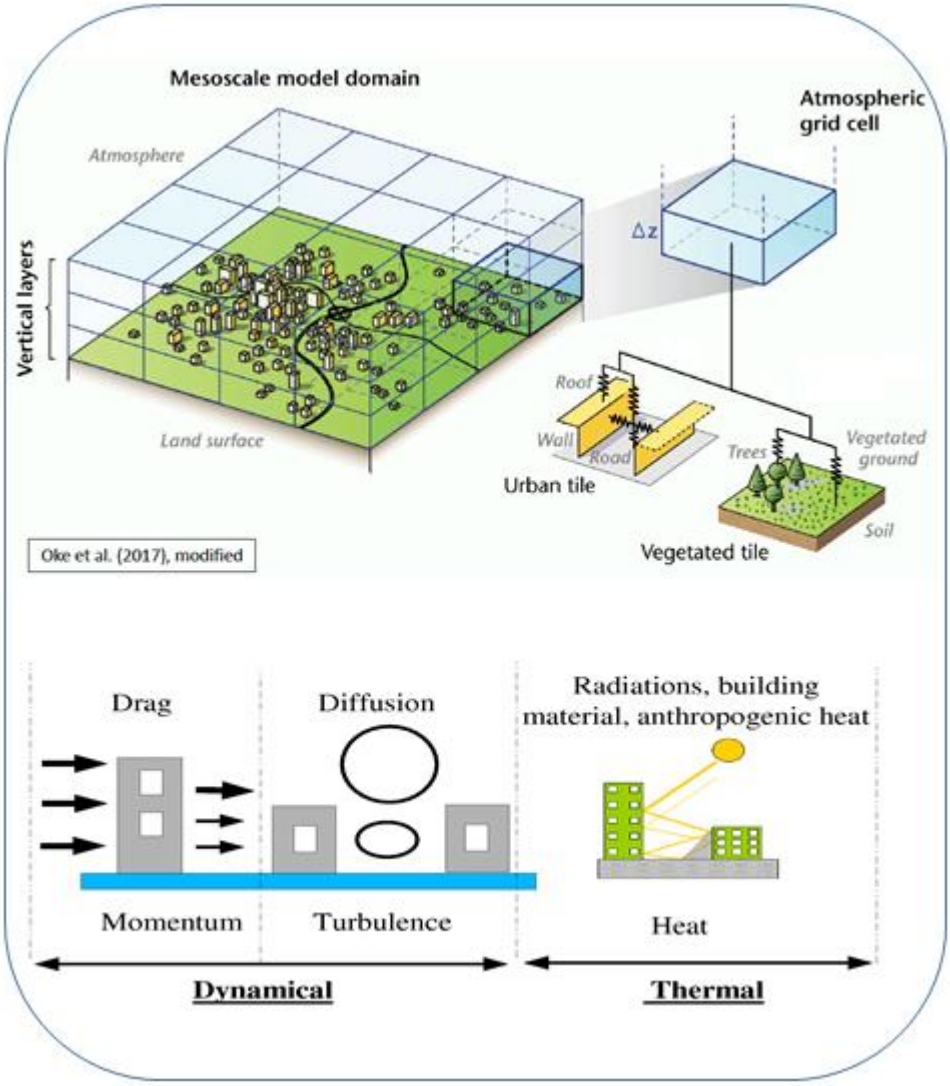


**Figure 10.4:** Single-layer urban canopy parametrization in the land surface model of RCMs. [For the SOD, more text will be given explaining the processes and models.]

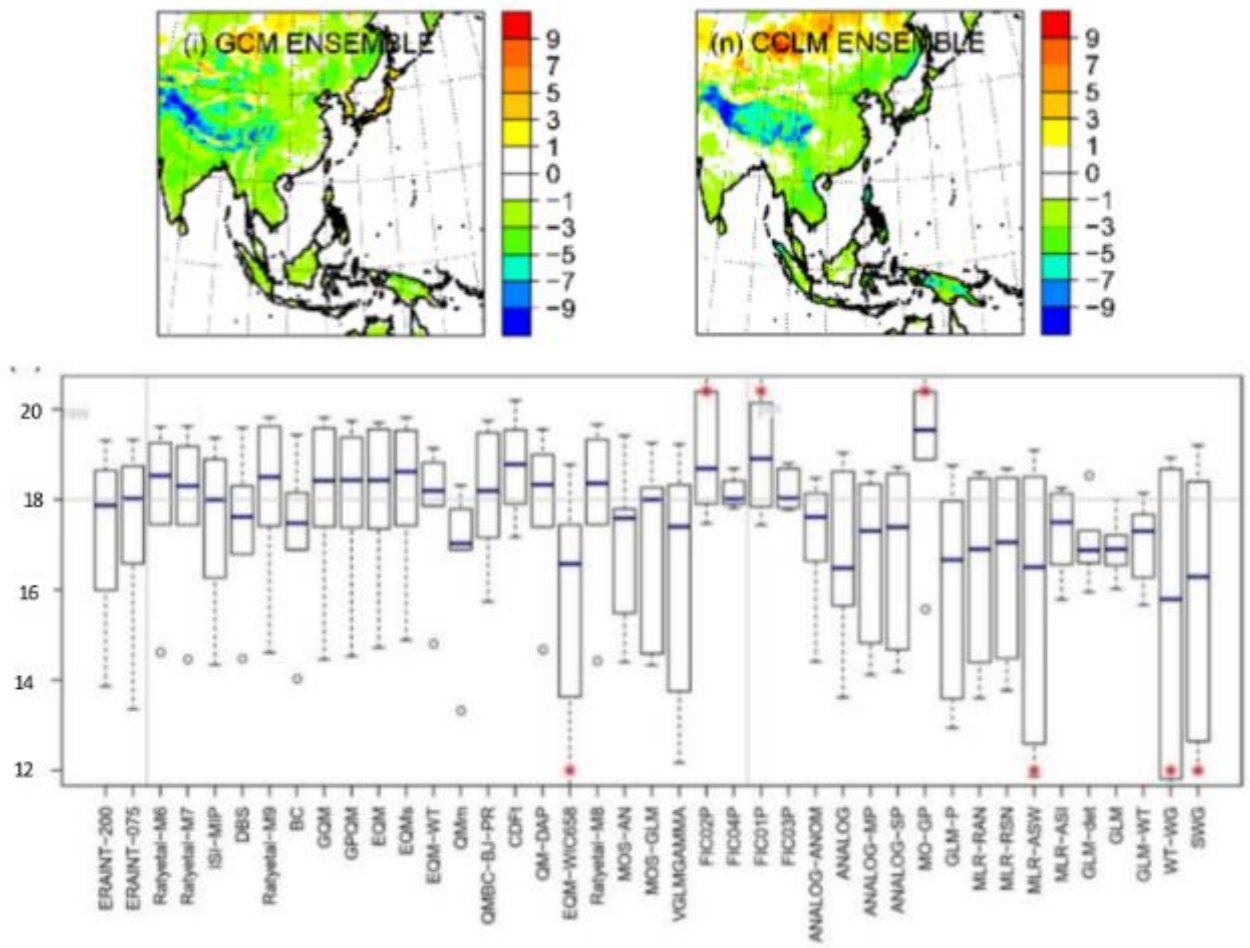


**Figure 10.5:** [Placeholder: Multipanel with, on the top row, mean bias of the GCM (left) and RCM (right) simulations over the East Asia (ASO), Western Europe (DJF) and/or West Africa (JAS) regions and, at the bottom, sets of box-and-whiskers with one box-and-whisker for each observational reference (observations and/or reanalyses) available and for each simulation considered (CMIP5, CMIP6, CORDEX). One multipanel for temperature and another one for precipitation. The box-and-whisker corresponds to the seasonal mean values for each year and for each point of the region (samples with N points x M years), where the region is a subsection (illustrated in the maps) of the area shown in the maps above. The box-and-whiskers for each region displayed with a different colour or shade, but if the panel becomes too cluttered then each region displayed separately with one multipanel per region: East Asia and West Africa precipitation and Western Europe temperature.]

| Aspect | MOS | | | | PP | | | | WG[a] | | | |
|---|---|---|---|---|---|---|---|---|---|---|---|---|
| | BC | QM emp. | QM para. | QM extreme | REG det. | REG infl. | REG stoch. | ANA SS/MS | RI U SS/MS | RI C SS/MS | POI SS/MS | HM U/C |
| Temperature, marginal | | | | | | | | | | | | |
| mean | + | + | + | + | + | + | + | ○ | + | + | + | + |
| variance | ○ | + | + | + | - | ○ | + | ○ | + | + | + | + |
| extremes[b] | ○ | + | + | + | - | ○ | + | + | + | + | + | + |
| Temperature, temporal variability | | | | | | | | | | | | |
| autocorrelation | + | + | + | + | + | + | - | - | + | + | + | + |
| mean spells | + | + | + | + | ○ | ○ | - | - | + | + | + | + |
| extreme spells | + | + | + | + | + | + | - | ○ | + | + | + | + |
| interannual variance | + | ○ | ○ | ○ | - | ○ | - | - | - | ○ | - | -/○ |
| climate change | + | ○ | ○ | ○ | + | - | + | - | + | + | + | + |
| Temperature, spatial variability | | | | | | | | | | | | |
| means | + | + | + | + | ○ | ○ | - | -/+ | -/? | -/? | -/? | ? |
| extremes | + | + | + | + | - | - | - | -/+ | -/? | -/? | -/? | ? |
| Precipitation, marginal | | | | | | | | | | | | |
| wet-day probabilities | + | + | + | + | - | - | + | + | + | + | + | + |
| mean intensity | + | + | + | + | - | - | + | + | + | + | + | + |
| extremes[b] | ○ | + | ○ | + | - | - | + | + | ○ | ○ | ○ | ○ |
| Precipitation, temporal variability | | | | | | | | | | | | |
| transition probabilities | ○ | + | + | + | - | - | + | + | + | + | + | + |
| mean spells | ○ | + | + | + | - | - | + | + | ○ | + | ○ | ○/+ |
| extreme spells | + | + | + | + | - | - | + | + | - | ○ | - | -/○ |
| interannual variance | + | ○ | ○ | ○ | - | ○ | ○ | ○ | - | ○ | - | -/○ |
| climate change | + | ○ | ○ | ○ | + | - | + | ○ | + | + | + | + |
| Precipitation, spatial variability | | | | | | | | | | | | |
| means | ○ | + | + | + | - | - | - | -/+ | -/○ | -/○ | -/○ | ○ |
| extremes | ○ | ○ | ○ | ○ | - | - | - | -/+ | -/? | -/? | -/? | ? |
| Multivariable | | | | | | | | | | | | |
| bulk | + | + | + | + | - | - | - | + | + | + | + | + |

[a] We consider standard WGs with Gaussian distribution for temperature and, for example, gamma distribution for precipitation.

[b] We consider extreme events within the range of observed values. No extrapolation is assessed.

**Figure 10.6:** [This figure is a placeholder. The abbreviations will be written out, and – depending on the available literature – more aspects may be added] performance of different statistical downscaling methods for daily resolution. BC: bias correction, QM: quantile mapping, REG: (generalised) linear model, det: deterministic, infl.: inflated variance, stoch: white noise randomisation; WT: weather typing; ANA: analog; RI: Richardson-type; POI: Possion clustering; HM: hidden Markov; SS: single-site; MS: multisite; U: unconditional; C: conditional; "+": should work reasonably well based on empirical evidence and/or expert judgement; “o”: problems may arise depending on the specific context; "-": weak performance either by construction or inferred from empirical evidence; "?": not studied. The categorisation assumes that predictors are provided by a well performing dynamical model simulating informative and representative predictors, also for climate change. Statements about extremes refer to moderate events occurring at least once every 20 years. From (Maraun and Widmann, 2018)]

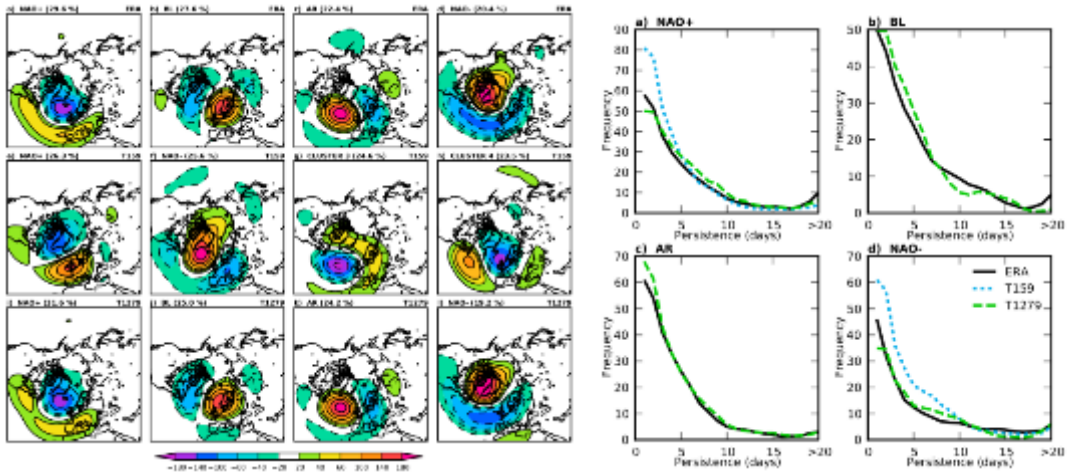


**Figure 10.7:** [Placeholder for a figure showing issues (e.g., blocking) with standard GCMs in simulating specific large-scale phenomena which are relevant for regional climate, and how high resolution GCMs may add value. It should be replaced by a more recent figure, include an intermediate resolution (say T512) and should, if possible, link to a phenomenon from the showcases in Section 10.4. From Dawson et al., GRL, 2012]

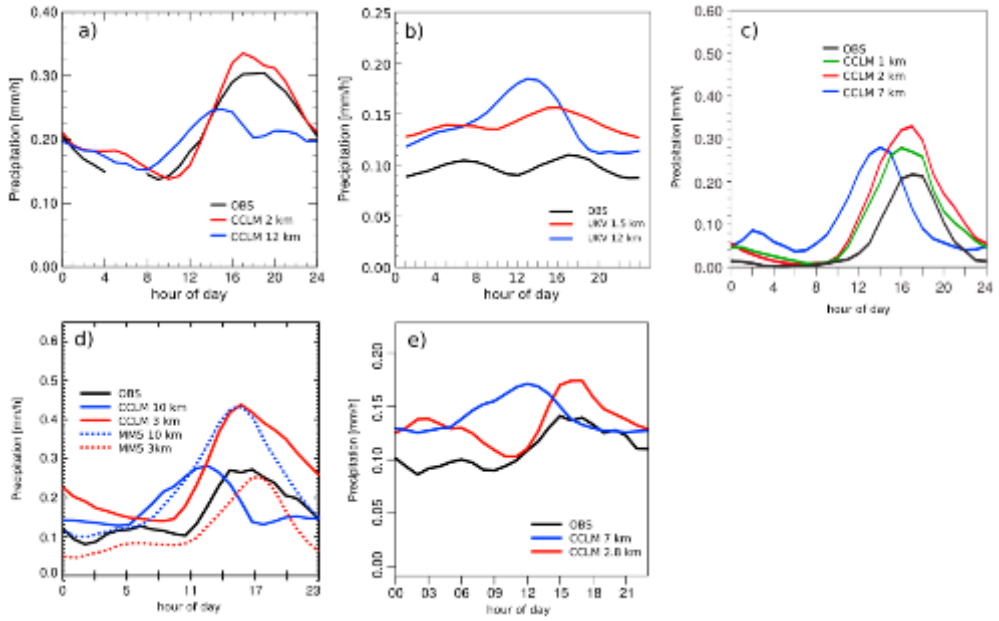


**Figure 10.8:** [Placeholder: Diurnal cycle of precipitation and added value by convection permitting resolution. Black: observations, blue: RCM with parameterised deep convection. Red: RCM at convection permitting resolution. From Prein et al., Rev. Geophys. 2015]

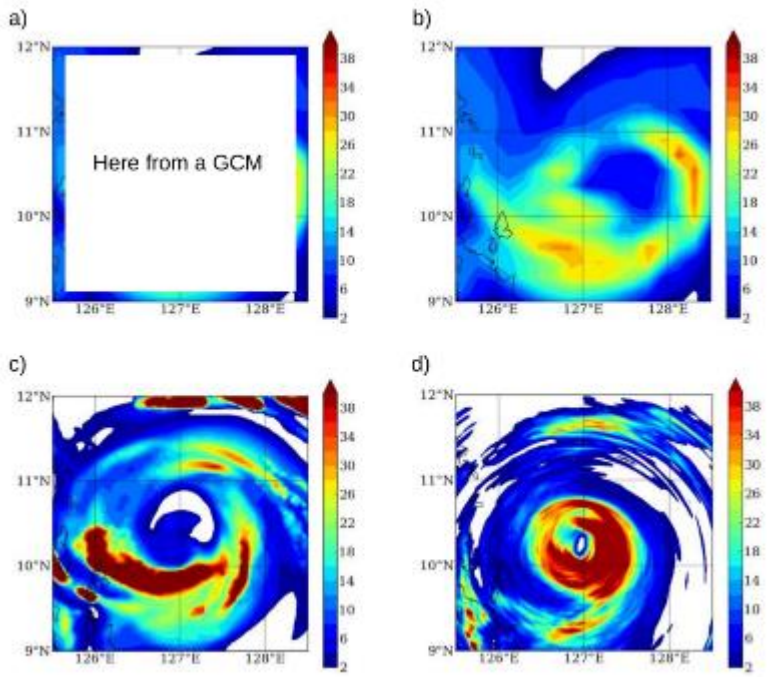


**Figure 10.9:** [Placeholder: Hourly accumulated precipitation profiles (mm/hour) around the eye of Typhoon Haiyan, simulated by the (a) Reanalysis, (b) NHRCM (20km), (c) NHRCM (5km), and (d) WRF (1km) models. From Takayabu et al. Env. Res. Lett., 2015]

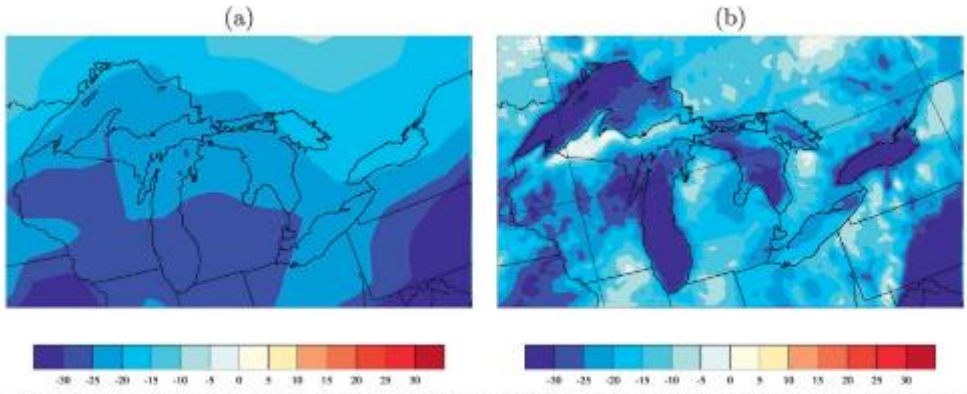


FIG. 13. Changes for the 2050–60 period relative to the historical period (1979–2001) over the Great Lakes Basin for snow precipitation (%) from (a) CCSM and (b) WRF.

**Figure 10.10:**[Placeholder: Projected changes in lake effect snow (in percent for the 2050-60 period compared to the 1979-2001 period) over the Great Lakes Basin. (a) GCM CCSM, (b) RCM WRF. From Gula and Peltier, J. Climate, 2012]

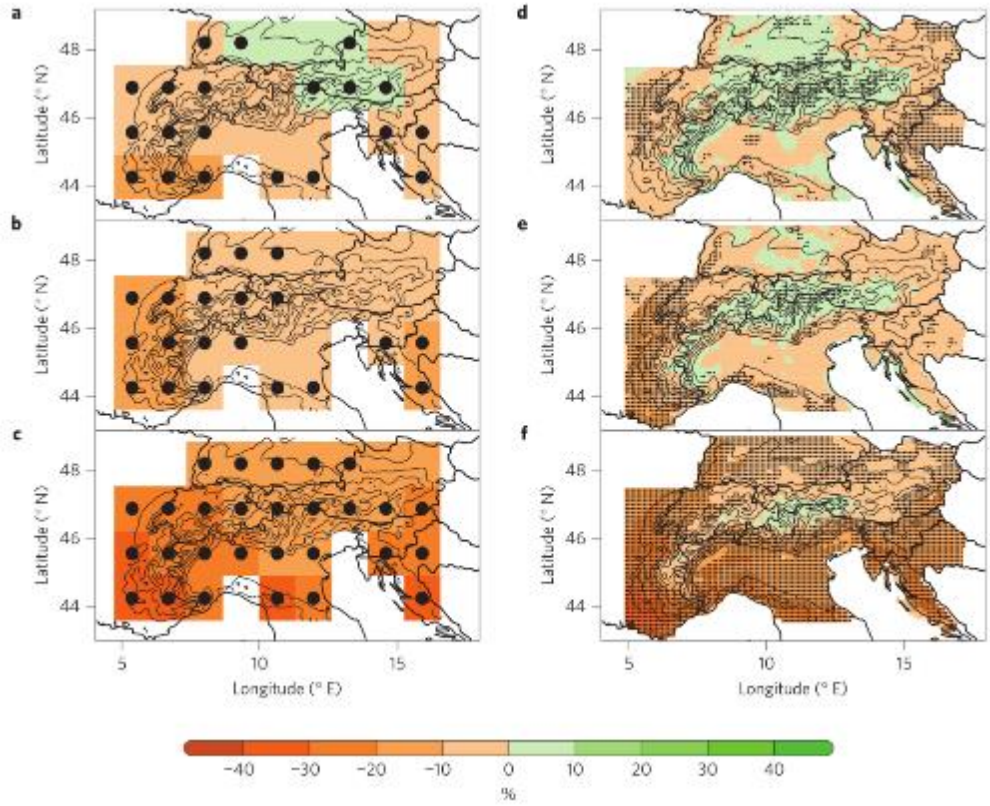


**Figure 10.11:**[Placeholder: Changes in summer precipitation over the Alps simulated by 4 GCMs (a-c) and 6 RCMs driven with the same GCMs (d-f) for three future time slices (top to bottom: 2010–2039; 2040–2069; 2070–2099). Further analysis, comparison with convection permitting simulations and physical arguments indicate that the RCM signal is more credible. From Giorgi et al., Nat. Geosci. 2016].

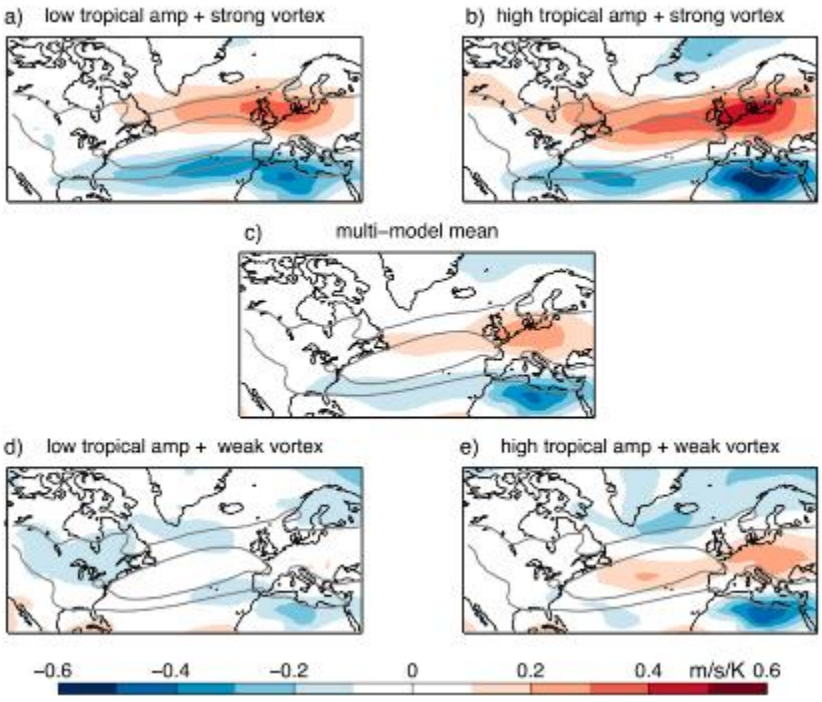


**Figure 10.12:**[Placeholder: Cold season U850 response per degree of global warming (m s-1 K-1) according to four plausible storylines in the CMIP5 models. (a) stronger stratospheric vortex and lower tropical amplification; (b) stronger stratospheric vortex and higher tropical amplification; (c) multi model mean response scaled by global warming; (d) weaker stratospheric vortex and lower tropical amplification; (e) weaker stratospheric vortex and higher tropical amplification. From Zappa and Shepherd, J. Climate, 2017]

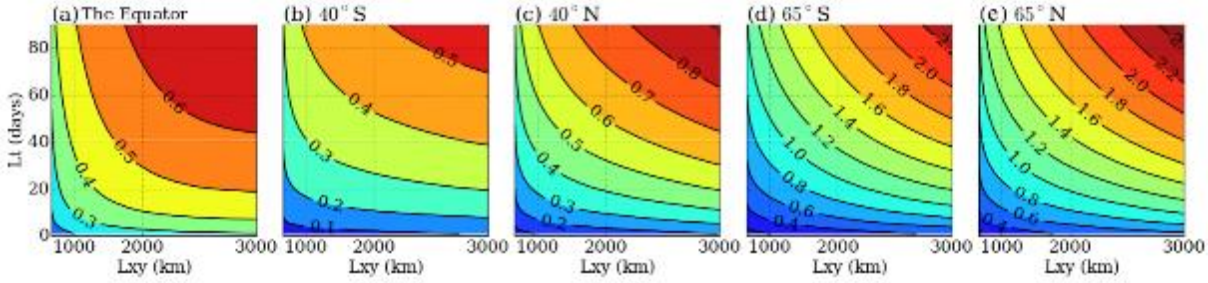


**Figure 10.13:**[Placeholder: Signal-to-noise ratio of precipitation changes (2075-2099 average minus 1979-2003 average according to the RCP8.5) in the MRI-AGCM3.2 atmospheric GCM at a 60km resolution as function of spatial (Lxy) and temporal (Lt) averaging scale for different latitudes. From Hibino and Takayabu, J. Met. Soc. Jap. 2016]

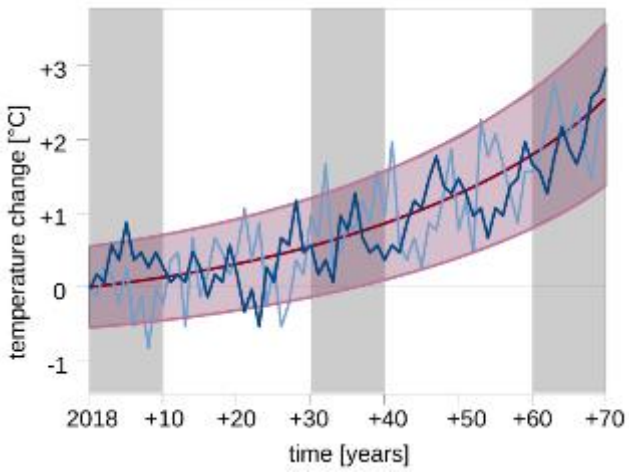


**Figure 10.14:**[Placeholder: Role of internal variability at different lead times. Sketch to be replaced by example from model simulation for SOD. Dark red: forced signal. Blue: two possible realisations. Magenta shading: likely range of future values. Pink lines: extreme thresholds. The longer the lead time, the stronger the forcing, the higher the signal-to-noise ratio, and thus the more robust statements can be drawn. But even at short lead times with low signal-to-noise ratio, the risk of exceeding high thresholds is steadily increasing, and the risk of exceeding a low threshold is steadily decreasing.]

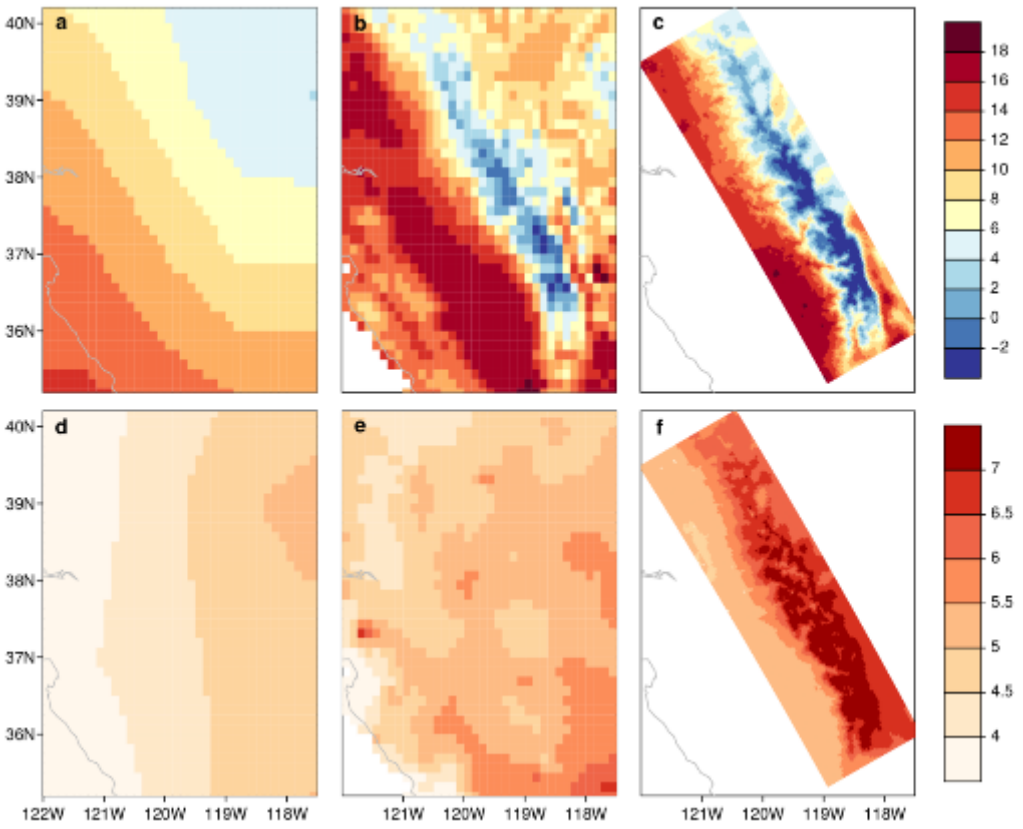


**Box 10.2, Figure 1:** [Placeholder: Spring (MAM) daily mean temperature in the Sierra Nevada region in California. Top: present climate (1981-2000 average) in (a) the GFDL-CM3 GCM, interpolated to 8km, (b) observations at 8km resolution, (c) WRF RCM at 3km horizontal resolution. Bottom: climate change signal (2081-2100 average minus 1981-2000 average according to RCP8.5) in (d) the GCM, (e) the bias adjusted GCM using quantile mapping, and (f) the RCM. As the GCM does not resolve the snow-albedo feedback, it simulates an implausible regional warming signal. The bias adjustment cannot improve the missing feedback. Only the high-resolution RCM simulation simulates a plausible elevation-dependent climate change signal. From Maraun et al., Nat. Clim. Change, 2017].

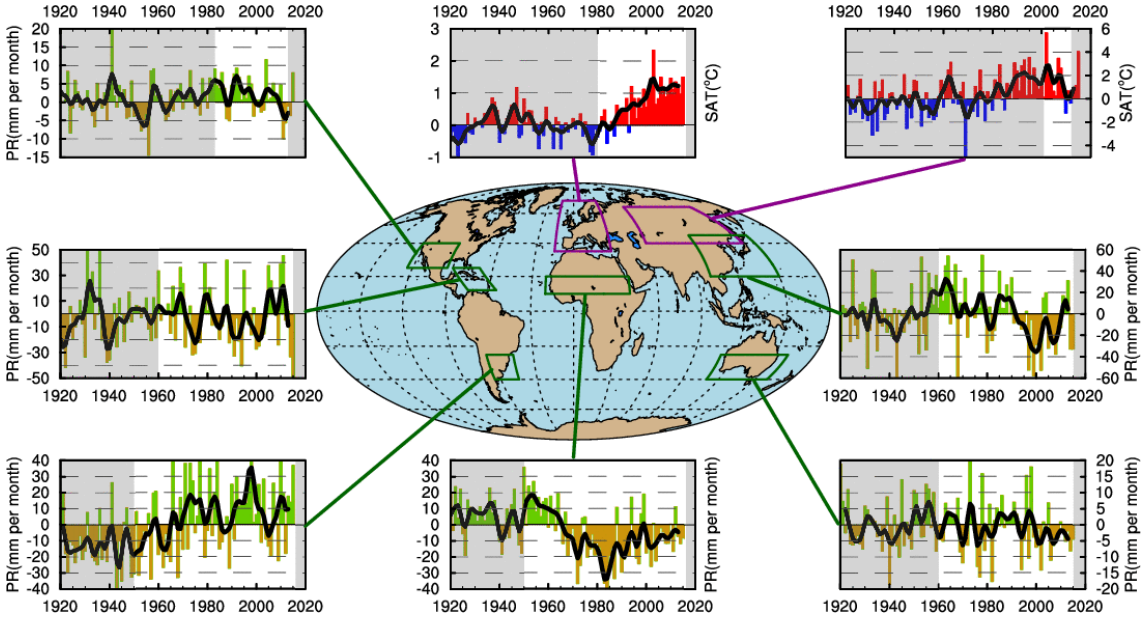


**Figure 10.15:** Time series of surface air temperature (SAT in °C, blue and red colours) or precipitation (PR in mm per month, green and ochre colours) anomalies (relative to the 1951–1980 period) area-averaged over appropriate regions of 8 out of the 10 selected case studies. The regions are broadly defined by the green (PR) and magenta (SAT) rectangles. The precise region boundaries and case studies are from top to bottom and left to right: a. The south-western North and Central America (25°N–40°N, 94°W–124°W) drought b. The Caribbean small islands (11°N–25°N, 60°W–85°W) summer (JJA) drought c. The south-eastern South America (25°S–40°S, 45°W–65°W) Austral summer (DJF) drought d. The Sahel and the West African monsoon (10°N–20°N, 20°W–40°E) drought and recovery e. The southern Australia (25°S–40°S, 110°E–150°E) rainfall decline f. The East Asia summer (JJA) monsoon weakening and recovery; here the time series is the difference of mean precipitation between two regions: PR (110°E–125°E, 35°N–45°N) – PR (105°E–125°E, 20°N–35°N) g. The central and eastern Eurasia (40°N–65°N, 60°E–140°E) winter (DJF) cooling h. The western Europe (35°N–70°N, 15°W–30°E) summer (JJA) warming. SAT is from the Berkeley surface temperature dataset (Rohde et al., 2013) and PR from GPCC v8 (Becker et al., 2013; Schneider et al., 2017). The white area on each graphic represents the period of interest for attribution. The black line is a simple low-pass filter that has been used in AR4. It has 5 weights 1/12 [1-3-4-3-1] and for annual data, its half-amplitude point is for a 6-year period, and the half-power point is near 8.4 years. The remaining two case studies concerned the Himalaya mountain range and Asian cities. The relevant data and graphics will be included in the figure for the SOD.

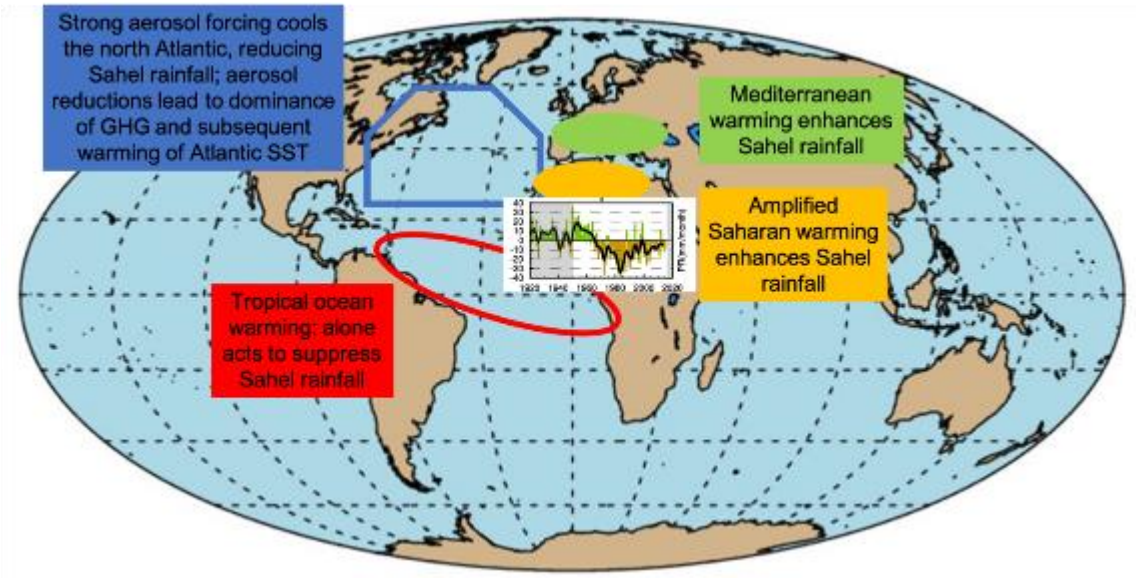


**Figure 10.16:**[Placeholder: Schematic diagram illustrating the main drivers of West African monsoon/Sahel rainfall demise and recovery across the 20th century historical period and under future RCPs in the 21st century. The Sahel domain used in the time series is as in Figure 10.15].

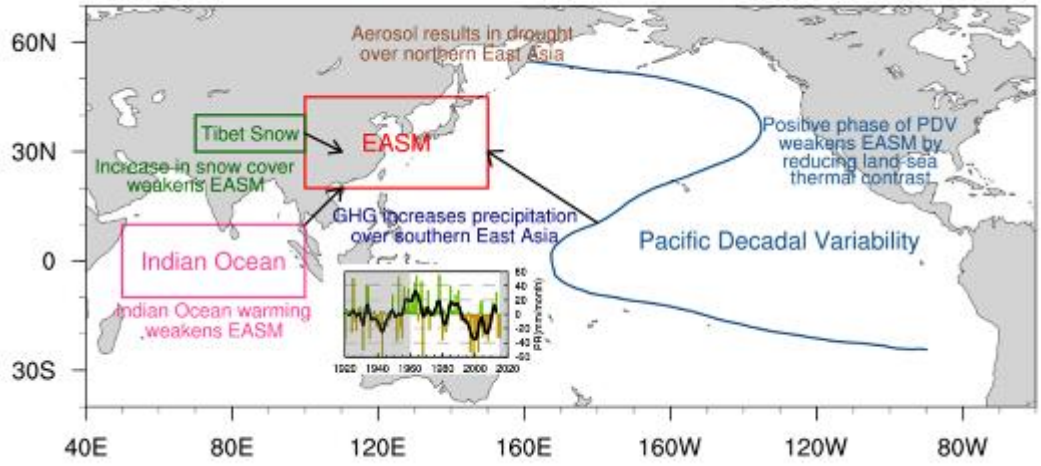


**Figure 10.17:**[Placeholder: Schematic diagram illustrating main contributing drivers on the decadal change (weakening and recovery) of the East Asia Summer Monsoon (EASM) since the 1970s. The time series shown is the difference of the mean summer (JJA) precipitation (PR) between two regions: PR (110°E–125°E, 35°N–45°N) – PR (105°E–125°E, 20°N–35°N).]

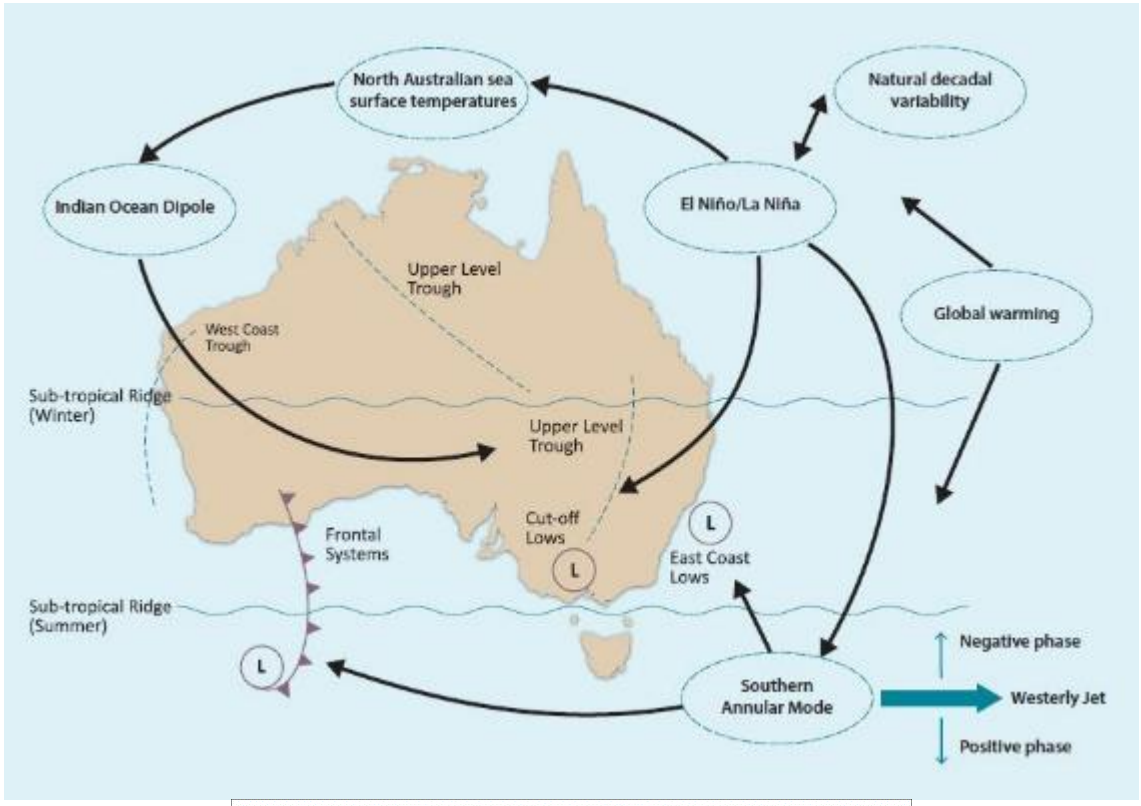


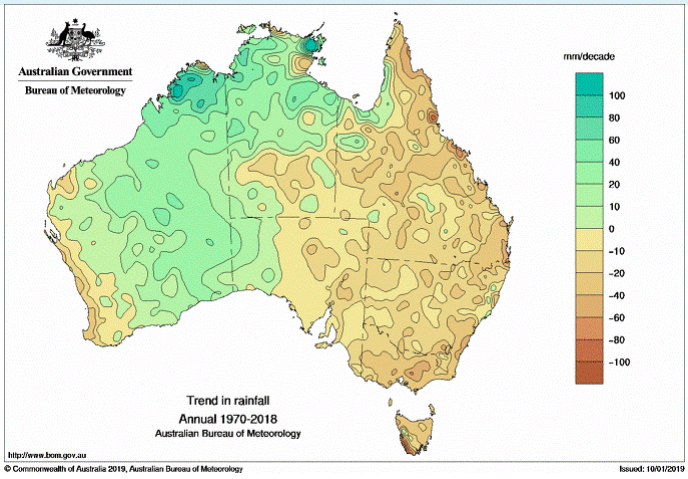


**Figure 10.18:**[Placeholder top) schematic showing the main drivers that can influence southern Australia's rainfall; their influence can vary strongly with season; bottom) Trend in annual rainfall from 1970 to 2018 shows a decline in the far south-west and the whole east coast.]

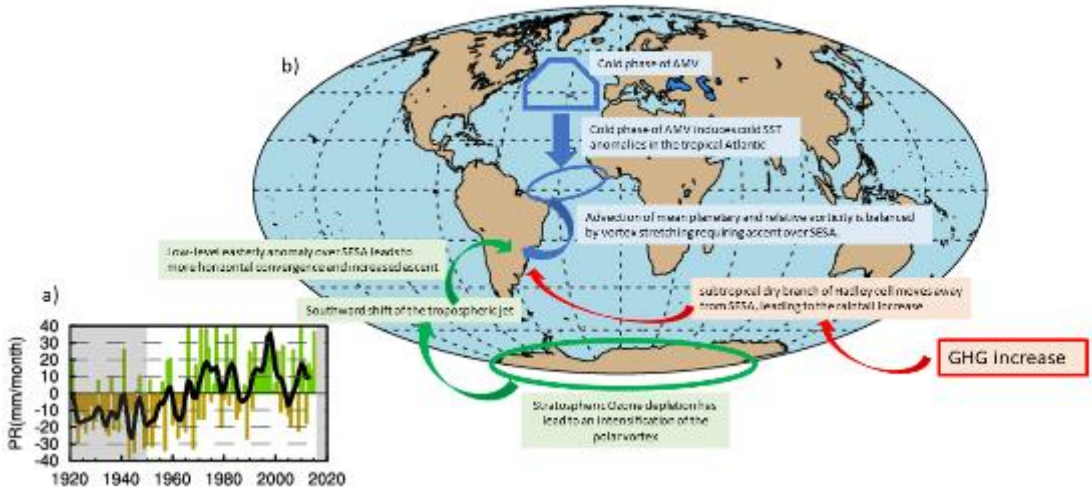


**Figure 10.19:**[Placeholder a) Austral summer (DJF) precipitation anomaly over SESA (25°S–40°S, 65°W–45°W) from 1920 to 2017 b) Mechanisms that have been suggested to contribute to SESA summer wetting since the beginning of the 20th century.]

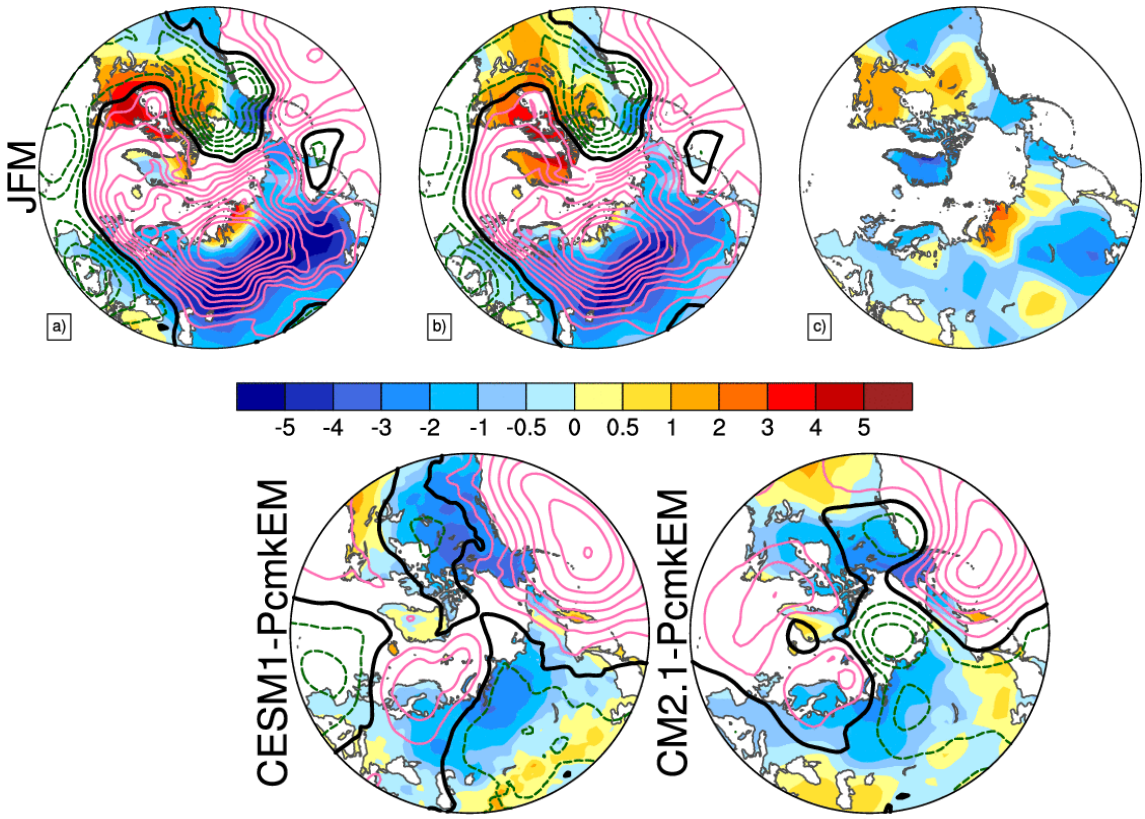


**Figure 10.20:**[Placeholder: Attribution of winter (JFM) Eurasian winter cooling: surface air temperature (SAT, shading) and sea level pressure (SLP, contours every 1hPa yr-1 interval) 2002-2013 linear trends in °C 12yr-1 and hPa 12yr-1, respectively. a) Observed raw SAT and SLP data b) SAT changes purely due to changes in atmospheric circulation (through dynamical adjustment) and reconstructed SLP based on best analogues c) SAT thermodynamic residual (a)-(b). Bottom row: influence of tropical Pacific changes as simulated by two pacemaker ensembles based on the CESM1 and GFDL-CM2.1 models; the response to anthropogenic and natural forcing has been subtracted from the pacemaker ensemble means based on the ensemble means of large ensembles of historical simulations performed with the two models. The figure will be adapted for the SOD to show other possible influences (for instance from Arctic sea-ice and anthropogenic drivers based on CMIP6 simulations).]

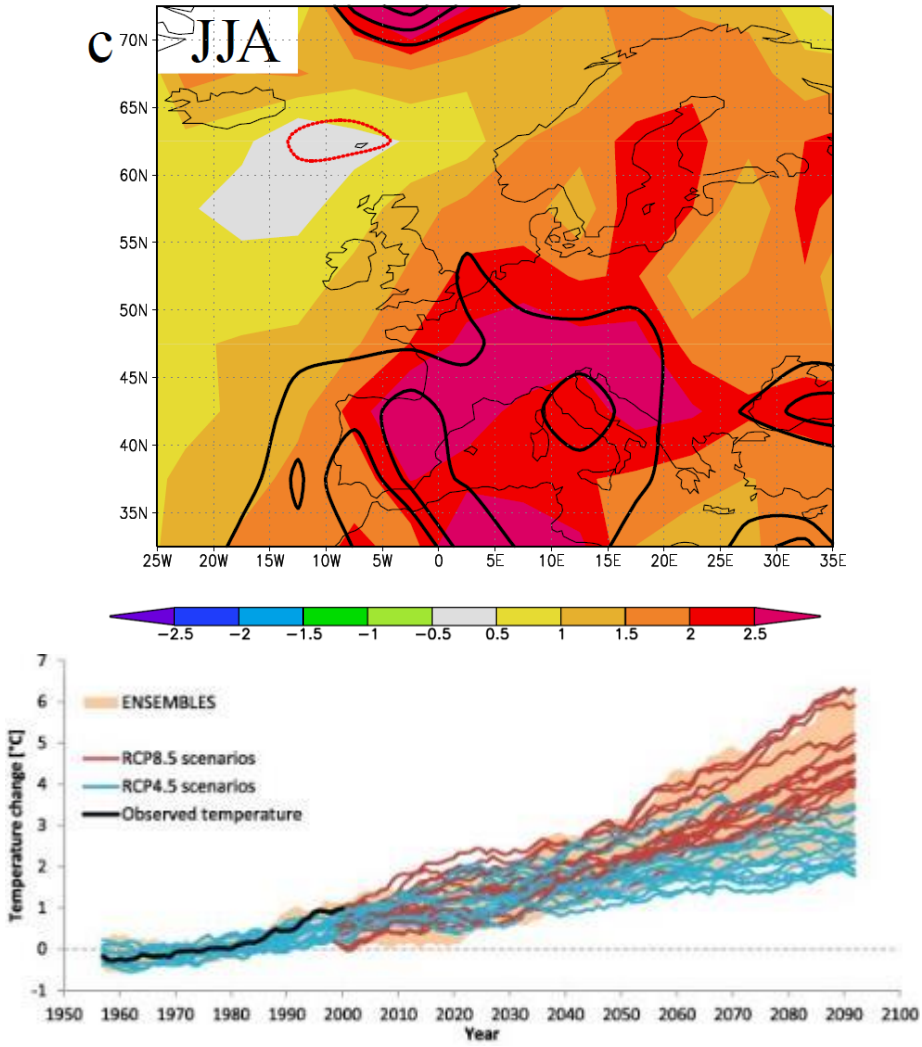


**Figure 10.21:**[Placeholder: The present plot is from the ENSEMBLES project, but should be made for different scenarios and based on CMIP6, HighResMIP, and CORDEX simulations] a) Historical warming (summer SAT 1950-2008 trend) over Europe relative to global mean warming (1 means European warming is equal to global mean warming). [Placeholder figure from Oldenborgh et al. 2008, will be updated for the SOD] b) Summer (JJA) European SAT change for historical period and future scenario.]

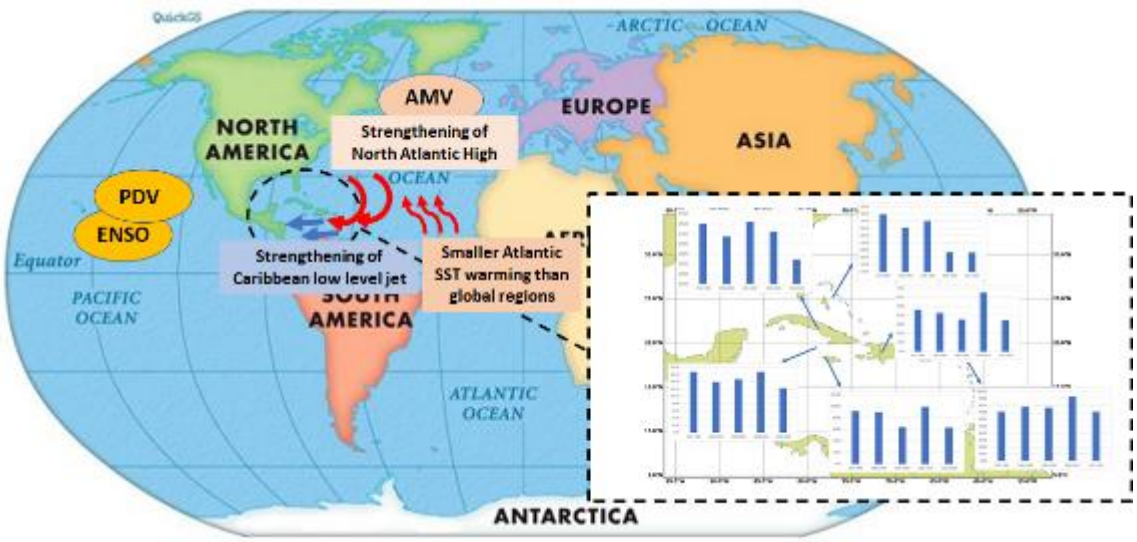


**Figure 10.22:**[Placeholder: Influences that have been suggested to contribute to an intensification of June-August rainfall over Caribbean. Inset shows average June-August rainfall in mm/month for some northern Caribbean stations by decade from 1971–1980 to 2011–2018 (2016 for station over Cuba).]

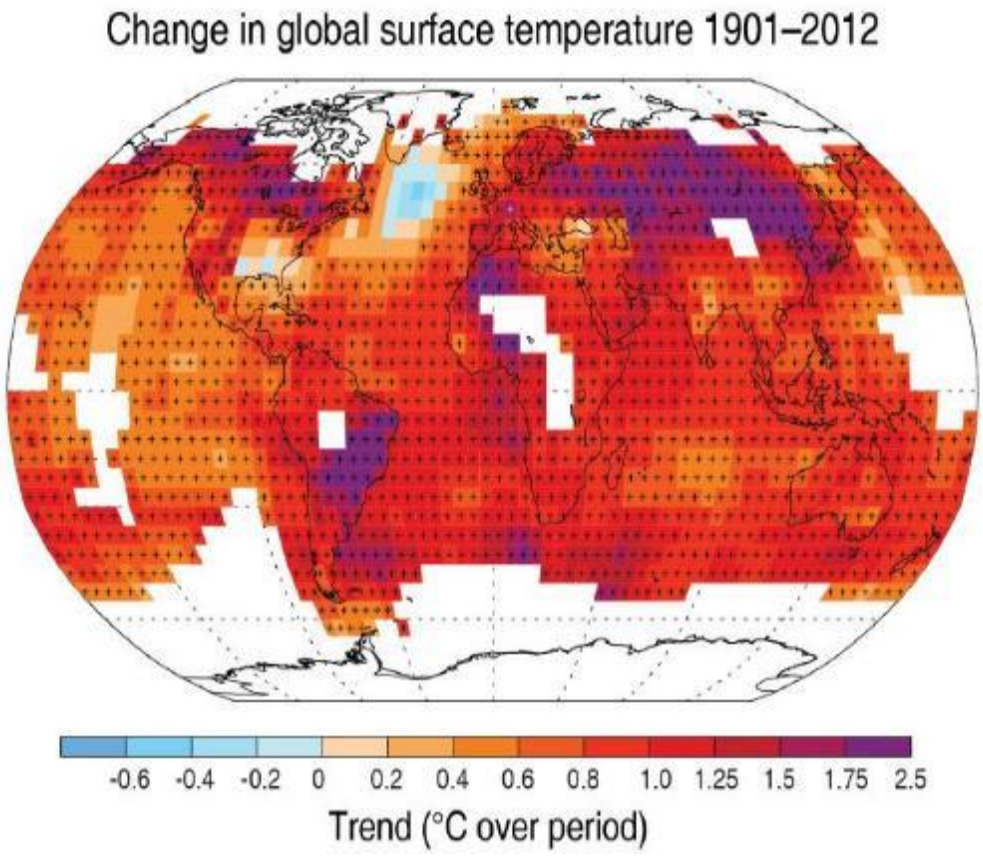


**Figure 10.23:**[Placeholder: A figure with time series of urban warming reported in the literature in different cities around the world and the spatial map of observed long-term trends in the background]

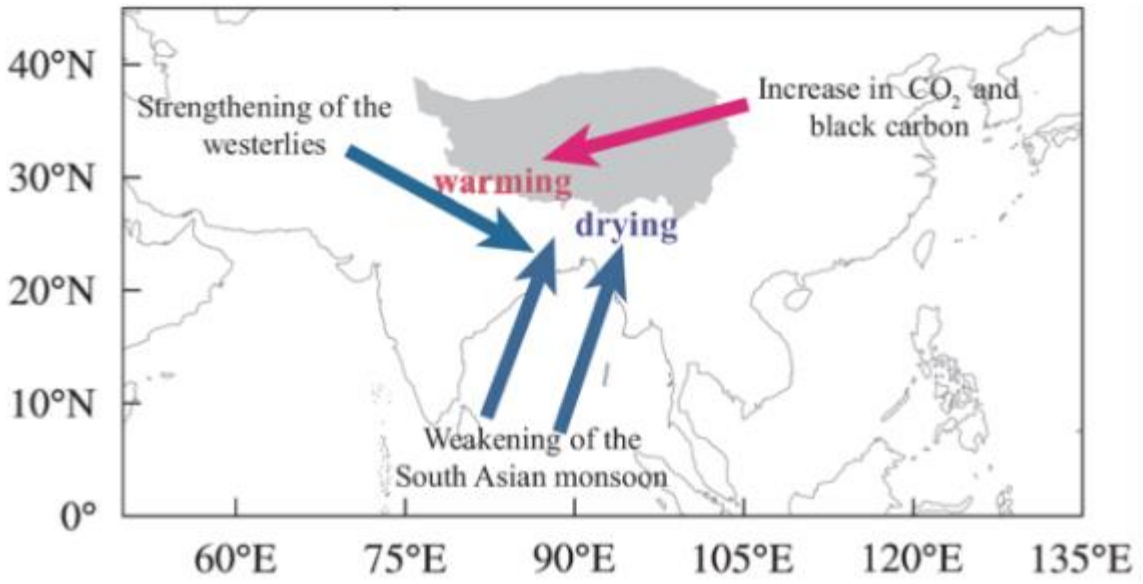


**Figure 10.24:**[Placeholder: Schematic diagram illustrating main contributing drivers on the decadal change of the Himalayas since 1960s.]

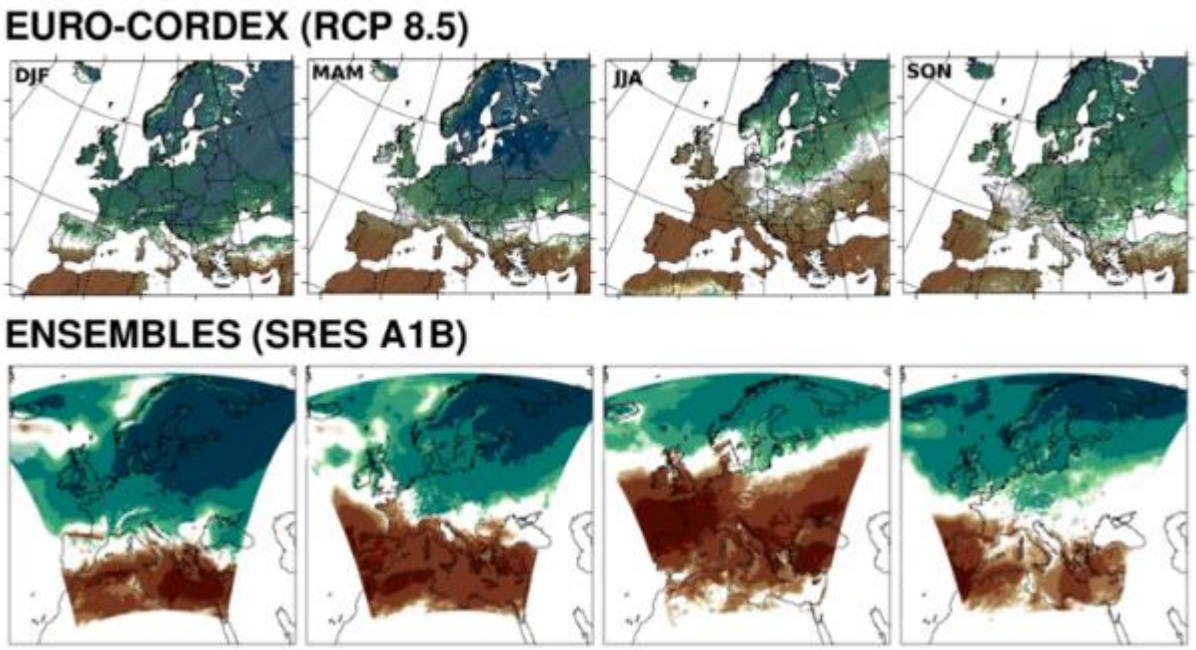


**Figure 10.25:**[Placeholder: Illustration of different and potentially conflicting information. The projected rainfall changes for the end of the century shows substantial differences between the EURO-CORDEX ensemble and the ENSEMBLES ensemble. For instance, for Northern France during MAM EURO-CORDEX projects wetting and ENSEMBLES no-change to drying. The difference is due to the different position of the North Atlantic jet in the EURO-CORDEX ensemble (driven by CMIP5 GCMs) and ENSEMBLES ensemble (driven by CMIP3 GCMs). The plan for evolving the figure after FOD consists in addressing two important questions that are still not answered by these figures: 1) Are the differences significant or just reflection of natural variability. 2) What are the positions of the North Atlantic jet in CMIP3 and CMIP5? To answer these questions: 1) In the SOD a difference map with significance should be included, or probabilistic maps instead of ensemble means, 2) the position of the jet or storm tracks in CMIP will be added.]

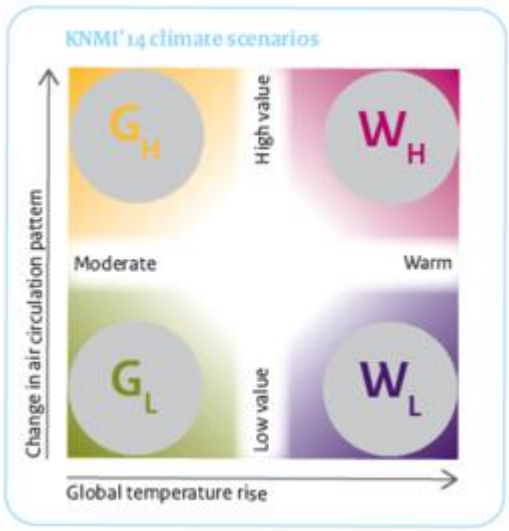


**Figure 10.26:**[Placeholder: Illustration of a story line approach in conveying regional climate projection. Four possible scenarios are presented depending on the rise of global mean temperature and change in circulation pattern. Source: KNMI 2014 climate scenarios http://www.climatescenarios.nl/scenarios_summary/index.html.]

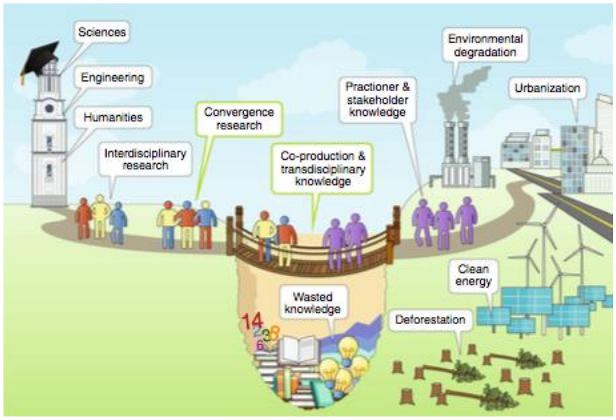


**Figure 10.27:**[Placeholder: To forge this bridge of saliency and relevance, co-producing knowledge with stakeholders is needed. This bridge is now often not existing resulting in wasted knowledge and hampering climate adaptation. Source (Irwin et al., 2018). The plan for evolving after FOD consists in based on this figure to design a new one that in addition also illustrates how a message can be distilled from this bridge.]

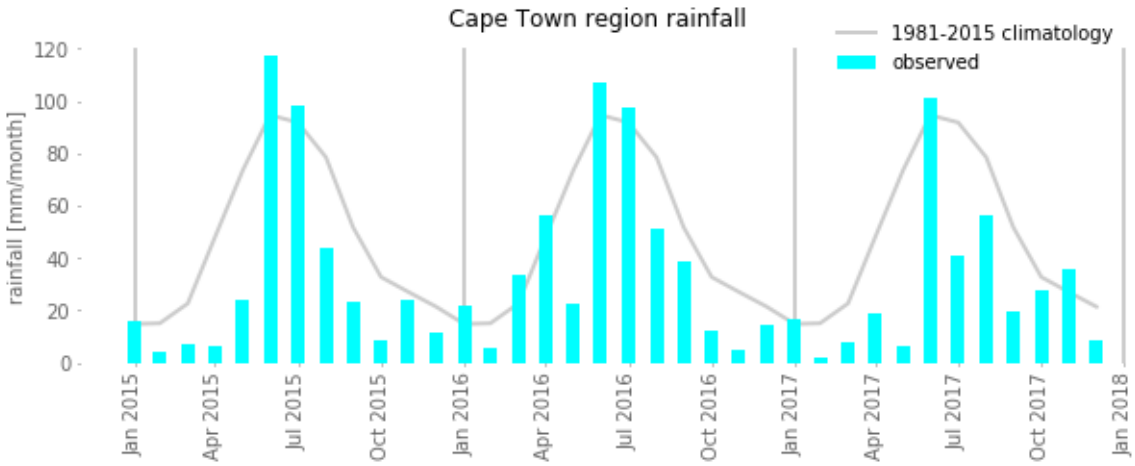


**Figure 10.28:**[Placeholder: Monthly rainfall during the 2015-2017 period. Average of 51 quality controlled and gap-filled series from stations within the Cape Town region.]

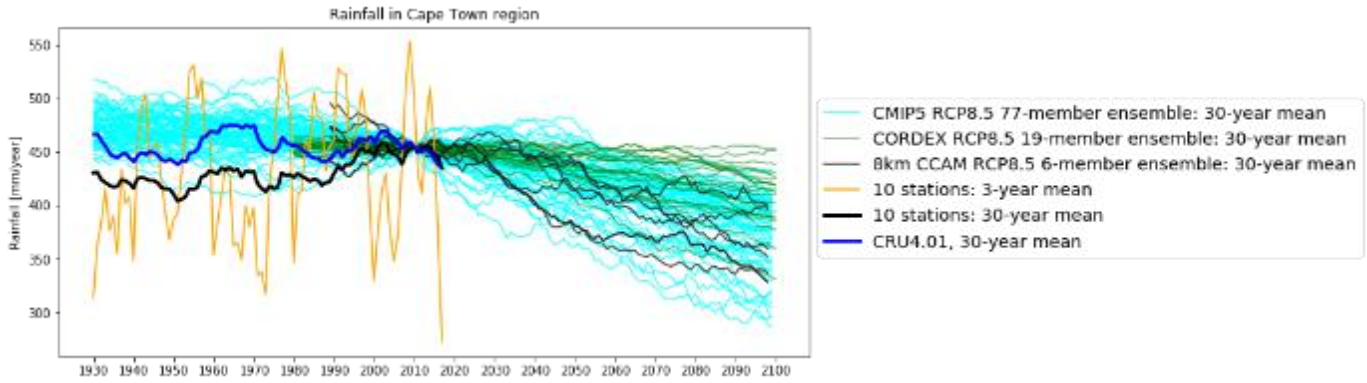


**Figure 10.29:**[Placeholder: Historical and projected rainfall over Cape Town region. Gridded datasets: averaged over 17ºE-19ºE, 32ºS-35ºS, with the observations an average of 10 quality-controlled, gap-filled time series for station located within the same bounding box. All data, apart from station-based data, are bias corrected in mean (but not in variance) over the 1981-2010 period. CMIP5 data include multiple runs of individual models. CORDEX data are simulations with 6 RCMs forced by one to ten GCMs. High-resolution simulations with C-CAM use forcings from 6 GCMs. Note that CRU4.01 dataset in the Cape Town region uses data from eight stations prior to 2000, and only 3-4 stations afterwards.]

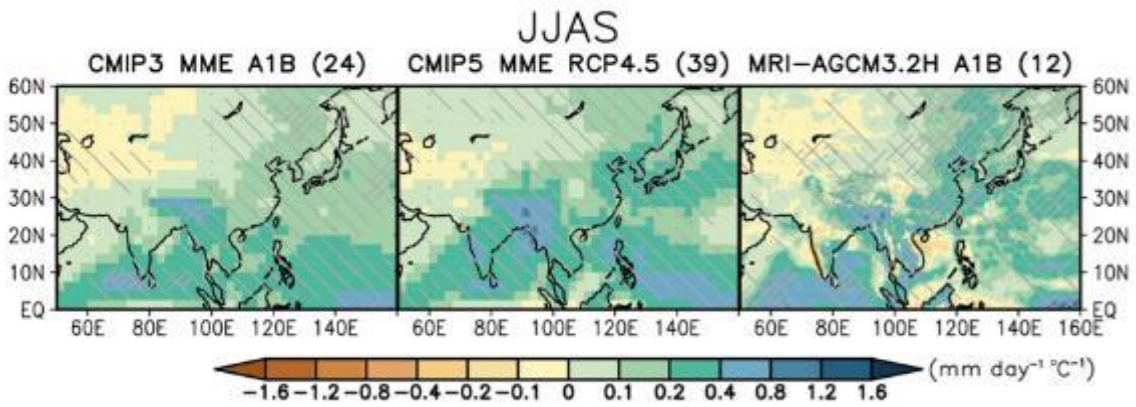


**Figure 10.30:**[Placeholder: Maps of precipitation changes for Central, North, East and South Asia in 2080-2099 with respect to 1986-2005 in June to August in the SRES A1B scenario with 24 CMIP3 models (left), and in the RCP4.5 scenario with 39 CMIP5 models (middle). Right figures are the precipitation changes in 2075-2099 with respect to 1979-2003 in the SRES A1B scenario with the 12 member 60 km mesh Meteorological Research Institute (MRI)-Atmospheric General Circulation Model 3.2 (AGCM3.2) multi-physics, multi-sea surface temperature (SST) ensembles (Kitoh et al., 2013). Precipitation changes are normalized by the global annual mean surface air temperature changes in each scenario. Light hatching denotes where more than 66% of models (or members) have the same sign with the ensemble mean changes, while dense hatching denotes where more than 90% of models (or members) have the same sign with the ensemble mean changes. Adapted from Fig. 14.24 of Christensen et al. (2013). To be replaced in SOD by corresponding figure using CMIP5, CMIP6 and CORDEX output.]

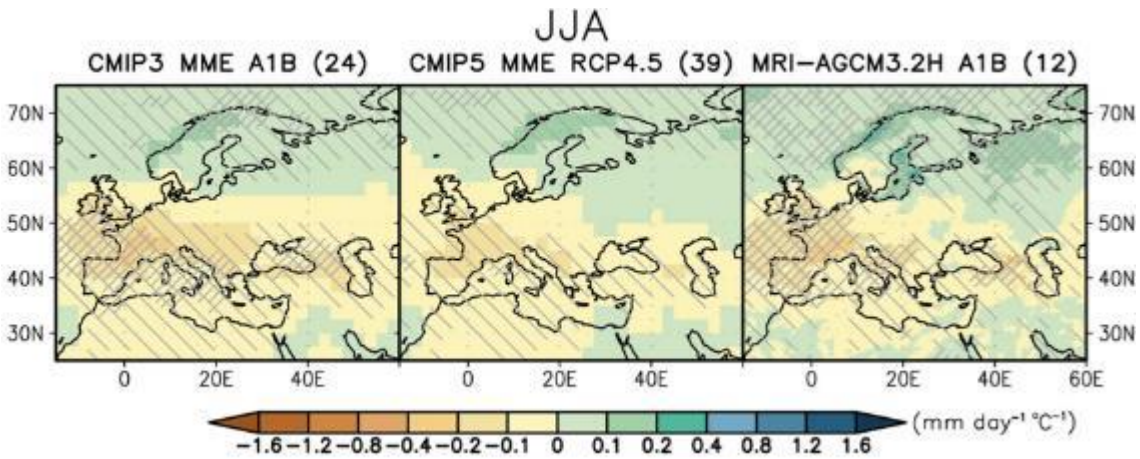


**Figure 10.31:**[Placeholder: Maps of precipitation changes for Europe and Mediterranean in 2080-2099 with respect to 1986-2005 in June to August in the SRES A1B scenario with 24 CMIP3 models (left), and in the RCP4.5 scenario with 39 CMIP5 models (middle). Right figures are the precipitation changes in 2075-2099 with respect to 1979-2003 in the SRES A1B scenario with the 12 member 60 km mesh Meteorological Research Institute (MRI)-Atmospheric General Circulation Model 3.2 (AGCM3.2) multi-physics, multi-sea surface temperature (SST) ensembles (Endo et al., 2012). Precipitation changes are normalized by the global annual mean surface air temperature changes in each scenario. Light hatching denotes where more than 66% of models (or members) have the same sign with the ensemble mean changes, while dense hatching denotes where more than 90% of models (or members) have the same sign with the ensemble mean changes. Adapted from Fig. 14.22 Christensen et al. (2013). To be replaced in SOD by corresponding figure using CMIP6 and CORDEX output.]

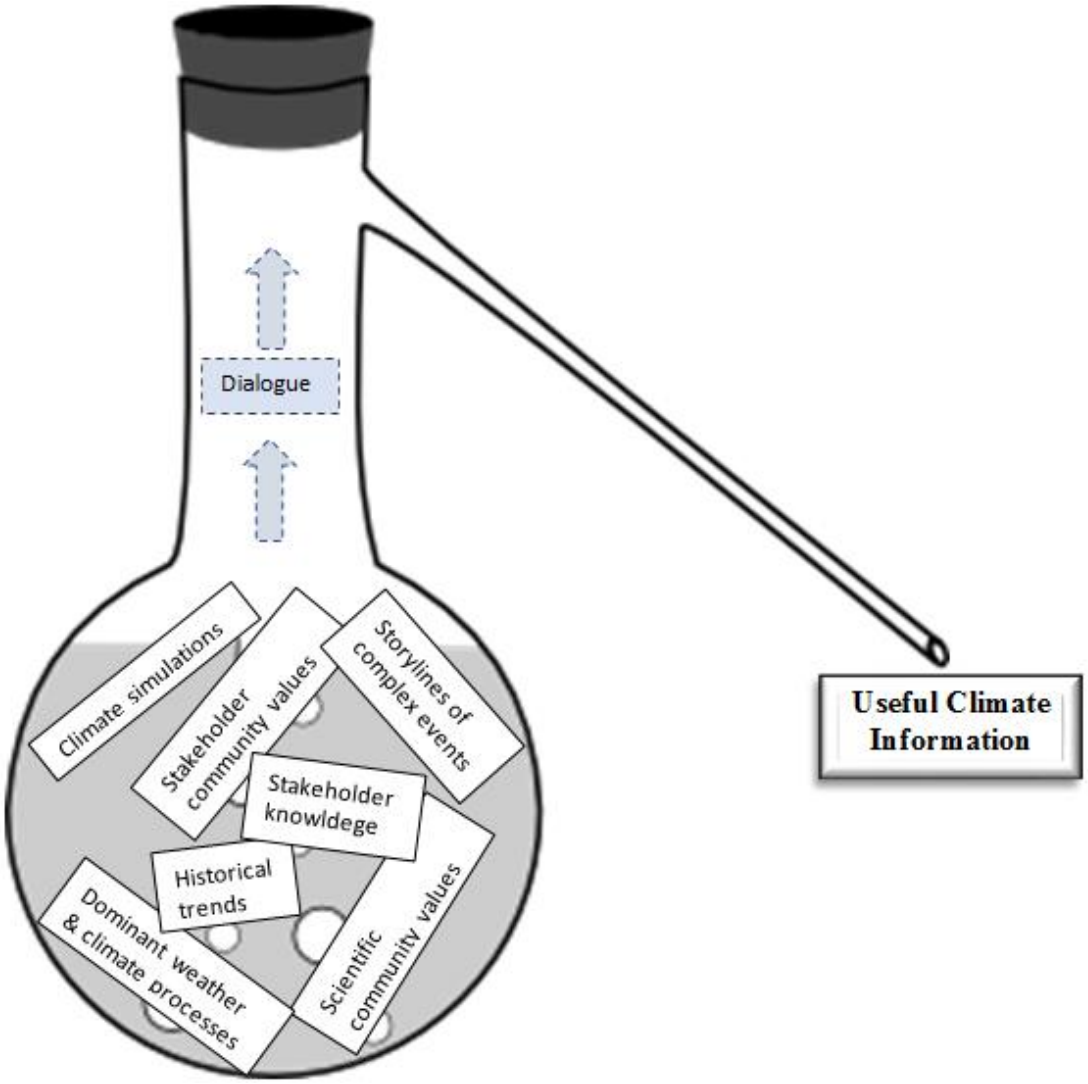


**FAQ 10.1, Figure 1:** [Placeholder: Schematic of possible figure showing the distillation of multiple factors into useful climate information. Underlying figure of the distillation flask found at http://www.clker.com/clipart-23858.html]